

Functionalized Photochromic Scaffolds

Dissertation

Zur Erlangung des Doktorgrades der Naturwissenschaften

(Dr. rer. nat.)

an der Fakultät für Chemie und Pharmazie

der Universität Regensburg



vorgelegt von

Karin Rustler

aus Regenstauf

2019

Der experimentelle Teil der vorliegenden Arbeit wurde in der Zeit von November 2016 bis Mai 2019 unter der Betreuung von Prof. Dr. Burkhard König am Institut für Organische Chemie der Universität Regensburg durchgeführt. Zusätzlicher Betreuer war von Juni 2019 bis August 2019 Prof. Dr. Itaru Hamachi am Department of Synthetic Chemistry and Biological Chemistry an der Graduate School of Engineering der Kyoto Universität, Japan.

Date of submission: 09.10.2019

Date of colloquium: 27.11.2019

Board of examiners:	Prof. Dr. Julia Rehbein	(chair)
	Prof. Dr. Burkhard König	(1 st referee)
	PD Dr. Hans-Heiner Gorris	(2 nd referee)
	Prof. Dr. Frank-Michael Matysik	(examiner)

„Man merkt nie, was schon getan wurde, man sieht immer nur, was noch zu tun bleibt.“

- Marie Curie

TABLE OF CONTENTS

1	PHOTOCHROMIC SURFACTANTS BASED ON AZOBENZENE.....	1
1.1	Introduction.....	3
1.2	Results and Discussion	4
1.2.1	Design and Syntheses	4
1.2.2	Photochemical Characterization.....	7
1.2.3	Drop Shape Analysis (DSA)	9
1.3	Conclusion.....	12
1.4	Experimental Part	12
1.4.1	General Procedures and Materials	12
1.4.2	Synthetic Procedures and Characterization.....	13
1.5	Supporting Information.....	18
1.5.1	¹ H- and ¹³ C-NMR Spectra.....	18
1.5.2	UV-Vis Absorption Spectra, Cycle Performances, and Thermal Half-Lives.....	27
1.6	References.....	33
2	PHOTOCHROMIC EVALUATION OF ARYLAZO <i>NH</i>-PYRAZOLES	37
2.1	Introduction.....	39
2.2	Results and Discussion	40
2.2.1	Design and Syntheses	40
2.2.2	Photochemical Characterization.....	42
2.3	Conclusion.....	46
2.4	Experimental Part	47
2.4.1	General Procedures and Materials	47
2.4.2	Synthetic Procedures and Characterization.....	48
2.4.3	Laser Flash Photolysis.....	51
2.5	Supporting Information.....	52

2.5.1	¹ H- and ¹³ C-NMR Spectra.....	52
2.5.2	UV-Vis Absorption Spectra, Cycle Performances, and Thermal Half-Lives.....	63
2.5.3	PSS Determination <i>via</i> NMR.....	107
2.6	References.....	118
3	DEVELOPMENT OF PHOTOSWITCHABLE INHIBITORS FOR β-GALACTOSIDASE	123
3.1	Introduction.....	125
3.2	Results and Discussion	127
3.2.1	Design and Syntheses	127
3.2.2	Photochemical Characterization.....	130
3.2.3	Enzyme Inhibition	132
3.2.4	Docking Experiments.....	134
3.3	Conclusion.....	135
3.4	Experimental Part.....	135
3.4.1	General Procedures and Materials.....	135
3.4.2	Synthetic Procedures and Characterization.....	137
3.4.3	Enzymatic Inhibition Studies.....	147
3.4.4	Molecular Docking	148
3.5	Supporting Information.....	149
3.5.1	¹ H- and ¹³ C-NMR Spectra.....	149
3.5.2	UV-Vis Absorption Spectra, Cycle Performances, and Thermal Half-Lives.....	169
3.5.3	HPLC- and NMR-Based Photochromic Characterization	182
3.5.4	Enzymatic Inhibition.....	183
3.6	References.....	184
4	LIGHT-SWITCHABLE ANTAGONISTS FOR THE HISTAMINE H₁ RECEPTOR AT THE ISOLATED GUINEA PIG ILEUM.....	189
4.1	Introduction.....	191

4.2	Results and Discussion	193
4.2.1	Design and Syntheses	193
4.2.2	Photochemical Characterization.....	197
4.2.3	Studies on the Isolated Guinea Pig Ileum	199
4.3	Conclusion.....	201
4.4	Experimental Part	202
4.4.1	General Procedures and Materials	202
4.4.2	Synthetic Procedures and Characterization.....	203
4.4.3	Organ-Pharmacological Testing	208
4.5	Supporting Information.....	210
4.5.1	¹ H- and ¹³ C-NMR Spectra.....	210
4.5.2	HSQC and HMBC spectra	223
4.5.3	UV-Vis Absorption Spectra and Cycle Performances	237
4.5.4	Thermal Half-Lives (THL).....	241
4.5.5	Additional Photochemical Data	245
4.5.6	Analytical HPLC Traces for Purity Determination	246
4.5.7	Analytical HPLC Traces for PSS Determination.....	253
4.5.8	PSS Determination <i>via</i> NMR.....	255
4.5.9	Single Crystal X-ray Crystallography	259
4.5.10	Additional Pharmacological Data	267
4.5.11	Additional Chemical Structures	267
4.6	References.....	268
5	A PHOTOCROMIC GLYCINE POTENTIATOR AZOLOG.....	273
5.1	Introduction.....	275
5.2	Results and Discussion	277
5.2.1	Design and Syntheses	277
5.2.2	Photochemical Characterization.....	278
5.2.3	<i>In Vivo</i> Behavioral Studies.....	280

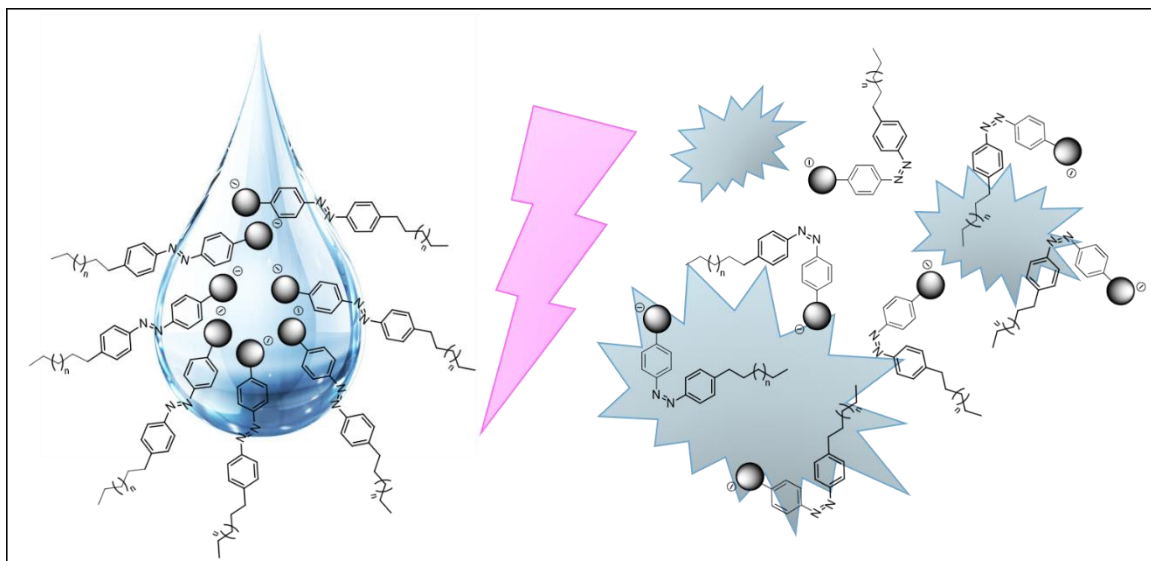
5.2.4	Molecular Docking	281
5.3	Conclusion.....	284
5.4	Experimental Part	284
5.4.1	General Procedures and Materials	284
5.4.2	Synthetic Procedures and Characterization.....	285
5.4.3	<i>In Vivo</i> Behavioral Studies.....	286
5.4.4	Molecular Docking	287
5.5	Supporting Information.....	289
5.5.1	¹ H- and ¹³ C-NMR Spectra.....	289
5.5.2	UV-Vis Absorption Spectra and Cycle Performances	291
5.5.3	Thermal Half-Lives.....	292
5.5.4	Analytical HPLC Traces for Purity Determination	293
5.5.5	Analytical HPLC Traces for PSS Determination	295
5.5.6	PSS Determination <i>via</i> NMR	296
5.5.7	Single Crystal X-ray Crystallography	297
5.6	References.....	301
6	FULGAZEPAM: A FULGIMIDE-BASED POTENTIATOR OF GABA_A RECEPTORS	305
6.1	Introduction.....	307
6.2	Results and Discussion	311
6.2.1	Syntheses.....	311
6.2.2	Photochemical Characterization.....	312
6.2.3	<i>In Vitro</i> Patch-Clamp Testing.....	314
6.2.4	<i>In Vivo</i> Behavioral Studies.....	315
6.3	Conclusion.....	317
6.4	Experimental Part	318
6.4.1	General Procedures and Materials	318
6.4.2	Synthetic Procedures and Characterization.....	319

6.4.3	<i>In Vitro</i> Studies	321
6.4.4	Behavioral Studies	323
6.5	Supporting Information.....	325
6.5.1	¹ H- and ¹³ C-NMR Spectra.....	325
6.5.2	UV-Vis Absorption Spectra and Cycle Performances	329
6.5.3	Analytical HPLC Traces for Purity Determination	331
6.5.4	Analytical HPLC Traces for PSS Determination.....	333
6.5.5	Single Crystal X-ray Crystallography	335
6.5.6	Additional <i>in Vitro</i> Patch-Clamp Data of Compound 3.....	337
6.6	References.....	338
7	AZOLOGIZATION OF SEROTONIN 5-HT₃ RECEPTOR ANTAGONISTS	345
7.1	Introduction.....	347
7.2	Results and Discussion	349
7.2.1	Design and Syntheses	349
7.2.2	Photochemical Characterization.....	353
7.2.3	<i>In Vitro</i> Patch-Clamp Studies.....	355
7.3	Conclusion.....	356
7.4	Experimental Part.....	357
7.4.1	General Procedures and Materials.....	357
7.4.2	Synthetic Procedures and Characterization.....	358
7.4.3	<i>In Vitro</i> Studies	363
7.5	Supporting Information.....	365
7.5.1	¹ H- and ¹³ C-NMR Spectra.....	365
7.5.2	UV-Vis Absorption Spectra, Cycle Performances, and Thermal Half-Lives.....	375
7.5.3	Tabular Summarized Photochemical Data	385
7.5.4	Single Crystal X-ray Crystallography	386
7.6	References.....	390

8	PHOTOCHROMIC METAL COMPLEX-AGONIST CONJUGATES	397
8.1	Introduction.....	399
8.2	Results and Discussion	401
8.2.1	Design and Syntheses	401
8.2.2	Photochemical Characterization.....	405
8.2.3	<i>In Vitro</i> Fluorescence Ca ²⁺ Imaging	407
8.3	Conclusion.....	409
8.4	Experimental Part	410
8.4.1	General Procedures and Materials	410
8.4.2	Synthetic Procedures and Characterization.....	411
8.4.3	<i>In Vitro</i> Studies	417
8.5	Supporting Information.....	419
8.5.1	¹ H- and ¹³ C-NMR Spectra.....	419
8.5.2	UV-Vis Absorption Spectra, Cycle Performances, and Thermal Half-Lives.....	429
8.5.3	<i>In Vitro</i> Fluorescence Ca ²⁺ Imaging	431
8.6	References.....	434
9	SUMMARY	439
10	ZUSAMMENFASSUNG	445
11	APPENDIX.....	453
11.1	Abbreviations	453
11.2	Curriculum Vitae.....	458
12	DANKSAGUNG	463

CHAPTER 1

1 Photochromic Surfactants Based on Azobenzene



This chapter has not been published.

This project was performed in collaboration with A. Dietz (Prof. H. Motschmann, University of Regensburg). K. Rustler performed the synthesis and (photo-)chemical characterization of all compounds. A. Dietz performed the drop shape analysis. Mass spectrometry analysis were performed by the analytical department at the University of Regensburg. Prof. B. König and Prof. H. Motschmann supervised the project.

1.1 Introduction

The equilibrium of assembly and disruption of amphiphilic molecules into ordered structures such as monolayers, bilayers, vesicles and micelles is based on their divided character containing both a hydrophilic and a hydrophobic moiety in one molecule.^[1] Besides their use for solubilization, emulsification, foaming, and detergency,^[2] the dynamics of those clusters allow to control and manipulate motion of particles,^[2-5] including reaction control *via* storage and release of reactants on demand.^[6-11] Besides redox activity^[12-15] and magnetic-field-sensitivity^[16] as triggers for destabilizing responses, optical control *via* light allows modulation with high spatial and temporal resolution. Several classes of photoreactions interfering with organized structures of surfactants bearing a light-responsive hydrophilic/hydrophobic change are reported. So-called “destructible surfactants” undergo irreversible photoscission between their hydrophilic headgroups and hydrophobic tails. For reversible structural modulations, the most common tool is represented by a photoinduced *cis-trans* isomerization^[1] of either an unsaturated double bond or an azobenzene within the hydrophobic chain of the surfactant.

Photochromic scaffolds, *e.g.*, dithienylethenes (DTEs), fulgides, and the above mentioned azobenzenes have achieved increasing interest as small molecular devices enabling non-invasive, reversible light-control without any waste or side-products. Especially azobenzenes are frequently exploited for industrial and biomedical applications benefiting of their large change in sterics and polarity upon isomerization. In the case of azobenzene-based surfactants, the isomerization enhances either the hydrophobic character of the tail (*trans* isomer) or the hydrophilic character of the surfactant’s head group (*cis* isomer). Furthermore, the change in dipole moment and end-to-end distance leads to a variation in the organization of the surfactant molecules disrupting their arrangements.^[17-19] It is reported that the addition of an azo moiety to the hydrophobic part of linear alkanesulfonates and -carboxylates promotes micellization.^[20] In addition, it

induces preassociation of surfactant monomers below the critical micellar concentration (cmc).^[21] Furthermore, the *cis-trans* isomerization affects the surface tension of liquids resulting in changes up to 20 mN/m,^[22,23] which can be determined using the hanging drop experiment.^[24] A pendant drop is a small column of liquid provided at the end of a low diameter vertical tube and is defined by gravitation and surface tension. The latter one is related to the drop's shape as described by the Young-Laplace equation.^[25]

In the presented work, we envisioned that functionalizing amphiphilic molecules with an azobenzene as photochromic core between the polar head group and the hydrophobic chain could result in bursting of a hanging drop upon light-induced *trans-cis* isomerization and resulting change in organization of the molecules and overall surface tension. Hence, we synthesized and (photo-)chemically characterized differently substituted azo-surfactants, which were tested in cooperation with the group of Prof. Motschmann.

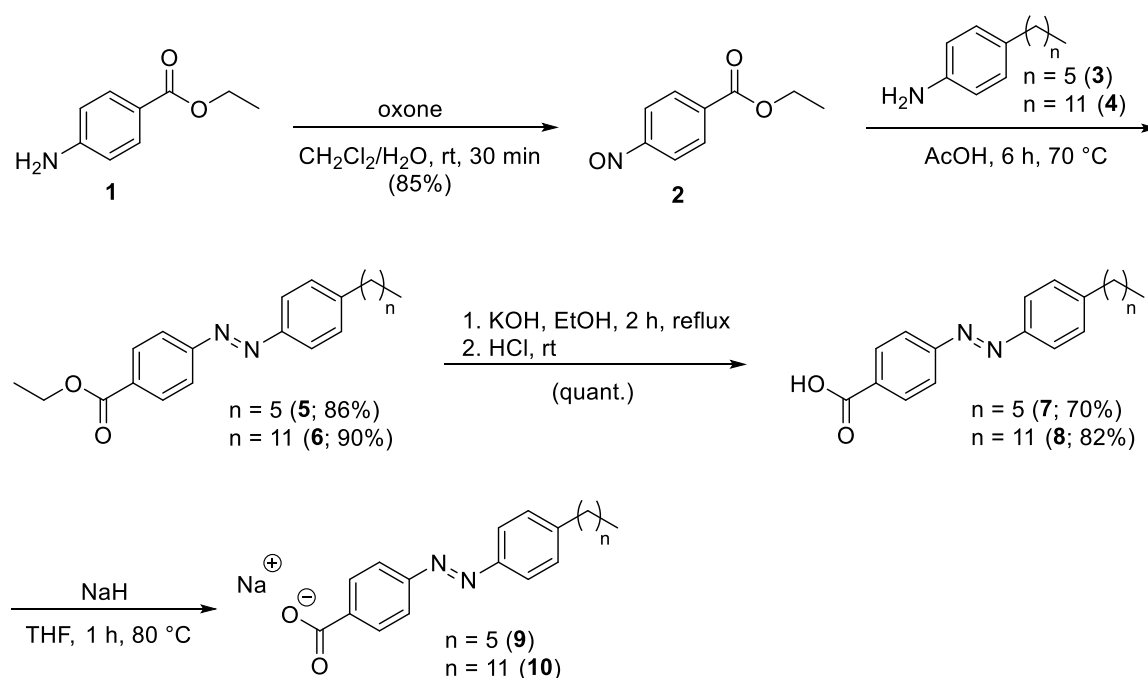
1.2 Results and Discussion

1.2.1 Design and Syntheses

Design. In a first attempt, alkane-azo-sulfonates and -carboxylates with different lengths of their hydrophobic tails are synthesized. To further increase the speed of the light-triggered *trans-cis* isomerization, push-pull azo-surfactants bearing an electron withdrawing nitro substitution as headgroup and a hydrophobic alkyl chain linked to the azo *via* an electron donating substituent are synthesized.

Synthesis of alkane-azo-carboxylates. The synthesis of differently substituted alkane-azo-carboxylates is based on a Baeyer^[26]-Mills^[27]-reaction of an aromatic nitroso and an arylamine (Scheme 1). In a first synthetic step, ethyl-4-aminobenzoate (**1**) is oxidized to its corresponding nitroso derivative **2** using potassium peroxymonosulfate as oxidant in a biphasic solvent mixture preventing overoxidation.^[28] The subsequent reaction of nitroso **2** with *para* alkyl substituted anilines ($n = 5$, **3**; $n = 11$, **4**) afforded alkane-azo-esters **5** ($n = 5$) and **6** ($n = 11$).

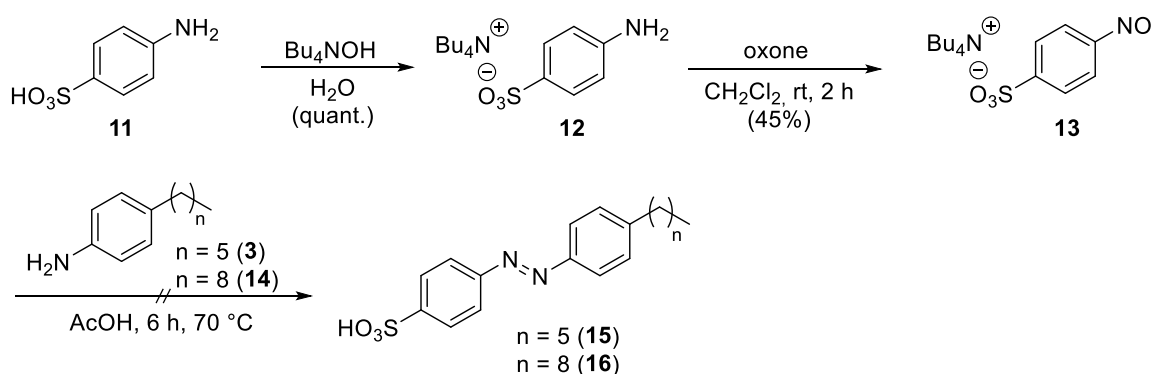
Cleavage of the ester in basic media using potassium hydroxide provided the corresponding alkane-azo-carboxylates **7** ($n = 5$) and **8** ($n = 11$).^[29] To increase both the solubility in aqueous media and the polarity of the head group, samples of the carboxylic acids **7** and **8** were converted into their sodium salts **9** ($n = 5$) and **10** ($n = 11$). As the corresponding carboxylic acids **7** and **8** are not deprotonated in water (pH = 7) due to their low pK_a value (pK_a of benzenecarboxylic acid = 4.2;^[30] pK_a of azobenzene carboxylic acid = 3.8^[31]), the sodium salts provide the presence of a charged species during the investigations.



Scheme 1. Synthesis of alkane-azo-carboxylates **7** ($n = 5$) and **8** ($n = 11$) and their corresponding sodium salts **9** ($n = 5$) and **10** ($n = 11$).^[26-29]

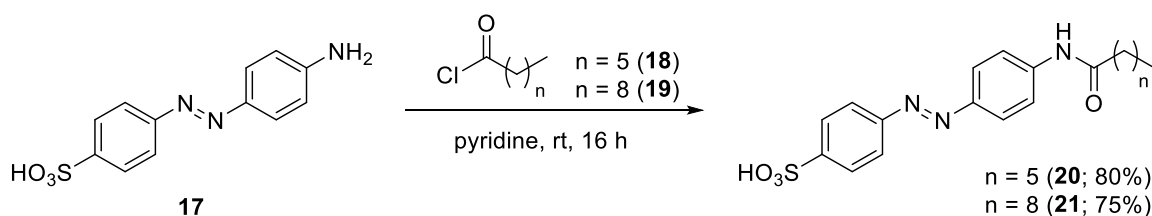
Synthesis of alkane-azo-sulfonates. In a first approach, a Baeyer^[26]-Mills^[27]-reaction in analogy to Scheme 1 starting from benzene sulfonic acid was attempted for the synthesis of alkane-azo-sulfonates (Scheme 2). Sulfanilic acid (**11**) was converted into its tetrabutylammonium salt **12**, which is soluble in organic solvents. Subsequent nitroso formation using oxone in a biphasic reaction mixture prevents overoxidation.^[32] Due to low or no yields in the azo forming step, the synthetic strategy was changed. Byproducts are the overoxidized nitro-substituted

sulfanilic acid as well as the symmetric azobenzene upon reaction of **13** with its precursor **12**.



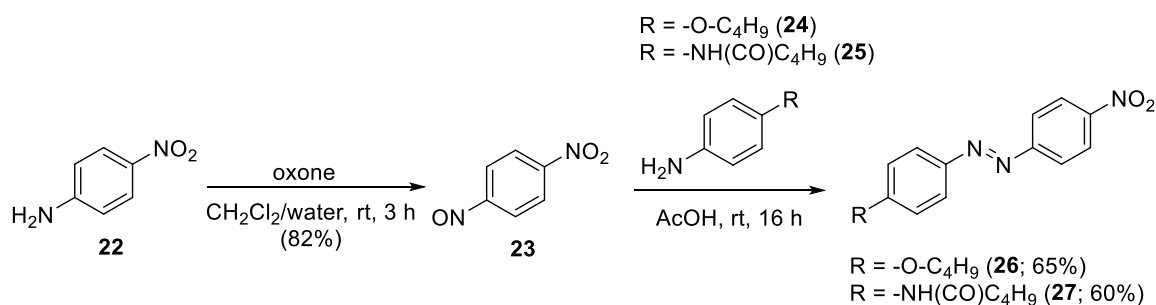
Scheme 2. Attempted synthesis of alkane-azo-sulfonates **15** ($n = 5$) and **16** ($n = 8$).^[26,27,32]

In a second approach, commercially available aminoazobenzene sulfonic acid **17** was reacted with alkanoyl chlorides **18** ($n = 5$) and **19** ($n = 8$) to generate the alkanoyl amido azobenzene sulfonic acids **20** ($n = 5$) and **21** ($n = 8$) in high yields. In contrast to the above mentioned carboxylic acid derivatives, the sulfonic acid derivatives **20** and **21** are completely deprotonated in water (pH = 7) bearing an overall negative charge (pK_a of benzenesulfonic acid = 0.7)^[32].



Scheme 3. Synthesis of the sulfonic acid substituted alkanamide azobenzene derivatives **20** and **21**.

Synthesis of the push-pull derivatives. The synthesis of the push-pull azobenzenes **26** and **27** is based on a Baeyer^[26]-Mills^[27]-reaction. *Para* nitro aniline **22** was oxidized to its nitroso derivative and reacted with alkanoyl ether- **24** and alkanoyl amide-substituted aniline **25**, respectively.



Scheme 4. Synthesis of the push-pull azobenzene derivatives **26** and **27**.^[26,27]

1.2.2 Photochemical Characterization

The decision for one type of photochromic scaffold is strongly dependent on its application. In the case of amphiphiles, azobenzene as light-responsive moiety can easily be incorporated between the polar head group and the hydrophobic tail. In addition to their synthetic accessibility, azobenzenes undergo efficient light-induced photoisomerization without photodegradation, loss of responsiveness or photobleaching.^[34,35]

The in general thermally more stable, planar *trans* isomer^[35] (except bridged azobenzenes^[36]) interconverts to its metastable, bent *cis* isomer upon irradiation with light of an appropriate wavelength resulting in a large change in geometry and dipole moment. Regeneration of the *trans* state occurs either quantitatively by thermal back relaxation or by irradiation with light only partially due to a substantial overlap of the absorption band of the *trans* and *cis* isomer.^[35]

The photochemical properties of compounds **7**, **8**, **20**, **21**, **26**, and **27** were investigated by UV-Vis spectroscopy in DMSO. Figure 1 shows exemplarily the UV-Vis absorption spectrum (left panel) and cycle performance (right panel) of alkane-azo-carboxylate **8** measured 50 μM in DMSO. The changes in absorption maxima upon irradiation are indicated with black arrows. Dotted black arrows label the isosbestic points indicating a clear two component switching without decomposition or side-reaction upon isomerization. The black curve represents the UV-Vis spectrum of compound **8** in its thermal equilibrium. Upon irradiation induced *trans-cis* isomerization using $\lambda = 365$ nm, the maximum around 350 nm

decreased and a new maximum around 440 nm arised representing the compound in its *cis*-photostationary state (*cis*-PSS; red curve). Reisomerization is triggered by irradiation with visible light of $\lambda = 455$ nm (blue curve, *trans*-PSS). The performance of the repetitive cycle measurement shows excellent fatigue resistance. After ten cycles no signs of photodegradation were observed.

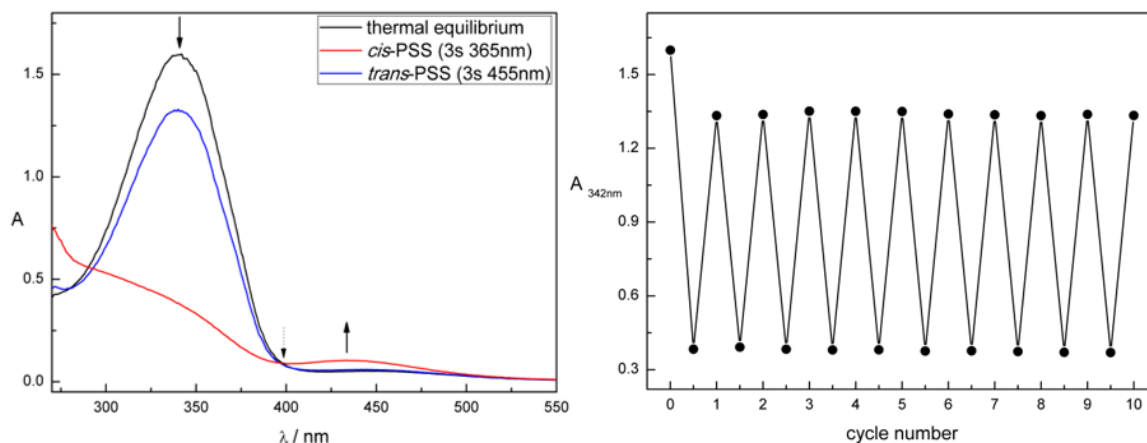


Figure 1. Compound **8** measured 50 μ M in DMSO. Left: UV-Vis spectrum. Right: Repetitive cycle performance.

In comparison, the photochromic properties of the alkane-azo-sulfonates **20** and **21** (Table 1) show a slight shift in the absorption spectrum due to the stronger electron withdrawing character of the sulfonic acid moiety compared to the carboxylic acid moiety. This tendency is more pronounced for the push-pull derivatives **26** and **27**. Figure 2 shows the UV-Vis spectrum (left panel) and cycle performance (right panel) of compound **27** measured 50 μ M in DMSO. The *trans* absorption maximum is shifted to the visible range. Both isomerizations are triggered using visible light: blue light of $\lambda = 400$ nm triggers the *trans* to *cis* and green light of $\lambda = 505$ nm the *cis* to *trans* isomerization. Furthermore, a broadening and overlap of the *trans* absorption band with the *cis* absorption band can be observed. In addition, as reported for push-pull azobenzenes, the thermal half-lives of **26** and **27** are shorter compared to the alkane-azo-sulfonate and -carboxylate derivatives (Table 1).

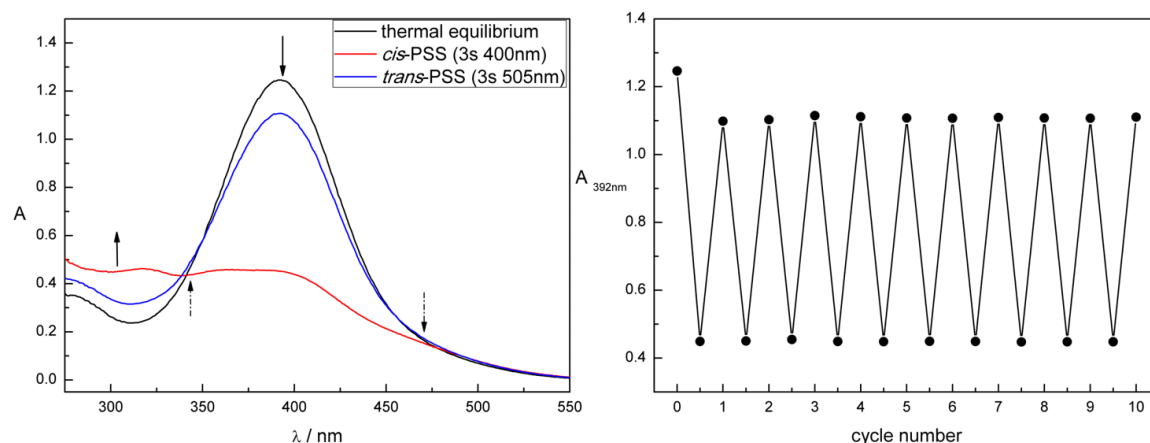


Figure 2. Compound **27** measured 50 μM in DMSO. Left: UV-Vis spectrum. Right: Repetitive cycle performance.

All synthesized compounds featured excellent photochromic properties. Table 1 summarizes the characteristic photochemical data (absorption maxima, isosbestic points, thermal half-lives) of compounds **7**, **8**, **20**, **21**, **26**, and **27** measured 50 μM in DMSO.

Table 1. Summary of the characteristic photochemical data of compounds **7**, **8**, **20**, **21**, **26**, and **27** measured 50 μM in DMSO.

Entry	Compound	λ_{\max} <i>trans</i> isomer [nm]	λ_{\max} <i>cis</i> isomer [nm]	Isosbestic points [nm]	THL ^(a)
1	7	341	439	292, 401	32 h
2	8	342	434	291, 397	26 h
3	20	367	443	316, 434	20 h
4	21	368	446	316, 433	24 h
5	26	382	-	332, 460	12 min
6	27	392	-	343, 464	18 min

(a) Determined by thermal relaxation of an irradiated sample (*cis*-PSS) in the dark at room temperature.

1.2.3 Drop Shape Analysis (DSA)

The change in the surface tension of a water drop containing a monolayer of the synthesized photochromic surfactant was measured in its *trans* and *cis* state using drop shape analysis (DSA) of a hanging drop. Due to insufficient solubility of compounds **20**, **21**, **26** and **27** the experiment could only be performed for carboxylic acids **7** and **8** and their sodium salts **9** and **10**. Figure 3 depicts the

experimental DSA setup. A camera and a lamp are used to record the changes in the drop's shape. Cut-off filters are used to ensure, that no light of the lamp or the camera might induce isomerization of the azobenzene surfactants. Two LEDs are switched on alternately to accumulate a substantial amount of the desired isomer. Using this method, changes in the surface tension of the hanging drop upon continuous irradiation can be analyzed.

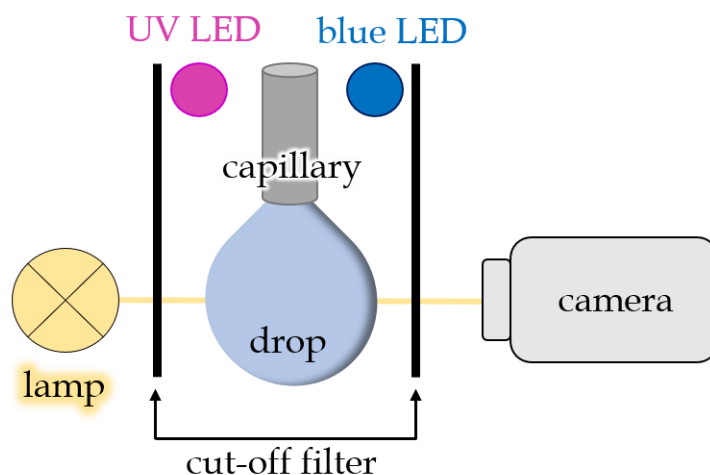


Figure 3. Schematic drawing of the DSA setup.

Figure 4 shows the plots of the measurement of the surface tension of compounds **7** and **8**, respectively **9** and **10**, depending on the subphase. As the solubility of the compounds in aqueous media was very low, the compounds were dissolved in chloroform and filtered to generate a saturated solution. The chloroform solution of the compound was applied to a hanging drop of water (compounds **7** and **8**) and 10 mM aqueous NaOH (compounds **9** and **10**), respectively. Upon evaporation of chloroform, the measurement of the surface tension was started. Irradiation with blue light ($\lambda = 460$ nm), triggering the *cis* to *trans* isomerization is labeled with a blue box. Irradiation with UV light ($\lambda = 365$ nm) for *trans* to *cis* isomerization is highlighted with a purple box. The surface tension of the protonated carboxylic acid **7** (subphase water) is shown in the upper left panel A; its deprotonated form **9** (subphase 10 mM NaOH) in the lower left panel B. The surface tension of

protonated compound **8** (subphase water) is shown in the upper right panel C; its deprotonated form **10** (subphase 10 mM NaOH) in the lower right panel D.

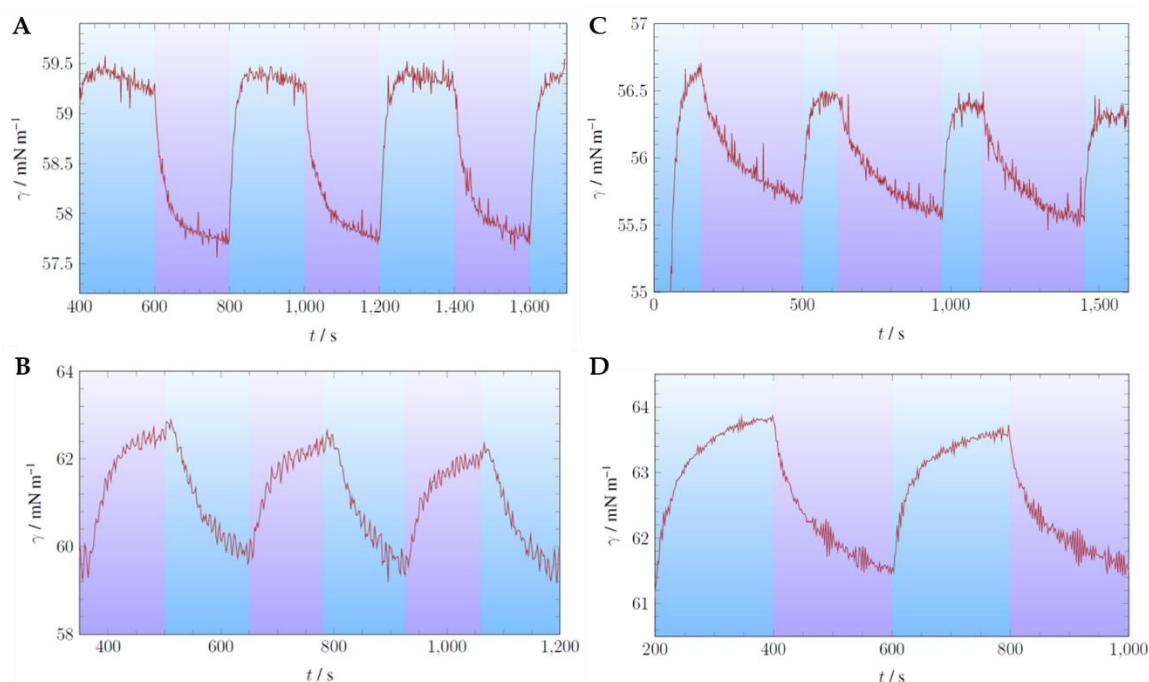


Figure 4. Measurement of the surface tension using drop shape analysis. (A) Compound **7**. Subphase water. (B) Compound **9**. Subphase 10 mM aq. NaOH. (C) Compound **8**. Subphase water. (D) Compound **10**. Subphase 10 mM aq. NaOH.

Table 2 summarizes the surface tension values for the *trans* isomers, the *cis* isomers and the change in surface tension upon isomerization. The change in surface tension $\Delta\gamma$ is increasing upon use of 10 mM aqueous NaOH as subphase compared to water. This might be explained by a higher solubility of the compound upon deprotonation of the carboxylic acid. The packing of the molecules in the monolayer is tighter and results in a stronger disorganization of the molecules upon *trans* to *cis* isomerization and in a larger change of the surface tension. The changes in surface tension for the shorter alkyl chain ($n = 5$) are higher than for the longer alkyl chain ($n = 11$). This might also be explained by a higher solubility of the shorter linked compound and a tighter packing of the molecules in the monolayer. Interestingly, for compound **9** the surface tension of the *cis* isomer is higher than for the *trans* isomer whereas in all other cases the surface tension of the *trans* isomer is higher. An explanation might be, that the in general more soluble *cis* isomer, its shorter tail and the charged moiety allow for molecules of

the interface to enter the subphase. Thus, more molecules are packed in the subphase resulting in an increase of the surface tension, whereas in all other cases the *trans* isomer allows for tighter packing of the molecules.

Table 2. Surface tension of both isomeric states of compounds **7-10** analyzed using DSA.

Entry	Compound	γ <i>trans</i> isomer [mN/m]	γ <i>cis</i> isomer [mN/m]	$\Delta\gamma$ (<i>trans-cis</i>) [mN/m]	Subphase
1	7	59.5	57.7	+1.80	water
2	9	59.8	62.8	-3.00	10 mM aq. NaOH
3	8	56.5	55.6	+0.90	water
4	10	63.8	61.4	+2.40	10 mM aq. NaOH

1.3 Conclusion

In summary, we synthesized azobenzene derivatives equipped with a rather soluble, polar head group (carboxylic acid, sulfonic acid, nitro) in *para* position and a hydrophobic alkyl chain of different lengths in *para'* position. The compounds were synthesized based on a Baeyer^[26]-Mills^[27]-reaction or functionalization of commercially available azobenzene precursors. In the used setup, only the carboxylic acid substituted derivatives were soluble enough to be tested using drop shape analysis. Changes in surface tension upon light-induced isomerization could be triggered but were not strong enough to cause bursting of the hanging drop. As the azobenzene moiety seems to enhance the hydrophobic character of the surfactant stronger than expected, the azobenzene moiety should be placed in the middle of an alkyl chain bearing a positively charged head group on one end to behave similar as non-photochromic alkane-substituted surfactants.

1.4 Experimental Part

1.4.1 General Procedures and Materials

Commercial reagents and starting materials were purchased from the commercial suppliers abcr, Acros Organics, Alfa-Aesar, Fisher Scientific, Fluorochem, Merck, Sigma Aldrich, TCI, or VWR and used without any further purification. Solvents

were used in p.a. quality and dried according to common procedures, if necessary. Flash column chromatography was performed using Sigma Aldrich MN silica gel 60 M (40-63 μm , 230-400 mesh) for normal phase chromatography. Reaction monitoring *via* thin layer chromatography was performed on alumina plates coated with silica gel (Merck silica gel 60 F₂₅₄, layer thickness 0.2 mm). Melting points were determined using a Stanford Research System OptiMelt MPA 100 and are uncorrected. NMR spectra were measured on a Bruker Avance 300 (¹H 300.13 MHz, ¹³C 75.48 MHz), Bruker Avance III HD 400 (¹H 400.13 MHz, ¹³C 100.61 MHz), Bruker Avance III HD 600 (¹H 600.25 MHz, ¹³C 150.95 MHz) and Bruker Avance III 600 (¹H 600.25 MHz, ¹³C 150.95 MHz). The spectra are referenced against the NMR solvent (DMSO-*d*₆: δ_{H} = 2.50 ppm, δ_{C} = 39.52 ppm; CDCl₃-*d*: δ_{H} = 7.26 ppm, δ_{C} = 77.16 ppm) and chemical shifts δ are reported in ppm. Resonance multiplicity is abbreviated as: s (singlet), d (doublet), t (triplet), q (quartet), p (pentet), and m (multiplet). Carbon NMR signals are assigned using DEPT 135 and ¹H-¹³C HSQC spectra with (+) for primary/tertiary, (-) for secondary, and (q) for quaternary carbons. Mass spectra were recorded on a Finnigan MAT-SSQ 710 A, ThermoQuest Finnigan TSQ 7000, Agilent Q-TOF 6540 UHD, or a Jeol AccuTOF GCX instrument. UV-Vis absorption spectroscopy was performed in 10 mm quartz cuvettes using an Agilent 8543, Agilent Cary 100, or Agilent Varian Cary 50 spectrometer. Light sources for irradiation: λ = 365 nm (Seoul Viosys CUN6GB1A, 1000 mA, 1.4 W), λ = 400 nm (Luxeon 400 nm SZ-01-S2, 500 mA, 0.48 W), λ = 455 nm (Osram OSRON SSL 80 LD-CQ7P-1U3U, 1000 mA, 0.45 W), and λ = 505 nm (Osram OSRON SSL 80 LVCK7P-JYKZ, 800 mA, 163 lm). The power of the light is given based on the specifications supplied by the company when the LEDs were purchased.

1.4.2 Synthetic Procedures and Characterization

Ethyl (*E*)-4-((4-hexylphenyl)diazenyl)benzoate (5). Compound **5** was synthesized as orange solid in 86% yield (8.1 g, 24 mmol) using an adapted literature reported procedure^[29] starting from hexylaniline **5** (5.0 g, 28 mmol, 1.0 eq) and nitroso

benzoic acid ethyl ester **2**^[28] (5.0 g, 28 mmol, 1.0 eq). M.p.: 63 °C. ¹H-NMR (300 MHz, CDCl₃-*d*): δ = 8.24 – 8.15 (m, 2H), 7.98 – 7.84 (m, 4H), 7.38 – 7.28 (m, 2H), 4.41 (q, *J* = 7.1 Hz, 2H), 2.68 (t, 2H), 1.73 – 1.57 (m, 2H), 1.42 (t, *J* = 7.1 Hz, 3H), 1.36 – 1.24 (m, 5H), 0.98 – 0.81 (m, 3H). ¹³C-NMR (75 MHz, CDCl₃-*d*): δ = 166.1 (q), 155.2 (q), 150.9 (q), 147.4 (q), 131.9 (q), 130.6 (+), 129.2 (+), 123.2 (+), 122.5 (+), 61.2 (-), 36.0 (-), 31.7 (-), 31.2 (-), 29.0 (-), 22.6 (-), 14.4 (+), 14.1 (+). HR-MS (ESI): calcd. for C₂₁H₂₇N₂O₂⁺ [M+H]⁺ 339.2067; found 339.2072. MF: C₂₁H₂₆N₂O₂. MW: 338.45 g/mol.

Ethyl (E)-4-((4-dodecylphenyl)diazenyl)benzoate (6). Compound **6** was synthesized as orange solid in 95% yield (1.5 g, 3.6 mmol) using an adapted literature reported procedure^[29] starting from dodecylaniline **4** (1.0 g, 3.8 mmol, 1.0 eq) and nitroso benzoic acid ethyl ester **2**^[28] (0.70 g, 3.8 mmol, 1.0 eq). M.p.: 71 °C. ¹H-NMR (400 MHz, CDCl₃-*d*): δ = 8.19 (d, *J* = 8.7 Hz, 2H), 7.93 (d, *J* = 8.3 Hz, 2H), 7.87 (d, *J* = 8.2 Hz, 2H), 7.33 (d, *J* = 8.1 Hz, 2H), 4.42 (q, *J* = 7.1 Hz, 2H), 2.69 (t, *J* = 7.7 Hz, 2H), 1.66 (p, *J* = 7.3 Hz, 2H), 1.43 (t, *J* = 7.1 Hz, 3H), 1.35 – 1.19 (m, 18H), 0.88 (t, *J* = 6.6 Hz, 3H). ¹³C-NMR (101 MHz, CDCl₃-*d*): δ = 166.1 (q), 155.3 (q), 150.9 (q), 147.5 (q), 131.9 (q), 130.6 (+), 129.2 (+), 123.2 (+), 122.5 (+), 61.2 (-), 36.0 (-), 31.9 (-), 31.3 (-), 29.7 (-), 29.7 (-), 29.7 (-), 29.6 (-), 29.5 (-), 29.4 (-), 29.3 (-), 22.7 (-), 14.4 (+), 14.1 (+). HR-MS (ESI): calcd. for C₂₇H₃₉N₂O₂⁺ [M+H]⁺ 423.3006; found 423.2997. MF: C₂₇H₃₈N₂O₂. MW: 422.61 g/mol.

(E)-4-((4-hexylphenyl)diazenyl)benzoic acid (7). Compound **7** was synthesized as orange solid in 70% yield (2.6 g, 8.4 mmol) using an adapted literature reported procedure^[29] starting from ethyl ester benzoic acid azobenzene **5** (4.2 g, 12 mmol, 1.0 eq) and KOH (38 g, 0.68 mol, 55 eq). M.p.: 228 °C. ¹H-NMR (400 MHz, DMSO-*d*₆): δ = 13.22 (s, 1H), 8.16 – 8.10 (m, 2H), 7.97 – 7.91 (m, 2H), 7.87 – 7.82 (m, 2H), 7.45 – 7.39 (m, 2H), 2.67 (t, *J* = 7.7 Hz, 2H), 1.60 (p, *J* = 7.5 Hz, 2H), 1.36 – 1.20 (m, 6H), 0.89 – 0.79 (m, 3H). ¹³C-NMR (101 MHz, DMSO-*d*₆): δ = 167.2 (q), 154.8 (q), 150.7 (q), 147.8 (q), 133.1 (q), 131.1 (+), 129.9 (+), 123.4 (+), 122.9 (+), 35.5 (-), 31.5 (-), 31.1 (-), 28.8 (-), 22.5 (-), 14.4 (+). HR-MS (ESI): calcd. for C₁₉H₂₃N₂O₂⁺ [M+H]⁺ 311.1754; found 311.1760. MF: C₁₉H₂₂N₂O₂. MW: 310.40 g/mol.

(E)-4-((4-dodecylphenyl)diazenyl)benzoic acid (8). Compound **8** was synthesized as orange solid in 82% yield (1.1 g, 2.9 mmol) using an adapted literature reported procedure^[29] starting from ethyl ester benzoic acid azobenzene **6** (1.5 g, 3.5 mmol, 1.0 eq) and KOH (11 g, 0.20 mol, 55 eq). M.p.: 198 °C. ¹H-NMR (400 MHz, DMSO-*d*₆): δ = 13.23 (s, 1H), 8.16 – 8.10 (m, 2H), 7.97 – 7.91 (m, 2H), 7.89 – 7.83 (m, 2H), 7.47 – 7.40 (m, 2H), 2.72 – 2.64 (m, 2H), 1.62 (t, *J* = 7.4 Hz, 2H), 1.32 – 1.21 (m, 18H), 0.89 – 0.81 (m, 3H). ¹³C-NMR (151 MHz, DMSO-*d*₆): δ = 166.5 (q), 154.8 (q), 150.7 (q), 147.9 (q), 133.2 (q), 131.1 (+), 129.9 (+), 123.4 (+), 122.9 (+), 35.5 (-), 31.8 (-), 31.1 (-), 29.5 (-), 29.5 (-), 29.5 (-), 29.4 (-), 29.3 (-), 29.2 (-), 29.1 (-), 22.6 (-), 14.4 (+). HR-MS (ESI): calcd. for C₂₅H₃₅N₂O₂⁺ [M+H]⁺ 395.2693; found: 395.2692. MF: C₂₅H₃₄N₂O₂. MW: 394.56 g/mol.

(E)-4-((4-heptanamidophenyl)diazenyl)benzenesulfonic acid (20). *Para* amino *para'* sulfonic acid azobenzene (**17**) (1.0 g, 3.6 mmol, 1.0 eq) was dissolved in pyridine (0.20 L) and heptanoyl chloride (**18**) (0.54 g, 3.6 mmol, 1.0 eq) was added dropwise. The reaction mixture was stirred at room temperature for 16 hours. The solvent was evaporated. Purification by recrystallization from methanol afforded the desired product (1.1 g, 2.9 mmol, 80%). M.p.: decomposition over 300 °C. ¹H-NMR (400 MHz, DMSO-*d*₆): δ = 10.24 (s, 1H), 7.91 – 7.85 (m, 2H), 7.85 – 7.72 (m, 6H), 2.36 (t, *J* = 7.4 Hz, 2H), 1.60 (p, *J* = 7.4, 6.6 Hz, 2H), 1.36 – 1.24 (m, 6H), 0.86 (t, 3H). ¹³C-NMR (101 MHz, DMSO-*d*₆): δ = 172.3 (q), 152.2 (q), 150.8 (q), 147.8 (q), 143.0 (q), 127.1 (+), 124.2 (+), 122.3 (+), 119.6 (+), 37.0 (-), 31.5 (-), 28.8 (-), 25.4 (-), 22.5 (-), 14.4 (+). HR-MS (ESI): calcd. for C₁₉H₂₄N₃O₄S⁺ [M+H]⁺ 390.1482; found: 390.1487. MF: C₁₉H₂₃N₃O₄S. MW: 389.47 g/mol.

(E)-4-((4-decanamidophenyl)diazenyl)benzenesulfonic acid (21). *Para* amino *para'* sulfonic acid azobenzene (**17**) (1.0 g, 3.6 mmol, 1.0 eq) was dissolved in pyridine (0.20 L) and decanoyl chloride (**19**) (0.69 g, 3.6 mmol, 1.0 eq) was added dropwise. The reaction mixture was stirred at room temperature for 16 hours. Purification by recrystallization from methanol afforded the desired product (1.2 g, 2.7 mmol, 75%). M.p.: decomposition over 300 °C. ¹H-NMR (400 MHz, DMSO-*d*₆): δ = 10.24 (s, 1H), 7.91 – 7.77 (m, 8H), 2.35 (t, *J* = 7.4 Hz, 2H), 1.60 (t, *J* =

7.2 Hz, 2H), 1.32 – 1.20 (m, 12H), 0.89 – 0.79 (m, 3H). ^{13}C -NMR (101 MHz, DMSO- d_6): δ = 172.3 (q), 152.2 (q), 150.7 (q), 147.8 (q), 143.1 (q), 127.2 (+), 124.2 (+), 122.3 (+), 119.6 (+), 37.0 (-), 31.7 (-), 29.4 (-), 29.3 (-), 29.2 (-), 29.1 (-), 25.5 (-), 22.6 (-), 14.4 (+). HR-MS (ESI): calcd. for $\text{C}_{22}\text{H}_{30}\text{N}_3\text{O}_4\text{S}^+$ $[\text{M}+\text{H}]^+$ 432.1952; found: 432.1955. MF: $\text{C}_{22}\text{H}_{29}\text{N}_3\text{O}_4\text{S}$. MW: 431.55 g/mol.

(E)-1-(4-butoxyphenyl)-2-(4-nitrophenyl)diazene (26). Nitroaniline **22** (2.0 g, 14 mmol, 1.0 eq) was dissolved in CH_2Cl_2 (0.10 L) and stirred under a nitrogen atmosphere. Oxone (8.9 g, 14 mmol, 1.0 eq) was dissolved in water (0.10 L) and added to the solution. The biphasic reaction mixture was stirred at room temperature for three hours. The organic phase containing nitroso **23** was separated, dried, and used in the next step without further purification. A solution of butoxy aniline **24** (2.4 g, 14 mmol, 1.0 eq) in acetic acid (0.10 L) was added to the nitroso solution and the mixture stirred at room temperature for 16 hours. The product was purified by column chromatography using PE/EA 3/1 as eluent. The solvent was evaporated yielding **26** as orange solid in good yield (2.6 g, 8.7 mmol, 60%). M.p.: 115 °C. ^1H -NMR (400 MHz, DMSO- d_6): δ = 8.45 – 8.34 (m, 2H), 8.08 – 7.99 (m, 2H), 7.99 – 7.91 (m, 2H), 7.21 – 7.11 (m, 2H), 4.11 (t, J = 6.5 Hz, 2H), 1.73 (p, 2H), 1.45 (h, J = 7.4 Hz, 2H), 0.94 (t, J = 7.4 Hz, 3H). ^{13}C -NMR (101 MHz, DMSO- d_6): δ = 163.1 (q), 155.9 (q), 148.5 (q), 146.6 (q), 125.9 (+), 125.5 (+), 123.6 (+), 115.7 (+), 68.4 (-), 31.1 (-), 19.2 (-), 14.2 (+). HR-MS (ESI): calcd. for $\text{C}_{16}\text{H}_{18}\text{N}_3\text{O}_3^+$ $[\text{M}+\text{H}]^+$ 300.1343; found: 300.1349. MF: $\text{C}_{16}\text{H}_{17}\text{N}_3\text{O}_3$. MW: 299.33 g/mol.

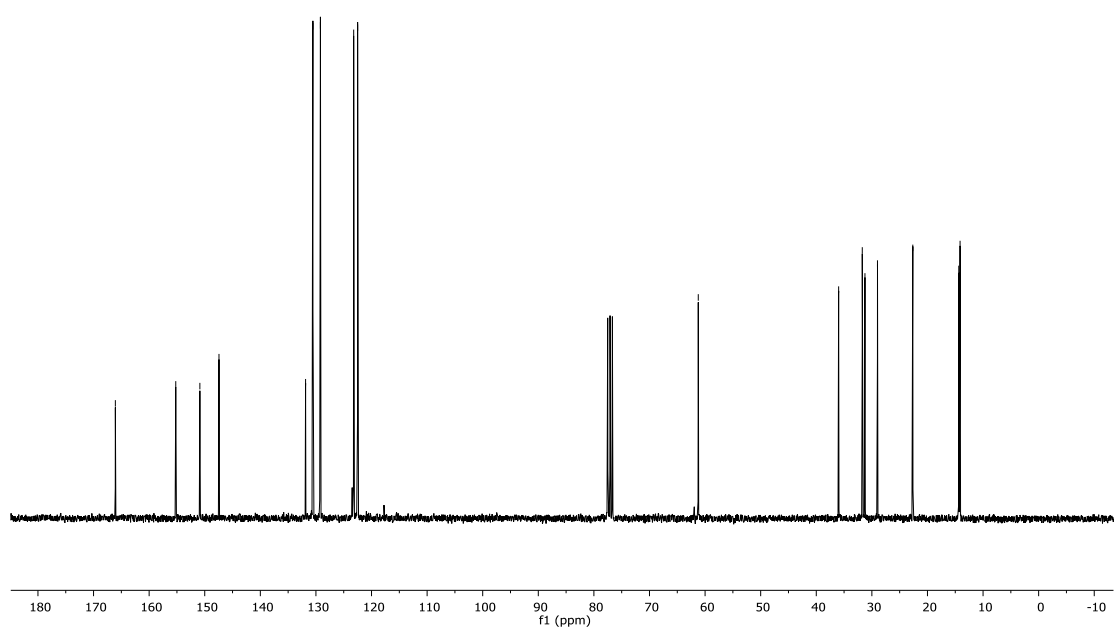
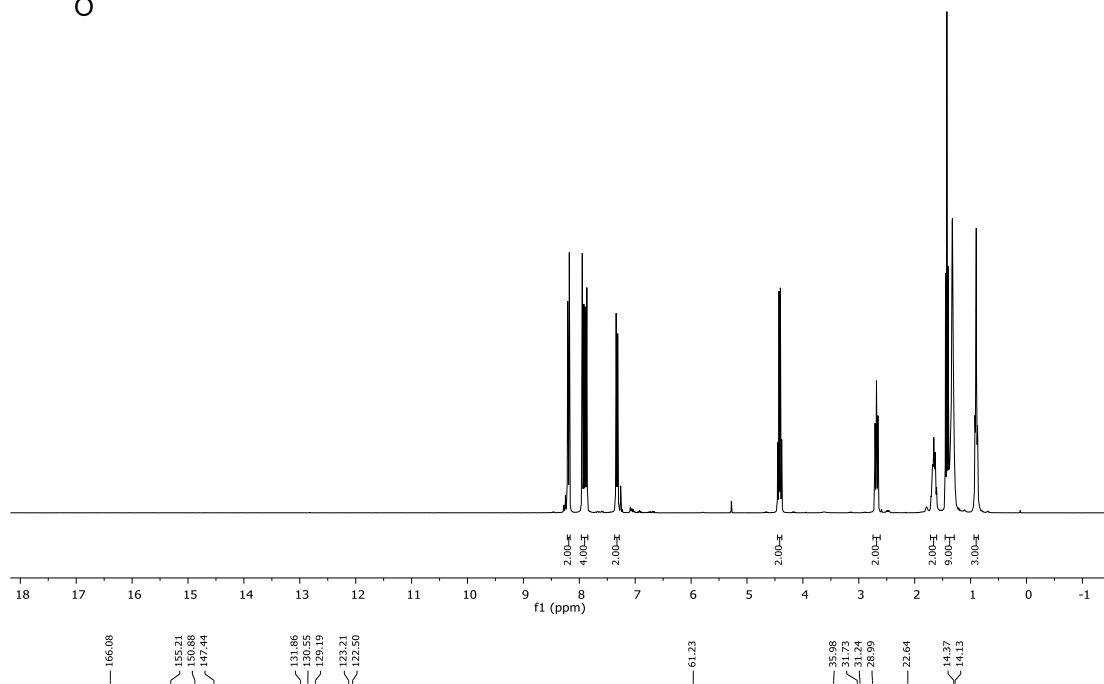
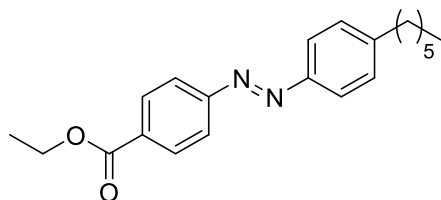
(E)-N-(4-((4-nitrophenyl)diazenyl)phenyl)pentanamide (27). Nitroaniline **22** (2.0 g, 14 mmol, 1.0 eq) was dissolved in CH_2Cl_2 (0.10 L) and stirred under a nitrogen atmosphere. Oxone (8.9 g, 14 mmol, 1.0 eq) was dissolved in water (0.10 L) and added. The biphasic reaction mixture was stirred at room temperature for three hours. The organic phase containing nitroso **23** was separated, dried, and used in the next step without further purification. A solution of pentanamide aniline **25** (2.8 g, 14 mmol, 1.0 eq) in acetic acid (0.10 L) was added to the nitroso solution and the mixture stirred at room temperature for 16 hours. The product was purified by column chromatography using PE/EA 3/1 as eluent. The solvent

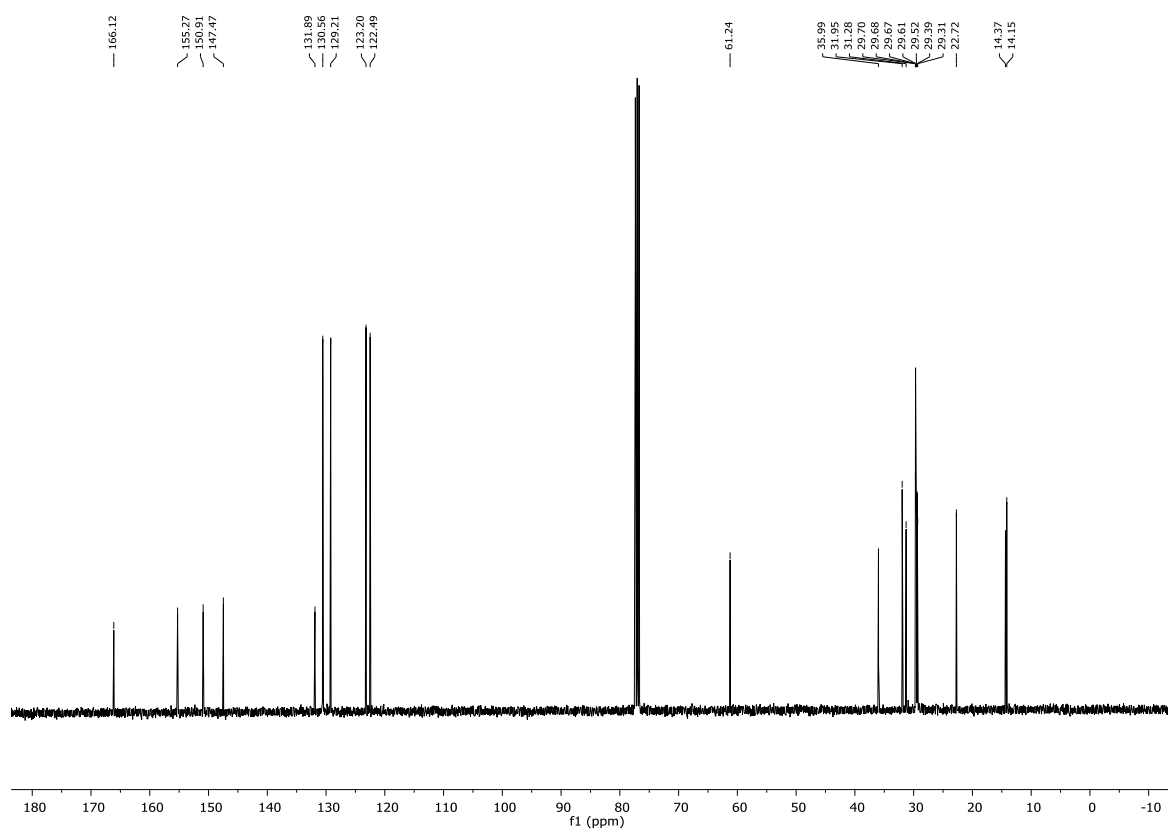
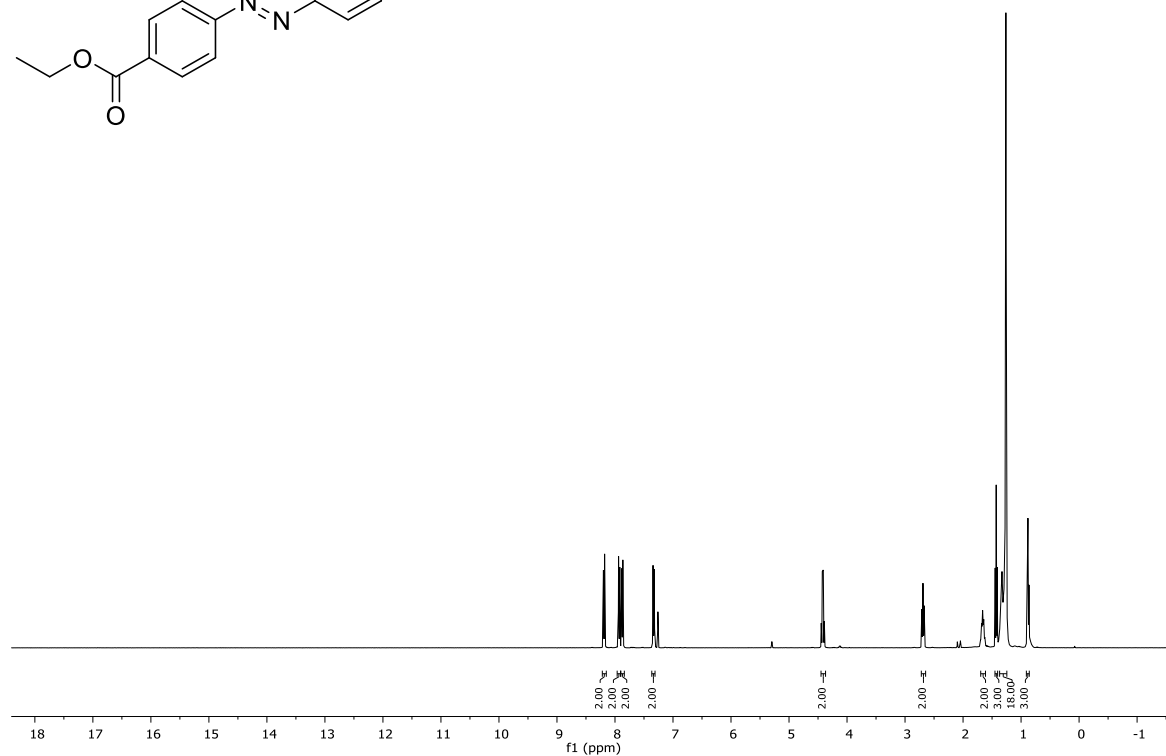
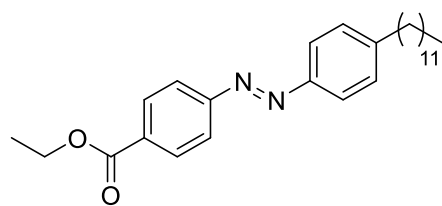
was evaporated yielding **27** as orange solid in good yield (3.1 g, 9.4 mmol, 65%). M.p.: 187 °C. ¹H-NMR (400 MHz, DMSO-*d*₆): δ = 10.33 (s, 1H), 8.46 – 8.37 (m, 2H), 8.11 – 7.99 (m, 2H), 7.99 – 7.89 (m, 2H), 7.89 – 7.80 (m, 2H), 2.38 (t, *J* = 7.5 Hz, 2H), 1.60 (p, *J* = 7.5 Hz, 2H), 1.34 (h, *J* = 7.3 Hz, 2H), 0.91 (t, *J* = 7.4 Hz, 3H). ¹³C-NMR (101 MHz, DMSO): δ = 172.5 (q), 155.8 (q), 148.5 (q), 147.8 (q), 144.2 (q), 125.5 (+), 125.0 (+), 123.7 (+), 119.6 (+), 36.8 (-), 27.6 (-), 22.3 (-), 14.2 (+). HR-MS (ESI): calcd. for C₁₇H₁₉N₄O₃⁺ [M+H]⁺ 327.1452; found: 327.1458. MF: C₁₇H₁₈N₄O₃. MW: 326.36 g/mol.

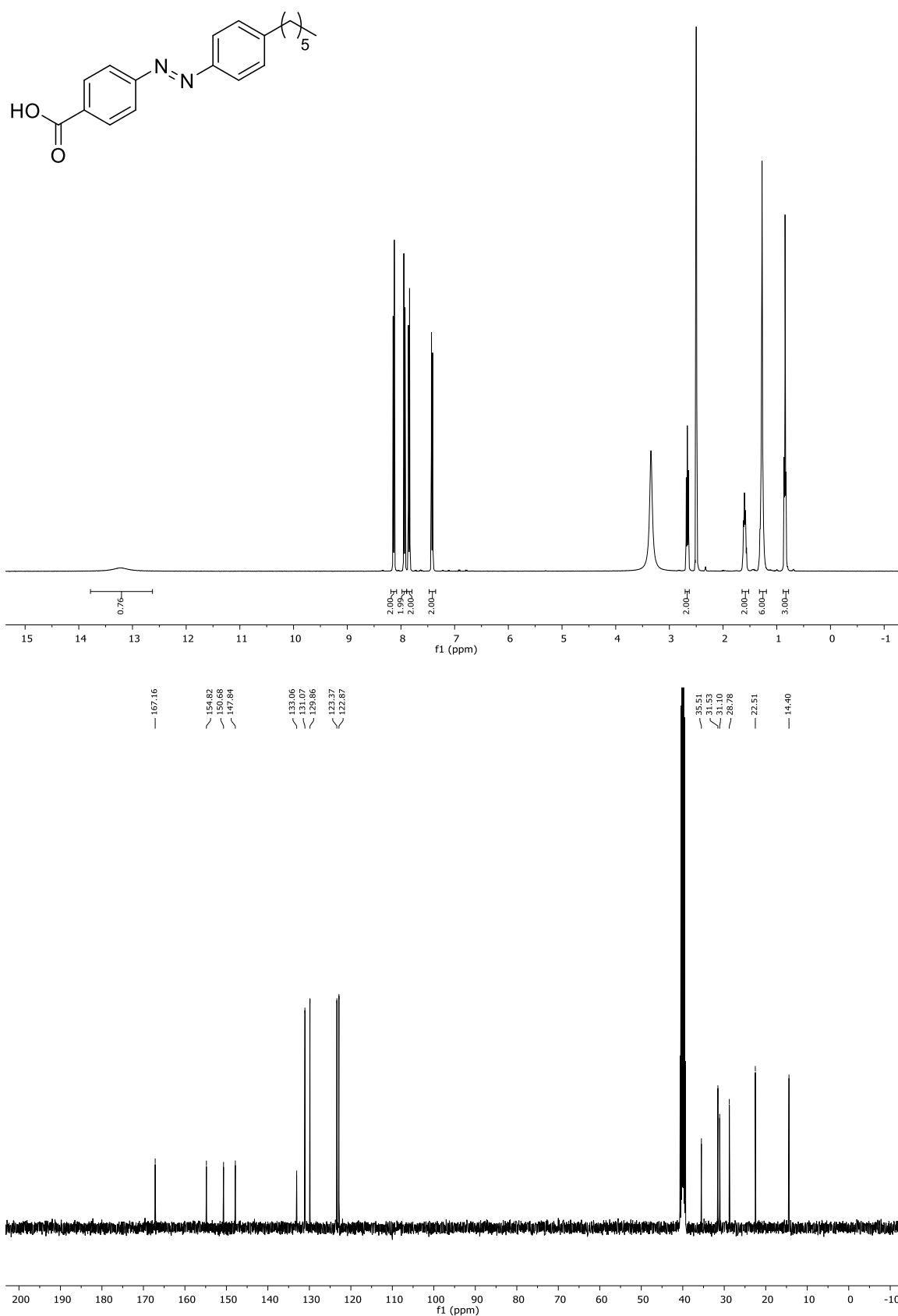
1.5 Supporting Information

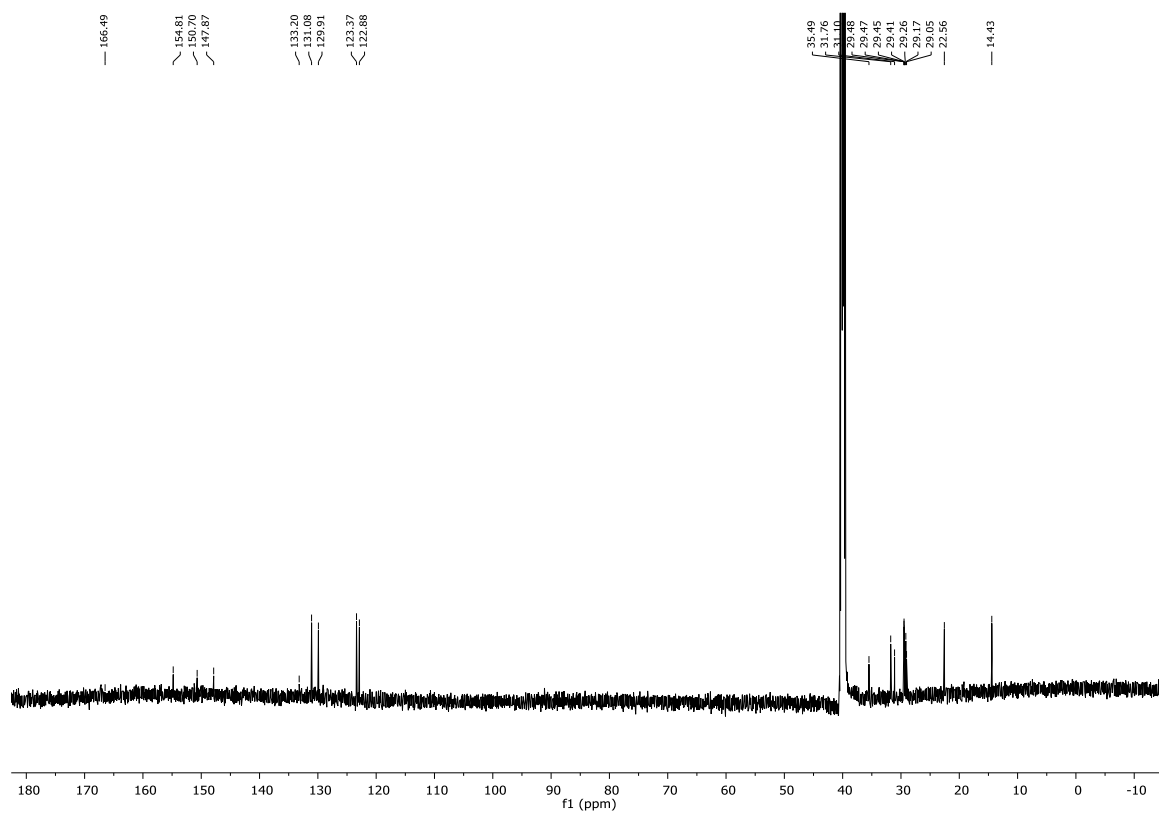
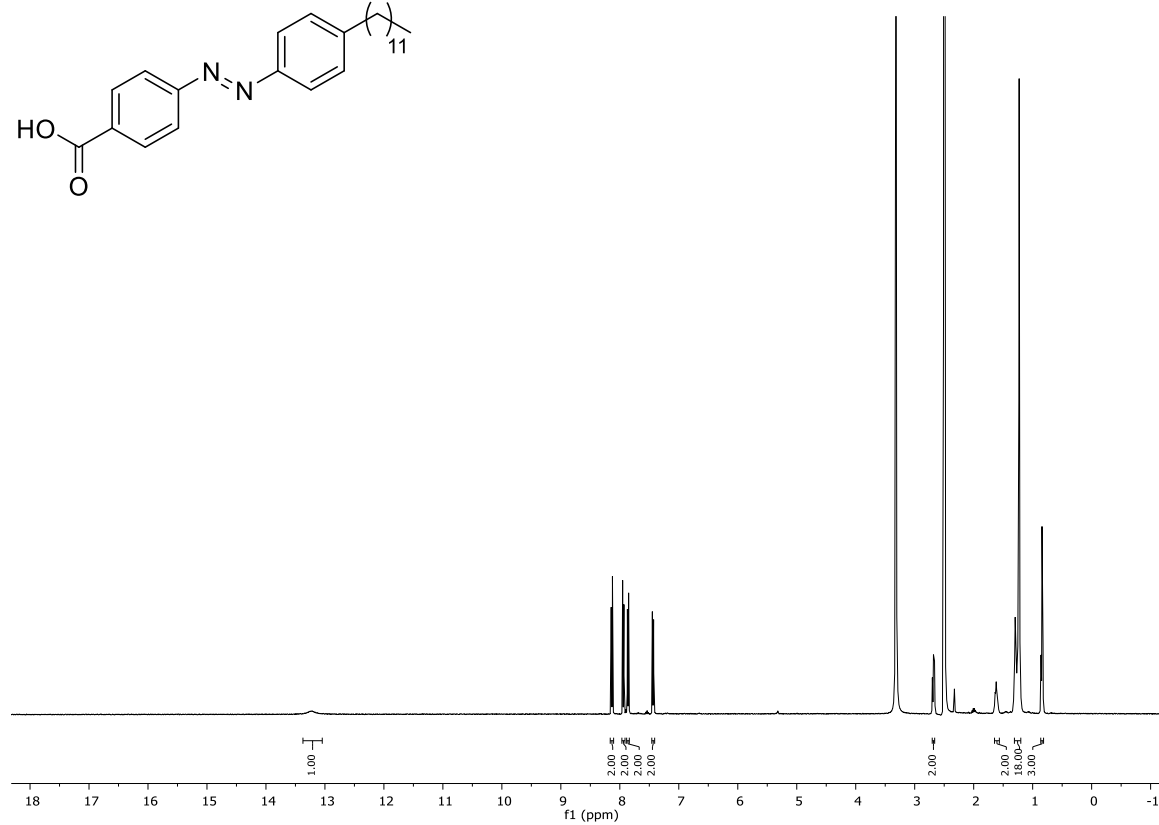
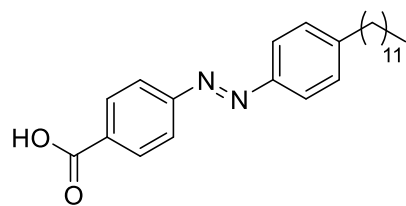
1.5.1 ^1H - and ^{13}C -NMR Spectra

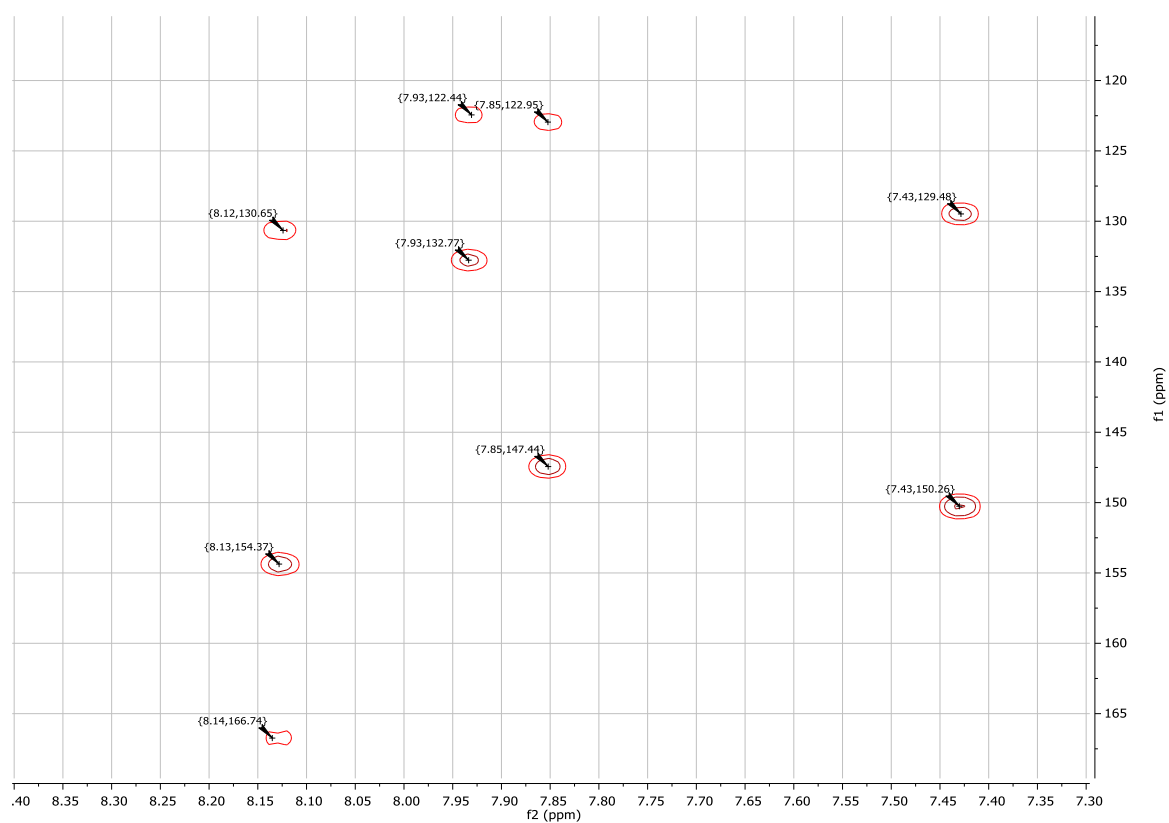
Compound 5 (CDCl_3 - d)

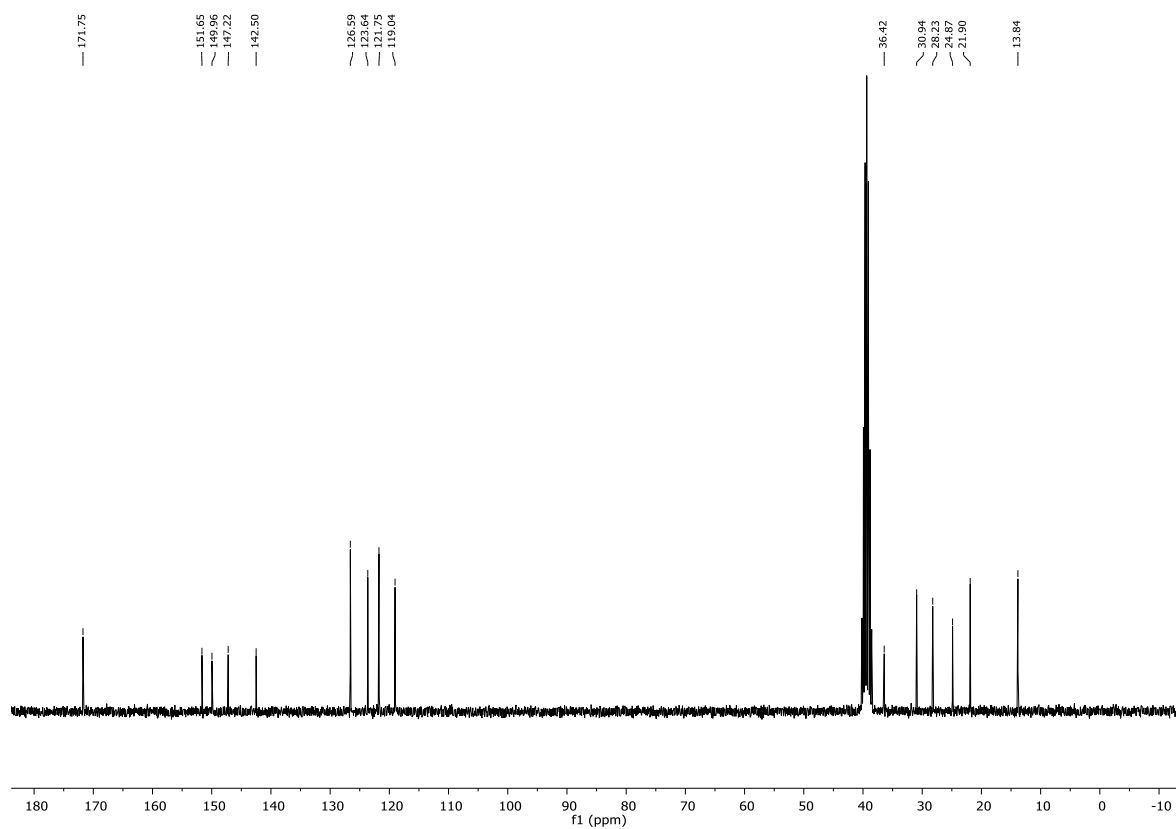
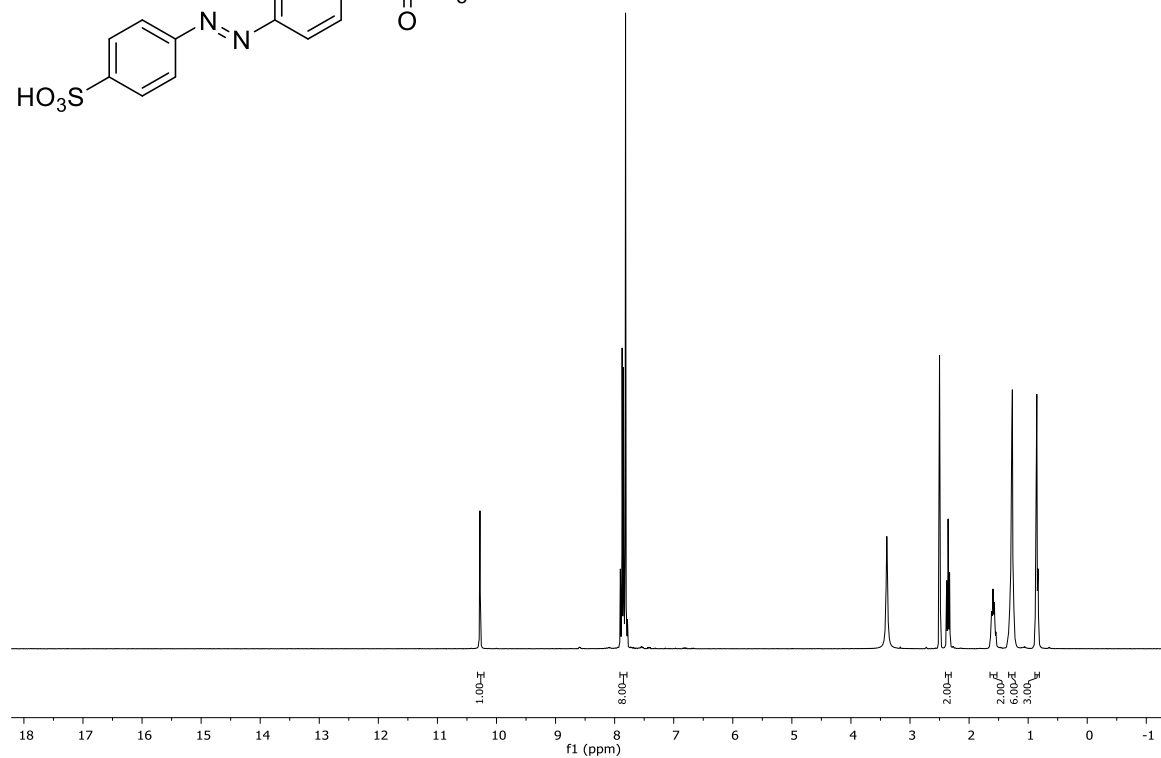
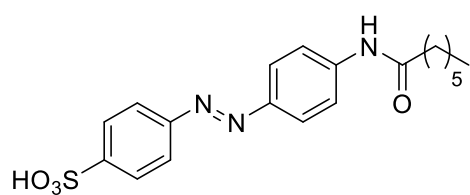


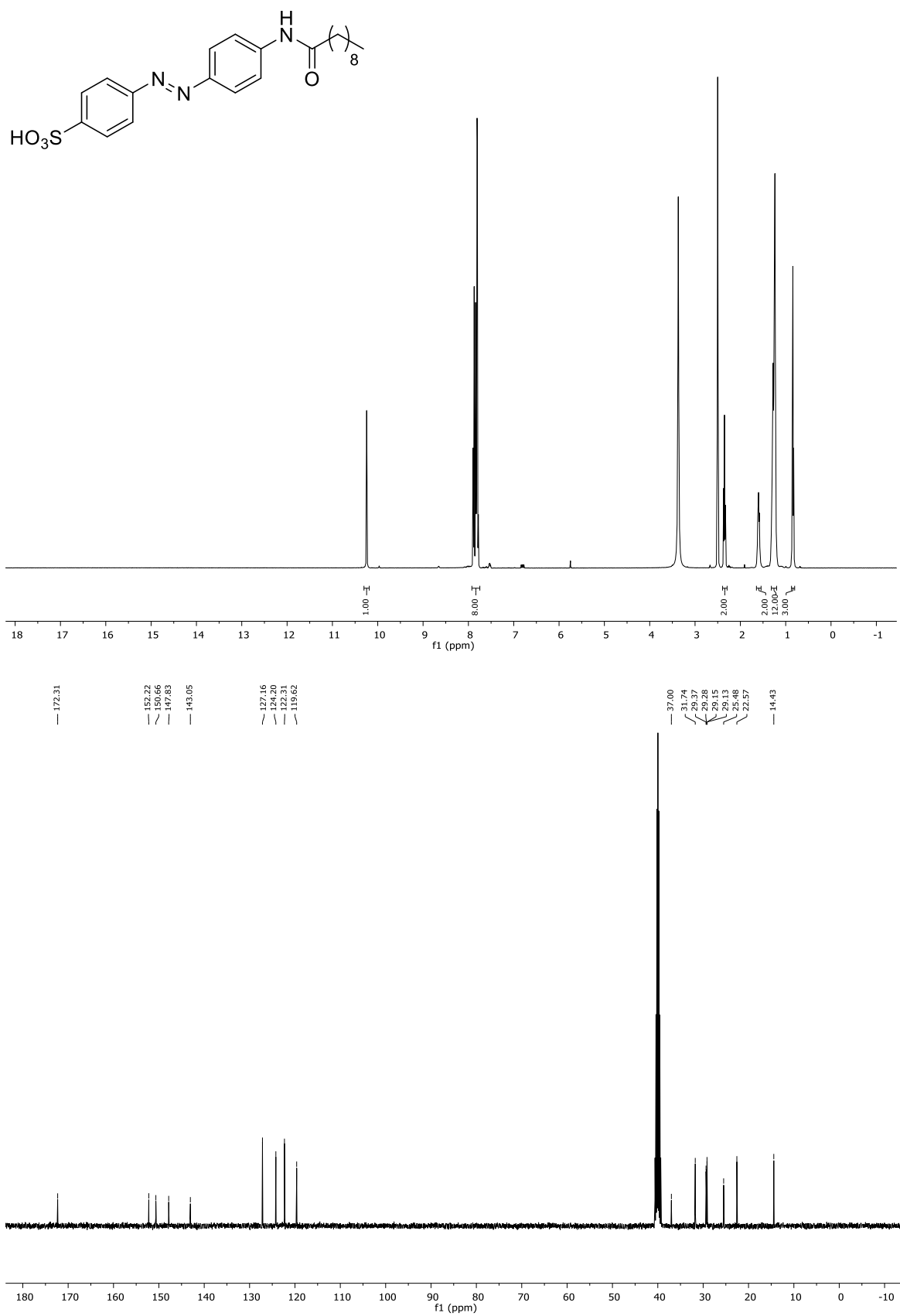
Compound 6 (CDCl_3 - d)

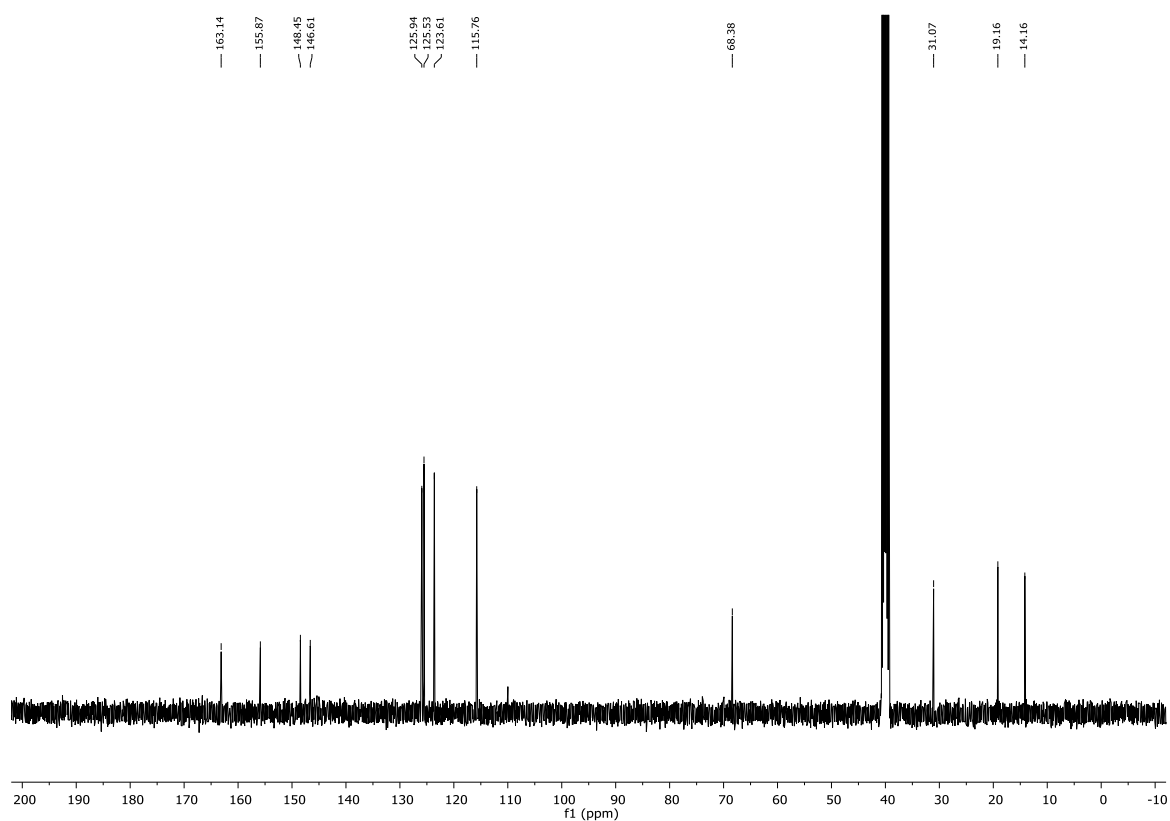
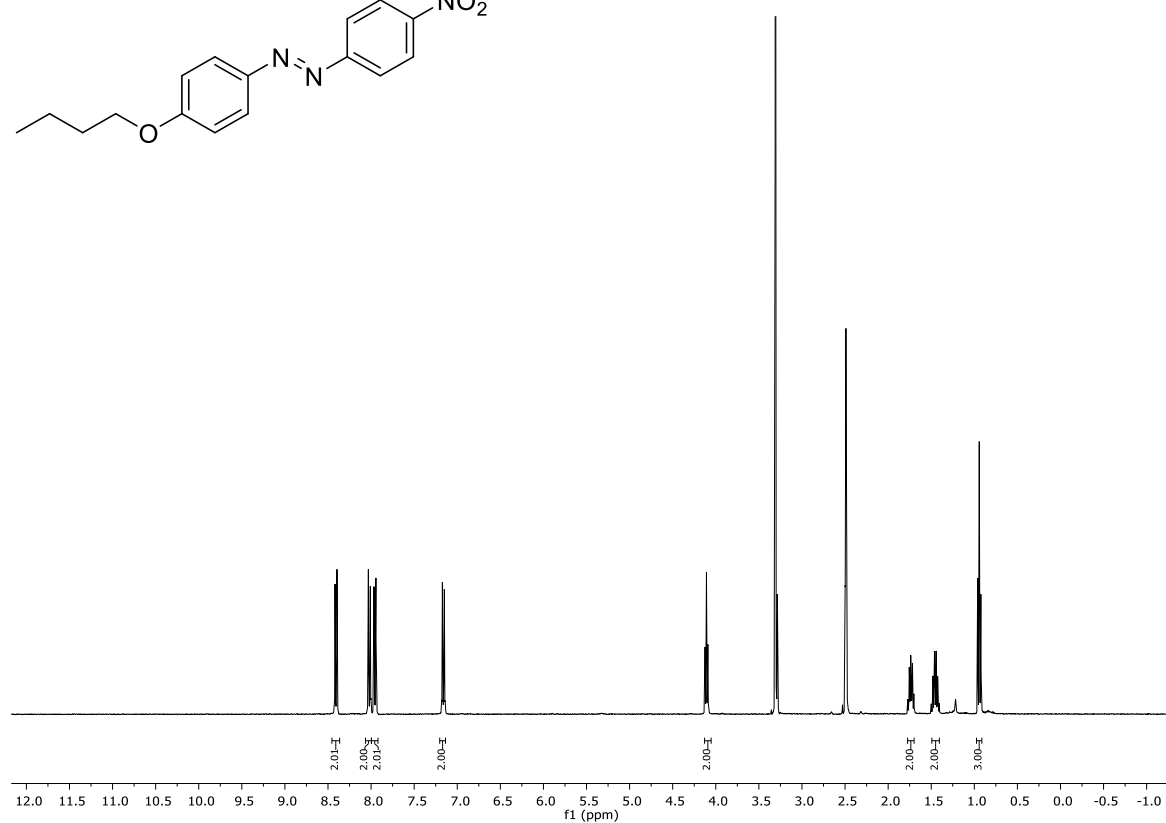
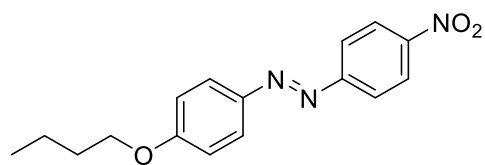
Compound 7 (DMSO-*d*₆)


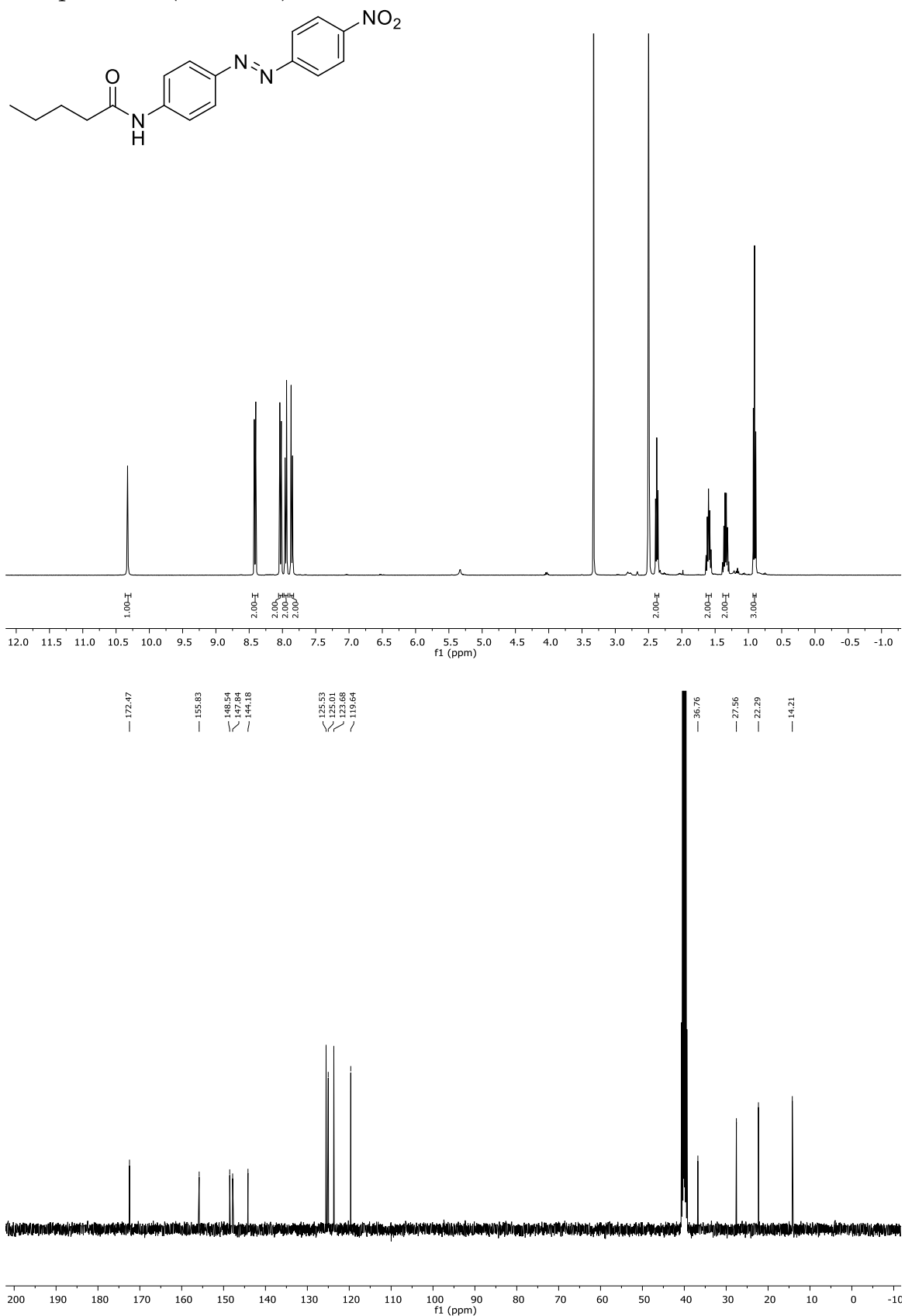
Compound 8 (DMSO- d_6)

Compound 8 (DMSO- d_6): HMBC spectrum

Compound **20** (DMSO-*d*₆)

Compound **21** (DMSO-*d*₆)


Compound **26** (DMSO-*d*₆)

Compound 27 (DMSO-*d*₆)


1.5.2 UV-Vis Absorption Spectra, Cycle Performances, and Thermal Half-Lives

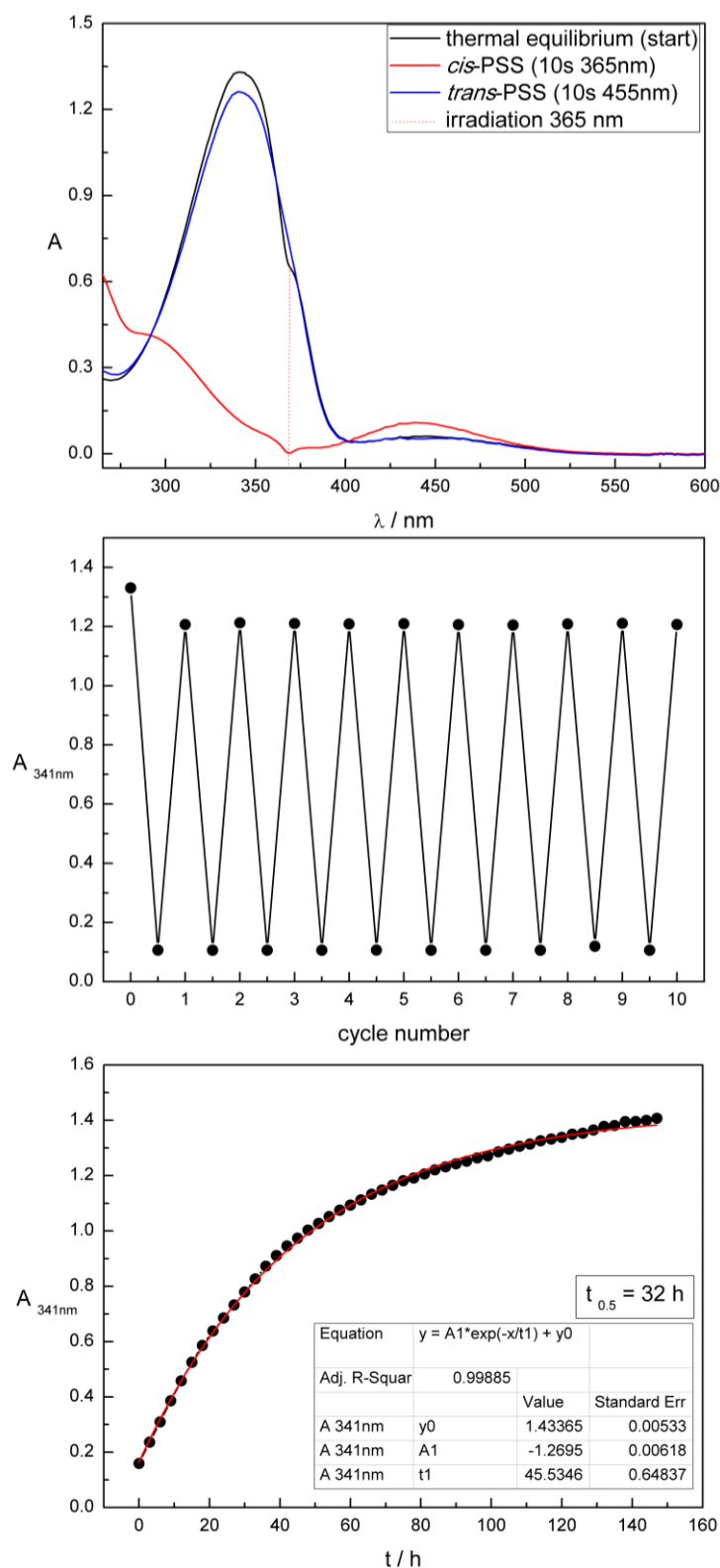


Figure S1. UV-Vis absorption spectroscopy of compound 7 measured 50 μM in DMSO. Upper panel: Absorption spectra (thermal equilibrium, *cis*-PSS, *trans*-PSS). Middle panel: Cycle performance. Lower panel: Thermal half-life.

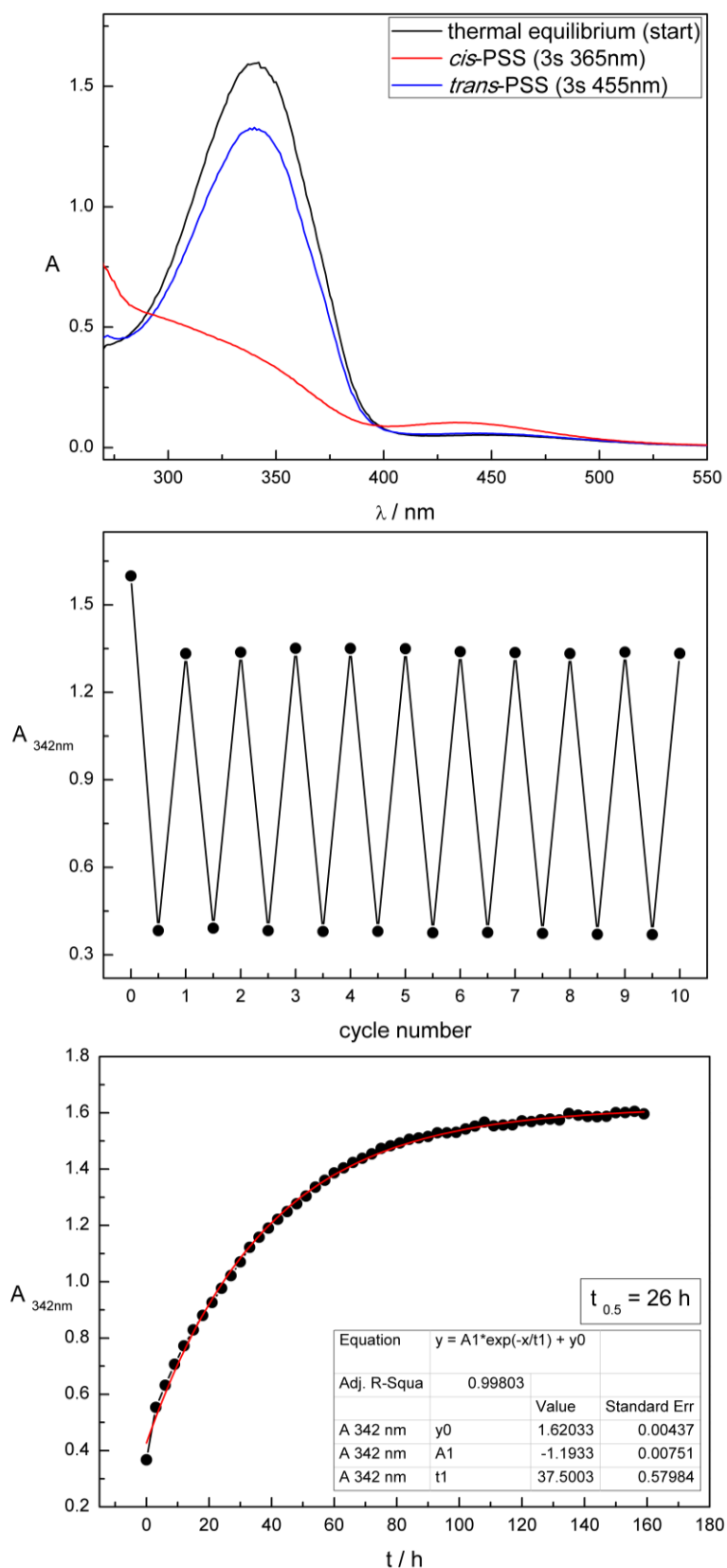


Figure S2. UV-Vis absorption spectroscopy of compound **8** measured 50 μM in DMSO. Upper panel: Absorption spectra (thermal equilibrium, *cis*-PSS, *trans*-PSS). Middle panel: Cycle performance. Lower panel: Thermal half-life.

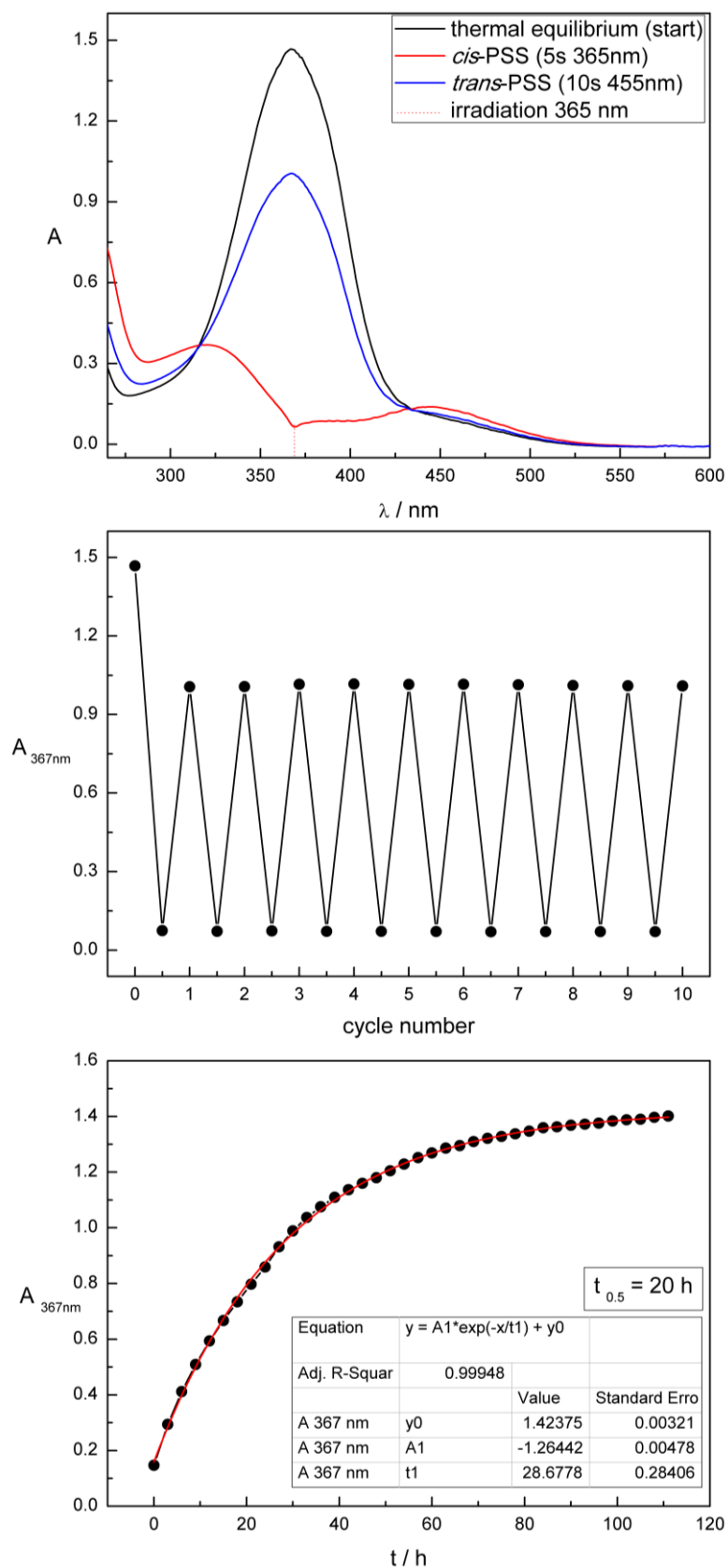


Figure S3. UV-Vis absorption spectroscopy of compound **9** measured 50 μM in DMSO. Upper panel: Absorption spectra (thermal equilibrium, *cis*-PSS, *trans*-PSS). Middle panel: Cycle performance. Lower panel: Thermal half-life.

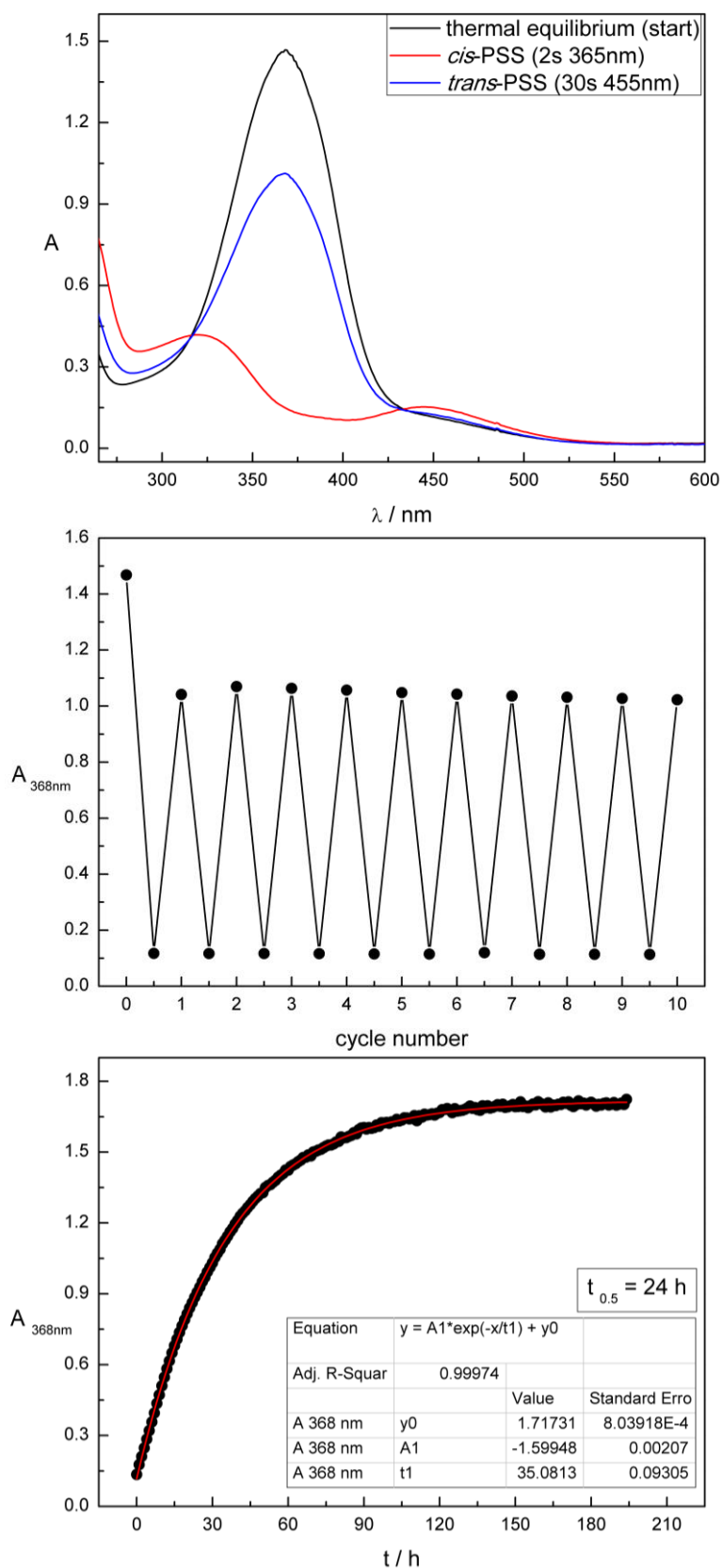


Figure S4. UV-Vis absorption spectroscopy of compound **21** measured 50 μM in DMSO. Upper panel: Absorption spectra (thermal equilibrium, *cis*-PSS, *trans*-PSS). Middle panel: Cycle performance. Lower panel: Thermal half-life.

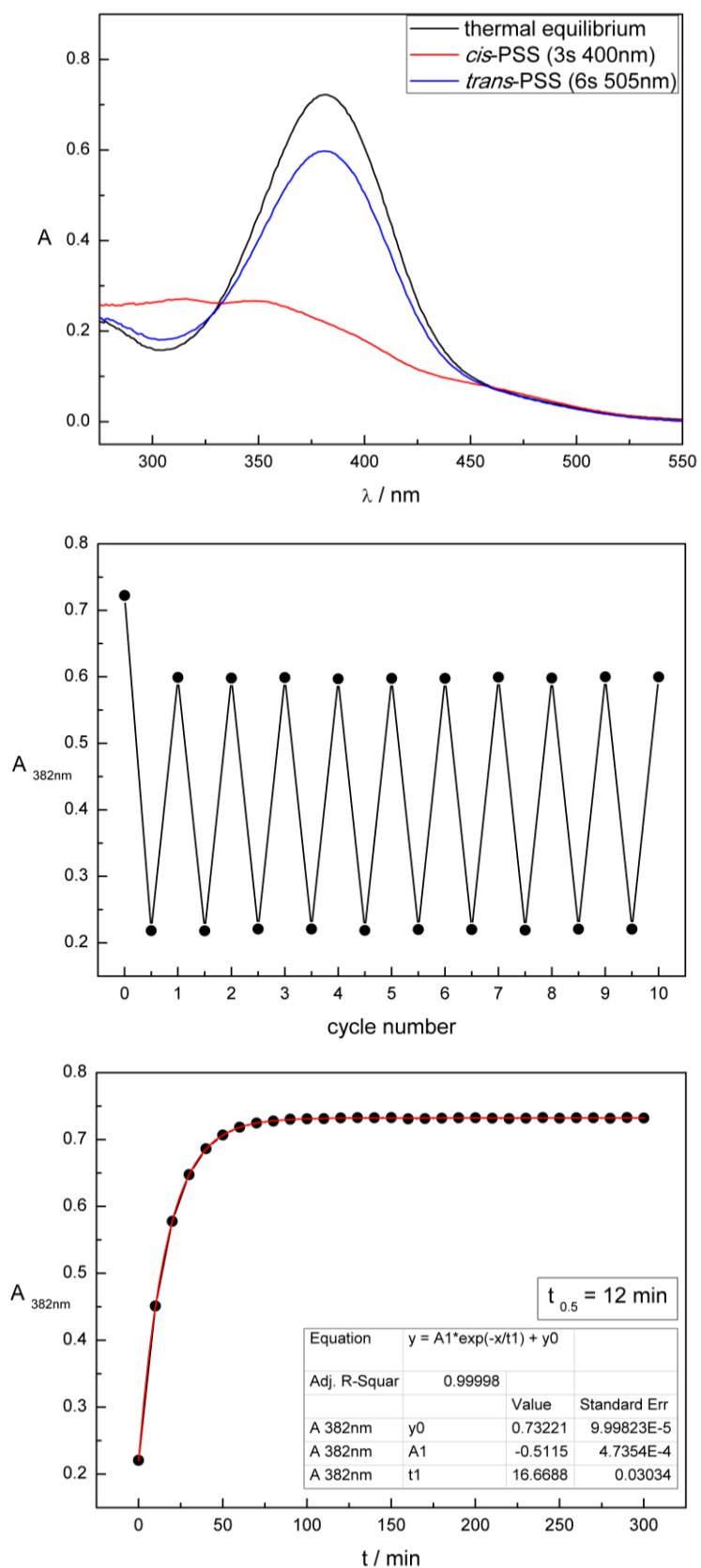


Figure S5. UV-Vis absorption spectroscopy of compound **26** measured 50 μM in DMSO. Upper panel: Absorption spectra (thermal equilibrium, *cis*-PSS, *trans*-PSS). Middle panel: Cycle performance. Lower panel: Thermal half-life.

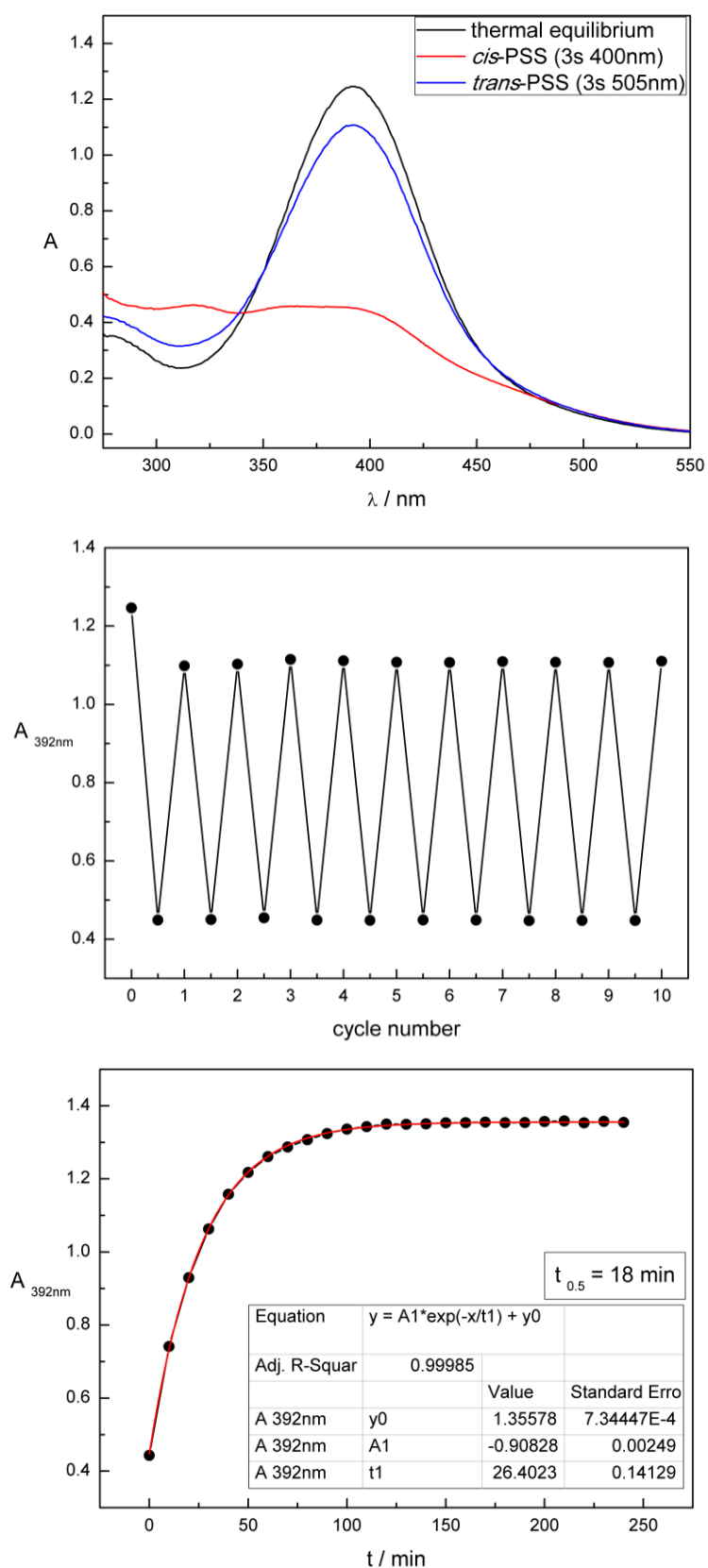


Figure S6. UV-Vis absorption spectroscopy of compound **27** measured 50 μM in DMSO. Upper panel: Absorption spectra (thermal equilibrium, *cis*-PSS, *trans*-PSS). Middle panel: Cycle performance. Lower panel: Thermal half-life.

1.6 References

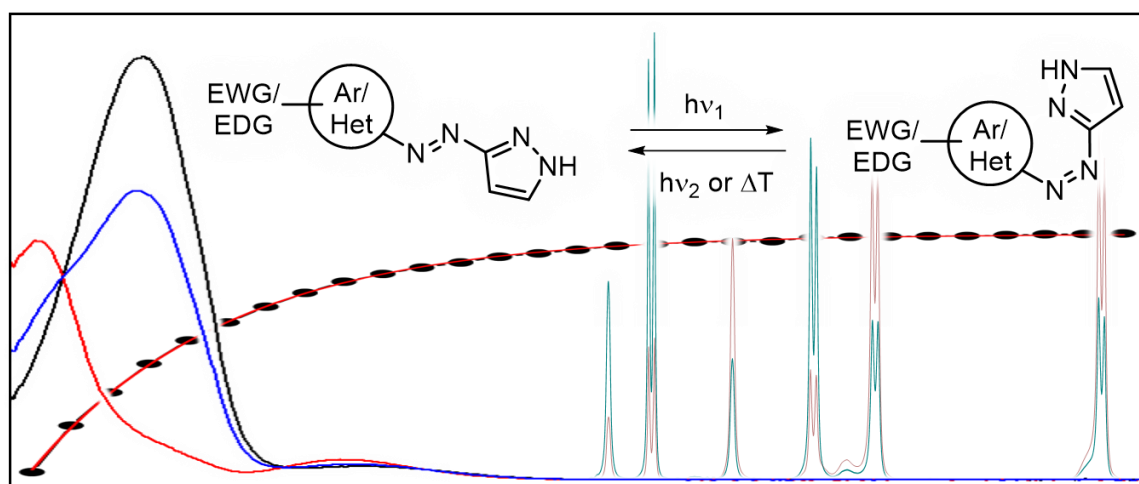
- [1] I. R. Dunkin, A. Gittinger, D. C. Sherrington, P. Whittaker, *J. Chem. Soc., Perkin Trans.* **1996**, 2, 1837-1842.
- [2] R. Lund, G. Brun, E. Chevallier, T. Narayanan, C. Tribet, *Langmuir* **2016**, 32, 2539-2548.
- [3] D. Yang, M. Piech, N. S. Bell, D. Gust, S. Vail, A. A. Garcia, J. Schneider, C.-D. Park, M. A. Hayes, S. T. Picraux, *Langmuir* **2007**, 23, 10864-10872.
- [4] S. N. Varanakkottu, S. D. George, T. Baier, S. Hardt, M. Ewald, M. Biesalski, *Lab Chip* **2012**, 12, 3637-3653.
- [5] S. J. Ebbens, J. R. Howse, *Soft Matter* **2010**, 6, 726-738.
- [6] N. Drillaud, E. Banaszak-Léonard, I. Pezron, C. Len, *J. Org. Chem.* **2012**, 77, 9553-9561.
- [7] T. Dwar, E. Paetzold, G. Oehme, *Angew. Chem., Int. Ed.* **2005**, 44, 7174-7199.
- [8] P. Cotanda, A. Lu, J. P. Patterson, N. Petzetakis, R. K. O'Reilly, *Macromolecules* **2012**, 45, 2377-2384.
- [9] E. Monflier, P. Bourdauducq, J.-L. Couturier, J. Kervennal, A. Mortreux, *Appl. Catal. A: Gen.* **1995**, 131, 167-178.
- [10] E. Monflier, P. Bourdauducq, J.-L. Couturier, I. Suisse, J. Kervennal, A. Mortreux, *A. Catal. Lett.* **1995**, 34, 201-212.
- [11] E. Monflier, P. Bourdauducq, J.-L. Couturier, J. Kervennal, E. Mortreux, *J. Mol. Catal. A: Chem.* **1995**, 97, 29-33.
- [12] X. Liu, N. L. Abbott, *J. Colloid Interface Sci.* **2009**, 339, 1-18.
- [13] T. Saji, K. Hoshino, S. Aoyagui, *J. Chem. Soc., Chem. Commun.* **1985**, 0, 865-866.
- [14] S. Sakai, H. Takayanagi, N. Suminoto, S. Fukuzawa, T. Fujinami, H. Saeki, *Appl. Organomet. Chem.* **1990**, 4, 35.

- [15] T. Saji, K. Ebata, K. Sugawara, S. Liu, K. Kobayashi, *J. Am. Chem. Soc.* **1994**, *116*, 6053-6054.
- [16] P. Brown, A. M. Khan, J. P. K. Armstrong, A. W. Perriman, C. P. Butts, J. Eastoe, *Adv. Mater.* **2012**, *24*, 6244-6247.
- [17] H. M. D. Bandara, S. C. Burdette, *Chem. Soc. Rev.* **2012**, *41*, 1809-1825.
- [18] W. Szymański, J. M. Beierle, H. A. V. Kistemaker, W. A. Velema, B. L. Feringa, *Chem. Rev.* **2013**, *113*, 6114-6178.
- [19] E. Merino, *Chem. Soc. Rev.* **2011**, *40*, 3835-3853.
- [20] T. Koźlecki, A. Sokolowski, K. A. Wilk, *Langmuir* **1997**, *13*, 6889-6895.
- [21] E. Chevallier, C. Monteux, F. Lequeux, C. Tribet, *Langmuir* **2012**, *28*, 2308-2312.
- [22] T. G. Shang, K. A. Smith, T. A. Hatton, *Langmuir* **2003**, *19*, 10764-10773.
- [23] B. A. Ciccirelli, J. A. Elia, T. A. Hatton, K. A. Smith, *Langmuir* **2007**, *23*, 8323-8330.
- [24] H. A. Ewart, K. E. Hyde, *J. Chem. Educ.* **1992**, *69*, 814-815.
- [25] L. Sigalotti, F. Pena-Polo, L. Trujillo, *Journal of Computational Methods in Sciences and Engineering* **2012**, *12*, 371-382.
- [26] A. Baeyer, *Chem. Ber.* **1874**, *7*, 1638-1640.
- [27] C. J. Mills, *J. Chem. Soc.* **1895**, *67*, 925-933.
- [28] A. D. Wong, T. M. Güngör, E. R. Gillies, *ACS Macro Lett.* **2014**, *3*, 1191-1195.
- [29] R. Yamakado, M. Hara, S. Nagano, T. Seki, H. Maeda, *Chem. Eur. J.* **2017**, *23*, 9244-9248.
- [30] W. N. Olmstead, Z. Margolin, F. G. Bordwell, *J. Org. Chem.* **1980**, *45*, 3295-3299.
- [31] Calculated using Advanced Chemistry Development (ACD/Labs) Software V11.02 (© 1994-2019 ACD/Labs)

- [32] H. Kim, J. Gao, D. J. Burgess, *Int. J. Pharm.* **2009**, 377, 105-111.
- [33] B. Priewisch, K. Rück-Braun, *J. Org. Chem.* **2005**, 70, 2350-2352.
- [34] W. Szymański, J. M. Beierle, H. A. V. Kistemaker, W. A. Velema, B. L. Feringa, *Chem. Rev.* **2013**, 113, 6114-6178.
- [35] A. A. Beharry, G. A. Woolley, *Chem. Soc. Rev.* **2011**, 40, 4422-4437.
- [36] H. Sell, C. Näther, R. Herges, *Beilstein J. Org. Chem.* **2013**, 9, 1-7.

CHAPTER 2

2 Photochromic Evaluation of Arylazo *NH*-Pyrazoles



This chapter has not been published.

This project was performed in collaboration with Dr. S. Crespi (Prof. B. L. Feringa, University of Groningen, Netherlands) and Dr. P. Nitschke (Prof. R. Gschwind, University of Regensburg). K. Rustler performed the synthesis of all compounds besides **4e** (synthesized by Dr. S. Crespi). K. Rustler performed the (photo-)chemical characterization of the compounds except the thermal half-lives of compounds **4b**, **4c**, **4e**, **4f**, **4h**, and **4j** in DMSO, **4a**, **4b**, **4c**, **4e-4h**, **4j** in DMSO:water, and **4a** in methanol (performed by Dr. S. Crespi). Dr. P. Nitschke measured the photostationary states *via* NMR spectroscopy under constant irradiation. Dr. S. Crespi performed laser flash photolysis. Mass spectrometry analysis were performed by the analytical department at the University of Regensburg. Prof. B. König supervised the project.

2.1 Introduction

Light is unsurpassed in nature as noninvasive, orthogonal, abundant fuel triggering diverse chemical and biological processes.^[1,2] Recently, this spatiotemporal tool is exploited in the emerging field of photopharmacology.^[3-8] Irradiation with light induces a reversible isomerization between at least two states of a photochromic scaffold each characterized by a certain absorption spectrum and specific structural and electronical properties. Such photoswitches are used as small molecular tools allowing to control molecular properties, biological activity^[9-10] or even motion as shown for molecular machines.^[11] Amongst others, *e.g.*, dithienylethenes and fulgides, azobenzenes are frequently reported for investigations in various scientific fields.^[9,10,12-14] Depending on the required criteria for a specific application, efforts are made to control their thermal stability and the wavelengths triggering their isomerization. Azobenzenes are favored because of their synthetic accessibility, tuneability, and high fatigue resistance. Besides, they show high extinction coefficients and quantum yields, allowing switching with low light intensity. Their thermodynamically stable, planar *trans* isomer can be converted to the metastable *cis* isomer by irradiation with light resulting in a huge change in geometry, end-to-end distance, solubility, and dipole moment. Regeneration of the usually thermally more stable *trans* isomer^[9,10,12] (except bridged azobenzenes)^[15] can be achieved either by irradiation with light or by thermal relaxation. Due to a substantial overlap of the absorption bands of the *trans* and *cis* isomer of classical azobenzenes, a quantitative generation of one or the other isomer by irradiation is not feasible.^[16] Depending on the substitution pattern, the thermal lifetime of the metastable *cis* isomer is strongly varying.^[17] As a result of the increasing interest in finding a fitting azobenzene scaffold for each application with predictable optimized properties, more and more attention is paid to new azobenzene derivatives *e.g.*, bearing heterocyclic rings as a substitute for the phenyl group.^[18-23] This led to the discovery of arylazo pyrazoles (AAPs) benefiting of almost quantitative photoswitching in both directions (for dimethyl

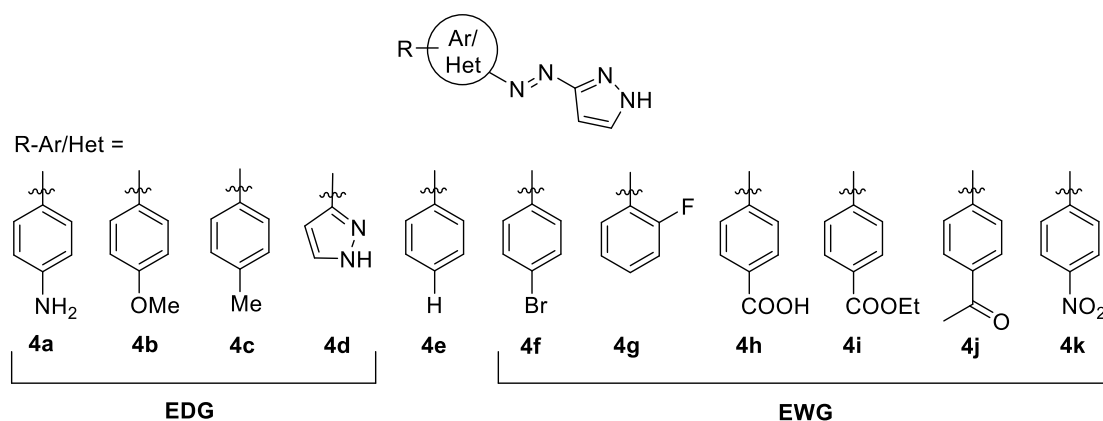
pyrazoles)^[24] and their stability against glutathione is beneficial for their use in biological environments.^[25] Other systems, containing imidazole, indole, and pyridine moieties are also explored.^[26-29] The introduction of a heterocycle as part of the switch offers further modes of interaction as coordination or hydrogen bond formation. Furthermore, nitrogen containing heterocycles are vastly represented as natural product sub moieties and drug elements.^[30] Despite investigations on unmethylated arylazo pyrazoles,^[32] mainly the more promising methylated derivatives^[22,24-26] are explored as hydrazone tautomerism and thermal stability are discussed controversial for unmethylated pyrazole azobenzenes. Tautomerism might occur in the same way as reported for hydroxy- or amino-substituted azobenzenes if the proton is shifted intra- or intermolecularly to the azo bond.^[21]

In this study, we focus on the experimental investigation of arylazo *NH*-pyrazoles as extension of the present knowledge on arylazo pyrazoles. This class of photochromic scaffold allows for post-functionalization of the *NH* and is sterically less demanding compared to its methylated derivatives. As for all classes of azobenzenes, solvent and substitution dependencies were expected and investigated. To evaluate the switching performance the wavelengths of maximum light absorption, thermal half-lives, photostationary states, and repetitive cycle performances were determined unraveling new insights into arylazo *NH*-pyrazoles.

2.2 Results and Discussion

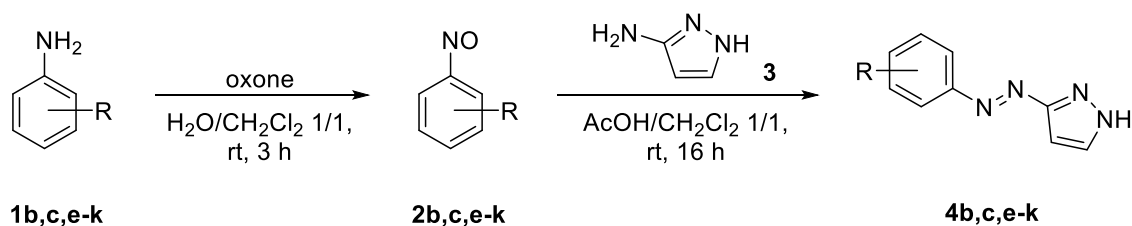
2.2.1 Design and Syntheses

Design. To unravel the photochromic properties of this type of photoswitchable scaffold, differently substituted arylazo pyrazoles bearing electron donating groups (EDGs) and electron withdrawing groups (EWGs) as substituents, respectively, were synthesized.



Scheme 1. Scope of the synthesized (hetero-)arylazo pyrazoles.

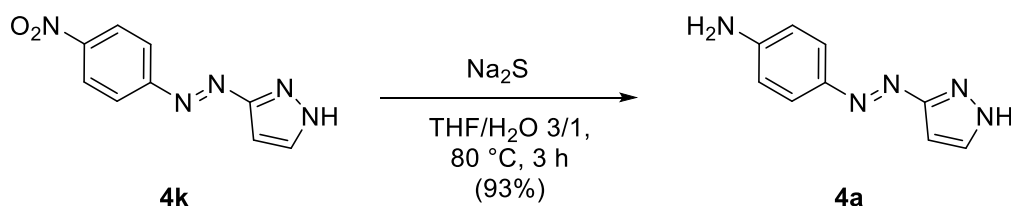
Syntheses. Arylazo pyrazoles **4b**, **4c**, and **4e-4k** were synthesized *via* Baeyer^[33]-Mills^[34] reaction – a well-known reported procedure for the synthesis of azobenzenes *via* reaction of an aryl nitroso with an arylamine (Scheme 2). The corresponding arylamines **1b**, **1c**, and **1e-1k**, respectively, were oxidized to their nitroso derivatives **2b**, **2c**, and **2e-2k** using potassium monopersulfate as oxidant in a biphasic reaction system preventing overoxidation. The resulting nitroso derivatives are reacted with the commercially available amino-substituted pyrazole **3** in a mixture of acetic acid and dichloromethane providing the substituted arylazo pyrazoles **4b**, **4c**, and **4e-4k** in moderate to good yields regardless of the presence of EDGs or EWGs.



R = *p*OMe (**b**; 20%), *p*Me (**c**; 48%), *p*H (**e**; 87%), *p*Br (**f**; 65%), *o*F (**g**; 8%), *p*COOH (**h**; 53%), *p*COOEt (**i**; 67%), *p*COMe (**j**; 33%), *p*NO₂ (**k**; 82%)

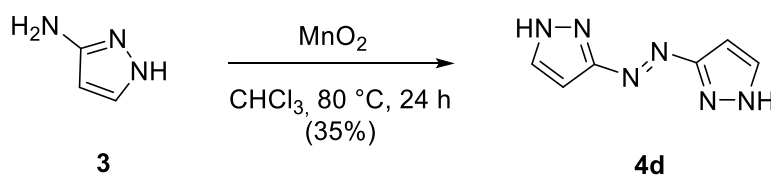
Scheme 2. Baeyer^[33]-Mills^[34] reaction for the synthesis of arylazo pyrazoles **4b**, **4c**, **4e-4k**.

The amino-substituted arylazo pyrazole **4a** was synthesized in good yield *via* reduction of its corresponding nitro-precursor **4k** using sodium sulfide as mild reductant (Scheme 3).^[35]



Scheme 3. Reduction of the nitro-substituted arylazo pyrazole **4k**.^[35]

In contrast, the symmetric arylazo pyrazole **4d** was synthesized *via* an oxidative coupling of amino pyrazole **3** in the presence of manganese(IV)oxide (Scheme 4).^[36]



Scheme 4. Oxidative coupling of amino pyrazole **3** for the synthesis of the symmetric azo pyrazole **4d**.^[36]

2.2.2 Photochemical Characterization

To investigate the influence of the different electron donating and electron withdrawing substituents on the photochromic performance of the arylazo pyrazole derivatives, the cycle performances, thermal half-lives and photostationary states of compounds **4a-4k** were determined using UV-Vis absorption spectroscopy. Furthermore, the effect of different solvents ranging from apolar (toluene, DMSO) to polar (DMSO/water, methanol) on the switching performance was investigated.

As an example, Figure 1 shows the normalized UV-Vis absorption spectra of compounds **4a** (amino-substituted), **4e** (unsubstituted), and **4k** (nitro-substituted) in their thermal equilibrium, their *cis*-PSS, and their *trans*-PSS state measured 50 μM in DMSO. The more bathochromically shifted the UV-Vis spectrum of the respective compound, the broader is the absorption peak. In DMSO, the unsubstituted arylazo pyrazole **4e** absorbs in its thermal equilibrium mainly at around 320 nm and its *cis* isomer at 430 nm. The EWG-substitution leads to a shift of the absorption spectrum towards longer wavelengths for the *trans* isomer (λ_{max}

~ 340 nm) whereas the *cis* absorption band is almost unaffected ($\lambda_{\text{max}} \sim 430$ nm). The strongest shift can be observed for the amino-substituted azo pyrazole **4a** with a maximum absorption at 400 nm for its *trans* isomer, which can be photoisomerized in both directions using visible light irradiation.

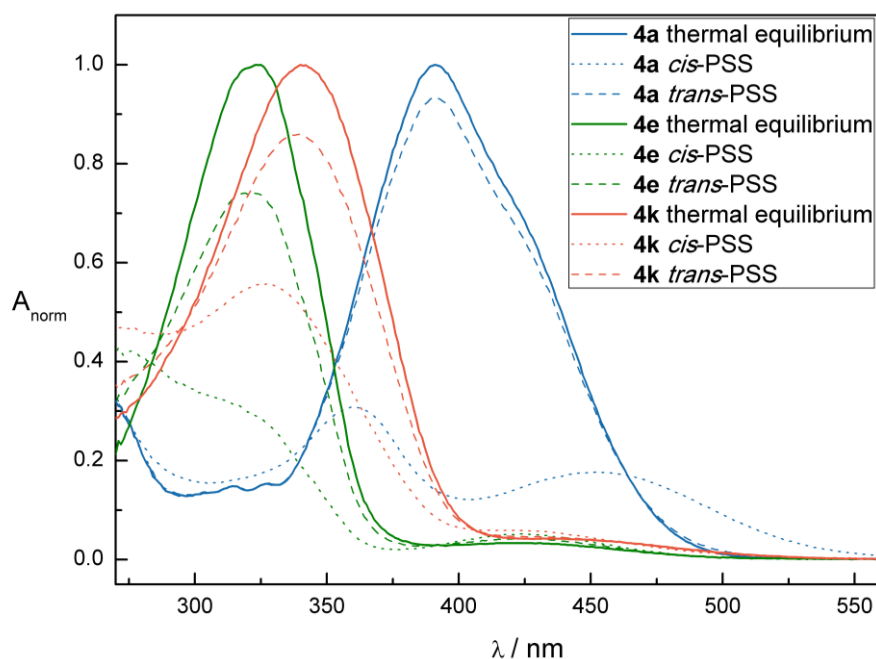


Figure 1. Normalized UV-Vis spectra of compounds **4a**, **4e**, and **4k** as example for an electron donating- (**4a**, R = NH₂) and an electron withdrawing- (**4k**, R = NO₂) substituted azo pyrazole compared to the unsubstituted reference (**4e**, R = H).

Considering all substitutions and solvents, the absorption maximum representing the *trans* isomer ranges from 300-400 nm. The weaker absorption band in the visible range representing the *cis* maximum tails around 400-450 nm. The formation of the *cis* isomer is generally triggered most efficiently using 365 nm (expect 400 nm for **4a**) and can be followed by a decrease in the absorption maximum in the UV-range and an increase of the absorption band in the visible region until the *cis*-photostationary state (*cis*-PSS; dotted line) is reached and no more changes in the absorption spectrum despite continuous irradiation are observed. Back-isomerization can be triggered using blue light irradiation ($\lambda = 455$ nm; except **4a**: green light, $\lambda = 505/528$ nm). Due to a substantial overlap of the absorption band of both isomeric species a quantitative generation of one or the other isomer by irradiation is not feasible. All compounds were subjected to alternate photoisomerization for ten cycles in each solvent and no significant

degradation was observed demonstrating high fatigue resistance. All compounds show fast switching proving high switching efficiency.

Table 1 summarizes all characteristic photochromic data (wavelengths of maximum absorption, extinction coefficients, isosbestic points, thermal half-lives) for compounds **4a-4k** measured 50 μ M in apolar (toluene, DMSO) and polar (DMSO/water 1/1, methanol) solvents.

Table 2 summarizes the photostationary states of compounds **4a-4k** determined by online NMR measurements under constant irradiation in deuterated DMSO. All compounds show moderate to high *cis*-photostationary states and moderate *trans*-photostationary states. For the determined values, the higher concentrated NMR solutions (\sim 50 mM) compared to the lower concentrated UV-Vis measurements (50 μ M) need to be considered. A discrepancy of the PSS values may be explained by a higher optical density of the NMR sample and resulting lower light penetration as well as the reduced light intensity of the light fiber irradiation (NMR) compared to the direct irradiation using high power LEDs (UV-Vis).

Table 1. Summary of the characteristic photochemical data of compounds **4a-4k** measured 50 μ M in toluene^(a) (entry 1-11), DMSO^(b) (entry 12-22), DMSO:water 1:1^(c) (entry 23-33), methanol^(d) (entry 34-44). Cpd. = Compound. Isosb. points = Isosbestic points. THL = thermal half-life.

Entry	Cpd.	Substituent	λ_{\max} $\pi\pi^*$ <i>trans</i> isomer [nm]	ϵ $\pi\pi^*$ <i>trans</i> isomer [M ⁻¹ cm ⁻¹]	λ_{\max} $n\pi^*$ <i>cis</i> isomer [nm]	ϵ $n\pi^*$ <i>cis</i> isomer [M ⁻¹ cm ⁻¹]	Isosb. points [nm]	THL ^(e)
1 ^(a)	4a	4-NH ₂ -C ₆ H ₄	373	23600	439	2868	314, 451	18 s
2 ^(a)	4b	4-OMe-C ₆ H ₄	339	12952	431	1632	297, 417	12 h
3 ^(a)	4c	4-Me-C ₆ H ₄	328	20714	433	1558	287, 399	84 h
4 ^(a)	4d	3(5)-Pyrazole	316	19944	425	1060	409	9.4 h
5 ^(a)	4e	4-H-C ₆ H ₄	321	12128	425	740.0	388	59 h
6 ^(a)	4f	4-Br-C ₆ H ₄	331	24630	429	1328	287, 397	93 h
7 ^(a)	4g	2-F-C ₆ H ₄	325	19734	424	1993	392	62 h
8 ^(a)	4h	4-COOH-C ₆ H ₄	325	12200	422	1068	289, 395	26 h
9 ^(a)	4i	4-COOEt-C ₆ H ₄	325	23460	425	1178	291, 396	23 h
10 ^(a)	4j	4-Ac-C ₆ H ₄	329	14328	426	904.0	295, 398	12 h
11 ^(a)	4k	4-NO ₂ -C ₆ H ₄	334	17914	427	1056	289, 403	11 h

12 ^(b)	4a	4-NH ₂ -C ₆ H ₄	391	24400	452	4296	343, 464	4.7 min
13 ^(b)	4b	4-OMe-C ₆ H ₄	344	20400	430	2460	296, 420	8.1 d ^(f)
14 ^(b)	4c	4-Me-C ₆ H ₄	332	20078	430	1200	285, 398	11 d ^(f)
15 ^(b)	4d	3(5)-Pyrazole	320	15980	430	1068	279, 390	22 h
16 ^(b)	4e	4-H-C ₆ H ₄	324	15440	423	880.0	283, 392	9.5 d ^(f)
17 ^(b)	4f	4-Br-C ₆ H ₄	331	21056	421	1096	286, 397	4.2 d ^(f)
18 ^(b)	4g	2-F-C ₆ H ₄	328	25600	421	2320	285, 391	21 h
19 ^(b)	4h	4-COOH-C ₆ H ₄	328	25930	425	1400	292, 394	1.6 d
20 ^(b)	4i	4-COOEt-C ₆ H ₄	331	25400	422	1300	293, 396	38 h ^(f)
21 ^(b)	4j	4-Ac-C ₆ H ₄	322	16740	415	1044	297, 401	5.1 h ^(f)
22 ^(b)	4k	4-NO ₂ -C ₆ H ₄	340	19524	418	1104	294, 406	42 s
23 ^(c)	4a	4-NH ₂ -C ₆ H ₄	388	20800	-(h)	-(h)	-(h)	96 ms ^(f,g)
24 ^(c)	4b	4-OMe-C ₆ H ₄	347	12960	430	2500	296, 420	7.6 d ^(f)
25 ^(c)	4c	4-Me-C ₆ H ₄	321	20360	417	2680	276, 391	20 d ^(f)
26 ^(c)	4d	3(5)-Pyrazole	311	19940	420	1614	270, 381	23 h
27 ^(c)	4e	4-H-C ₆ H ₄	322	12054	420	776.0	282, 381	15 d ^(f)
28 ^(c)	4f	4-Br-C ₆ H ₄	322	22800	410	1340	277, 387	6.4 d ^(f)
29 ^(c)	4g	2-F-C ₆ H ₄	318	20440	408	1800	284, 391	20 h ^(f)
30 ^(c)	4h	4-COOH-C ₆ H ₄	319	14080	409	1100	279, 383	18 h ^(f)
31 ^(c)	4i	4-COOEt-C ₆ H ₄	320	24000	409	1236	280, 381	16 h
32 ^(c)	4j	4-Ac-C ₆ H ₄	322	17600	403	1180	285, 386	20 h ^(f)
33 ^(c)	4k	4-NO ₂ -C ₆ H ₄	328	17600	403	1440	286, 392	43 min
34 ^(d)	4a	4-NH ₂ -C ₆ H ₄	380	25200	-(h)	-(h)	-(h)	0.10 s ^(f,g)
35 ^(d)	4b	4-OMe-C ₆ H ₄	340	17560	430	2600	292, 412	5.5 d
36 ^(d)	4c	4-Me-C ₆ H ₄	325	21000	425	1300	281, 390	31 h
37 ^(d)	4d	3(5)-Pyrazole	315	18530	420	900.0	274, 387	51 h
38 ^(d)	4e	4-H-C ₆ H ₄	315	14518	415	718.0	279, 384	11 h
39 ^(d)	4f	4-Br-C ₆ H ₄	325	24760	420	1170	282, 384	10 h
40 ^(d)	4g	2-F-C ₆ H ₄	320	20708	420	1358	279, 383	37 h
41 ^(d)	4h	4-COOH-C ₆ H ₄	325	18784	420	700.0	285, 386	5.8 h
42 ^(d)	4i	4-COOEt-C ₆ H ₄	320	21368	420	1058	286, 385	15 h
43 ^(d)	4j	4-Ac-C ₆ H ₄	325	17650	415	682.0	291, 392	16 h
44 ^(d)	4k	4-NO ₂ -C ₆ H ₄	330	18846	420	1054	290, 394	4.6 h

(e) Determined by thermal relaxation of an irradiated sample (*cis* isomer) in the dark at room temperature and following of the increase in the absorption of λ_{\max} (*trans* isomer) *via* UV-Vis absorption spectroscopy. (f) Measurement performed by Dr. S. Crespi. (g) Determined by laser flash photolysis. (h) n.d. = not determined due to very short thermal half-life of the *cis* isomer.

Table 2. Determined photostationary states by online NMR spectroscopy under constant irradiation. n.d. = not determined due to very short thermal half-life of the *cis* isomer. Measurements performed by Dr. P. Nitschke.

Entry	PSS	4a	4b	4c	4d	4e	4f	4g	4h	4i	4h	4k
1	% <i>cis</i> (<i>E</i> → <i>Z</i>)	73	76	79	74	62	88	58	69	73	70	45
2	% <i>trans</i> (<i>Z</i> → <i>E</i>)	n.d.	66	61	79	60	54	61	62	63	64	n.d.

2.3 Conclusion

In summary, we synthesized a series of substituted arylazo *NH*-pyrazoles bearing electron donating and electron withdrawing substituents, respectively. All compounds showed moderate to high photostationary states, especially for the *trans* to *cis* isomerization. The thermal stabilities of their corresponding *cis* isomers are within the hours to days range, with the exception of the amino-substituted azo pyrazole **4a** and the nitro-substituted derivative **4k** in DMSO and DMSO/water 1/1 as solvents, which show high thermal instability. This is beneficial especially for different types of analysis, as constant irradiation during the testing can be avoided. All compounds showed high fatigue. Despite the lower switching efficiency compared to their literature reported dimethyl azo pyrazole derivatives^[24], especially for the *cis* to *trans* isomerization, this new class benefits of a reduced steric demand, which might be beneficial for applications in biological systems as well as the possibility of post-functionalization of its free *NH*. Nevertheless, especially the *trans* to *cis* isomerization shows good photostationary states. Furthermore, the compounds show highly efficient fast switching in both directions. This is beneficial for biological applications, as short irradiation times during online measurements are sufficient to reach the photostationary state. In ongoing studies performed by Dr. S. Crespi, the quantum yields of the isomerization of all compounds will be determined.

2.4 Experimental Part

2.4.1 General Procedures and Materials

Commercial reagents and starting materials were purchased from the commercial suppliers abcr, Acros Organics, Alfa-Aesar, Fisher Scientific, Merck, Sigma Aldrich, TCI, or VWR and used without any further purification. Solvents were used in p.a. quality and dried according to common procedures, if necessary. Dry nitrogen was used as an inert gas atmosphere. Flash column chromatography was performed using Sigma Aldrich MN silica gel 60 M (40-63 μm , 230-400 mesh) for normal phase chromatography. Reaction monitoring *via* thin layer chromatography was performed on alumina plates coated with silica gel (Merck silica gel 60 F₂₅₄, layer thickness 0.2 mm). Melting points were determined using a Stanford Research System OptiMelt MPA 100 and are uncorrected. NMR spectra were measured on a Bruker Avance 300 (¹H 300.13 MHz, ¹³C 75.48 MHz) and a Bruker Avance III HD 400 (¹H 400.13 MHz, ¹³C 100.61 MHz). The spectra are referenced against the NMR solvent (DMSO-*d*₆: δ_{H} = 2.50 ppm, δ_{C} = 39.52 ppm) and chemical shifts δ are reported in ppm. Resonance multiplicity is abbreviated as: s (singlet), d (doublet), t (triplet) and m (multiplet). Carbon NMR signals are assigned using DEPT 135 and ¹H-¹³C HSQC spectra with (+) for primary/tertiary, (-) for secondary, and (q) for quaternary carbons. Mass spectra were recorded on a Finnigan MAT-SSQ 710 A, ThermoQuest Finnigan TSQ 7000, Agilent Q-TOF 6540 UHD, or a Jeol AccuTOF GCX instrument. UV-Vis absorption spectroscopy was performed in 10 mm quartz cuvettes using an Agilent 8543, Agilent Cary 100, or Agilent Varian Cary 50 spectrometer. Light sources for irradiation: λ = 365 nm (Seoul Viosys CUN6GB1A, 1000 mA, 1.4 W), λ = 405 nm (Nichia NVSU233A SMD-LED UV, 1000 mA, 1.4 W), λ = 455 nm (Osram OSOLON SSL 80 LD-CQ7P-1U3U, 1000 mA, 0.45 W), λ = 505 nm (Osram OSOLON SSL 80 LVCK7P-JYKZ, 800 mA, 163 lm), and λ = 528 nm (Osram LTCP7P-KXKZ, 350 mA, 71 lm). The power of the light is given based on the specifications supplied by the company when the LEDs were purchased. Light sources used for PSS determination *via* online NMR

spectroscopy under constant irradiation: λ = 365 nm (LEUVA66; operated at 1000-1500 mA); λ = 450 nm (Osilon SSL80; operated at 1000 mA); λ = 405 nm (Nichia NVSU233 B; operated at 1400 mA); λ = 500 nm (Nichia NCSE119 A; operated at 700 mA).

2.4.2 Synthetic Procedures and Characterization

General procedure for the Baeyer^[33]-Mills^[34] reaction. The respective arylamines **1b**, **1c**, and **1e-1k** (1.0 eq) were dissolved in CH₂Cl₂ under an inert gas atmosphere and a solution of oxone (1.0 eq) in water (ratio CH₂Cl₂/water 1/1) was added. The biphasic reaction mixture was stirred at room temperature for three hours. The organic phase was separated, dried, and the solvent evaporated. The crude nitroso derivatives **2a**, **2c**, and **2e-2k**, respectively, were used in the next reaction step without further purification. The nitroso derivatives were dissolved in a mixture of acetic acid and CH₂Cl₂ (ratio 1/1) and amino pyrazole **3** (1.0 eq) was added and the reaction stirred at room temperature for 16 hours. After removal of the solvent, the product was purified by flash column chromatography using CH₂Cl₂ + 5% MeOH as eluent.

(E)-3-((4-methoxyphenyl)diazenyl)-1H-pyrazole (4b). The compound was synthesized as brown solid in 20% yield following the general procedure for the Baeyer^[33]-Mills^[34] reaction starting from *para* methoxy aniline **1b**. M.p.: 143 °C. ¹H-NMR (400 MHz, DMSO-*d*₆): δ = 13.36 (s, 1H), 7.87 – 7.81 (m, 3H), 7.14 – 7.10 (m, 2H), 6.52 (d, *J* = 2.5 Hz, 1H), 3.86 (s, 3H). ¹³C-NMR (101 MHz, DMSO-*d*₆): δ = 162.2 (q), 146.8 (q), 124.7 (+), 115.1 (+), 56.1 (+). HRMS (ESI): calcd. for (C₁₀H₁₁N₄O⁺) [M+H]⁺: *m/z* = 203.0927; found 203.0930. MF: C₁₀H₁₀N₄O. MW: 202.22 g/mol.

(E)-3-(*p*-tolyl diazenyl)-1H-pyrazole (4c). The compound was synthesized as yellow solid in 48% yield following the general procedure for the Baeyer^[33]-Mills^[34] reaction starting from *para* methyl aniline **1c**. M.p.: 157 °C. ¹H-NMR (400 MHz, DMSO-*d*₆): δ = 13.42 (s, 1H), 7.89 – 7.82 (m, 1H), 7.77 – 7.74 (m, 2H), 7.39 – 7.36 (m, 2H), 6.53 (t, *J* = 2.2 Hz, 1H), 2.39 (s, 3H). ¹³C-NMR (101 MHz, DMSO-*d*₆): δ = 152.6 (q), 131.7 (+), 131.2 (+), 129.9 (+), 122.7 (+), 94.2 (+). HRMS (ESI): calcd.

for (C₁₀H₁₁N₄⁺) [M+H]⁺: m/z = 187.0978; found 187.0978. MF: C₁₀H₁₀N₄. MW: 186.22 g/mol.

(E)-3-(phenyldiazenyl)-1H-pyrazole (4e). The compound was synthesized as yellow solid in 87% yield following the general procedure for the Baeyer^[33]-Mills^[34] reaction starting from aniline **1e**. M.p.: 126 °C. ¹H-NMR (400 MHz, DMSO-*d*₆): δ = 13.49 (s, 1H), 7.88 – 7.83 (m, 3H), 7.60 – 7.52 (m, 3H), 6.58 (d, *J* = 2.5 Hz, 1H). ¹³C-NMR (101 MHz, DMSO-*d*₆): δ = 152.6 (q), 131.7 (+), 131.2 (+), 129.9 (+), 122.7 (+), 94.2 (+). HRMS (ESI): calcd. for (C₉H₉N₄⁺) [M+H]⁺: m/z = 173.0822; found 173.0823. MF: C₉H₈N₄. MW: 172.19 g/mol.

(E)-3-((4-bromophenyl)diazenyl)-1H-pyrazole (4f). The compound was synthesized as yellow solid in 65% yield following the general procedure for the Baeyer^[33]-Mills^[34] reaction starting from *para* bromo aniline **1f**. M.p.: 151 °C. ¹H-NMR (400 MHz, DMSO-*d*₆): δ = 13.54 (s, 1H), 7.89 (t, *J* = 2.0 Hz, 1H), 7.79 (s, 4H), 6.56 (t, *J* = 2.1 Hz, 1H). ¹³C NMR (101 MHz, DMSO-*d*₆): δ = 151.5 (q), 133.0 (+), 125.0 (q), 124.6 (+). HRMS (ESI): calcd. for (C₉H₈BrN₄⁺) [M+H]⁺: m/z = 250.9927; found 250.9928. MF: C₉H₇BrN₄. MW: 251.09 g/mol.

(E)-3-((2-fluorophenyl)diazenyl)-1H-pyrazole (4g). The compound was synthesized by Dr. S. Crespi as brown solid in 8% yield following the general procedure for the Baeyer^[33]-Mills^[34] reaction starting from *ortho* fluoro aniline **1g**. M.p.: 103 °C. ¹H-NMR (400 MHz, DMSO-*d*₆): δ = 13.56 (s, 1H), 7.89 (dd, *J* = 2.6, 1.5 Hz, 1H), 7.71 (td, *J* = 7.9, 1.8 Hz, 1H), 7.59 (s, 1H), 7.51 – 7.44 (m, 1H), 7.34 (td, *J* = 7.7, 1.3 Hz, 1H), 6.55 (t, *J* = 2.2 Hz, 1H). ¹³C-NMR (101 MHz, DMSO-*d*₆): δ = 164.6 (q), 160.7 (q), 158.2 (q), 140.5 (q), 140.5 (q), 133.6 (+), 133.6 (+), 131.3 (+), 125.5 (+), 125.5 (+), 117.9 (+), 117.8 (+), 117.6 (+), 94.1 (+). HRMS (ESI): calcd. for (C₉H₈FN₄⁺) [M+H]⁺: m/z = 191.0728; found 191.0730. MF: C₉H₇FN₄. MW: 190.18 g/mol.

(E)-4-((1H-pyrazol-3-yl)benzoic acid) (4h). The compound was synthesized as orange solid in 53% yield following the general procedure for the Baeyer^[33]-Mills^[34] reaction starting from *para* carboxy aniline **1h**. M.p.: 270 °C. ¹H-NMR (300 MHz, DMSO-*d*₆): δ = 13.48 (s, 2H), 8.15 – 8.09 (m, 2H), 7.95 – 7.87 (m, 3H), 6.61

(d, $J = 2.5$ Hz, 1H). ^{13}C -NMR (75 MHz, $\text{DMSO-}d_6$): δ 166.58 (q), 154.47 (q), 132.44 (q), 130.52 (+), 122.18 (+). HRMS (ESI): calcd. for $(\text{C}_{10}\text{H}_9\text{N}_4\text{O}_2^+)$ $[\text{M}+\text{H}]^+$: $m/z = 217.0720$; found 217.0719. MF: $\text{C}_{10}\text{H}_8\text{N}_4\text{O}_2$. MW: 216.20 g/mol.

Ethyl (E)-4-((1H-pyrazol-3-yl)diazenyl)benzoate (4i). The compound was synthesized as yellow solid in 67% yield following the general procedure for the Baeyer^[33]-Mills^[34] reaction starting from *para* ethylbenzoate aniline **1i**. M.p.: 149 °C. ^1H -NMR (300 MHz, $\text{DMSO-}d_6$): $\delta = 13.65$ (s, 1H), 8.16 – 8.12 (m, 2H), 7.96 – 7.92 (m, 2H), 7.91 (d, $J = 2.5$ Hz, 1H), 6.61 (d, $J = 2.5$ Hz, 1H), 4.34 (q, $J = 7.1$ Hz, 2H), 1.34 (t, $J = 7.1$ Hz, 3H). ^{13}C -NMR (75 MHz, $\text{DMSO-}d_6$): $\delta = 165.6$ (q), 155.2 (q), 135.0 (q), 132.0 (q), 130.9 (+), 122.9 (+), 94.2 (q), 61.5 (-), 14.6 (+). HRMS (ESI): calcd. for $(\text{C}_{12}\text{H}_{13}\text{N}_4\text{O}_2^+)$ $[\text{M}+\text{H}]^+$: 245.1033; found: 245.1037. MF: $\text{C}_{12}\text{H}_{12}\text{N}_4\text{O}_2$. MW: 244.25 g/mol.

(E)-1-(4-((1H-pyrazol-3-yl)diazenyl)phenyl)ethan-1-one (4j): The compound was synthesized as orange solid in 33% yield following the general procedure for the Baeyer^[33]-Mills^[34] reaction starting from *para* acetyl aniline **1j**. M.p.: 127 °C. ^1H -NMR (400 MHz, $\text{DMSO-}d_6$): $\delta = 13.62$ (s, 1H), 8.15 (d, $J = 8.4$ Hz, 2H), 7.94 (d, $J = 8.4$ Hz, 2H), 7.90 (d, $J = 2.5$ Hz, 1H), 6.61 (d, $J = 2.5$ Hz, 1H), 2.64 (s, 3H). ^{13}C -NMR (75 MHz, $\text{DMSO-}d_6$): $\delta = 197.9$ (q), 155.0 (q), 138.6 (q), 131.9 (q), 130.1 (+), 122.9 (+), 116.3 (q), 94.4 (q), 27.4 (+). HRMS (ESI): calcd. for $(\text{C}_{11}\text{H}_{11}\text{N}_4\text{O}^+)$ $[\text{M}+\text{H}]^+$: $m/z = 215.0927$; found 215.0931. MF: $\text{C}_{11}\text{H}_{10}\text{N}_4\text{O}$. MW: 214.23 g/mol.

(E)-3-((4-nitrophenyl)diazenyl)-1H-pyrazole (4k): The compound was synthesized as orange solid in 82% yield following the general procedure for the Baeyer^[33]-Mills^[34] reaction starting from *para* carboxy aniline **1k**. M.p.: 200 °C. ^1H -NMR (300 MHz, $\text{DMSO-}d_6$): $\delta = 13.72$ (s, 1H), 8.42 – 8.37 (m, 2H), 8.04 – 7.99 (m, 2H), 7.93 (d, $J = 2.5$ Hz, 1H), 6.63 (s, 1H). ^{13}C -NMR (75 MHz, $\text{DMSO-}d_6$): $\delta = 163.9$ (q), 155.3 (q), 148.1 (q), 131.0 (+), 124.9 (+), 123.1 (+), 93.9 (+). HRMS (ESI): calcd. for $(\text{C}_9\text{H}_8\text{N}_5\text{O}_2^+)$ $[\text{M}+\text{H}]^+$: $m/z = 218.9673$; found 218.0674. MF: $\text{C}_9\text{H}_7\text{N}_5\text{O}_2$. MW: 217.19 g/mol.

(E)-4-((1H-pyrazol-5-yl)diazenyl)aniline (4a). Compound **4a** was synthesized *via* an adapted literature reported procedure as orange solid in 93% yield *via* reduction of its nitro-substituted precursor **4k** using sodium sulfide.^[35] M.p.: 184 °C. ¹H-NMR (400 MHz, DMSO-*d*₆): δ = 13.10 (s, 1H), 7.75 (s, 1H), 7.62 – 7.58 (m, 2H), 6.67 – 6.63 (m, 2H), 6.41 (s, 1H), 6.01 (s, 2H). ¹³C-NMR (101 MHz, DMSO-*d*₆): δ = 153.0 (q), 143.3 (q), 130.4 (+), 130.4 (q), 125.2 (+), 113.8 (+), 93.3 (+). HRMS (ESI): calcd. for (C₉H₁₀N₅⁺) [M+H]⁺: m/z = 188.0931; found 188.0929. MF: C₉H₉N₅. MW: 187.21 g/mol.

(E)-1,2-di(1H-pyrazol-5-yl)diazene (4d). Compound **4d** was synthesized as brown solid in 35% yield *via* oxidative coupling following an adapted literature reported procedure.^[36] M.p.: decomposition over 300 °C. ¹H-NMR (400 MHz, DMSO-*d*₆): δ = 13.42 (s, 2H), 7.84 (s, 2H), 6.54 (s, 2H). ¹³C-NMR (101 MHz, DMSO-*d*₆): δ = 164.5 (q), 131.1 (+), 93.8 (+). HRMS (ESI): calcd. for (C₆H₇N₆⁺) [M+H]⁺: m/z = 163.0727; found 163.0727. MF: C₆H₆N₆. MW: 162.16 g/mol.

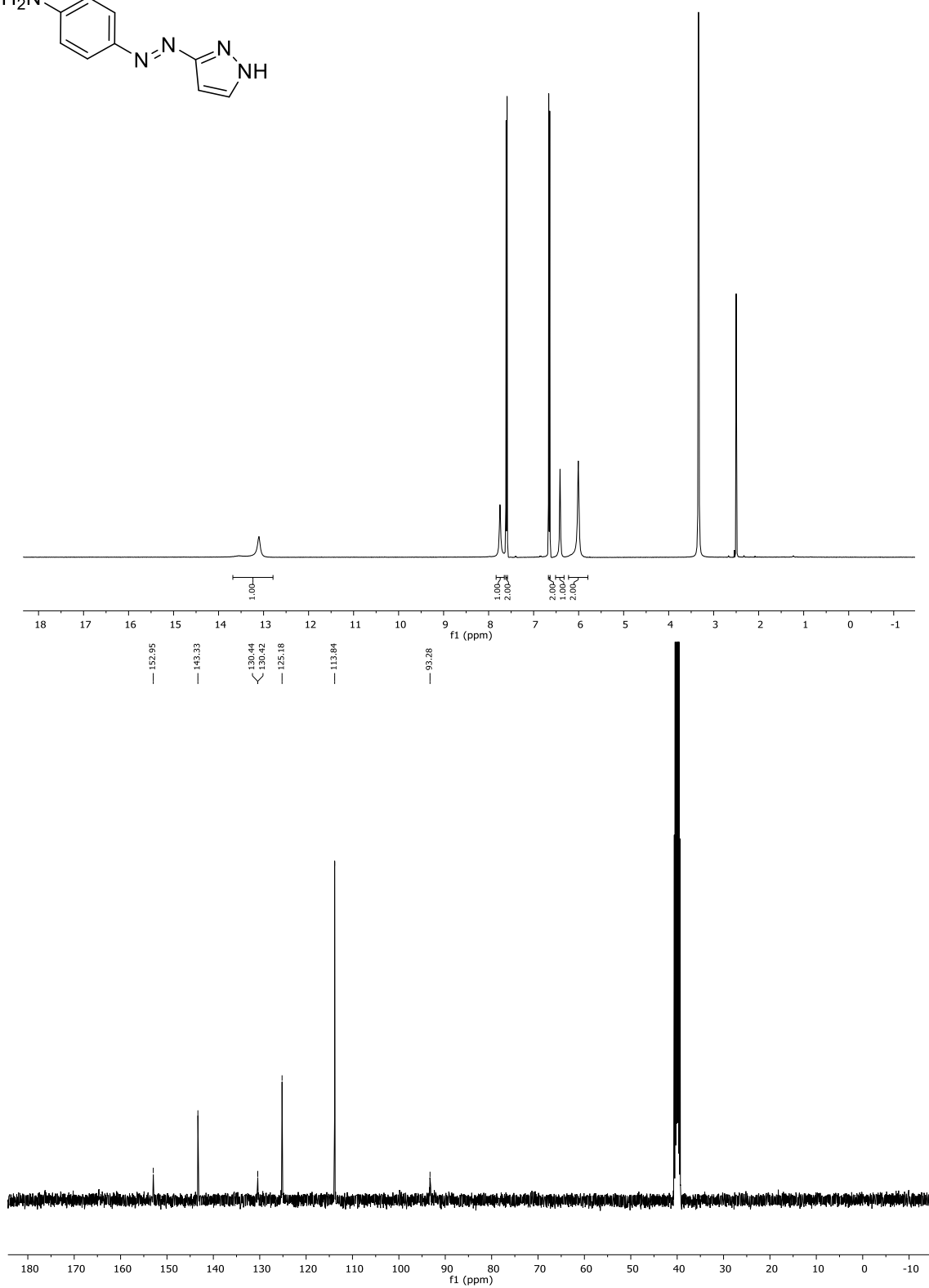
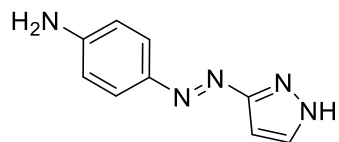
2.4.3 Laser Flash Photolysis

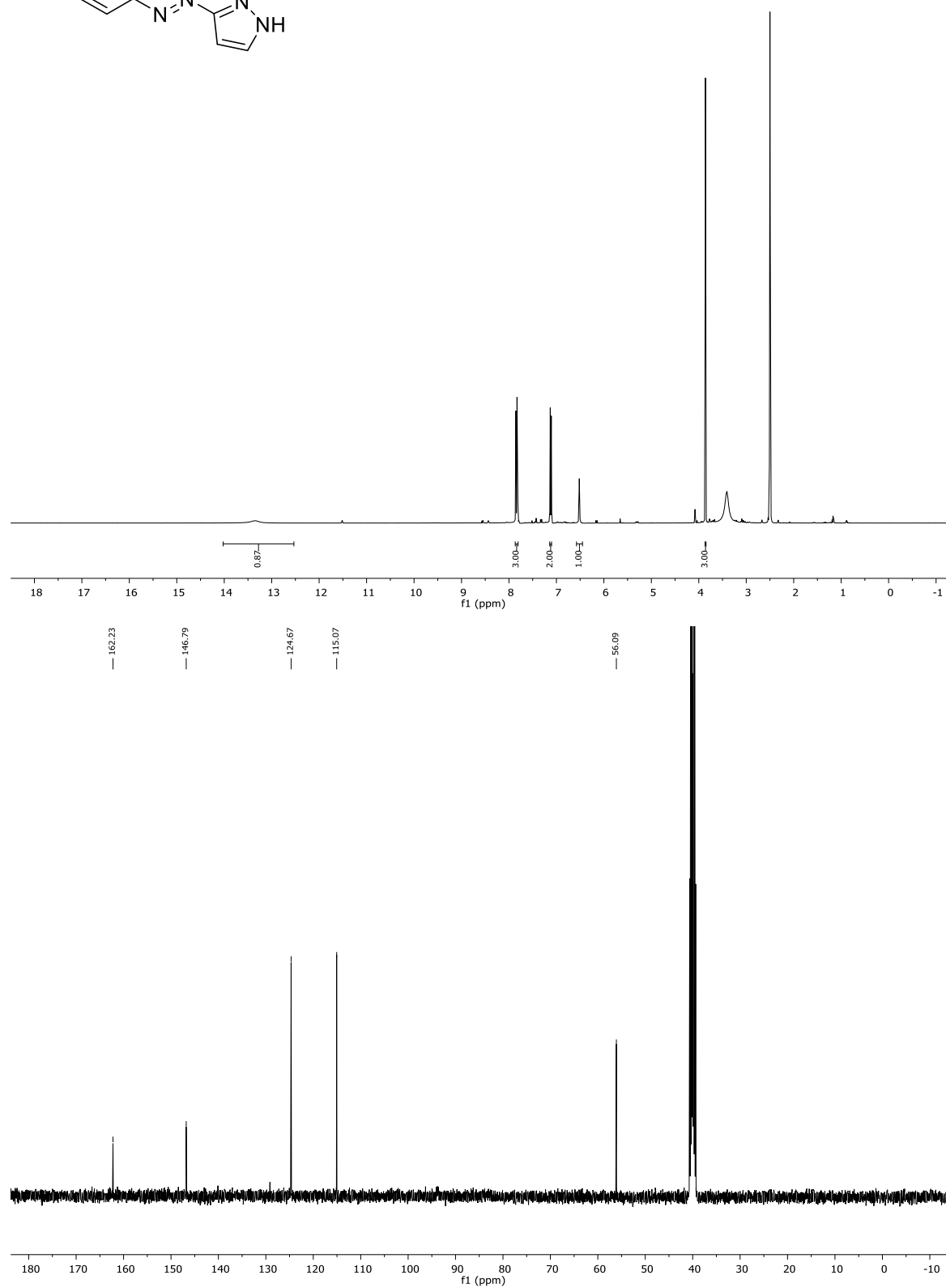
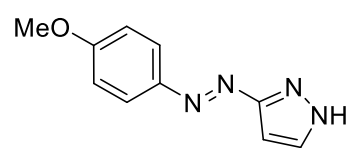
The laser pulse photolysis apparatus consisted of a Flash lamp pumped Q-switched SpitLight-100 Nd:YAG laser from InnoLas, used at the third harmonic of its fundamental wavelength. It delivered a maximum power of 10 mJ at 355 nm with 6 ns pulse duration. The LP920-K monitor system (supplied by Edinburgh Instruments), arranged in a cross-beam configuration, consisted of a high-intensity 450 W ozone free Xe arc lamp (operating both in pulsed and in continuous wave), a Czerny-Turner with Triple Grating Turret monochromator, and a five-stage dynode photomultiplier. The signals were captured by means of a Tektronix TDS 3012C digital phosphor oscilloscope, and the data was processed with the L900 software supplied by Edinburgh Instruments. The solutions to be analysed were placed in a fluorescence cuvette (d = 10 mm) without any further treatment (all the signals are thus registered in the presence of the atmospheric oxygen). All the decays reported are an average of 10 signals.

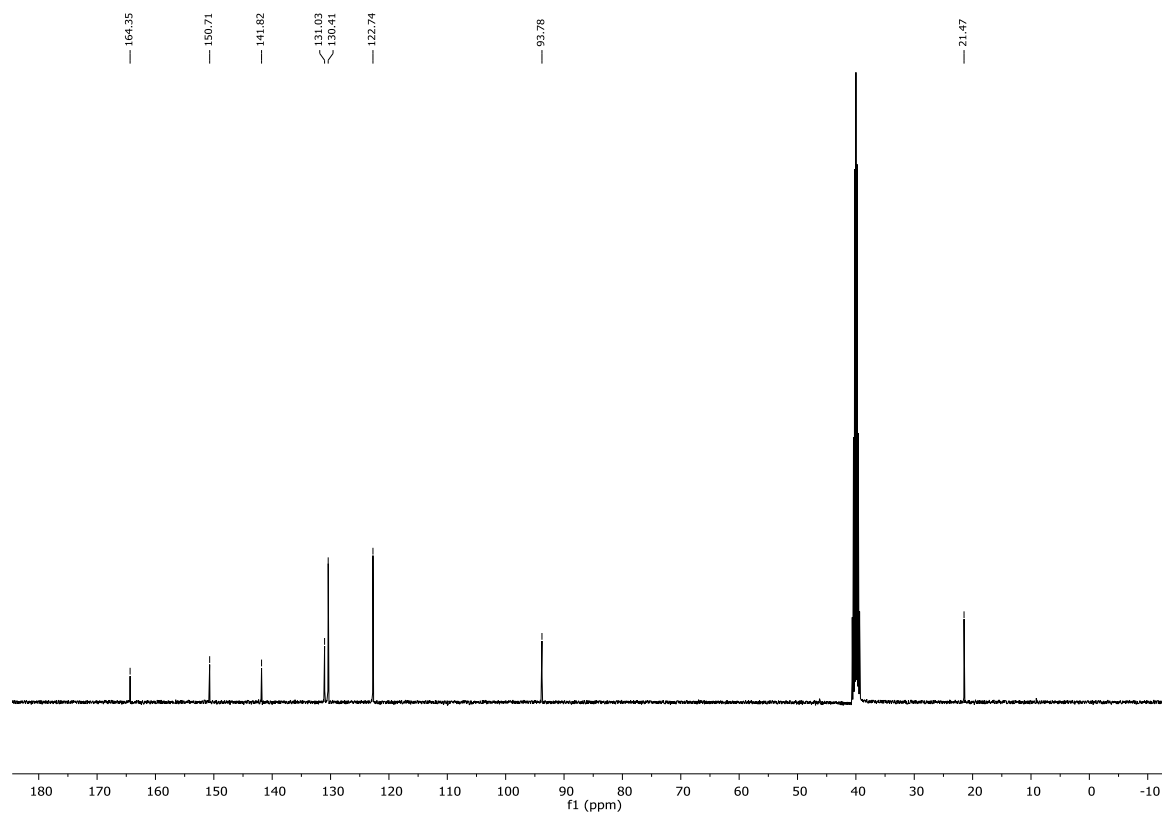
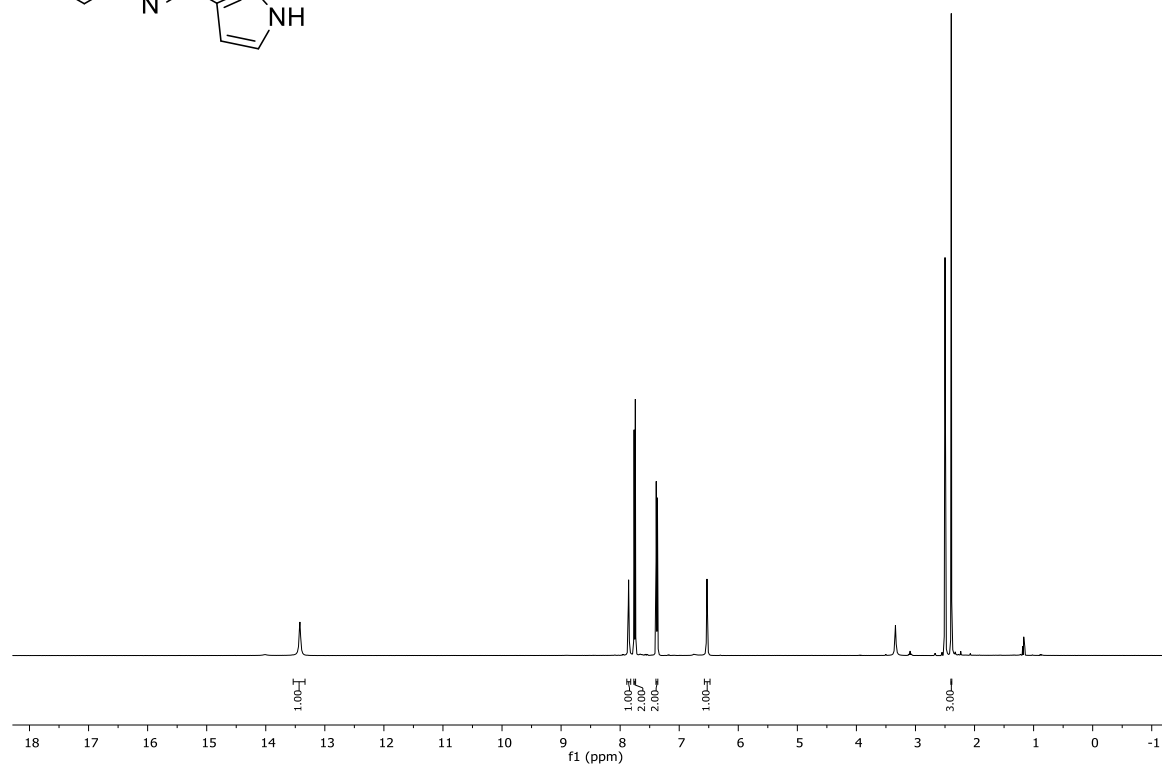
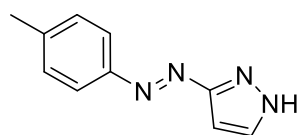
2.5 Supporting Information

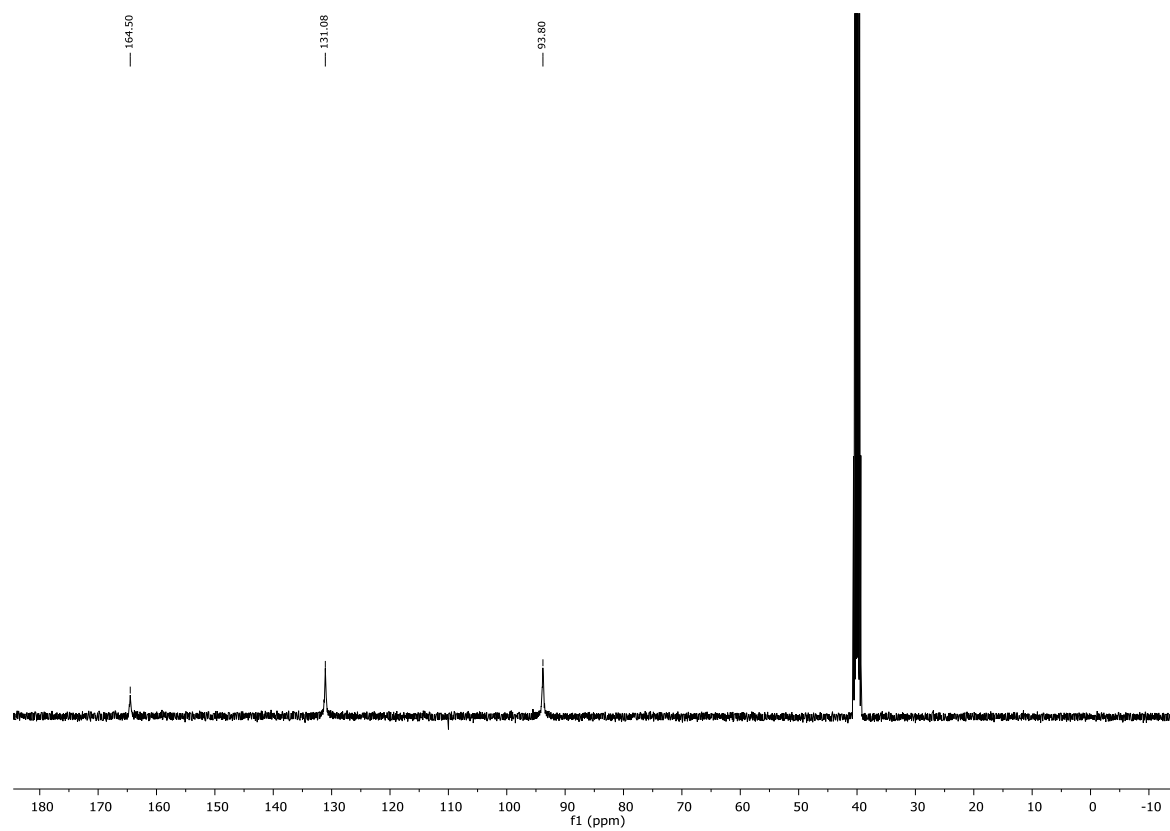
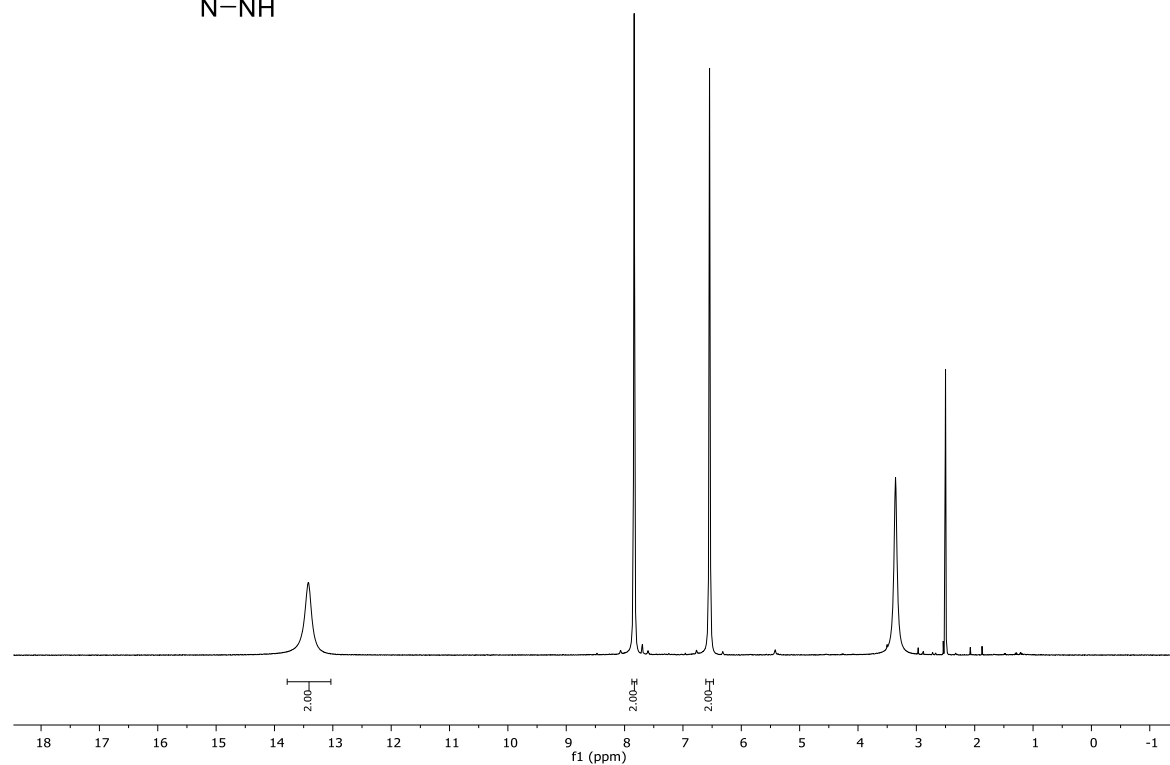
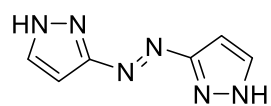
2.5.1 ^1H - and ^{13}C -NMR Spectra

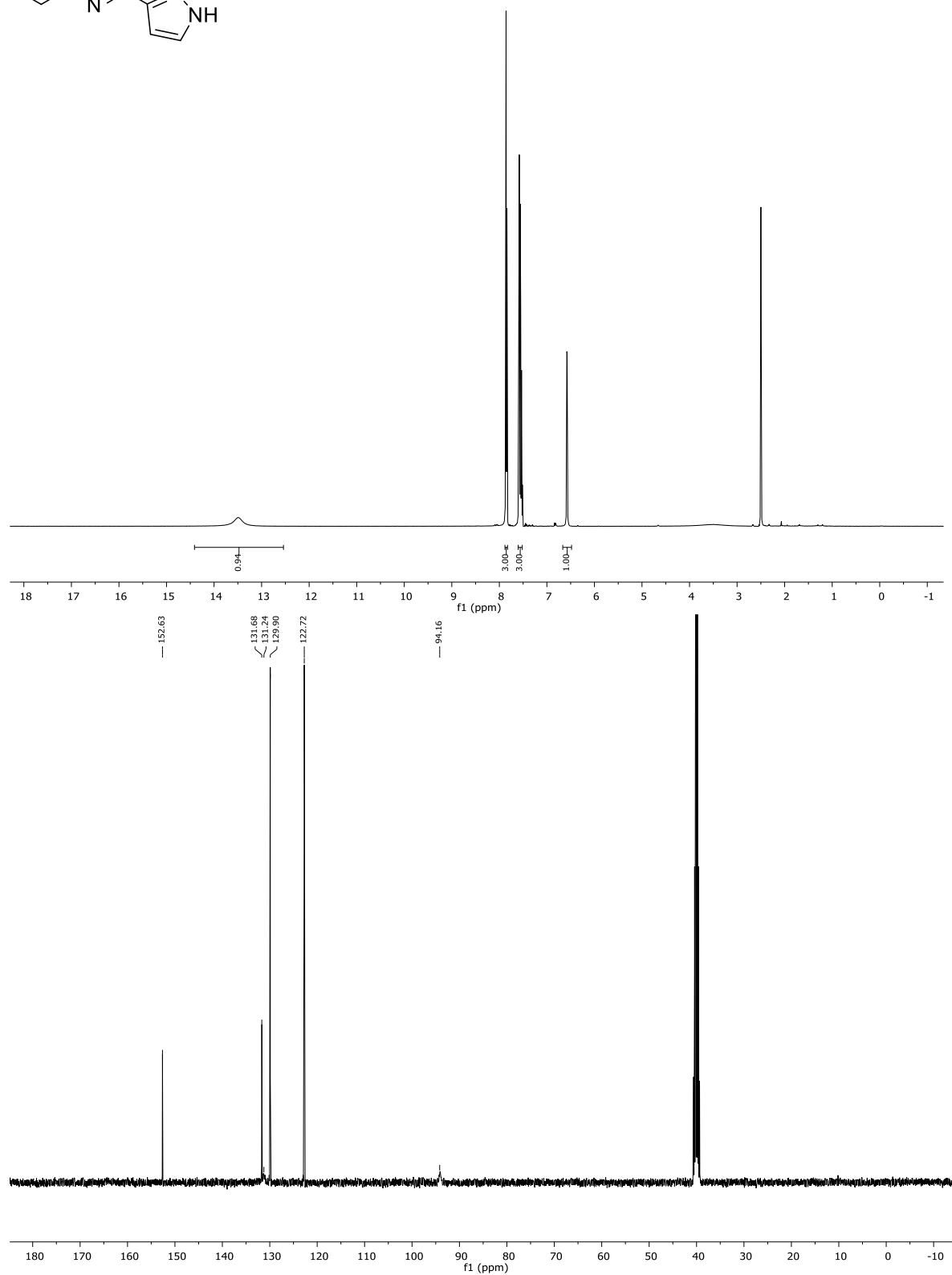
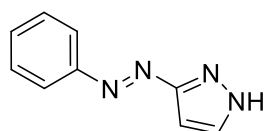
Compound **4a** ($\text{DMSO}-d_6$)

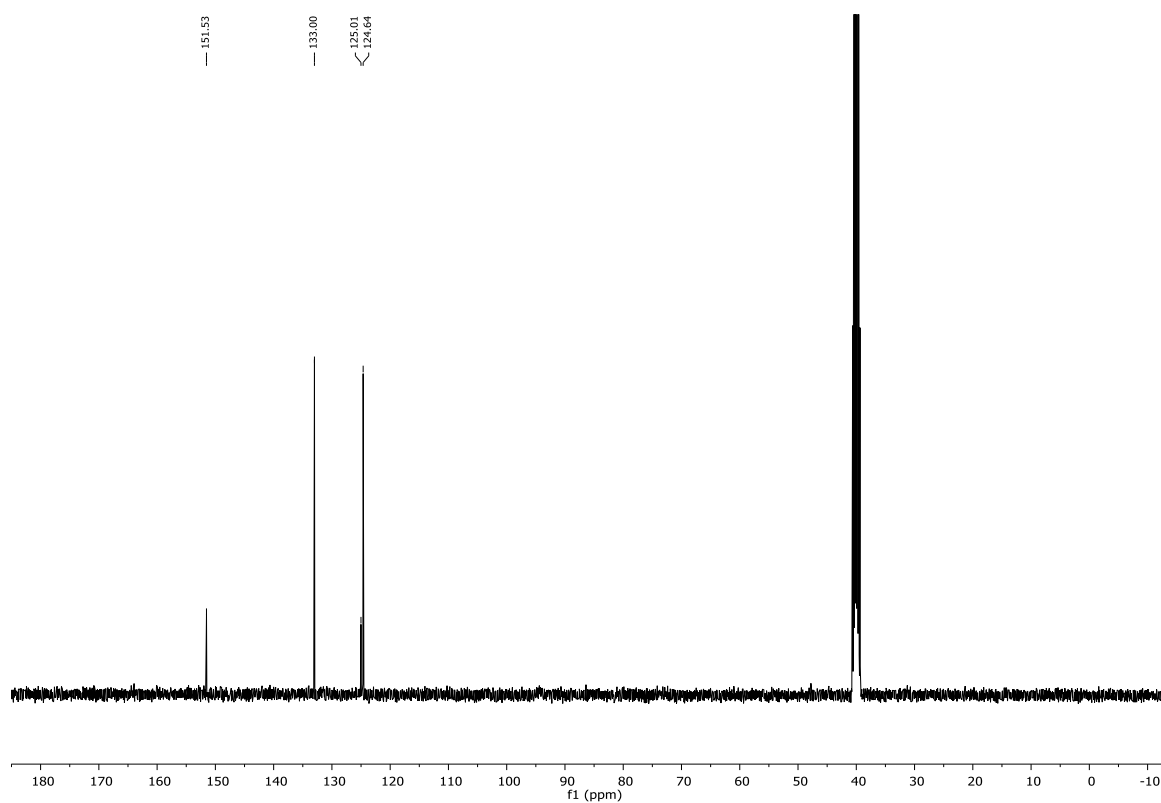
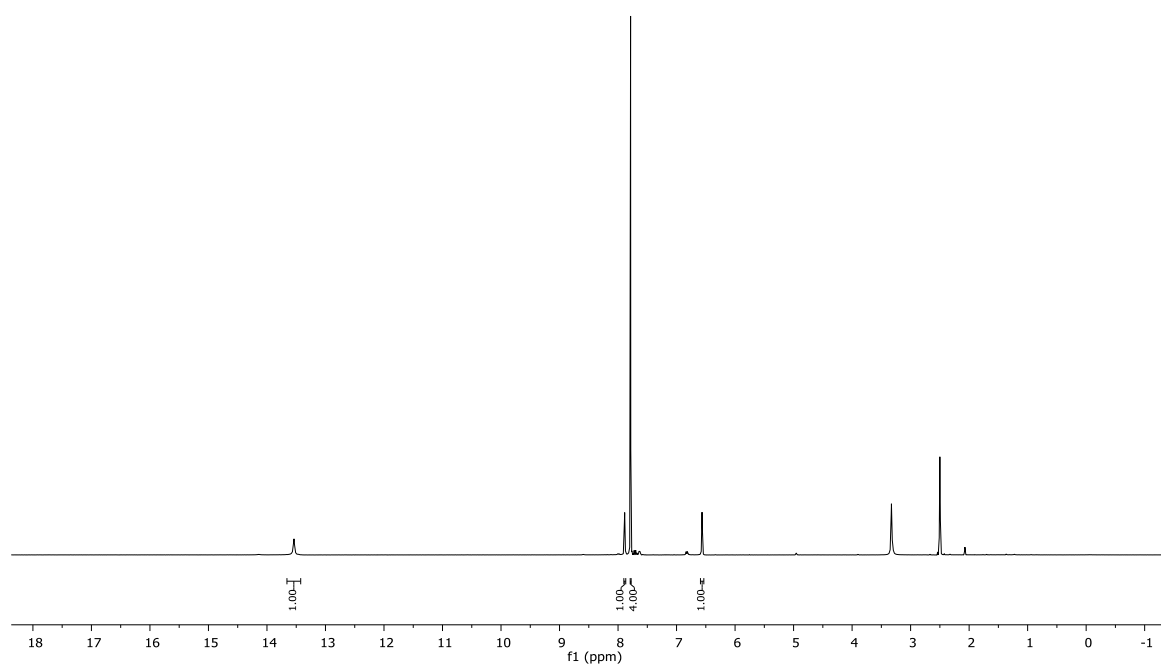
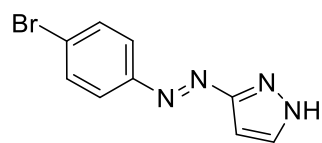


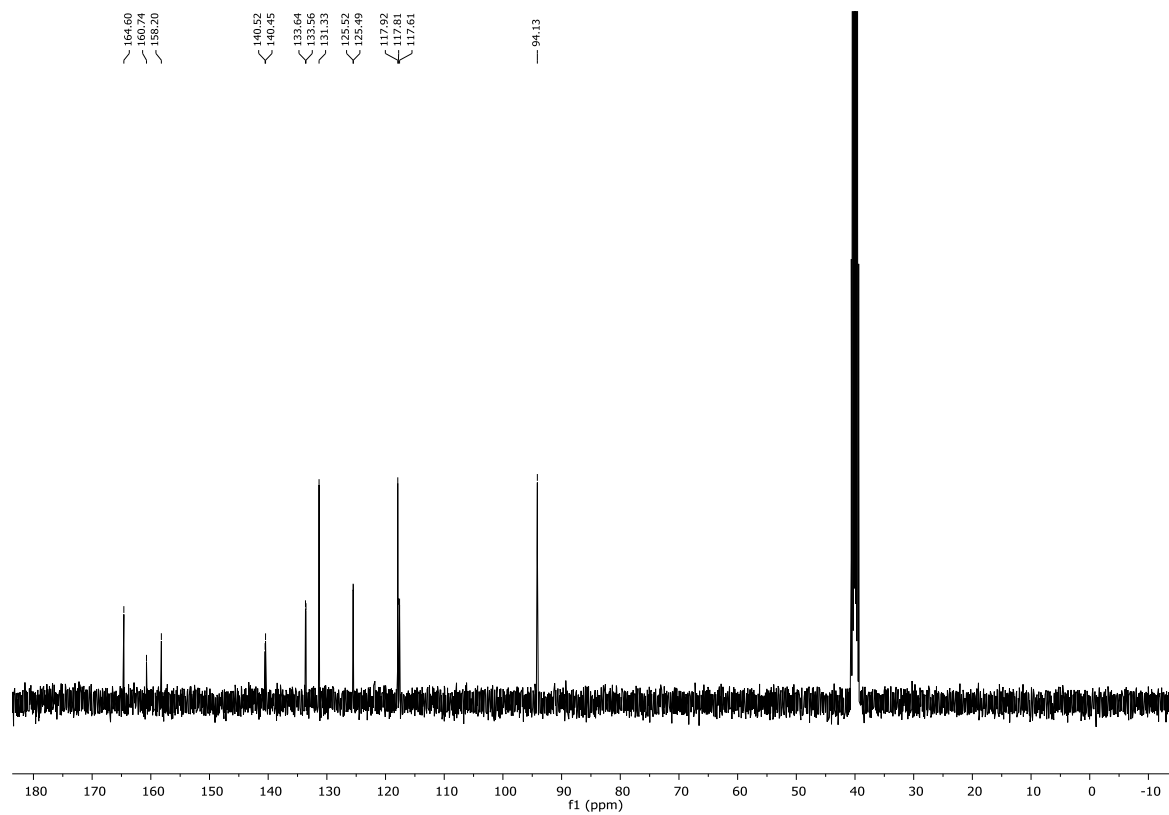
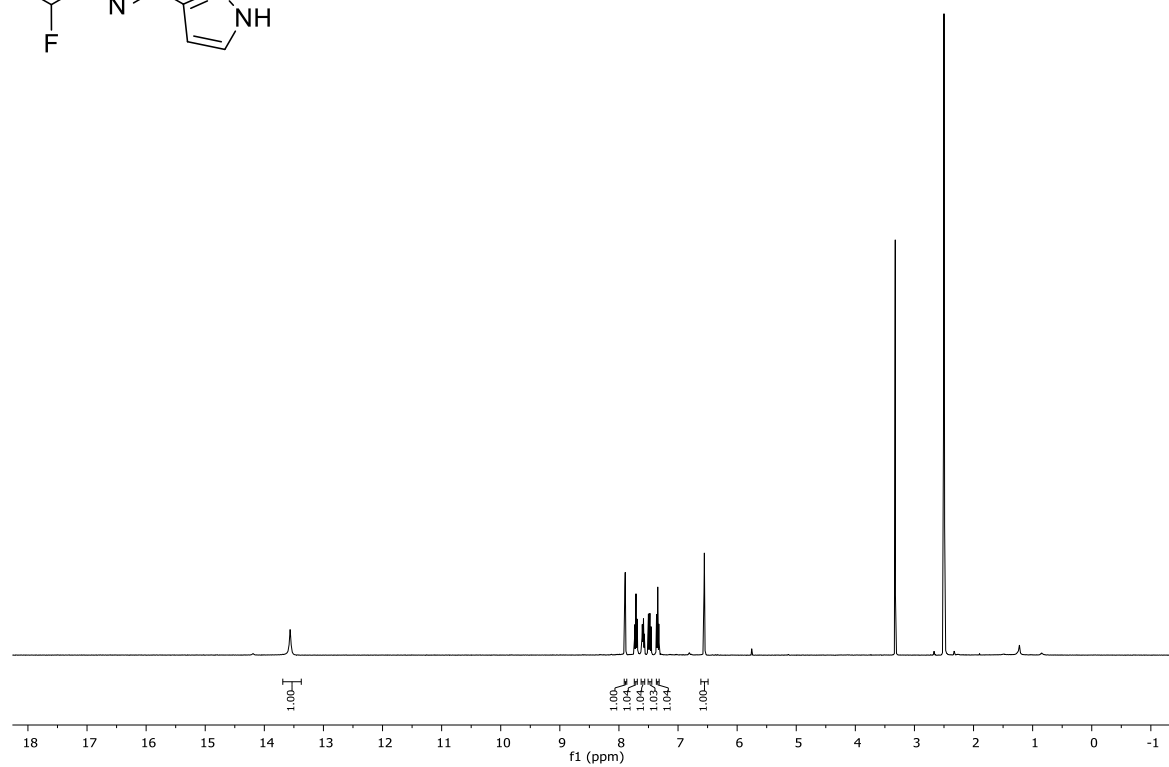
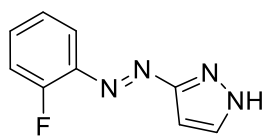
Compound **4b** (DMSO-*d*₆)

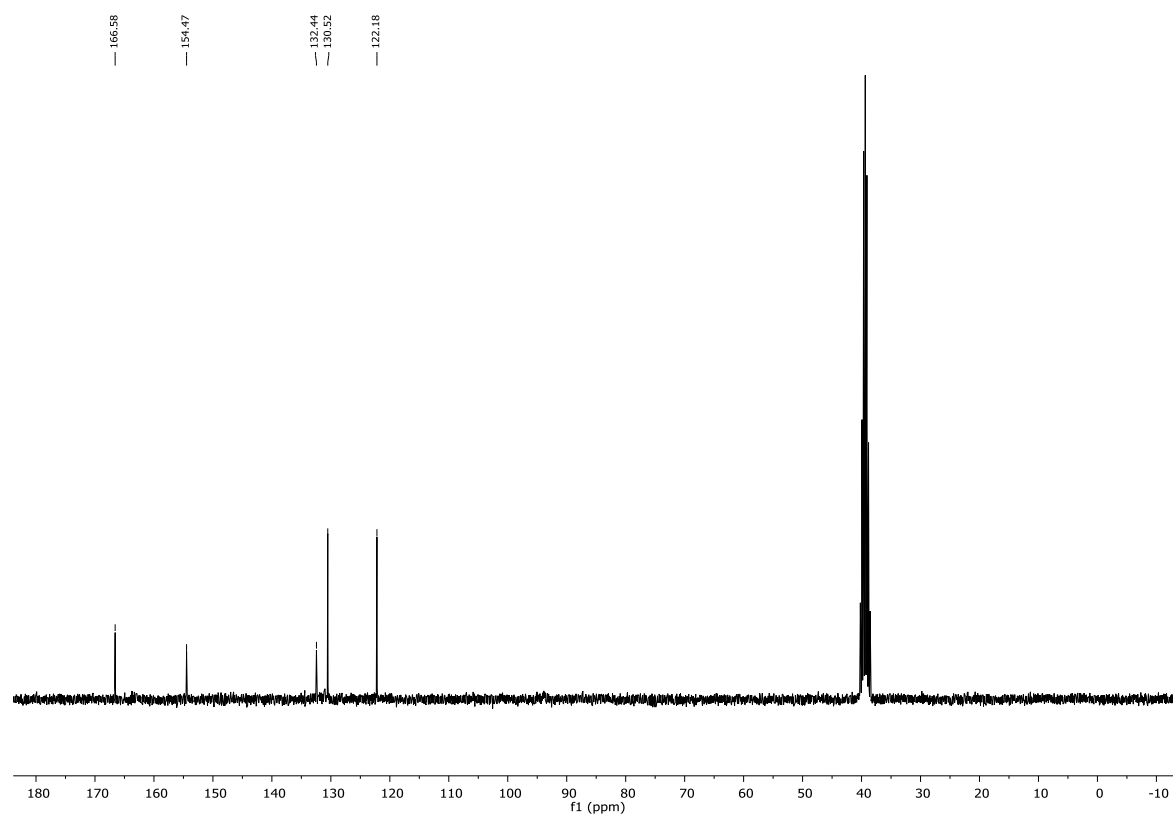
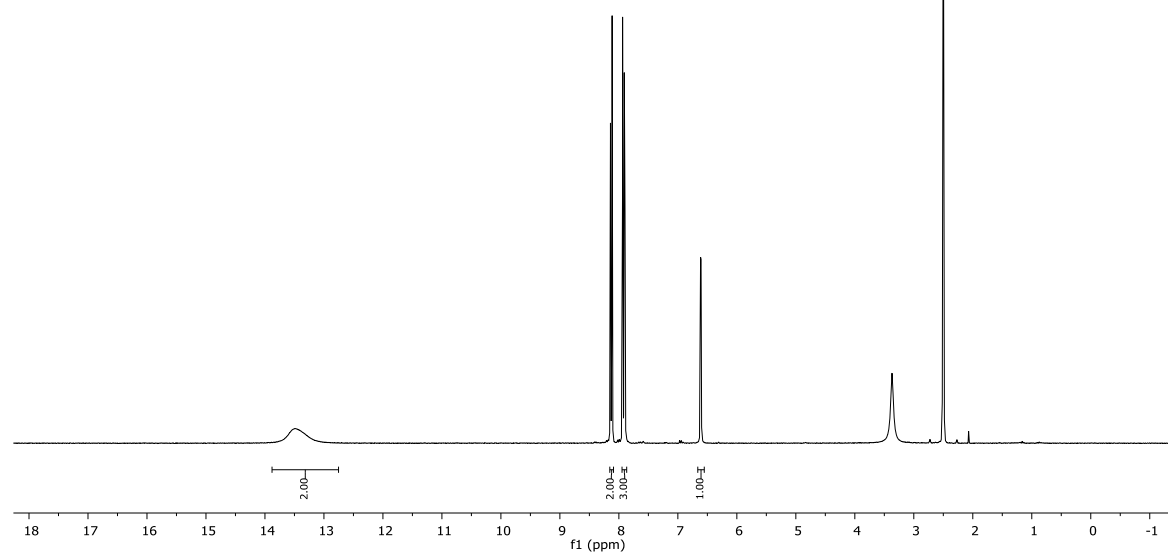
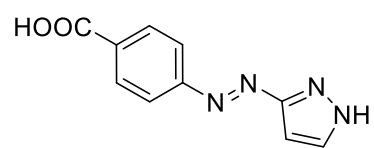
Compound **4c** (DMSO-*d*₆)


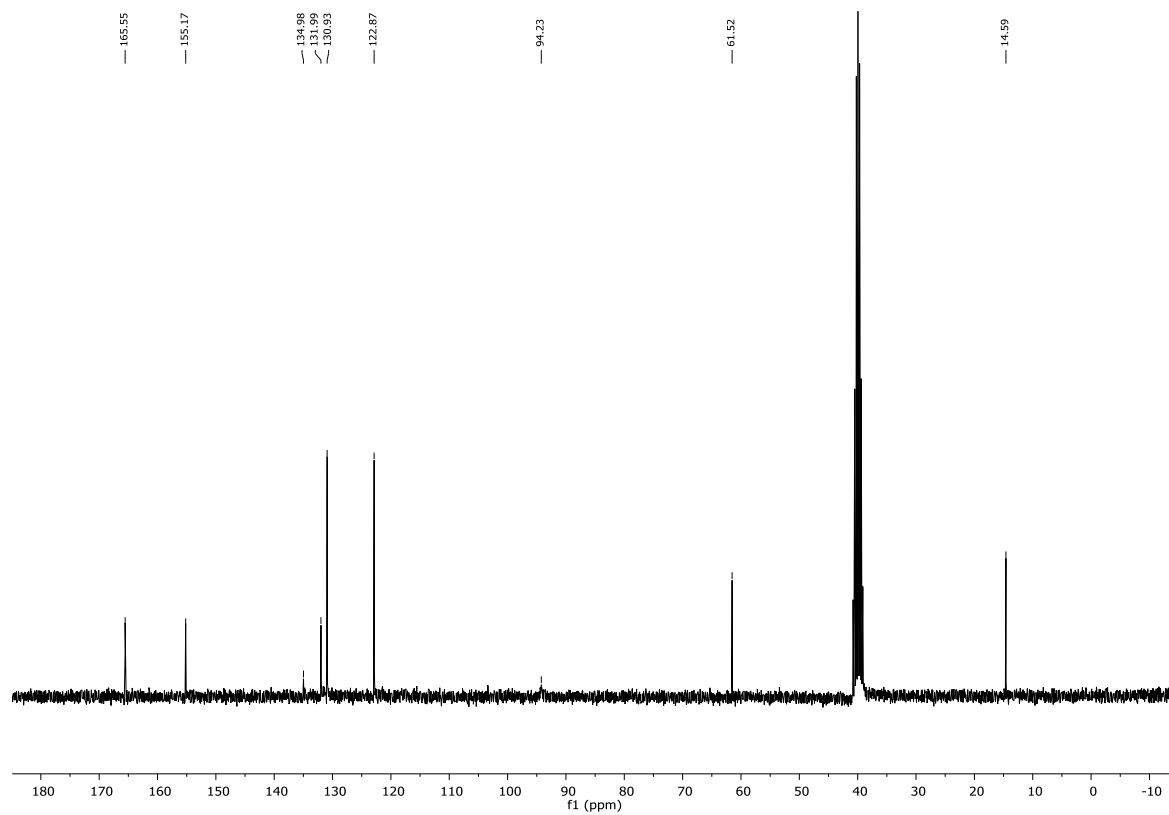
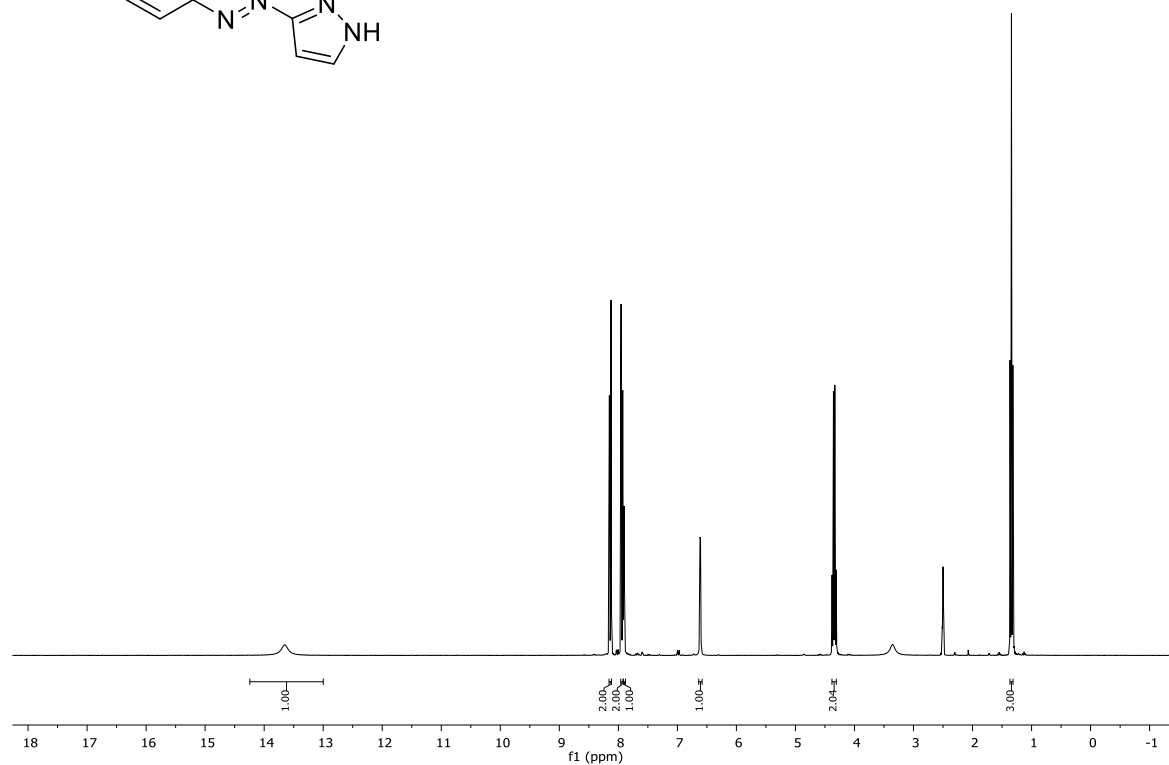
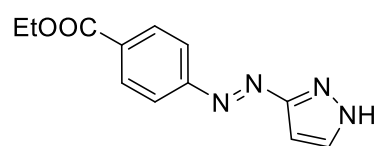
Compound **4d** (DMSO-*d*₆)

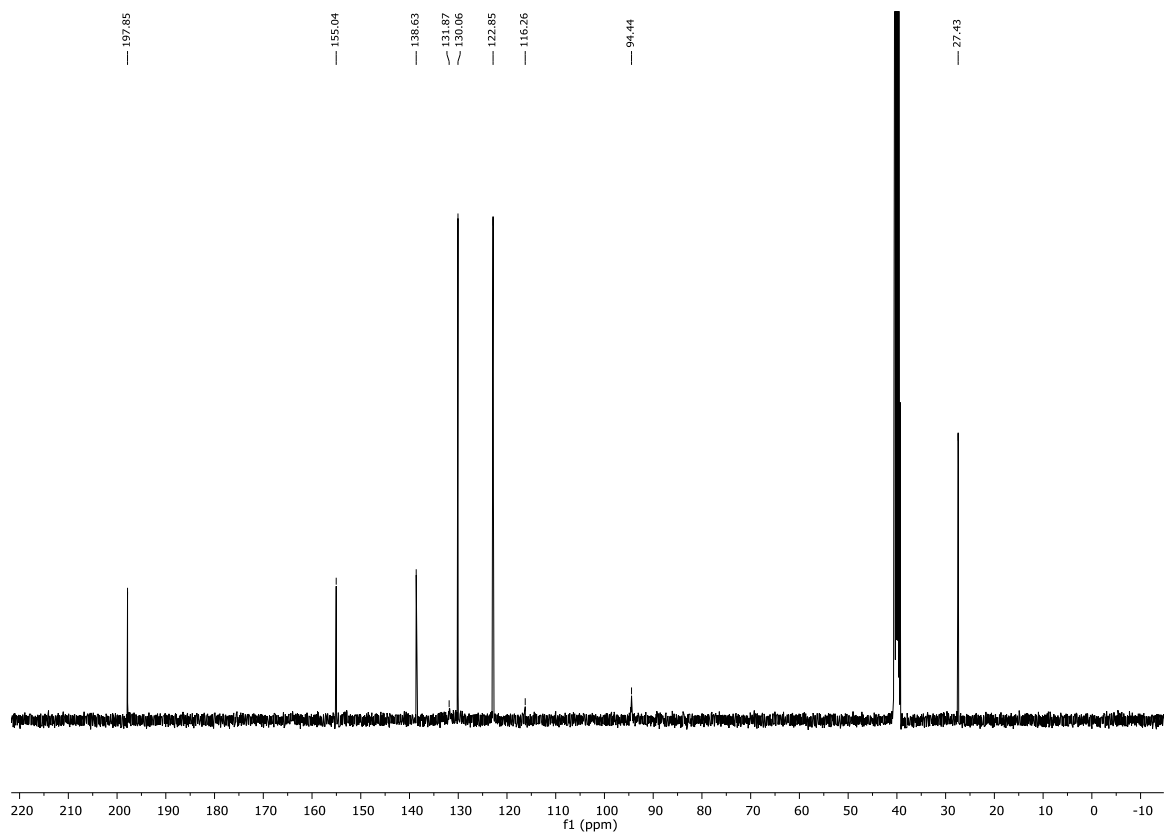
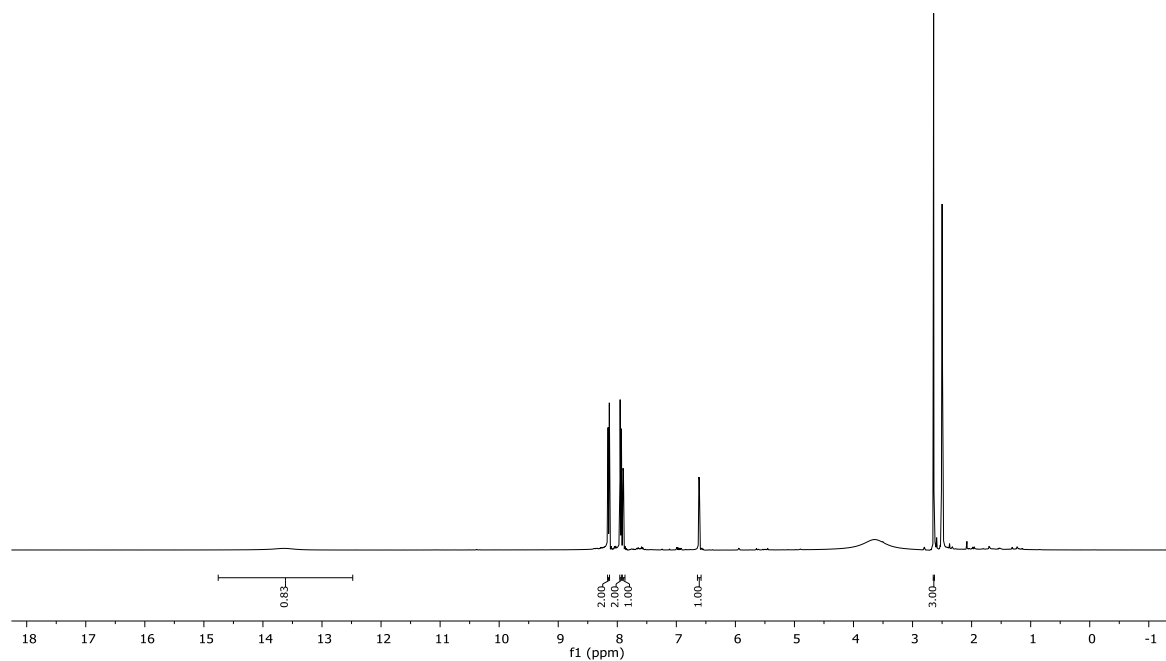
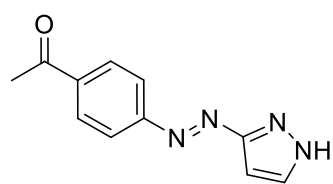
Compound **4e** (DMSO-*d*₆)


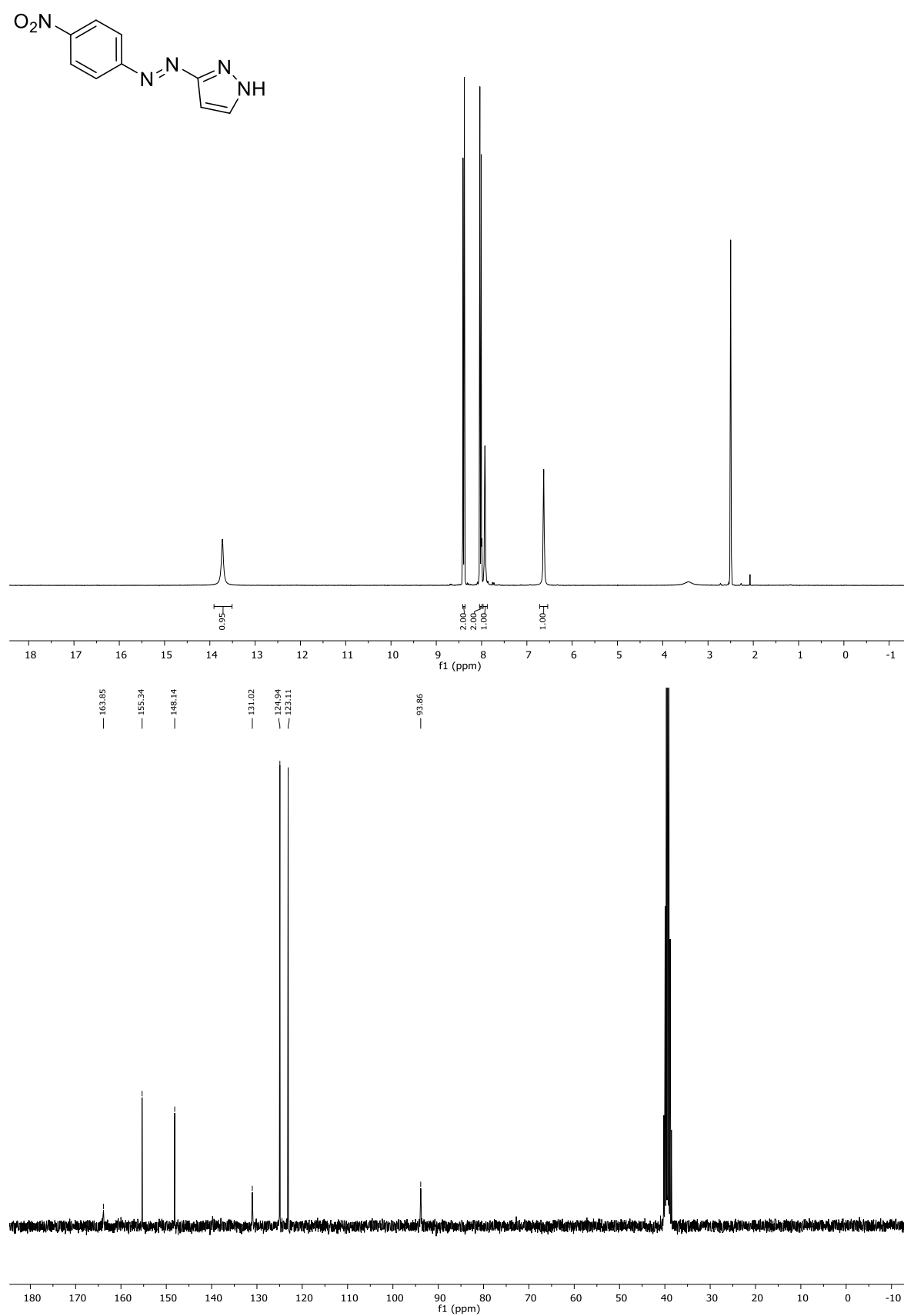
Compound **4f** (DMSO-*d*₆)

Compound **4g** (DMSO-*d*₆)


Compound **4h** (DMSO-*d*₆)

Compound **4i** (DMSO-*d*₆)


Compound **4j** (DMSO-*d*₆)

Compound **4k** (DMSO-*d*₆)


2.5.2 UV-Vis Absorption Spectra, Cycle Performances, and Thermal Half-Lives

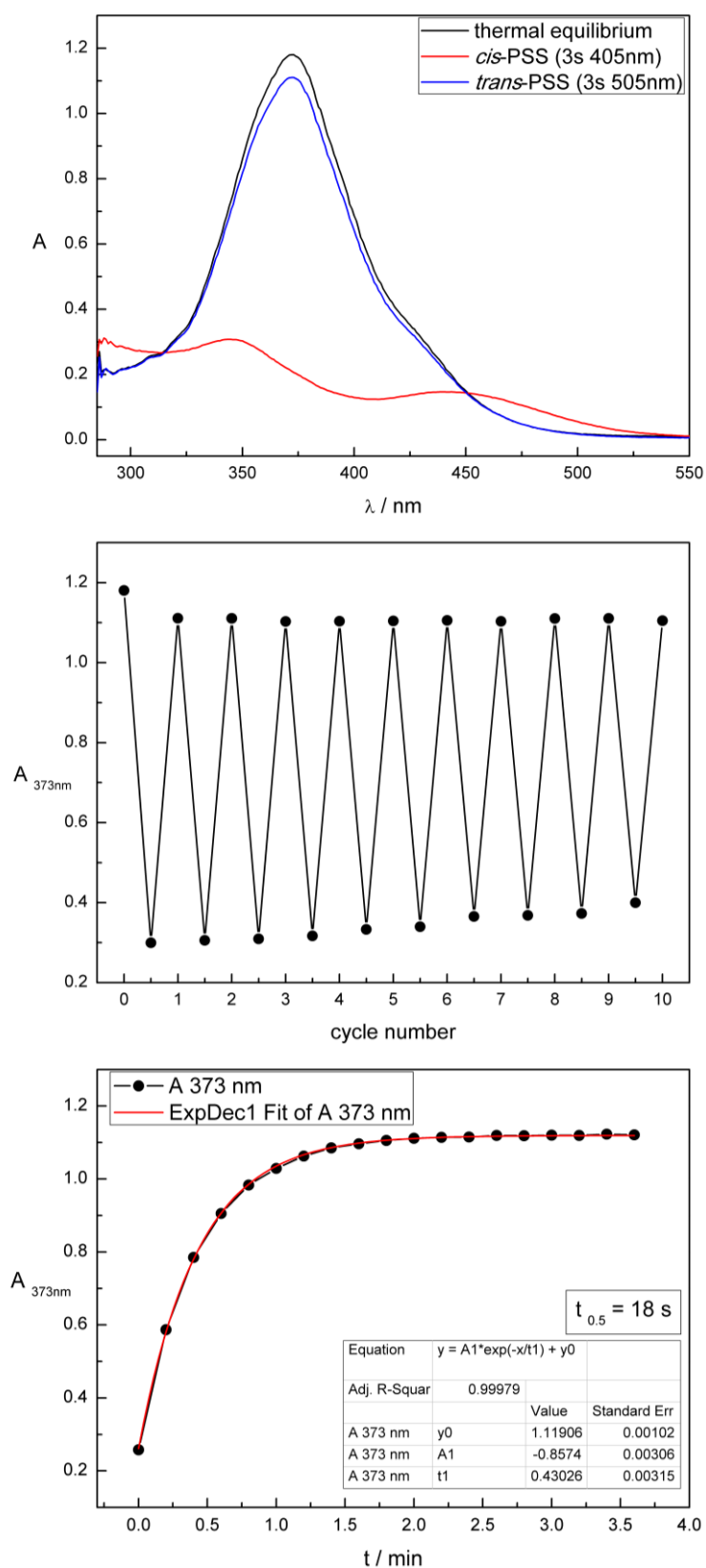


Figure S1. Compound **4a** measured 50 μM in toluene. Upper panel: UV-Vis absorption spectra. Middle panel: Cycle performance upon alternate irradiation. Lower panel: Thermal half-life.

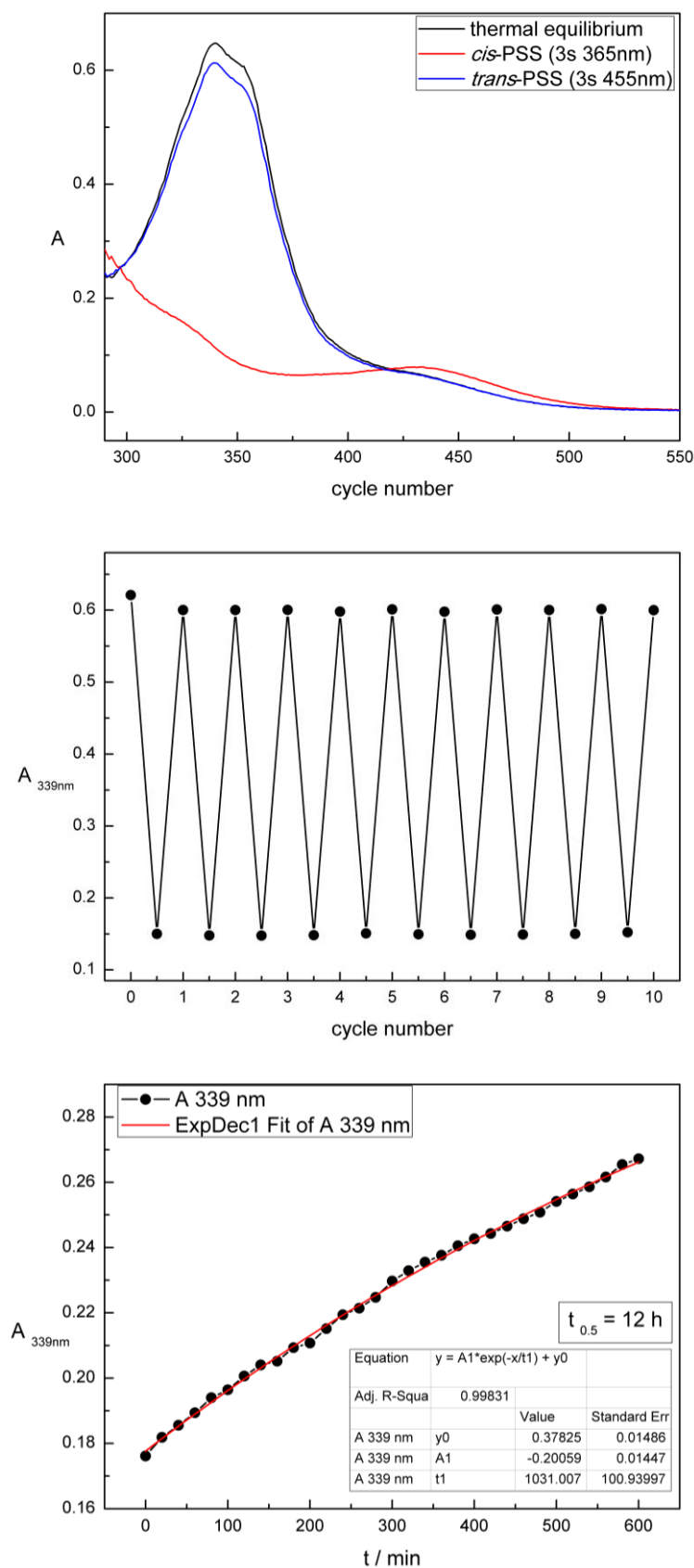


Figure S2. Compound **4b** measured 50 μM in toluene. Upper panel: UV-Vis absorption spectra. Middle panel: Cycle performance upon alternate irradiation. Lower panel: Thermal half-life.

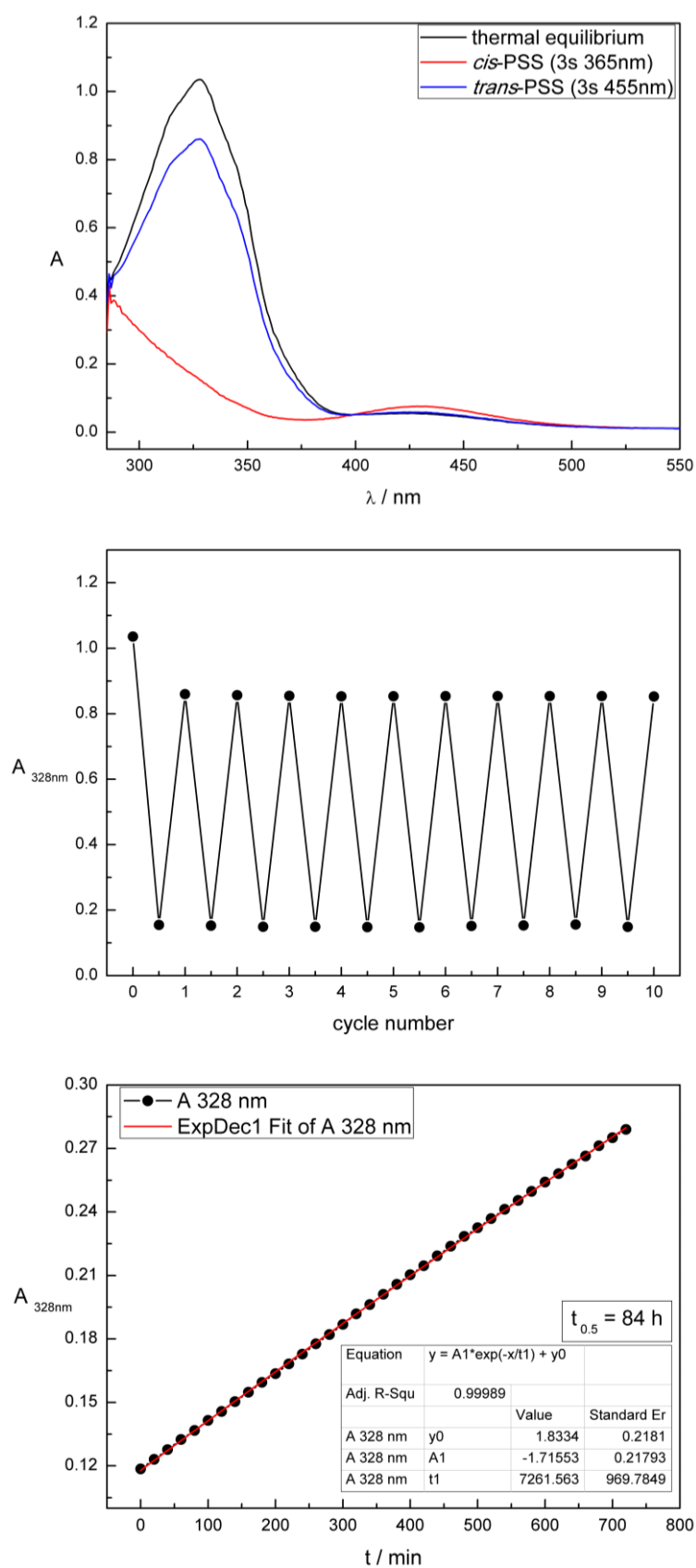


Figure S3. Compound **4c** measured 50 μM in toluene. Upper panel: UV-Vis absorption spectra. Middle panel: Cycle performance upon alternate irradiation. Lower panel: Thermal half-life.

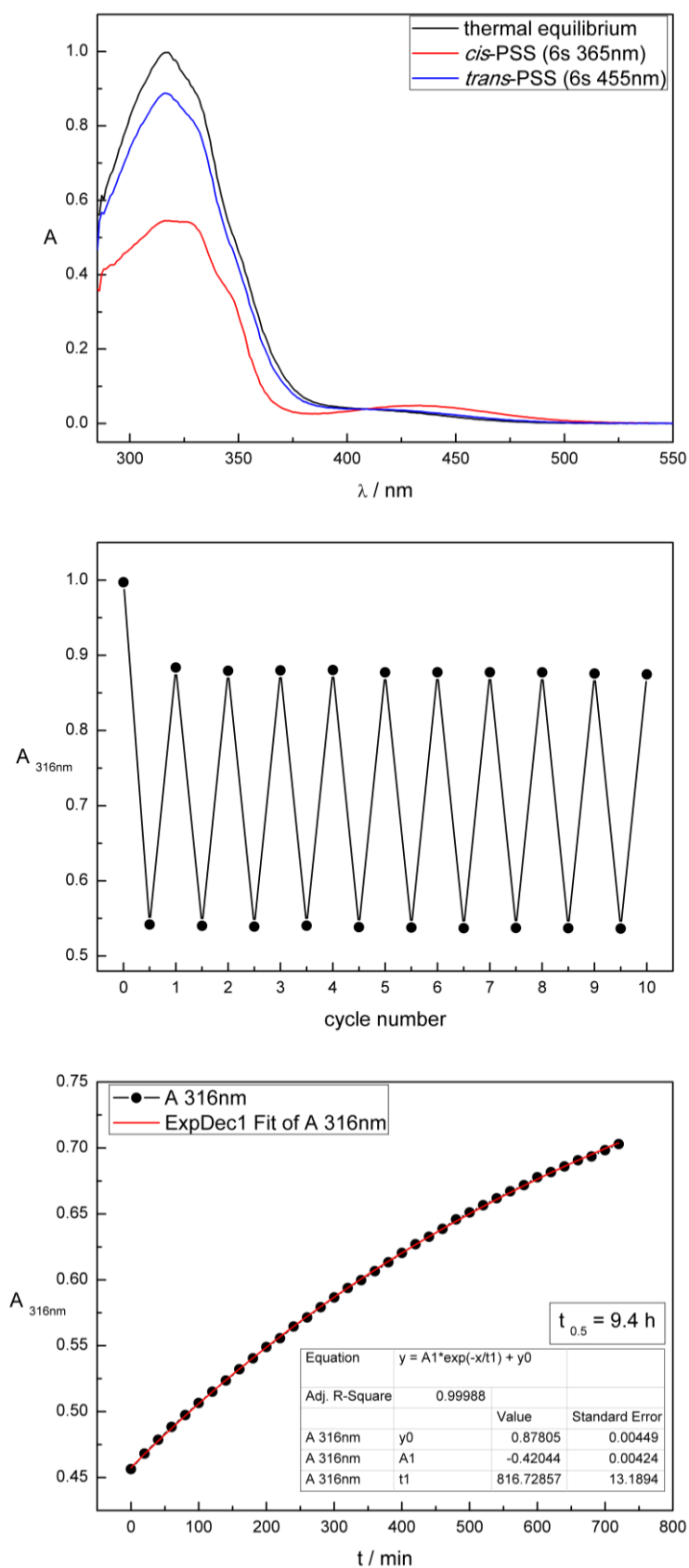


Figure S4. Compound **4d** measured 50 μM in toluene. Upper panel: UV-Vis absorption spectra. Middle panel: Cycle performance upon alternate irradiation. Lower panel: Thermal half-life.

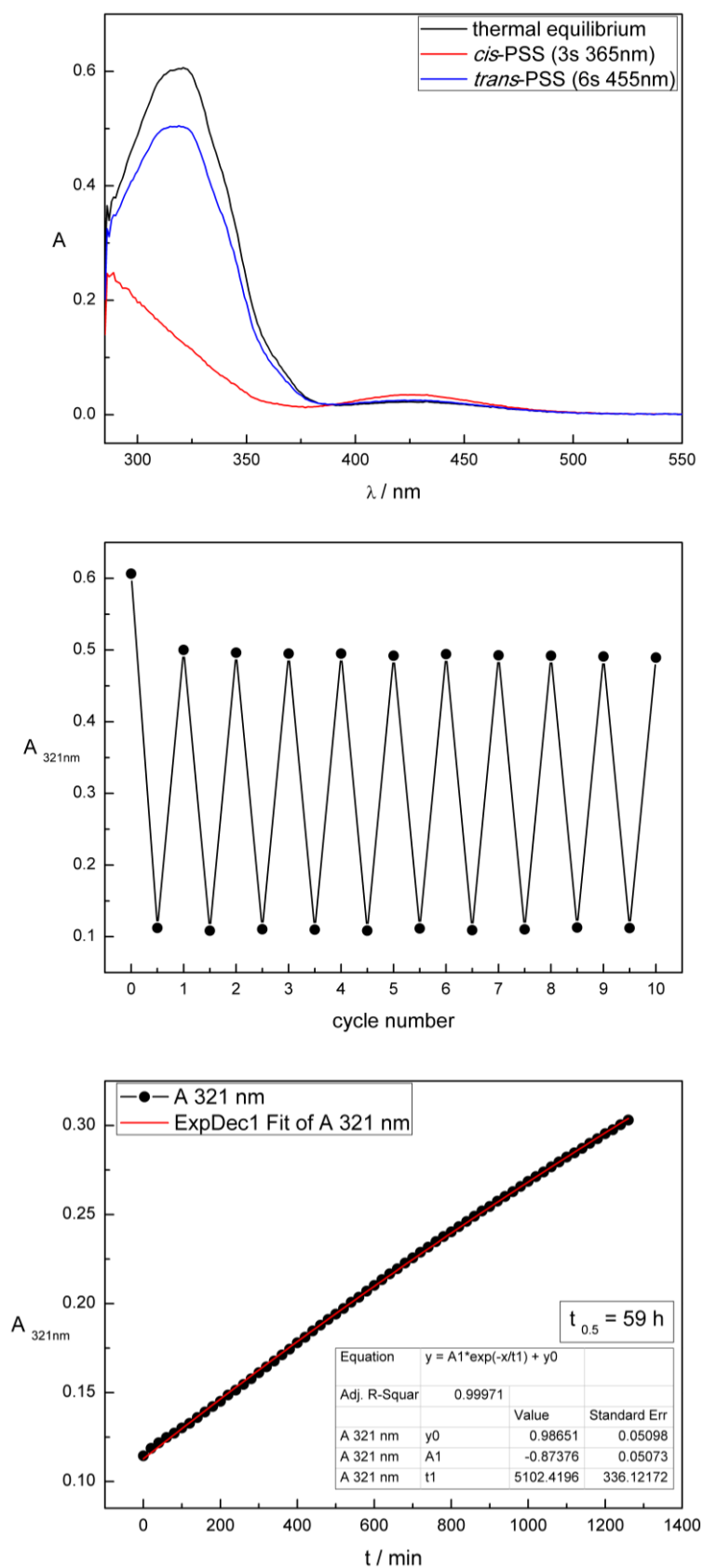


Figure S5. Compound **4e** measured 50 μM in toluene. Upper panel: UV-Vis absorption spectra. Middle panel: Cycle performance upon alternate irradiation. Lower panel: Thermal half-life.

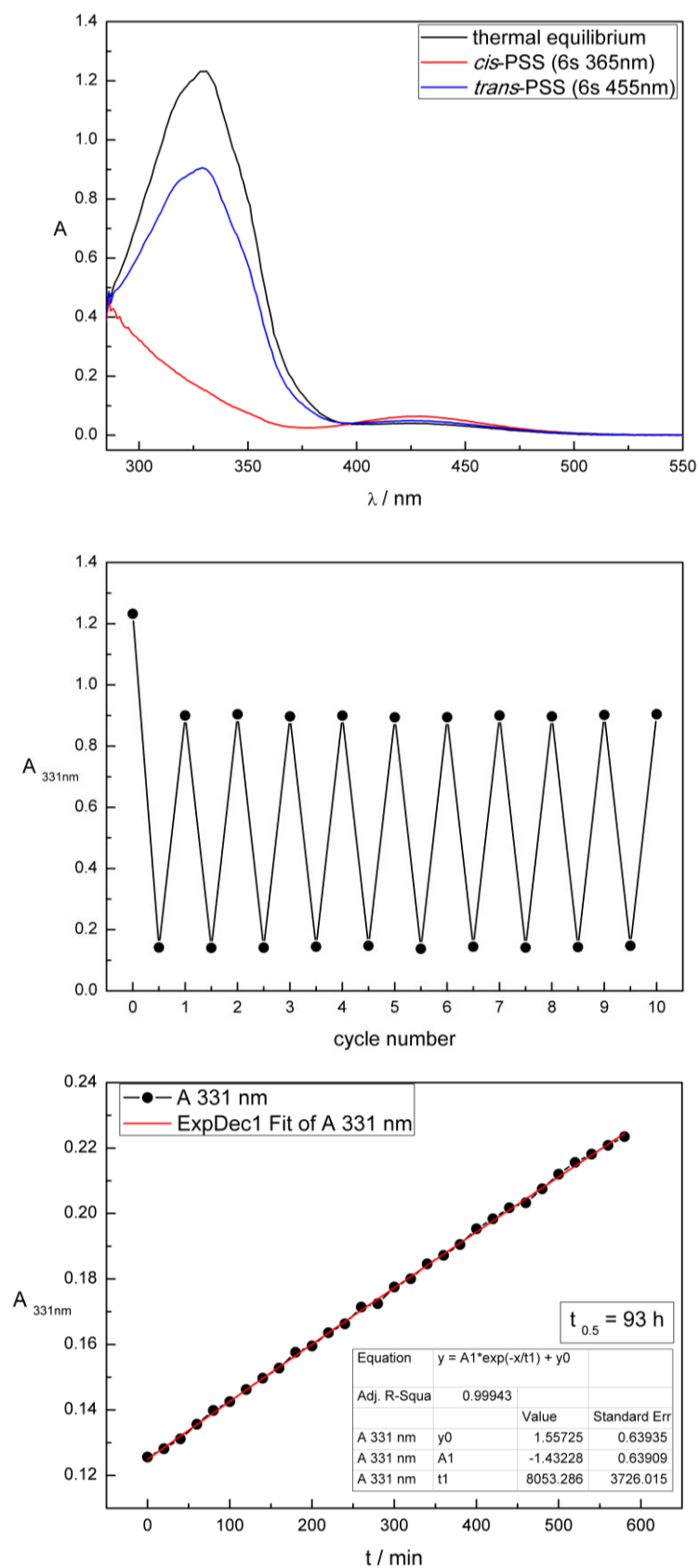


Figure S6. Compound **4f** measured 50 μM in toluene. Upper panel: UV-Vis absorption spectra. Middle panel: Cycle performance upon alternate irradiation. Lower panel: Thermal half-life.

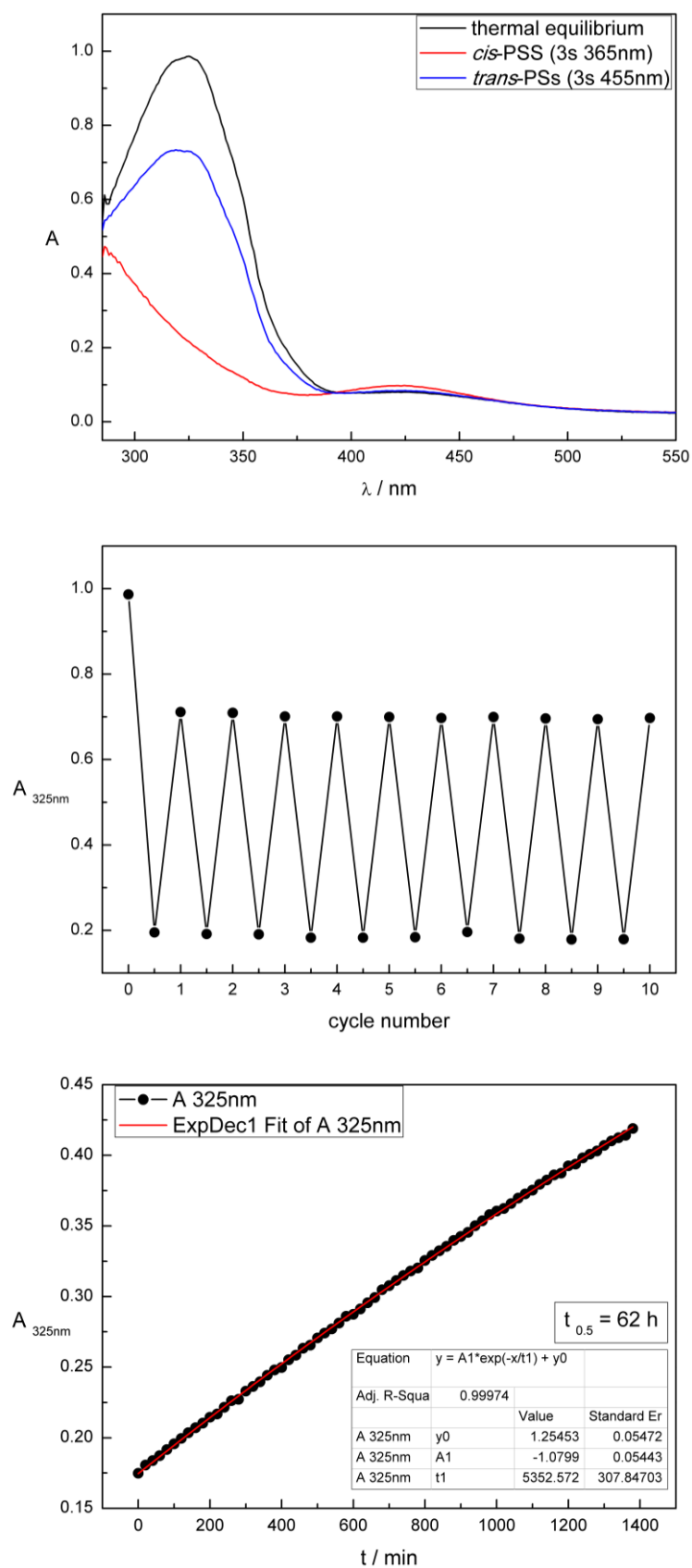


Figure S7. Compound **4g** measured 50 μM in toluene. Upper panel: UV-Vis absorption spectra. Middle panel: Cycle performance upon alternate irradiation. Lower panel: Thermal half-life.

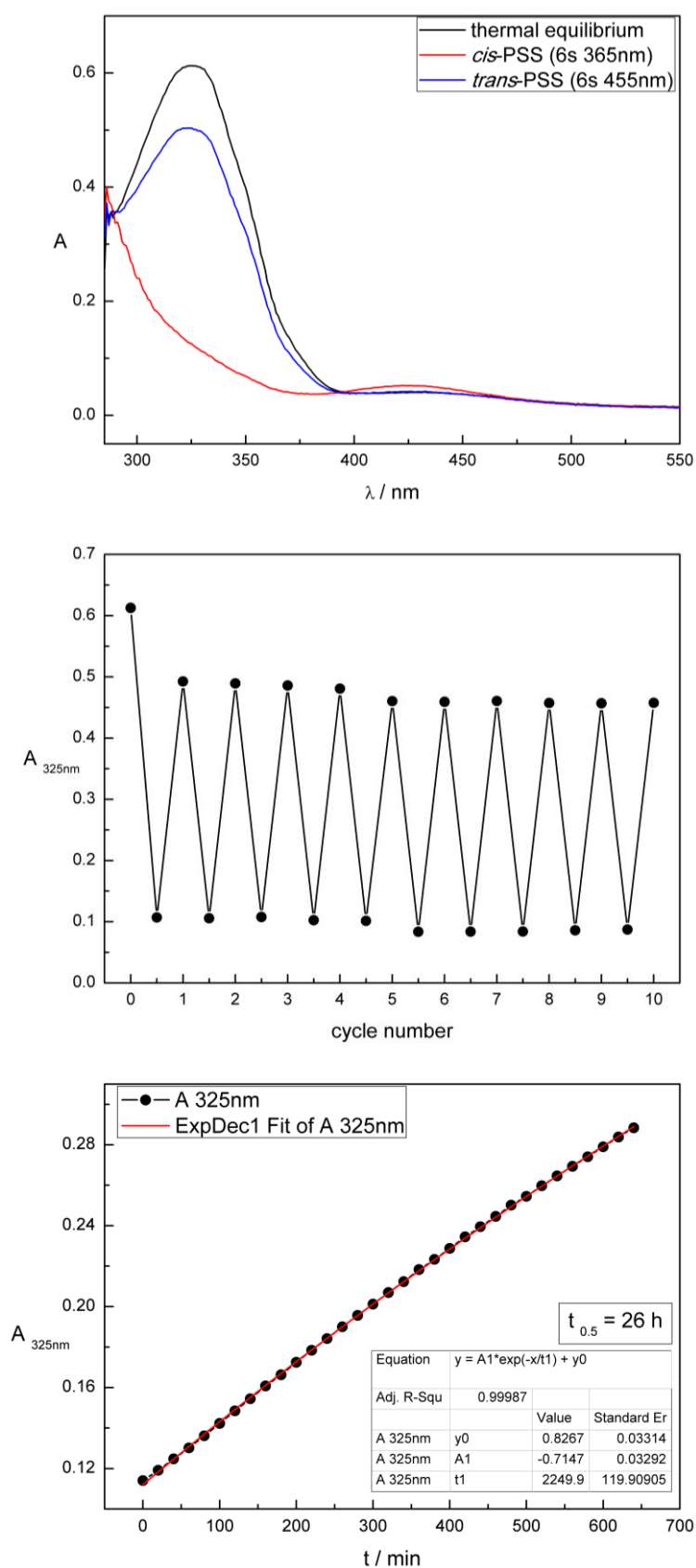


Figure S8. Compound **4h** measured 50 μM in toluene. Upper panel: UV-Vis absorption spectra. Middle panel: Cycle performance upon alternate irradiation. Lower panel: Thermal half-life.

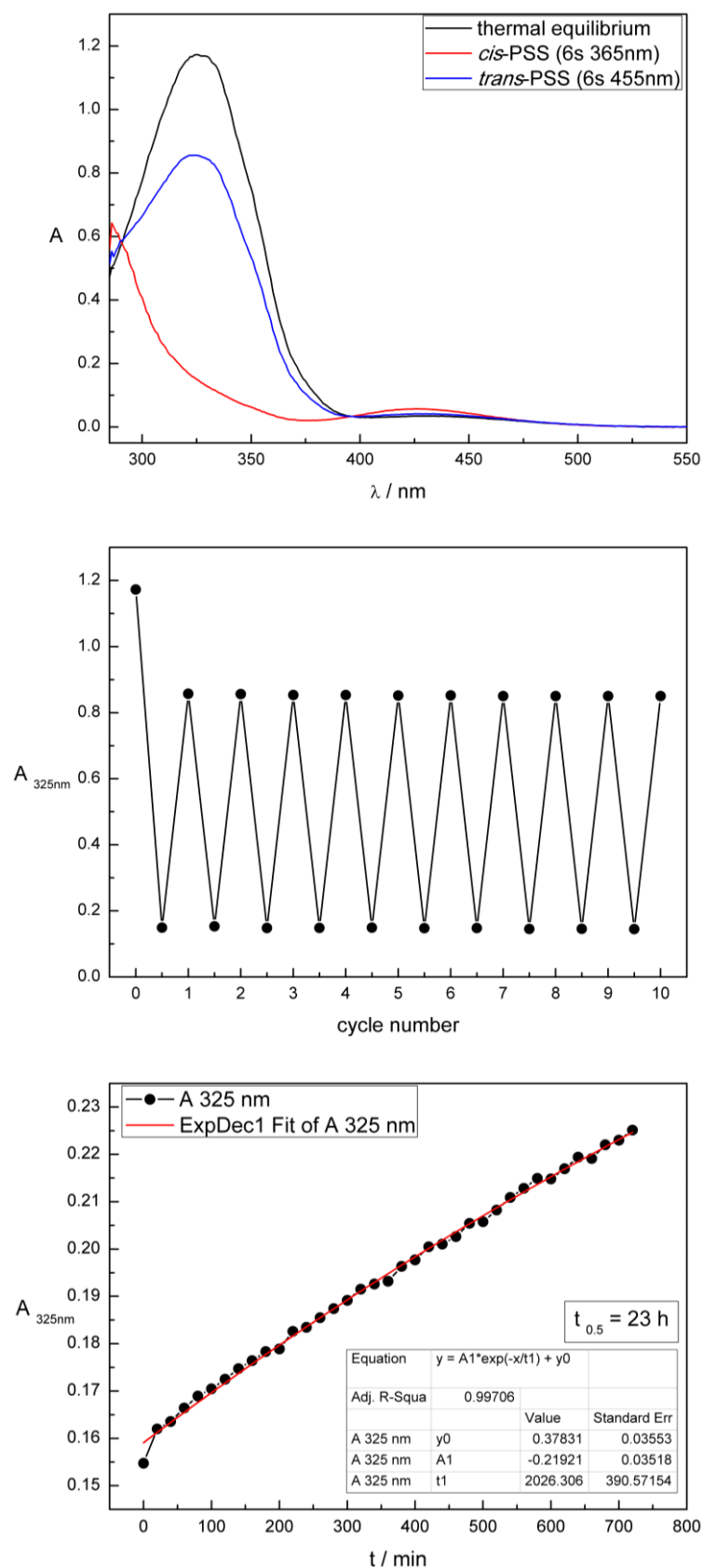


Figure S9. Compound **4i** measured 50 μM in toluene. Upper panel: UV-Vis absorption spectra. Middle panel: Cycle performance upon alternate irradiation. Lower panel: Thermal half-life.

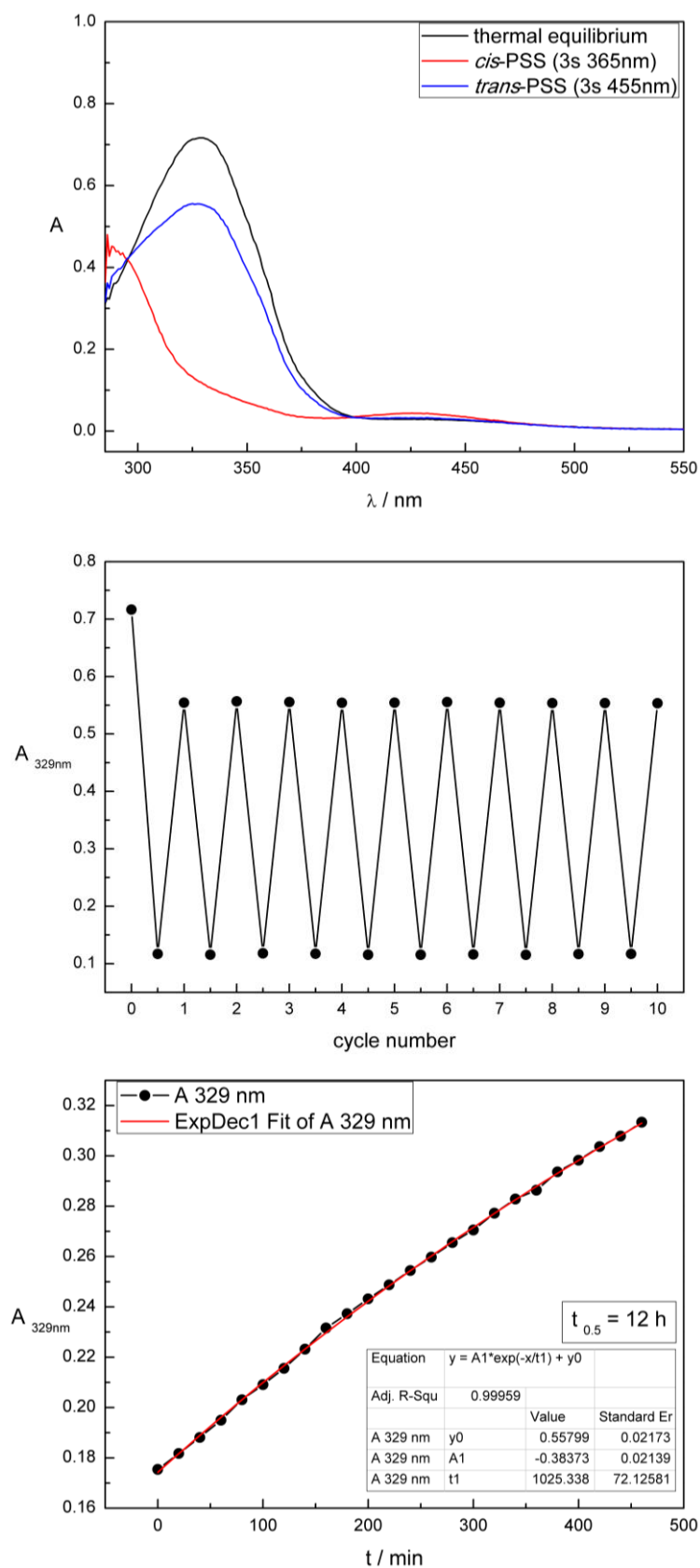


Figure S10. Compound **4j** measured 50 μM in toluene. Upper panel: UV-Vis absorption spectra. Middle panel: Cycle performance upon alternate irradiation. Lower panel: Thermal half-life.

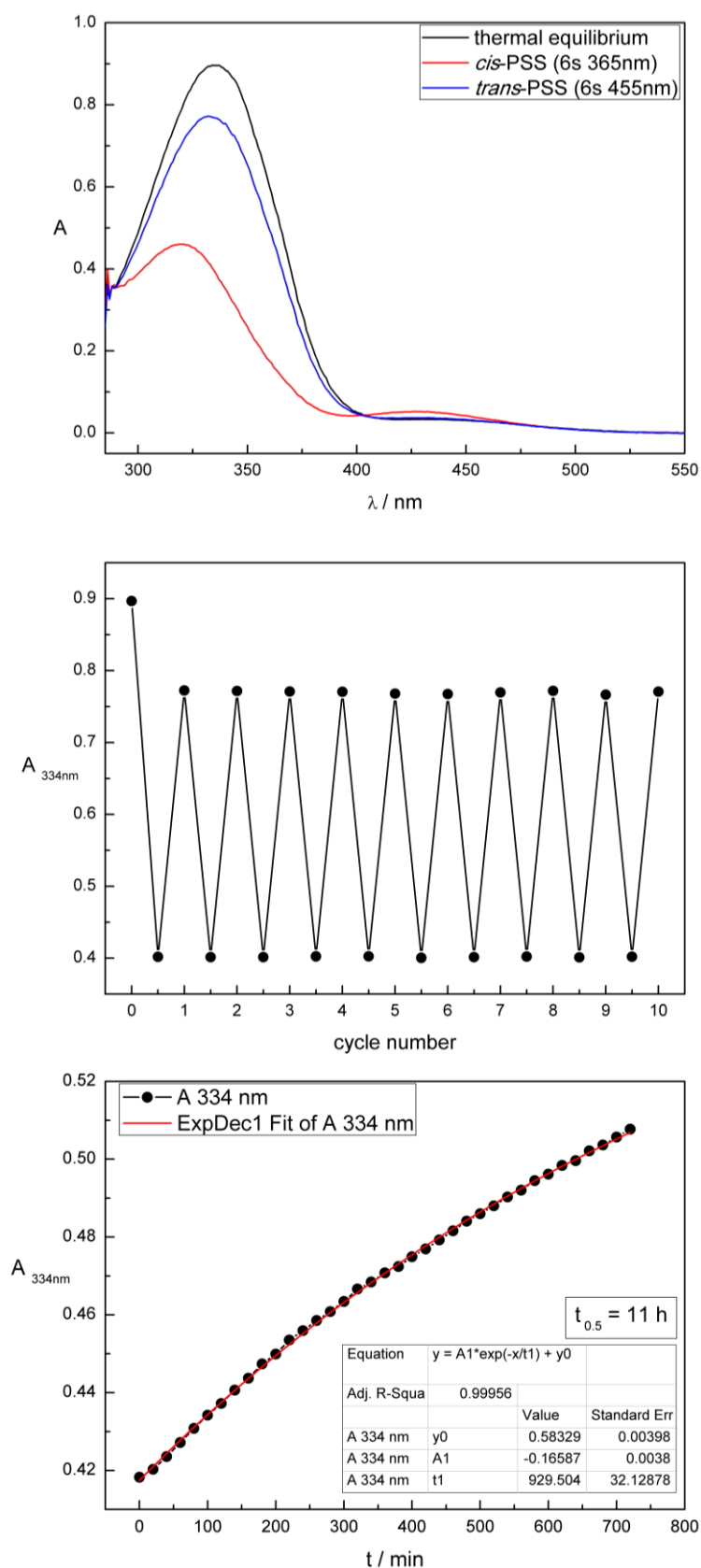


Figure S11. Compound **4k** measured 50 μM in toluene. Upper panel: UV-Vis absorption spectra. Middle panel: Cycle performance upon alternate irradiation. Lower panel: Thermal half-life.

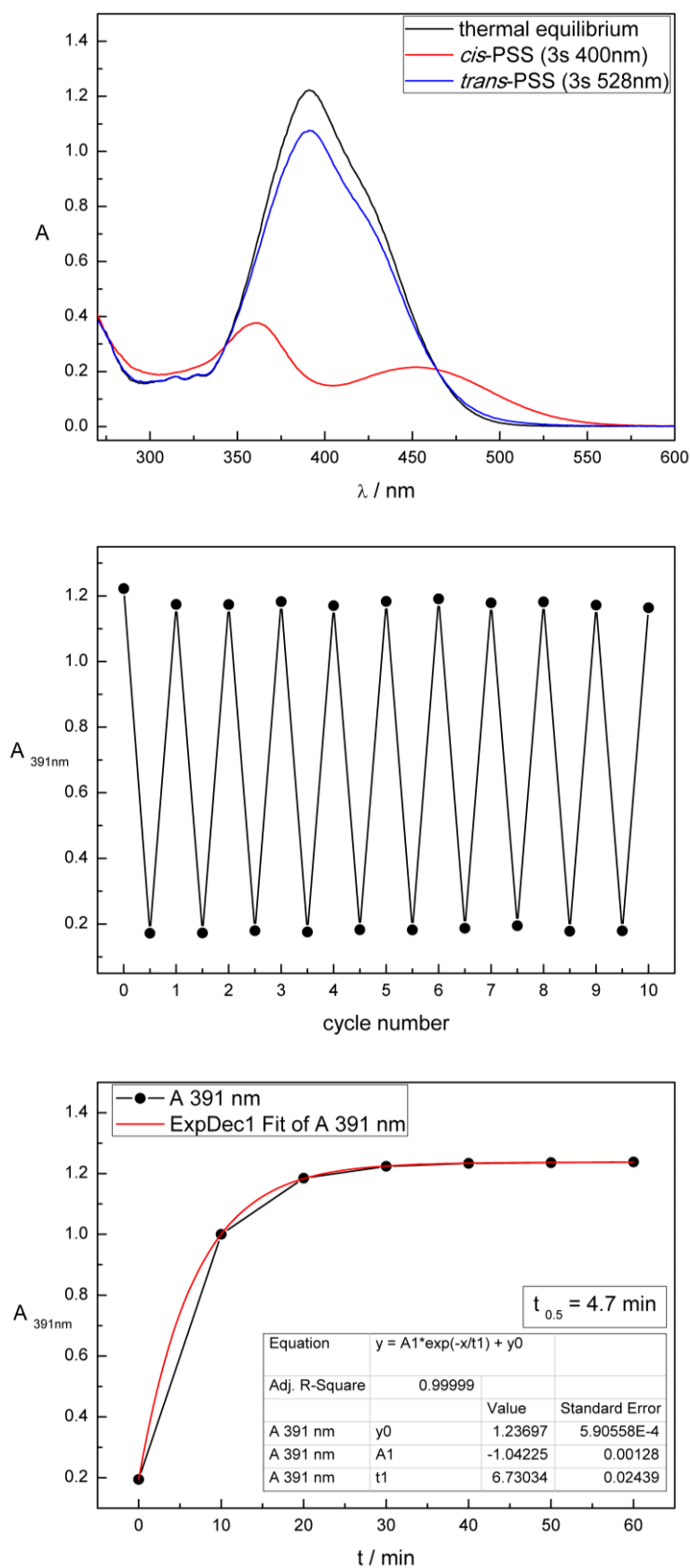


Figure S12. Compound **4a** measured 50 μ M in DMSO. Upper panel: UV-Vis absorption spectra. Middle panel: Cycle performance upon alternate irradiation. Lower panel: Thermal half-life.

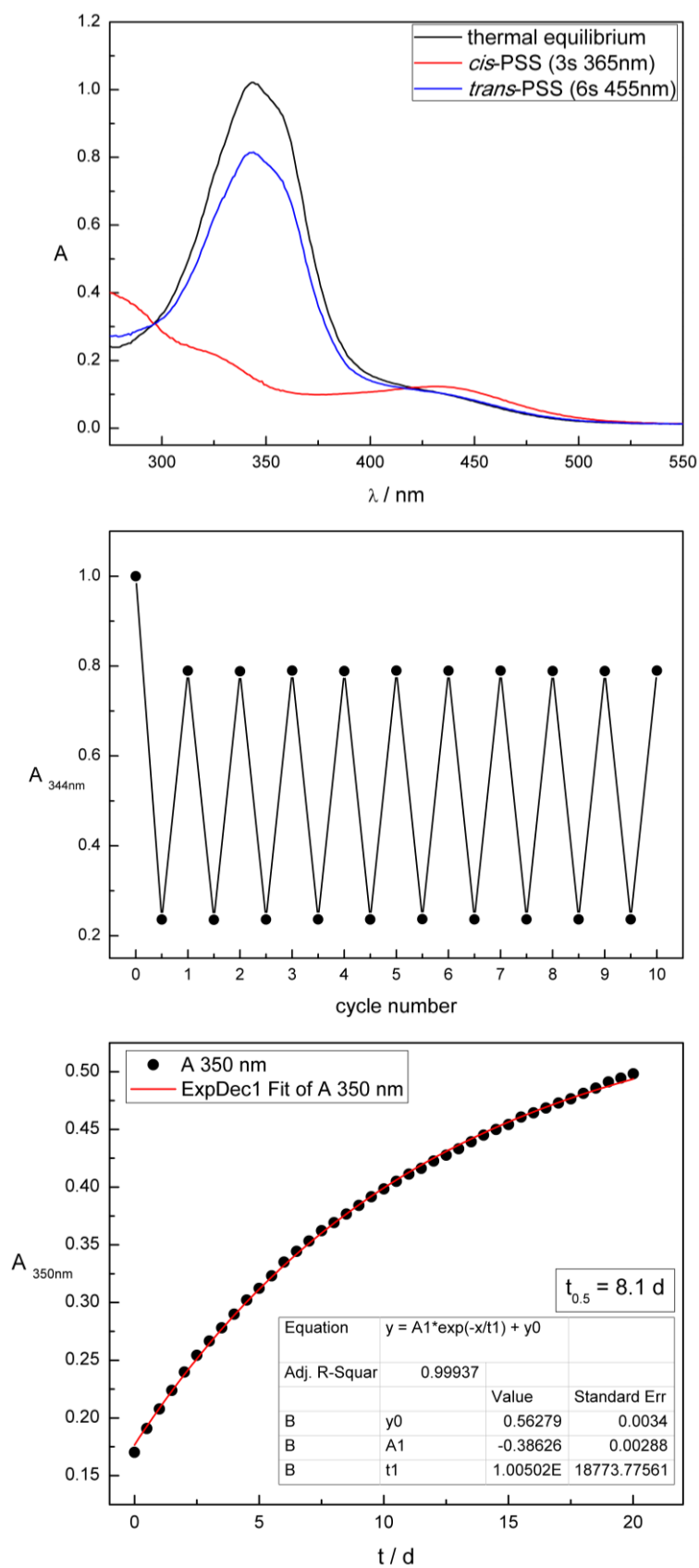


Figure S13. Compound **4b** measured 50 μM in DMSO. Upper panel: UV-Vis absorption spectra. Middle panel: Cycle performance upon alternate irradiation. Lower panel: Thermal half-life.

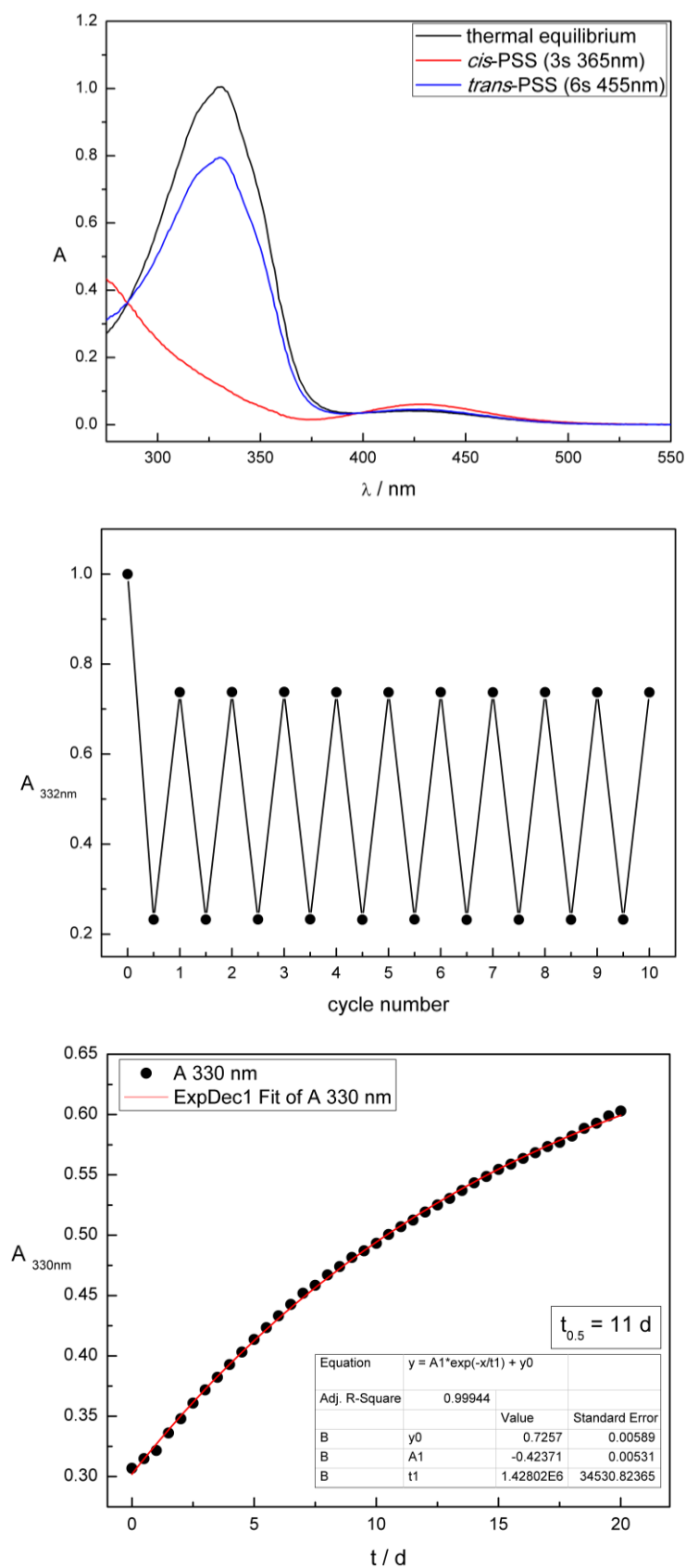


Figure S14. Compound **4c** measured 50 μM in DMSO. Upper panel: UV-Vis absorption spectra. Middle panel: Cycle performance upon alternate irradiation. Lower panel: Thermal half-life.

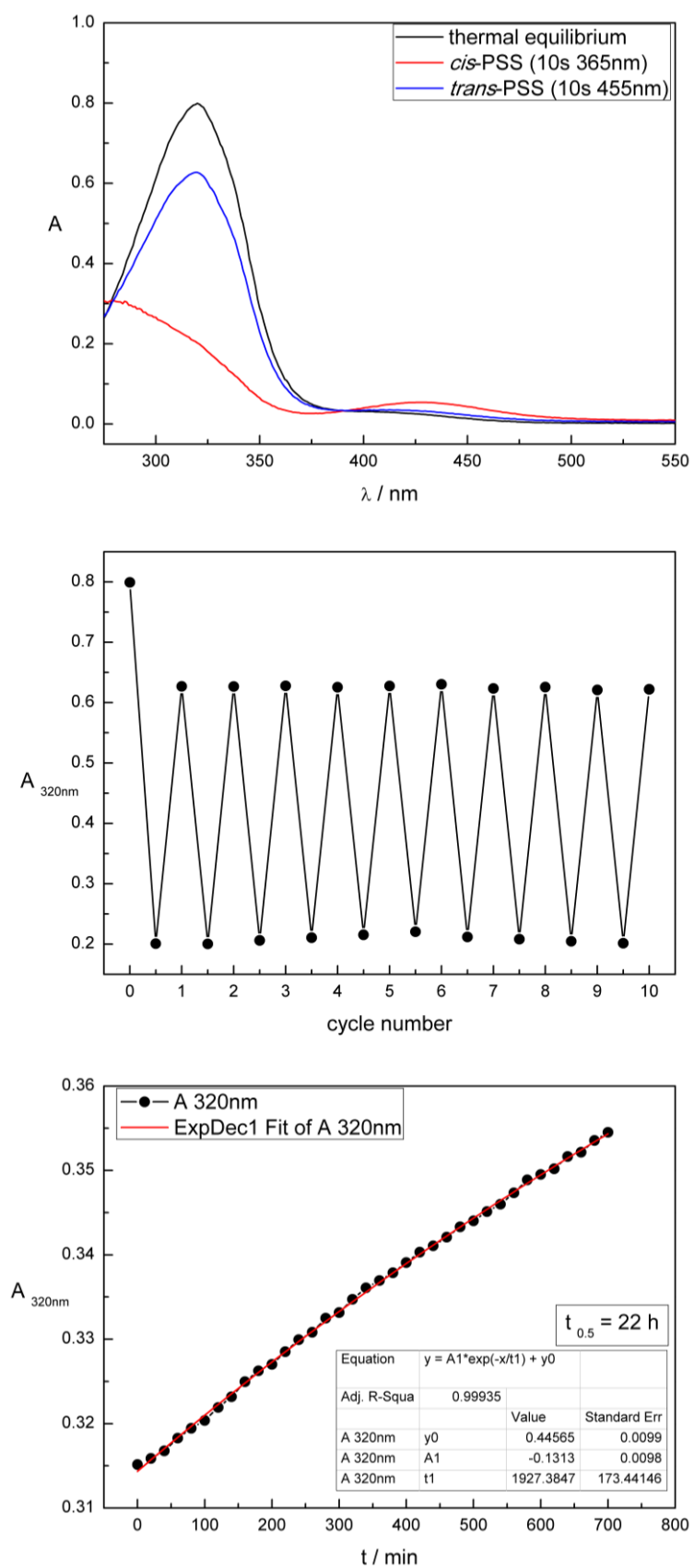


Figure S15. Compound **4d** measured 50 μM in DMSO. Upper panel: UV-Vis absorption spectra. Middle panel: Cycle performance upon alternate irradiation. Lower panel: Thermal half-life.

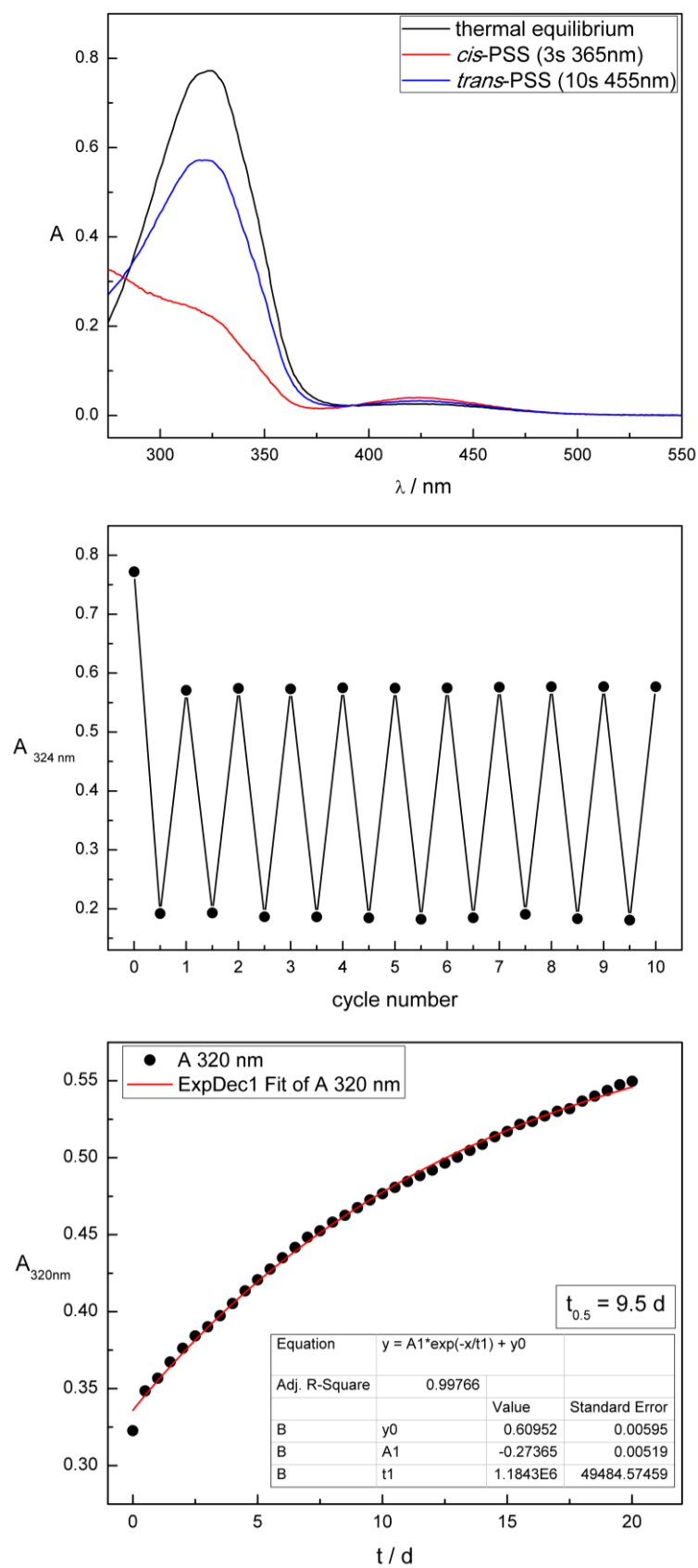


Figure S16. Compound **4e** measured 50 μM in DMSO. Upper panel: UV-Vis absorption spectra. Middle panel: Cycle performance upon alternate irradiation. Lower panel: Thermal half-life.

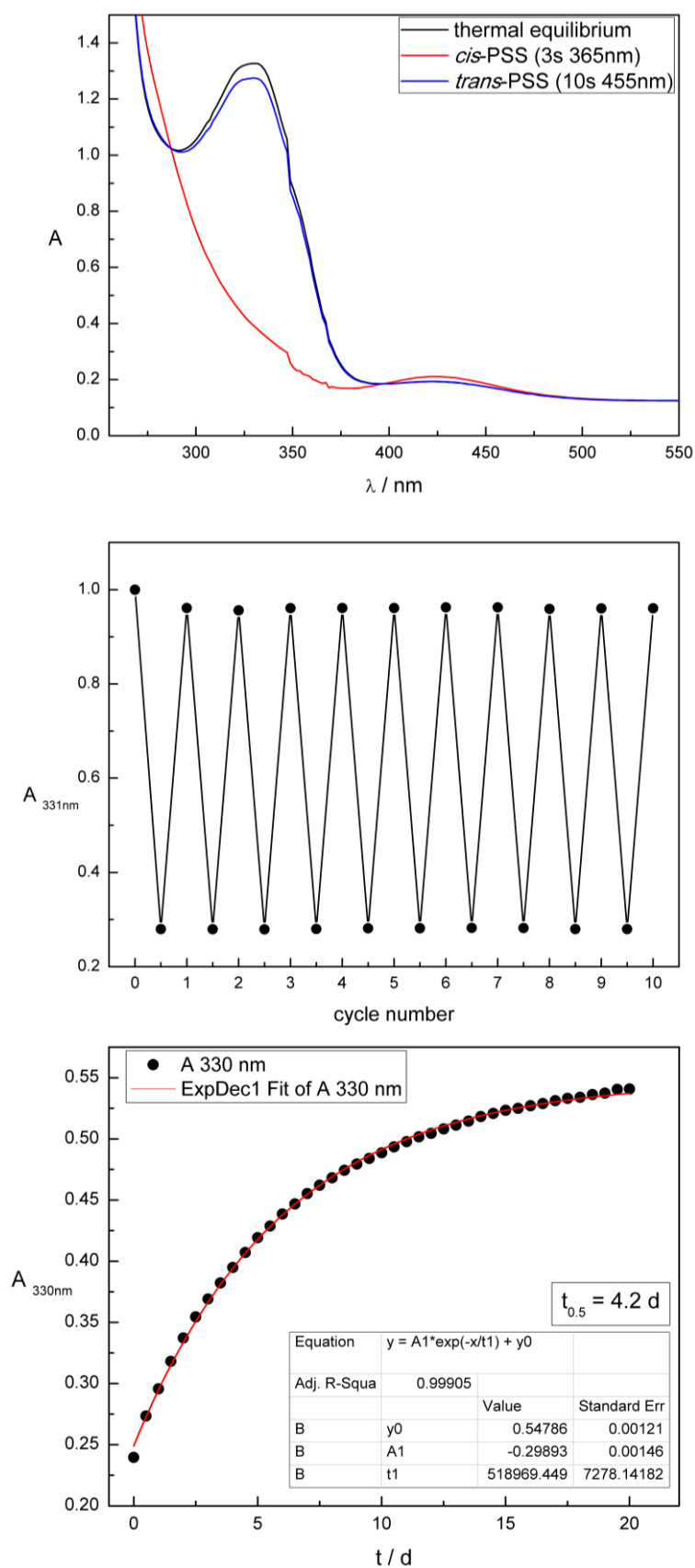


Figure S17. Compound **4f** measured 50 μM in DMSO. Upper panel: UV-Vis absorption spectra. Middle panel: Cycle performance upon alternate irradiation. Lower panel: Thermal half-life.

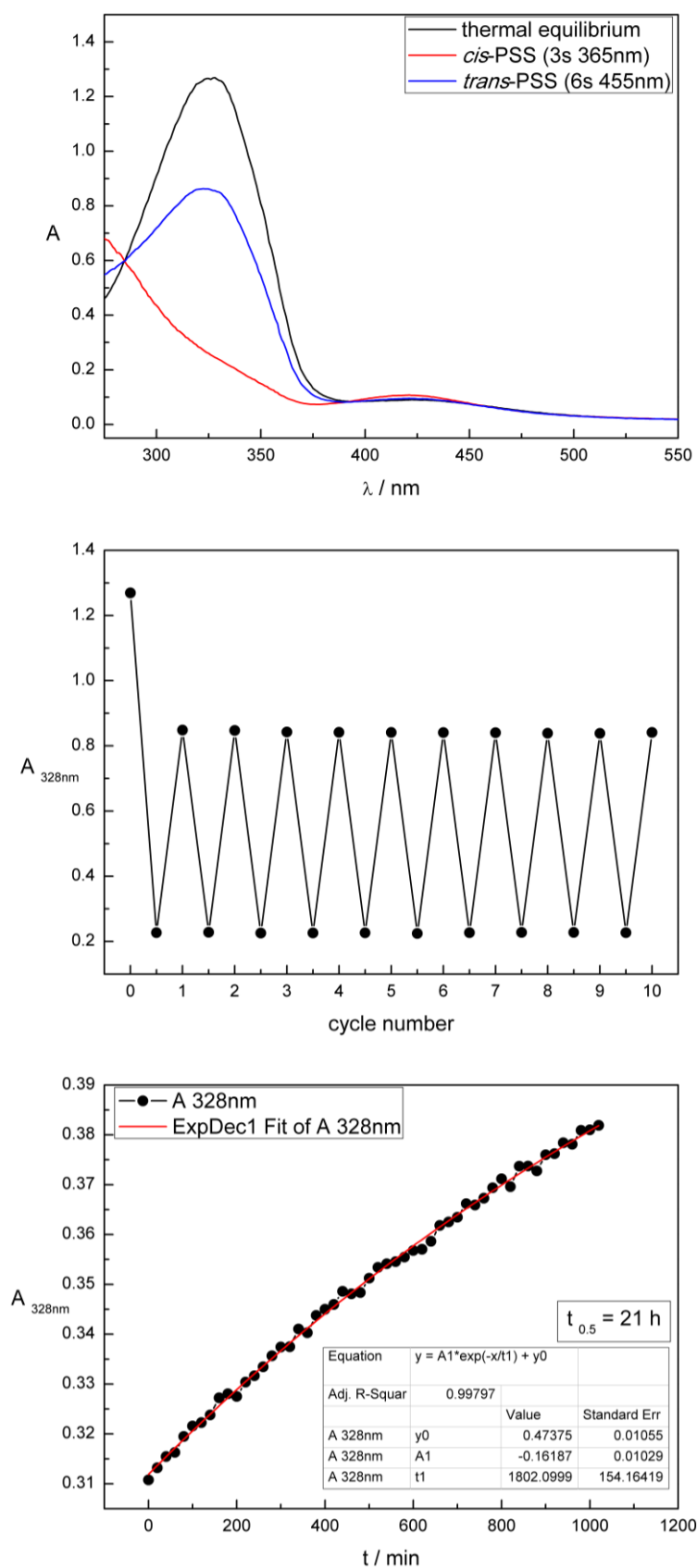


Figure S18. Compound **4g** measured 50 μM in DMSO. Upper panel: UV-Vis absorption spectra. Middle panel: Cycle performance upon alternate irradiation. Lower panel: Thermal half-life.

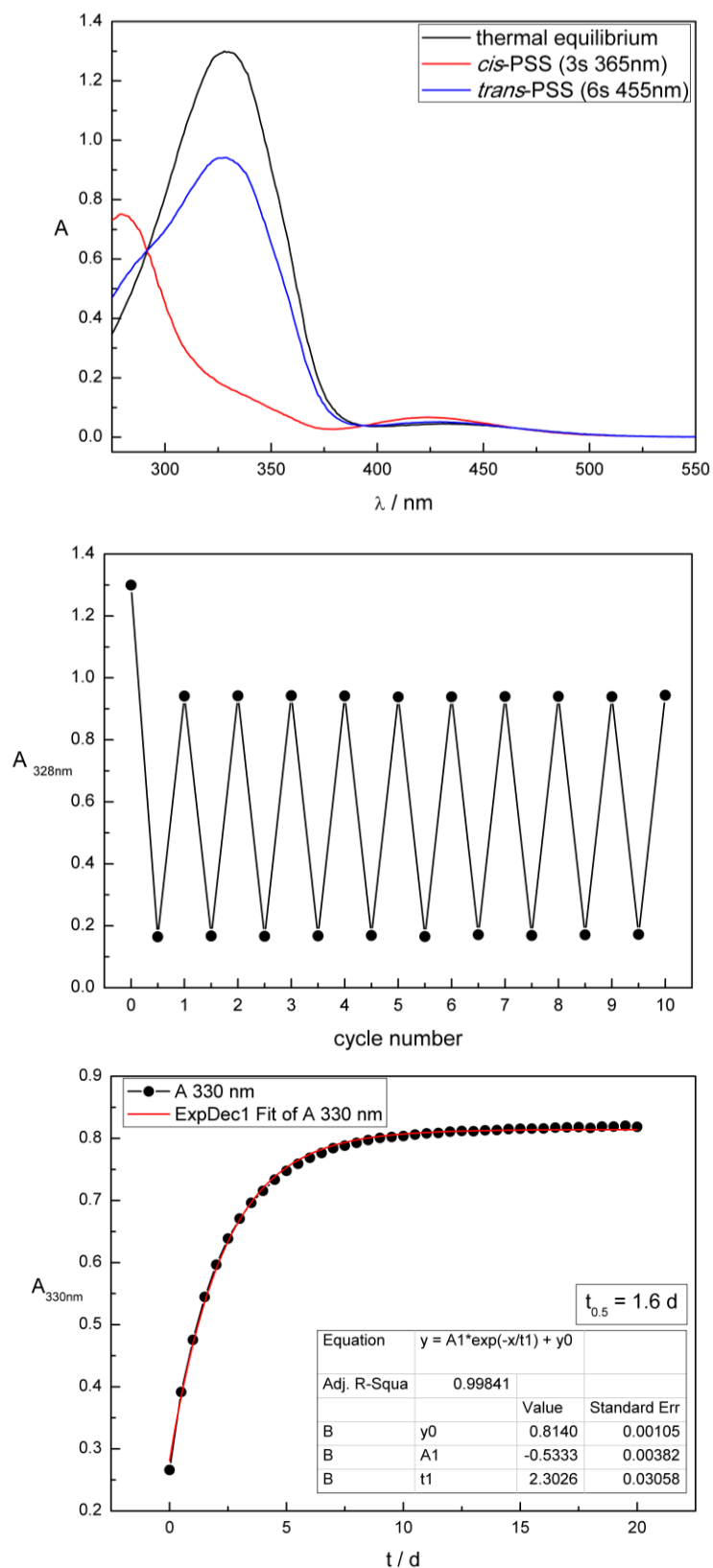


Figure S19. Compound **4h** measured 50 μM in DMSO. Upper panel: UV-Vis absorption spectra. Middle panel: Cycle performance upon alternate irradiation. Lower panel: Thermal half-life.

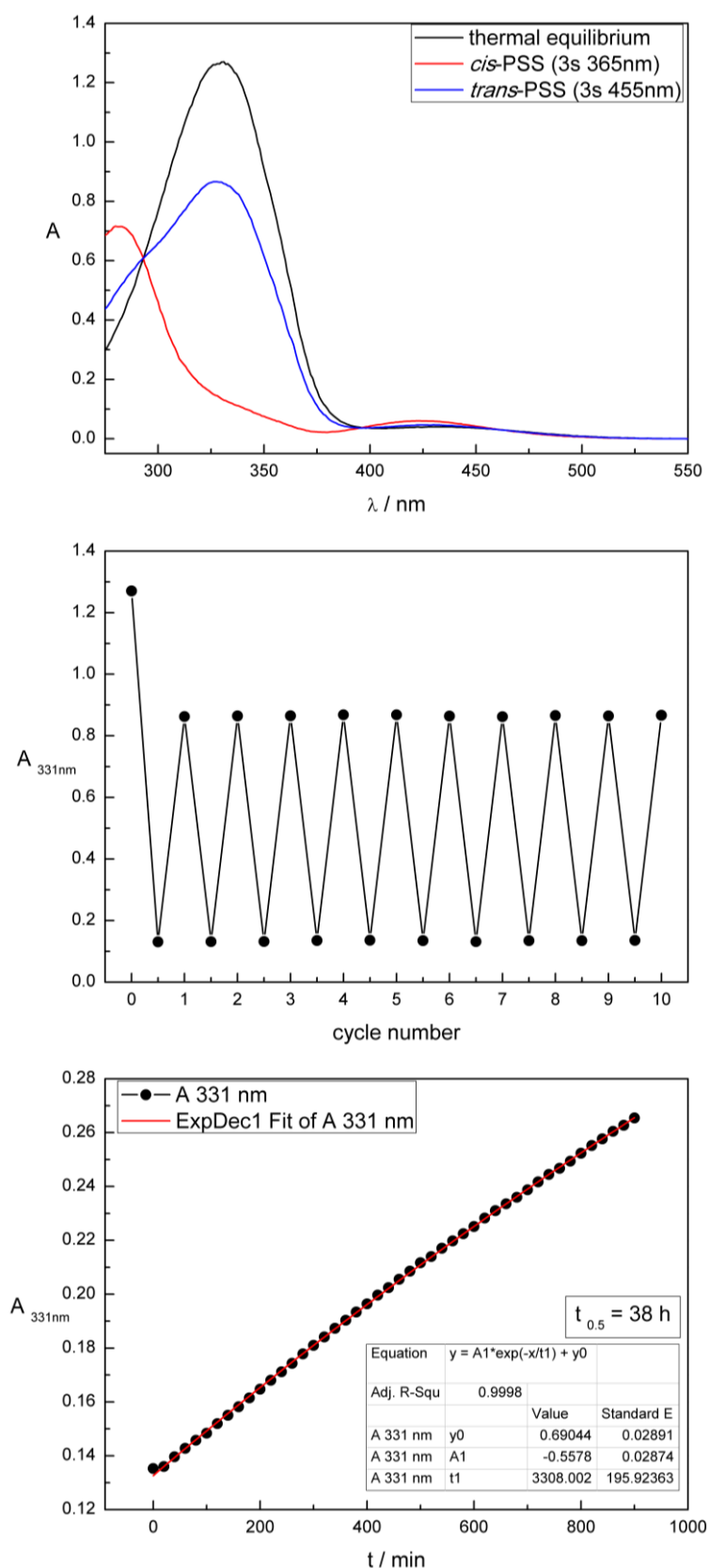


Figure S20. Compound **4i** measured 50 μM in DMSO. Upper panel: UV-Vis absorption spectra. Middle panel: Cycle performance upon alternate irradiation. Lower panel: Thermal half-life.

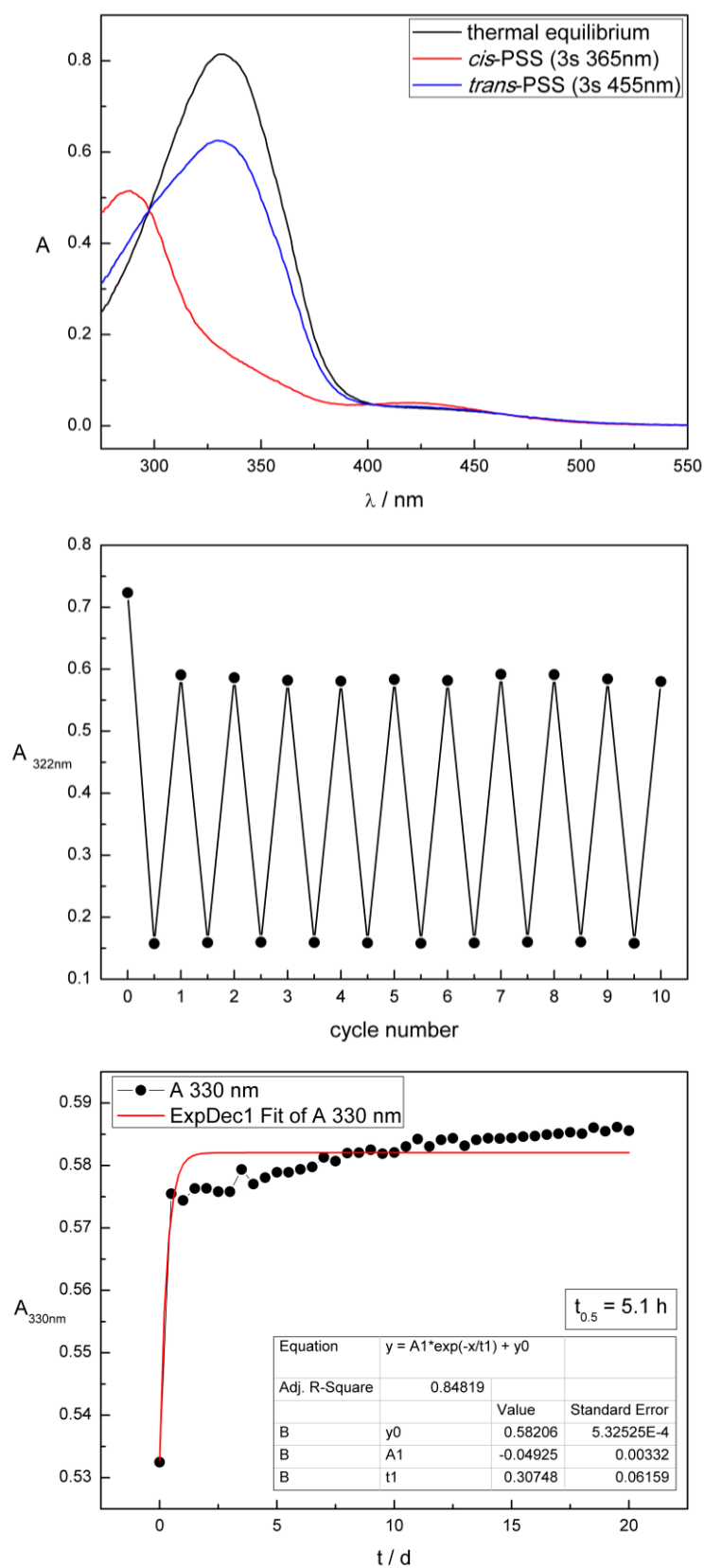


Figure S21. Compound **4j** measured 50 μM in DMSO. Upper panel: UV-Vis absorption spectra. Middle panel: Cycle performance upon alternate irradiation. Lower panel: Thermal half-life.

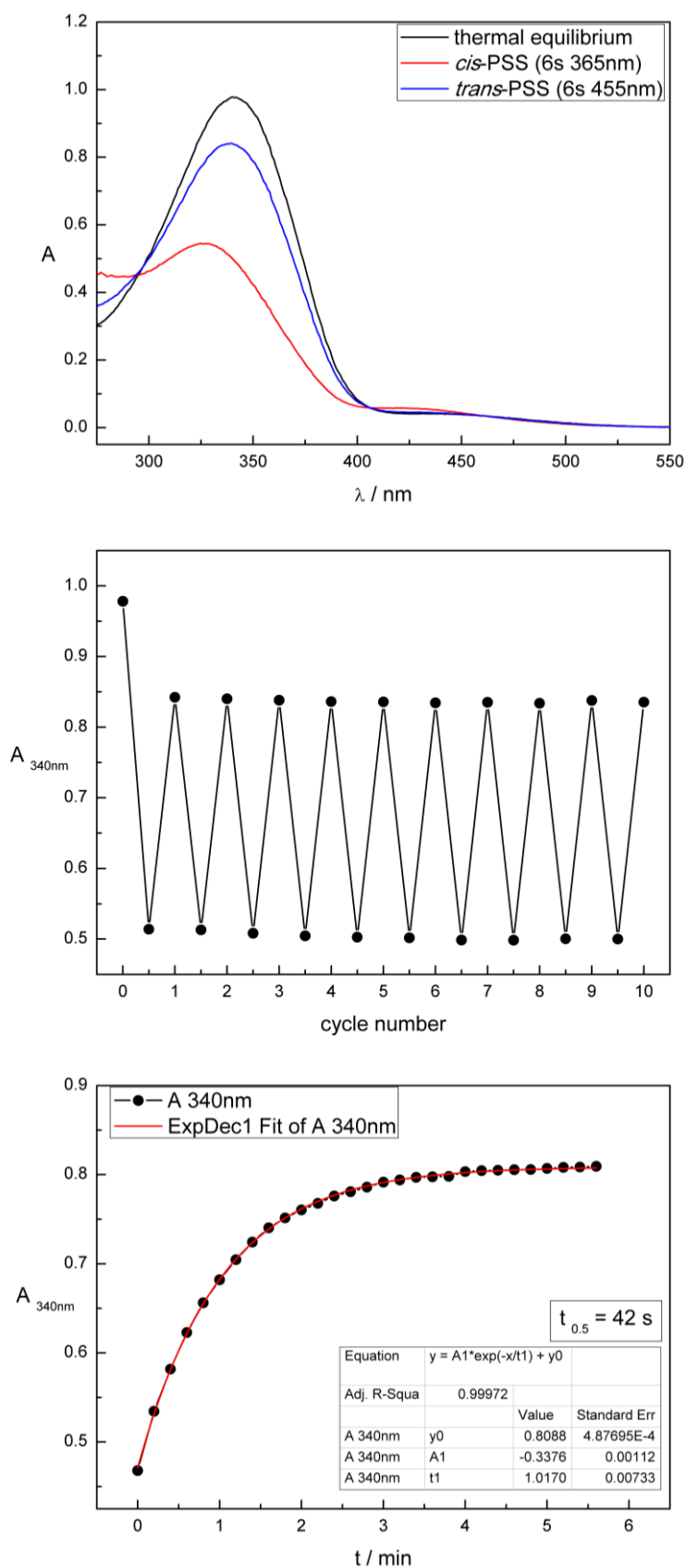


Figure S22. Compound **4k** measured 50 μ M in DMSO. Upper panel: UV-Vis absorption spectra. Middle panel: Cycle performance upon alternate irradiation. Lower panel: Thermal half-life.

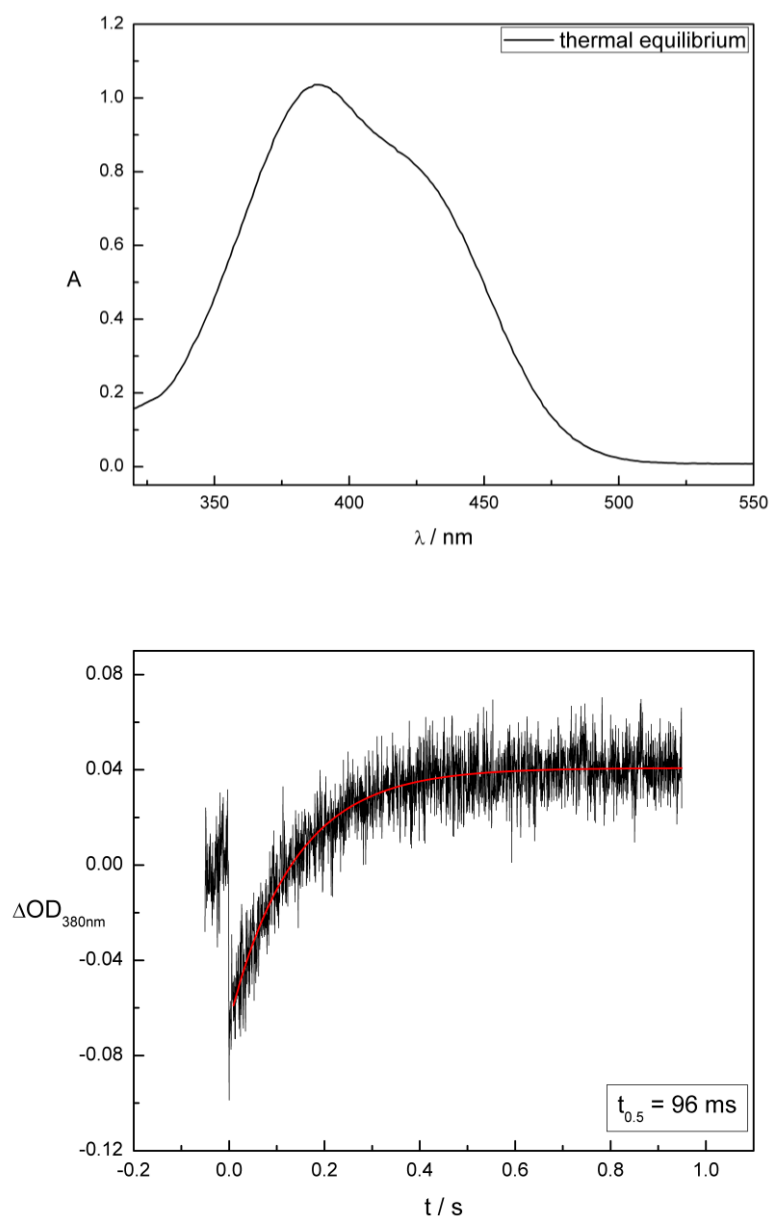


Figure S23. Compound **4a** measured 50 μM in DMSO:water 1:1. Upper panel: UV-Vis absorption spectrum. Lower panel: Thermal half-life.

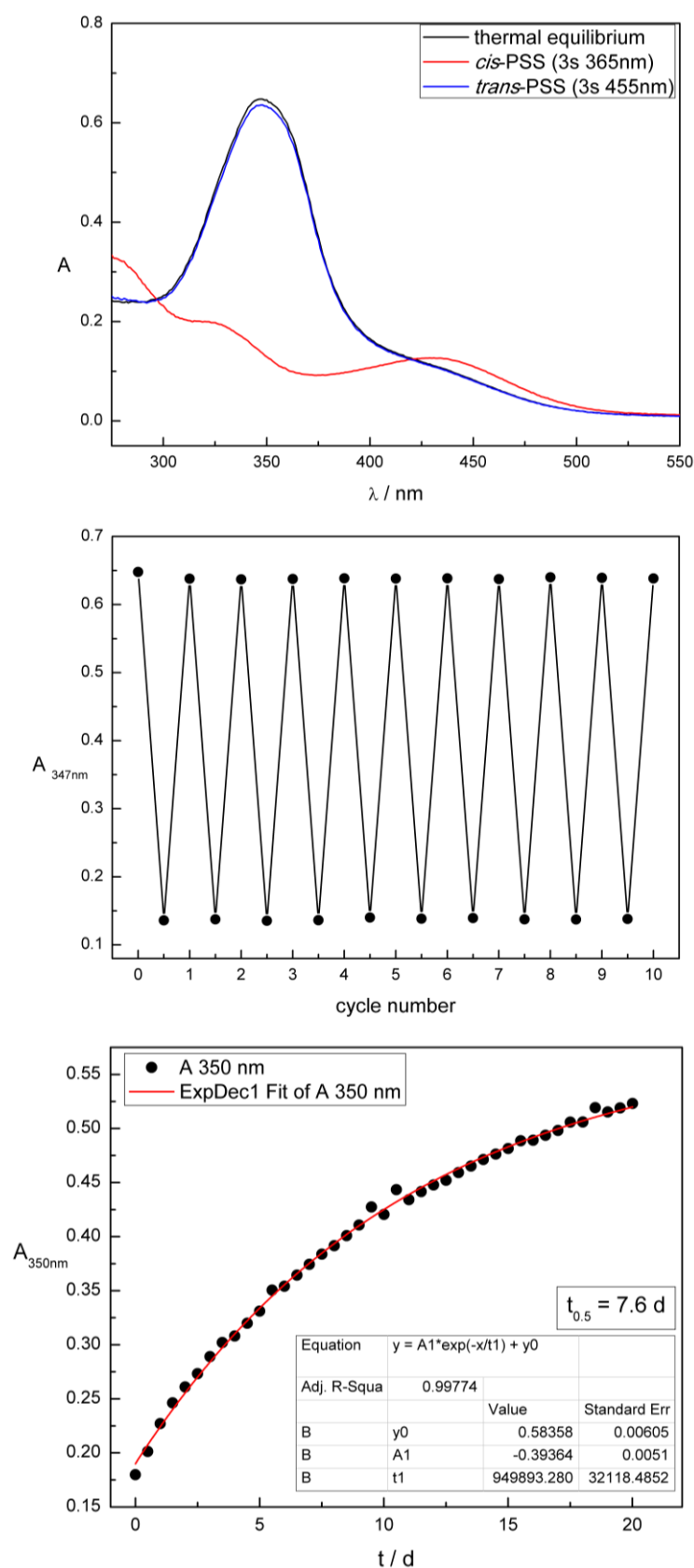


Figure S24. Compound **4b** measured 50 μM in DMSO:water 1:1. Upper panel: UV-Vis absorption spectra. Middle panel: Cycle performance upon alternate irradiation. Lower panel: Thermal half-life.

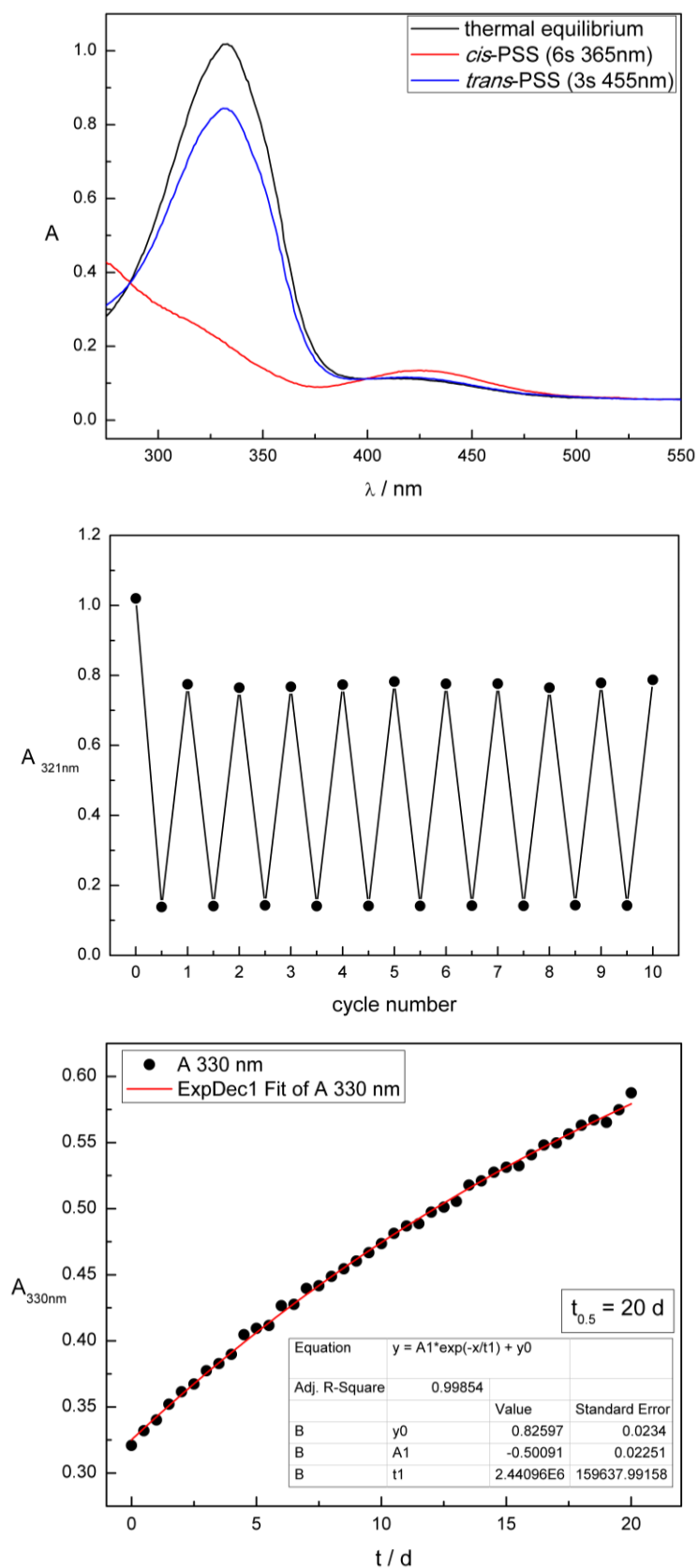


Figure S25. Compound **4c** measured 50 μM in DMSO:water 1:1. Upper panel: UV-Vis absorption spectra. Middle panel: Cycle performance upon alternate irradiation. Lower panel: Thermal half-life.

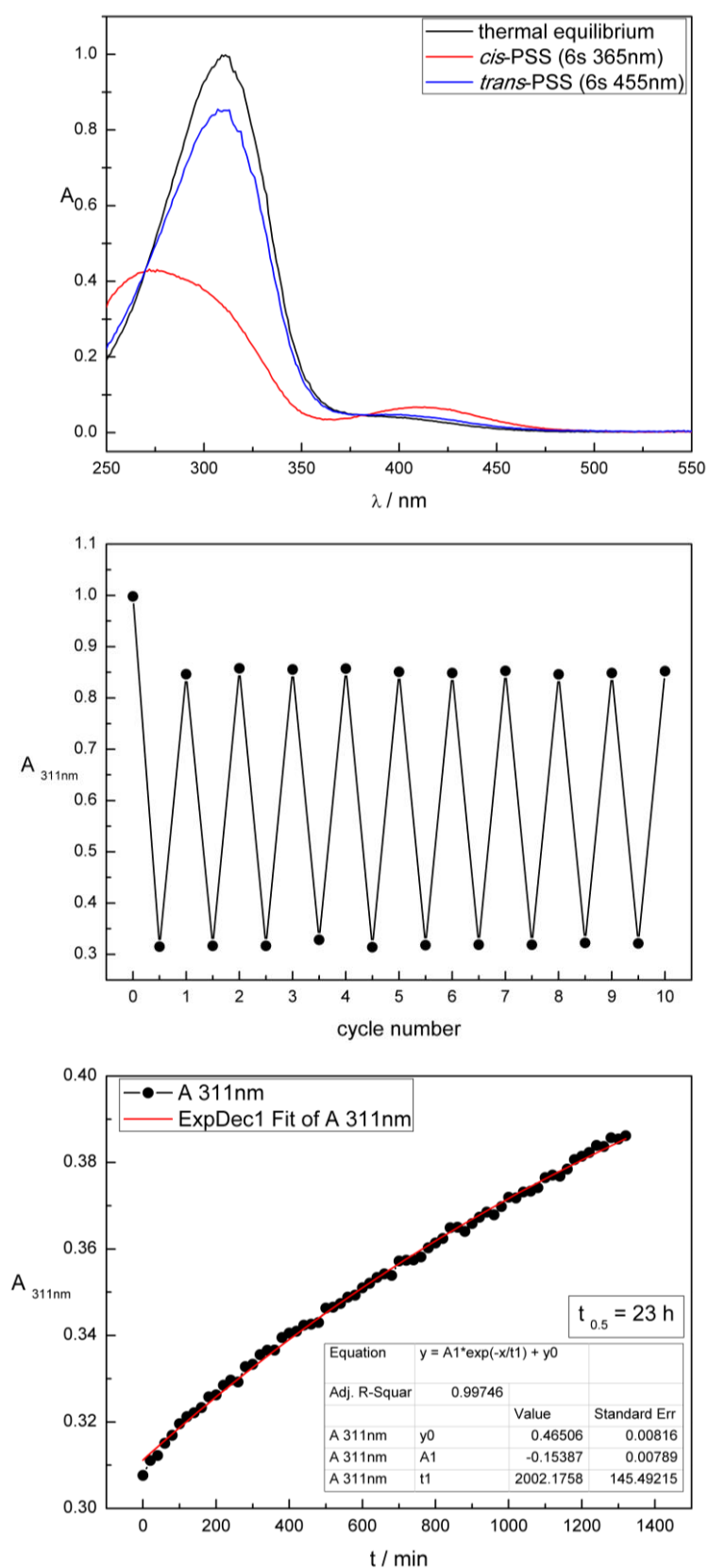


Figure S26. Compound **4d** measured 50 μM in DMSO:water 1:1. Upper panel: UV-Vis absorption spectra. Middle panel: Cycle performance upon alternate irradiation. Lower panel: Thermal half-life.

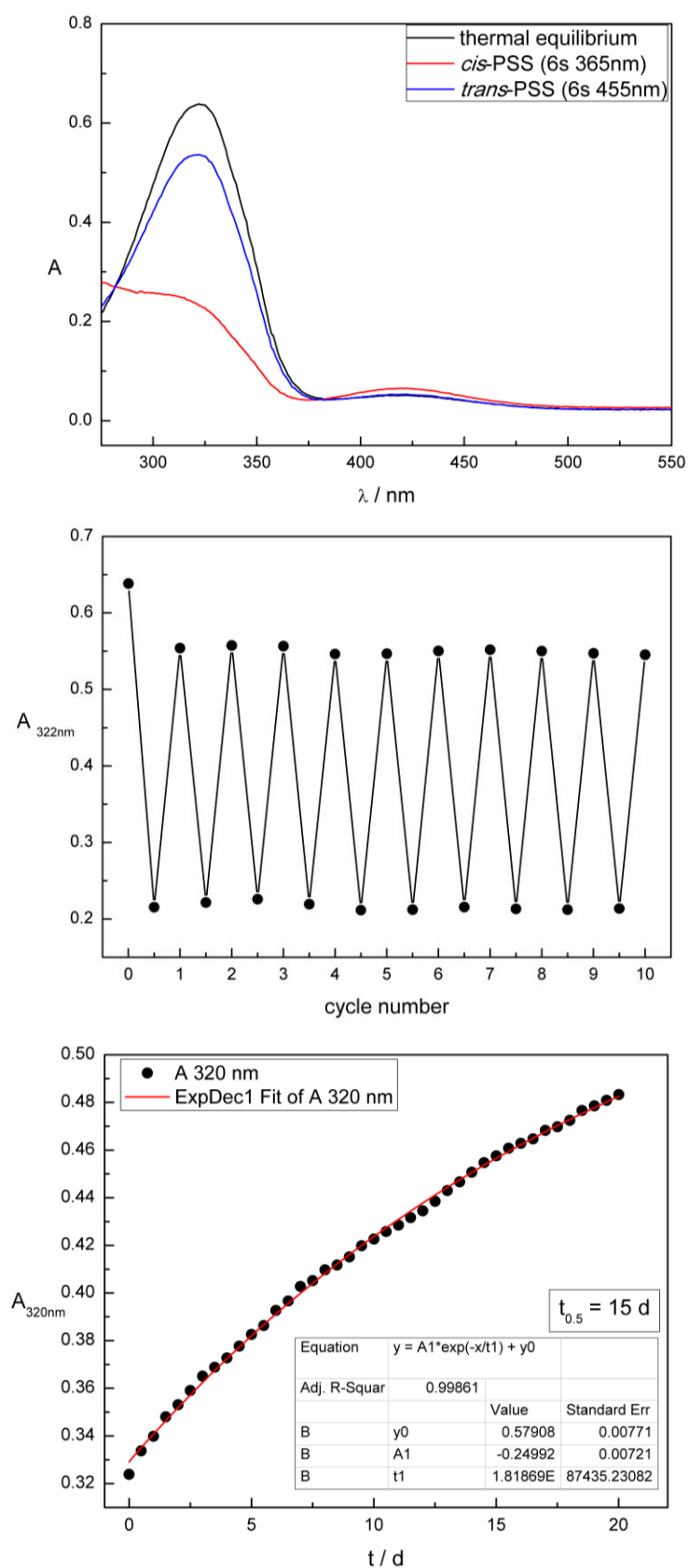


Figure S27. Compound **4e** measured 50 μM in DMSO:water 1:1. Upper panel: UV-Vis absorption spectra. Middle panel: Cycle performance upon alternate irradiation. Lower panel: Thermal half-life.

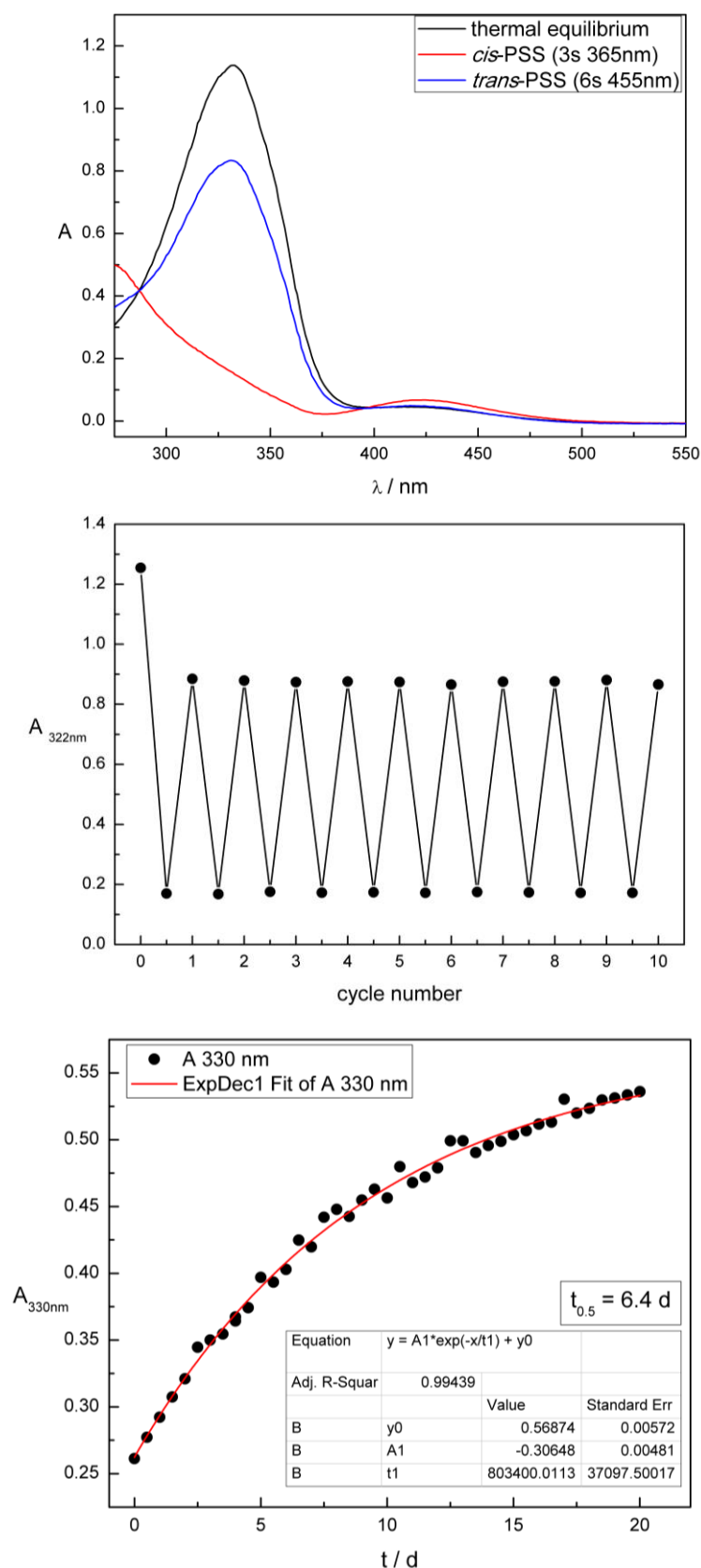


Figure S28. Compound **4f** measured 50 μM in DMSO:water 1:1. Upper panel: UV-Vis absorption spectra. Middle panel: Cycle performance upon alternate irradiation. Lower panel: Thermal half-life.

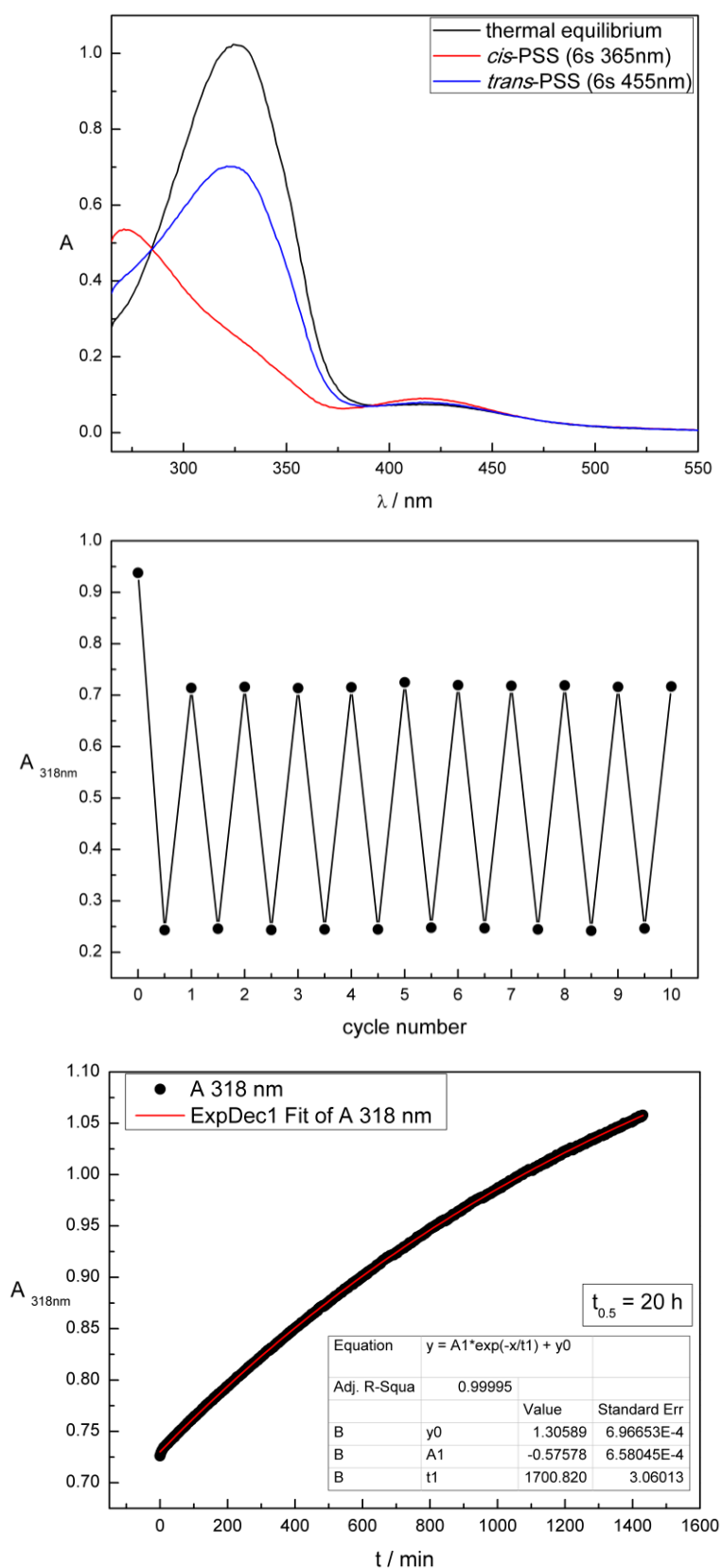


Figure S29. Compound **4g** measured 50 μM in DMSO:water 1:1. Upper panel: UV-Vis absorption spectra. Middle panel: Cycle performance upon alternate irradiation. Lower panel: Thermal half-life.

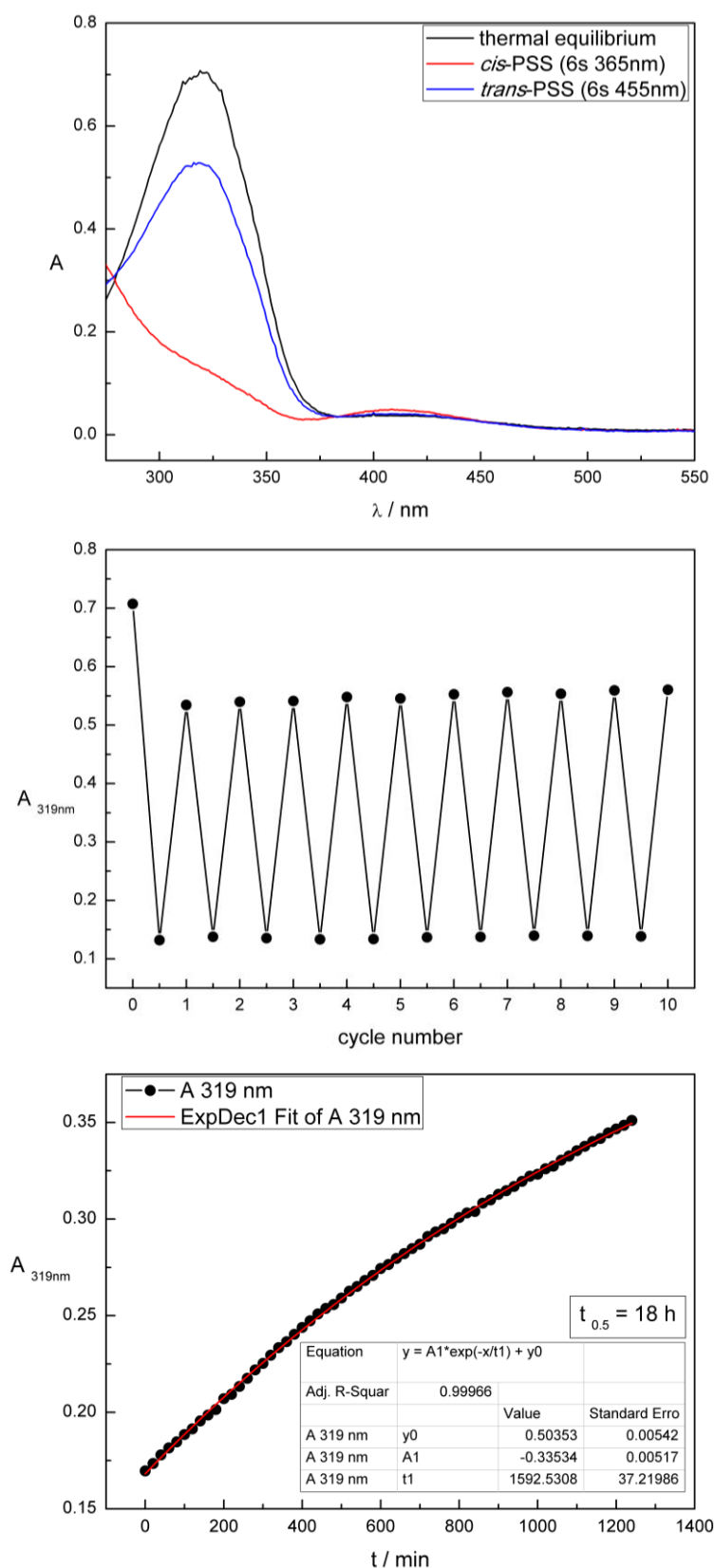


Figure S30. Compound **4h** measured 50 μM in DMSO:water 1:1. Upper panel: UV-Vis absorption spectra. Middle panel: Cycle performance upon alternate irradiation. Lower panel: Thermal half-life.

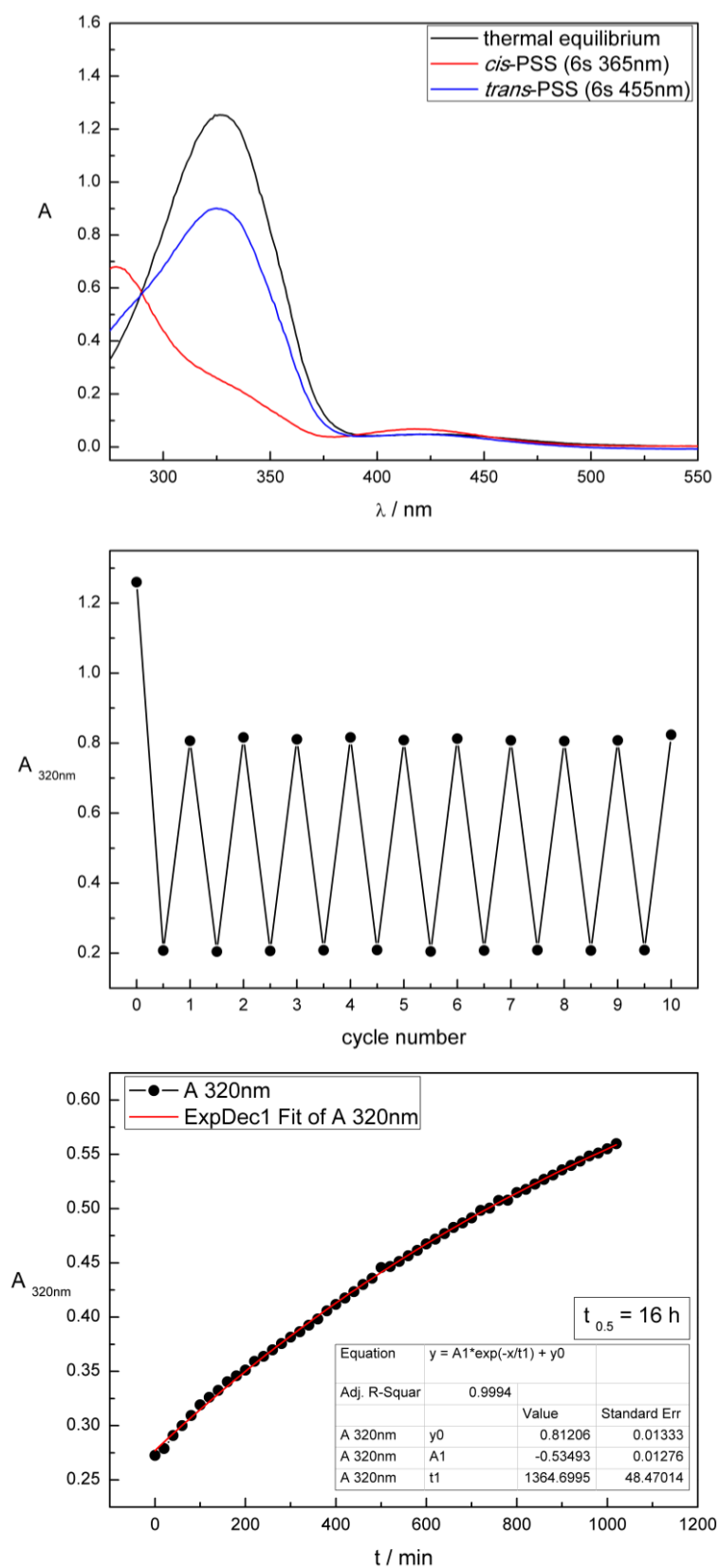


Figure S31. Compound **4i** measured 50 μM in DMSO:water 1:1. Upper panel: UV-Vis absorption spectra. Middle panel: Cycle performance upon alternate irradiation. Lower panel: Thermal half-life.

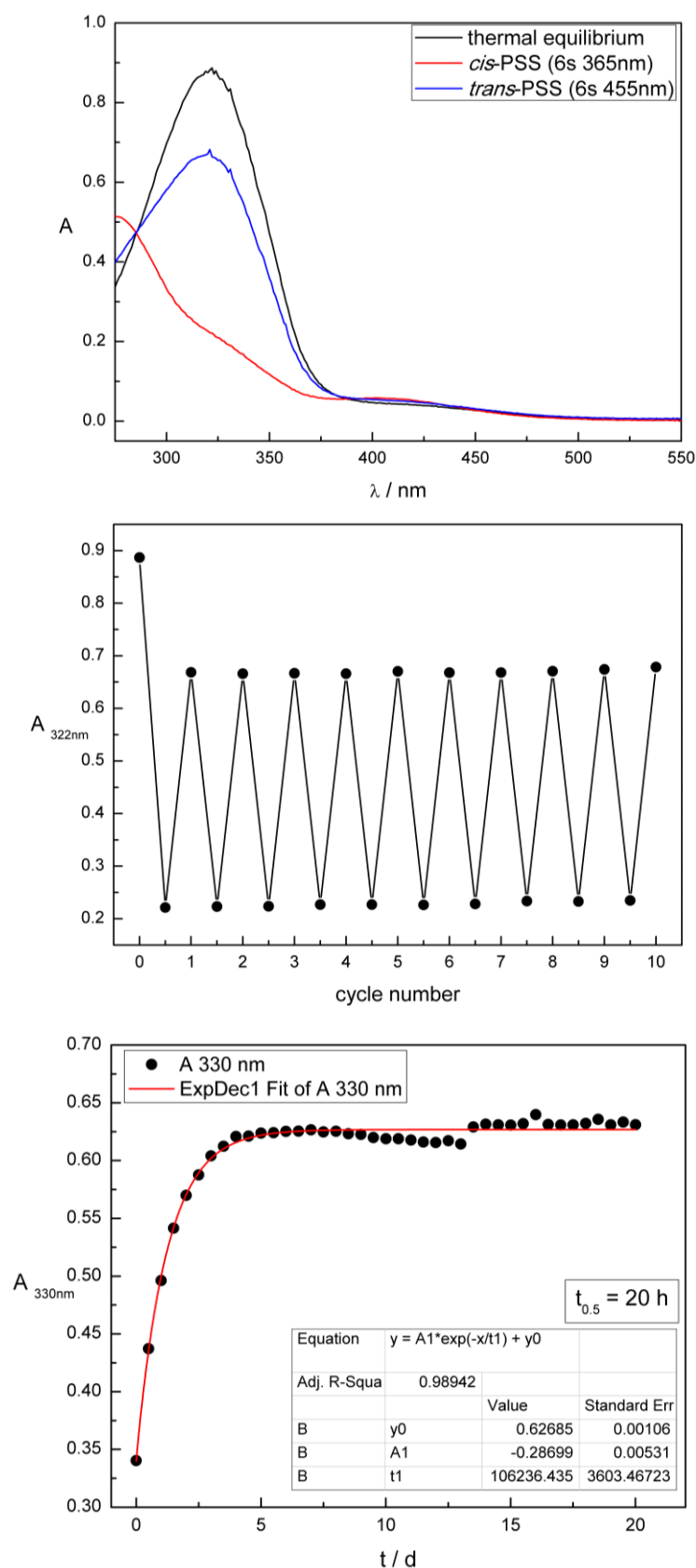


Figure S32. Compound **4j** measured 50 μM in DMSO:water 1:1. Upper panel: UV-Vis absorption spectra. Middle panel: Cycle performance upon alternate irradiation. Lower panel: Thermal half-life.

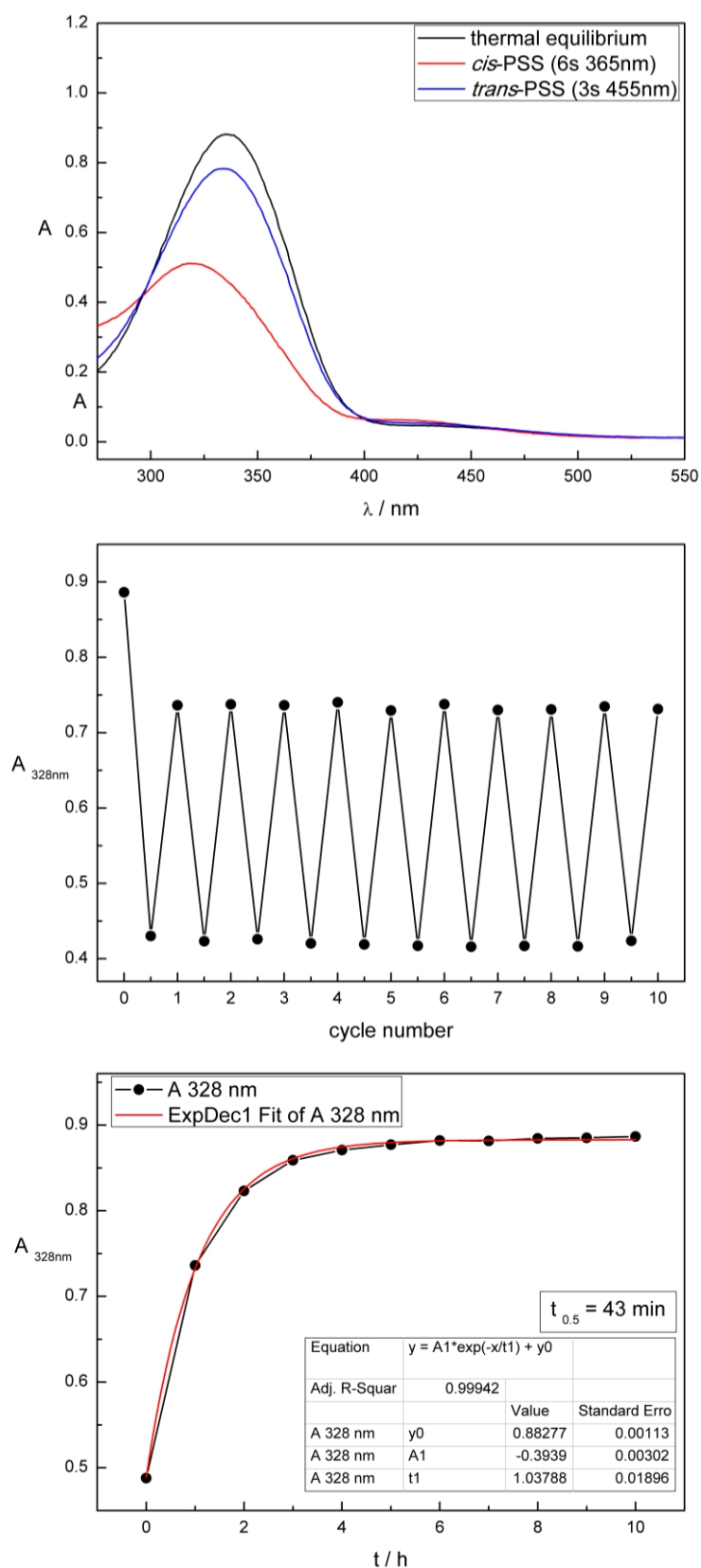


Figure S33. Compound **4k** measured 50 μM in DMSO:water 1:1. Upper panel: UV-Vis absorption spectra. Middle panel: Cycle performance upon alternate irradiation. Lower panel: Thermal half-life.

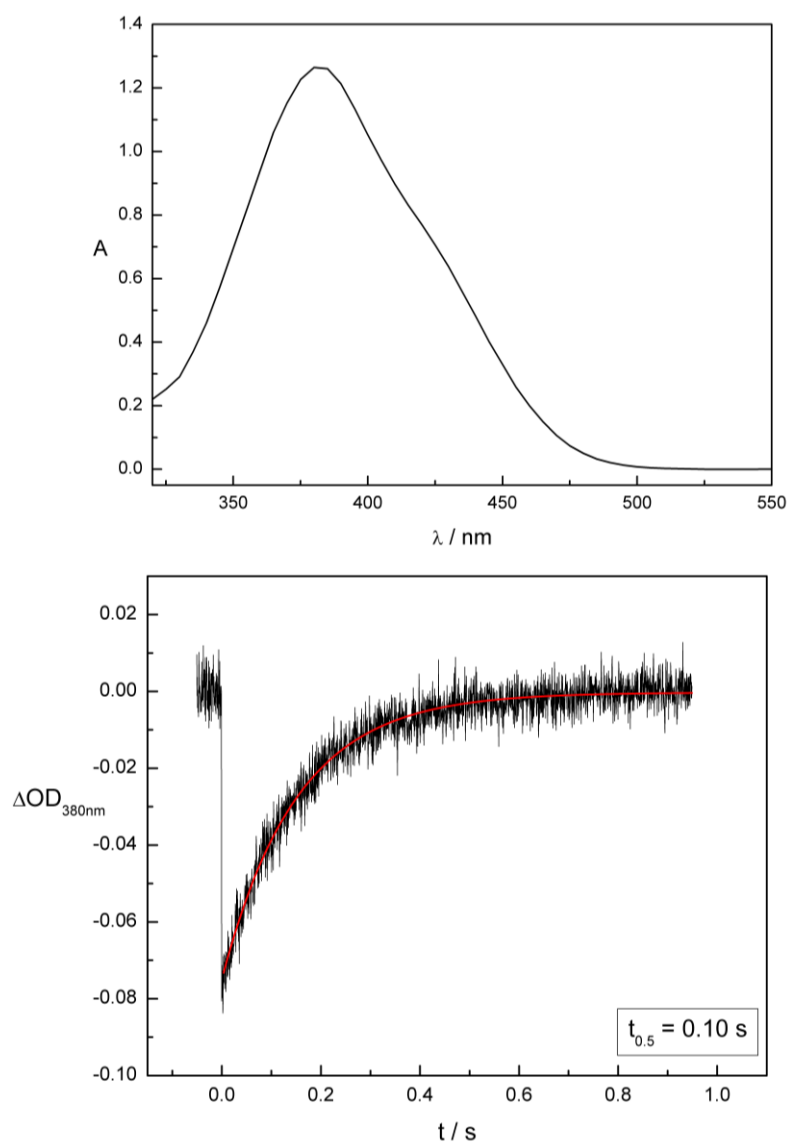


Figure S34. Compound **4a** measured 50 μM in methanol. Upper panel: UV-Vis absorption spectrum. Lower panel: Thermal half-life.

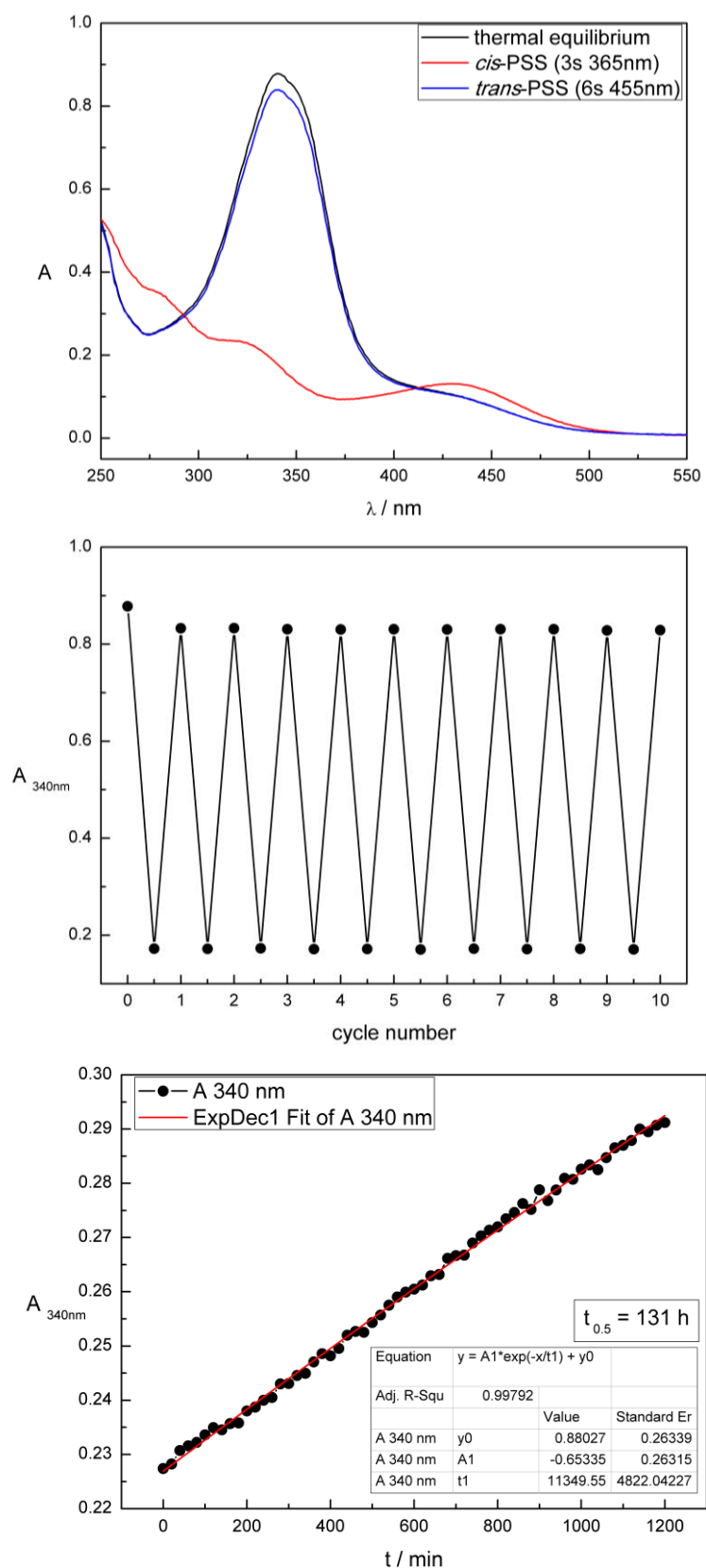


Figure S35. Compound **4b** measured 50 μM in methanol. Upper panel: UV-Vis absorption spectra. Middle panel: Cycle performance upon alternate irradiation. Lower panel: Thermal half-life.

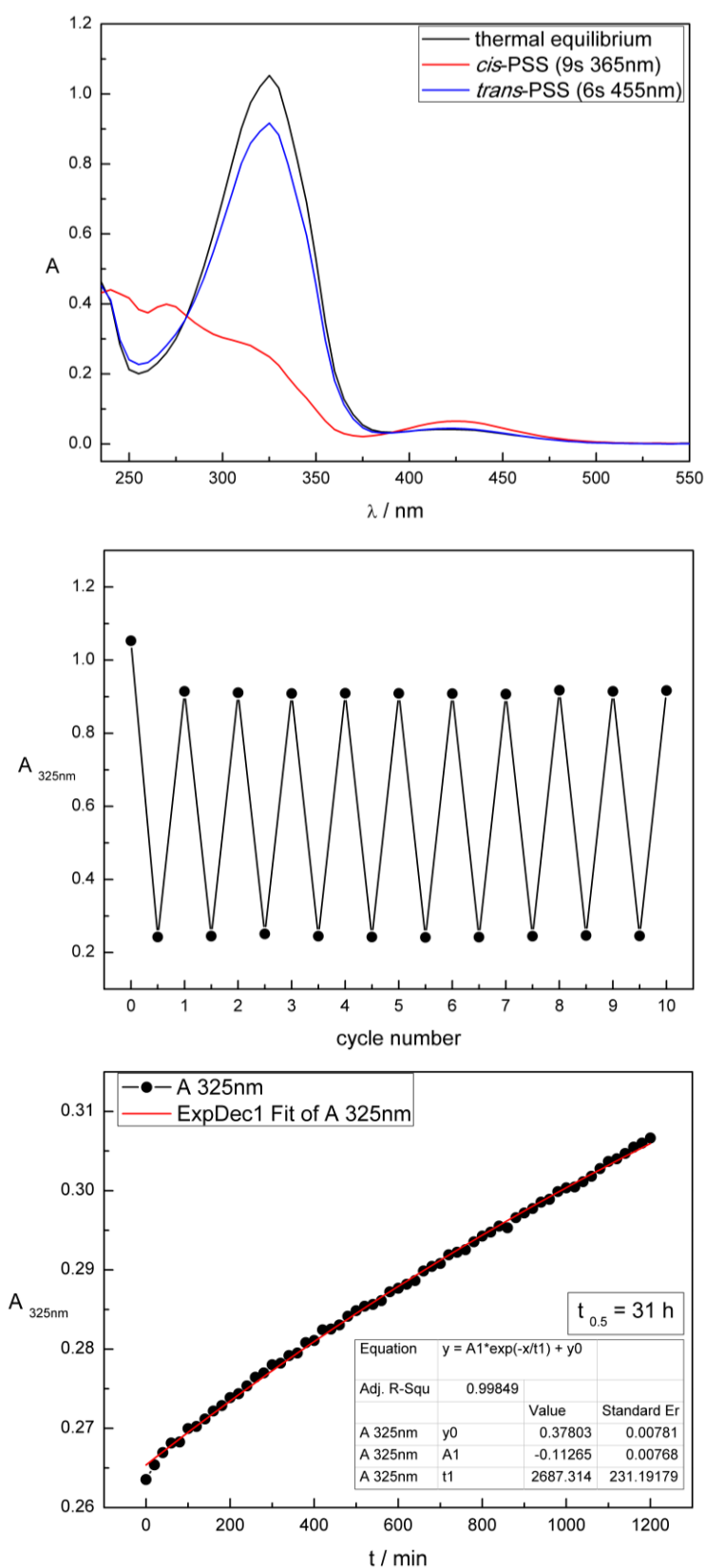


Figure S36. Compound **4c** measured 50 μM in methanol. Upper panel: UV-Vis absorption spectra. Middle panel: Cycle performance upon alternate irradiation. Lower panel: Thermal half-life.

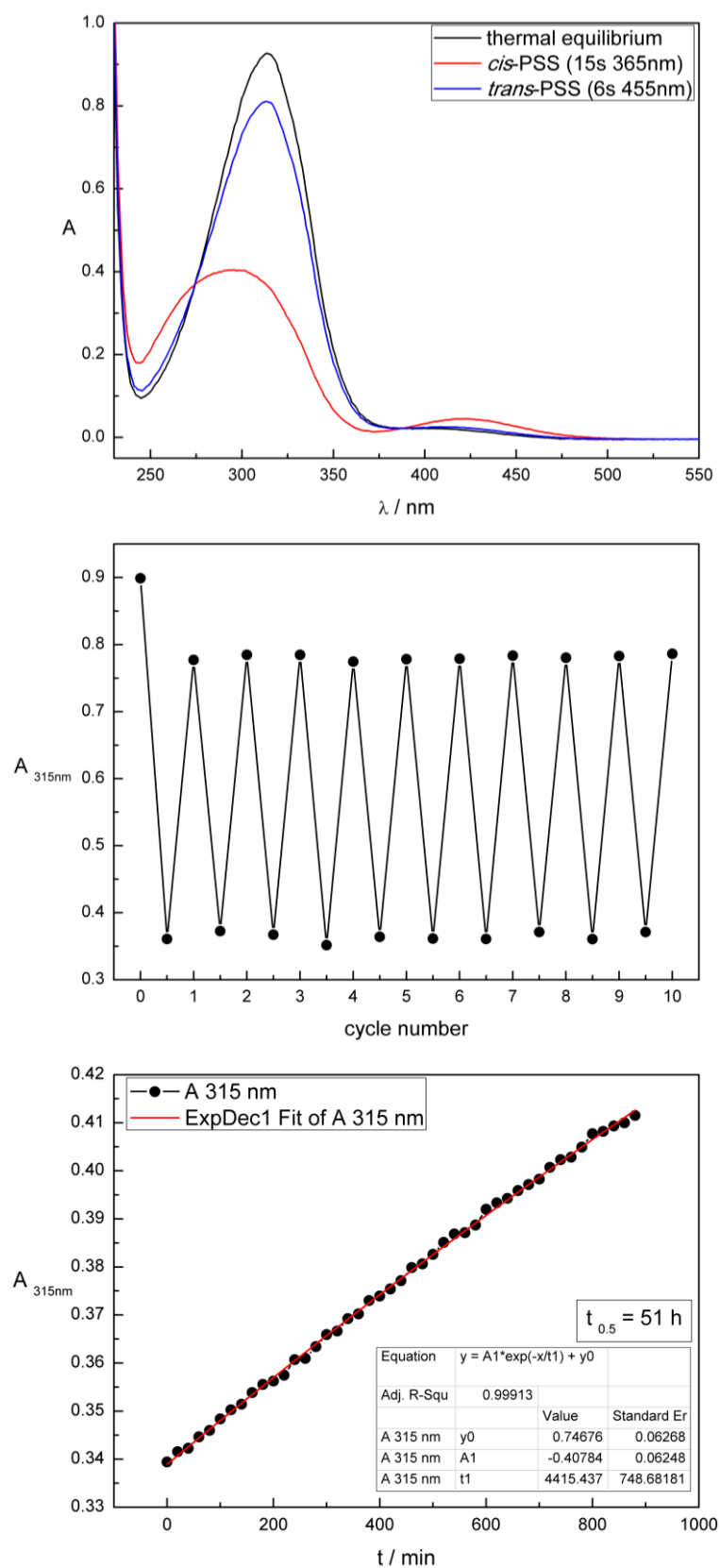


Figure S37. Compound **4d** measured 50 μM in methanol. Upper panel: UV-Vis absorption spectra. Middle panel: Cycle performance upon alternate irradiation. Lower panel: Thermal half-life.

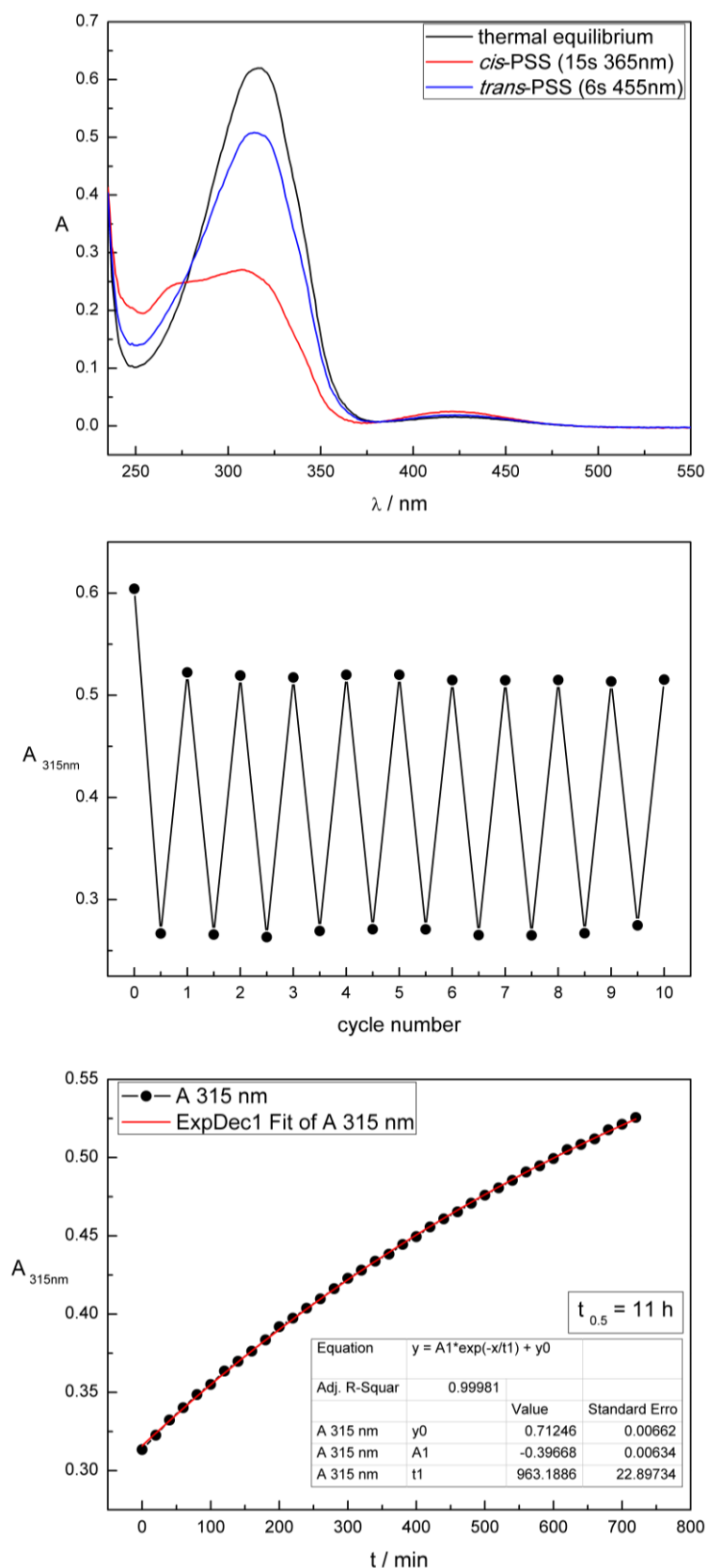


Figure S38. Compound **4e** measured 50 μM in methanol. Upper panel: UV-Vis absorption spectra. Middle panel: Cycle performance upon alternate irradiation. Lower panel: Thermal half-life.

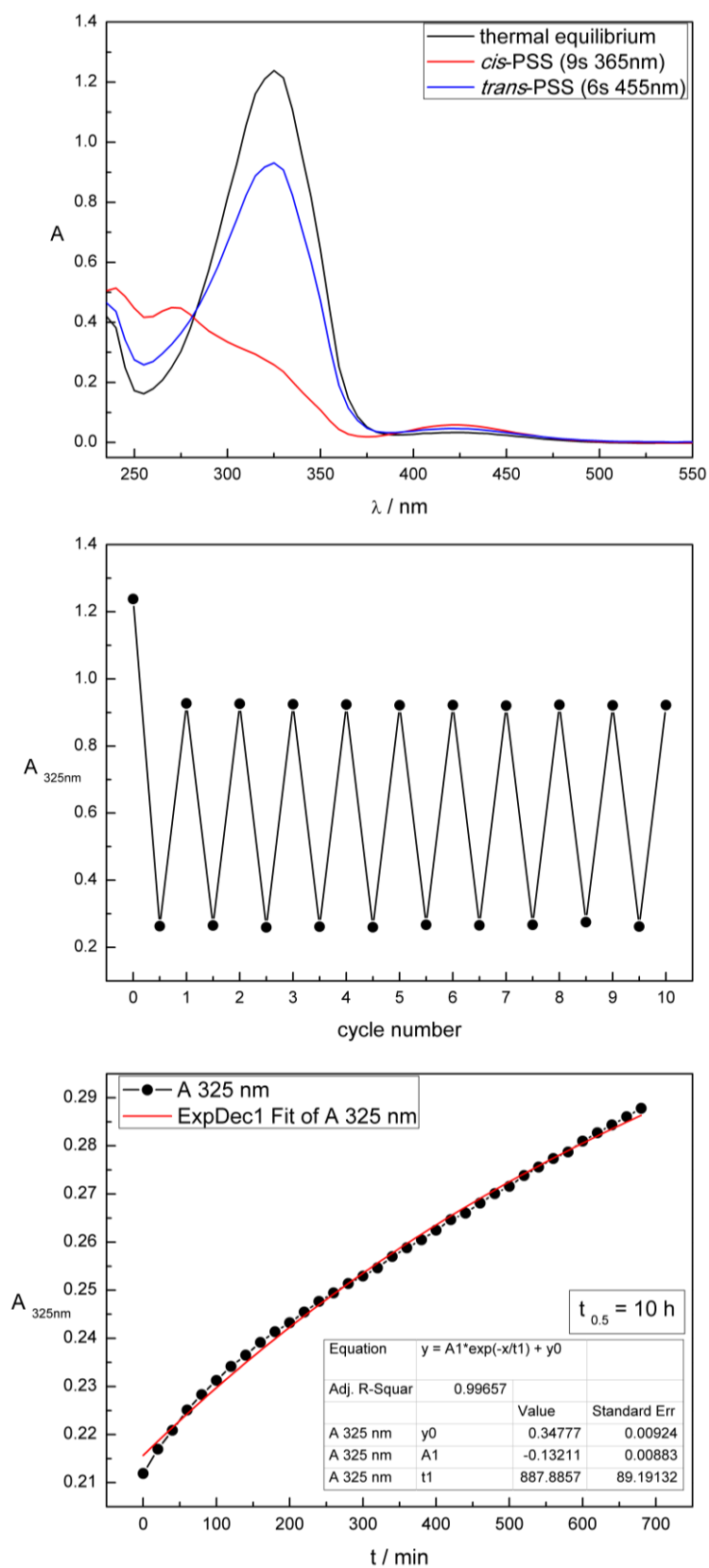


Figure S39. Compound **4f** measured 50 μM in methanol. Upper panel: UV-Vis absorption spectra. Middle panel: Cycle performance upon alternate irradiation. Lower panel: Thermal half-life.

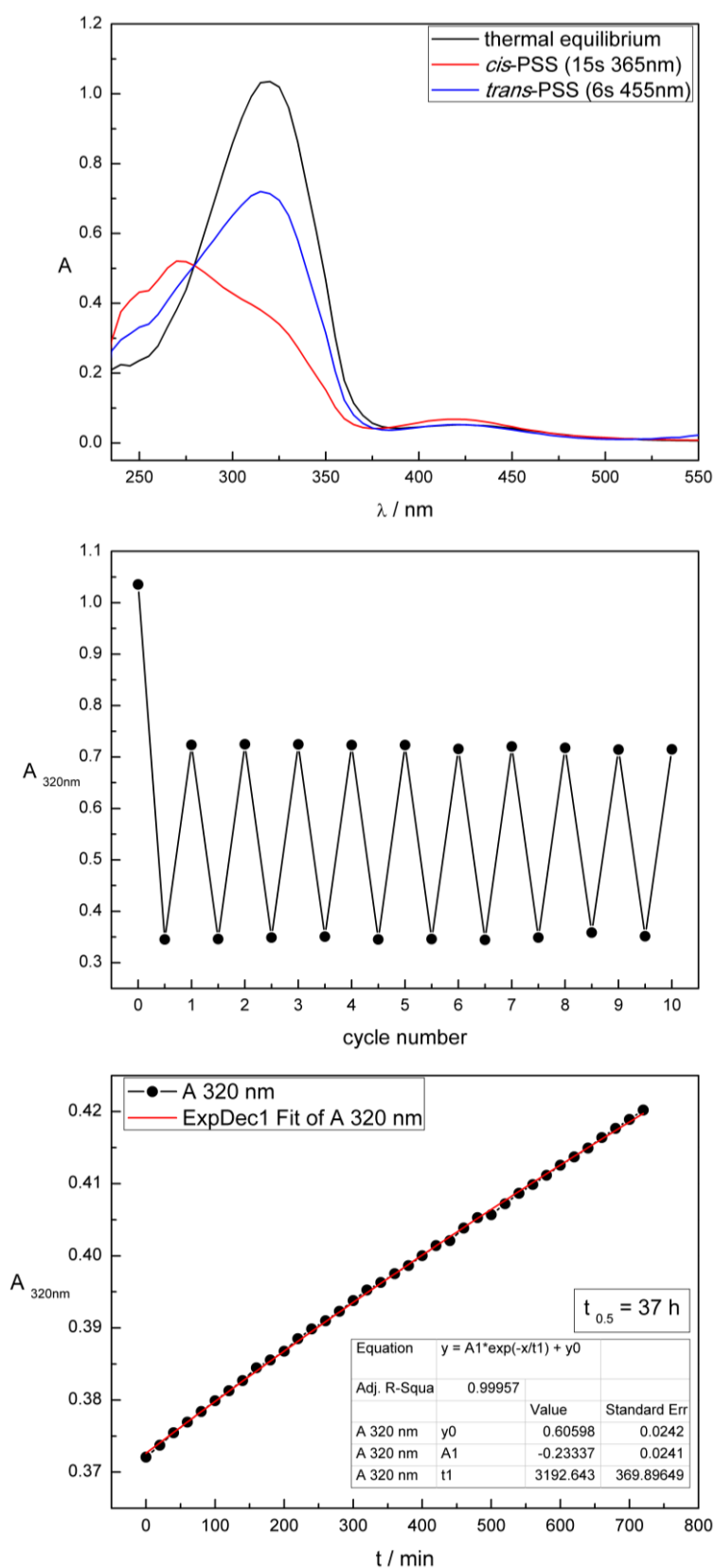


Figure S40. Compound **4g** measured 50 μM in methanol. Upper panel: UV-Vis absorption spectra. Middle panel: Cycle performance upon alternate irradiation. Lower panel: Thermal half-life.

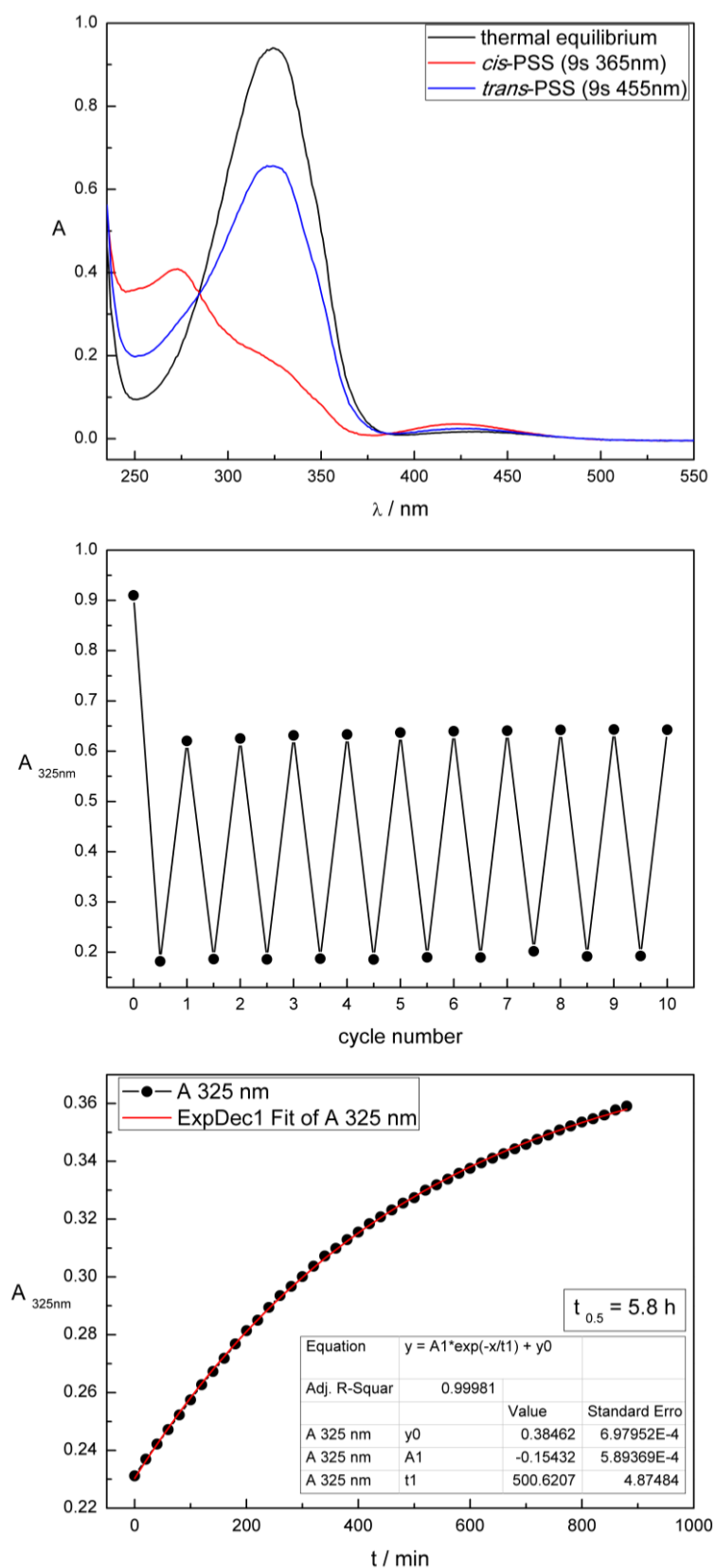


Figure S41. Compound **4h** measured 50 μM in methanol. Upper panel: UV-Vis absorption spectra. Middle panel: Cycle performance upon alternate irradiation. Lower panel: Thermal half-life.

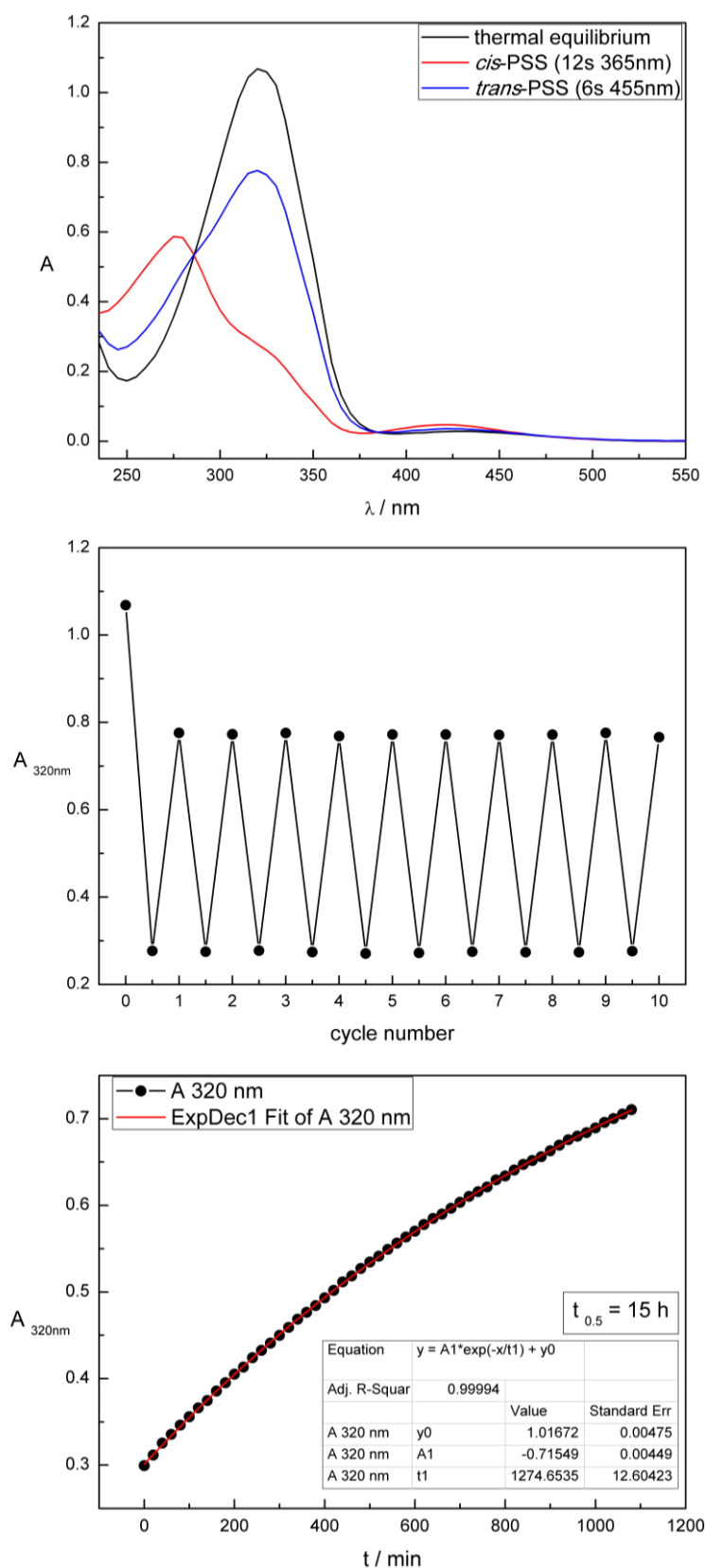


Figure S42. Compound **4i** measured 50 μM in methanol. Upper panel: UV-Vis absorption spectra. Middle panel: Cycle performance upon alternate irradiation. Lower panel: Thermal half-life.

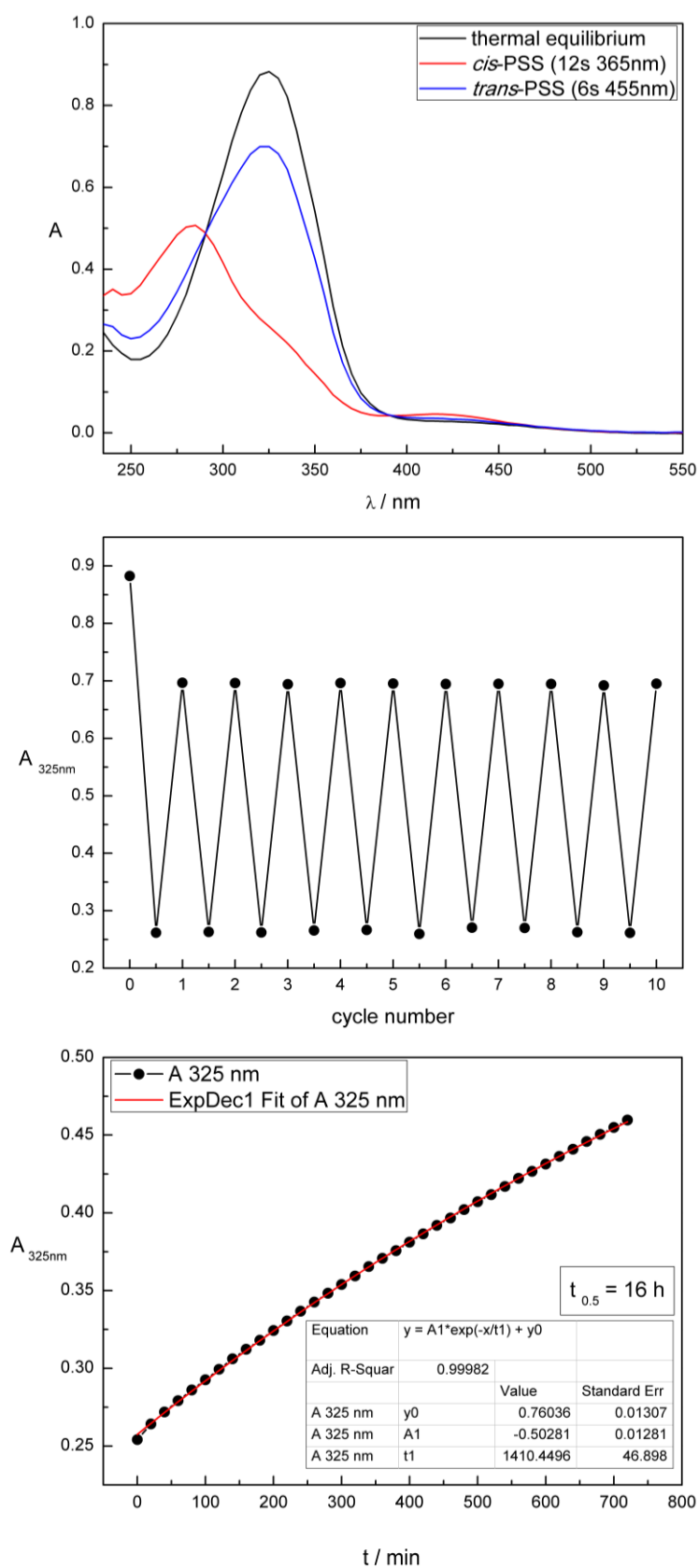


Figure S43. Compound **4j** measured 50 μM in methanol. Upper panel: UV-Vis absorption spectra. Middle panel: Cycle performance upon alternate irradiation. Lower panel: Thermal half-life.

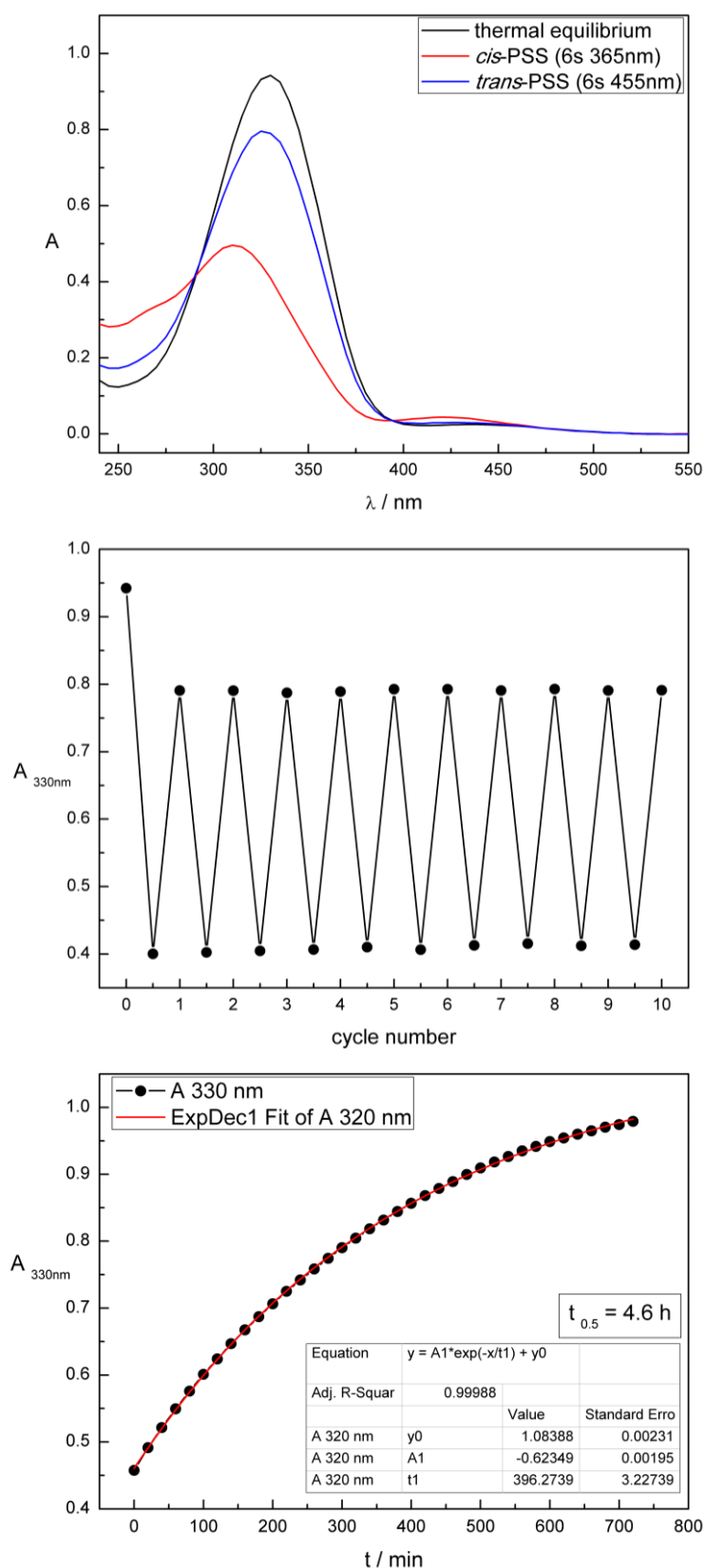
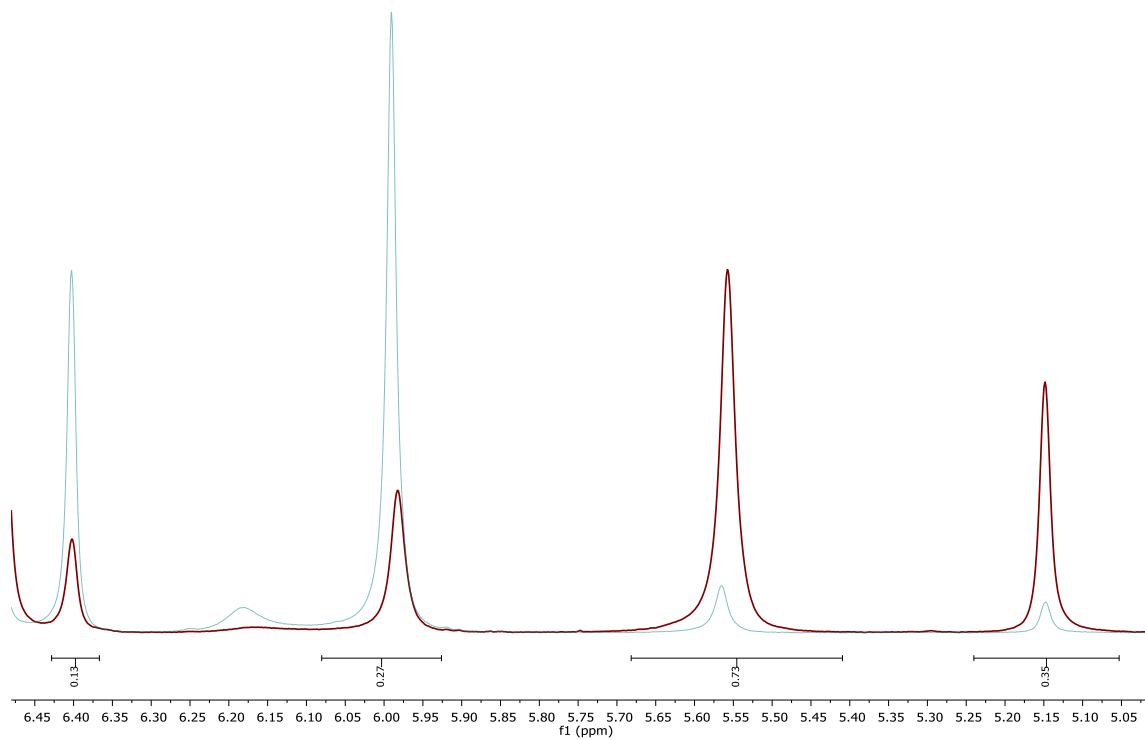


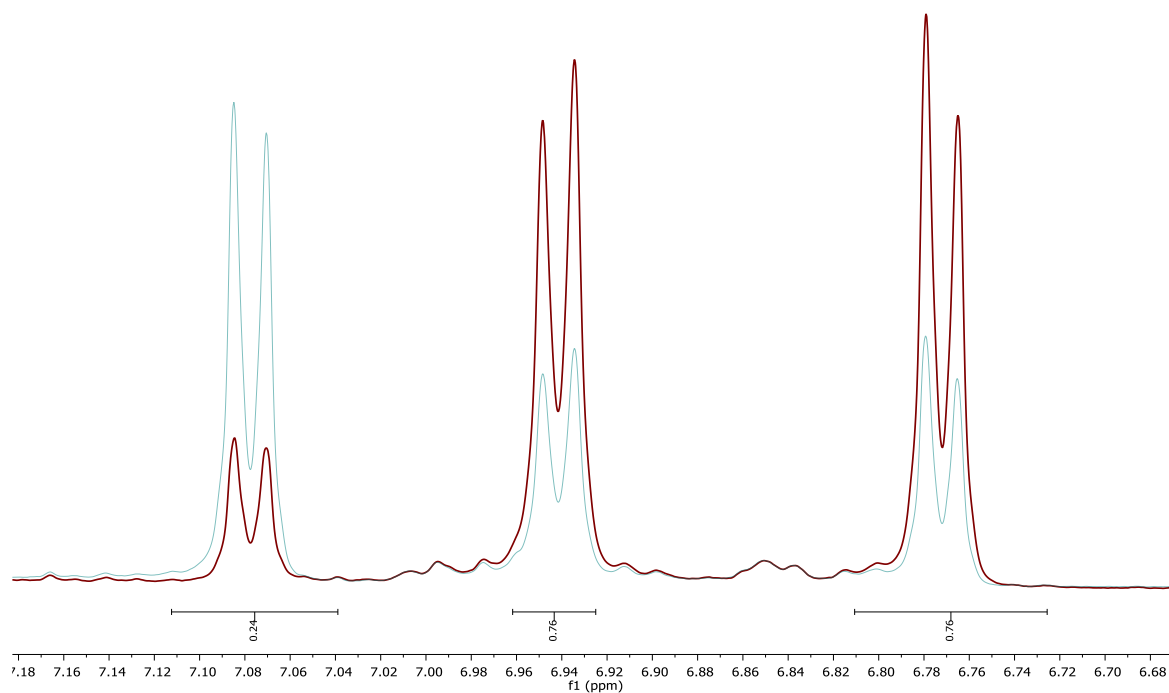
Figure S44. Compound **4k** measured 50 μM in methanol. Upper panel: UV-Vis absorption spectra. Middle panel: Cycle performance upon alternate irradiation. Lower panel: Thermal half-life.

2.5.3 PSS Determination *via* NMR

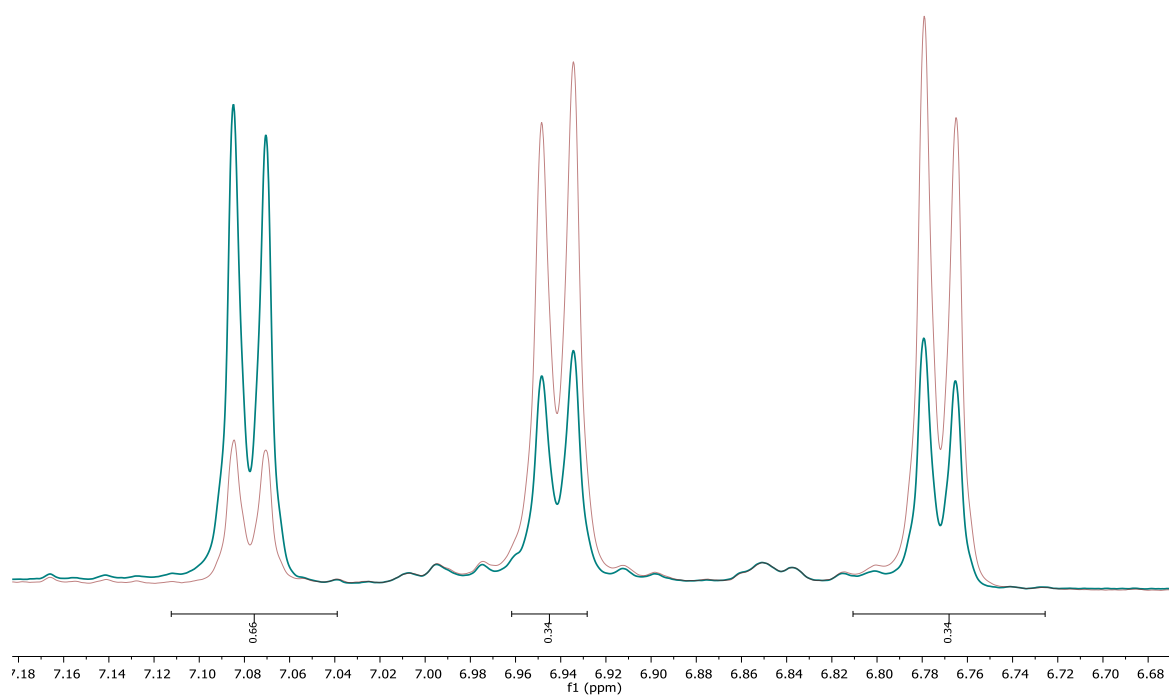
Compound **4a**: red spectrum = *cis* PSS 73% (DMSO- d_6)



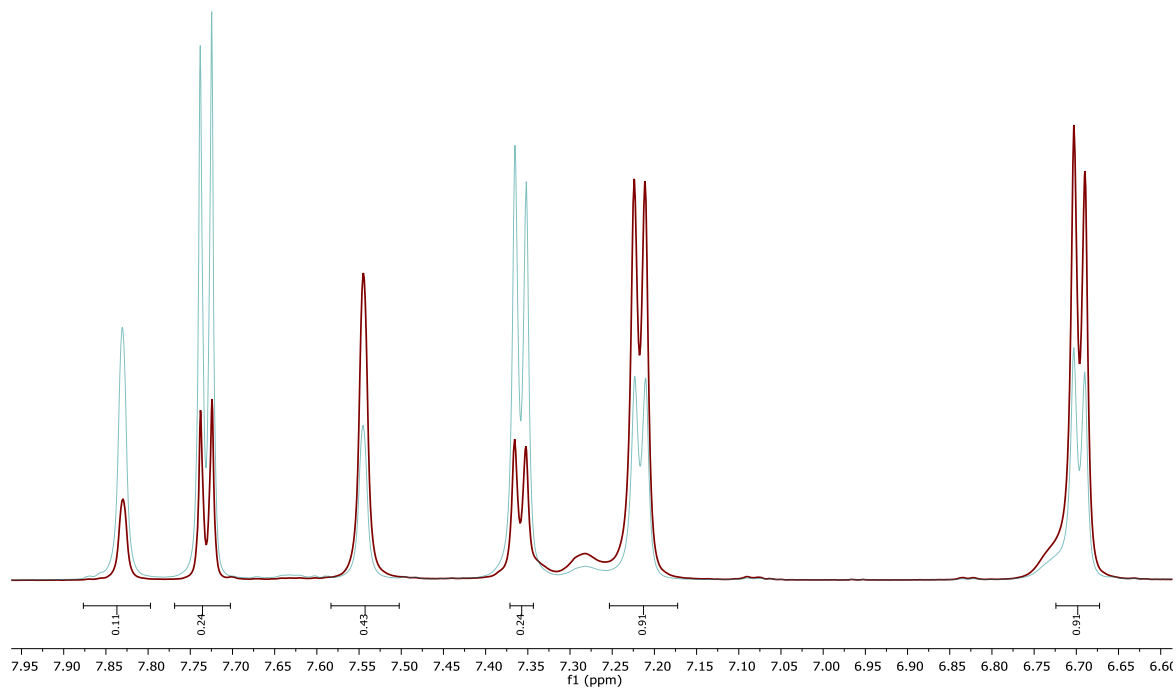
Compound **4b**: red spectrum = *cis* PSS 76% (DMSO-*d*₆)



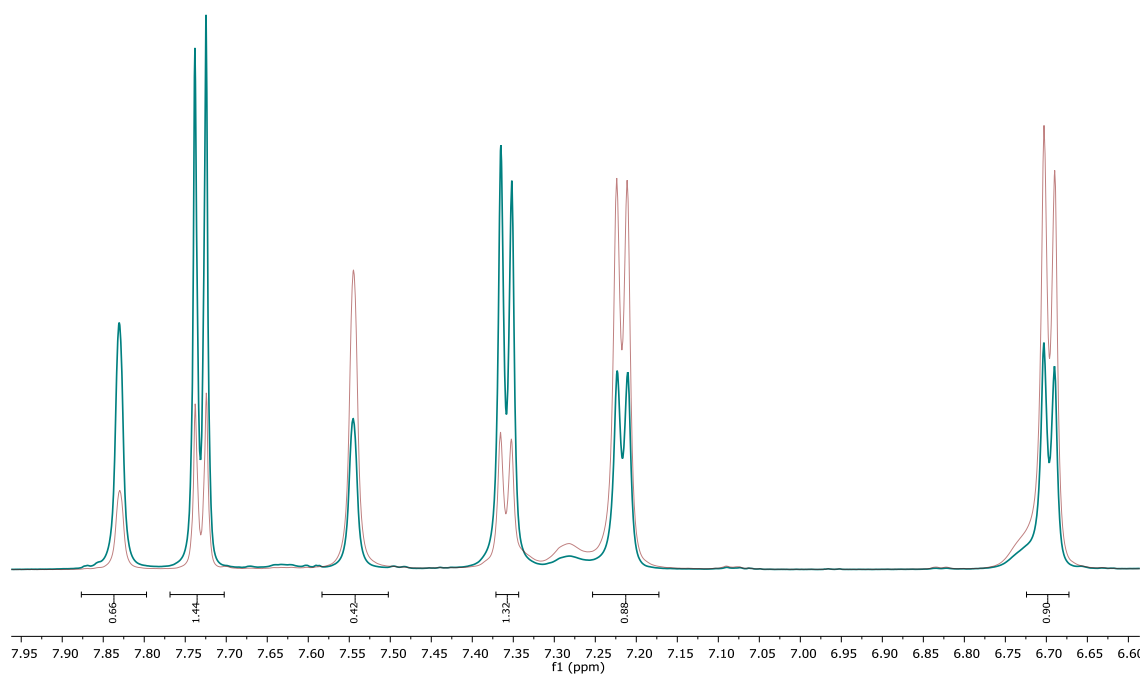
Compound **4b**: blue spectrum = *trans* PSS 66% (DMSO-*d*₆)



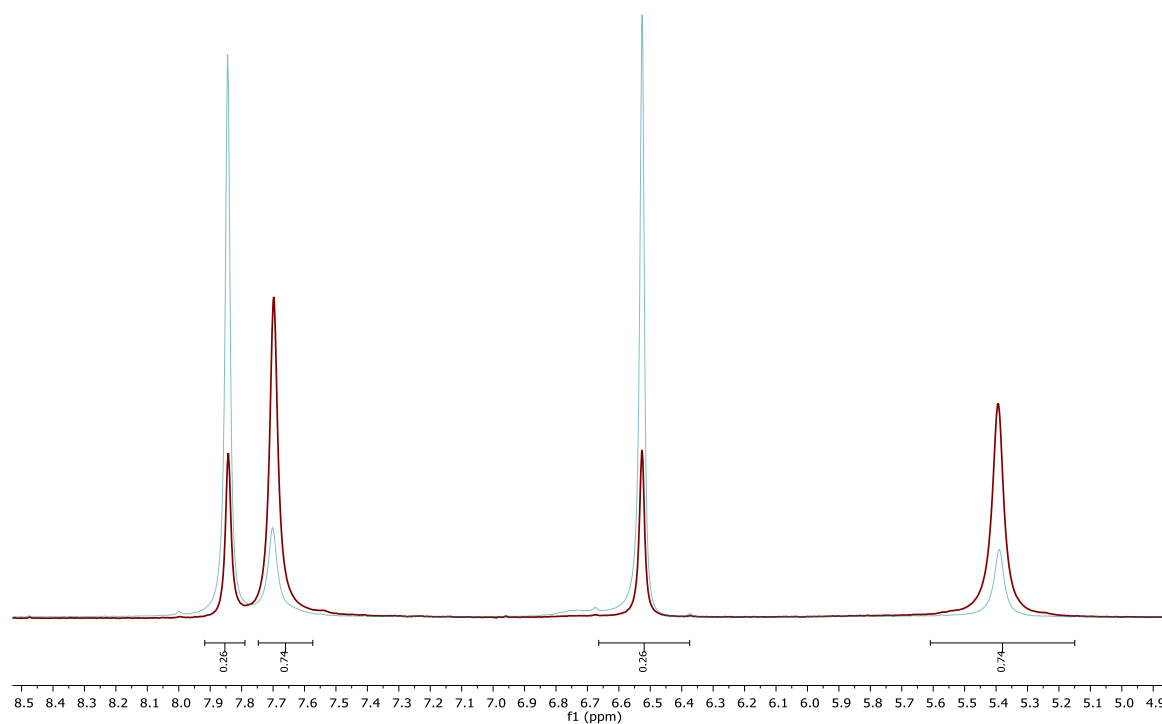
Compound **4c**: red spectrum = *cis* PSS 79% (DMSO-*d*₆)



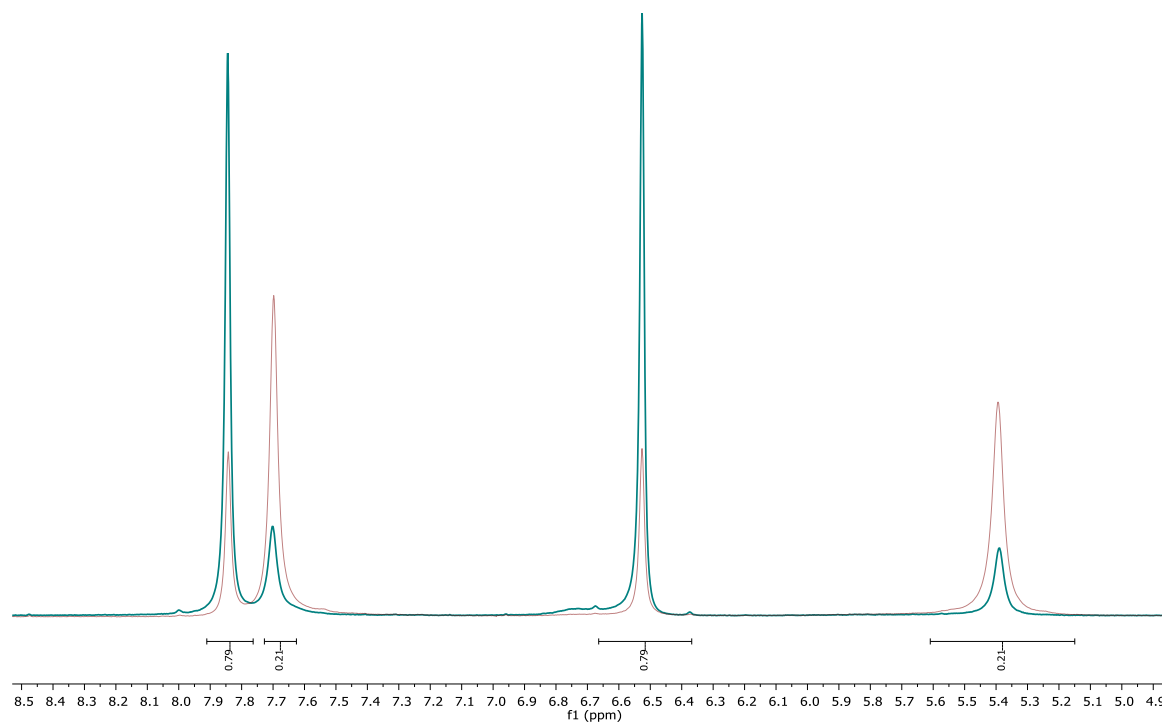
Compound **4c**: blue spectrum = *trans* PSS 61% (DMSO-*d*₆)



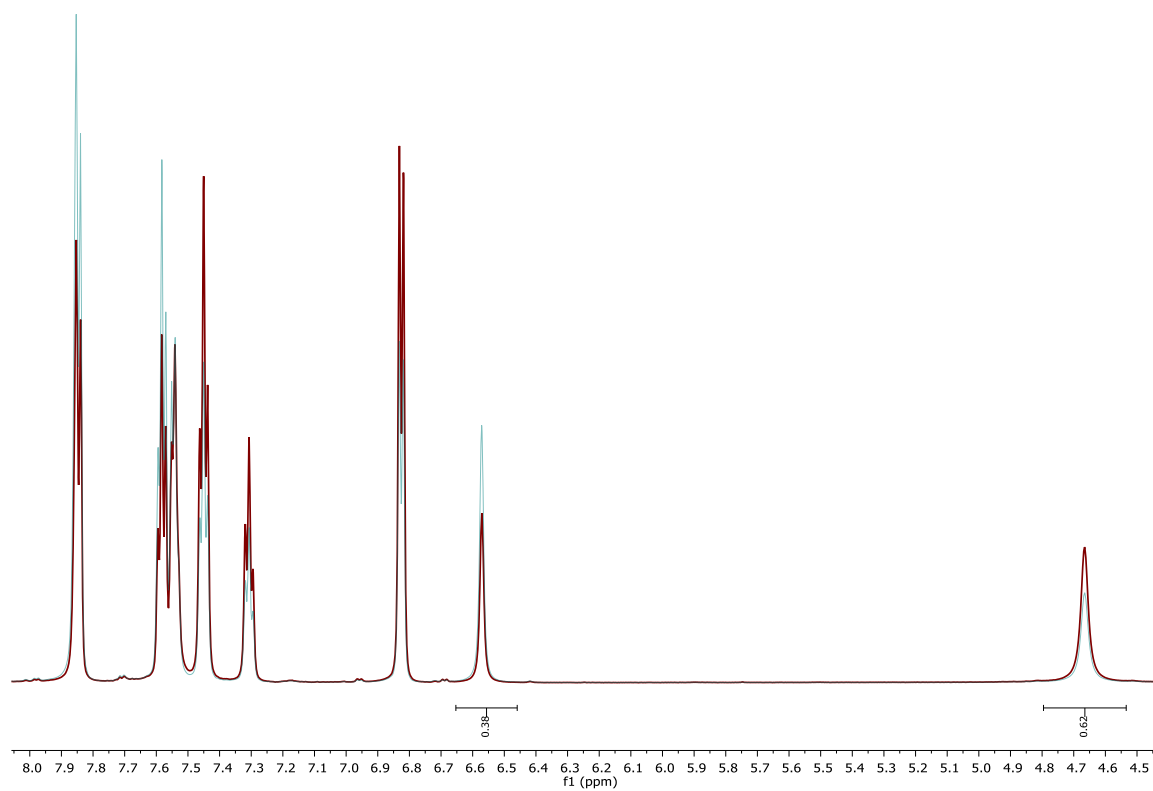
Compound **4d**: red spectrum = *cis* PSS 74% (DMSO-*d*₆)



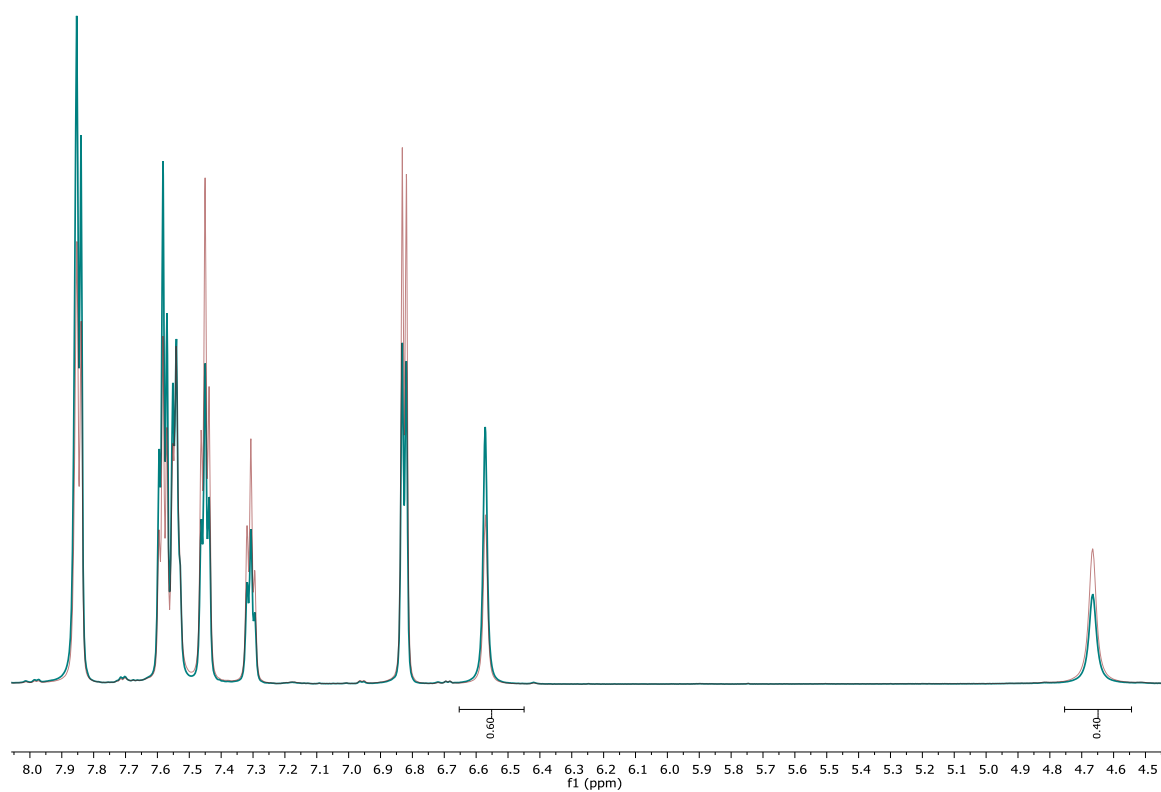
Compound **4d**: blue spectrum = *trans* PSS 79% (DMSO-*d*₆)



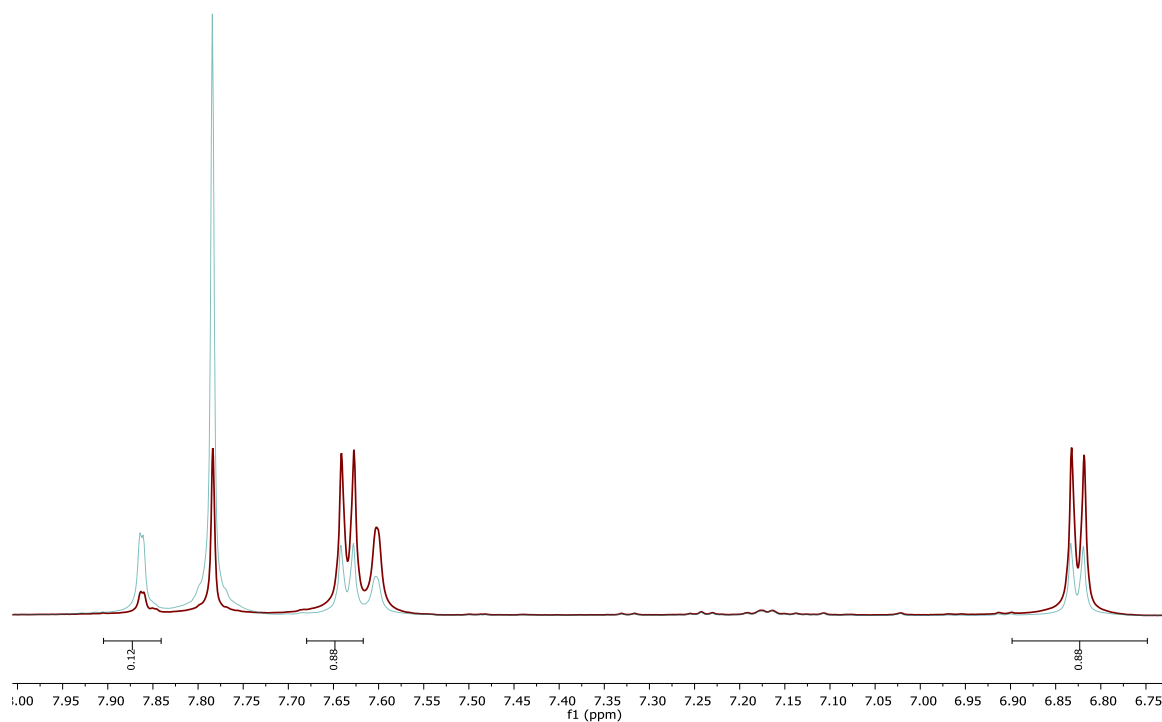
Compound **4e**: red spectrum = *cis* PSS 62% (DMSO-*d*₆)



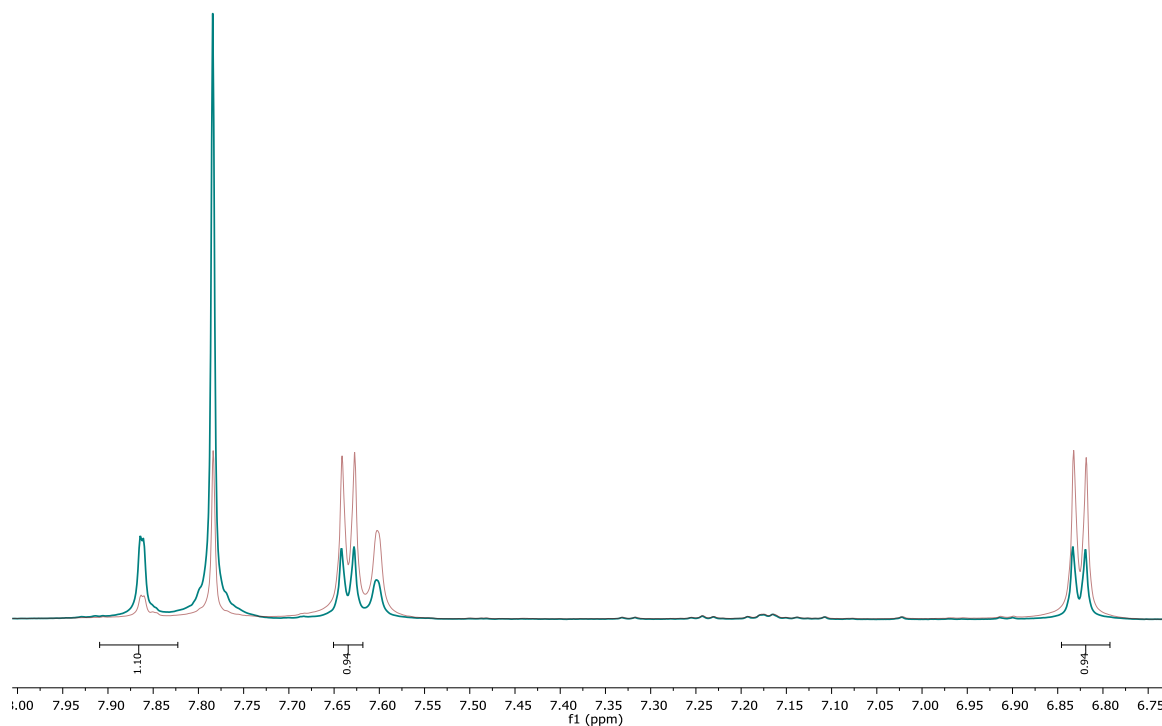
Compound **4e**: blue spectrum = *trans* PSS 60% (DMSO-*d*₆)



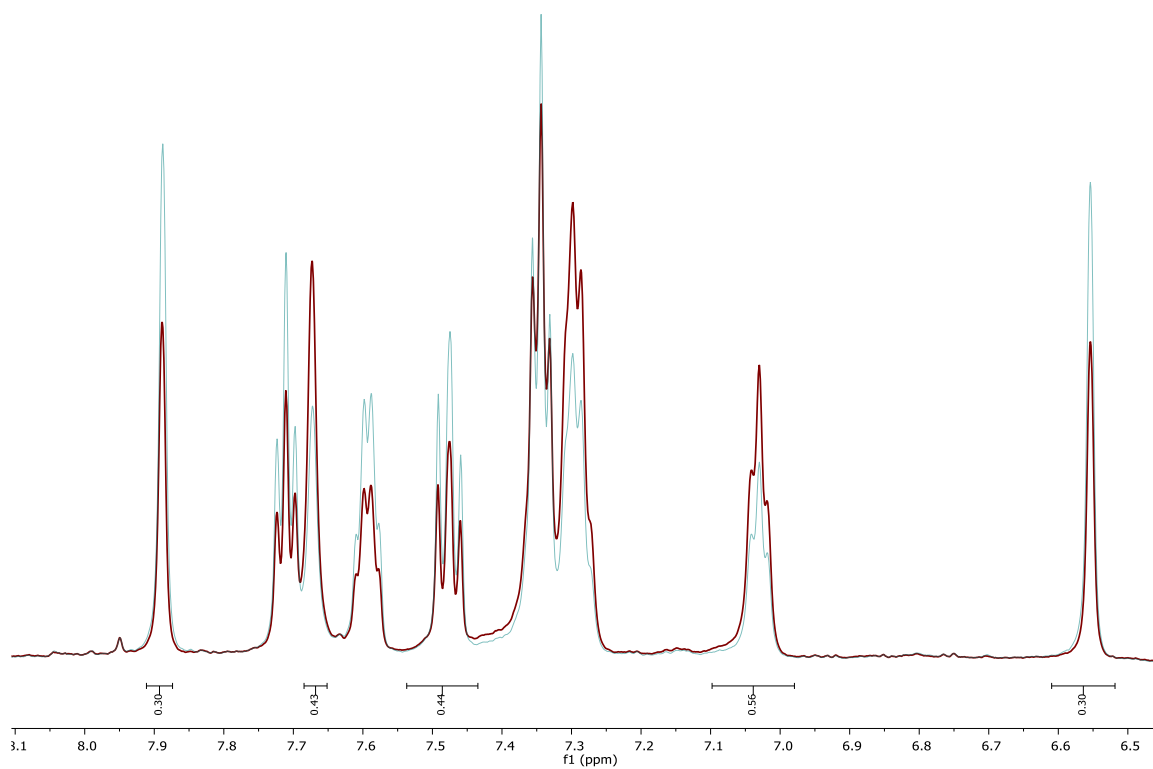
Compound **4f**: red spectrum = *cis* PSS 88% (DMSO-*d*₆)



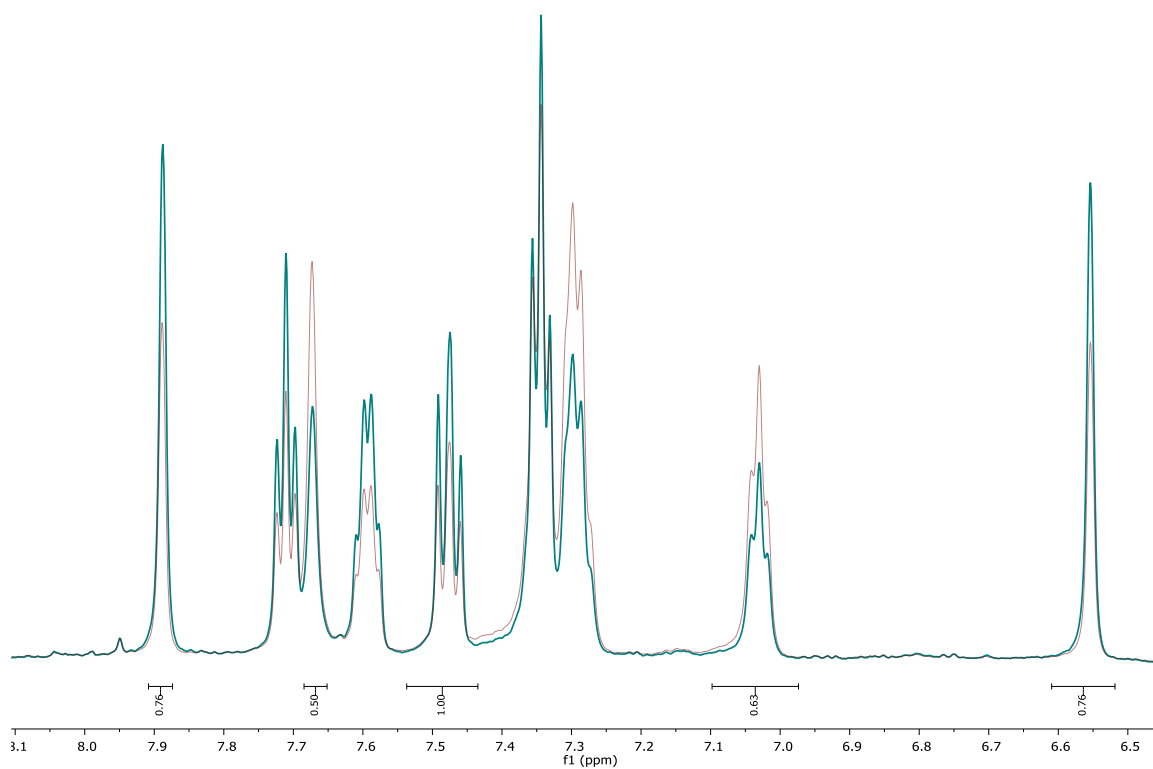
Compound **4f**: blue spectrum = *trans* PSS 54% (DMSO-*d*₆)



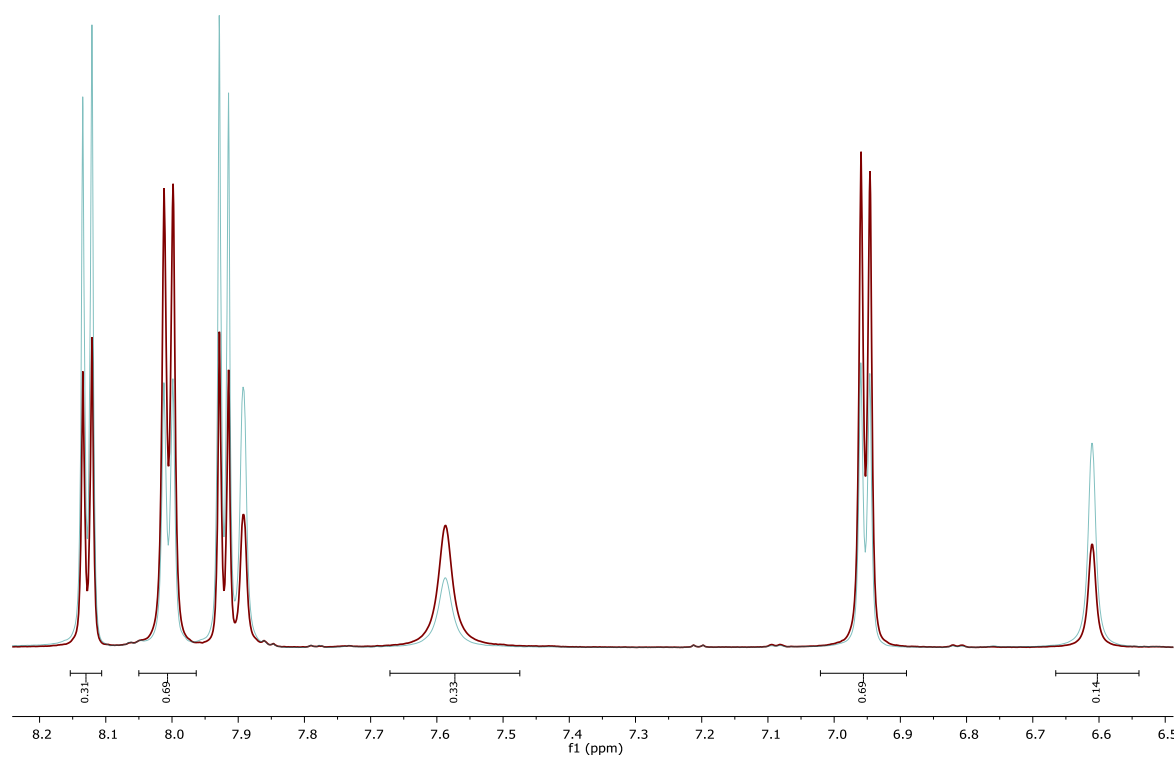
Compound **4g**: red spectrum = *cis* PSS 58% (DMSO-*d*₆)



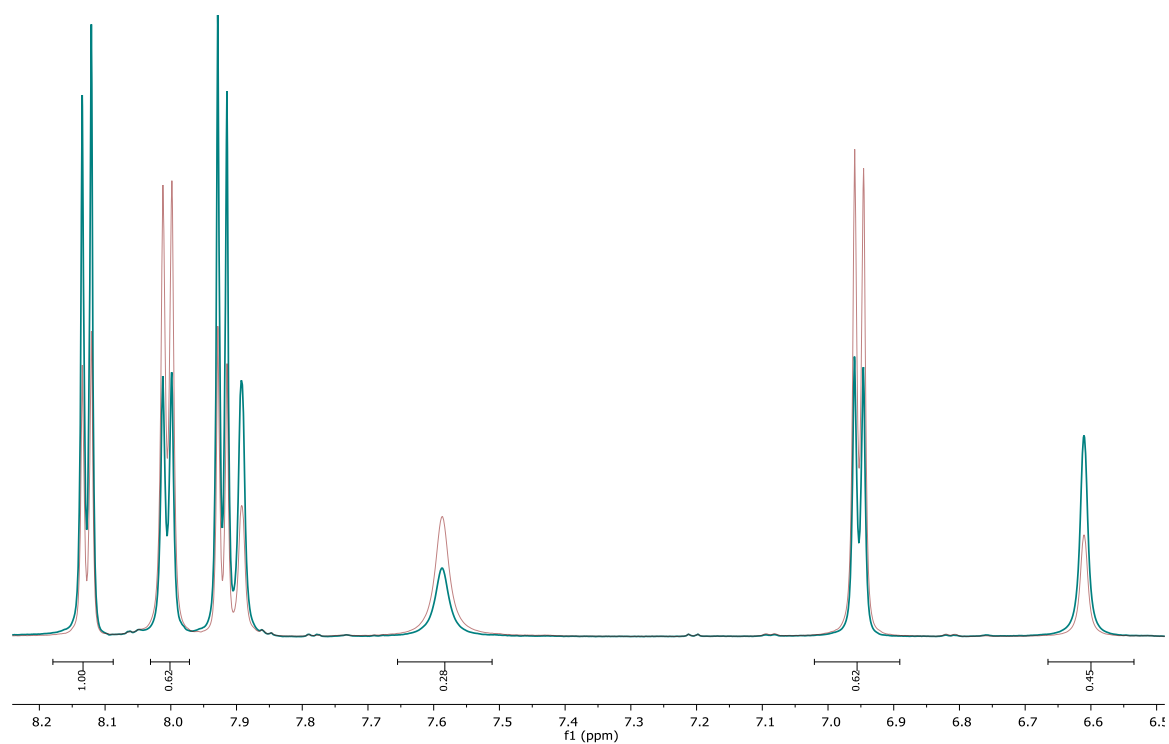
Compound **4g**: blue spectrum = *trans* PSS 61% (DMSO-*d*₆)



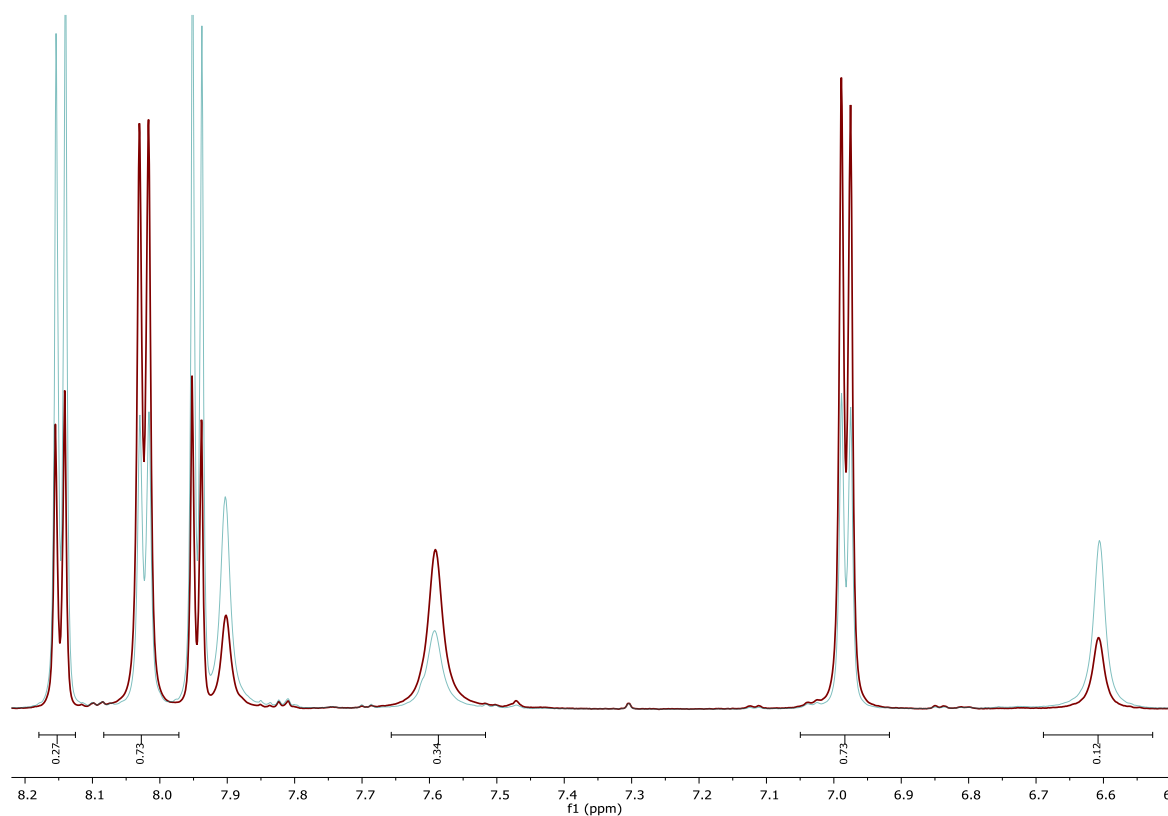
Compound **4h**: red spectrum = *cis* PSS 69% (DMSO-*d*₆)



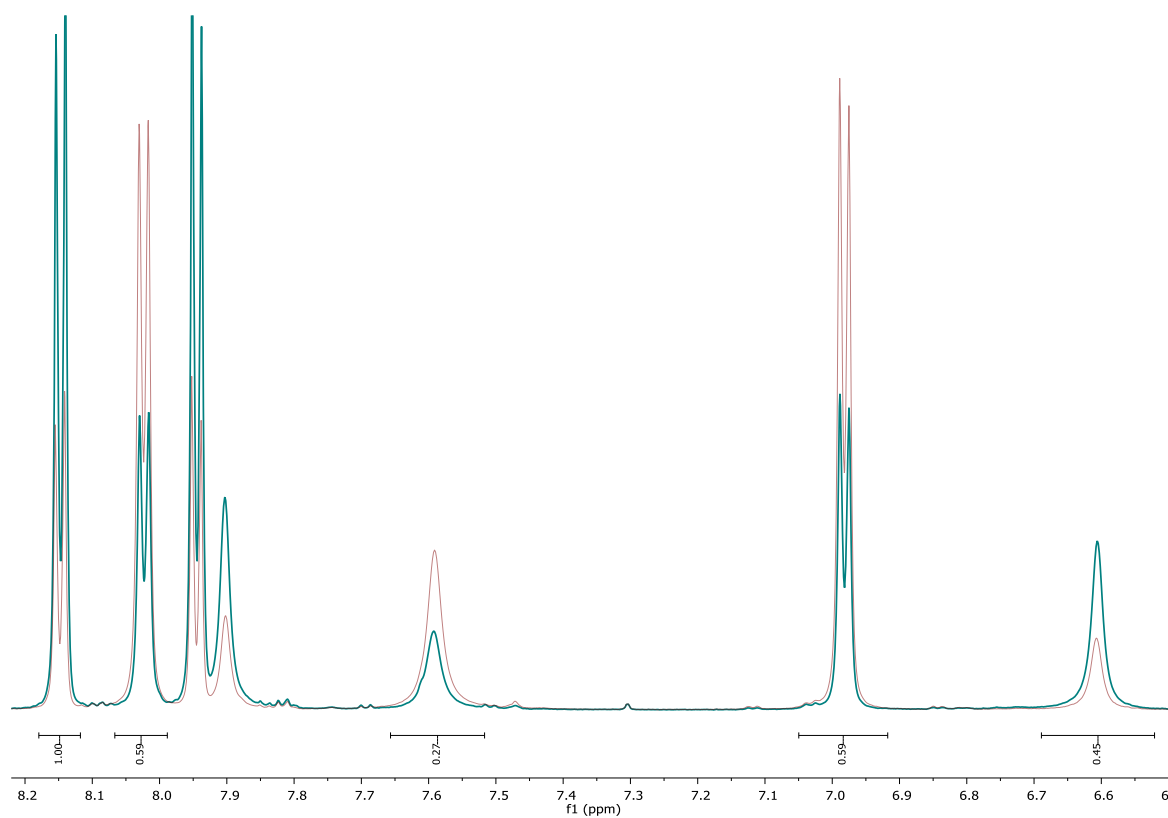
Compound **4h**: blue spectrum = *trans* PSS 62% (DMSO-*d*₆)



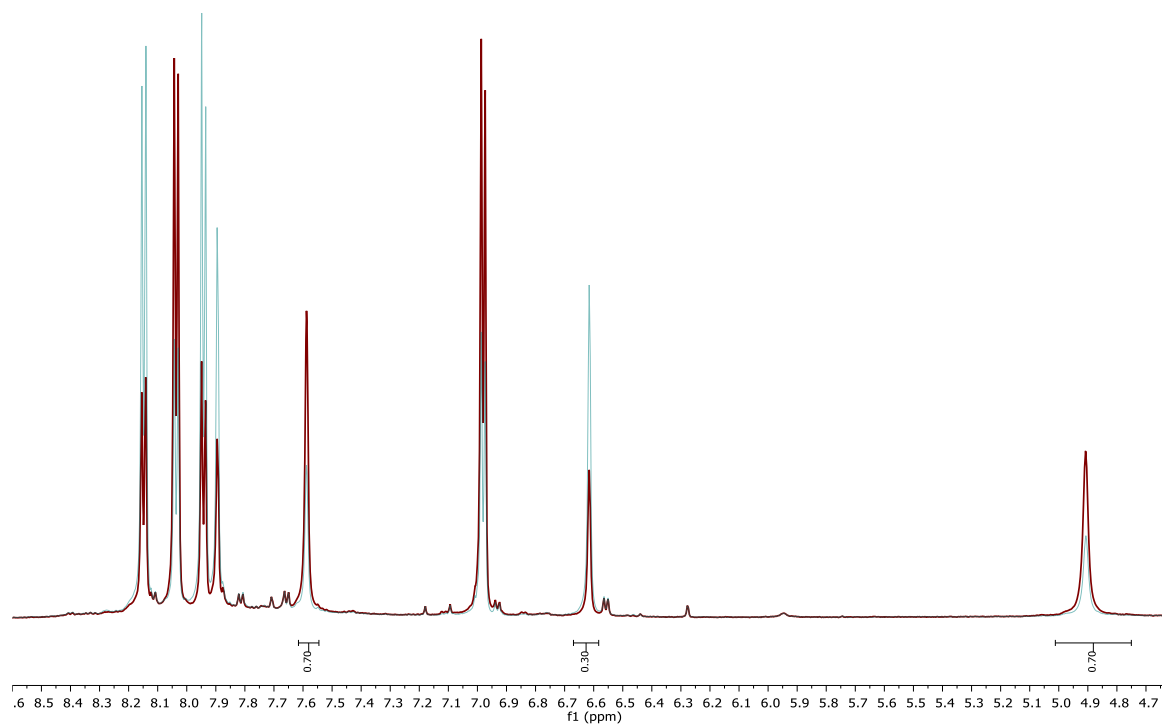
Compound **4i**: red spectrum = *cis* PSS 73% (DMSO-*d*₆)



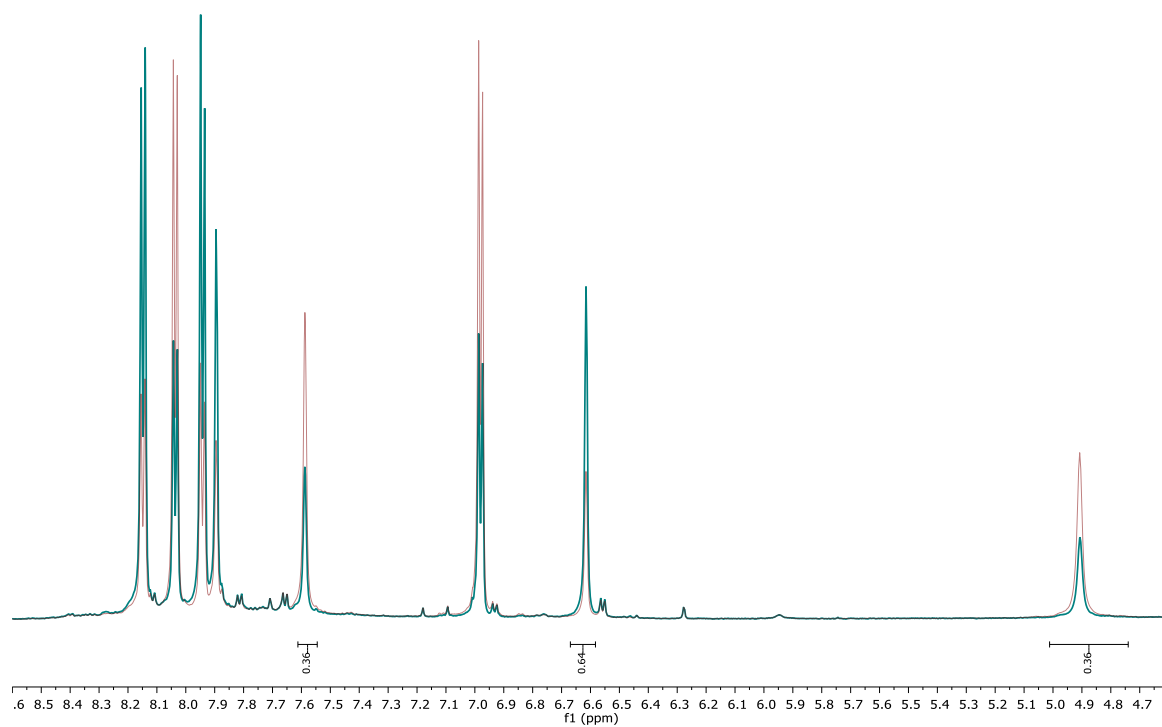
Compound **4i**: blue spectrum = *trans* PSS 63% (DMSO-*d*₆)



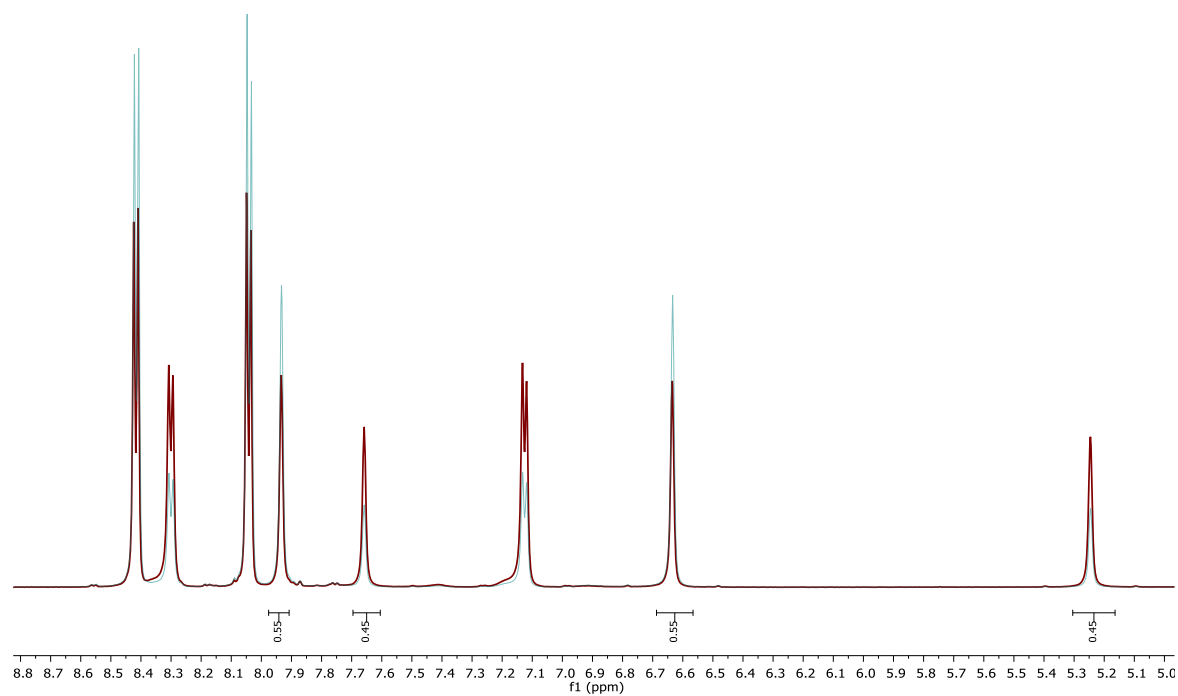
Compound **4j**: red spectrum = *cis* PSS 70% (DMSO-*d*₆)



Compound **4j**: blue spectrum = *trans* PSS 64% (DMSO-*d*₆)



Compound **4k**: red spectrum = *cis* PSS 45% (DMSO-*d*₆)



2.6 References

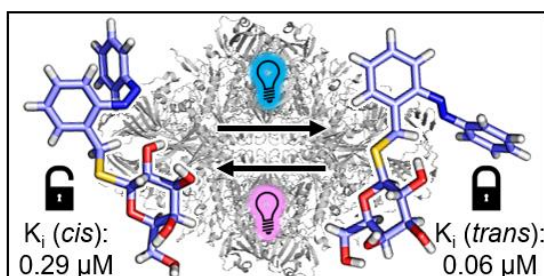
- [1] Editorial, *Nat. Chem. Biol.* **2014**, 10, 483.
- [2] I. Ahmed, L. Fruk, *Mol. BioSyst.* **2013**, 9, 565-570.
- [3] J. Broichhagen, J. A. Frank, D. Trauner, *Acc. Chem. Res.* **2015**, 48, 1947-1960.
- [4] W. A. Velema, W. Szymanski, B. L. Feringa, *J. Am. Chem. Soc.* **2014**, 136, 2178-2191.
- [5] K. Hüll, J. Morstein, D. Trauner, *Chem. Rev.* **2018**, 118, 10710-10747.
- [6] J. Morstein, D. Trauner, *Curr. Opin. Chem. Biol.* **2019**, 50, 145-151.
- [7] P. Sarma, B. Medhi, *Indian J. Pharmacol.* **2017**, 49, 221-222.
- [8] M. M. Lerch, M. J. Hansen, G. M. van Dam, W. Szymanski, B. L. Feringa, *Angew. Chem. Int. Ed.* **2016**, 55, 10978-10999.
- [9] C. Brieke, F. Rohrbach, A. Gottschalk, G. Mayer, A. Heckel, *Angew. Chem. Int. Ed.* **2012**, 51, 8446-8476.
- [10] W. Szymanski, J. M. Beierle, H. A. V. Kistemaker, W. A. Velema, B. L. Feringa, *Chem. Rev.* **2013**, 113, 6114-6178.
- [11] *Molecular Switches*; B. L. Feringa, W. R. Browne, Eds.; Wiley-VCH Verlag GmbH & Co. KGaA: Weinheim, Germany **2011**.
- [12] E. Merino, M. Ribagorda, *Beilstein J. Org. Chem.* **2012**, 8, 1071-1090.
- [13] M.-M. Russew, S. Hecht, *Adv. Mater.* **2010**, 22, 3348-3360.
- [14] Z. L. Pianowski, *Chem. Eur. J.* **2019**, 25, DOI: 10.1002/chem.201805814.
- [15] R. Siewertsen, H. Neumann, B. Buchheim-Stehn, R. Herges, C. Näther, F. Renth, F. Temps, *J. Am. Chem. Soc.* **2009**, 131, 15594-15595.
- [16] A. A. Beharry, G. A. Woolley, *Chem. Soc. Rev.* **2011**, 40, 4422-4437.

- [17] A. Goulet-Hanssens, C. J. Barrett, *Wiley Periodicals, Inc. J. Polym. Sci., Part A: Polym. Chem.* **2013**, *51*, 3058-3070.
- [18] S. Crespi, N. A. Simeth, B. König, *Nat. Rev. Chem.* **2019**, *3*, 133-146.
- [19] N. A. Simeth, A. Bellisario, S. Crespi, M. Fagnoni, B. König, *J. Org. Chem.* **2019**, *84*, 6565-6575.
- [20] N. A. Simeth, S. Crespi, M. Fagnoni, B. König, *J. Am. Chem. Soc.* **2018**, *140*, 2940-2946.
- [21] S. Crespi, N. A. Simeth, A. Bellisario, M. Fagnoni, B. König, *J. Phys. Chem. A.* **2019**, *123*, 1814-1823.
- [22] J. Calbo, C. E. Weston, A. J. P. White, H. S. Rzepa, J. Contreras-García, M. J. Fuchter, *J. Am. Chem. Soc.* **2017**, *139*, 3, 1261-1274.
- [23] R. Siewertsen, H. Neumann, B. Buchheim-Stehn, R. Herges, C. Näther, F. Renth, F. Temps, *J. Am. Chem. Soc.* **2009**, *131*, 15594-15595.
- [24] C. E. Weston, R. D. Richardson, P. R. Haycock, A. J. P. White, M. J. Fuchter, *J. Am. Chem. Soc.* **2014**, *136*, 11878-11881.
- [25] L. Stricker, M. Böckmann, T. M. Kirse, N. L. Doltsinis, B. J. Ravoo, *Chem. Eur. J.* **2018**, *24*, 8639-8647.
- [26] Y.-T. Wang, X.-Y. Liu, G. Cui, W.-H. Fang, W. Thiel, *Angew. Chem. Int. Ed.* **2016**, *55*, 14009-14013.
- [27] J. Garcia-Amorós, M. Díaz-Lobo, S. Nonell, D. Velasco, *Angew. Chem. Int. Ed.* **2012**, *51*, 12820-12823.
- [28] S. Venkataramani, U. Jana, M. Dommaschk, F. D. Sonnichsen, F. Tuczek, R. Herges, *Science* **2011**, *331*, 445-448.
- [29] R. Travieso-Puente, S. Budzak, J. Chen, P. Stacko, J. T. B. H. Jastrzebski, E. Otten, *J. Am. Chem. Soc.* **2017**, *139*, 3328-3331.
- [30] R. D. Taylor, M. MacCoss, A. D. G. Lawson, *J. Med. Chem.* **2014**, *57*, 5845-5859.

- [31] L. Stricker, E.-C. Fritz, M. Peterlechner, N. L. Doltsinis, B. J. Ravoo, *J. Am. Chem. Soc.* **2016**, *138*, 4547-4554.
- [32] S. Devi, M. Saraswat, S. Grewal, S. Venkataramani, *J. Org. Chem.* **2018**, *83*, 4307-4322.
- [33] A. Baeyer, *Chem. Ber.* **1874**, *7*, 1638-1640.
- [34] C. J. Mills, *J. Chem. Soc.* **1895**, *67*, 925-933.
- [35] M. Schönberger, D. Trauner, *Angew. Chem. Int. Ed.* **2014**, *53*, 3264-3267.
- [36] P. López-Tarifa, G. Sánchez-Sanz, I. Alkorta, J. Elguero, D. Sanz, A. Perona, R. M. Claramunt, *J. Mol Struct.* **2012**, *1015*, 138-146.

CHAPTER 3

3 Development of Photoswitchable Inhibitors for β -Galactosidase



This chapter has been published as:

K. Rustler, M. J. Mickert, J. Nazet, R. Merkl, H. H. Gorris, B. König, *Org. Biomol. Chem.* **2018**, 16, 7430-7437.

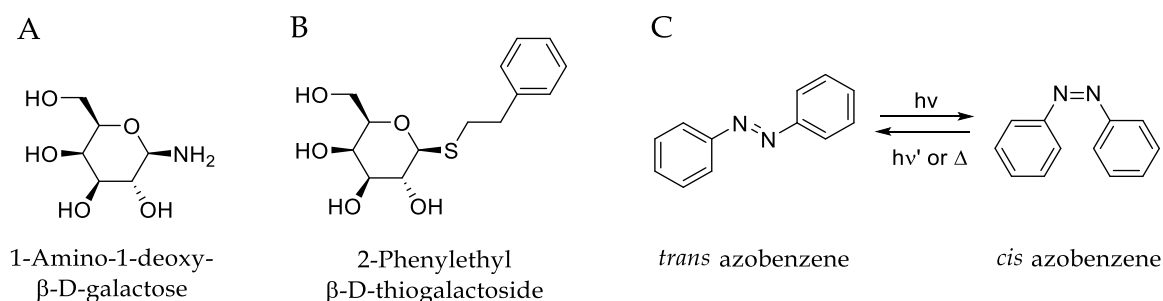
This project was performed in collaboration with M. J. Mickert (PD Dr. H.-H. Gorris, University of Regensburg) and J. Nazet (Prof. R. Merkl, University of Regensburg). K. Rustler performed the synthesis and (photo-)chemical investigation of all compounds. M. J. Mickert performed all enzymatic inhibition studies. J. Nazet performed docking analysis. Mass spectrometry analysis were performed by the analytical department at the University of Regensburg. K. Rustler, M. J. Mickert, and J. Nazet wrote the manuscript. PD Dr. H.-H. Gorris, Prof. R. Merkl, and B. König supervised the project. B. König is the corresponding author.

3.1 Introduction

By incorporating photochromic scaffolds into the molecular structure of known bioactive compounds, photons can be used as an orthogonal control element providing high spatiotemporal precision in a – depending on the applied wavelength – non-invasive manner without risking contamination of the studied sample.^[1-5] In contrast to photolyzable moieties, the reversible approach of photoswitches and the absence of a cleaved side-product is beneficial.^[6-8] Introducing this photochromic tool into a bioactive target leads – upon irradiation with light – to a reversible toggling between two states, affecting geometry, polarity, and charge distribution.^[1,7,9] A variety of such photoresponsive scaffolds has been investigated, including dithienylethenes (DTEs), fulgi(mi)des, and azobenzenes, which can be characterized by their distinct switching mechanism either based on a 6π -electrocyclic rearrangement (cyclization/ring-opening: DTEs, fulgi(mi)des) or an *E-Z* double-bond photoisomerization (azobenzenes). Their thermal stability differs from bistable (P-type: DTEs, fulgi(mi)des) to a tuneable thermal reversibility ranging from ns to years (T-type: azobenzenes).^[1,3,5,10-12] After the first publication of azobenzene in the late 1960s for the photoregulation of the activity of chymotrypsin,^[13] the applications for photoactive moieties expanded towards the reversible light-triggered control of receptors,^[14-17] bacterial growth,^[18] vision restoration,^[19,20] the respiratory chain,^[21] and enzymatic activity.^[13,22-27] The homotetrameric enzyme β -galactosidase from *Escherichia coli* catalyzes the hydrolysis of glycosidic bonds in β -D-galactosides.^[28] β -Galactosidase has been extensively investigated^[29] and several competitive inhibitors including 2-phenylethyl β -D-thiogalactoside (PETG)^[32] and 1-amino-1-deoxy- β -D-galactose (galactosylamine)^[33] have been developed. One of the strongest competitive inhibitors of β -galactosidase (K_i : 0.6 nM; tight binding inhibitor) based on a mannostatin derivative was developed by Greul *et al.*^[35,36] More recently, the inhibition of β -galactosidase has been investigated on the single molecule level in so-called femtoliter arrays.^[30,37] This method provides statistic information about the individual behavior of enzyme molecules in a population. The substrate

turnover of a single β -galactosidase molecule – observable by the generation of a fluorescent product – is interrupted if an inhibitor binds to the active site, and the turnover resumes when the inhibitor is released. From the intermittency of the substrate turnover, stochastic information on individual binding and unbinding events can be retrieved. While it has not been possible to exert any control over these random events so far, a photochromic inhibitor would allow for switching the activity of single enzyme molecules on and off on demand. By extending the PETG-benzene moiety, we have designed a photochromic β -galactosidase inhibitor, whose inhibitory activity can be controlled by irradiation with light orthogonal to the fluorescent read-out system resorufin ($\lambda_{\text{Ex/Em}} = 574/589 \text{ nm}$).^[31,32]

Azobenzenes form one of the largest and most studied classes of photochromic molecules. First described in 1834,^[38] their photoinduced *cis-trans* isomerization, which is accompanied by a large geometrical change and a considerable change in polarity, was discovered one century later in 1937 by G. S. Hartley.^[39] Back-switching to the thermodynamically more stable *trans* isomer can be achieved by irradiation with light of a different wavelength or may proceed by thermal relaxation.^[1,3,5] Benefiting from those properties, we aimed for a strong difference in inhibitory activity upon light-induced switching between the two isomers. In this work, we report the design, synthesis, photochromic characterization, and inhibitory performance of water-soluble photochromic competitive β -galactosidase inhibitors based on the structures of PETG and galactosylamine (Scheme 1).

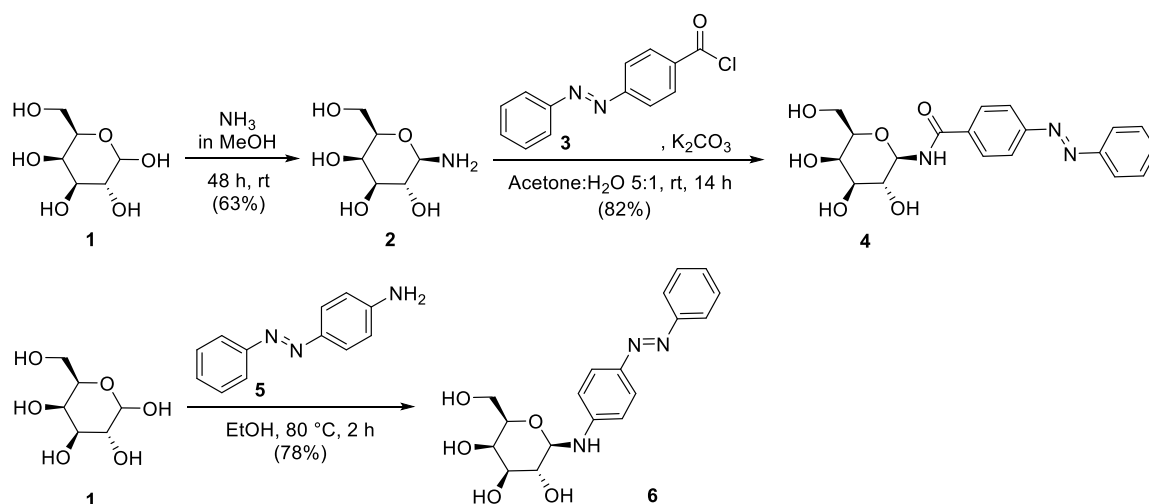


Scheme 1. Chemical structures of β -galactosidase inhibitors. (A) 1-Amino-1-deoxy- β -D-galactose (Galactosylamine).^[33] (B) 2-Phenylethyl β -D-thiogalactoside (PETG).^[32] (C) Photochromic azobenzene in its *trans*- and *cis*-isomeric state.

3.2 Results and Discussion

3.2.1 Design and Syntheses

Design and synthesis of photochromic galactosylamine derivatives. Because of its high inhibitory activity, synthetic accessibility, and high reactivity at its C1 position for further functionalization, galactosylamine was chosen as one inhibitory scaffold for the introduction of a photoresponsive moiety. To attach the photoswitch azobenzene to the galactopyranoside moiety two different syntheses were conducted (Scheme 2). In a first synthetic attempt, *D*-galactose (**1**) was converted into its C1-amino derivative **2** (galactosylamine) in moderate yield upon reaction with ammonia in methanol for 48 hours at room temperature. Under these conditions the β -pyranose isomer was isolated as pure precipitate beside its α -pyranose and α/β -furanose form.^[40] In the next step the β -pyranose product **2** was transformed into its photochromic amide **4** upon reaction with the carboxylic acid chloride azobenzene **3** in basic media in good yield; an acetone/water solvent mixture (5/1) allowed the solution of all reactants.^[41] As compound **4** is based on a carboxy azobenzene core its photochromic properties are characterized by a long thermal half-life of its *cis* isomer. To vary the photochromic properties (*e.g.*, thermal half-life, absorption maxima), in addition, a second derivative, bearing an amino azobenzene moiety directly attached to the galactosylamine, was synthesized. Compound **6** was obtained in a one-step reaction starting from *D*-galactose (**1**) and *para* amino azobenzene **5**.^[42] In analogy to the formation of β -*D*-galactosylamine **2** from *D*-galactose (**1**) again the β -pyranose form was isolated as major product.

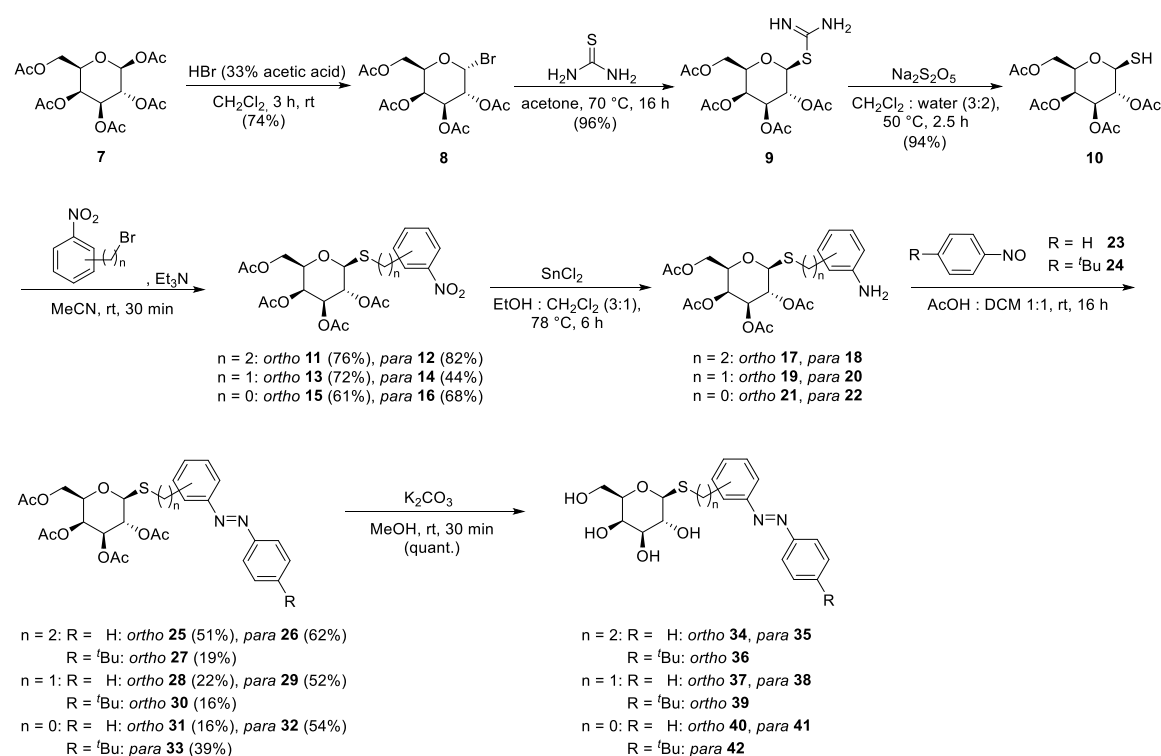


Scheme 2. Synthesis of azobenzene-based galactosylamine derivatives as competitive inhibitors for β -D-galactosidase (*Escherichia coli*).^[40–42]

Design of azobenzene-based PETG derivatives. Based on its benzene ring, PETG was selected for azo-formation as the structural necessary modification is less drastic compared to the complete *de novo* introduction of an azobenzene and the risk to lose inhibitory activity is consequently lower.

Synthesis of asymmetric azobenzene-based PETG derivatives. The asymmetric PETG-based azobenzene derivatives **34–42** were synthesized as outlined in Scheme 3. The general procedure is based on the transformation of the commercially available pentaacetylated β -D-galactose **7** into its C1- α -acetobromo-derivative **8** upon reaction with HBr in acetic acid.^[43] In the next step, compound **8** was converted into its imino-methanamine salt **9** by reaction with thiourea and subsequently reduced to obtain the pentaacetylated β -D-thiogalactopyranoside **10**.^[44] This thiosugar derivative was used for the reaction with differently bromo-substituted nitrobenzenes affording the corresponding pentaacetylated nitrobenzene β -D-thiogalactopyranosides **11–16**.^[45] Besides the use of the native PETG moiety containing two CH_2 linking groups, the steric influence of the linker length and substitution position was further investigated. Bromo-substituted nitrobenzenes vary in their linker length ($n = 0, 1, 2$) and their substitution position (*ortho*, *para*). In order to perform a classical Mills reaction for the formation of an azo bridge, the nitro group was reduced to its amino function.^[46] As reaction partner nitrosobenzene (**23**) and its sterically more demanding *para tert*-butyl

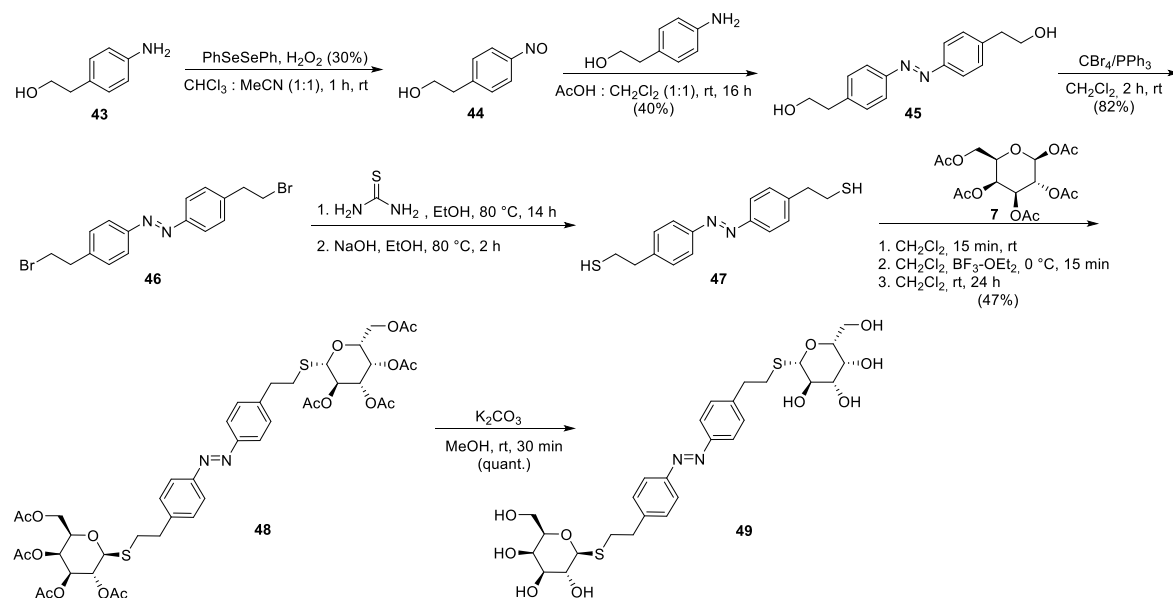
substituted derivative **24**^[47] were used affording the pentaacetylated β -D-thiogalactopyranoside azobenzenes **25–33** in low to moderate yields. Thereby, the *tert*-butyl group was introduced to increase the steric demand upon light-induced *trans*-*cis* isomerization. For synthetic reasons, the *tert*-butyl substitution was placed in *para* position as the *ortho*-substituted nitrosobenzene showed no product formation in the Mills reaction due to steric hindrance. To regain the free hydroxy groups necessary for the interaction with the biological target, the protected hydroxy groups were deacetylated in quantitative yield using potassium carbonate affording the desired photochromic thiogalactoside-based azobenzene derivatives **34–42**.^[48]



Scheme 3. Synthesis of asymmetric azobenzene-based PETG derivatives as competitive inhibitors for β -galactosidase (*E. coli*).^[43–47]

Synthesis of the symmetric azobenzene-based PETG derivative. As design for a sterically more demanding inhibitor with increased binding probability, a symmetrically phenethyl thiogalactopyranoside substituted azobenzene was synthesized. For the synthesis, a different synthetic strategy was used (Scheme 4). In a first step, the symmetric *para* hydroxyethyl substituted azobenzene **45** was synthesized. Therefore, commercially available *para* amino-phenethylalcohol **43**

was converted into its nitroso derivative **44** *via* organoselenium-catalyzed oxidation by hydrogen peroxide.^[49] The generated nitroso compound was subsequently reacted in a Mills reaction upon addition of amine **43** in acetic acid. The alcohol of the symmetric hydroxyethyl substituted azobenzene **45** was then converted to the bromide **46** using tetrabromomethane and triphenylphosphine. The thiol functional groups were introduced by reaction of **46** with thiourea followed by basic hydrolysis.^[50] The glycosylation of thiol **47** with pentaacetylated galactopyranoside **7** under activation of the Lewis acid boron trifluoride etherate yielded the symmetrically glycosylated ethylazobenzene **48**. Deacetylation of the hydroxy protecting groups under basic conditions afforded the desired symmetrical target compound **49**.^[48]



Scheme 4. Synthesis of the symmetric azobenzene-based PETG derivative as competitive inhibitor for β -galactosidase (*E. coli*).^[48-50]

3.2.2 Photochemical Characterization

Photoisomerization studies of the competitive photochromic β -galactosidase inhibitors **4**, **6**, **34-42**, and **49** were conducted in phosphate buffer and DMSO, respectively, by absorption and NMR-spectroscopy as well as HPLC-assisted analysis. Therefore, the dissolved compounds were irradiated with the indicated wavelengths to accumulate a substantial amount of their *cis* isomer until the

photostationary state (PSS) was reached. Thereby, the maximum representing the *trans* isomer decreased and a new shoulder in the visible range, characteristic for the *cis* isomer, evolved. For back isomerization the photochromic inhibitors were exposed to visible light. The resulting isosbestic points in the absorption spectra indicate a clear two-component switching without any degradation or formation of a side product.

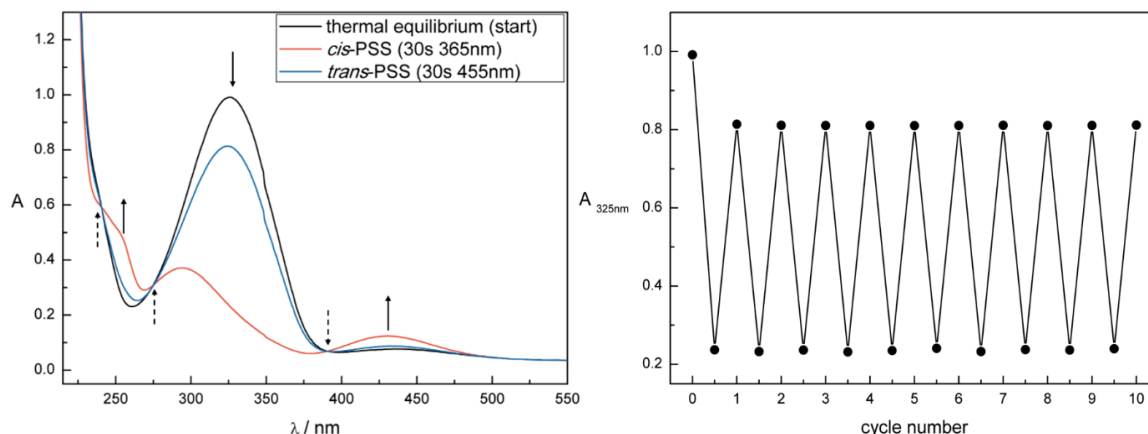


Figure 1. Photochromic properties of azobenzene-based PETG-derivative **37** (50 μ M in phosphate buffer + 0.1% DMSO). Left: UV-Vis absorption spectrum upon irradiation with $\lambda = 365$ nm until the *cis*-PSS is reached (30 s) and $\lambda = 455$ nm until the *trans*-PSS is reached (30 s). Black arrows indicate the characteristic changes in the absorption spectrum upon irradiation with the indicated wavelengths. Dotted black arrows indicate isosbestic points. Right: Repetitive switching cycles after alternate irradiation with UV ($\lambda = 365$ nm) and blue ($\lambda = 455$ nm) light determined at 325 nm.

For full UV-Vis absorption spectroscopic characterization see Figures S1-S12. In addition, the PSS was determined by HPLC and NMR measurements. The major photophysical properties of compounds **4**, **6**, **34-42**, and **49** are summarized in Table 1; for additional photochemical data see Supporting Information Tables S1-S3. All compounds showed excellent photochromic properties in DMSO, and phosphate buffer, respectively, with high photostationary states and fatigue resistance. Figure 1 shows exemplarily the UV-Vis absorption spectrum (left) and the cycle performance (right) for the competitive inhibitor **37**.

The thermal half-lives (THL) of the *cis* isomers of compounds **4**, **6**, **34-42**, and **49** were determined by monitoring the increase in absorbance which corresponds to the evolution of the *trans* isomer. The data indicate slow thermal reversal of the *cis*

isomer at room temperature (except compound **6**), which is beneficial because constant irradiation during the enzymatic testing can be avoided.

Table 1. Photochemical properties of azobenzene-based β -galactosidase inhibitors measured 50 μ M in phosphate buffer + 0.1% DMSO, and 1% DMSO (labeled by *), respectively. Cpd. = Compound.

Entry	Cpd.	λ_{\max} <i>trans</i> isomer [nm]	λ_{\max} <i>cis</i> isomer [nm]	Isosbestic points [nm]	THL	PSS distribution
1	4	323	425	237, 280, 385	536 h	67% <i>cis</i> (375 nm) ^(a) 75% <i>trans</i> (405 nm) ^(a)
2	6	379	-	279, 293, 335, 464	1.69 s	n.d.
3	34	325	431	234, 274, 390	98.2 h	93% <i>cis</i> (365 nm) ^(b) 74% <i>trans</i> (455 nm) ^(b)
4	35	329	426	238, 278, 396	252 h	88% <i>cis</i> (365 nm) ^(a) 72% <i>trans</i> (455 nm) ^(a)
5	36*	334	431	242, 287, 399	21.8 h	90% <i>cis</i> (365 nm) ^(b) 82% <i>trans</i> (455 nm) ^(b)
6	37	325	431	241, 275, 390	17.4 h	76% <i>cis</i> (365 nm) ^(b) 77% <i>trans</i> (455 nm) ^(b)
7	38	323	423	235, 273, 388	203 h	83% <i>cis</i> (365 nm) ^(a) 75% <i>trans</i> (455 nm) ^(a)
8	39*	335	434	245, 288, 399	25.3 h	90% <i>cis</i> (365 nm) ^(b) 82% <i>trans</i> (455 nm) ^(b)
9	40	322	428	235, 254, 273, 428	262 h	81% <i>cis</i> (365 nm) ^(a) 63% <i>trans</i> (455 nm) ^(a)
10	41	348	429	238, 280, 421	94.3 h	88% <i>cis</i> (365 nm) ^(a) 69% <i>trans</i> (455 nm) ^(a)
11	42*	352	433	241, 297, 432	37.0 h	90% <i>cis</i> (365 nm) ^(a) 76% <i>trans</i> (455 nm) ^(a)
12	49	338	430	240, 288, 407	104 h	93% <i>cis</i> (365 nm) ^(a) 74% <i>trans</i> (455 nm) ^(a)

(a) Determined by analytical HPLC measurement of a preirradiated 50 μ M solution at 20 °C. (b) Determined by NMR-measurement of a preirradiated sample in D₂O + 5% DMSO until the PSS was reached. n.d.: not detected due to fast thermal back relaxation.

3.2.3 Enzyme Inhibition

Based on the determined relative inhibitory activity (see Supporting Information Table S4) of the *trans* isomer in its thermal equilibrium and the *cis* isomer at its PSS of the competitive β -galactosidase inhibitors **4**, **6**, **34-42**, and **49**, the K_i values of the most promising derivatives were determined (Table 2).

Table 2. K_i [μ M] values of photochromic competitive β -galactosidase inhibitors. K_i was determined by varying the inhibitor concentration at three different substrate concentrations (50, 100, and 150 μ M). The standard deviation was calculated from the average of three independent measurements. Cpd. = Compound.

Entry	Cpd.	K_i [μ M] <i>trans</i> isomer	K_i [μ M] <i>cis</i> -PSS	Ratio (<i>cis/trans</i>)
1	34	0.7 ± 0.2	1.7 ± 0.5	2.4
2	37	0.06 ± 0.01	0.29 ± 0.08	4.8
3	41	62 ± 12	50 ± 11	0.8

From all tested photoswitchable inhibitors, the *ortho* substituted thiogalactosides with one (compound **37**) or two CH_2 spacers (compound **34**) between the sugar residue and the photochromic azobenzene part showed the strongest inhibition compared to the well-known inhibitor PETG, which has a K_i value of 7.2 μ M.^[34] Compared to PETG, the *trans* isomer of compound **34** had a 10x lower K_i (0.7 μ M) and the *trans* isomer of compound **37** a 100x lower K_i (60 nM). Irradiating both inhibitors with 365 nm until the *cis*-PSS was reached allowed the accumulation of a substantial amount of the sterically more demanding isomer, which increased the K_i values of **34** to 1.7 μ M (2.4x higher), and of **37** to 0.29 μ M (4.8x higher). The *trans* isomer of the *para* substituted thiogalactosyl compound **41** without CH_2 spacer had a 10x higher K_i compared to PETG. Switching to the *cis*-PSS had almost no effect on K_i as indicated by a *cis/trans* ratio of around 1. β -Galactosidase is a homotetramer comprising four identical active centers at the interface of two neighboring subunits. The large binding pockets make it difficult to design photochromic derivatives with high *cis/trans* ratios. Comparing the inhibitors **34**, **37**, and **41**, compound **41** is the least sterically demanding inhibitor, which resulted in no activity change upon switching the molecule (K_i ratio 1.2; Table 2). Changing the position of the azobenzene substitution from *para* (**41**) to *ortho* and extending the spacer length increased the *cis/trans* ratio by a factor of 2 for compound **34** (two CH_2 linking groups; ratio 2.4), and by a factor of 4 for compound **37** (one CH_2 linker; ratio 4.8). This implicates that the structural flexibility gained by one CH_2 group between sugar moiety and azobenzene (**37**) is sufficient for efficient binding into the enzyme's pocket.

3.2.4 Docking Experiments

Compound **37** was docked to the β -galactosidase in its *trans*- and *cis*-isomeric state using VINA docking^[51] as implemented in YASARA.^[52] The best-ranked *cis* isomer of **37** had an estimated dissociation constant of 31 nM, whereas the estimated dissociation constant of its best-ranked *trans* isomer is 27 nM, which supports a stronger binding of the *trans* isomer. Figure 2 indicates that the sugar moiety of the ligand fits well into the binding pocket and fills it completely. The two aromatic rings of azobenzene, which are involved in light-induced switching are located at the surface of the protein and protrude out of the binding pocket. This localization argues against a drastic effect in inhibitory activity upon light-induced isomerization.

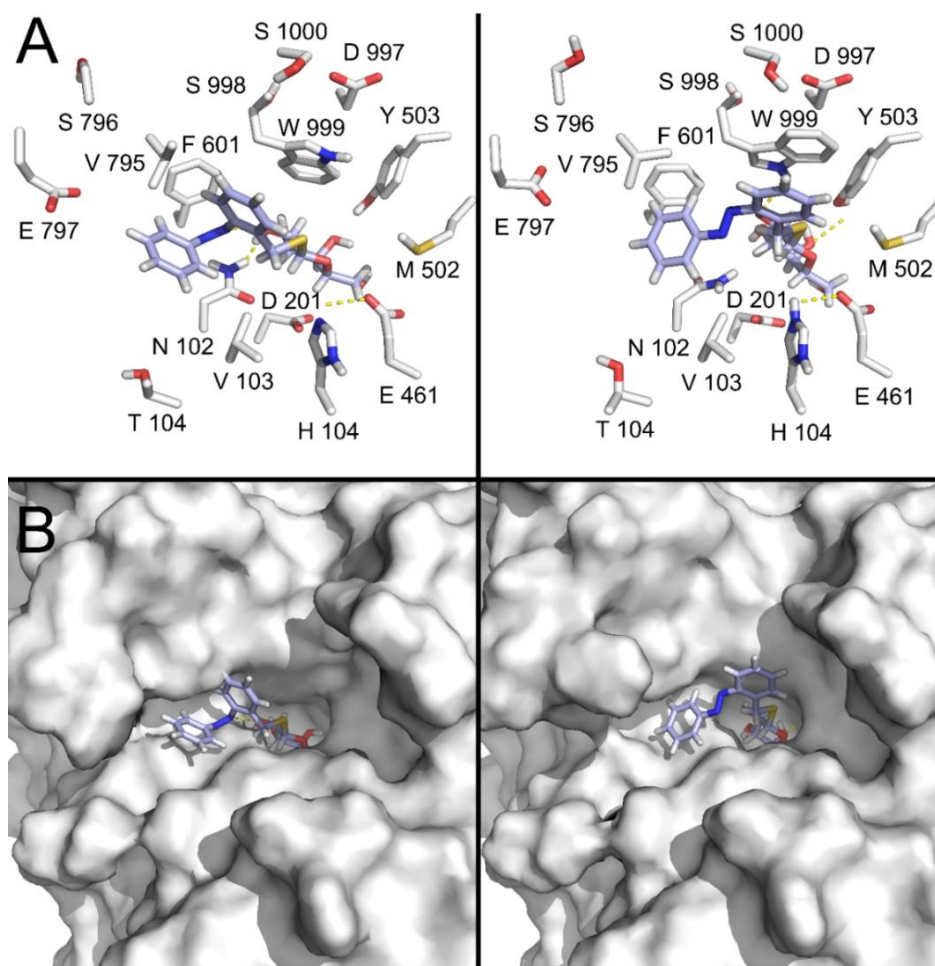


Figure 2. (A) A detailed view of the ligand **37** in its *cis*- (left panel) and *trans*-isomeric (right panel) state. The ligand is shown in blue; residues defined as flexible during docking are shown in white. Yellow dotted lines represent hydrogen bonds. (B) Surface view of the ligand in its *cis*- (left panel) and *trans*-isomeric (right panel) state.

3.3 Conclusion

In the presented work, we succeeded in the synthesis of thermally highly stable photochromic β -galactosidase inhibitors by modifying the chemical structure of potent inhibitors with an azobenzene moiety. All compounds show highly reversible photochromism in aqueous media with excellent fatigue resistance over ten measurement cycles. For the galactosylamine derivatives **4** and **6**, the high inhibitory activity of parent compound **2** (galactosylamine) could not be retained. In contrast, the PETG-based photochromic inhibitors **34-42** and **49** could be structurally optimized regarding their isomer-dependent activity by variation of their linker length, their substitution position, and their steric demand. Thereby, the photochromic moiety was first placed in *para* position to the inhibitory PETG moiety resulting in good inhibitory activity without significant isomer-dependent effect. To increase the effect of isomerization, the linker length was reduced resulting in a partial decrease of the inhibitory activity but no gain in isomer specific effects. Therefore, the switching moiety was placed in *ortho* position increasing on one hand inhibitory activity and on the other hand isomer dependent effects. Compound **37** could be identified as a highly inhibitory active photochromic PETG-derivative with 5-fold difference upon switching and a K_i value of 60 nM (*trans* isomer). Single-molecule experiments will provide additional information about the inhibition mechanism. Additional docking analysis explained the experimental observations.

3.4 Experimental Part

3.4.1 General Procedures and Materials

Commercial reagents and starting materials were purchased from the commercial suppliers abcr, Acros Organics, Alfa-Aesar, Fisher Scientific, Merck, Sigma Aldrich, TCI, or VWR and used without any further purification. Solvents were used in p.a. quality and dried according to common procedures, if necessary. Dry nitrogen was used as an inert gas atmosphere. Flash column chromatography was

performed using Sigma Aldrich MN silica gel 60 M (40-63 μm , 230-400 mesh) for normal phase chromatography. Reaction monitoring *via* thin layer chromatography was performed on alumina plates coated with silica gel (Merck silica gel 60 F₂₅₄, layer thickness 0.2 mm). Melting points were determined using a Stanford Research System OptiMelt MPA 100 and are uncorrected. NMR spectra were measured on a Bruker Avance 300 (¹H 300.13 MHz, ¹³C 75.48 MHz), Bruker Avance III HD 400 (¹H 400.13 MHz, ¹³C 100.61 MHz), Bruker Avance III HD 600 (¹H 600.25 MHz, ¹³C 150.95 MHz) and Bruker Avance III 600 (¹H 600.25 MHz, ¹³C 150.95 MHz). The spectra are referenced against the NMR solvent (DMSO-*d*₆: δ_{H} = 2.50 ppm, δ_{C} = 39.52 ppm; CDCl₃-*d*: δ_{H} = 7.26 ppm, δ_{C} = 77.16 ppm) and chemical shifts δ are reported in ppm. Resonance multiplicity is abbreviated as: s (singlet), d (doublet), t (triplet) and m (multiplet). Carbon NMR signals are assigned using DEPT 135 and ¹H-¹³C HSQC spectra with (+) for primary/tertiary, (-) for secondary, and (q) for quaternary carbons. Mass spectra were recorded on a Finnigan MAT-SSQ 710 A, ThermoQuest Finnigan TSQ 7000, Agilent Q-TOF 6540 UHD, or a Jeol AccuTOF GCX instrument. UV-Vis absorption spectroscopy was performed in 10 mm quartz cuvettes using an Agilent 8543, Agilent Cary 100, or Agilent Varian Cary 50 spectrometer. Analytical HPLC measurements were performed using an Agilent 1220 Infinity LC (column: Phenomenex Luna 3 μm C₁₈(2) 100 Å, 150 x 2.00 mm; flow 0.3 mL min⁻¹ at 20 °C for PSS determination or 30 °C for purity determination; solvent A: MilliQ water with 0.05 wt% TFA; solvent B: MeCN). The ratios at the PSSs were determined *via* analytical HPLC at 20 °C at the isosbestic points or *via* NMR spectroscopy. An Agilent 1260 system (column: Phenomenex Luna 10 μm C₁₈(2) 100 Å, 250 x 21.2 mm; flow: 22 mL min⁻¹; solvent A: MilliQ water; solvent B: MeCN) was used for preparative HPLC purification. Light sources for irradiation: λ = 365 nm (Seoul Viosys CUN6GB1A, 1000 mA, 1.4 W), λ = 385 nm (Seoul Viosys CUN8GF1A, 1000 mA, 1.6 W), λ = 455 nm (Osram OSOLON SSL 80 LD-CQ7P-1U3U, 1000 mA, 0.45 W), λ = 470 nm (Osram OSOLON SSL 80 LBCP7P-GYHY, 1000 mA, 50.4 lm), and λ = 505 nm (Osram OSOLON SSL 80 LVCK7P-JYKZ, 800 mA, 163 lm). The power of the light is given based on the

specifications supplied by the company when the LEDs were purchased. All tested final compounds possess a purity $\geq 93\%$ determined by HPLC measurements at 30 °C with detection at 220 nm or 254 nm, respectively.

Compounds **8**,^[43] **9**,^[44] **10**,^[44] **24**^[47] were prepared according to previously reported procedures.

3.4.2 Synthetic Procedures and Characterization

(2R,3R,4S,5R,6R)-2-amino-6-(hydroxymethyl)tetrahydro-2H-pyran-3,4,5-triol (2). Galactosylamine **2** was synthesized *via* an adapted literature reported procedure.^[40] Therefore, *D*-Galactose (1.0 g, 5.5 mmol, 1.0 eq) was dissolved in a solution of ammonia in methanol (40 mL, 7.0 M, 0.28 mol, 50 eq) and stirred at room temperature for 48 hours until a colorless solid precipitated. The product was filtered, washed with cold methanol (2 x 5.0 mL) and diethyl ether (2 x 5.0 mL) and dried *in vacuo* to afford **2** in its β -pyranose form in 63% yield (3.5 mmol, 0.62 g). The measured NMR spectrum was in accordance with the literature reported spectrum.

4-((E)-phenyldiazenyl)-N-((2R,3R,4S,5R,6R)-3,4,5-trihydroxy-6-hydroxymethyl)tetrahydro-2H-pyran-2-yl)benzamide (4). To a stirred solution of galactosylamine **2** (0.17 g, 0.94 mmol, 2.3 eq) and potassium carbonate (56 mg, 0.41 mmol, 1.0 eq) in water (2.0 mL) was added a solution of phenylazobenzoylchloride **3** (0.25 g, 1.0 mmol, 2.4 eq) in acetone (8.0 mL) and stirred at room temperature for 14 hours.^[41] Thin layer chromatography indicated complete consumption of the phenylazobenzoylchloride. Purification by column chromatography (CH₂Cl₂ + 5% MeOH) afforded the desired product which was further purified by preparative HPLC (column: Phenomenex Luna 10 μ m C₁₈(2) 100 Å, gradient 0-16 min 75:25 - 66:34, *t_R* = 12.5 min) to afford the product as orange solid in good yield (0.30 g, 0.77 mmol, 82%). M.p.: 189 °C. ¹H-NMR (400 MHz, DMSO-*d*₆): δ = 8.56 (d, *J* = 8.7 Hz, 1H), 8.10 (d, *J* = 8.3 Hz, 2H), 7.99 – 7.91 (m, 4H), 7.65 – 7.58 (m, 3H), 5.68 (dd, *J* = 8.7, 5.4 Hz, 1H), 5.02 – 4.92 (m, 1H), 4.69 – 4.50 (m, 2H), 4.40 (d, *J* = 4.5 Hz, 1H), 4.01 – 3.91 (m, 1H), 3.87 (s, 1H), 3.78 – 3.73 (m, 1H), 3.71 (t, *J* = 6.2 Hz, 1H), 3.57

– 3.50 (m, 1H), 3.44 – 3.38 (m, 1H). ^{13}C -NMR (101 MHz, $\text{DMSO}-d_6$): δ = 167.1 (q), 153.4 (q), 151.9 (q), 136.8 (q), 132.1 (+), 129.6 (+), 129.2 (+), 122.8 (+), 122.2 (+), 77.2 (+), 72.3 (+), 69.0 (+), 68.5 (+), 67.0 (+), 60.4 (-). HRMS (ESI) calcd. for $(\text{C}_{19}\text{H}_{22}\text{N}_3\text{O}_6)^+$ $[\text{M}+\text{H}]^+$: m/z = 388.1503; found 388.1502. MF: $\text{C}_{19}\text{H}_{21}\text{N}_3\text{O}_6$. MW: 387.39 g/mol.

(2R,3R,4S,5R,6R)-2-(hydroxymethyl)-6-((4-((E)-phenyldiazenyl)phenyl)amino) tetrahydro-2H-pyran-3,4,5-triol (6). Compound **6** was synthesized according to an adapted literature reported procedure.^[42] *Para* aminoazobenzene (1.0 g, 5.2 mmol, 1.0 eq) was added to a solution of β -D-galactose (0.90 g, 5.0 mmol, 1.0 eq) in a mixture of EtOH and water (20 mL, 3:1). The reaction was heated to reflux for four hours and at room temperature for additional 16 hours. The mixture was extracted with ethyl acetate (3x 20 mL). The organic phase was dried over MgSO_4 and the solvent was evaporated. The product was purified by column chromatography (CH_2Cl_2 + 5% MeOH) and preparative HPLC (column: Phenomenex Luna 10 μm C_{18} (2) 100 Å, gradient 0-12 min 10:90 -37:63, t_R = 10.0 min) to yield the desired product in good yield as orange solid (1.4 g, 3.9 mmol, 78%). M.p.: 131 °C. ^1H -NMR (400 MHz, $\text{DMSO}-d_6$): δ = 7.81 – 7.70 (m, 4H), 7.57 – 7.47 (m, 2H), 7.45 – 7.39 (m, 1H), 7.17 (d, J = 7.7 Hz, 1H), 6.90 – 6.82 (m, 2H), 4.81 (t, J = 5.2 Hz, 2H), 4.60 (t, J = 5.1 Hz, 1H), 4.54 – 4.41 (m, 2H), 3.76 (t, J = 3.8 Hz, 1H), 3.62 – 3.51 (m, 3H), 3.51 – 3.41 (m, 2H). ^{13}C -NMR (101 MHz, $\text{DMSO}-d_6$): δ = 152.8 (q), 151.5 (q), 144.2 (q), 130.2 (+), 129.7 (+), 125.2 (+), 122.3 (+), 113.5 (+), 85.0 (+), 76.3 (+), 74.8 (+), 70.5 (+), 68.9 (+), 61.0 (-). HRMS (ESI) calcd. for $(\text{C}_{18}\text{H}_{22}\text{N}_3\text{O}_5)^+$ $[\text{M}+\text{H}]^+$: m/z = 360.1554; found 360.1558. MF: $\text{C}_{18}\text{H}_{21}\text{N}_3\text{O}_5$. MW: 359.38 g/mol.

General procedure for the synthesis of pentaacetylated-thiogalactoside nitrobenzene precursors 11-16. The compounds were synthesized following an adapted literature procedure.^[45] To a solution of β -D-thiogalactoside **10** (2.0 g, 5.5 mmol, 1.0 eq) in CH_3CN (20 mL) was added the respective bromo-substituted nitrobenzene (6.0 mmol, 1.1 eq) and triethylamine (0.80 mL, 6.0 mmol, 1.1 eq) and stirred at room temperature until TLC indicated consumption of the starting material. The solvent was evaporated, and the mixture separated between water and ethyl acetate. The organic phase was dried (MgSO_4), the solvent evaporated,

and the residue purified by flash column chromatography (PE/EA 1/1) to afford the desired products in moderate to good yields.

(2R,3S,4S,5R,6S)-2-(acetoxymethyl)-6-((2-nitrophenethyl)thio)tetrahydro-2H-pyran-3,4,5-triyl triacetate (11). White foam: 76% yield; $^1\text{H-NMR}$ (300 MHz, CDCl_3 -*d*): δ = 7.95 (dd, J = 8.5, 1.4 Hz, 1H), 7.60 – 7.49 (m, 1H), 7.45 – 7.32 (m, 2H), 5.44 (dd, J = 3.4, 1.1 Hz, 1H), 5.25 (t, J = 10.0 Hz, 1H), 5.06 (dd, J = 10.0, 3.4 Hz, 1H), 4.58 (d, J = 9.9 Hz, 1H), 4.13 (dd, 2H), 4.04 – 3.92 (m, 1H), 3.33 – 3.12 (m, 2H), 3.11 – 2.95 (m, 1H), 2.98 – 2.77 (m, 1H), 2.15 (s, 3H), 2.05 (s, 3H), 1.99 (s, 3H), 1.97 (s, 3H). $^{13}\text{C-NMR}$ (75 MHz, CDCl_3 -*d*): δ = 170.5 (q), 170.4 (q), 170.1 (q), 169.7 (q), 149.2 (q), 135.1 (q), 133.4 (+), 132.7 (+), 127.9 (+), 125.1 (+), 84.5 (+), 74.7 (+), 72.0 (+), 67.4 (+), 67.3 (+), 61.6 (-), 34.7 (-), 31.0 (-), 20.9 (+), 20.8 (+), 20.8 (+), 20.7 (+). HRMS (ESI) calcd. for $(\text{C}_{22}\text{H}_{27}\text{NO}_{11}\text{SNa}^+)$ $[\text{M}+\text{Na}]^+$: m/z = 536.1197; found 536.1197. MF: $\text{C}_{22}\text{H}_{27}\text{NO}_{11}\text{S}$. MW: 513.51 g/mol.

(2R,3S,4S,5R,6S)-2-(acetoxymethyl)-6-((4-nitrophenethyl)thio)tetrahydro-2H-pyran-3,4,5-triyl triacetate (12). White foam: 82% yield; $^1\text{H-NMR}$ (400 MHz, CDCl_3 -*d*): δ = 8.03 (d, J = 8.7 Hz, 2H), 7.29 (d, J = 8.7 Hz, 2H), 5.34 (d, J = 3.4, 1.1 Hz, 1H), 5.15 (t, J = 10.0 Hz, 1H), 4.98 (dd, J = 10.0, 3.4 Hz, 1H), 4.45 (d, J = 9.9 Hz, 1H), 4.06 – 3.98 (m, 2H), 3.91 (t, 1H), 3.00 – 2.90 (m, 3H), 2.90 – 2.81 (m, 1H), 2.04 (s, 3H), 1.93 (s, 3H), 1.91 (s, 3H), 1.87 (s, 3H). $^{13}\text{C-NMR}$ (101 MHz, CDCl_3 -*d*): δ = 170.2 (q), 170.0 (q), 169.9 (q), 169.5 (q), 147.8 (q), 146.6 (q), 129.5 (+), 123.6 (+), 83.8 (+), 74.5 (+), 71.7 (+), 67.3 (+), 66.9 (+), 61.6 (-), 35.9 (-), 30.4 (-), 20.7 (+), 20.6 (+), 20.6 (+), 20.5 (+). HRMS (ESI) calcd. for $(\text{C}_{22}\text{H}_{27}\text{NO}_{11}\text{SNa}^+)$ $[\text{M}+\text{Na}]^+$: m/z = 536.1197; found 536.1196. MF: $\text{C}_{22}\text{H}_{27}\text{NO}_{11}\text{S}$. MW: 513.51 g/mol.

(2R,3S,4S,5R,6S)-2-(acetoxymethyl)-6-((2-nitrobenzyl)thio)tetrahydro-2H-pyran-3,4,5-triyl triacetate (13). White viscous solid: 72% yield; $^1\text{H-NMR}$ (300 MHz, CDCl_3 -*d*): δ = 7.92 (dd, J = 8.1, 1.5 Hz, 1H), 7.57 – 7.47 (m, 1H), 7.46 – 7.35 (m, 2H), 5.35 (dd, J = 3.3, 1.2 Hz, 1H), 5.17 (t, J = 10.0 Hz, 1H), 4.92 (dd, J = 10.0, 3.4 Hz, 1H), 4.30 (d, J = 10.0 Hz, 1H), 4.19 (s, 2H), 4.04 – 3.98 (m, 2H), 3.79 (td, J = 6.6, 1.2 Hz, 1H), 2.11 (s, 3H), 2.01 (s, 3H), 1.96 (s, 3H), 1.91 (s, 3H). $^{13}\text{C-NMR}$ (75 MHz, CDCl_3 -*d*):

δ = 170.4 (q), 170.2 (q), 170.0 (q), 169.6 (q), 148.7 (q), 133.5 (q), 133.0 (+), 132.2 (+), 128.6 (+), 125.3 (+), 83.2 (+), 74.5 (+), 71.7 (+), 67.2 (+), 67.0 (+), 61.4 (-), 31.3 (-), 20.7 (+), 20.7 (+), 20.7 (+), 20.6 (+). HRMS (ESI) calcd. for (C₂₁H₂₅NO₁₁SNa⁺) [M+Na]⁺: m/z = 522.1041; found 522.1044. MF: C₂₁H₂₅NO₁₁S. MW: 499.49 g/mol.

(2R,3S,4S,5R,6S)-2-(acetoxymethyl)-6-((4-nitrobenzyl)thio)tetrahydro-2H-pyran-3,4,5-triyl triacetate (14). White foam: 44% yield; ¹H-NMR (300 MHz, CDCl₃-d): δ = 8.19 – 8.13 (m, 2H), 7.51 – 7.45 (m, 2H), 5.41 (dd, J = 3.4, 1.2 Hz, 1H), 5.28 (t, J = 10.0 Hz, 1H), 4.99 (dd, J = 10.0, 3.4 Hz, 1H), 4.32 (d, J = 9.9 Hz, 1H), 4.12 – 4.00 (m, 3H), 3.95 – 3.84 (m, 2H), 2.15 (s, 3H), 2.05 (s, 3H), 2.04 (s, 3H), 1.96 (s, 3H). ¹³C-NMR (75 MHz, CDCl₃-d): δ = 170.3 (q), 170.1 (q), 170.0 (q), 169.7 (q), 147.2 (q), 144.9 (q), 130.0 (+), 123.8 (+), 82.4 (+), 74.7 (+), 71.6 (+), 67.2 (+), 66.9 (+), 61.5 (-), 32.8 (-), 20.8 (+), 20.7 (+), 20.7 (+), 20.6 (+). HRMS (ESI) calcd. for (C₂₁H₂₅NO₁₁SNa⁺) [M+Na]⁺: m/z = 522.1041; found 522.1045. MF: C₂₁H₂₅NO₁₁S. MW: 499.49 g/mol.

(2R,3S,4S,5R,6S)-2-(acetoxymethyl)-6-((2-nitrophenyl)thio)tetrahydro-2H-pyran-3,4,5-triyl triacetate (15). White viscous solid: 61% yield; ¹H-NMR (300 MHz, CDCl₃-d): δ = 8.09 (dd, J = 8.1, 1.5 Hz, 1H), 7.82 (dd, J = 8.1, 1.3 Hz, 1H), 7.57 (ddd, J = 8.1, 7.3, 1.5 Hz, 1H), 7.40 (ddd, J = 8.4, 7.3, 1.3 Hz, 1H), 5.48 (dd, J = 3.4, 1.0 Hz, 1H), 5.35 (t, J = 10.0 Hz, 1H), 5.10 (dd, J = 9.9, 3.3 Hz, 1H), 4.85 (d, J = 10.0 Hz, 1H), 4.22 – 4.10 (m, 2H), 4.08 – 4.02 (m, 1H), 2.17 (s, 3H), 2.06 (s, 3H), 2.03 (s, 3H), 1.98 (s, 3H). ¹³C-NMR (75 MHz, CDCl₃-d): δ = 170.3 (q), 170.1 (q), 170.0 (q), 169.3 (q), 148.4 (q), 133.2 (+), 132.5 (q), 130.2 (+), 127.1 (+), 125.5 (+), 84.6 (+), 74.7 (+), 71.9 (+), 67.1 (+), 66.4 (+), 61.8 (-), 20.7 (+), 20.7 (+), 20.7 (+), 20.6 (+). HRMS (ESI) calcd. for (C₂₀H₂₃NO₁₁SNa⁺) [M+Na]⁺: m/z = 508.0884; found 508.0882. MF: C₂₀H₂₃NO₁₁S. MW: 485.46 g/mol.

(2R,3S,4S,5R,6S)-2-(acetoxymethyl)-6-((4-nitrophenyl)thio)tetrahydro-2H-pyran-3,4,5-triyl triacetate (16). White foam: 68% yield; ¹H-NMR (400 MHz, DMSO-*d*₆): δ = 8.19 (d, J = 8.9 Hz, 2H), 7.66 (d, J = 9.0 Hz, 2H), 5.56 (d, J = 10.0 Hz, 1H), 5.42 – 5.38 (m, 1H), 5.31 (dd, J = 9.9, 3.4 Hz, 1H), 5.13 (t, J = 9.9 Hz, 1H), 4.47 – 4.40 (m, 1H), 4.14 – 4.01 (m, 2H), 2.15 (s, 3H), 2.05 (s, 3H), 2.01 (s, 3H), 1.94 (s, 3H). ¹³C-NMR

(101 MHz, DMSO- d_6): δ = 170.4 (q), 170.3 (q), 169.9 (q), 169.8 (q), 146.3 (q), 143.7 (q), 129.2 (+), 124.4 (+), 82.6 (+), 74.3 (+), 71.3 (+), 68.0 (+), 67.0 (+), 62.2 (-), 21.0 (+), 20.9 (+), 20.9 (+), 20.8 (+). HRMS (ESI) calcd. for (C₂₀H₂₃NO₁₁SN⁺) [M+Na]⁺: m/z = 508.0884; found 508.0882. MF: C₂₀H₂₃NO₁₁S. MW: 485.46 g/mol.

General procedure for reduction to pentaacetylated-thiogalactoside aminobenzenes 17-22. For the reduction of the nitro-groups of the pentaacetylated-thiogalactosides, nitrobenzenes **11-16** (4.0 mmol, 1.0 eq) were dissolved in a mixture of EtOH (60 mL) and CH₂Cl₂ (20 mL). Tin(II)chloride dihydrate (3.6 g, 16 mmol, 4.0 eq) was added and the mixture heated to reflux at 80 °C for four to six hours until TLC indicated complete consumption of the starting material and ninhydrin stain positive amine formation. The solvent was removed, and the residue portioned between EtOAc (200 mL) and NaHCO₃. The organic phase was dried over MgSO₄, the solvent was evaporated, and the crude product directly used in the next step without further purification.^[46]

General preparation for the formation of PETG-based azobenzene derivatives 34-42. The pentaacetylated-thiogalactoside aminobenzenes **17-22** (1.0 eq) and the respective nitrosobenzene (1.0 eq) were dissolved in a mixture of acetic acid and CH₂Cl₂ (1:1) and stirred at room temperature for 16 hours. The solvent was evaporated, and the product purified by flash column chromatography (CH₂Cl₂). Deprotection of the sugar-moiety was achieved by dissolving the protected compound in methanol and addition of potassium carbonate (0.50 eq).^[53] The crude products were purified by flash column chromatography (CH₂Cl₂ + 5% MeOH) and preparative HPLC (column: Phenomenex Luna 10 μ m C₁₈(2) 100 Å) to afford the desired products in moderate to good yields.

(2R,3R,4S,5R,6S)-2-(hydroxymethyl)-6-((2-((E)-phenyldiazenyl)phenethyl)thio) tetrahydro-2H-pyran-3,4,5-triol (34). Orange solid (51%). Gradient 0-20 min 10:90 -98:2, t_R = 11.7 min. M.p.: 139 °C. ¹H-NMR (400 MHz, DMSO- d_6): δ = 7.94 - 7.85 (m, 2H), 7.65 - 7.54 (m, 4H), 7.53 - 7.44 (m, 2H), 7.41 - 7.33 (m, 1H), 4.92 (d, J = 5.7 Hz, 1H), 4.76 (d, J = 5.6 Hz, 1H), 4.54 (t, J = 5.6 Hz, 1H), 4.38 (d, J = 4.4 Hz, 1H), 4.25 (d,

$J = 9.4$ Hz, 1H), 3.67 (t, $J = 3.9$ Hz, 1H), 3.52 – 3.32 (m, 6H), 3.29 – 3.19 (m, 1H), 3.00 – 2.83 (m, 2H). ^{13}C -NMR (101 MHz, DMSO- d_6): $\delta = 152.8$ (+), 149.9 (+), 141.0 (+), 132.1 (+), 131.9 (+), 131.6 (+), 130.0 (+), 127.8 (+), 123.1 (+), 115.5 (+), 86.3 (+), 79.6 (+), 75.2 (+), 70.3 (+), 68.8 (+), 61.0 (-), 32.4 (-), 31.7 (-). HRMS (ESI) calcd. for ($\text{C}_{20}\text{H}_{25}\text{N}_2\text{O}_5\text{S}^+$) $[\text{M}+\text{H}]^+$: $m/z = 405.1479$; found 405.1482. MF: $\text{C}_{20}\text{H}_{24}\text{N}_2\text{O}_5\text{S}$. MW: 404.48 g/mol.

(2R,3R,4S,5R,6S)-2-(hydroxymethyl)-6-((4-((E)-phenyldiazenyl)phenethyl)thio)tetrahydro-2H-pyran-3,4,5-triol (35). Orange solid (62%). Gradient 0-11 min 28:72 - 70:30, $t_R = 8.57$ min. M.p.: 162 °C. ^1H -NMR (400 MHz, DMSO- d_6): $\delta = 7.90$ – 7.86 (m, 2H), 7.85 – 7.81 (m, 2H), 7.62 – 7.53 (m, 3H), 7.51 – 7.45 (m, 2H), 4.97 (d, $J = 5.7$ Hz, 1H), 4.80 (d, $J = 5.6$ Hz, 1H), 4.60 (t, $J = 5.6$ Hz, 1H), 4.42 (d, $J = 4.4$ Hz, 1H), 4.29 (d, $J = 9.4$ Hz, 1H), 3.70 (t, $J = 3.9$ Hz, 1H), 3.52 (t, $J = 5.6$ Hz, 2H), 3.43 – 3.36 (m, 2H), 3.32 – 3.27 (m, 1H), 3.01 – 2.92 (m, 3H), 2.92 – 2.82 (m, 1H). ^{13}C -NMR (101 MHz, DMSO- d_6): $\delta = 152.4$ (-), 150.9 (-), 145.4 (-), 131.8 (+), 130.1 (+), 129.9 (+), 123.0 (+), 122.9 (+), 86.1 (+), 79.7 (+), 75.2 (+), 70.2 (+), 69.0 (+), 61.2 (-), 36.3 (-), 30.7 (-). HRMS (ESI) calcd. for ($\text{C}_{20}\text{H}_{24}\text{N}_2\text{O}_5\text{SNa}^+$) $[\text{M}+\text{Na}]^+$: $m/z = 427.1300$; found 427.1298. MF: $\text{C}_{20}\text{H}_{24}\text{N}_2\text{O}_5\text{S}$. MW: 404.48 g/mol.

(2R,3S,4S,5R,6S)-2-(acetoxymethyl)-6-((2-((E)-(4-(tert-butyl)phenyl)diazenyl)phenethyl)thio)tetrahydro-2H-pyran-3,4,5-triyl triacetate (36). Orange solid (19%). Gradient 0-20 min 10:90 - 98:2, $t_R = 15.7$ min. M.p.: 109 °C. ^1H -NMR (400 MHz, DMSO- d_6): $\delta = 7.83$ (d, $J = 8.6$ Hz, 2H), 7.62 (d, $J = 8.5$ Hz, 2H), 7.59 – 7.56 (m, 1H), 7.51 – 7.44 (m, 2H), 7.38 – 7.34 (m, 1H), 5.34 – 4.29 (m, 5H), 4.24 (d, $J = 9.4$ Hz, 1H), 3.67 (d, $J = 3.1$ Hz, 1H), 3.52 – 3.37 (m, 4H), 3.30 – 3.18 (m, 2H), 2.94 – 2.85 (m, 2H), 1.33 (s, 9H). ^{13}C -NMR (101 MHz, DMSO- d_6): $\delta = 154.5$ (q), 150.4 (q), 149.5 (q), 140.3 (q), 131.3 (+), 131.1 (+), 127.3 (+), 126.3 (+), 122.4 (+), 115.0 (+), 85.9 (+), 79.1 (+), 74.7 (+), 69.9 (+), 68.3 (+), 60.5 (-), 34.8 (q), 32.0 (-), 31.3 (-), 31.0 (+). HRMS (ESI) calcd. for ($\text{C}_{24}\text{H}_{32}\text{N}_2\text{O}_5\text{SNa}^+$) $[\text{M}+\text{Na}]^+$: $m/z = 483.1924$; found 483.1924. MF: $\text{C}_{24}\text{H}_{32}\text{N}_2\text{O}_5\text{S}$. MW: 460.59 g/mol.

(2R,3R,4S,5R,6S)-2-(hydroxymethyl)-6-((2-((E)-phenyldiazenyl)benzyl)thio)tetrahydro-2H-pyran-3,4,5-triol (37). Orange solid (22%). Gradient 0-20 min 10:90 - 98:2, $t_R = 11.1$ min. M.p.: 179 °C. $^1\text{H-NMR}$ (400 MHz, $\text{DMSO-}d_6$): $\delta = 7.96 - 7.91$ (m, 2H), 7.65 - 7.55 (m, 5H), 7.52 - 7.47 (m, 1H), 7.43 - 7.39 (m, 1H), 4.90 (d, $J = 5.9$ Hz, 1H), 4.76 (d, $J = 5.6$ Hz, 1H), 4.66 (t, $J = 5.6$ Hz, 1H), 4.44 - 4.38 (m, 2H), 4.33 (d, $J = 12.6$ Hz, 1H), 4.15 (d, $J = 9.5$ Hz, 1H), 3.68 (t, $J = 4.0$ Hz, 1H), 3.54 (t, $J = 5.8$ Hz, 2H), 3.41 - 3.33 (m, 2H), 3.23 - 3.18 (m, 1H). $^{13}\text{C-NMR}$ (101 MHz, $\text{DMSO-}d_6$): $\delta = 152.8$ (q), 149.5 (q), 139.5 (q), 131.9 (+), 131.8 (+), 131.6 (+), 129.9 (+), 128.3 (+), 123.3 (+), 115.7 (+), 84.7 (+), 79.7 (+), 75.2 (+), 70.4 (+), 68.9 (+), 61.1 (-), 28.6 (-). HRMS (ESI) calcd. for $(\text{C}_{19}\text{H}_{22}\text{N}_2\text{O}_5\text{SNa}^+)$ $[\text{M}+\text{Na}]^+$: $m/z = 413.1142$; found 413.1143. MF: $\text{C}_{19}\text{H}_{22}\text{N}_2\text{O}_5\text{S}$. MW: 390.45 g/mol.

(2R,3R,4S,5R,6S)-2-(hydroxymethyl)-6-((4-((E)-phenyldiazenyl)benzyl)thio)tetrahydro-2H-pyran-3,4,5-triol (38). Orange solid (52%). Gradient 0-20 min 10:90 - 98:2, $t_R = 10.6$ min. M.p.: 128 °C. $^1\text{H-NMR}$ (400 MHz, $\text{DMSO-}d_6$): $\delta = 7.93 - 7.80$ (m, 4H), 7.63 - 7.53 (m, 5H), 4.98 (d, $J = 5.9$ Hz, 1H), 4.79 (d, $J = 5.5$ Hz, 1H), 4.69 (t, $J = 5.7$ Hz, 1H), 4.44 (d, $J = 4.4$ Hz, 1H), 4.09 - 3.98 (m, 2H), 3.87 (d, $J = 13.0$ Hz, 1H), 3.68 (t, $J = 3.8$ Hz, 1H), 3.62 - 3.50 (m, 2H), 3.44 - 3.38 (m, 1H), 3.34 - 3.31 (m, 1H), 3.26 - 3.20 (m, 1H). $^{13}\text{C-NMR}$ (101 MHz, $\text{DMSO-}d_6$): $\delta = 152.4$ (q), 151.1 (q), 143.2 (q), 131.9 (+), 130.6 (+), 130.9 (+), 123.1 (+), 123.0 (+), 84.0 (+), 79.9 (+), 75.2 (+), 70.5 (+), 69.0 (+), 61.3 (-), 32.5 (-). HRMS (ESI) calcd. for $(\text{C}_{19}\text{H}_{22}\text{N}_2\text{O}_5\text{SNa}^+)$ $[\text{M}+\text{Na}]^+$: $m/z = 413.1142$; found 413.1143. MF: $\text{C}_{19}\text{H}_{22}\text{N}_2\text{O}_5\text{S}$. MW: 390.45 g/mol.

(2S,3R,4S,5R,6R)-2-((2-((E)-(4-(tert-butyl)phenyl)diazenyl)benzyl)thio)-6-(hydroxymethyl)tetrahydro-2H-pyran-3,4,5-triol (39). Light brown solid (16%). Gradient 0-20 min 10:90 - 98:2, $t_R = 14.8$ min. M.p.: 143 °C. $^1\text{H-NMR}$ (400 MHz, $\text{DMSO-}d_6$): $\delta = 7.90 - 7.82$ (m, 2H), 7.64 - 7.58 (m, 3H), 7.54 (dd, $J = 7.7, 1.5$ Hz, 1H), 7.46 (td, $J = 7.4, 1.4$ Hz, 1H), 7.39 (td, $J = 7.6, 1.5$ Hz, 1H), 4.88 (d, $J = 5.9$ Hz, 1H), 4.75 (d, $J = 5.6$ Hz, 1H), 4.66 (t, $J = 5.6$ Hz, 1H), 4.43 - 4.35 (m, 2H), 4.30 (d, $J = 12.6$ Hz, 1H), 4.14 (d, $J = 9.5$ Hz, 1H), 3.67 (t, $J = 3.9$ Hz, 1H), 3.53 (t, $J = 5.7$ Hz, 2H), 3.40 - 3.34 (m, 2H), 3.22 - 3.16 (m, 1H), 1.33 (s, 9H). $^{13}\text{C-NMR}$ (101 MHz, $\text{DMSO-}d_6$): $\delta = 154.5$ (q), 150.4 (q), 149.1 (q), 138.8 (q), 131.1 (+), 131.1 (+), 127.8 (+), 126.3 (+),

122.6 (+), 115.2 (+), 84.3 (+), 79.3 (+), 74.7 (+), 70.0 (+), 68.4 (+), 60.6 (-), 34.8 (q), 31.0 (+), 28.2 (-). HRMS (ESI) calcd. for (C₂₃H₃₀N₂O₅SNa⁺) [M+Na]⁺: m/z = 469.1768; found 469.1769. MF: C₂₃H₃₀N₂O₅S. MW: 446.56 g/mol.

(2R,3R,4S,5R,6S)-2-(hydroxymethyl)-6-((2-((E)-phenyldiazenyl)phenyl)thio)tetrahydro-2H-pyran-3,4,5-triol (40). Orange solid (16%). Gradient 0-10 min 32:68 - 78:22, t_R = 5.8 min. M.p.: 166 °C. ¹H-NMR (400 MHz, DMSO-*d*₆): δ = 7.90 - 7.86 (m, 2H), 7.72 (dd, *J* = 8.2, 1.2 Hz, 1H), 7.64 - 7.56 (m, 4H), 7.47 (ddd, *J* = 8.3, 7.3, 1.5 Hz, 1H), 7.27 (ddd, *J* = 8.2, 7.2, 1.2 Hz, 1H), 5.26 (d, *J* = 6.0 Hz, 1H), 4.96 (s, 1H), 4.86 (d, *J* = 9.7 Hz, 1H), 4.67 (t, *J* = 5.4 Hz, 1H), 4.55 (d, *J* = 4.5 Hz, 1H), 3.77 (t, *J* = 3.7 Hz, 1H), 3.64 - 3.48 (m, 4H), 3.46 - 3.41 (m, 1H). ¹³C-NMR (101 MHz, DMSO-*d*₆): δ = 152.6 (q), 148.6 (q), 139.7 (q), 132.5 (+), 132.1 (+), 130.0 (+), 127.8 (+), 125.7 (+), 123.2 (+), 116.6 (+), 85.3 (+), 79.6 (+), 75.3 (+), 69.7 (+), 68.9 (+), 61.0 (-). HRMS (ESI) calcd. for (C₁₈H₂₀N₂O₅SNa⁺) [M+Na]⁺: m/z = 399.0985; found 399.0986. MF: C₁₈H₂₀N₂O₅S. MW: 376.43 g/mol.

(2R,3R,4S,5R,6S)-2-(hydroxymethyl)-6-((4-((E)-phenyldiazenyl)phenyl)thio)tetrahydro-2H-pyran-3,4,5-triol (41). Orange solid (54%). Gradient 0-10 min 23:77 - 67:33, t_R = 8.2 min. M.p.: 188 °C. ¹H-NMR (400 MHz, DMSO-*d*₆): δ = 7.90 - 7.85 (m, 2H), 7.85 - 7.81 (m, 2H), 7.65 - 7.54 (m, 5H), 5.26 (d, *J* = 6.1 Hz, 1H), 4.94 (d, *J* = 5.7 Hz, 1H), 4.78 (d, *J* = 9.6 Hz, 1H), 4.68 (t, *J* = 5.4 Hz, 1H), 4.55 (d, *J* = 4.4 Hz, 1H), 3.75 (t, *J* = 3.9 Hz, 1H), 3.60 - 3.49 (m, 4H), 3.44 - 3.38 (m, 1H). ¹³C-NMR (101 MHz, DMSO-*d*₆): δ = 152.4 (q), 150.2 (q), 141.3 (q), 131.9 (+), 129.9 (+), 129.1 (+), 123.4 (+), 123.0 (+), 87.1 (+), 79.8 (+), 75.1 (+), 69.6 (+), 68.9 (+), 61.0 (-). HRMS (ESI) calcd. for (C₁₈H₂₁N₂O₅S⁺) [M+H]⁺: m/z = 377.1166; found 377.1164. MF: C₁₈H₂₀N₂O₅S. MW: 376.43 g/mol.

(2S,3R,4S,5R,6R)-2-((4-((E)-(4-(tert-butyl)phenyl)diazenyl)phenyl)thio)-6-(hydroxymethyl)tetrahydro-2H-pyran-3,4,5-triol (42). Orange solid (39%). Gradient 0-20 min 10:90 - 98:2, t_R = 9.7 min. M.p.: 146 °C. ¹H-NMR (400 MHz, DMSO-*d*₆): δ = 7.85 - 7.77 (m, 4H), 7.64 - 7.58 (m, 4H), 5.26 (d, *J* = 6.0 Hz, 1H), 4.94 (d, *J* = 5.3 Hz, 1H), 4.77 (d, *J* = 9.6 Hz, 1H), 4.68 (t, *J* = 5.5 Hz, 1H), 4.55 (d, *J* = 4.4 Hz, 1H), 3.75 (t,

$J = 3.8$ Hz, 1H), 3.58 – 3.48 (m, 4H), 3.44 – 3.39 (m, 1H), 1.33 (s, 9H). ^{13}C -NMR (101 MHz, DMSO- d_6): $\delta = 154.9$ (q), 150.4 (q), 150.3 (q), 140.8 (q), 129.2 (+), 126.7 (+), 123.3 (+), 122.8 (+), 87.2 (+), 79.8 (+), 75.1 (+), 69.7 (+), 68.8 (+), 61.0 (-), 35.3 (+), 31.4 (+). HRMS (ESI) calcd. for ($\text{C}_{22}\text{H}_{28}\text{N}_2\text{O}_5\text{SNa}^+$) $[\text{M}+\text{Na}]^+$: $m/z = 455.1611$; found 455.1610. MF: $\text{C}_{22}\text{H}_{28}\text{N}_2\text{O}_5\text{S}$. MW: 432.54 g/mol.

(*E*)-2,2'-(diazene-1,2-diylbis(4,1-phenylene))bis(ethan-1-ol) (45). The symmetric phenethyl-alcohol azobenzene **45** was synthesized in a twostep procedure starting from 2-(4-aminophenyl)ethan-1-ol (**43**). In order to perform a Mills reaction the amino-group of **43** was transformed into its nitroso derivative following an adapted literature procedure.^[49] The PhSeSePh catalyst (57 mg, 5.0 mol-%), the aniline **43** (0.50 g, 3.6 mmol, 1.0 eq), and 30% aqueous H_2O_2 (0.24 mL, 7.9 mmol, 2.2 eq) were mixed $\text{CHCl}_3/\text{MeCN}$ (1:1, 5.0 mL) and stirred at room temperature for one hour. The solvent was evaporated and the generated nitroso **44** was used without further purification. For the following Mills reaction, the nitroso-derivative **44** was dissolved in acetic acid (15 mL) and the aniline **43** (0.50 g, 3.6 mmol, 1.0 eq) was added and the mixture stirred at room temperature for 16 hours. Purification by flash column chromatography (CH_2Cl_2) afforded the desired product **45** as orange solid in moderate yield (0.39 g, 1.4 mmol, 40%). ^1H -NMR (400 MHz, DMSO- d_6): $\delta = 7.80$ (d, $J = 8.3$ Hz, 4H), 7.43 (d, $J = 8.4$ Hz, 4H), 4.70 (t, $J = 5.2$ Hz, 2H), 3.71 – 3.60 (m, 4H), 2.82 (t, $J = 6.9$ Hz, 4H). ^{13}C -NMR (101 MHz, DMSO- d_6): $\delta = 150.4$ (q), 143.6 (q), 129.9 (+), 122.3 (+), 61.8 (-), 38.8 (-). HRMS (ESI) calcd. for ($\text{C}_{16}\text{H}_{18}\text{N}_2\text{O}_2\text{Na}^+$) $[\text{M}+\text{Na}]^+$: $m/z = 293.1260$; found 293.1261. MF: $\text{C}_{16}\text{H}_{18}\text{N}_2\text{O}_2$. MW: 270.33 g/mol.

(*E*)-1,2-bis(4-(2-bromoethyl)phenyl)diazene (46). Compound **46** was synthesized according to a literature adapted procedure.^[50] A solution of triphenyl phosphine (1.1 g, 4.2 mmol, 3.0 eq) was dissolved in anhydrous CH_2Cl_2 (10 mL) and added to a suspension of the symmetric phenethyl alcohol azobenzene **45** (0.39 g, 1.4 mmol, 1.0 eq) and tetra bromomethane (1.1 g, 3.4 mmol, 2.4 eq) in anhydrous CH_2Cl_2 (20 mL) under an inert gas atmosphere. The reaction mixture was stirred at room temperature for two hours until TLC indicated full conversion of the starting

material. The solution was diluted with CH_2Cl_2 , filtered, and concentrated under reduced pressure. Purification by flash column chromatography (CH_2Cl_2) and evaporation of the solvent afforded the desired product **46** as red solid in high yield (0.46 g, 1.1 mmol, 82%). ^1H -NMR (300 MHz, $\text{DMSO}-d_6$): δ = 7.84 (d, J = 8.3 Hz, 4H), 7.50 (d, J = 8.4 Hz, 4H), 3.80 (t, J = 7.1 Hz, 4H), 3.24 (t, J = 7.1 Hz, 4H). ^{13}C -NMR (75 MHz, $\text{DMSO}-d_6$): δ = 150.8 (q), 142.7 (q), 129.9 (+), 122.5 (+), 38.0 (-), 34.2 (-). HRMS (ESI) calcd. for $(\text{C}_{16}\text{H}_{16}\text{N}_2\text{Br}_2\text{Na}^+)$ $[\text{M}+\text{Na}]^+$: m/z = 418.9553; found 418.9554. MF: $\text{C}_{16}\text{H}_{16}\text{N}_2\text{Br}_2$. MW: 396.13 g/mol.

(2*R*,2'*R*,3*R*,3'*R*,4*S*,4'*S*,5*R*,5'*R*,6*S*,6'*S*)-6,6'-((((*E*)-diazene-1,2-diyl)bis(4,1-phenylene))bis(ethane-2,1-diyl))bis(sulfanediyl))bis(2-(hydroxymethyl)tetrahydro-2*H*-pyran-3,4,5-triol) (49). The compound was synthesized in a two-step procedure starting from **46** following a literature adapted procedure. Under a nitrogen atmosphere thiourea (0.36 g, 4.4 mmol, 4.0 eq) was added to a solution of symmetric bromoethylazobenzene **46** (0.46 g, 1.1 mmol, 1.0 eq) in ethanol (20 mL) and heated to reflux for 16 hours. 10% aqueous NaOH (20 mL) was added and the solution heated to reflux for additional two hours.^[50] The solvent was removed under reduced pressure and the residue extracted with CH_2Cl_2 and water. The organic phase was dried (MgSO_4), filtered, and concentrated under reduced pressure. The orange product (0.24 g, 0.78 mmol, 71%) was directly used in the next step without further purification to avoid disulfide formation or degradation. (*E*)-2-2'-(diazene-1,2-diylbis(4,1-phenylene))bis(ethane-1-thiol) (**47**) (0.24 g, 0.78 mmol, 1.0 eq) was added to a solution of 1,2,3,4,6-penta-*O*-acetyl-*D*-galactose (**7**) (0.61 g, 1.6 mmol, 2.0 eq) in CH_2Cl_2 (7.0 mL). The reaction mixture was stirred for 15 minutes at room temperature, cooled to 0 °C and boron trifluoride diethyl etherate (2.0 mL, 5.5 mmol, 7.0 eq) was added dropwise. The mixture was stirred for 15 minutes, warmed to room temperature, and stirred for additional 24 hours. The reaction mixture was diluted with CH_2Cl_2 and poured into ice water under stirring. The organic phase was separated, washed with saturated NaHCO_3 , water, dried (Na_2SO_4), filtered, and concentrated.^[53] Purification by flash column chromatography (CH_2Cl_2 + 10% MeOH) and evaporation of the solvent afforded

the pentaacetylated galactopyranose azobenzene derivative **48** (0.36 g, 0.37 mmol, 47%) as orange solid. Deacetylation was achieved by dissolving the compound in MeOH (10 mL) and addition of potassium carbonate (51 mg, 0.37 mmol, 1.0 eq). The reaction mixture was stirred at room temperature for 30 minutes, filtered, and concentrated under reduced pressure. Purification by preparative HPLC (gradient 0-9 min 10:90 – 60:40, t_R = 8.06 min) afforded the desired product as orange solid in quantitative yield (0.23 g, 0.37 mmol). M.p.: 202 °C. $^1\text{H-NMR}$ (400 MHz, DMSO- d_6): δ = 7.81 (d, J = 8.3 Hz, 4H), 7.47 (d, J = 8.4 Hz, 4H), 4.96 (d, J = 5.7 Hz, 2H), 4.79 (d, J = 5.4 Hz, 2H), 4.60 (t, J = 5.6 Hz, 2H), 4.41 (d, J = 4.4 Hz, 2H), 4.28 (d, J = 9.4 Hz, 2H), 3.69 (t, J = 3.9 Hz, 2H), 3.51 (t, J = 5.4 Hz, 4H), 3.42 – 3.35 (m, 4H), 3.32 – 3.27 (m, 2H), 3.02 – 2.92 (m, 6H), 2.91 – 2.81 (m, 2H). $^{13}\text{C-NMR}$ (101 MHz, DMSO- d_6): δ = 151.0 (q), 145.1 (q), 130.1 (+), 122.9 (+), 86.1 (+), 79.7 (+), 75.2 (+), 70.2 (+), 68.9 (+), 61.1 (-), 36.3 (-), 30.7 (-). HRMS (ESI) calcd. for ($\text{C}_{28}\text{H}_{39}\text{N}_2\text{O}_{10}\text{S}_2^+$) $[\text{M}+\text{H}]^+$: m/z = 627.2041; found 627.2040. MF: $\text{C}_{28}\text{H}_{38}\text{N}_2\text{O}_{10}\text{S}_2$. MW: 626.74 g/mol.

3.4.3 Enzymatic Inhibition Studies

A 2 μM β -galactosidase stock solution was diluted to 720 pM in sterile filtered assay buffer (137 mM NaCl, 10 mM Na_2HPO_4 , 2 mM KH_2PO_4 , 2.7 mM KCl, pH 7.5) containing 0.05 mg mL^{-1} bovine serum albumin, 0.005% Tween 20 and 1 mM MgCl_2 . Prior to each measurement, 10 μl of β -galactosidase was added to 190 μl of substrate or substrate/inhibitor mix resulting in a final enzyme concentration of 36 pM. Inhibitors were dissolved in DMSO to a concentration of 20 mM, diluted in assay buffer and mixed either directly 1:1 with the substrate (*trans* isomer in its thermal equilibrium) or irradiated at 365 nm for 1 minute in a fused silica microplate and then mixed with the substrate (*cis* isomer at its photostationary state). Fluorescence measurements (λ_{Ex} : 565 nm; λ_{Em} : 590 nm) were performed in a Synergy neo 2 multi-mode microplate reader (BioTek) at 25 °C. The formation of the fluorescent product resorufin was observed in intervals of 30 seconds over a period of 5 minutes. The inhibitory activity of all compounds was pre-tested at a concentration of typically 100 μM (Table S4). Three of these compounds showed a high inhibitory activity and were investigated in detail. The initial increase of the

fluorescence was normalized to the uninhibited reaction and the inhibitor concentrations $[I]$ were varied at three different substrate concentrations ($[S] = 50, 100$ and $150 \mu\text{M}$). K_i values were determined by non-linear regression using the Michaelis Menten model for competitive inhibition (Eq. 1). The velocity at substrate saturation (V_{\max}) was set to 1000 s^{-1} [31] and the Michaelis constant K_M was determined as a curve fit parameter.

$$v = \frac{V_{\max} \cdot [S]}{K_M \cdot \left(1 + \frac{[I]}{K_i}\right) + [S]} \quad \text{Eq. 1}$$

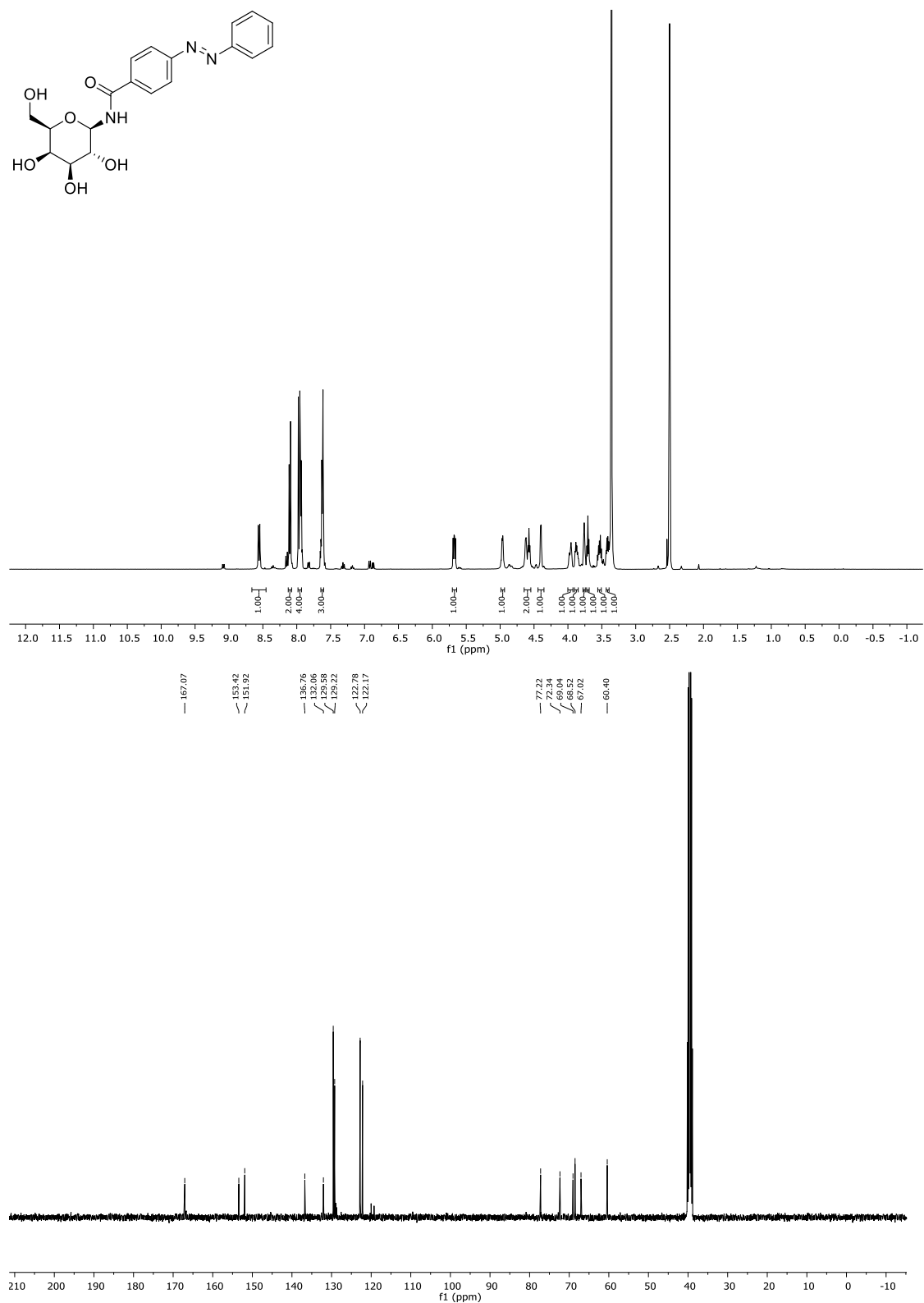
3.4.4 Molecular Docking

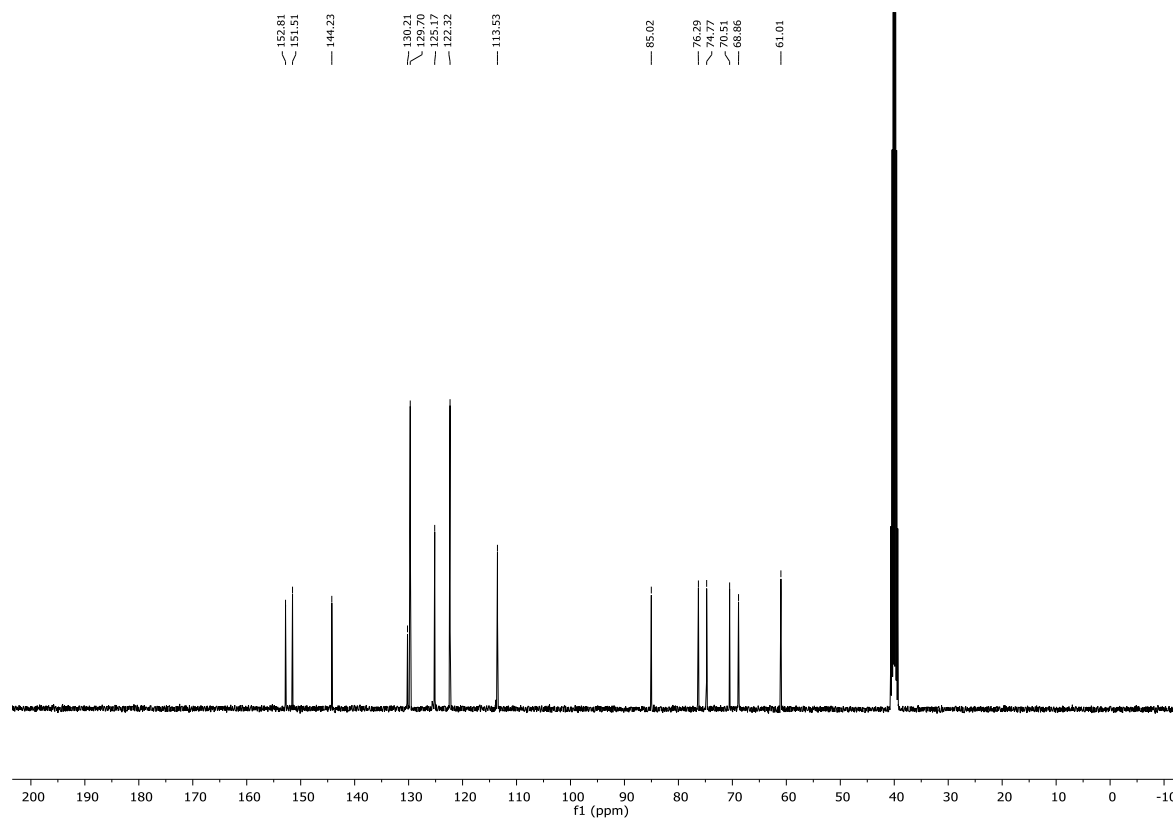
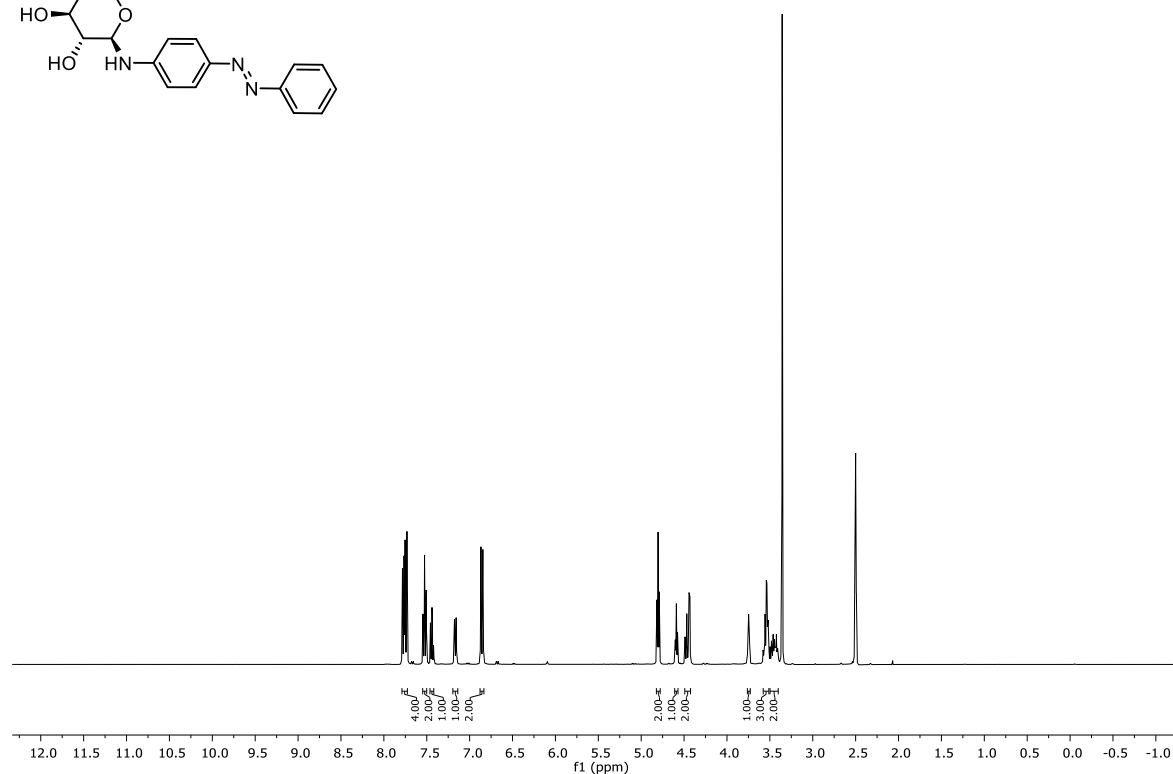
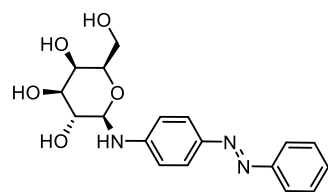
The ligands were docked to an ensemble of β -galactosidases using VINA^[51] as implemented in YASARA^[52]. The ensemble consisted of the following 3D structures indicated by their PDB IDs: 1dp0, 1f4a, 1f4h, 1hn1, 1jyn, 1jyv, 1jyw, 1jyx, 1jz2, 1jz3, 1jz4, 1jz5, 1jz6, 1jz7, 1jz8, 1px3, 1px4, 3czj, 3dym, 3dyo, 3dyp, 3e1f, 3i3b, 3i3d, 3i3e, 3iap, 3iaq, 3j7h, 3muy, 3muz, 3mv0, 3mv1, 3sep, 3t08, 3t09, 3t0a, 3t0b, 3t0d, 3t2o, 3t2p, 3t2q, 3vd3, 3vd4, 3vd5, 3vd7, 3vd9, 3vda, 3vdb, 3vdc, 4ckd, 4duv, 4duw, 4dux, 4ttg, 5a1a. Residues with a distance of $\leq 10 \text{ \AA}$ to the ligand-binding site were made flexible; all other ones were kept rigid. For a comprehensive sampling of the search space, every ligand was docked 32 times to each receptor, resulting in 1760 dockings per ligand. The results were ranked according to their estimated dissociation constant.

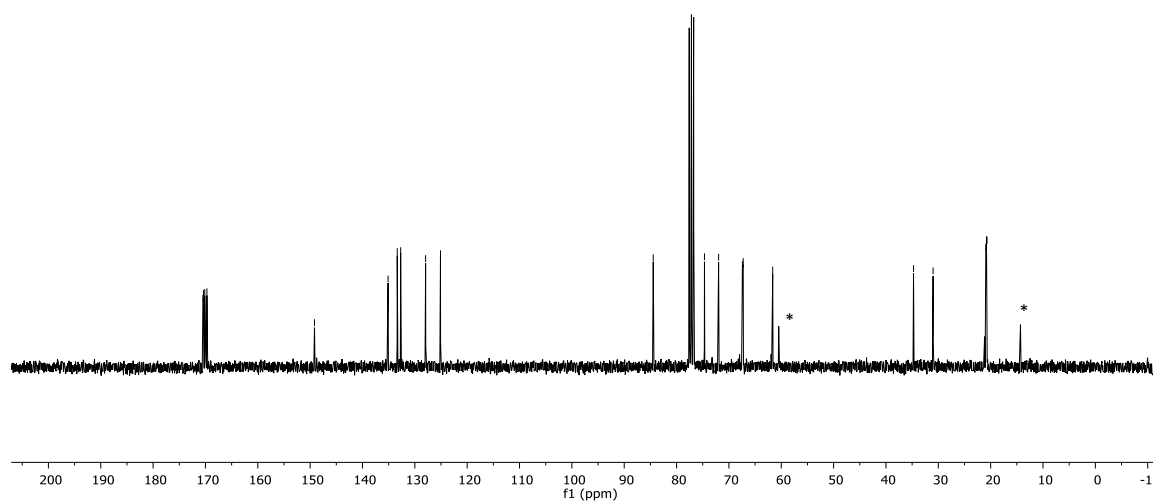
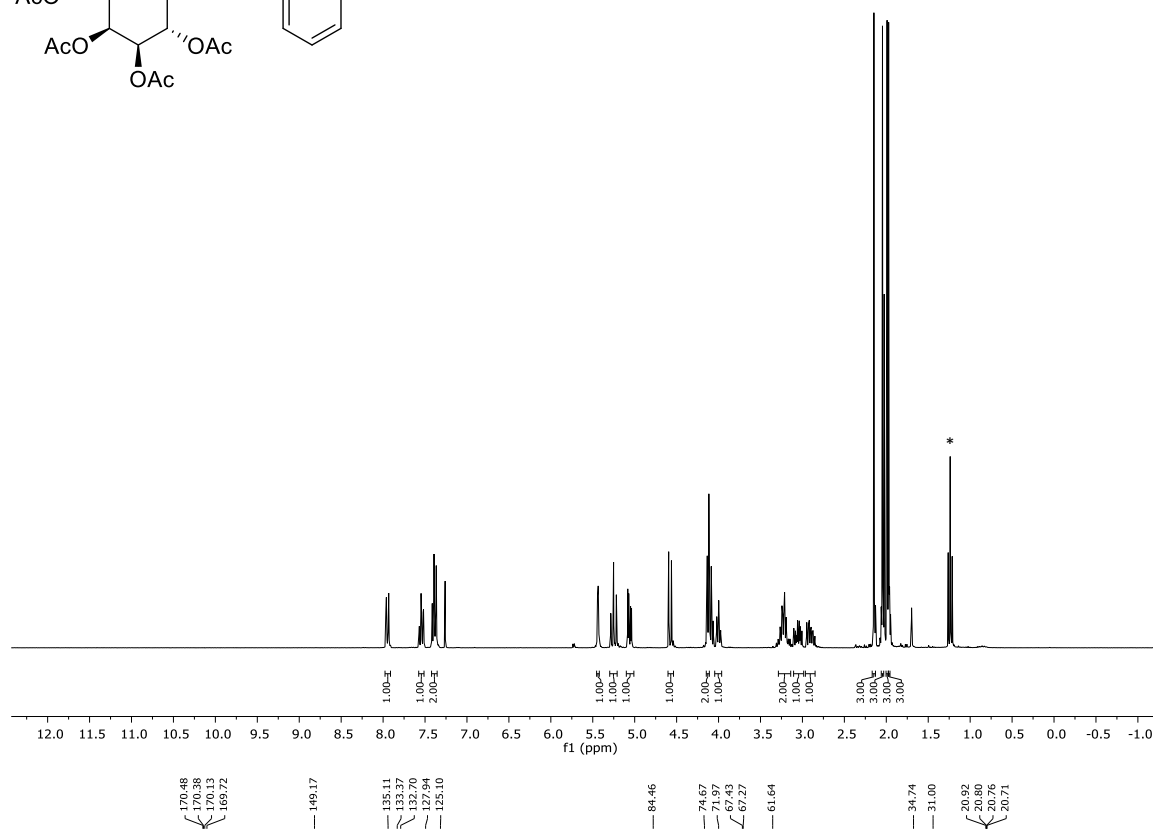
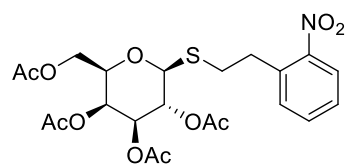
3.5 Supporting Information

3.5.1 ^1H - and ^{13}C -NMR Spectra

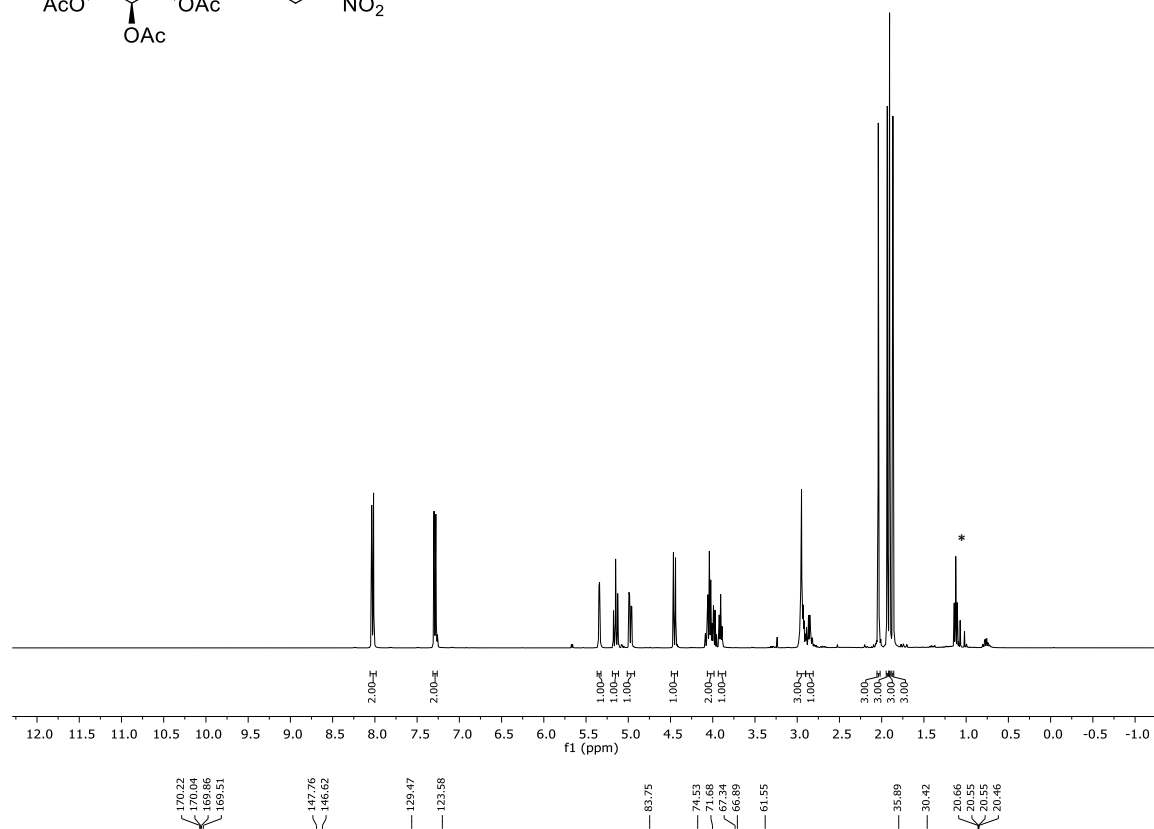
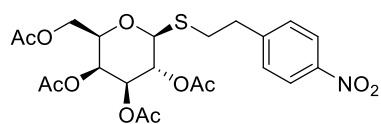
Compound **4** ($\text{DMSO-}d_6$)

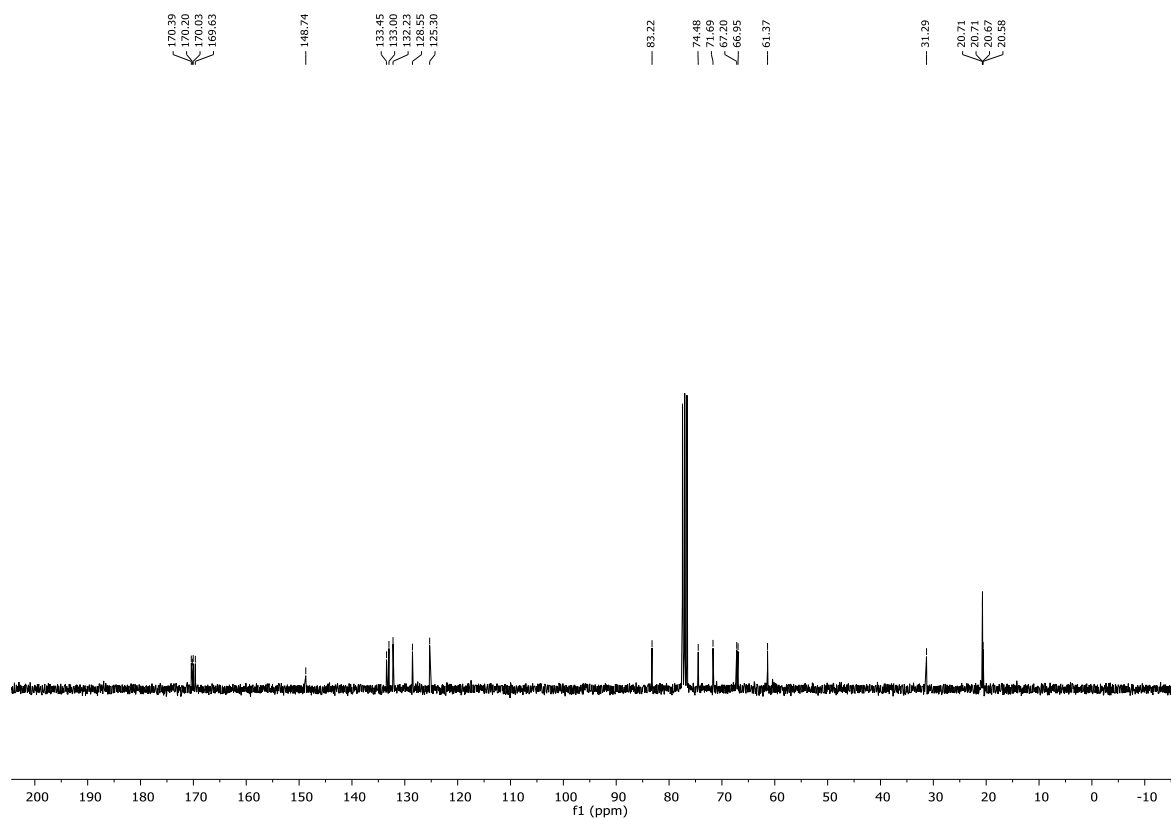
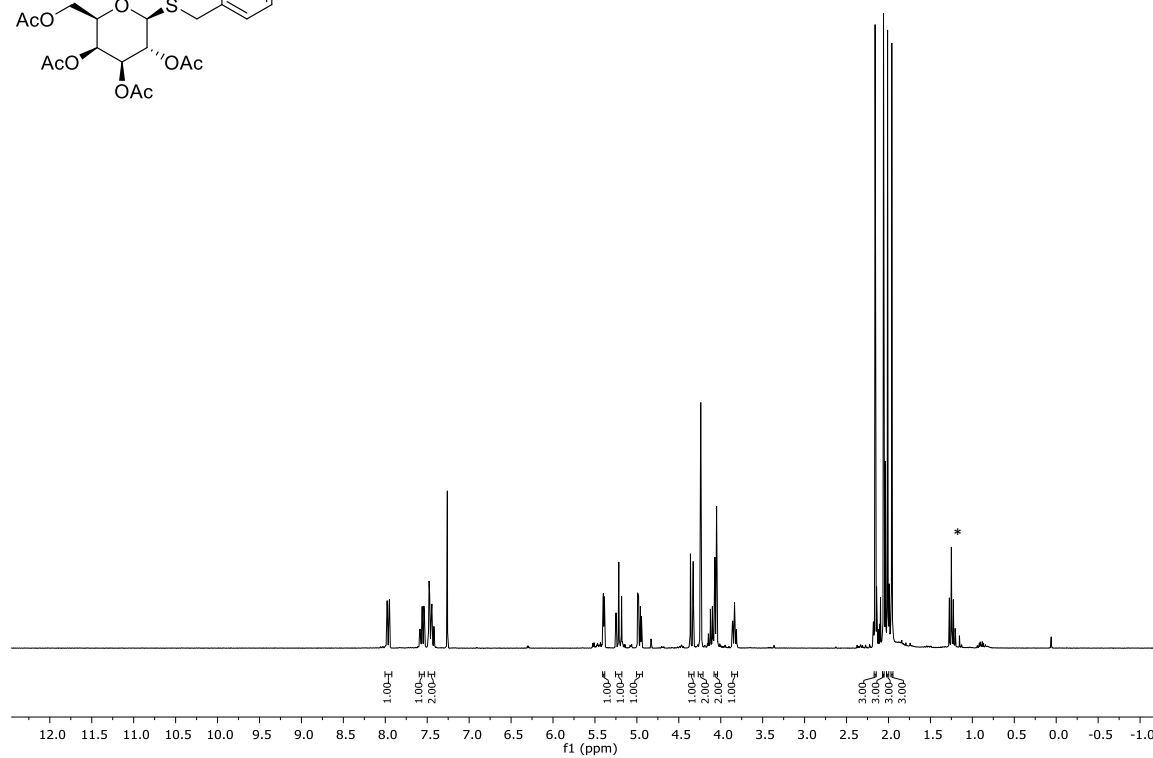
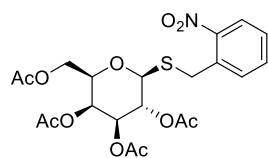


Compound 6 (DMSO- d_6)

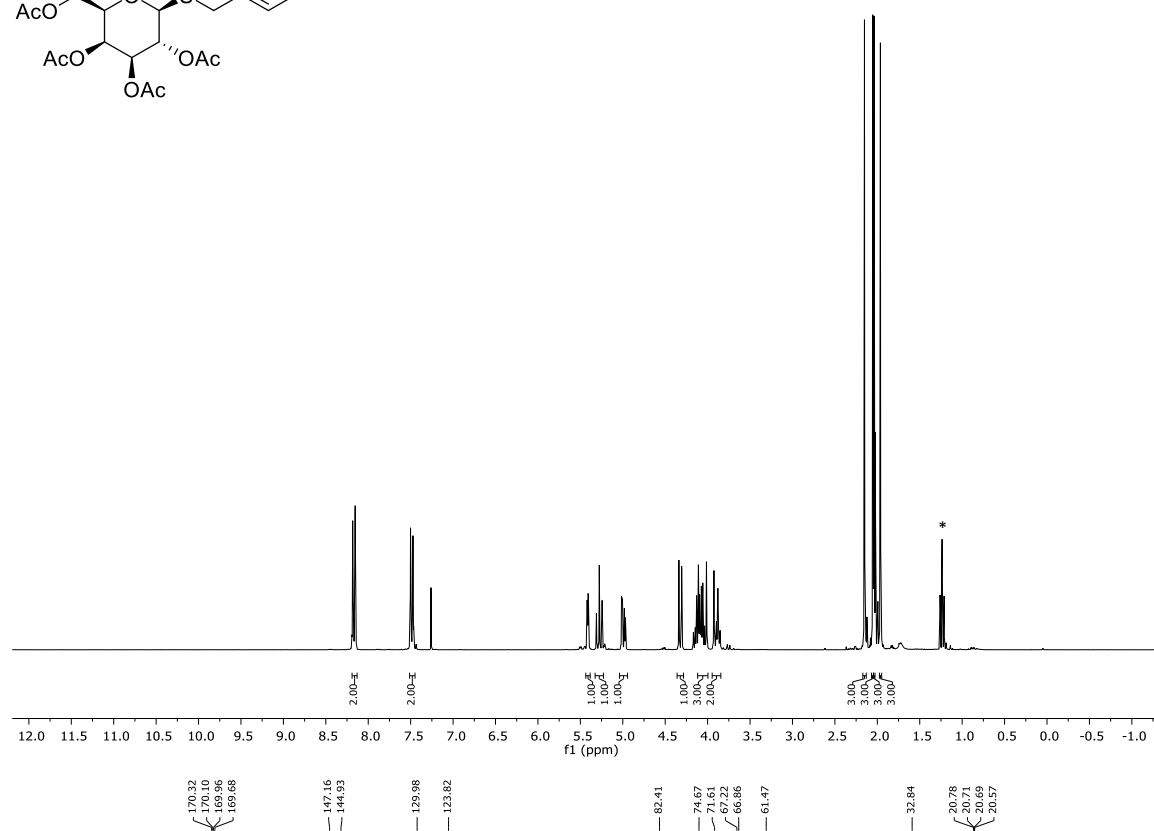
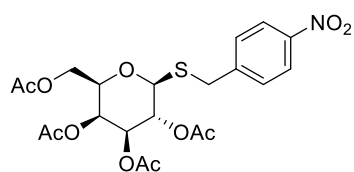
Compound **11** (CDCl₃-d)

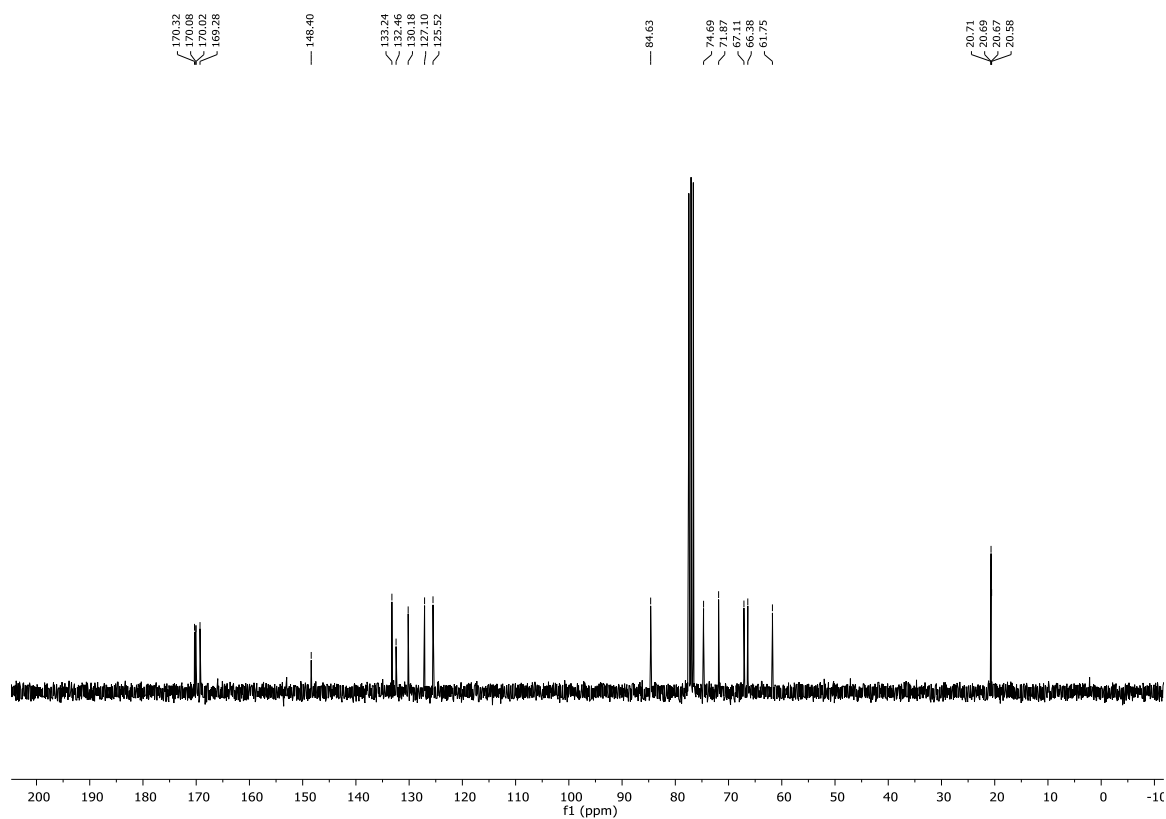
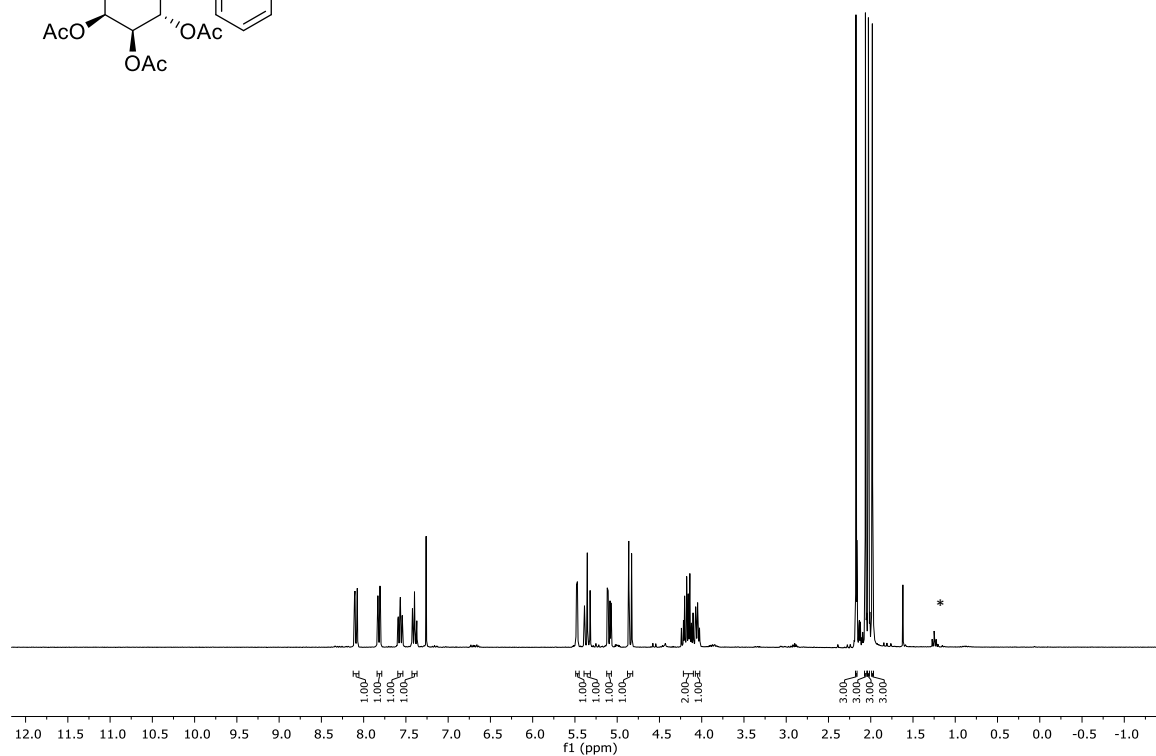
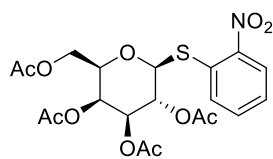
* solvent residual signal: ethyl acetate

Compound **12** (CDCl_3 -*d*)

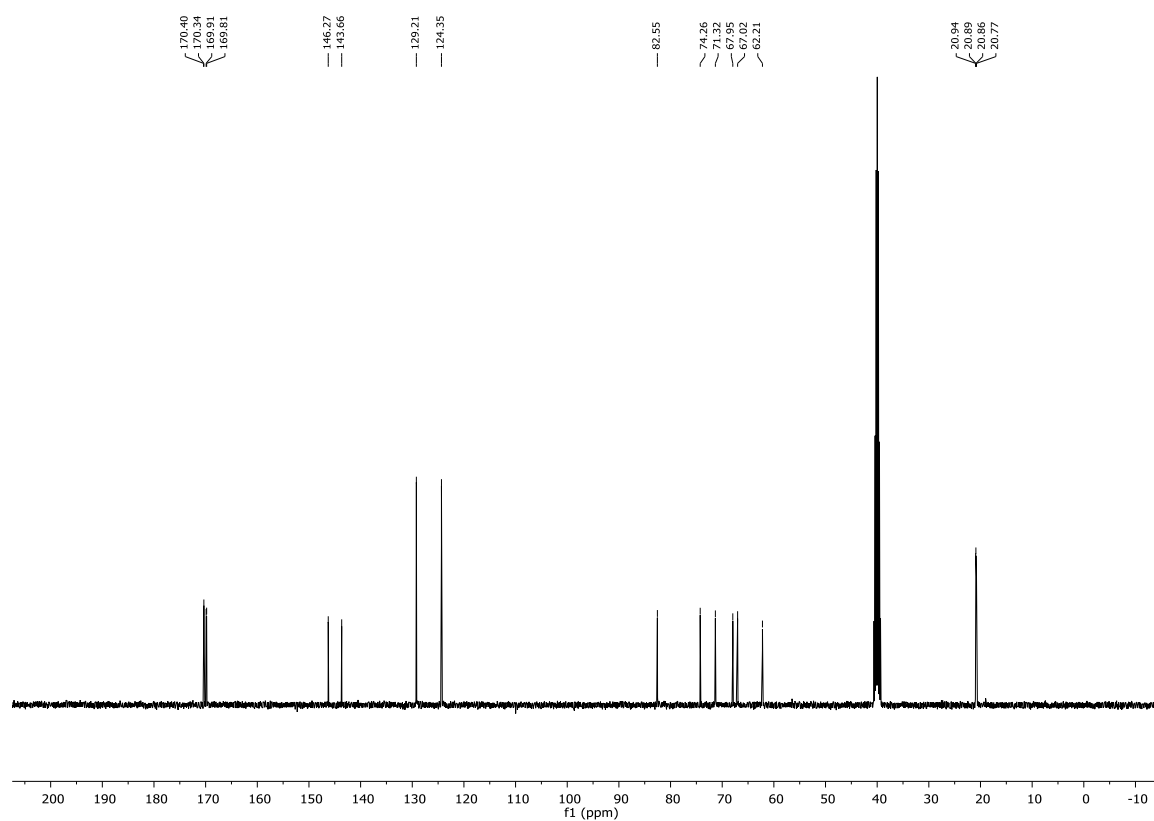
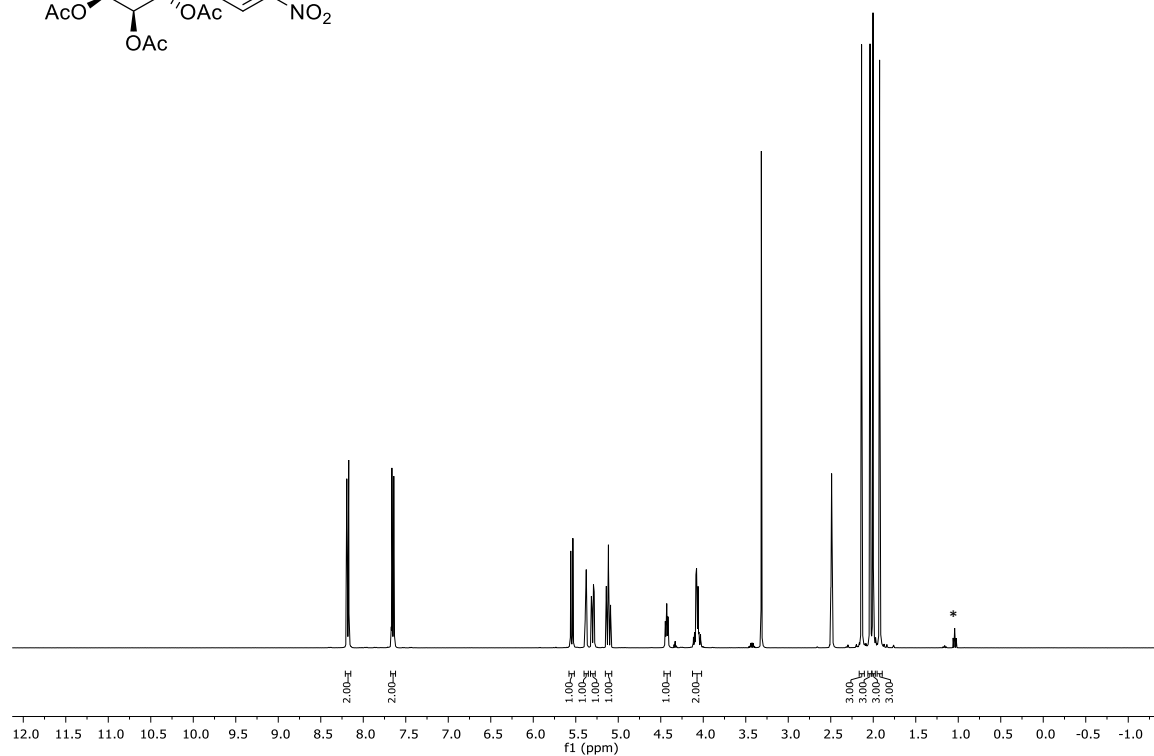
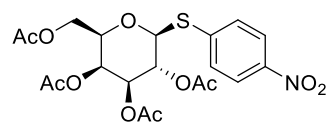
Compound **13** (CDCl₃-*d*)

* solvent residual signal: ethyl acetate

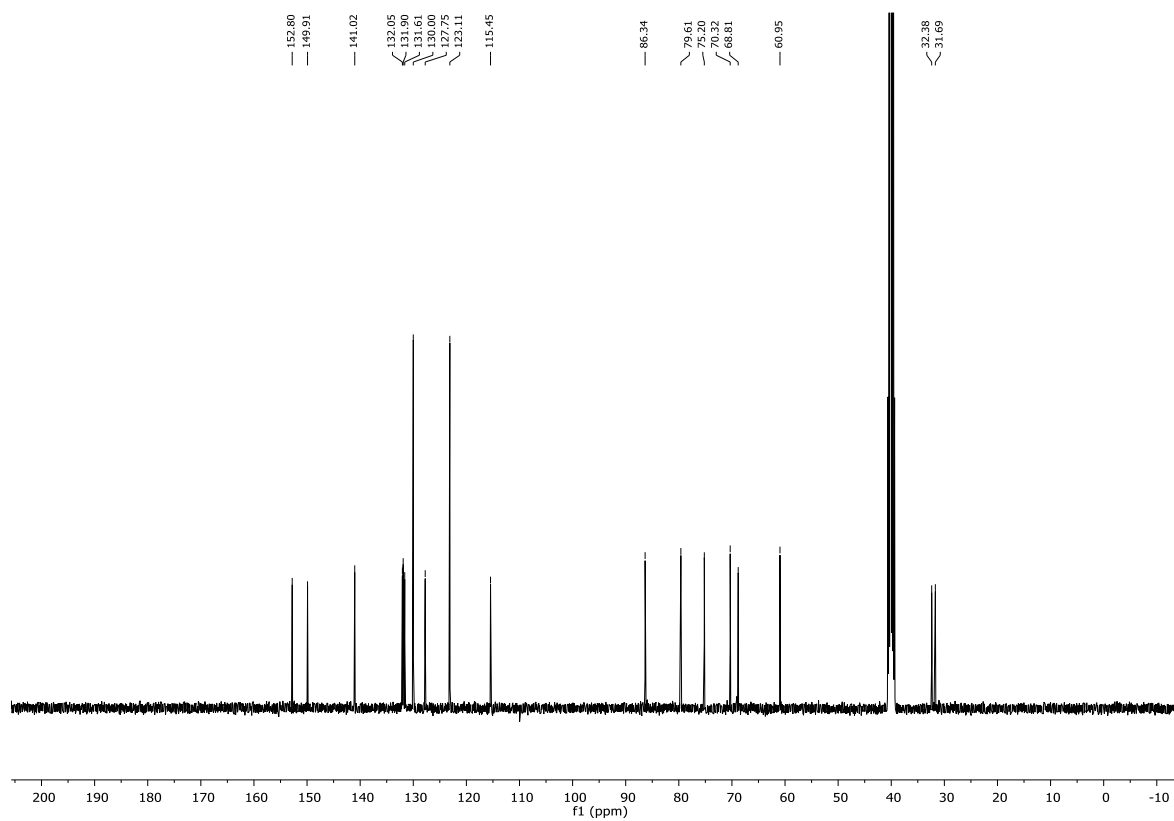
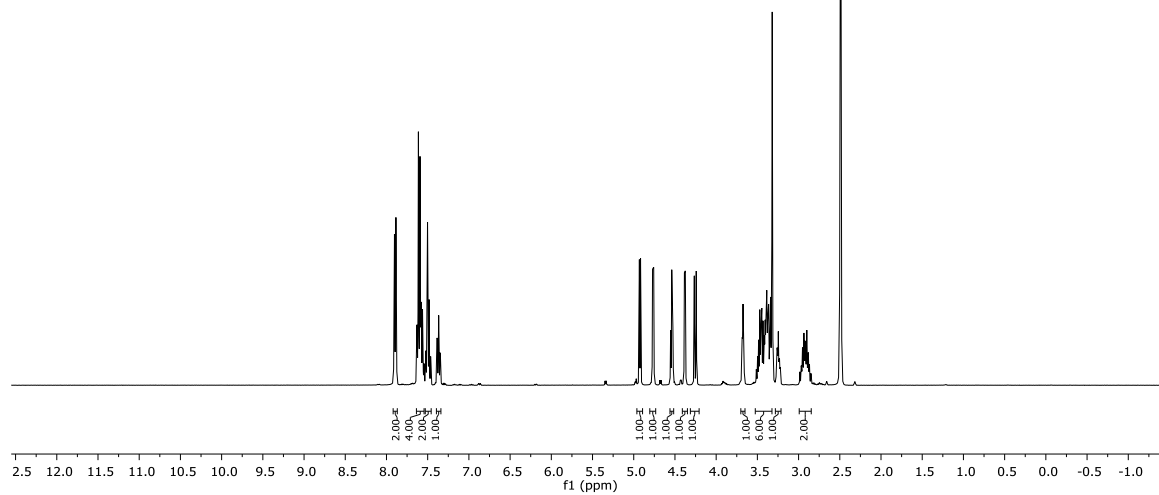
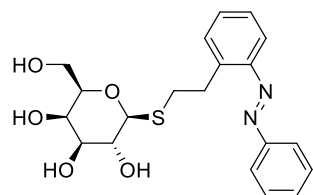
Compound **14** (CDCl_3 -*d*)

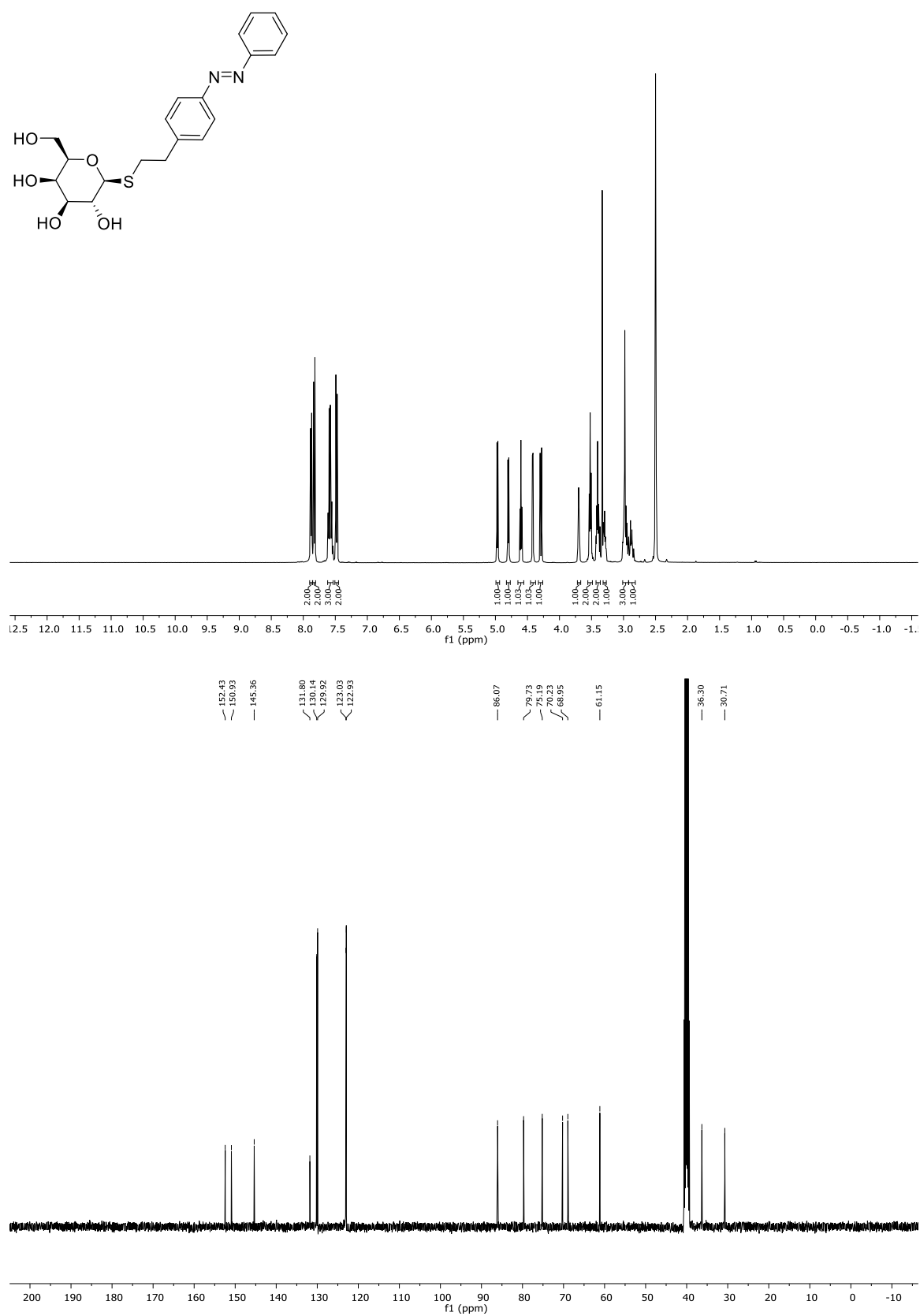
Compound **15** (CDCl₃-*d*)

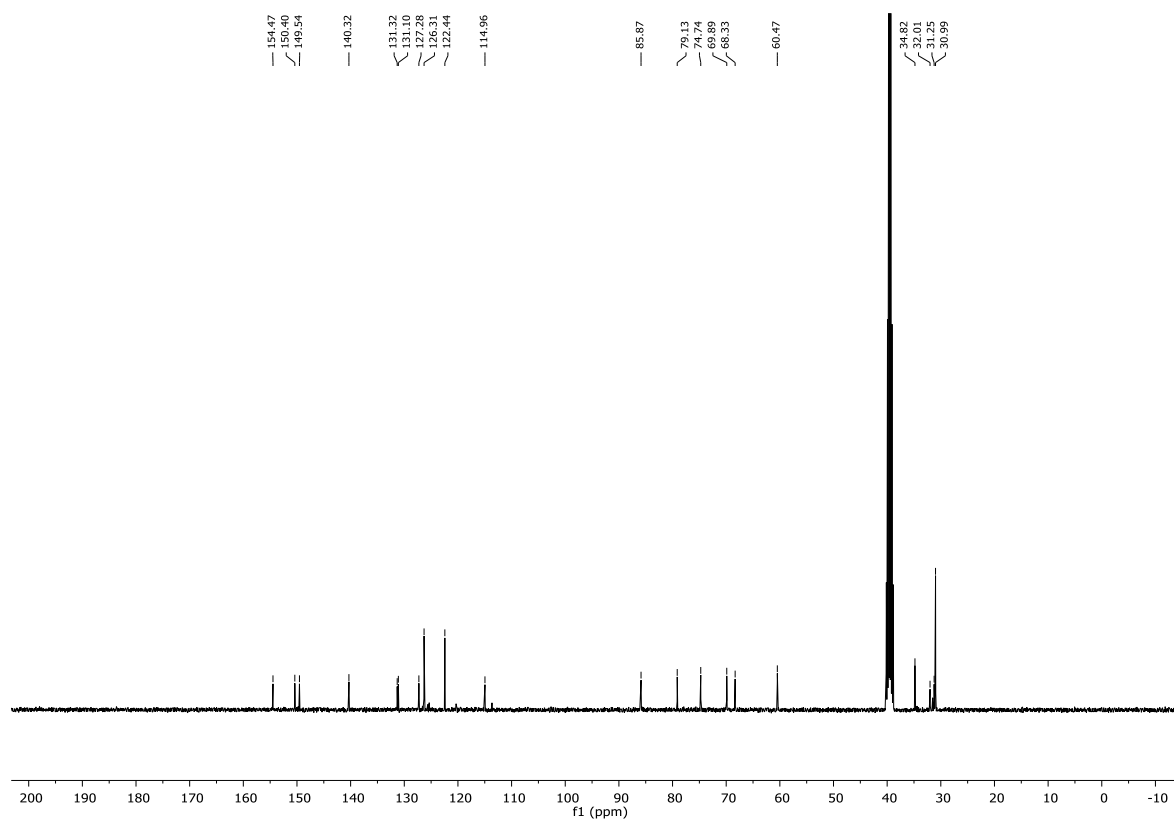
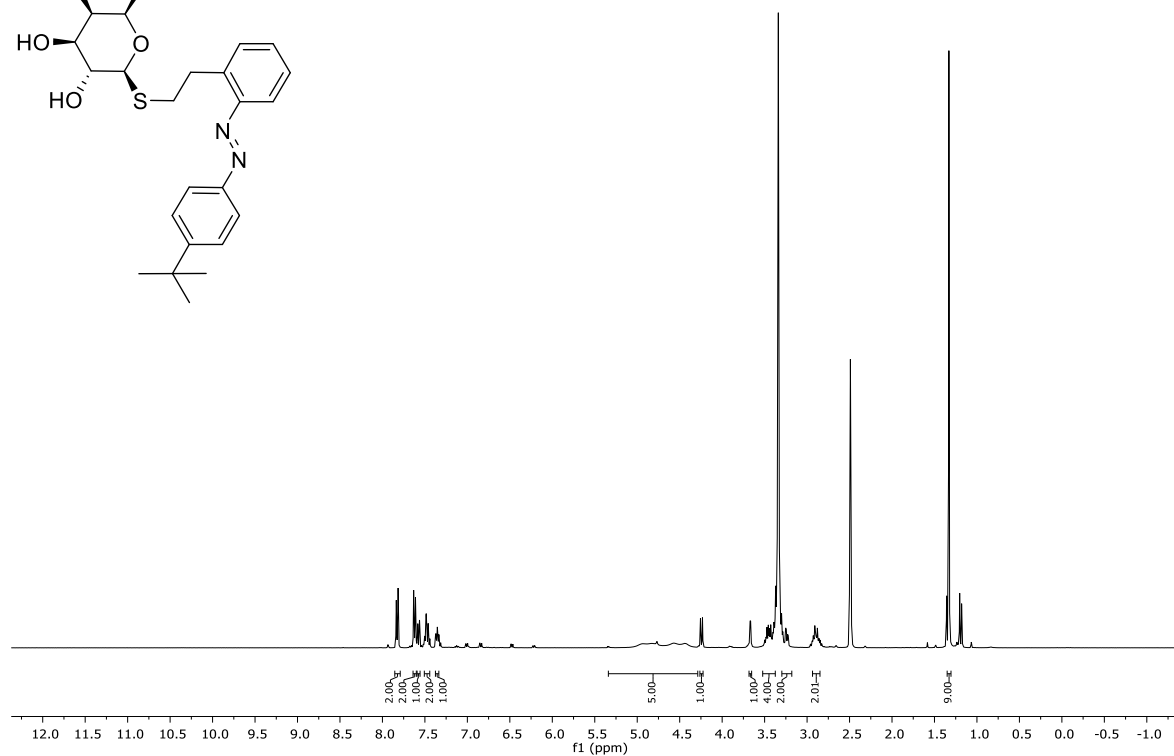
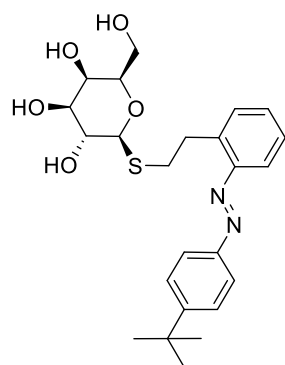
* solvent residual signal: ethyl acetate

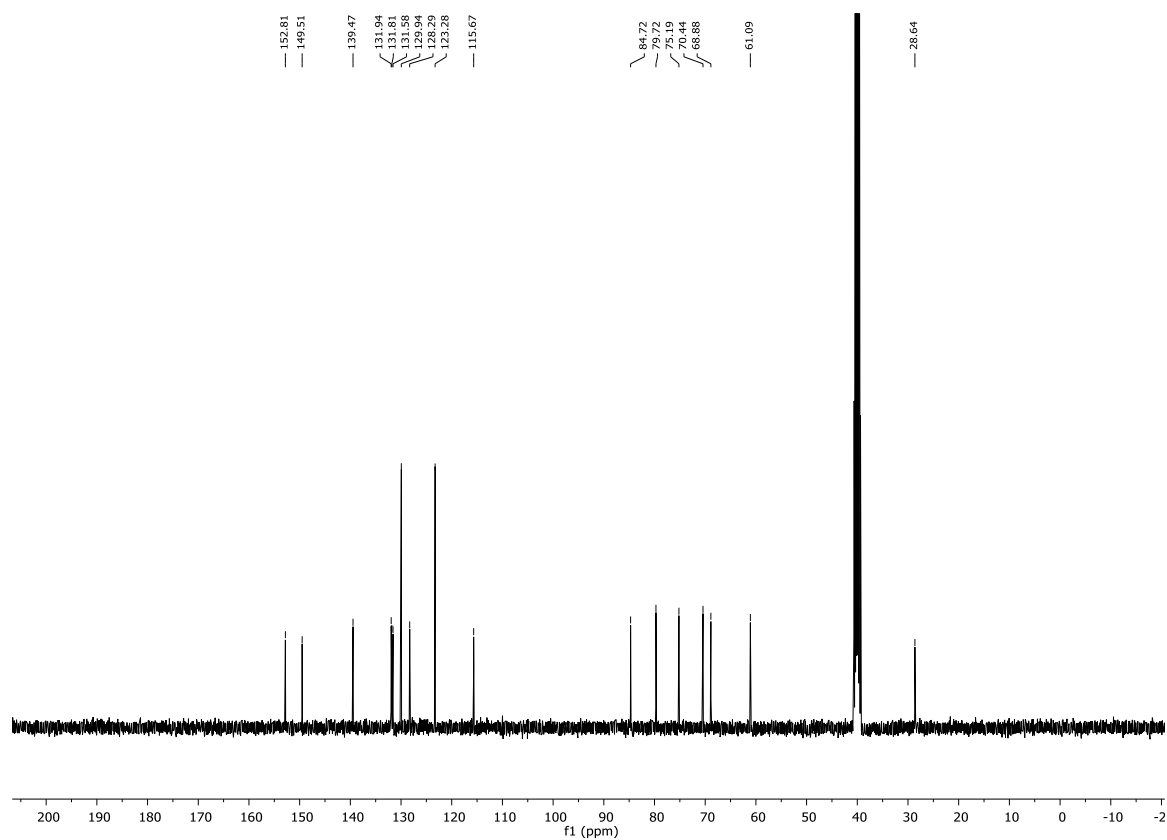
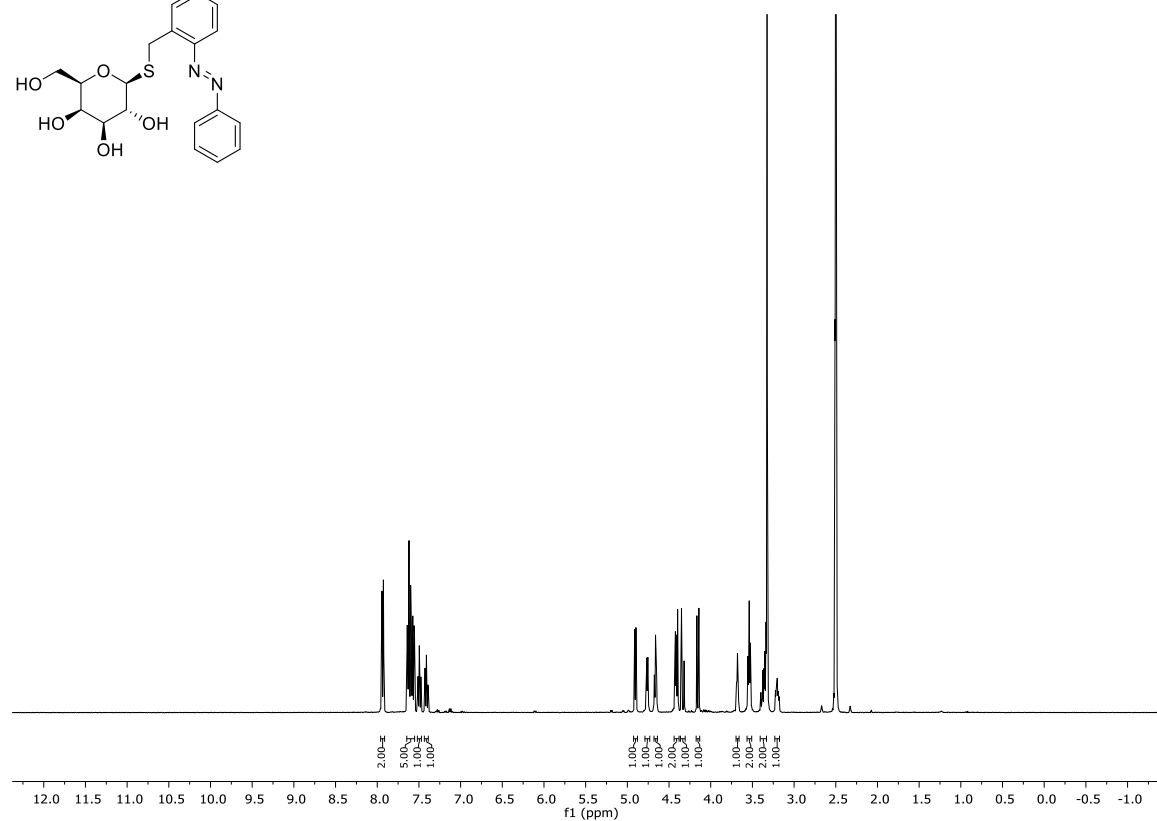
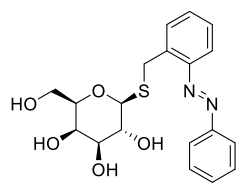
Compound **16** (DMSO- d_6)

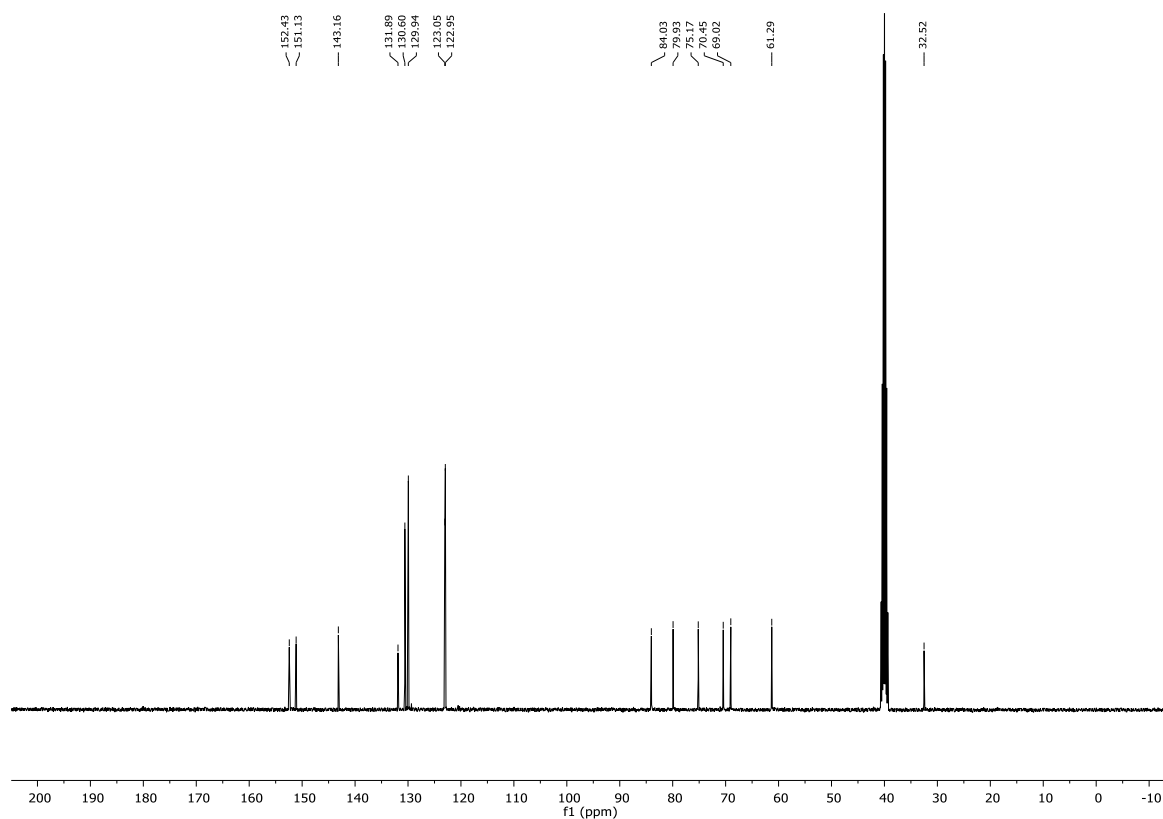
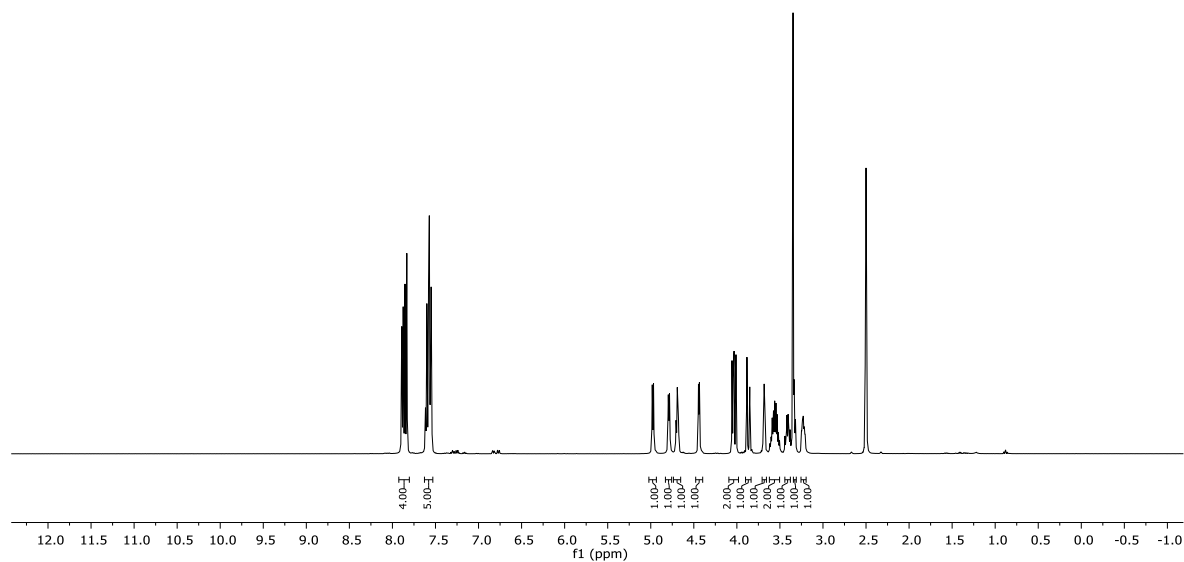
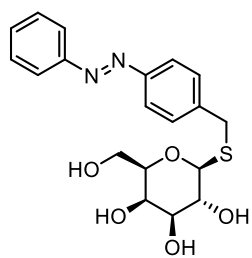
* solvent residual signal: ethyl acetate

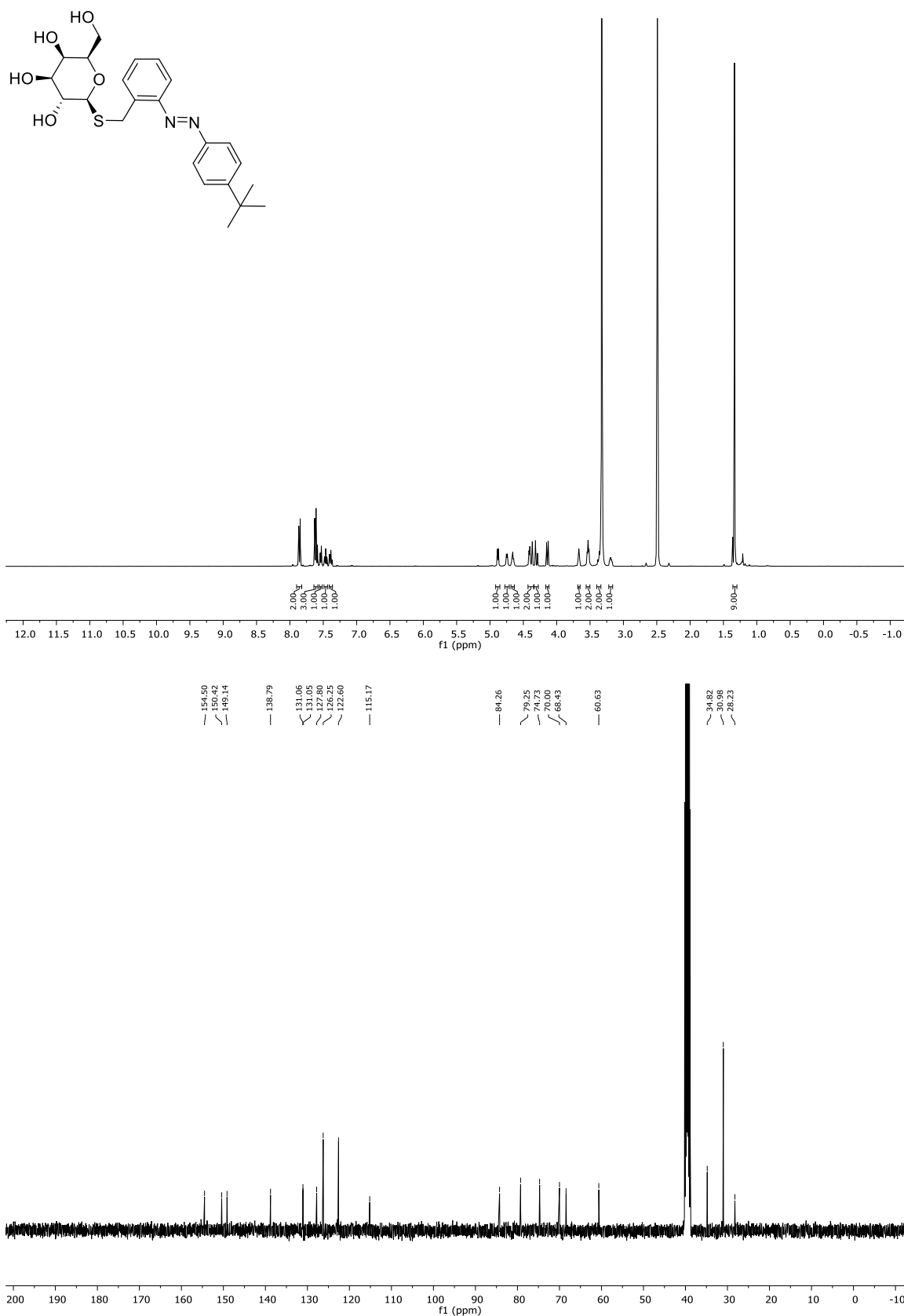
Compound **34** (DMSO-*d*₆)

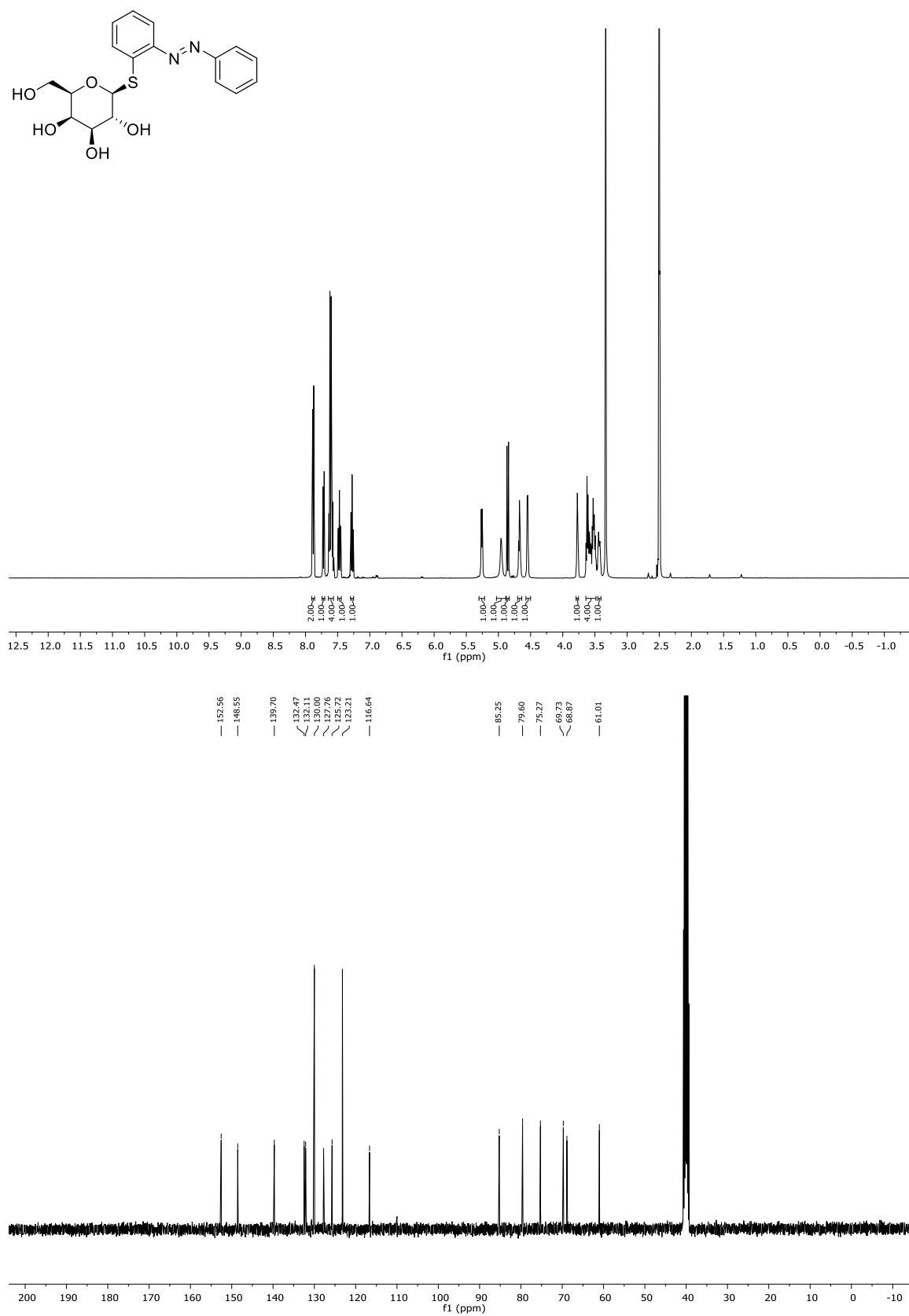
Compound **35** (DMSO- d_6)

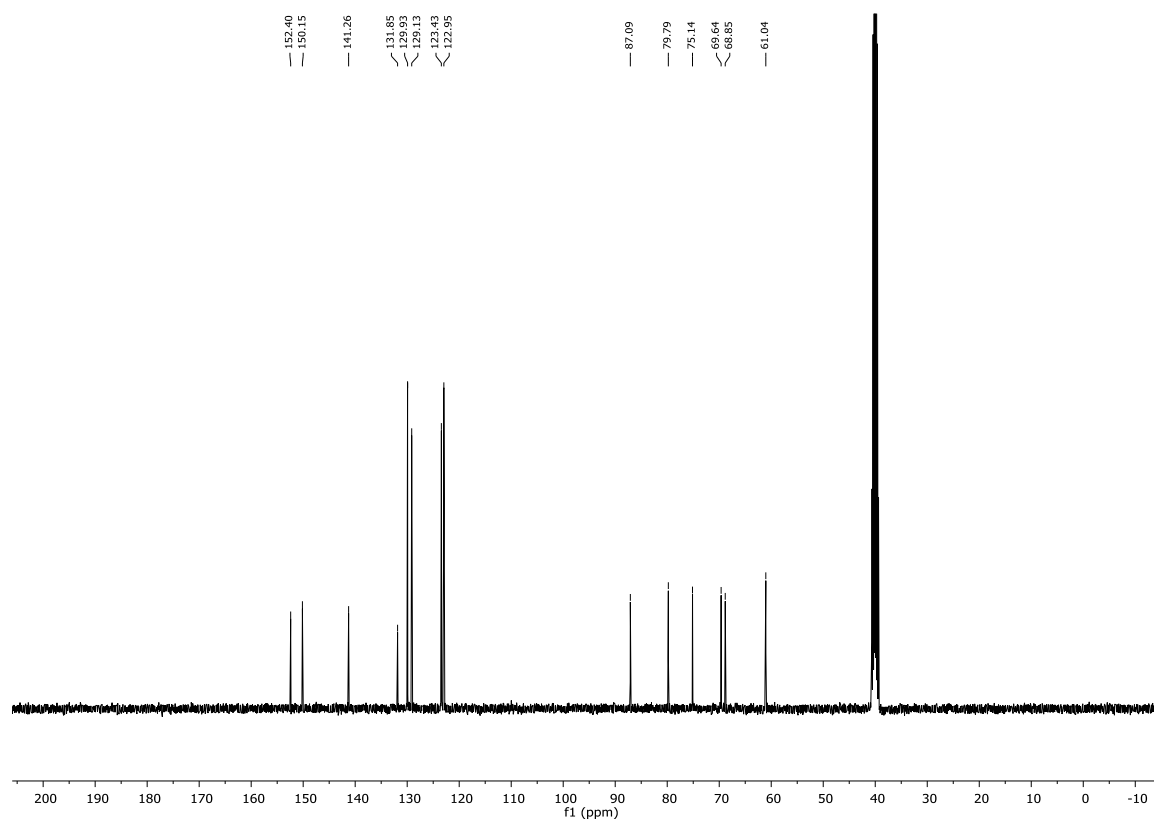
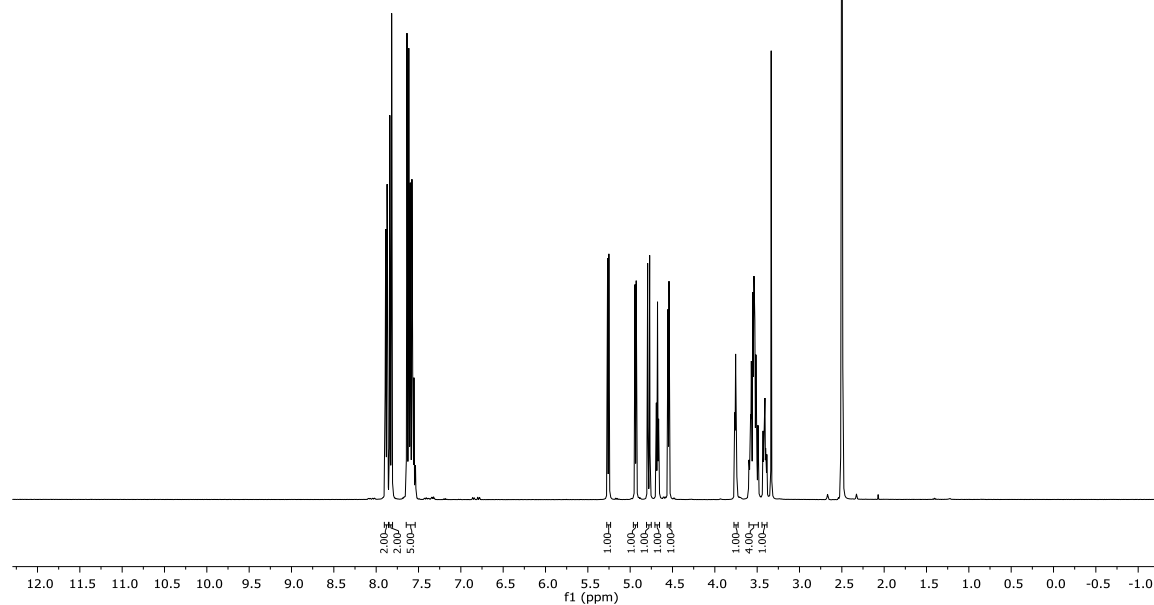
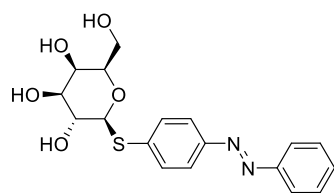
Compound **36** (DMSO-*d*₆)

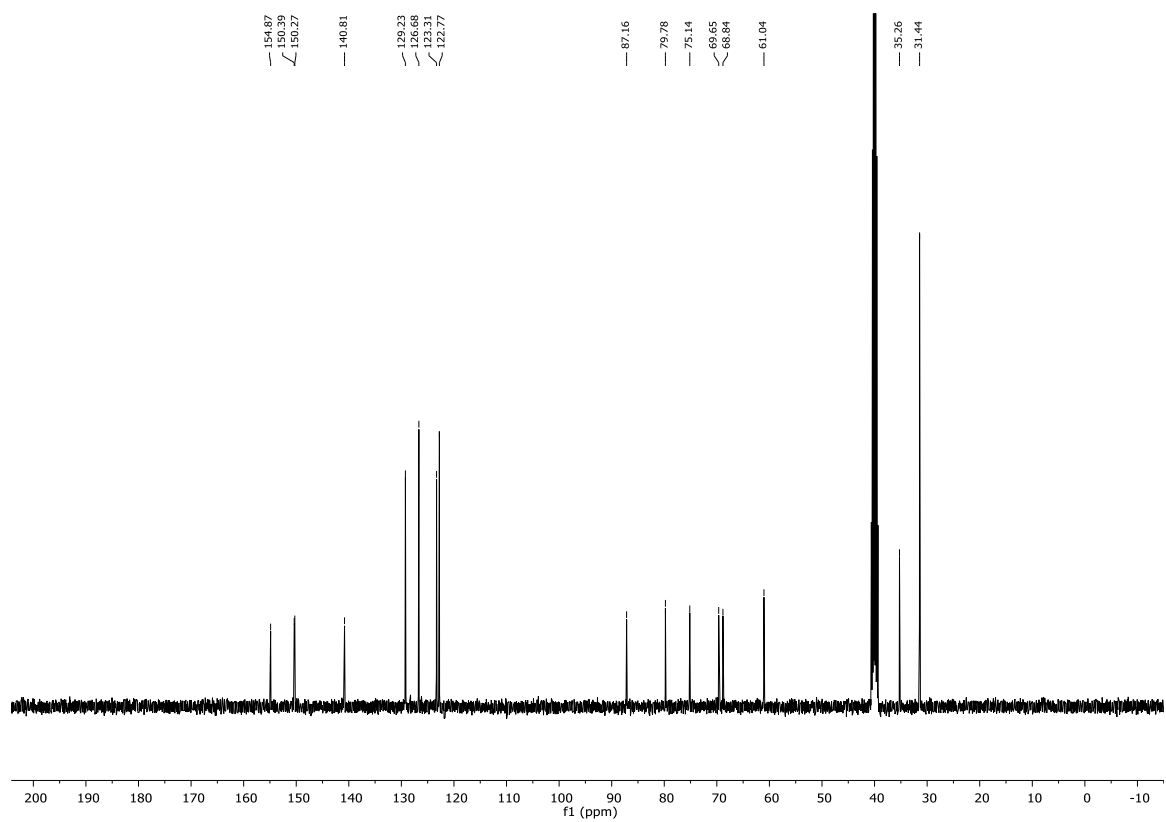
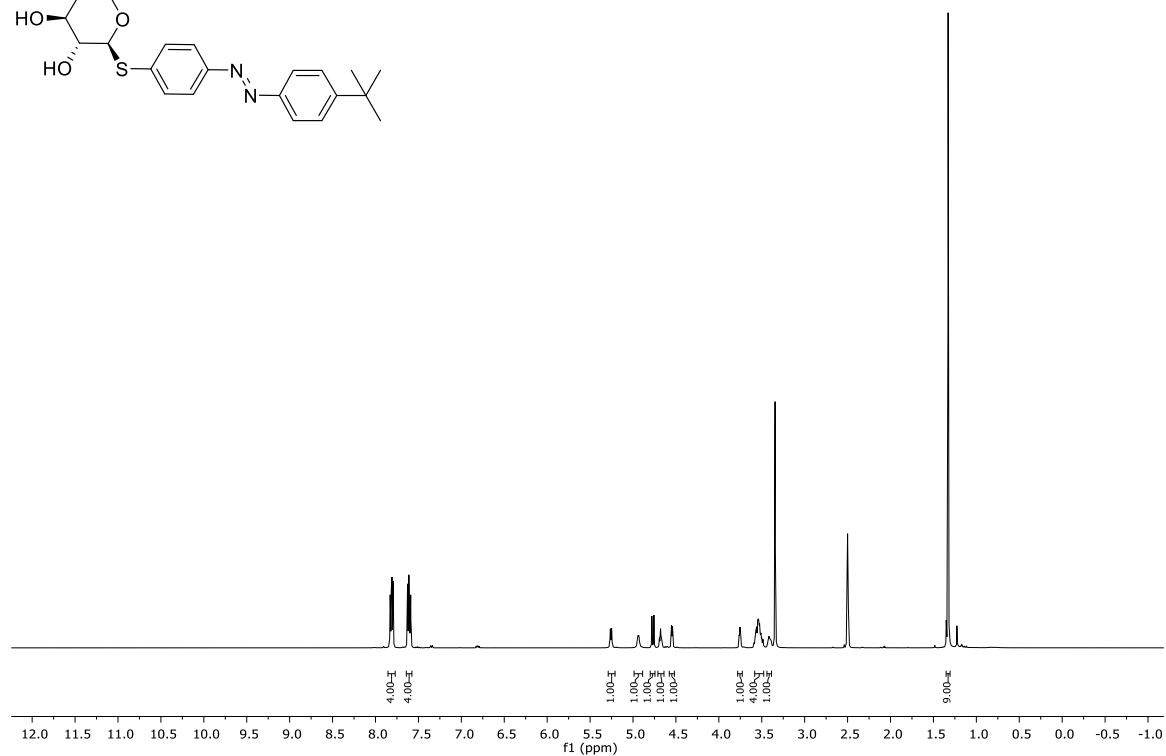
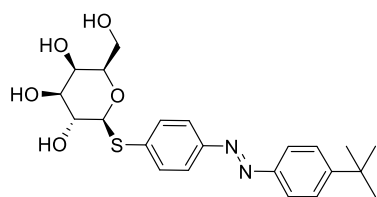
Compound **37** (DMSO- d_6)

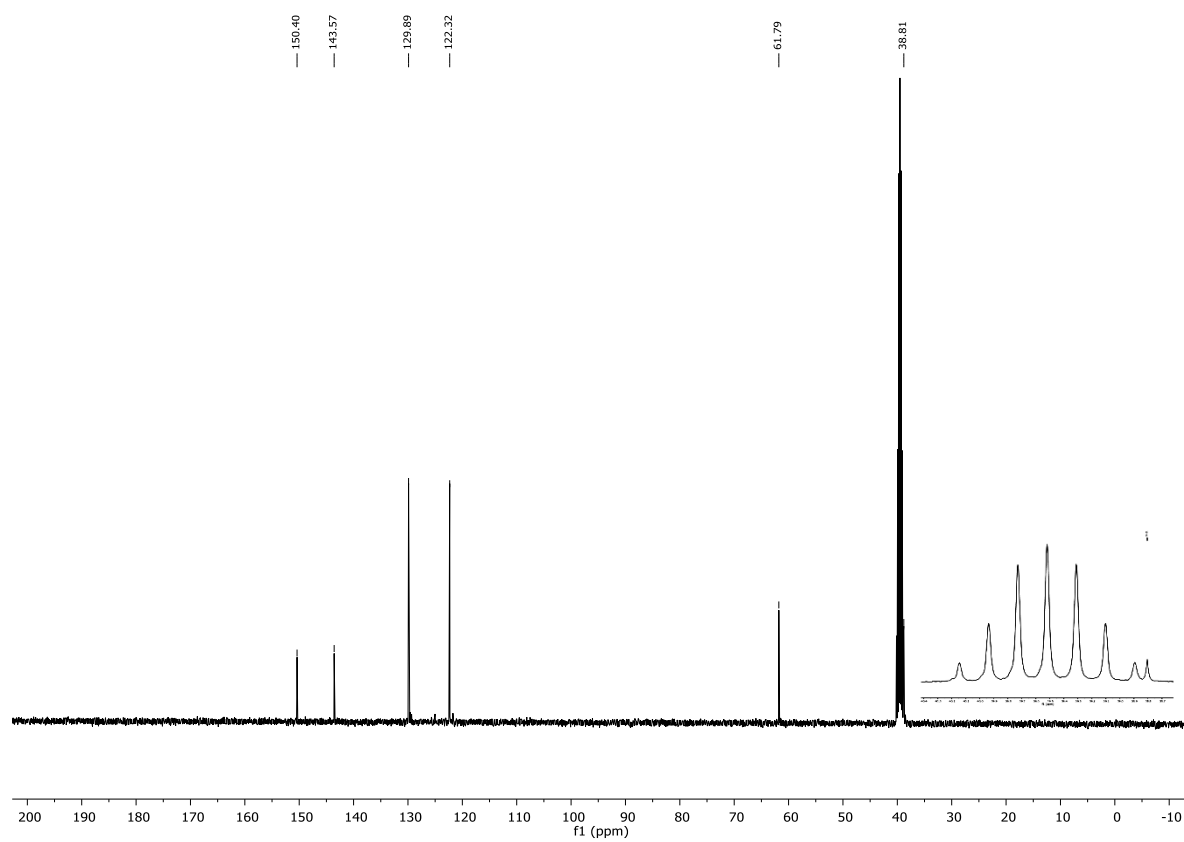
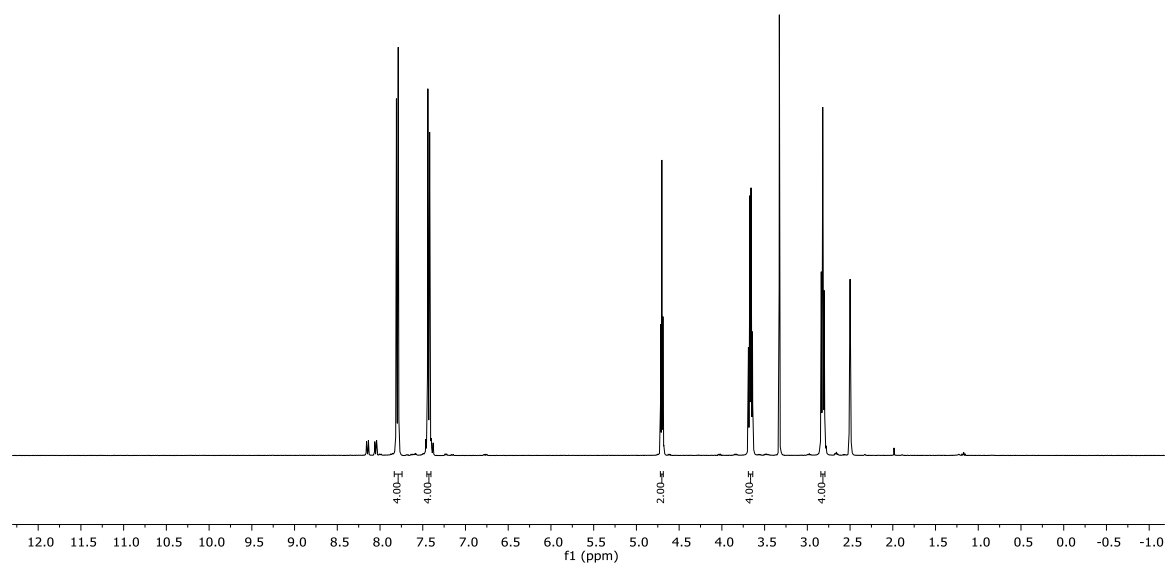
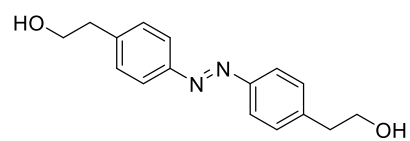
Compound **38** (DMSO-*d*₆)

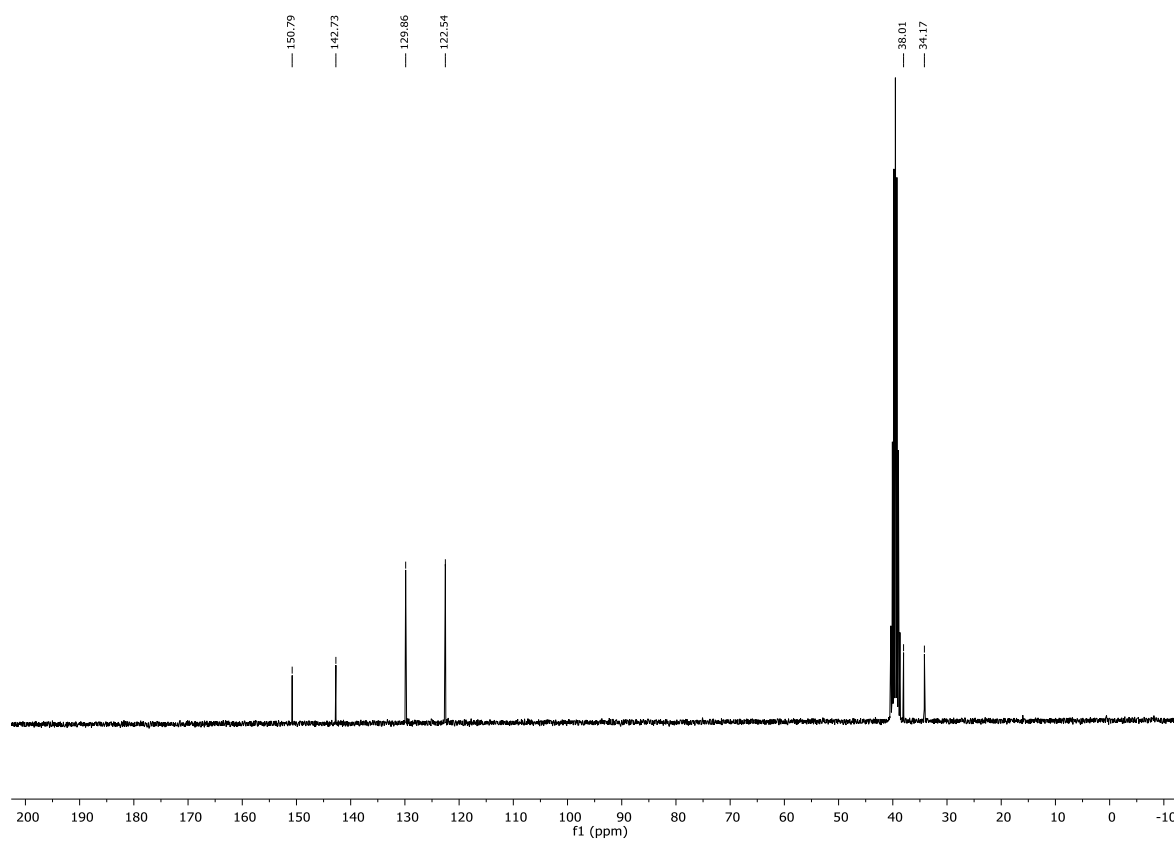
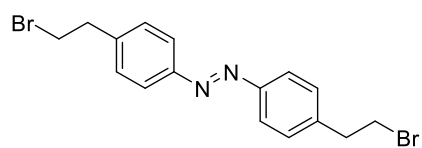
Compound **39** (DMSO- d_6)

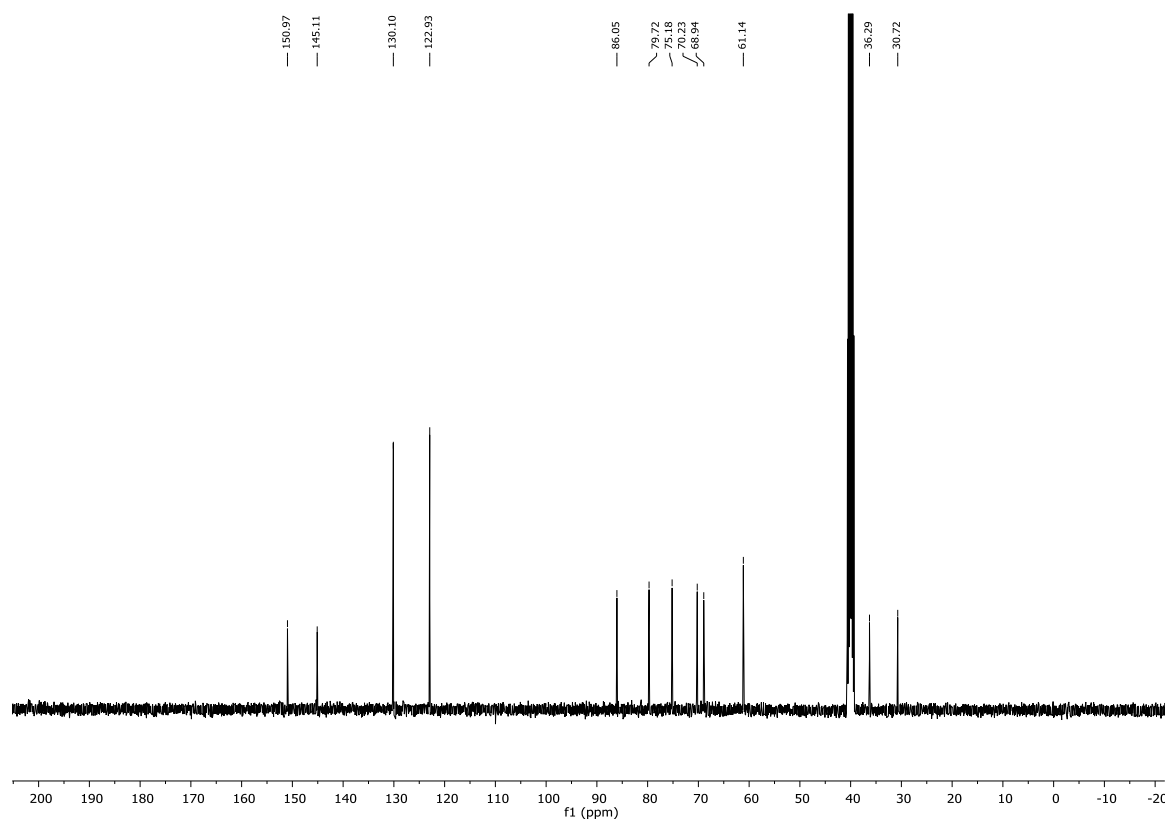
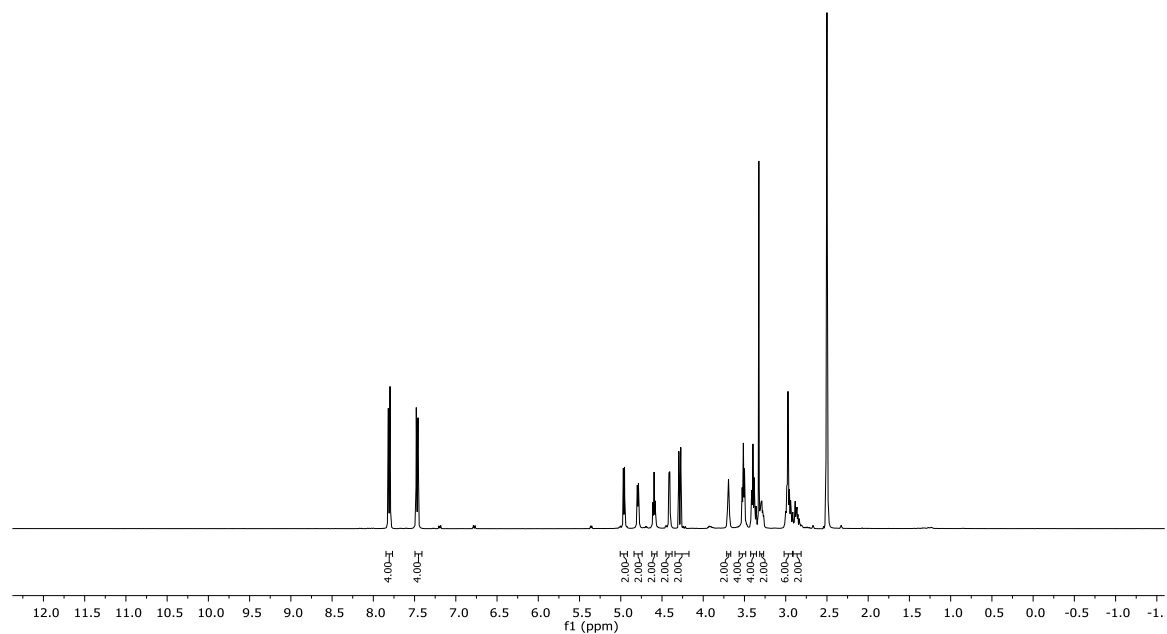
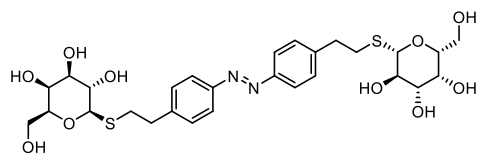
Compound **40** (DMSO-*d*₆)

Compound **41** (DMSO- d_6)

Compound **42** (DMSO-*d*₆)

Compound **45** (DMSO- d_6)

Compound **46** (DMSO-*d*₆)

Compound **49** (DMSO- d_6)

3.5.2 UV-Vis Absorption Spectra, Cycle Performances, and Thermal Half-Lives

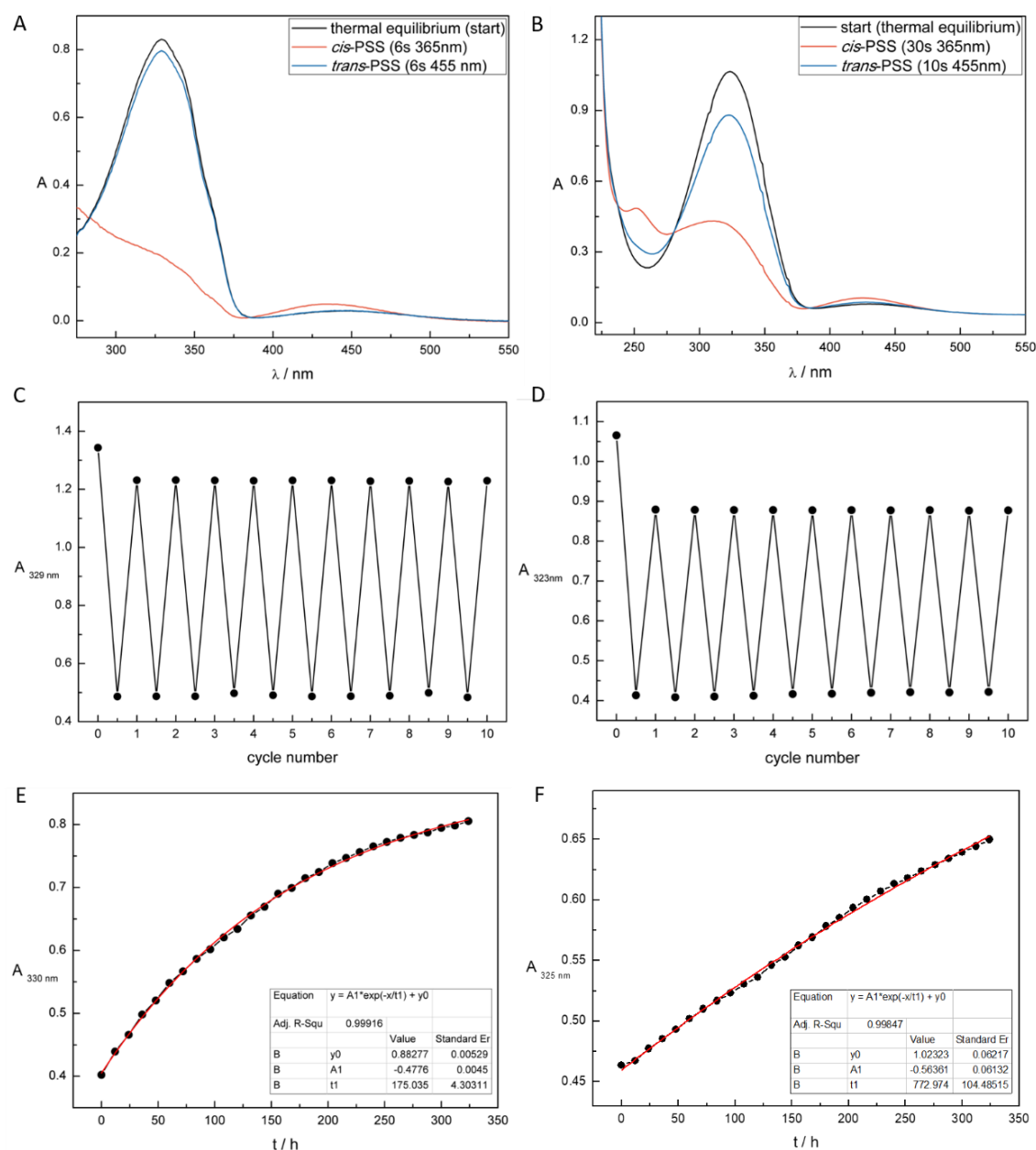
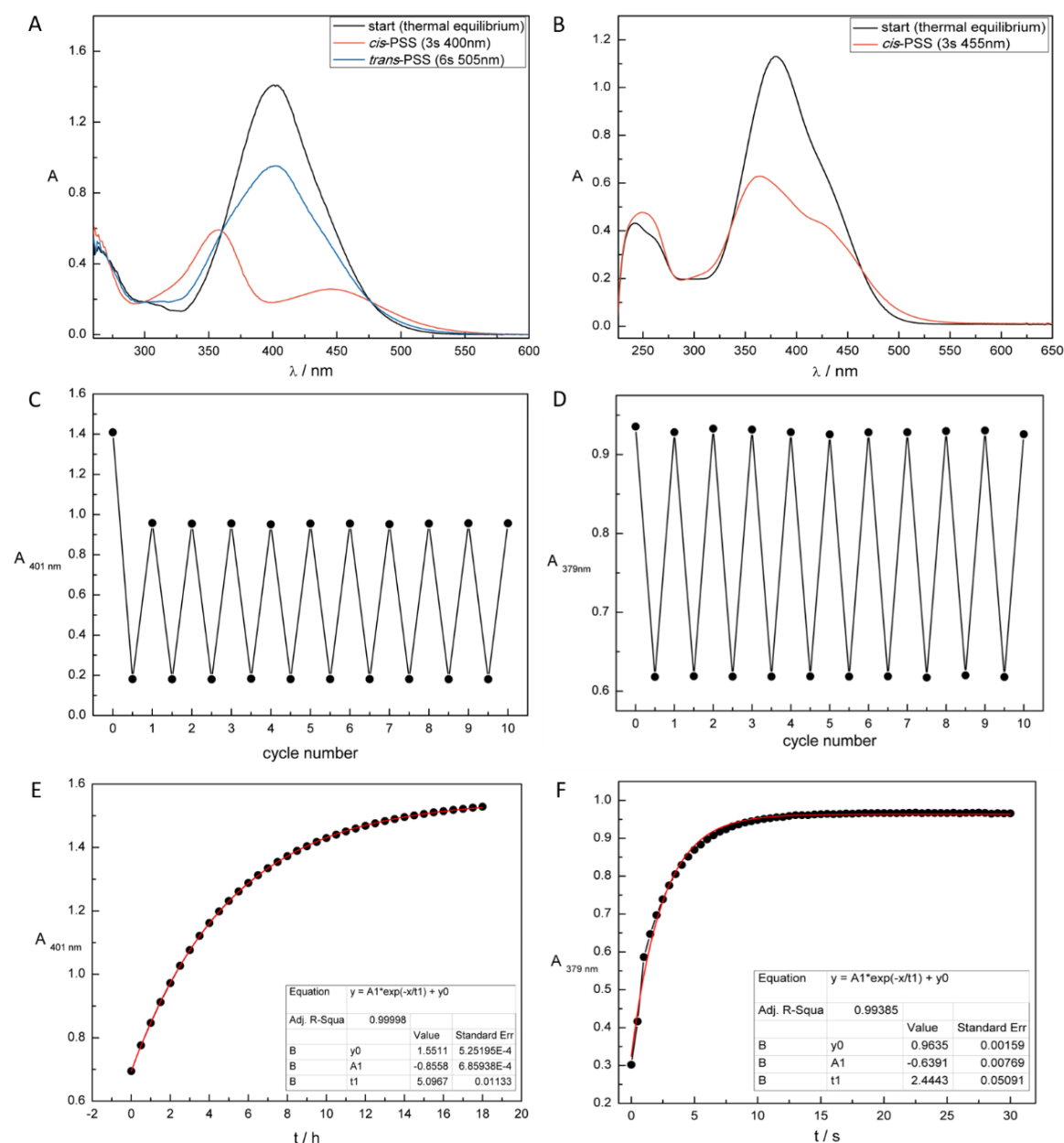


Figure S1. Changes in absorption spectra of 4 upon continuous irradiation until the PSS is reached. (A) 50 μ M in DMSO. λ (cis-PSS) = 365 nm, λ (trans-PSS) = 455 nm. (B) 50 μ M in phosphate buffer + 0.1% DMSO. λ (cis-PSS) = 365 nm, λ (trans-PSS) = 455 nm. **Cycle performance of 4.** (C) 50 μ M in DMSO. Changes in absorption at 329 nm (λ_{\max} of the trans isomer) were measured during alternate irradiation with light of $\lambda = 365$ nm and $\lambda = 455$ nm until the PSS is reached. (D) 50 μ M in phosphate buffer + 0.1% DMSO. Changes in absorption at 323 nm (λ_{\max} of the trans isomer) were measured during alternate irradiation with light of $\lambda = 365$ nm and $\lambda = 455$ nm until the PSS is reached. **Thermal stability of the cis isomer of 4 measured at 25 $^{\circ}$ C.** Black dots represent the absorption at the indicated wavelength dependent on the time of relaxation [h]. Red curve represents an exponential nonlinear curve fit. (E) 50 μ M in DMSO. Changes in absorption maxima measured at 330 nm (λ_{\max} of the trans isomer) after irradiation with $\lambda = 365$ nm until the PSS is reached. $t_{0.5} = 121$ h. (F) 50 μ M solution in phosphate buffer + 0.1% DMSO. Changes in absorption maxima measured at 323 nm (λ_{\max} of the trans isomer) after irradiation with $\lambda = 365$ nm until the PSS is reached. $t_{0.5} = 536$ h.



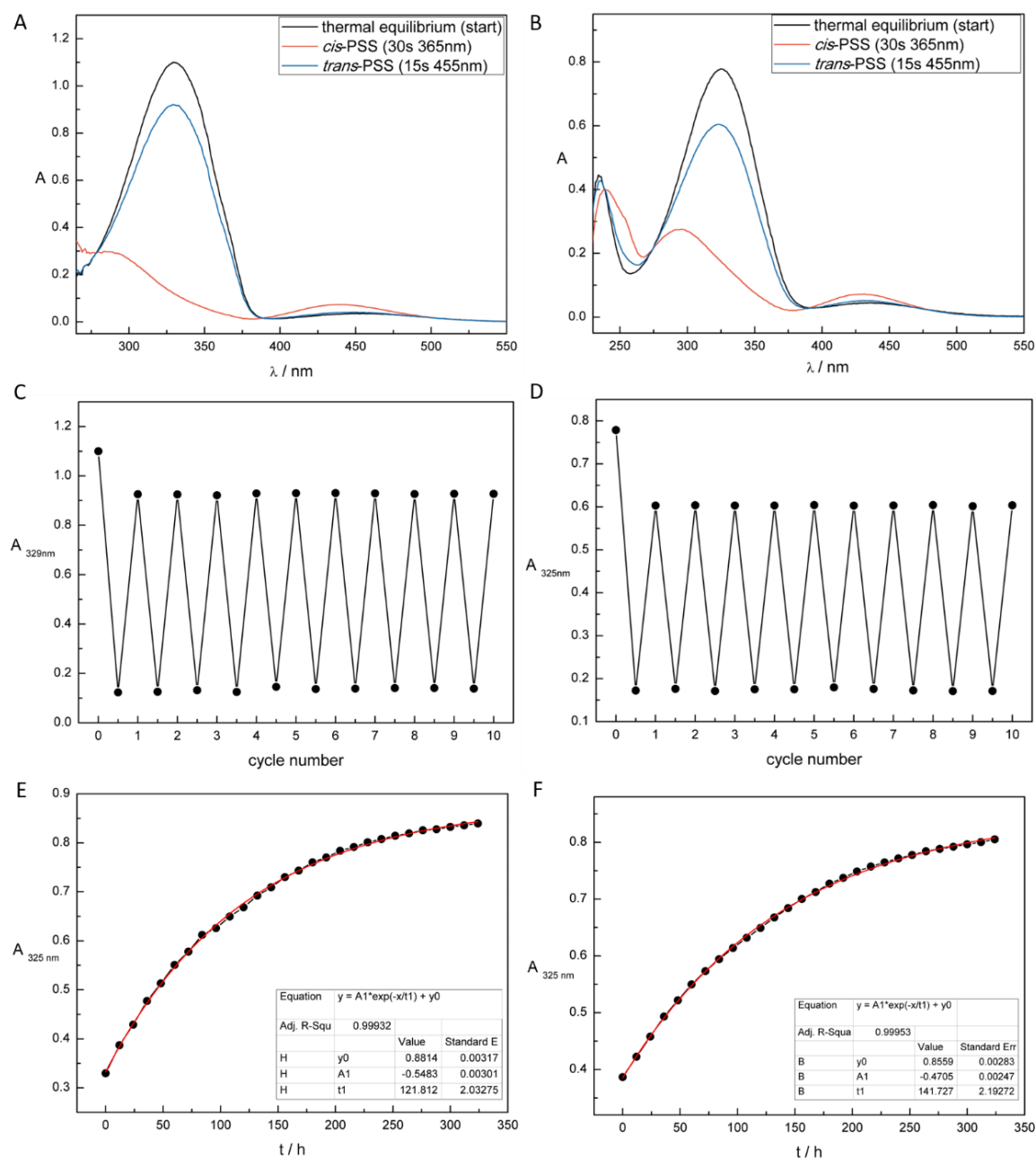


Figure S3. Changes in absorption spectra of 34 upon continuous irradiation until the PSS is reached. (A) 50 μ M in DMSO. λ (*cis*-PSS) = 365 nm, λ (*trans*-PSS) = 455 nm. (B) 50 μ M in phosphate buffer + 0.1% DMSO. λ (*cis*-PSS) = 365 nm, λ (*trans*-PSS) = 455 nm. **Cycle performance of 34.** (C) 50 μ M in DMSO. Changes in absorption at 329 nm (λ_{max} of the *trans* isomer) were measured during alternate irradiation with light of λ = 365 nm and λ = 455 nm until the PSS is reached. (D) 50 μ M in phosphate buffer + 0.1% DMSO. Changes in absorption at 325 nm (λ_{max} of the *trans* isomer) were measured during alternate irradiation with light of λ = 365 nm and λ = 455 nm until the PSS is reached. **Thermal stability of the *cis* isomer of 34 measured at 25 °C.** Black dots represent the absorption at the indicated wavelength dependent on the time of relaxation [h]. Red curve represents an exponential nonlinear curve fit. (E) 50 μ M in DMSO. Changes in absorption maxima measured at 325 nm after irradiation with λ = 365 nm until the PSS is reached. $t_{0.5}$ = 84.4 h. (F) 50 μ M solution in phosphate buffer + 0.1% DMSO. Changes in absorption maxima measured at 325 nm (λ_{max} of the *trans* isomer) after irradiation with λ = 365 nm until the PSS is reached. $t_{0.5}$ = 98.2 h.

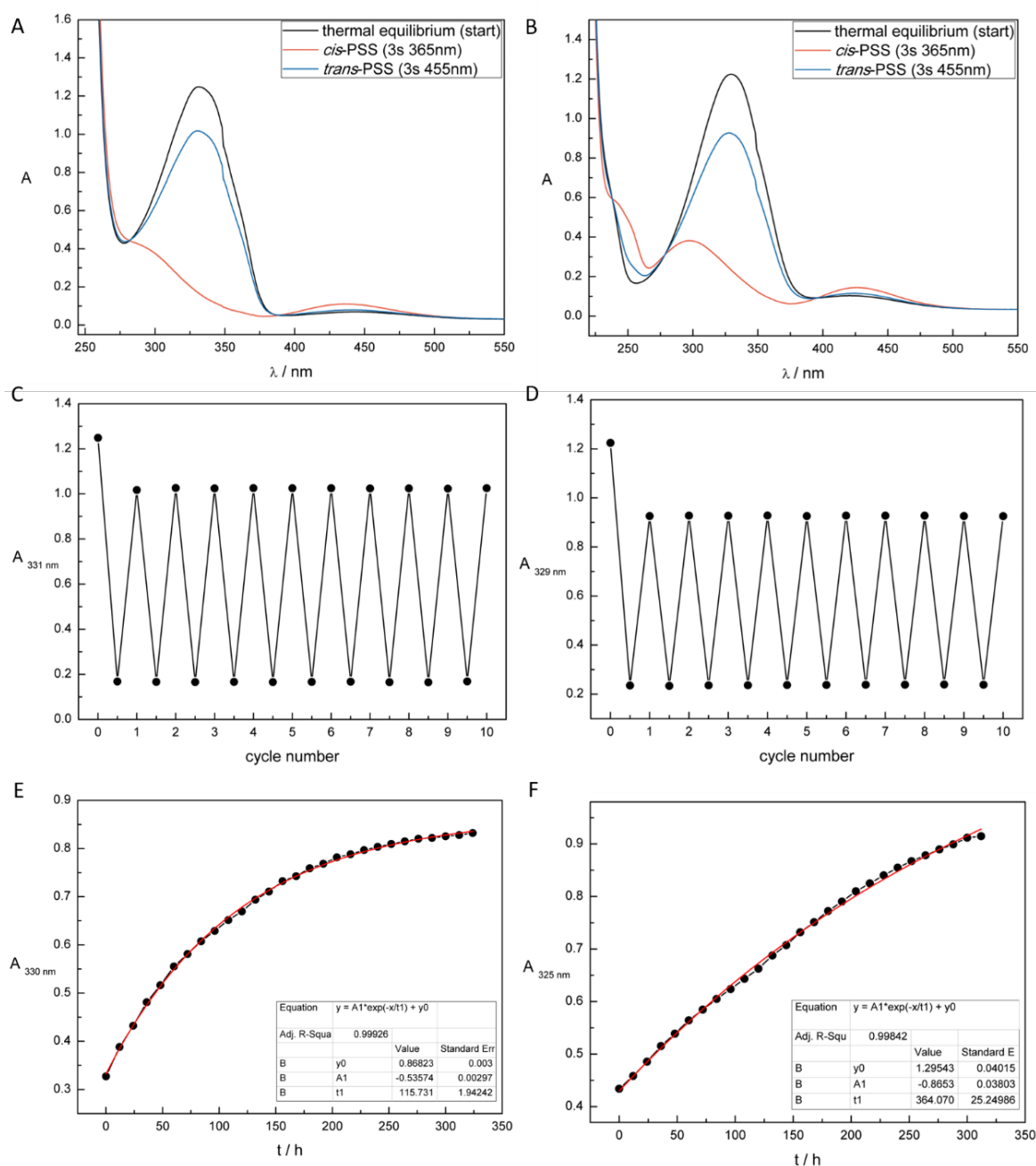


Figure S4. Changes in absorption spectra of 35 upon continuous irradiation until the PSS is reached. (A) 50 μ M in DMSO. λ (*cis*-PSS) = 365 nm, λ (*trans*-PSS) = 455 nm. (B) 50 μ M in phosphate buffer + 0.1% DMSO. λ (*cis*-PSS) = 365 nm, λ (*trans*-PSS) = 455 nm. **Cycle performance of 35.** (C) 50 μ M in DMSO. Changes in absorption at 331 nm (λ_{max} of the *trans* isomer) were measured during alternate irradiation with light of λ = 365 nm and λ = 455 nm until the PSS is reached. (D) 50 μ M in phosphate buffer + 0.1% DMSO. Changes in absorption at 329 nm (λ_{max} of the *trans* isomer) were measured during alternate irradiation with light of λ = 365 nm and λ = 455 nm until the PSS is reached. **Thermal stability of the *cis* isomer of 35 measured at 25 °C.** Black dots represent the absorption at the indicated wavelength dependent on the time of relaxation [h]. Red curve represents an exponential nonlinear curve fit. (E) 50 μ M in DMSO. Changes in absorption maxima measured at 330 nm after irradiation with λ = 365 nm until the PSS is reached. $t_{0.5}$ = 80.2 h. (F) 50 μ M solution in phosphate buffer + 0.1% DMSO. Changes in absorption maxima measured at 325 nm after irradiation with λ = 365 nm until the PSS is reached. $t_{0.5}$ = 252 h.

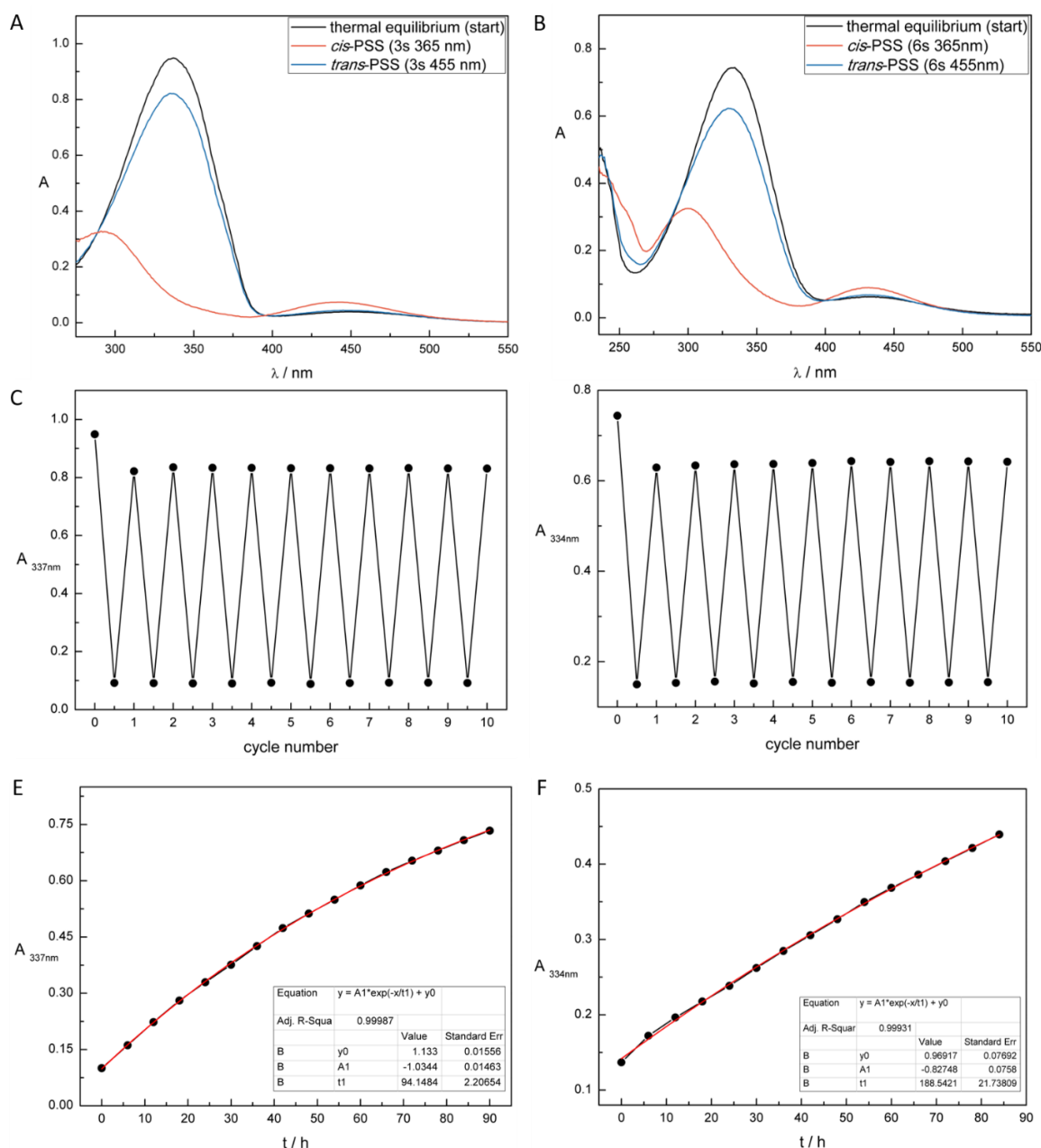


Figure S5. Changes in absorption spectra of 36 upon continuous irradiation until the PSS is reached. (A) 50 μM in DMSO. λ (*cis*-PSS) = 365 nm, λ (*trans*-PSS) = 455 nm. (B) 50 μM in phosphate buffer + 1% DMSO. λ (*cis*-PSS) = 365 nm, λ (*trans*-PSS) = 455 nm. **Cycle performance of 36.** (C) 50 μM in DMSO. Changes in absorption at 337 nm (λ_{max} of the *trans* isomer) were measured during alternate irradiation with light of λ = 365 nm and λ = 455 nm until the PSS is reached. (D) 50 μM in phosphate buffer + 1% DMSO. Changes in absorption at 334 nm (λ_{max} of the *trans* isomer) were measured during alternate irradiation with light of λ = 365 nm and λ = 455 nm until the PSS is reached. **Thermal stability of the *cis* isomer of 36 measured at 25 °C.** Black dots represent the absorption at the indicated wavelength dependent on the time of relaxation [h]. Red curve represents an exponential nonlinear curve fit. (E) 50 μM in DMSO. Changes in absorption maxima measured at 337 nm (λ_{max} of the *trans* isomer) after irradiation with λ = 365 nm until the PSS is reached. $t_{0.5}$ = 65.2 h. (F) 50 μM solution in phosphate buffer + 1% DMSO. Changes in absorption maxima measured at 334 nm after irradiation with λ = 365 nm until the PSS is reached. $t_{0.5}$ = 131 h.

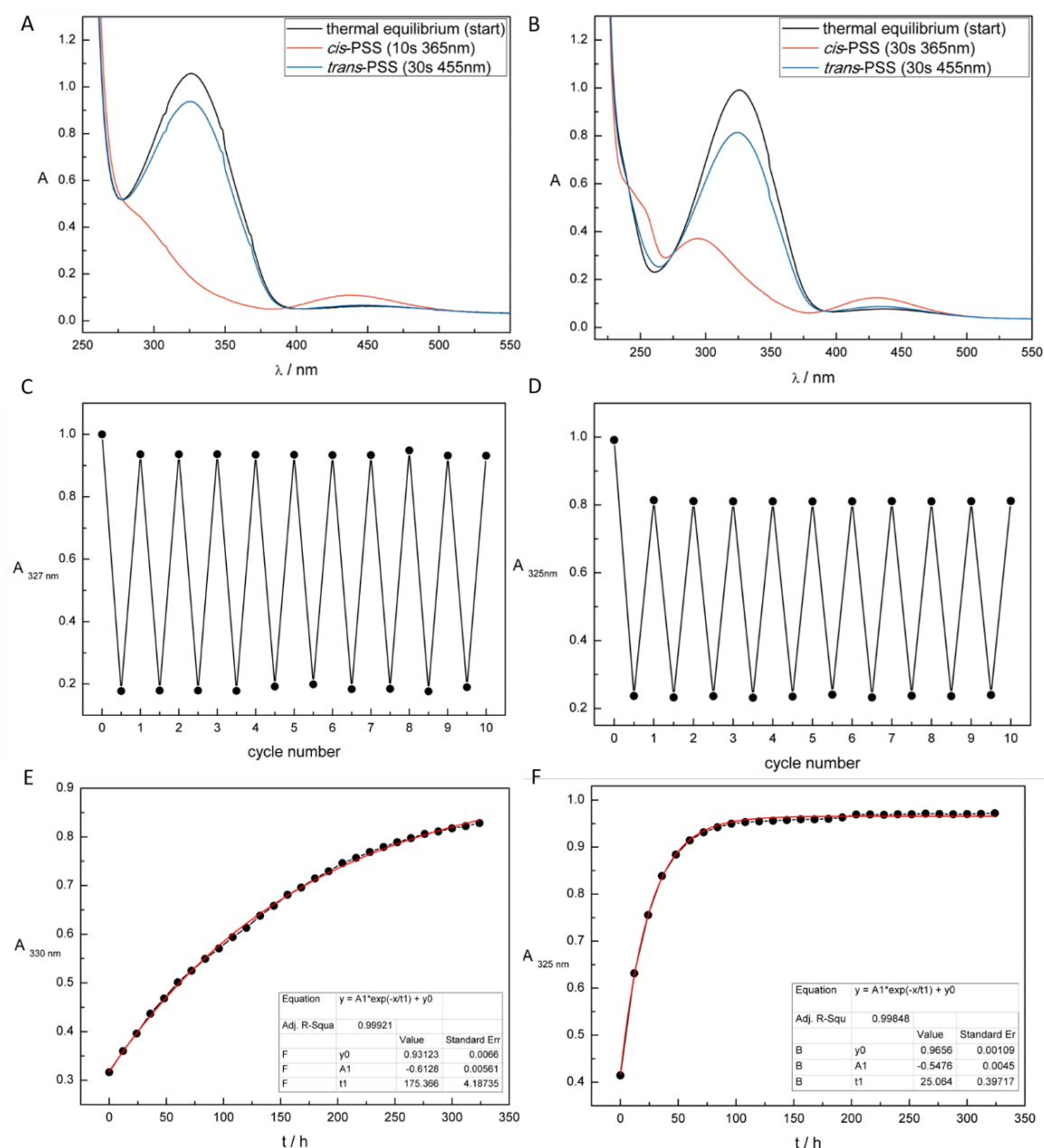


Figure S6. Changes in absorption spectra of 37 upon continuous irradiation until the PSS is reached. (A) 50 μ M in DMSO. λ (*cis*-PSS) = 365 nm, λ (*trans*-PSS) = 455 nm. (B) 50 μ M in phosphate buffer + 0.1% DMSO. λ (*cis*-PSS) = 365 nm, λ (*trans*-PSS) = 455 nm. **Cycle performance of 37.** (C) 50 μ M in DMSO. Changes in absorption at 327 nm (λ_{\max} of the *trans* isomer) were measured during alternate irradiation with light of λ = 365 nm and λ = 455 nm until the PSS is reached. (D) 50 μ M in phosphate buffer + 0.1% DMSO. Changes in absorption at 325 nm (λ_{\max} of the *trans* isomer) were measured during alternate irradiation with light of λ = 365 nm and λ = 455 nm until the PSS is reached. **Thermal stability of the *cis* isomer of 37 measured at 25 °C.** Black dots represent the absorption at the indicated wavelength dependent on the time of relaxation [h]. Red curve represents an exponential nonlinear curve fit. (E) 50 μ M in DMSO. Changes in absorption maxima measured at 340 nm after irradiation with λ = 365 nm until the PSS is reached. $t_{0.5}$ = 122 h. (F) 50 μ M solution in phosphate buffer + 0.1% DMSO. Changes in absorption maxima measured at 325 nm (λ_{\max} of the *trans* isomer) after irradiation with λ = 365 nm until the PSS is reached. $t_{0.5}$ = 17.4 h.

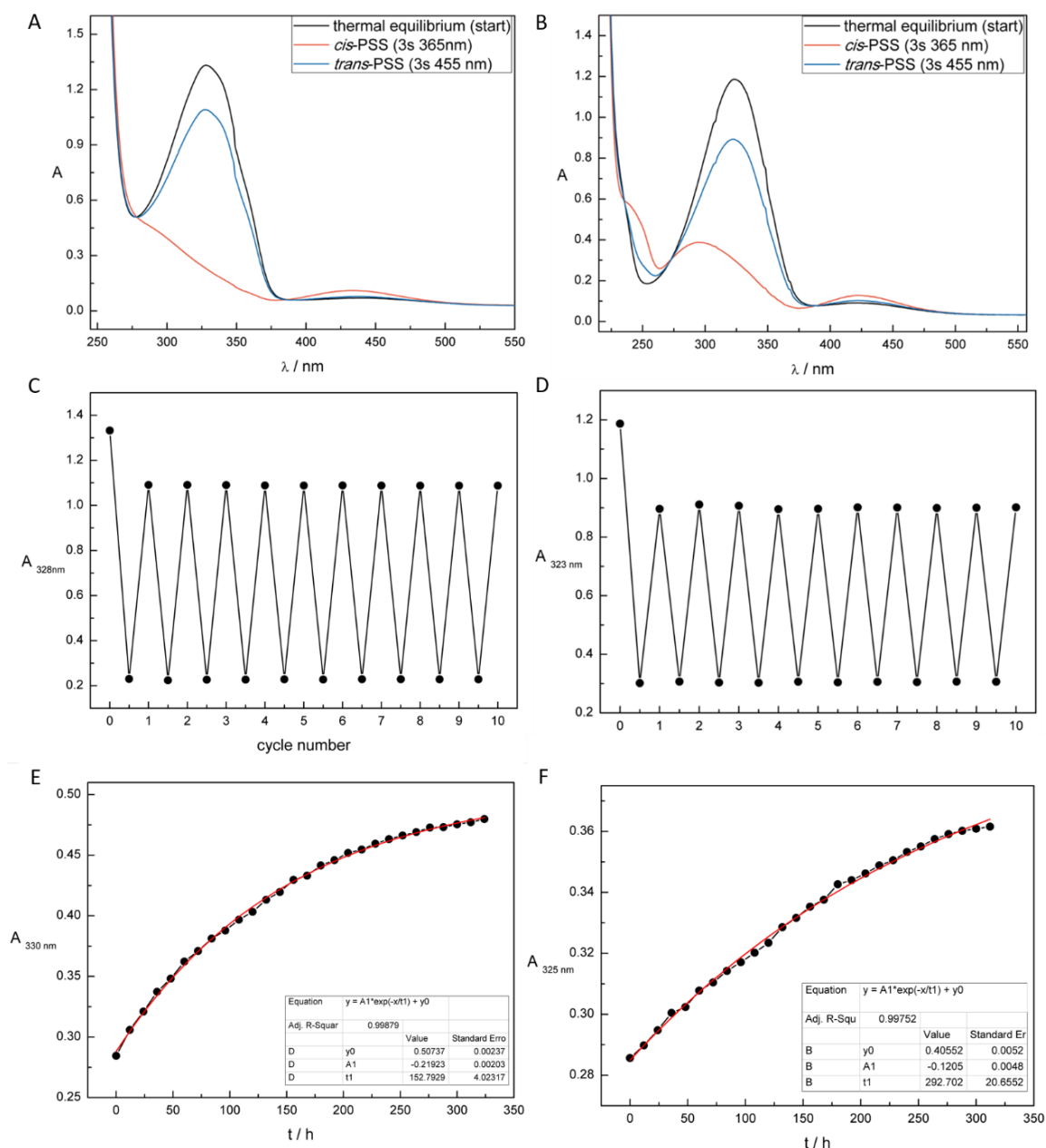


Figure S7. **Changes in absorption spectra of 38 upon continuous irradiation until the PSS is reached.** (A) 50 μM in DMSO. λ (*cis*-PSS) = 365 nm, λ (*trans*-PSS) = 455 nm. (B) 50 μM in phosphate buffer + 0.1% DMSO. λ (*cis*-PSS) = 365 nm, λ (*trans*-PSS) = 455 nm. **Cycle performance of 38.** (C) 50 μM in DMSO. Changes in absorption at 328 nm (λ_{max} of the *trans* isomer) were measured during alternate irradiation with light of λ = 365 nm and λ = 455 nm until the PSS is reached. (D) 50 μM in phosphate buffer + 0.1% DMSO. Changes in absorption at 323 nm (λ_{max} of the *trans* isomer) were measured during alternate irradiation with light of λ = 365 nm and λ = 455 nm until the PSS is reached. **Thermal stability of the *cis* isomer of 38 measured at 25 °C.** Black dots represent the absorption at the indicated wavelength dependent on the time of relaxation [h]. Red curve represents an exponential nonlinear curve fit. (E) 50 μM in DMSO. Changes in absorption maxima measured at 330 nm after irradiation with λ = 365 nm until the PSS is reached. $t_{0.5}$ = 106 h. (F) 50 μM solution in phosphate buffer + 0.1% DMSO. Changes in absorption maxima measured at 325 nm after irradiation with λ = 365 nm until the PSS is reached. $t_{0.5}$ = 203 h.

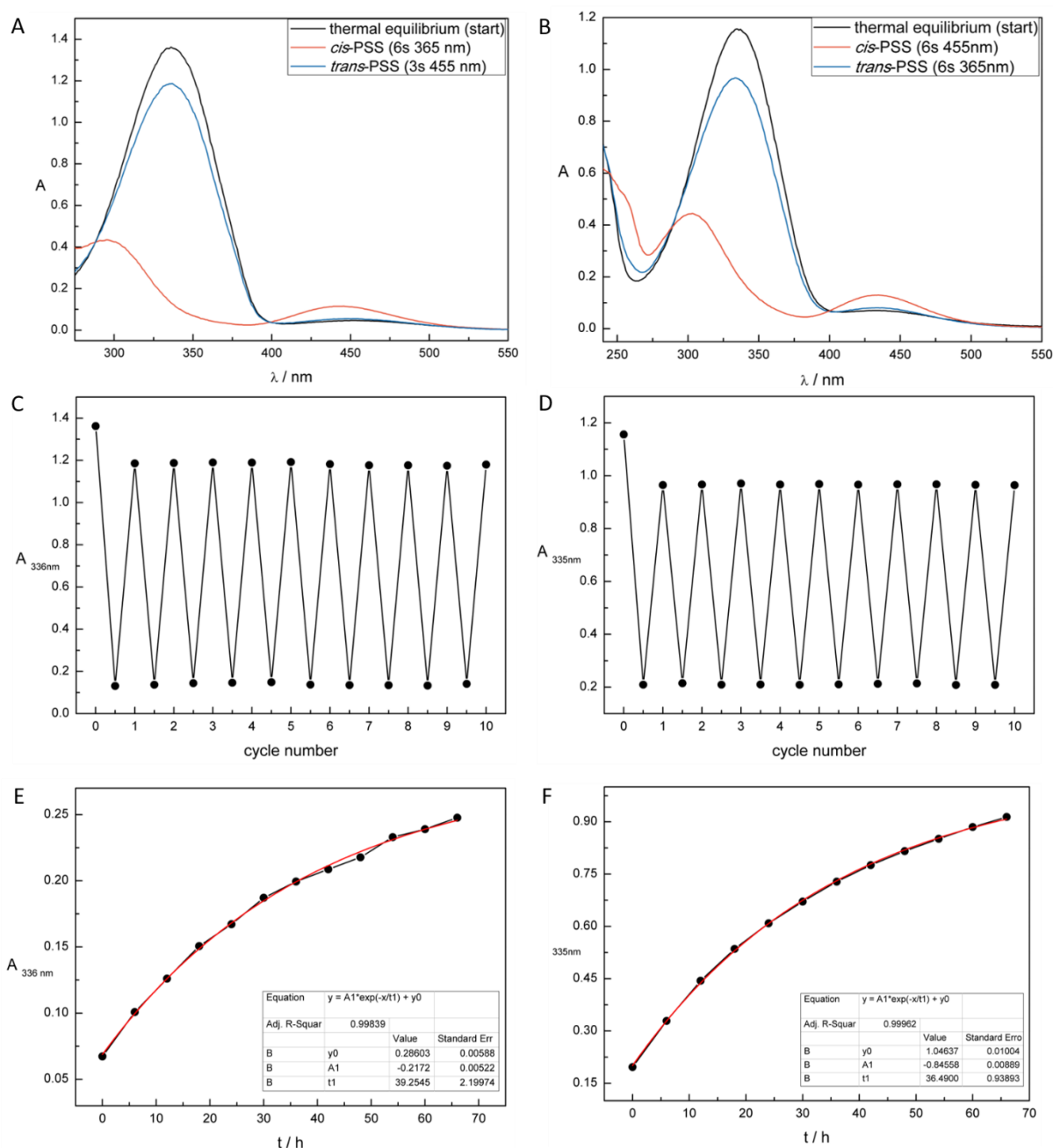
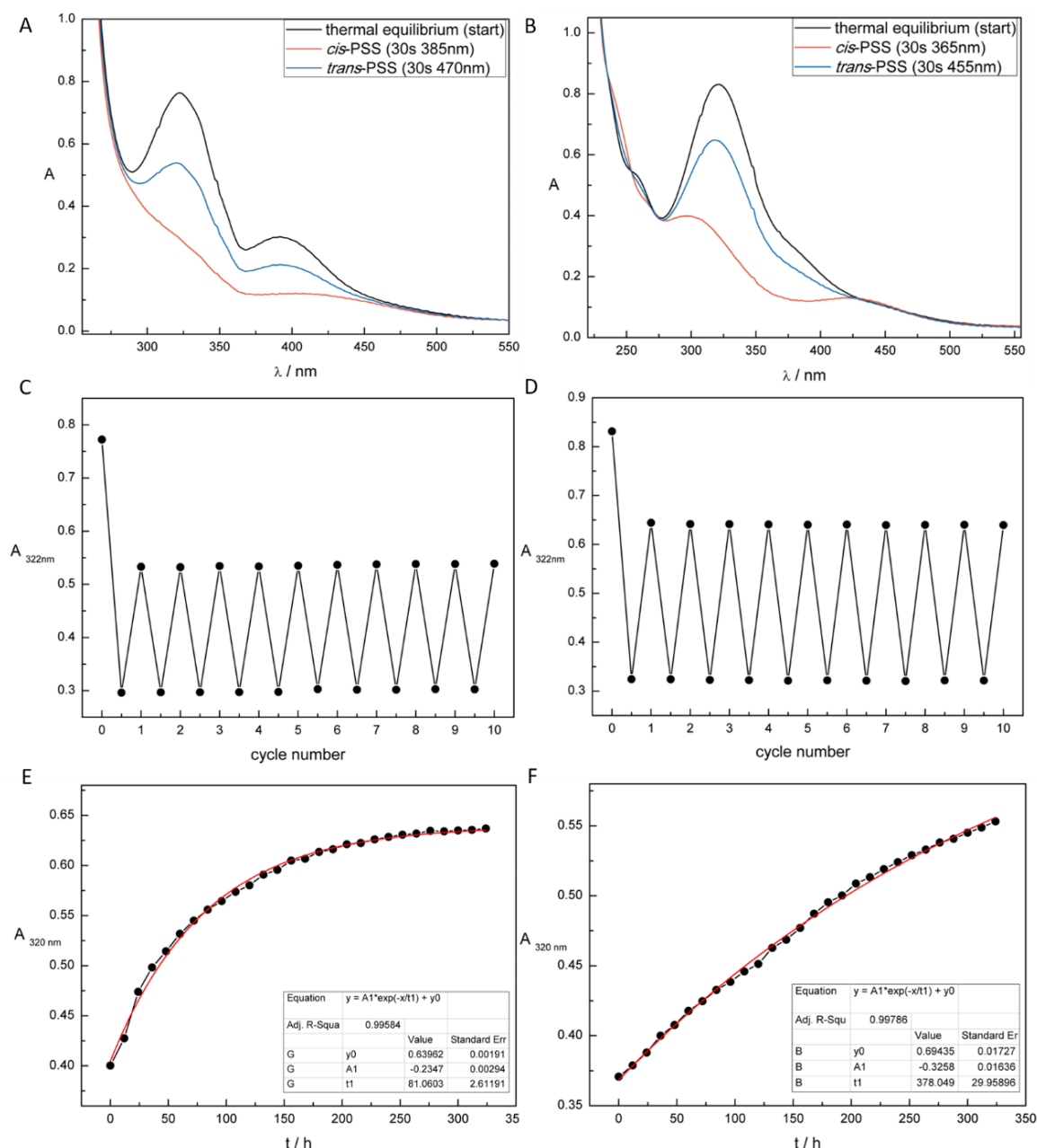


Figure S8. Changes in absorption spectra of 39 upon continuous irradiation until the PSS is reached. (A) 50 μ M in DMSO. λ (*cis*-PSS) = 336 nm, λ (*trans*-PSS) = 446 nm. (B) 50 μ M in phosphate buffer + 1% DMSO. λ (*cis*-PSS) = 335 nm, λ (*trans*-PSS) = 434 nm. **Cycle performance of 39.** (C) 50 μ M in DMSO. Changes in absorption at 336 nm (λ_{max} of the *trans* isomer) were measured during alternate irradiation with light of λ = 365 nm and λ = 455 nm until the PSS is reached. (D) 50 μ M in phosphate buffer + 1% DMSO. Changes in absorption at 335 nm (λ_{max} of the *trans* isomer) were measured during alternate irradiation with light of λ = 365 nm and λ = 455 nm until the PSS is reached. **Thermal stability of the *cis* isomer of 39 measured at 25 °C.** Black dots represent the absorption at the indicated wavelength dependent on the time of relaxation [h]. Red curve represents an exponential nonlinear curve fit. (E) 25 μ M in DMSO. Changes in absorption maxima measured at 336 nm (λ_{max} of the *trans* isomer) after irradiation with λ = 365 nm until the PSS is reached. $t_{0.5}$ = 27.2 h. (F) 50 μ M solution in phosphate buffer + 1% DMSO. Changes in absorption maxima measured at 350 nm after irradiation with λ = 365 nm until the PSS is reached. $t_{0.5}$ = 25.3 h.



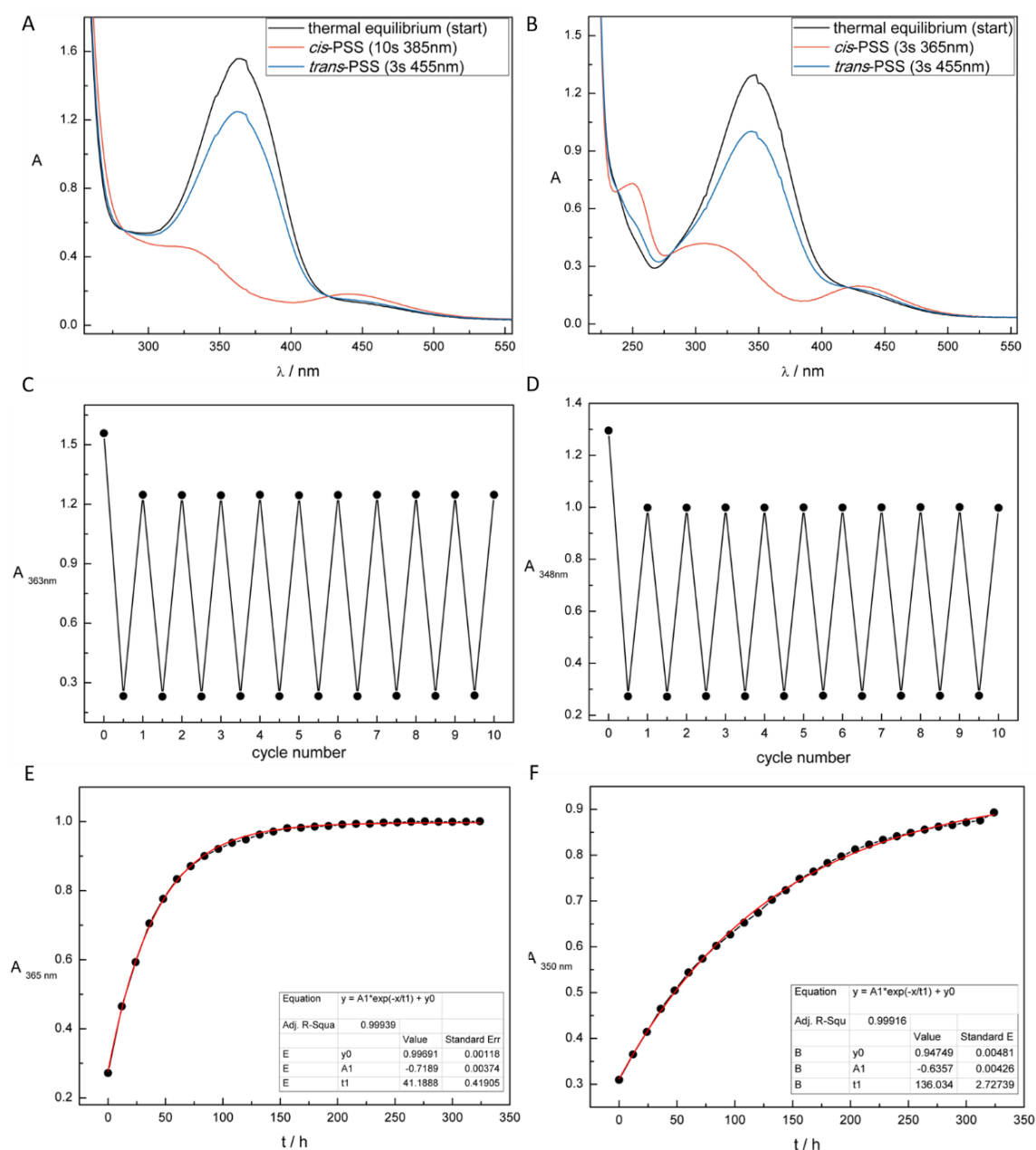


Figure S10. Changes in absorption spectra of 41 upon continuous irradiation until the PSS is reached. (A) 50 μ M in DMSO. λ (*cis*-PSS) = 385 nm, λ (*trans*-PSS) = 455 nm. (B) 50 μ M in phosphate buffer + 0.1% DMSO. λ (*cis*-PSS) = 365 nm, λ (*trans*-PSS) = 455 nm. **Cycle performance of 41.** (C) 50 μ M in DMSO. Changes in absorption at 363 nm (λ_{\max} of the *trans* isomer) were measured during alternate irradiation with light of λ = 365 nm and λ = 455 nm until the PSS is reached. (D) 50 μ M in phosphate buffer + 0.1% DMSO. Changes in absorption at 348 nm (λ_{\max} of the *trans* isomer) were measured during alternate irradiation with light of λ = 365 nm and λ = 455 nm until the PSS is reached. **Thermal stability of the *cis* isomer of 41 measured at 25 °C.** Black dots represent the absorption at the indicated wavelength dependent on the time of relaxation [h]. Red curve represents an exponential nonlinear curve fit. (E) 50 μ M in DMSO. Changes in absorption maxima measured at 365 nm after irradiation with λ = 385 nm until the PSS is reached. $t_{0.5}$ = 28.5 h. (F) 50 μ M solution in phosphate buffer + 0.1% DMSO. Changes in absorption maxima measured at 350 nm after irradiation with λ = 365 nm until the PSS is reached. $t_{0.5}$ = 94.3 h.

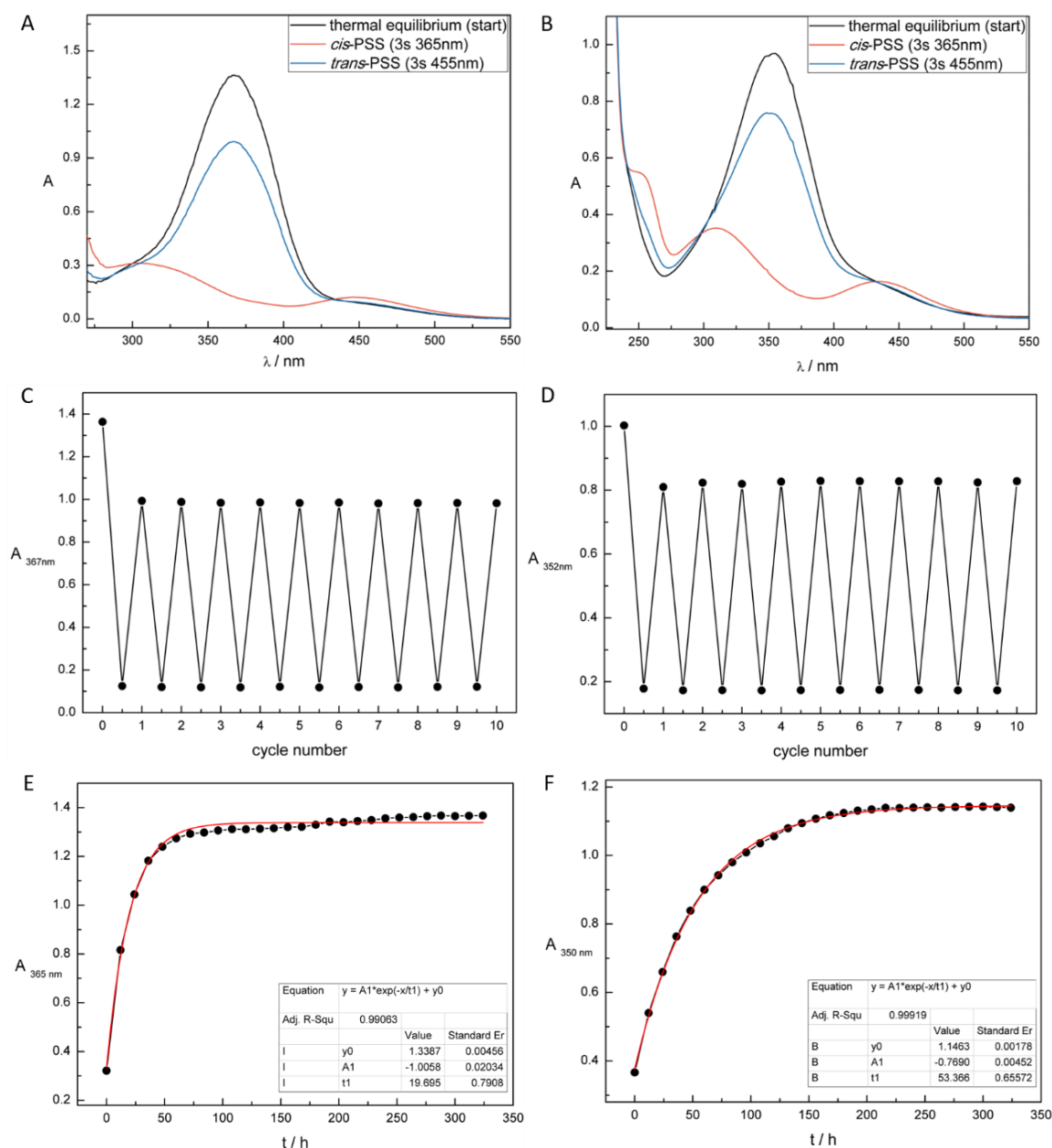


Figure S11. Changes in absorption spectra of 42 upon continuous irradiation until the PSS is reached. (A) 50 μ M in DMSO. λ (*cis*-PSS) = 365 nm, λ (*trans*-PSS) = 455 nm. (B) 50 μ M in phosphate buffer + 0.1% DMSO. λ (*cis*-PSS) = 365 nm, λ (*trans*-PSS) = 455 nm. **Cycle performance of 42.** (C) 50 μ M in DMSO. Changes in absorption at 367 nm (λ_{\max} of the *trans* isomer) were measured during alternate irradiation with light of λ = 365 nm and λ = 455 nm until the PSS is reached. (D) 50 μ M in phosphate buffer + 1% DMSO. Changes in absorption at 352 nm (λ_{\max} of the *trans* isomer) were measured during alternate irradiation with light of λ = 365 nm and λ = 455 nm until the PSS is reached. **Thermal stability of the *cis* isomer of 42 measured at 25 °C.** Black dots represent the absorption at the indicated wavelength dependent on the time of relaxation [h]. Red curve represents an exponential nonlinear curve fit. (E) 50 μ M in DMSO. Changes in absorption maxima measured at 367 nm (λ_{\max} of the *trans* isomer) after irradiation with λ = 365 nm until the PSS is reached. $t_{0.5}$ = 13.6 h. (F) 50 μ M solution in phosphate buffer + 1% DMSO. Changes in absorption maxima measured at 350 nm after irradiation with λ = 365 nm until the PSS is reached. $t_{0.5}$ = 37.0 h.

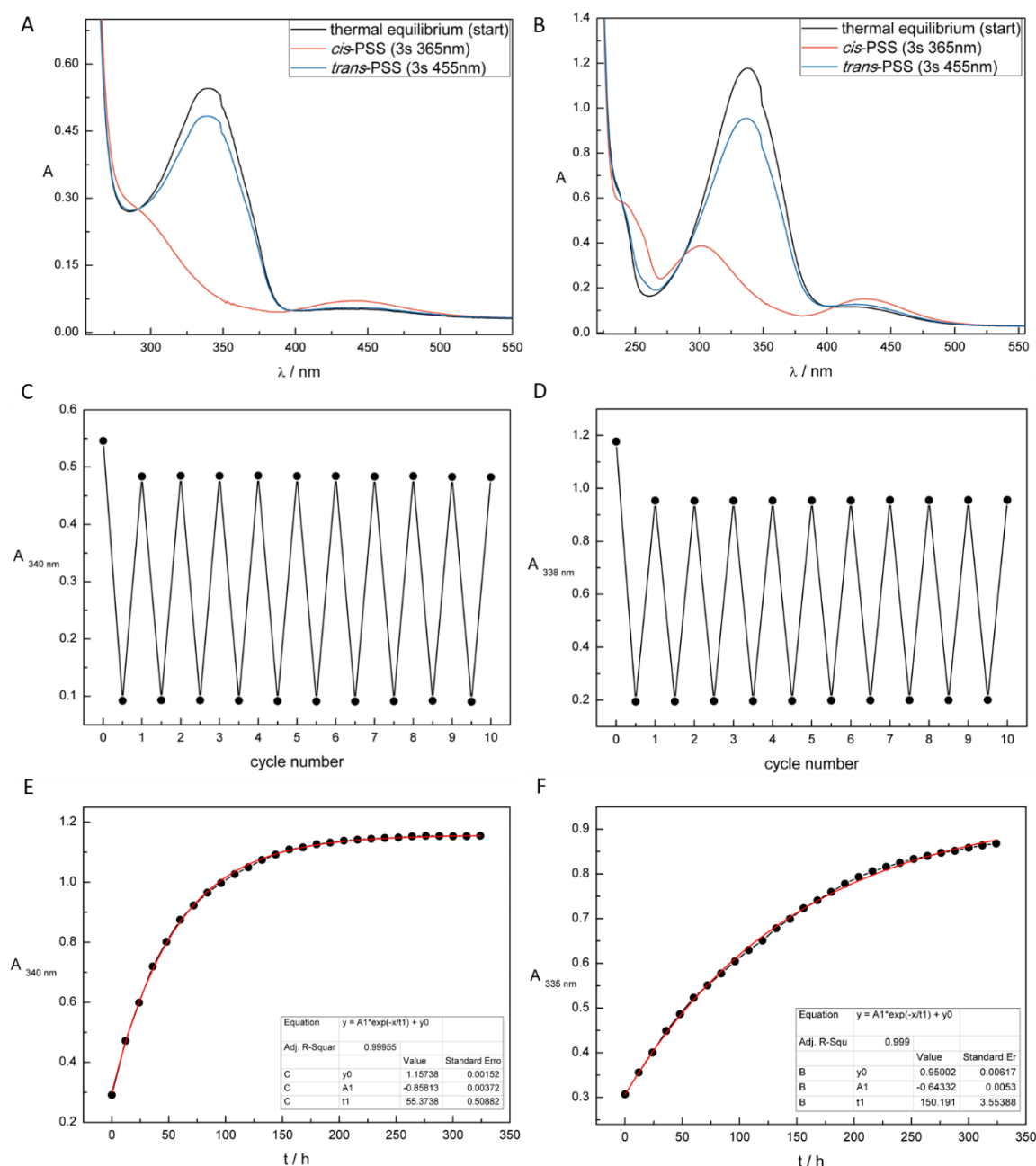


Figure S12. Changes in absorption spectra of 49 upon continuous irradiation until the PSS is reached. (A) 50 μ M in DMSO. λ (*cis*-PSS) = 365 nm, λ (*trans*-PSS) = 455 nm. (B) 50 μ M in phosphate buffer + 0.1% DMSO. λ (*cis*-PSS) = 365 nm, λ (*trans*-PSS) = 455 nm. **Cycle performance of 49.** (C) 50 μ M in DMSO. Changes in absorption at 340 nm (λ_{\max} of the *trans* isomer) were measured during alternate irradiation with light of λ = 365 nm and λ = 455 nm until the PSS is reached. (D) 50 μ M in phosphate buffer + 0.1% DMSO. Changes in absorption at 338 nm (λ_{\max} of the *trans* isomer) were measured during alternate irradiation with light of λ = 365 nm and λ = 455 nm until the PSS is reached. **Thermal stability of the *cis* isomer of 49 measured at 25 °C.** Black dots represent the absorption at the indicated wavelength dependent on the time of relaxation [h]. Red curve represents an exponential nonlinear curve fit. (E) 50 μ M in DMSO. Changes in absorption maxima measured at 340 nm (λ_{\max} of the *trans* isomer) after irradiation with λ = 365 nm until the PSS is reached. $t_{0.5}$ = 38.4 h. (F) 50 μ M solution in phosphate buffer + 0.1% DMSO. Changes in absorption maxima measured at 335 nm after irradiation with λ = 365 nm until the PSS is reached. $t_{0.5}$ = 104 h.

Table S1. Photochemical properties of azobenzene-based galactosidase inhibitors measured 50 μ M in DMSO at 25 °C. Cpd. = Compound.

Entry	Cpd.	λ_{max} <i>trans</i> isomer [nm]	λ_{max} <i>cis</i> isomer [nm]	Isosbestic points [nm]	Fatigue resistance	λ_{irr} <i>trans-cis</i> [nm]	λ_{irr} <i>cis-trans</i> [nm]
1	4	329	435	283, 386	excellent	365	455
2	6	401	445	271, 300, 360, 477	excellent	400	505
3	34	329	441	279, 389	excellent	365	455
4	35	331	436	282, 389	excellent	365	455
5	36	337	442	289, 396	excellent	365	455
6	37	327	440	278, 394	excellent	365	455
7	38	328	432	278, 386	excellent	365	455
8	39	336	446	288, 399	excellent	365	455
9	40	322	-	-	excellent	385	470
10	41	363	440	283, 426	excellent	385	455
11	42	367	446	302, 433	excellent	365	455
12	49	340	441	291, 398	excellent	365	455

Table S2. Photochemical properties of azobenzene-based galactosidase inhibitors measured 50 μ M in phosphate buffer + 0.01% DMSO, and 1% DMSO*, respectively. Cpd. = Compound.

Entry	Cpd.	λ_{max} <i>trans</i> isomer [nm]	λ_{max} <i>cis</i> isomer [nm]	Isosbestic points [nm]	Fatigue resistance	λ_{irr} <i>trans-cis</i> [nm]	λ_{irr} <i>cis-trans</i> [nm]
1	4	323	425	237, 280, 385	excellent	365	455
2	6	379	-	279, 293, 335, 464	excellent	455	-
3	34	325	431	234, 274, 390	excellent	365	455
4	35	329	426	238, 278, 396	excellent	365	455
5	36*	334	431	242, 287, 399	excellent	365	455
6	37	325	431	241, 275, 390	excellent	365	455
7	38	323	423	235, 273, 388	excellent	365	455
8	39*	335	434	245, 288, 399	excellent	365	455
9	40	322	428	235, 254, 273, 428	excellent	365	455
10	41	348	429	238, 280, 421	excellent	365	455
11	42*	352	433	241, 297, 432	excellent	365	455
12	49	338	430	240, 288, 407	excellent	365	455

3.5.3 HPLC- and NMR-Based Photochromic Characterization

Table S3. Photochemical properties of azobenzene-based galactosidase inhibitors measured 50 μ M in DMSO at 25 °C. Cpd. = Compound.

Entry	Cpd.	PSS-distribution (DMSO)	PSS-distribution (aqueous media)	THL [h] (DMSO)	THL [h] (PBS+0.1% / 1%* DMSO)
1	4	74% <i>cis</i> (375 nm) ^(a)	67% <i>cis</i> (375 nm) ^(a)	121	536
		88% <i>trans</i> (405 nm) ^(a)	75% <i>trans</i> (405 nm) ^(a)		
2	6	91% <i>cis</i> (400 nm) ^(b)	n.d.	3.53	$4.70 \cdot 10^{-4}$
		64% <i>trans</i> (505 nm) ^(b)			
3	34	53% <i>cis</i> (365 nm) ^(b)	93% <i>cis</i> (365 nm) ^(b)	84.4	98.2
		78% <i>trans</i> (455 nm) ^(b)	74% <i>trans</i> (455 nm) ^(b)		
4	35	93% <i>cis</i> (365 nm) ^(a)	88% <i>cis</i> (365 nm) ^(a)	80.2	252
		82% <i>trans</i> (455 nm) ^(a)	72% <i>trans</i> (455 nm) ^(a)		
5	36*	63% <i>cis</i> (365 nm) ^(b)	90% <i>cis</i> (365 nm) ^(b)	65.2	131
		72% <i>trans</i> (455 nm) ^(b)	82% <i>trans</i> (455 nm) ^(b)		
6	37	86% <i>cis</i> (365 nm) ^(b)	76% <i>cis</i> (365 nm) ^(b)	122	17.4
		83% <i>trans</i> (455 nm) ^(b)	77% <i>trans</i> (455 nm) ^(b)		
7	38	89% <i>cis</i> (365 nm) ^(a)	83% <i>cis</i> (365 nm) ^(a)	106	203
		81% <i>trans</i> (455 nm) ^(a)	75% <i>trans</i> (455 nm) ^(a)		
8	39*	92% <i>cis</i> (365 nm) ^(b)	90% <i>cis</i> (365 nm) ^(b)	27.2	25.3
		82% <i>trans</i> (455 nm) ^(b)	82% <i>trans</i> (455 nm) ^(b)		
9	40	84% <i>cis</i> (385 nm) ^(a)	81% <i>cis</i> (365 nm) ^(a)	56.2	262
		63% <i>trans</i> (455 nm) ^(a)	63% <i>trans</i> (455 nm) ^(a)		
10	41	91% <i>cis</i> (385 nm) ^(a)	88% <i>cis</i> (365 nm) ^(a)	28.5	94.3
		73% <i>trans</i> (455 nm) ^(a)	69% <i>trans</i> (455 nm) ^(a)		
11	42*	89% <i>cis</i> (365 nm) ^(a)	90% <i>cis</i> (365 nm) ^(a)	13.6	37.0
		70% <i>trans</i> (455 nm) ^(a)	76% <i>trans</i> (455 nm) ^(a)		
12	49	96% <i>cis</i> (365 nm) ^(a)	93% <i>cis</i> (365 nm) ^(a)	38.4	104
		80% <i>trans</i> (455 nm) ^(a)	74% <i>trans</i> (455 nm) ^(a)		

(a) determined by analytical HPLC measurement of a preirradiated 50 μ M solution in DMSO and phosphate buffer + 0.1% DMSO, and 1% DMSO,* respectively, at 20 °C. (b) determined by NMR-measurement of a preirradiated solution in DMSO and D₂O + 5% DMSO,* respectively.

3.5.4 Enzymatic Inhibition

Table S4. Inhibitory activity of photochromic competitive β -galactosidase inhibitors measured at a substrate concentration of 100 μ M, an enzyme concentration of 36 pM. Inhibitor concentrations were chosen according to the compound solubility and are indicated below. Cpd. = Compound.

Entry	Cpd.	Relative activity <i>trans</i> isomer [%]	Relative activity <i>cis</i> -PSS [%]	Ratio (<i>cis</i> / <i>trans</i>)
1	4 ^(b)	77 \pm 29	85 \pm 15	1.1
2	6 ^(b,e)	78.5 \pm 1.7	n.d. ^(a)	-
3	34 ^(b,e)	0.48 \pm 0.16	0.88 \pm 0.09	1.8
4	35 ^(b,e)	16.6 \pm 1.6	11.8 \pm 2.1	0.7
5	36 ^(d,e)	23.7 \pm 2.4	15.2 \pm 1.0	0.6
6	37 ^(b)	-6.28 \pm 0.11	0.346 \pm 0.023	-
7	38 ^(b)	23 \pm 3	22 \pm 4	1.0
8	39 ^(d,e)	13.4 \pm 1.9	10.5 \pm 1.7	0.8
9	40 ^(b)	18.9 \pm 1.2	23.5 \pm 1.1	1.2
10	41 ^(b)	27 \pm 3	52 \pm 11	1.9
11	42 ^(c,e)	30.1 \pm 1.8	49 \pm 5	1.6
12	49 ^(b)	8.5 \pm 0.3	5.53 \pm 0.11	0.6

(a) n.d. due to thermal instability during enzymatic assay. (b) 100 μ M inhibitor concentration. (c) 50 μ M inhibitor concentration. (d) 25 μ M inhibitor concentration. (e) 1% DMSO present in assay buffer.

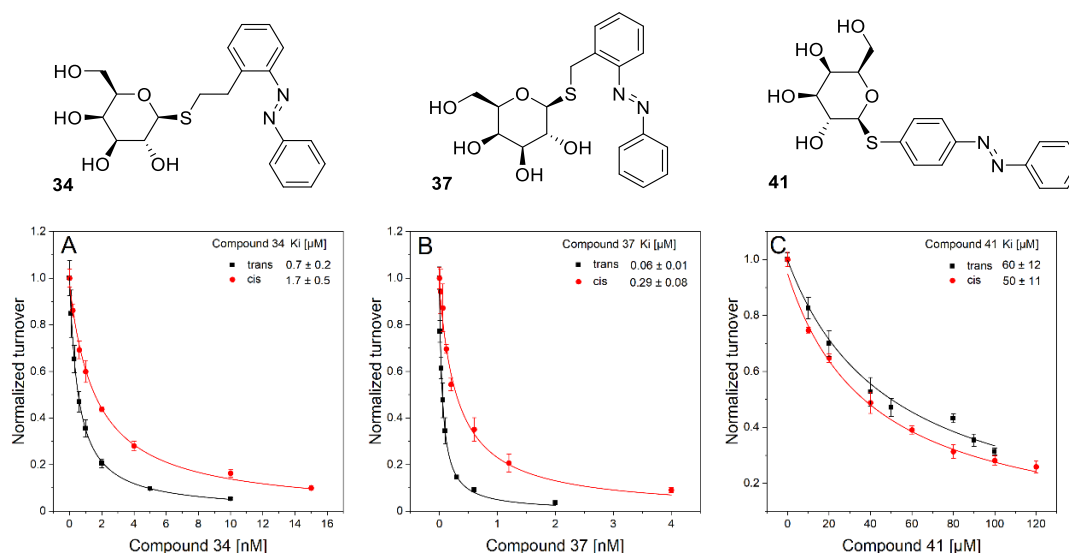


Figure S13. Normalized β -galactosidase kinetics at 100 μ M substrate concentration at different concentrations of (A) compound **34**; (B) compound **37** and (C) compound **41** either in its *trans*-isomeric state (black lines; thermal equilibrium) or its *cis*-PSS (red lines). An enzyme concentration of 36 pM was present in all experiments. Error bars indicate the standard deviation of three independent measurements. Enzyme kinetics were additionally measured at 50 and 150 μ M substrate concentration and the inhibition constant K_i was calculated as the average over these measurements.

3.6 References

- [1] W. A. Velema, W. Szymanski, B. L. Feringa, *J. Am. Chem. Soc.* **2014**, *136*, 2178-2191.
- [2] D. Bléger and S. Hecht, *Angew. Chem. Int. Ed.* **2015**, *54*, 11338-11349.
- [3] W. Szymanski, J. M. Beierle, H. A. V. Kistemaker, W. A. Velema, B. L. Feringa, *Chem. Rev.* **2013**, *113*, 6114-6178.
- [4] M. M. Lerch, M. J. Hansen, G. M. van Dam, W. Szymanski, B. L. Feringa, *Angew. Chem. Int. Ed.* **2016**, *55*, 10987-10999.
- [5] C. Brieke, F. Rohrbach, A. Gottschalk, G. Mayer, A. Heckel, *Angew. Chem. Int. Ed.* **2012**, *51*, 8446-8476.
- [6] M. M. Lerch, M. J. Hansen, W. A. Velema, W. Szymanski, B. L. Feringa, *Nat. Commun.* **2016**, *7*, 12054.
- [7] H. Bouas-Laurent and H. Dürr, *Pure Appl. Chem.* **2001**, *73*, 639-665.
- [8] P. Klán, T. Šolomek, C. G. Bochet, A. Blanc, R. Givens, M. Rubina, V. Popik, A. Kostikov, J. Wirz, *Chem. Rev.* **2013**, *113*, 119-191.
- [9] M. M. Lerch, W. Szymanski, B. L. Feringa, *Chem. Soc. Rev.* **2018**, *47*, 1910-1937.
- [10] J. Garcia-Amorós, M. Díaz-Lobo, S. Nonell, D. Velasco, *Angew. Chem. Int. Ed.* **2012**, *51*, 12820-12823.
- [11] J. Garcia-Amorós, M. C. R. Castro, P. Coelho, M. M. M. Raposo, D. Velasco, *Chem. Commun.* **2013**, *49*, 11427-11429.
- [12] J. Garcia-Amorós, S. Nonell, D. Velasco, *Chem. Commun.* **2012**, *48*, 3421-3423.
- [13] H. Kaufman, S. M. Vratsanos, B. F. Erlanger, *Science* **1968**, *162*, 1487-1489.
- [14] W. J. Deal, B. F. Erlanger, D. Nachmansohn, *Proc. Natl. Acad. Sci. U. S. A.* **1969**, *64*, 1230-1234.

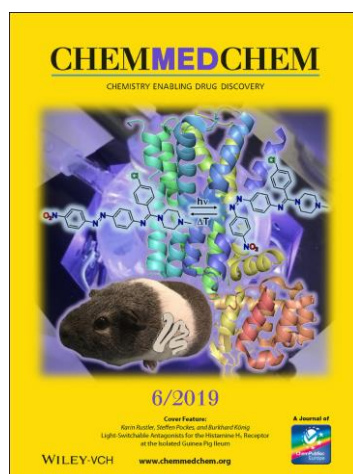
- [15] M. Volgraf, P. Gorostiza, R. Numano, R. H. Kramer, E. Y. Isacoff, D. Trauner, *Nat. Chem. Biol.* **2006**, 2, 47-52.
- [16] P. Gorostiza, M. Volgraf, R. Numano, S. Szobota, D. Trauner, E. Y. Isacoff, *Proc. Natl. Acad. Sci. U. S. A.* **2007**, 104, 10865-10870.
- [17] M. Volgraf, P. Gorostiza, S. Szobota, M. R. Helix, E. Y. Isacoff, D. Trauner, *J. Am. Chem. Soc.* **2007**, 129, 260-261.
- [18] M. Wegener, M. J. Hansen, A. J. M. Driessen, W. Szymanski, B. L. Feringa, *J. Am. Chem. Soc.* **2017**, 139, 17979-17986.
- [19] A. Polosukhina, J. Litt, I. Tochitsky, J. Nemargut, Y. Sychev, I. de Kouchkovsky, T. Huang, K. Borges, D. Trauner, R. N. van Gelder, R. H. Kramer, *Neuron* **2012**, 75, 271-282.
- [20] I. Tochitsky, A. Polosukhina, V. E. Degtyar, N. Gallerani, C. M. Smith, A. Friedman, R. N. van Gelder, D. Trauner, D. Kaufer, R. H. Kramer, *Neuron* **2014**, 81, 800-813.
- [21] N. A. Simeth, A. C. Kneuttinger, R. Sterner, B. König, *Chem. Sci.* **2017**, 8, 6474-6483.
- [22] N. A. Simeth, L. M. Altmann, N. Wössner, E. Bauer, M. Jung, B. König, *J. Org. Chem.* **2018**, 83, 7919-7927.
- [23] B. Eisel, F. Hartrampf, T. Meier, D. Trauner, *FEBS Lett.* **2018**, 592, 343-355.
- [24] D. Wilson, J. W. Li, N. R. Branda, *ChemMedChem* **2017**, 12, 284-287.
- [25] R. Ferreira, J. R. Nilsson, C. Solano, J. Andréasson, M. Grøtli, *Sci. Rep.* **2015**, 5, 9769-9776.
- [26] J. Broichhagen, I. Jurastow, K. Iwan, W. Kummer, D. Trauner, *Angew. Chem. Int. Ed.* **2014**, 53, 7657-7660.

- [27] D. Wutz, D. Gluhaceic, A. Chakrabarti, K. Schmidtkunz, D. Robaa, F. Erdmann, C. Romier, W. Sippl, M. Jung, B. König, *Org. Biomol. Chem.* **2017**, *15*, 4882-4896.
- [28] D. H. Juers, B. W. Matthews, R. E. Huber, *Protein Science* **2012**, *21*, 1792-1807.
- [29] Q. Husain, *Crit. Rev. Biotechnol.* **2010**, *30*, 41-62.
- [30] P. Mogalisetti, H. H. Gorris, M. J. Rojek, D. R. Walt, *Chem. Sci.* **2014**, *5*, 4467-4473.
- [31] M. J. Mickert, H. H. Gorris, *J. Phys. Chem. B* **2018**, *122*, 5809-5819.
- [32] A. G. Hadd, D. E. Raymond, J. W. Halliwell, S. C. Jacobson, J. M. Ramsey, *Anal. Chem.* **1997**, *69*, 3407-3412.
- [33] R. E. Huber, M. T. Gaunt, *Can. J. Biochem.* **1982**, *60*, 608-612.
- [34] R. B. Liebherr, A. Hutterer, M. J. Mickert, F. C. Vogl, A. Beutner, A. Lechner, H. Hummel, H. H. Gorris, *Anal. Bioanal. Chem.* **2015**, *407*, 7443-7452.
- [35] M. Kleban, P. Hilgers, J. N. Greul, R. D. Kugler, J. Li, S. Picasso, P. Vogel, V. Jäger, *ChemBioChem* **2001**, *2*, 365-368.
- [36] J. N. Greul, M. Kleban, B. Schneider, S. Picasso, V. Jäger, *ChemBioChem* **2001**, *2*, 368-370.
- [37] H. H. Gorris, D. M. Rissin, D. R. Walt, *PNAS* **2007**, *104*, 17680-17685.
- [38] E. Mitscherlich, *Ann. Pharm.* **1834**, *12*, 311-314.
- [39] G. S. Hartley, *Nature* **1937**, *140*, 281-282.
- [40] L. Lindner, P. Klüfers, *Z. Anorg. Allg. Chem.* **2015**, *641*, 1869-1873.
- [41] M. P. Seed, M. Burnet, H. J. Gutcke, *Assignee Diosamine Development Corporation Patent* **2008**, WO2008059003 A1.
- [42] R. Rajaganesh, A. Gopal, T. M. Das, A. Ajayaghosh, *Org. Lett.* **2012**, *14*, 748-751.

- [43] A. G. Watts, T. Kantner, A. B. MacKenzie, *Assignee The University of Bath* **2010**, WO2010070300A2.
- [44] L. M. Doyle, S. O'Sullivan, C. Di Salvo, M. McKinney, P. McArdle, P. V. Murphy, *Org. Lett.* **2017**, *19*, 5802-5805.
- [45] X. Xiao, Y. Zhao, P. Shu, X. Zhao, Y. Liu, J. Sun, Q. Zhang, J. Zeng, Q. Wan, *J. Am. Chem. Soc.* **2016**, *138*, 13402-13407.
- [46] X. Li, L. Huang, X. Hu, X. Huang, *Org. Biomol. Chem.* **2009**, *7*, 117-127.
- [47] H. Wang, S. Sun, J. Cheng, *Tetrahedron Letters* **2017**, *58*, 3875-3878.
- [48] M. Poláková, S. Šesták, E. Lattová, L. Petruš, J. Mucha, I. Tvaroška, J. Kóňa, *Eur. J. Med. Chem.* **2011**, *46*, 944-952.
- [49] D. Zhao, M. Johansson, J.-E. Bäckvall, *Eur. J. Org. Chem.* **2007**, *26*, 4431-4436.
- [50] N. Marquestaut, A. Martin, D. Talaga, L. Servant, S. Ravaine, S. Reculosa, D. M. Bassani, E. Gillies, F. Lagugné-Labarhet, *Langmuir* **2008**, *24*, 11313-11321.
- [51] O. Trott, A. J. Olson, *J. Comput. Chem.* **2010**, *31*, 455-461.
- [52] E. Krieger, G. Vriend, *Bioinformatics* **2014**, *30*, 2981-2982.
- [53] M. Polakova, S. Sestak, E. Lattova, L. Petrus, J. Mucha, I. Tvaroska, J. Kona, *Eur. J. Med. Chem.* **2011**, *46*, 944-952.

CHAPTER 4

4 Light-Switchable Antagonists for the Histamine H₁ Receptor at the Isolated Guinea Pig Ileum



This chapter has been published as:

K. Rustler, S. Pockes, B. König, *ChemMedChem* **2019**, 14, 636-644.

This project was performed in collaboration with Dr. S. Pockes (Prof. S. Elz, University of Regensburg). K. Rustler performed the synthesis and (photo-)chemical investigation of all compounds. Dr. S. Pockes performed tests at the isolated guinea pig ileum. Dr. P. Nitschke (Prof. R. Gschwind, University of Regensburg) measured the photostationary states *via* NMR spectroscopy under constant irradiation. Single crystal X-ray crystallography and mass spectrometry analysis were performed by the analytical department at the University of Regensburg. K. Rustler and Dr. S. Pockes wrote the manuscript. Prof. B. König supervised the project. Dr. S. Pockes and Prof. B. König are corresponding authors.

4.1 Introduction

The biogenic amine histamine is stored in vesicles or granules, and upon stimulation is released by various cell types, such as mast and enterochromaffin cells. Subsequent binding can occur at four different histamine receptors (H_1R , H_2R , H_3R , H_4R) present in various tissues, for example, smooth muscle and endothelial cells for H_1R . Those receptors belong to the rhodopsin-like family A of G protein-coupled receptors (GPCRs), a subfamily of the GPCR superfamily.^[1-7] GPCRs contain seven transmembrane domains including an extracellular N terminus and an intracellular C terminus – the latter being able to interact with G proteins.^[8,9] Amongst them, H_1R is related to symptoms of inflammatory processes and contraction of the intestinal smooth muscle,^[2,4,10,11] which is the basis for the organ-pharmacological studies presented herein. Although a multitude of H_1 antihistamines have been developed and are in clinical use, these drugs show a wide variety in chemical structure, pharmacology, side effects (*e.g.*, sedation), and toxicity.^[2,12,13] Furthermore, the complexity of GPCR function and the diversity of receptor subtypes makes it difficult to develop new structures and investigate their exact mode of operation. For a better understanding of the pharmacokinetics and pharmacodynamics, as well as spatial and temporal control of histamine antagonists, a photochromic H_1 receptor ligand may overcome some limitations of conventional drugs and could be an important tool to study the dynamics of this receptor at the molecular level.^[14-16]

Light is an ideal external trigger of pharmacological functions for a variety of reasons. It can be modulated in its intensity (dosage control) and it can be focused to very small areas (sub-micron accuracy) with high temporal and spatial precision in a non-invasive fashion, depending on wavelength, intensity, and duration.^[17-20] Light-responsive molecules with bioactivity are finding increasing use in biological and pharmaceutical applications in the emerging field of photopharmacology.^[17,19] Three main approaches to introduce light-responsiveness can be distinguished, some as irreversible or as reversible

processes. In the single-cycle irreversible caged-ligand (CL) approach, a deactivating photosensitive chemical protecting group (cage) renders the biologically interacting group ineffective. Restoration of the active structure occurs by light-stimulated cleavage with the formation of a by-product, such as the remnants of the protecting group.^[21-24] In contrast, a reversible multicycle approach is offered by photoswitchable tethered ligands (PTLs)^[25-27] and photoswitchable orthogonal remotely tethered ligands (PORTLs).^[15] Both approaches use a flexible linker that allows anchoring on a remote site of the engineered receptor.^[15,25-27] The most common technique is represented by photochromic ligands (PCLs) serving as freely diffusible light-controllable small-molecule drugs. Typically, the ligand carries a photosensitive unit that can be switched between two or more configurations, thereby changing the binding properties to the native receptor.^[18] Considering the limitations of the various approaches,^[28] PCLs were chosen as the mode of operation in our study, allowing an organ-pharmacological investigation on the native H₁R (guinea pig). Within the group of PCLs, different photoinduced mechanisms are used. For example, dithienylethenes (DTEs) and fulgimides are based on an intramolecular 6 π -electrocyclic reaction resulting in bond formation (closed isomer) and bond cleavage (open isomer).^[29-32] In contrast, azobenzenes rely on a light-inducible *trans*-*cis* isomerization. The thermodynamically more stable *trans* isomer takes up an extended planar configuration with a dipole moment near zero, compared with the higher energy, metastable nonplanar *cis* isomer. Although the *trans* isomer can be regenerated 100% by thermal relaxation, full conversion by irradiation with visible light is impossible owing to a substantial overlap of the absorption spectra of both isomers. Additional benefits, besides their large geometrical change, include reversibility of 10⁵ to 10⁶ cycles without detectable photodegradation or loss of responsiveness, synthetic accessibility *via* Mills reaction, oxidative/reductive coupling or azo coupling, and tunability of their photochromic properties.^[33-36] Furthermore, azobenzene-based photoresponsive systems have already been successfully applied in several biological systems.^[37-41]

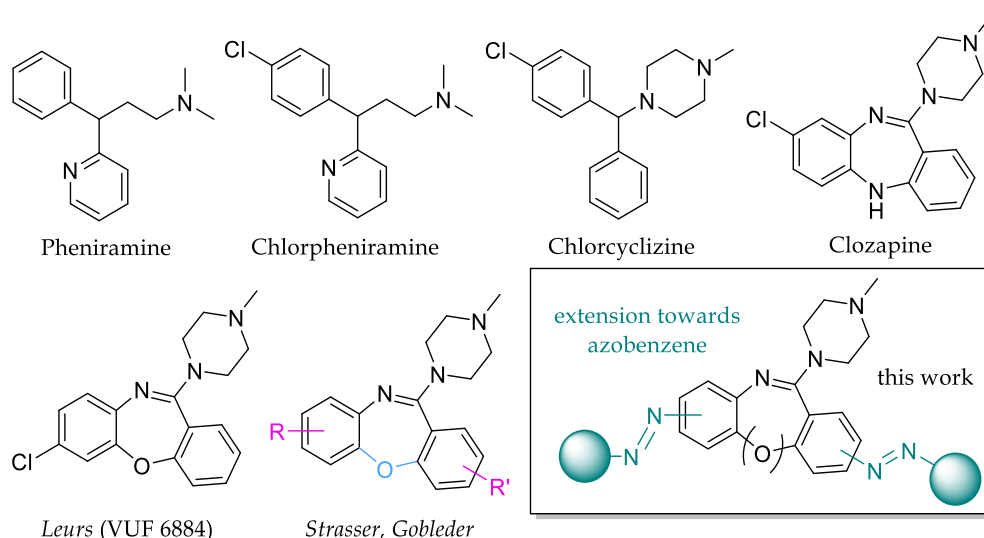
Recently, the research groups of Wijtmans and Leurs reported the use of a bidirectional photoswitchable antagonist toolbox for the H₃R, a GPCR, based on azobenzene.^[16]

We designed a photochromic antagonist for the H₁R based on azobenzene as the photochromic scaffold. The clozapine derivative VUF6884^[42,43] and dibenzo[*b,f*][1,4]oxazepine derivatives,^[5,44,45] showing antagonistic behavior at the H₁R, served as the molecular design models. Herein we report the design, synthesis, photochromic characterization, and organ-pharmacological investigations of azobenzene-based histamine H₁R ligands.

4.2 Results and Discussion

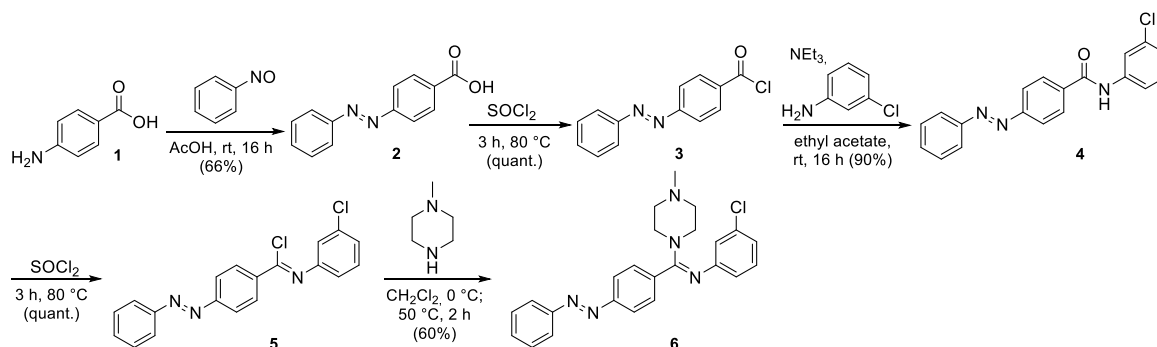
4.2.1 Design and Syntheses

Design. The design of the investigated photochromic histamine H₁ receptor ligands is derived from the work of Strasser^[5,44] and Gobleder^[45] based on substitution studies on the clozapine derivative VUF6884^[42,43] developed by the research group of Leurs (Scheme 1). In general, the beneficial effect of electron-withdrawing groups (*e.g.*, chlorine) and the addition of a basic moiety (*e.g.*, methylpiperazine) has been well investigated for the development of potent histamine antagonists.^[13,46-48] Derived from the standard antihistamines mepyramine (pA₂ = 8.95)^[46] and diphenhydramine (pA₂ = 7.68)^[46] compounds such as pheniramine (pA₂ = 7.82, Scheme 1),^[46] chlorpheniramine (pA₂ = 8.82, Scheme 1)^[46] and chlorcyclizine (pA₂ = 7.98, Scheme 1)^[46] were investigated in the 1940s and 1950s. Various substituted ring-open derivatives and one ring-closed tricyclic derivative containing an azobenzene photochromic moiety were synthesized. The best photochromic antagonist **19** was further optimized, resulting in the bathochromically shifted azobenzene derivatives **35** and **41**.



Scheme 1. Reported parent compounds and modifications towards a photochromic azobenzene derivative.^[5,44,45,42,43,46-48]

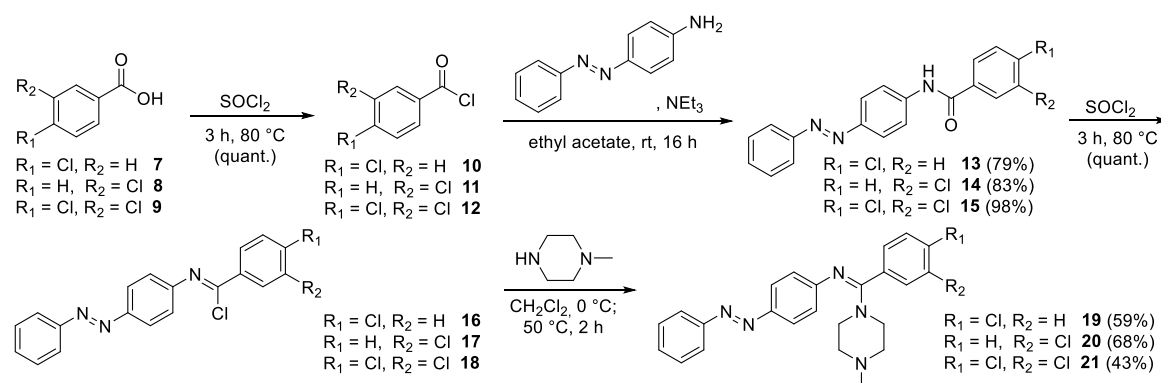
Synthesis of the azobenzene-4-methanimine derivative. The synthesis of azobenzene-4-methanimine **6** was performed as outlined in Scheme 2. In a first synthetic step the *para* carboxy-substituted azobenzene **2** was synthesized in a Mills reaction in acetic acid starting from 4-aminobenzoic acid (**1**) and nitrosobenzene.^[49] Activation of the carboxylic acid moiety of **2** using thionyl chloride^[50] afforded the acid chloride **3** and allowed the subsequent reaction with 3-chloroaniline in the presence of triethylamine to form the *meta* chloro-substituted azobenzene amide **4**.^[51] A second activation step of amide **4** using thionyl chloride^[52] to obtain imino chloride **5** afforded the target compound **6** upon reaction with *N*-methylpiperazine.^[5,45]



Scheme 2. Synthesis of the ring open azobenzene-4-methanimine derivative **6**.^[5,45,49-52]

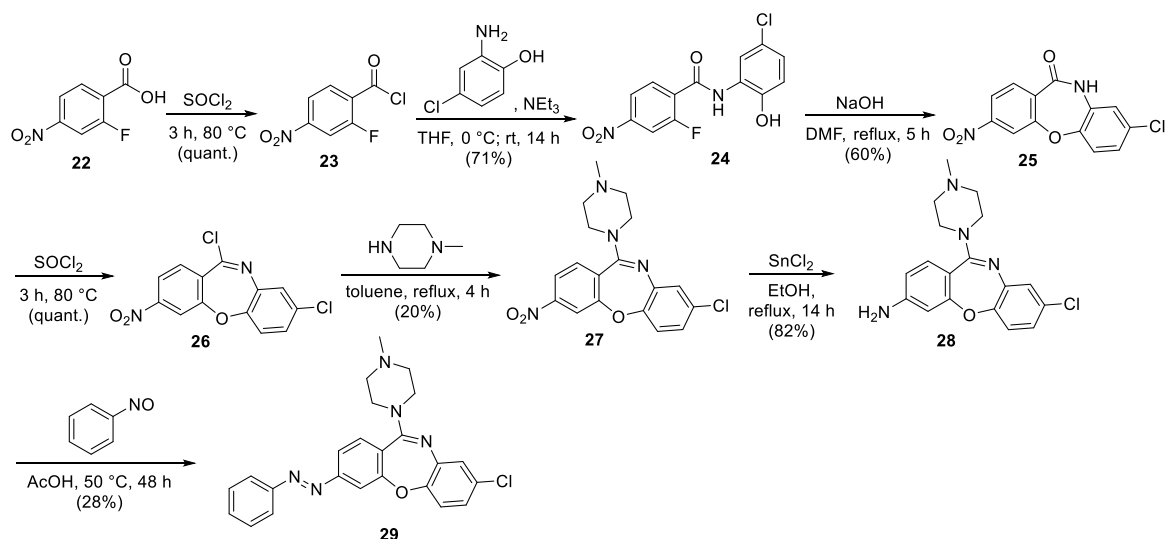
Synthesis of the *para* aminoazobenzene derivatives. In comparison with the substitution patterns analyzed by Strasser^[5,44] and Gobleder,^[45] the variously

chloro-substituted *para* aminoazobenzene derivatives **19-21** were synthesized as depicted in Scheme 3. The synthetic strategy was kept in analogy to the synthesis of the azobenzene-4-methanimine **6** (Scheme 2) using *para*-aminoazobenzene as starting material. The differently chloro-substituted benzoic acids **7-9** were activated as acid chlorides **10-12**^[50] and subsequently converted into the respective amide derivatives **13-15** by reaction with *para* aminoazobenzene.^[51] Formation of the highly reactive imino chlorides **16-18**^[52] allowed the introduction of *N*-methylpiperazine^[5,45] to afford target compounds **19-21**.



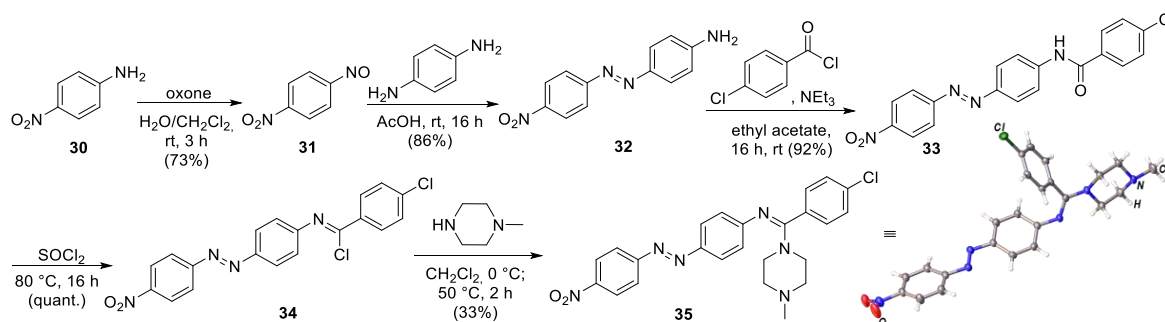
Scheme 3. Synthesis of the ring-open *para* aminoazobenzene derivatives **19-21**.^[5,45,50-52]

Synthesis of the ring-closed derivative. The synthesis of the photochromic ring-closed derivative was performed as reported for the non-photochromic amino precursor **28**,^[5,45] and adding a Mills reaction in the final step (Scheme 4). Carboxylic acid **22** was converted into its corresponding acid chloride **23**,^[50] which reacted with 2-amino-4-chlorophenol to yield the highly functionalized amide **24**. Ring closure was performed by the addition of pulverized sodium hydroxide and heating.^[5] The cyclic amide **25** was activated to its imino chloride **26**^[52] and reacted with *N*-methylpiperazine to give the nitro-substituted derivative **27**.^[5] Reduction of the nitro group of **27** to its amine **28**^[5] allowed installation of an azo bridge in a Mills reaction^[53] and provided the photochromic tricyclic ring-closed derivative **29**.



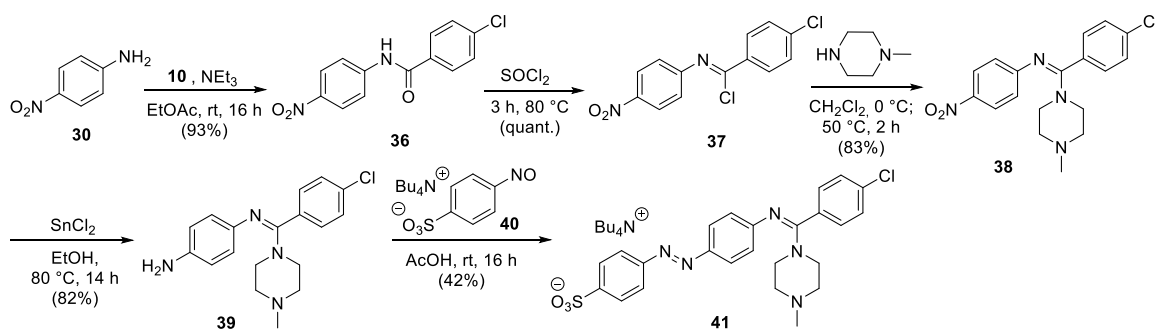
Scheme 4. Synthesis of the ring-closed photochromic derivative **29**.^[5,45,52,53]

Synthesis of the bathochromically shifted derivatives of **19.** To increase solubility and to avoid the use of UV light, a nitro-substituted push-pull azobenzene derivative **35** and a sulfonate-substituted derivative **41** (negatively charged at physiological pH) of the so-far most active compound **19** were synthesized. For the nitro-substituted derivative (Scheme 5), aminoazobenzene **32** was synthesized *via* a Mills reaction^[53] of the respective nitro-substituted nitrosobenzene **31**^[54] and subsequent reaction with phenylene diamine. Formation of the amide^[51] **33**, activation (**34**),^[52] and substitution with *N*-methylpiperazine^[5,45] (**35**) was performed in analogy to Scheme 3.



Scheme 5. Synthesis of the bathochromically shifted target compound **35** and its corresponding crystal structure.^[5,45,51-54]

Synthesis of the sulfonate-substituted derivative of **19** is based on a strategy in analogy to that shown in Scheme 4. First, the pharmacophore was synthesized and converted into the azobenzene in the final reaction step (Scheme 6).^[5,45,51,52,53]



Scheme 6. Synthesis of the sulfonate-substituted target compound **41**.^[5,45,51,52,55]

4.2.2 Photochemical Characterization

Azobenzenes are the most widely used class of photochromic compounds. Depending on their molecular structure, they differ in the absorption wavelength that triggers *trans*–*cis* isomerization and in the half-life of their thermal relaxation. Azobenzene-type derivatives show a strong UV absorption maximum around 320 nm (π – π^* transition) and a weaker one around 430 nm (n – π^* transition) with a thermodynamically long half-life. In our study, this type is represented by the azobenzene-4-methanimine derivatives **6** and **29**. *Ortho*/*para* electron-donating substituents (EDG, such as NH_2) shorten the lifetime and shift the π – π^* transition bathochromically, which was observed for the *para* aminoazobenzene-based ligands **19–21**, and **41**. The so-called push-pull azobenzene derivative **35** is characterized by an EDG (NR_2) in *para* and an electron-withdrawing group (EWG, NO_2) in *para'* position, resulting in a faster thermal reversion and a red-shifted absorption.^[53]

As dimethyl sulfoxide was used as stock solvent for the photochromic derivatives, it was used as solvent for the investigations of the photoisomerization of **6**, **19–21**, **29**, **35**, and **41** by UV-Vis absorption spectroscopy and NMR analysis. Due to poor solubility, only the negatively charged sulfonate derivative **41** was investigated by UV-Vis absorption spectroscopy in the organ bath solvent (Tyrode's solution). Solutions of the compounds in DMSO (50 μM), and Tyrode's solution (50 μM + 0.1% DMSO, compound **41**), respectively, were irradiated with UV light ($\lambda_{\text{irr}} = 365 \text{ nm}$; **6**, **19–21**, **29**) and visible light ($\lambda_{\text{irr}} = 420 \text{ nm}$, **35**; $\lambda_{\text{irr}} = 400 \text{ nm}$, **41**),

respectively, until the photostationary state (PSS) was reached and a substantial amount of the *cis* isomer had accumulated. Upon *trans*–*cis* isomerization the maximum representing the *trans* isomer decreased and a new absorption band in the visible range representing the *cis* isomer formed (Figure 1, black arrows). Back-isomerization to the thermally more stable *trans* isomer was triggered by irradiation with blue light ($\lambda_{\text{irr}} = 455 \text{ nm}$; **6**, **19–21**, **29**), green light ($\lambda_{\text{irr}} = 528 \text{ nm}$; **41**) or thermally (**35**). The resulting isosbestic points indicate a clean, two-component switching (Figure 1, dotted black arrows). Table S1 (Supporting Information) summarizes the characteristic absorption maxima, isosbestic points, and required irradiation wavelengths of **6**, **19–21**, **29**, **35**, and **41**. Due to a substantial overlap of the absorption maxima of the *trans* and the *cis* isomers, the *trans* isomer cannot be regenerated quantitatively by irradiation. Still, the investigated compounds show high photostationary states (Table S2, Supporting Information). Determination of the thermal stability of the *cis* isomers of **6**, **19–21**, **29**, **35**, and **41** revealed intermediate thermal stability for compounds **19–21**, and **29** relative to the thermally more stable derivative **6** and the less stable derivatives **35** and **41** (Table S2, Figures S9–S16, Supporting Information). Investigations of the repetitive cycle performance showed excellent fatigue over ten measured cycles for all analyzed compounds (Figures S1–S8, Supporting Information).

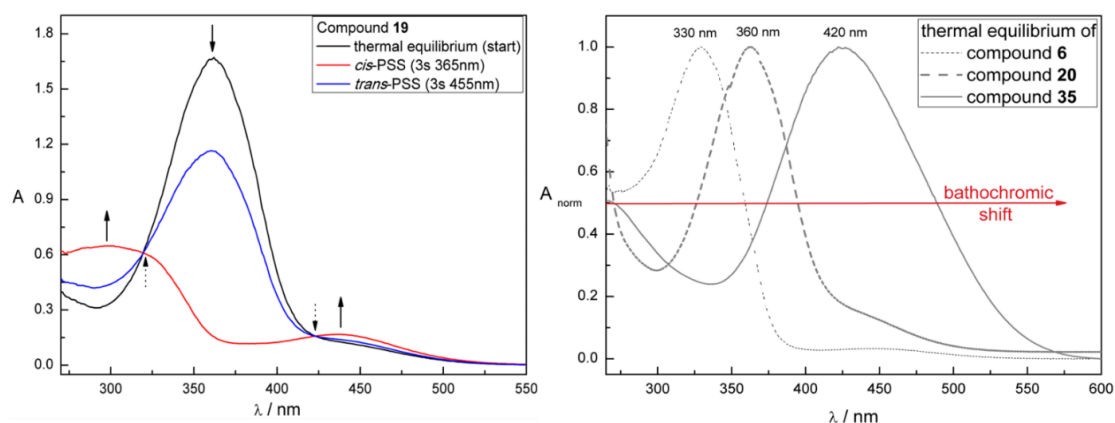


Figure 1. Left: Exemplary UV-Vis absorption spectrum representing the *para* aminoazobenzene derivative **19** in its thermal equilibrium (black), *cis*-PSS (red), and *trans*-PSS (blue). Black arrows indicate the characteristic changes in the absorption spectra upon switching to the *cis* isomer. Dotted black arrows indicate isosbestic points. Right: Depiction of the bathochromic shift of λ_{max} (*trans* isomer) for the differently substituted classes of azobenzenes. Carboxyazobenzene represented by compound **6** ($\lambda_{\text{max}} 330 \text{ nm}$); aminoazobenzene by compound **20** ($\lambda_{\text{max}} 360 \text{ nm}$); push-pull azobenzene by compound **35** ($\lambda_{\text{max}} 420 \text{ nm}$).

4.2.3 Studies on the Isolated Guinea Pig Ileum

The established organ-pharmacological setup (Figure 2) on the isolated guinea pig ileum allows investigation of the photochromic derivatives **6**, **19-21**, **29**, **35**, and **41** on native H₁R in comparison to the results obtained by Strasser^[5] and Gobleder.^[45] To guarantee the presence of the maximum amount of the *cis* isomer available by irradiation (*cis*-PSS), the thermally less stable derivatives **19-21** ($\lambda_{\text{irr}} = 365 \text{ nm}$), **35** ($\lambda_{\text{irr}} = 420 \text{ nm}$), and **41** ($\lambda_{\text{irr}} = 400 \text{ nm}$) were exposed to constant irradiation during the organ-pharmacological testing.

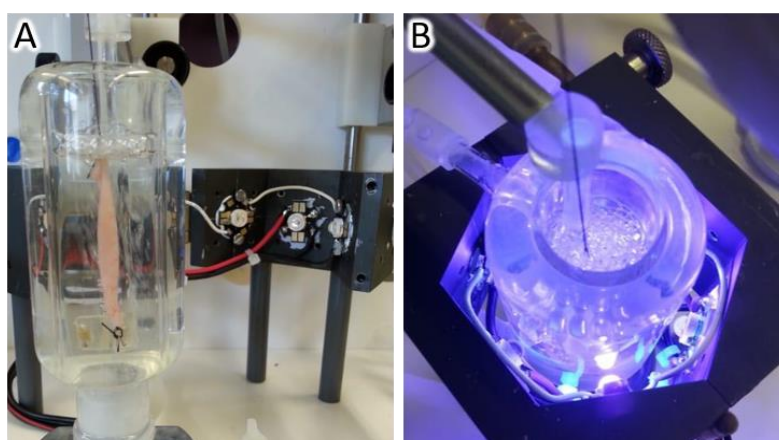


Figure 2. Organ-pharmacological setup. (A) Side view without irradiation. (B) Top view under constant irradiation.

Table 1 summarizes the antagonistic activities (pA_2) of the investigated compounds on the H₁R of the isolated guinea pig ileum. The pA_2 determination is based on the addition of various concentrations of histamine to the organ bath solution, resulting in contraction of the guinea pig ileum (histamine concentration-response curve, or CRC). The contraction is transmitted to a needle writer *via* a transducer.

Upon addition of the photochromic antagonist, either in its *trans* isomer (thermal equilibrium) or at its *cis*-PSS, the contraction of the ileum is reduced if the compounds behave as H₁R antagonists and thus displace histamine. The resulting Schild plot curves (see Supporting Information) allow calculation of the logarithmic pA_2 values as unit for an antagonist's effectiveness. Compared with their reference compounds (**SI-1**, **SI-2**, **SI-3**, and **SI-4**; see Supporting Information)

6, **20**, and **29** showed a remarkable decrease in pA₂ values. The most drastic collapse of at least three logarithmic units could be observed for **29** with its tricyclic pattern. It was conspicuous that **19** maintained its antagonistic activity with respect to its lead structure. Interestingly, the *trans* isomer of **19** demonstrated fourfold higher antagonistic activity than the *cis* form. Furthermore, additional substitution with an EWG (NO₂, **35**) or charged moiety (SO₃⁻, **41**) increased the *trans* isomer antagonistic activity relative to reference **SI-2** (**35**: eightfold, **41**: fourfold), as well as the solubility in aqueous solution. Upon light-induced *cis* isomer accumulation, the antagonistic activity of **41** decreased by a factor of 15, and for **35** even by a factor of 46. The use of longer wavelengths required for the *trans*–*cis* isomerization of **41** (λ_{irr} = 400 nm) and especially **35** (λ_{irr} = 420 nm) relative to their photochromic reference **19** (λ_{irr} = 365 nm) allows better light penetration toward the organ-pharmacological testing and hence increased *cis* isomer accumulation. Furthermore, the results obtained for the nitro-substituted derivative **35** suggest a positive effect of an EWG at the *para* position, on the antagonistic activity. This is in agreement with data obtained by Marshall^[46] and Gobleider^[45] proving the beneficial effect of chloro substituents.

Table 1. Overview of the determined pA₂ values determined at the guinea pig ileum. Cpd. = Compound.

Cpd.	pA ₂ ±SEM ^(a) <i>trans</i> isomer ^(b)	N ^{*(d)}	pA ₂ ±SEM ^(a) <i>cis</i> isomer ^(c)	N ^{*(d)}	pA ₂ ±SEM ^(a) reference	Ref. ^(e)	ratio pA ₂ <i>trans/cis</i>
6	5.04 ± 0.07	14/(40)	5.37 ± 0.24	9/(26)	6.22 ± 0.07	SI-1	0.5
19	5.27 ± 0.12	6/(9)	4.70 ± 0.17	3/(9)	5.27 ± 0.10	SI-2	3.7
20	n.a.	27	n.a.	19	4.74 ± 0.12	SI-3	-
21	4.84 ± 0.09	4/(9)	4.73 ± 0.16	4/(9)	-	-	1.3
29	5.69 ± 0.08	18/(36)	5.83 ± 0.12	12/(25)	8.88 ± 0.06	SI-4	0.7
35	6.16 ± 0.08	25/(30)	4.50 ± 0.07	4/(15)	5.27 ± 0.12	SI-2	46
41	5.85 ± 0.12	19/(30)	4.67 ± 0.11	5/(15)	5.27 ± 0.12	SI-2	15

(a) Data are the mean values ± SEM (standard error of mean) from *N* experiments; data were analyzed by nonlinear regression and were best fitted to sigmoidal concentration-response curves. pA₂ = -log₁₀(Ant)+log(*r*-1), where *r* = 10^{ΔpEC₅₀}; ΔpEC₅₀ was calculated from pEC₅₀ of histamine and pEC₅₀ of histamine in presence of the respective antagonist; n.a. = not active. (b) The *trans* isomer was tested in its thermal equilibrium. (c) The *cis* isomer was tested at its photostationary state (PSS) upon irradiation. (d) *N*^{*} represents the number of experiments in “X/(X+Y)”. Experiments were

carried out in presence of the respective antagonist at a concentration range from $10^{-7.5}$ to 10^{-4} M. "X" represents experiments in which an effect—a rightward shift of the histamine concentration-response curve (CRC) –could be measured. "Y" represents experiments in which no rightward-shifted histamine CRCs could be measured (especially for weak antagonists at lower concentration). (e) See the Supporting Information.

4.3 Conclusion

We report the design, synthesis, and photophysical characterization of seven photochromic oxazepine derivatives, as well as the establishment of an organopharmacological assay compatible with continuous tissue irradiation. Initially, three different structural leads were used, comprising a ring-closed oxazepine derivate (**29**), a ring-open azobenzene-4-methanimine derivative (**6**), and three *para* aminoazobenzene-based ring-open derivatives (**19-21**). The change in position of the azobenzene moiety, either as extension of the aniline-benzene or the carboxybenzene, and variation of the chloro substitution pattern varies the steric and electronic properties. Four compounds showed decreased antagonistic activity, whereas one compound – **19** – maintained its pharmacological activity relative to its non-photochromic lead. Compound **19** showed an isomer-dependent antagonistic activity by a factor of four. Optimization resulted in two bathochromically shifted compounds (**35** and **41**) to avoid the use of UV light and to improve both solubility and tissue penetration, resulting in increased *trans* isomer antagonistic activity compared with reference **SI-2** (factor of eight for *trans*-**35**, and a factor of four for *trans*-**41**). Upon irradiation-induced *trans*–*cis* isomerization, the antagonistic activity dropped remarkably by a factor of 15 (for **41**) and even 46 (for **35**). Ongoing attempts are aimed at a stronger bathochromic shift and the use of *ortho,ortho*-bridged azobenzenes^[56] for a *cis* active compound. Furthermore, the use of arylazo pyrazoles,^[57] known for almost quantitative switching in both directions, is considered to increase the amount of *cis* isomer accessible by irradiation.

4.4 Experimental Part

4.4.1 General Procedures and Materials

Commercial reagents and starting materials were purchased from the commercial suppliers abcr, Acros Organics, Alfa-Aesar, Fisher Scientific, Merck, Sigma-Aldrich, TCI, or VWR, and used without any further purification. Solvents were used in p.a. quality and dried according to common procedures, if necessary. Dry nitrogen was used as an inert gas atmosphere. Flash column chromatography was performed using Sigma-Aldrich MN silica gel 60M (40-63 μm , 230-400 mesh) for normal-phase chromatography. Reaction monitoring *via* thin-layer chromatography was performed on alumina plates coated with silica gel (Merck silica gel 60 F₂₅₄, layer thickness: 0.2 mm). Melting points were determined using a Stanford Research System OptiMelt MPA 100 and are uncorrected. NMR spectra were measured on a Bruker Avance 300 (¹H 300.13 MHz, ¹³C 75.48 MHz), Bruker Avance III HD 400 (¹H 400.13 MHz, ¹³C 100.61 MHz), Bruker Avance III HD 600 (¹H 600.25 MHz, ¹³C 150.95 MHz) and Bruker Avance III 600 (¹H 600.25 MHz, ¹³C 150.95 MHz). The spectra are referenced against the NMR solvent (DMSO-*d*₆: δ_{H} = 2.50 ppm, δ_{C} = 39.52 ppm), and chemical shifts (δ) are reported in ppm. Resonance multiplicity is abbreviated as: s (singlet), d (doublet), t (triplet), and m (multiplet). Carbon NMR signals are assigned using DEPT 135 and ¹H-¹³C HSQC spectra with (+) for primary/tertiary, (-) for secondary, and (q) for quaternary carbons. Mass spectra were recorded on a Finnigan MAT-SSQ 710 A, ThermoQuest Finnigan TSQ 7000, Agilent Q-TOF 6540 UHD, or a Jeol AccuTOF GCX instrument. UV-Vis absorption spectroscopy was performed in 10 mm quartz cuvettes using an Agilent Cary 100 or Agilent Varian Cary 50 spectrometer. Analytical HPLC measurements were performed using an Agilent 1220 Infinity LC (column: Phenomenex Luna 3 μm C₁₈(2) 100 Å, 150 x 2.00 mm; flow rate 0.3 mL min⁻¹ at 30 °C; solvent A: MilliQ water with 0.05 wt% TFA; solvent B: MeCN). The ratios at the PSSs were determined by analytical HPLC at 30 °C at the isosbestic points or by NMR spectroscopy of an irradiated sample. An Agilent 1260 system (column:

Phenomenex Luna 10 μm C₁₈(2) 100 Å, 250 x 21.2 mm; flow rate 22 mL min⁻¹; solvent A: MilliQ water with 0.05 wt% TFA; solvent B: MeCN) was used for preparative HPLC purification. Light sources for irradiation: λ = 365 nm (Herolab hand-held lamp UV-6 L, 6W; Seoul Viosys CUN6GB1A, 1000 mA, 1.4 W), λ = 400 nm (Luxeon 400 nm SZ-01-S2, 500 mA, 0.48 W), λ = 420 nm (Luxeon 420 nm SZ-01-S6, 500 mA, 0.63 W), λ = 455 nm (Osram OSRON SSL 80 LD-CQ7P-1U3U, 1000 mA, 0.45 W), λ = 528 nm (Osram LTCP7P-KXKZ, 350 mA, 71 lm). The power of the light is given based on the specifications supplied by the manufacturer for the case of purchased LEDs.

Compounds **2**,^[49] **24**,^[5,45] **25**,^[5,45] **27**,^[5,45] **28**,^[5,45] **31**,^[54] **39**,^[5,45] and **40**^[55] were synthesized by following literature reported procedures. Acid and imino chlorides **3**, **5**, **10-12**, **16-18**, **23**, **26**, **34**, and **37** were synthesized by following general procedure A.^[50,52] Amides **4**, **13-15**, **33**, and **36** were synthesized by following general procedure B.^[51] *N*-methylpiperazine derivatives **6**, **19-21**, **35**, and **38** were synthesized by following general procedure C.^[5,45] Mills reactions^[53] for the formation of compounds **29**, **32**, and **41** were performed according to general procedure D.

4.4.2 Synthetic Procedures and Characterization

General procedure A. The respective compound (carboxylic acid/amide; 1.0 eq) was suspended in thionyl chloride (10 eq) and heated at reflux for three hours until complete dissolution of the starting material.^[50,52] The solvent was evaporated under reduced pressure, and the reaction mixture was co-evaporated from CH₂Cl₂ three times to remove residual thionyl chloride. The crude products were used in the next step without further purification or characterization. The crystal structure of the imino chloride **16** is available in the Supporting Information.

General procedure B. The respective substituted aniline (1.0 eq) was dissolved in ethyl acetate (5.0 mL mmol⁻¹) in the presence of triethylamine (1.4 eq). A solution of the benzoic acid chloride derivative (1.2 eq) in ethyl acetate (2.0 mL mmol⁻¹) was added dropwise under stirring at room temperature. The reaction mixture was

stirred at room temperature overnight.^[51] The formed precipitate was collected and dried under vacuum to afford the desired products without further purification.

(E)-N-(3-chlorophenyl)-4-(phenyldiazenyl)benzamide (4). Brown solid (90%). M.p.: 176 °C. ¹H-NMR (400 MHz, DMSO-*d*₆): δ = 10.58 (s, 1H), 8.20 – 8.16 (m, 2H), 8.04 – 7.98 (m, 3H), 7.98 – 7.93 (m, 2H), 7.74 (ddd, *J* = 8.3, 2.0, 1.0 Hz, 1H), 7.67 – 7.59 (m, 3H), 7.41 (t, *J* = 8.1 Hz, 1H), 7.19 (ddd, *J* = 8.0, 2.1, 0.9 Hz, 1H). ¹³C-NMR (101 MHz, DMSO-*d*₆): δ = 165.4 (q), 154.1 (q), 152.4 (q), 141.0 (q), 137.1 (q), 133.4 (q), 132.6 (+), 130.8 (+), 130.0 (+), 129.6 (+), 124.0 (+), 123.3 (+), 122.9 (+), 120.3 (+), 119.2 (+). HRMS (ESI) calcd. for (C₁₉H₁₅ClN₃O⁺) [M+H]⁺: *m/z* = 336.0898; found 336.0903. MF: C₁₉H₁₄ClN₃O. MW: 335.79 g/mol.

(E)-4-chloro-N-(4-(phenyldiazenyl)phenyl)benzamide (13). Orange solid (79%). M.p.: 226 °C. ¹H-NMR (400 MHz, DMSO-*d*₆): δ = 10.64 (s, 1H), 8.06 – 8.00 (m, 4H), 7.96 – 7.92 (m, 2H), 7.90 – 7.85 (m, 2H), 7.65 – 7.53 (m, 5H). ¹³C-NMR (101 MHz, DMSO-*d*₆): δ = 165.3 (q), 152.5 (q), 148.4 (q), 142.6 (q), 137.2 (q), 133.8 (q), 131.6 (+), 130.2 (+), 129.9 (+), 129.0 (+), 124.0 (+), 122.8 (+), 121.0 (+). HRMS (ESI) calcd. for (C₁₉H₁₅ClN₃O⁺) [M+H]⁺: *m/z* = 336.0898; found 336.0902. MF: C₁₉H₁₄ClN₃O. MW: 335.79 g/mol.

(E)-3-chloro-N-(4-(phenyldiazenyl)phenyl)benzamide (14). Orange solid (83%). M.p.: 194 °C. ¹H-NMR (300 MHz, DMSO-*d*₆): δ = 10.69 (s, 1H), 8.08 – 8.00 (m, 3H), 7.99 – 7.92 (m, 3H), 7.91 – 7.85 (m, 2H), 7.70 (ddd, *J* = 8.0, 2.2, 1.1 Hz, 1H), 7.64 – 7.52 (m, 4H). ¹³C-NMR (101 MHz, DMSO-*d*₆): δ = 164.9 (q), 152.5 (q), 148.4 (q), 142.5 (q), 137.1 (q), 133.7 (q), 132.1 (+), 131.6 (+), 130.9 (+), 129.9 (+), 128.0 (+), 127.1 (+), 124.0 (+), 122.9 (+), 121.0 (+). HRMS (ESI) calcd. for (C₁₉H₁₅ClN₃O⁺) [M+H]⁺: *m/z* = 336.0898; found 336.0902. MF: C₁₉H₁₄ClN₃O. MW: 335.79 g/mol.

(E)-3,4-dichloro-N-(4-(phenyldiazenyl)phenyl)benzamide (15). Orange solid (98%). M.p.: 228 °C. ¹H-NMR (400 MHz, DMSO-*d*₆): δ = 10.71 (s, 1H), 8.25 (d, *J* = 2.1 Hz, 1H), 8.05 – 8.00 (m, 2H), 7.99 – 7.92 (m, 3H), 7.91 – 7.82 (m, 3H), 7.62 – 7.52 (m, 3H). ¹³C-NMR (101 MHz, DMSO-*d*₆): δ = 164.0 (q), 152.5 (q), 148.5 (q), 142.3 (q),

135.4 (q), 135.1 (q), 131.8 (q), 131.6 (+), 131.3 (+), 130.2 (+), 129.9 (+), 128.7 (+), 124.0 (+), 122.9 (+), 121.1 (+). HRMS (ESI) calcd. for (C₁₉H₁₄Cl₂N₃O⁺) [M+H]⁺: m/z = 370.0508; found 370.0513. MF: C₁₉H₁₃Cl₂N₃O. MW: 370.23 g/mol.

(E)-4-chloro-N-(4-((4-nitrophenyl)diazenyl)phenyl)benzamide (33). Red solid (92%). M.p.: 253 °C. ¹H-NMR (400 MHz, DMSO-*d*₆): δ = 10.73 (s, 1H), 8.45 – 8.37 (m, 2H), 8.09 – 7.98 (m, 8H), 7.65 – 7.60 (m, 2H). ¹³C-NMR (101 MHz, DMSO-*d*₆): δ = 165.4 (q), 155.8 (q), 148.6 (q), 148.3 (q), 143.9 (q), 137.27 (q), 133.7 (q), 130.3 (+), 129.0 (+), 125.5 (+), 124.8 (q), 123.7 (q), 120.9 (q). HRMS (ESI) calcd. for (C₁₉H₁₃ClN₄O₃Na⁺) [M+Na]⁺: m/z = 403.0568; found 403.0568. MF: C₁₉H₁₃ClN₄O₃. MW: 380.79 g/mol.

General procedure C. *N*-Methylpiperazine (1.3 eq) and triethylamine (1.7 eq) were dissolved in dry CH₂Cl₂ (5 mL mmol⁻¹) and stirred at 0 °C for ten minutes. To this mixture was added a solution of the respective imino chloride (1.0 eq) in dry CH₂Cl₂ (3 mL mmol⁻¹). The reaction mixture was stirred at 0 °C for 20 minutes and heated at 50 °C for two hours. After cooling to room temperature, the reaction mixture was extracted with ethyl acetate and washed with 1 M HCl. The organic layer was dried over anhydrous Na₂SO₄.^[5,45] Purification by preparative HPLC afforded the desired products.

(Z)-N-(3-chlorophenyl)-1-(4-methylpiperazin-1-yl)-1-(4-((E)phenyldiazenyl)phenyl)methanimine (6). Light orange solid (60%). Gradient 0-20 min 10:90-98:2, t_R = 10.1 min. M.p.: 144 °C. ¹H-NMR (400 MHz, DMSO-*d*₆): δ = 7.89 – 7.84 (m, 2H), 7.82 – 7.78 (m, 2H), 7.61 – 7.55 (m, 3H), 7.39 – 7.35 (m, 2H), 6.98 (t, *J* = 8.0 Hz, 1H), 6.71 (ddd, *J* = 8.0, 2.1, 1.0 Hz, 1H), 6.57 (t, *J* = 2.0 Hz, 1H), 6.46 (ddd, *J* = 8.0, 2.0, 0.9 Hz, 1H), 3.34 (s, 4H), 2.37 (s, 4H), 2.21 (s, 3H). ¹³C-NMR (101 MHz, DMSO-*d*₆): δ = 159.6 (q), 153.2 (q), 152.4 (q), 151.9 (q), 136.2 (q), 132.9 (q), 132.3 (+), 130.3 (+), 130.1 (+), 130.0 (+), 123.1 (+), 122.9 (+), 122.6 (+), 121.7 (+), 121.0 (+), 54.7 (-), 46.2 (+). HRMS (ESI) calcd. for (C₂₄H₂₅ClN₅⁺) [M+H]⁺: m/z = 418.1793; found 418.1795. MF: C₂₄H₂₄ClN₅. MW: 417.94 g/mol.

(Z)-1-(4-chlorophenyl)-1-(4-methylpiperazin-1-yl)-N-(4-((E)-phenyldiazenyl)phenyl)methanimine (19). Orange solid (59%). Gradient 0-9 min 32:68-70:30, t_R = 5.1 min. M.p.: 164 °C. ¹H-NMR (400 MHz, DMSO-*d*₆): δ = 7.79 – 7.72 (m, 2H), 7.60 – 7.45 (m, 5H), 7.42 – 7.36 (m, 2H), 7.24 – 7.19 (m, 2H), 6.67 – 6.61 (m, 2H), 3.33 (s, 4H), 2.38 (s, 4H), 2.22 (s, 3H). ¹³C-NMR (101 MHz, DMSO-*d*₆): δ = 159.1 (q), 155.3 (q), 152.6 (q), 146.7 (q), 134.1 (q), 132.1 (q), 131.0 (+), 131.0 (+), 129.8 (+), 129.0 (+), 123.7 (+), 123.6 (+), 122.6 (+), 54.7 (-), 46.1 (+). HRMS (ESI) calcd. for (C₂₄H₂₅ClN₅)⁺ [M+H]⁺: m/z = 418.1793; found 418.1795. MF: C₂₄H₂₄ClN₅. MW: 417.94 g/mol. The crystal structure of **19** is provided in the Supporting Information.

(Z)-1-(3-chlorophenyl)-1-(4-methylpiperazin-1-yl)-N-(4-((E)-phenyldiazenyl)phenyl)methanimine (20). Red solid (68%). Gradient 0-20 min 10:90-98:2, t_R = 10.3 min. M.p.: 143 °C. ¹H-NMR (400 MHz, DMSO-*d*₆): δ = 7.79 – 7.74 (m, 2H), 7.60 – 7.46 (m, 5H), 7.37 – 7.32 (m, 2H), 7.31 – 7.27 (m, 1H), 7.19 – 7.14 (m, 1H), 6.69 – 6.65 (m, 2H), 3.33 (s, 4H), 2.39 (s, 4H), 2.23 (s, 3H). ¹³C NMR (101 MHz, DMSO-*d*₆): δ = 158.4 (q), 155.2 (q), 152.6 (q), 146.8 (q), 135.4 (q), 133.7 (q), 131.0 (+), 130.8 (+), 129.8 (+), 129.5 (+), 128.7 (+), 127.8 (+), 123.7 (+), 123.6 (+), 122.6 (+), 54.6 (-), 46.1 (+). HRMS (ESI) calcd. for (C₂₄H₂₅ClN₅)⁺ [M+H]⁺: m/z = 418.1793; found 418.1797. MF: C₂₄H₂₄ClN₅. MW: 417.94 g/mol.

(Z)-1-(3,4-dichlorophenyl)-1-(4-methylpiperazin-1-yl)-N-(4-((E)-phenyldiazenyl)phenyl)methanimine (21). Orange solid (43%). Gradient 0-20 min 10:90-98:2, t_R = 11.6 min. M.p.: 156 °C. ¹H-NMR (400 MHz, DMSO-*d*₆): δ = 7.80 – 7.73 (m, 2H), 7.64 – 7.56 (m, 3H), 7.56 – 7.46 (m, 4H), 7.19 (dd, J = 8.2, 2.0 Hz, 1H), 6.72 – 6.66 (m, 2H), 3.32 (s, 4H), 2.39 (s, 4H), 2.23 (s, 3H). ¹³C-NMR (101 MHz, DMSO-*d*₆): δ = 157.5 (q), 155.0 (q), 152.6 (q), 146.8 (q), 133.9 (q), 132.2 (q), 131.9 (q), 131.2 (+), 131.1 (+), 131.0 (+), 129.8 (+), 129.4 (+), 123.8 (+), 123.6 (+), 122.6 (+), 54.6 (-), 46.1 (+). HRMS (ESI) calcd. for (C₂₄H₂₄Cl₂N₅)⁺ [M+H]⁺: m/z = 452.1403; found 452.1408. MF: C₂₄H₂₃Cl₂N₅. MW: 452.38 g/mol. The crystal structure of **21** is provided in the Supporting Information.

(Z)-1-(4-chlorophenyl)-1-(4-methylpiperazin-1-yl)-N-(4-((E)-(4-nitrophenyl)diaz-enyl)phenyl)methanimine (35). Red solid (33%). Gradient (A: MilliQ water; solvent B: MeCN) 0-20 min 10:90-98:2, t_R = 21.5 min. M.p.: 124 °C. $^1\text{H-NMR}$ (400 MHz, $\text{DMSO-}d_6$): δ = 8.40 – 8.33 (m, 2H), 7.97 – 7.91 (m, 2H), 7.68 – 7.62 (m, 2H), 7.42 – 7.38 (m, 2H), 7.25 – 7.22 (m, 2H), 6.70 – 6.65 (m, 2H), 3.38 (s, 4H), 2.37 (s, 4H), 2.22 (s, 3H). $^{13}\text{C-NMR}$ (101 MHz, $\text{DMSO-}d_6$): δ = 159.1 (q), 156.9 (q), 156.0 (q), 148.2 (q), 146.8 (q), 134.2 (q), 132.0 (q), 131.0 (+), 129.1 (+), 125.5 (+), 124.6 (+), 123.8 (+), 123.4 (+), 54.7 (-), 46.1 (+). HRMS (ESI) calcd. for $(\text{C}_{24}\text{H}_{24}\text{ClN}_6\text{O}_2)^+$ $[\text{M}+\text{H}]^+$: m/z = 463.1644; found 463.1640. MF: $\text{C}_{24}\text{H}_{23}\text{ClN}_6\text{O}_2$. MW: 462.94 g/mol. The crystal structure of **35** is provided in the Supporting Information.

(Z)-1-(4-chlorophenyl)-1-(4-methylpiperazin-1-yl)-N-(4-nitrophenyl)methanimine (38). Yellow oil (83%) Purification by column chromatography (CH_2Cl_2 + 5% MeOH). $^1\text{H-NMR}$ (300 MHz, $\text{DMSO-}d_6$): δ = 7.92 – 7.81 (m, 2H), 7.43 – 7.35 (m, 2H), 7.26 – 7.14 (m, 2H), 6.71 – 6.57 (m, 2H), 3.38 (s, 4H), 2.36 (s, 4H), 2.20 (s, 3H). $^{13}\text{C-NMR}$ (75 MHz, $\text{DMSO-}d_6$): δ = 158.6 (q), 158.2 (q), 140.6 (q), 133.9 (q), 130.9 (q), 130.4 (+), 128.6 (+), 124.2 (+), 122.7 (+), 54.1 (-), 45.4 (+). HRMS (ESI) calcd. for $(\text{C}_{18}\text{H}_{20}\text{ClN}_4\text{O}_2)^+$ $[\text{M}+\text{H}]^+$: m/z = 359.1270; found 359.1269. MF: $\text{C}_{18}\text{H}_{19}\text{ClN}_4\text{O}_2$. MW: 358.83 g/mol.

General procedure D. The amino-substituted benzene derivative (1.0 eq) and the respective substituted nitrosobenzene derivative (1.0 eq) were dissolved in a mixture of acetic acid and CH_2Cl_2 (1:1) and stirred at 50 °C for 48 hours (**29**) and at room temperature for 16 hours (**32**, **41**), respectively.

(E)-8-chloro-11-(4-methylpiperazin-1-yl)-3-(phenyldiazenyl)dibenzo[*b,f*][1,4]oxazepine (29). Purification by preparative HPLC (gradient 0-20 min 10:90-98:2, t_R = 15.5 min) afforded the desired product as light brown solid (28%). M.p.: 123 °C. $^1\text{H-NMR}$ (600 MHz, $\text{DMSO-}d_6$): δ = 7.95 – 7.90 (m, 2H), 7.89 – 7.84 (m, 2H), 7.74 – 7.71 (m, 1H), 7.66 – 7.61 (m, 3H), 7.37 (d, J = 8.6 Hz, 1H), 7.15 (d, J = 2.6 Hz, 1H), 7.12 (dd, J = 8.6, 2.6 Hz, 1H), 3.52 – 3.30 (broad, 8H), 2.88 (s, 3H). $^{13}\text{C-NMR}$ (151 MHz, $\text{DMSO-}d_6$): δ = 160.5 (q), 158.0 (q), 157.8 (q), 155.2 (q), 151.8 (q), 149.9

(q), 141.0 (q), 132.5 (q), 130.8 (+), 129.6 (+), 125.8 (+), 124.3 (+), 124.1 (+), 122.9 (+), 122.1 (+), 120.5 (+), 114.3 (+), 52.0 (-), 52.0 (-), 42.2 (+). HRMS (ESI) calcd. for (C₂₄H₂₃ClN₅O⁺) [M+H]⁺: m/z = 432.1586; found 432.1590. MF: C₂₄H₂₂ClN₅O. MW: 431.92 g/mol.

(E)-4-((4-nitrophenyl)diazenyl)aniline (32). Purification by column chromatography (CH₂Cl₂) afforded the desired product as dark-red solid (86%). The analytical data agree with published data.^[58]

4-((E)-4-(((Z)-(4-chlorophenyl)(4-methylpiperazin-1-yl)methylene)amino)phenyl)diazenyl)benzenesulfonate (41). The respective amino precursor was synthesized following an adapted reported procedure for the reduction of nitro groups.^[4,45] The amine was used in the next reaction step without further characterization or purification. Mills reaction afforded the desired product **41**, which was further purified by column chromatography (CH₂Cl₂ + 10% MeOH) and subsequent preparative HPLC (gradient MilliQ water/MeCN 0-20 min 10:90-98:2, t_R = 9.6 min; red viscous solid; 42%). M.p.: 141 °C. ¹H-NMR (300 MHz, DMSO-*d*₆): δ = 7.73 (d, *J* = 2.0 Hz, 4H), 7.60 – 7.56 (m, 2H), 7.41 – 7.37 (m, 2H), 7.21 (d, *J* = 8.5 Hz, 2H), 6.64 (d, *J* = 8.7 Hz, 2H), 3.59 (s, 4H), 3.10 – 3.18 (m, 8H), 2.38 (s, 4H), 2.22 (s, 3H), 1.60 – 1.49 (m, 8H), 1.29 (h, *J* = 7.4 Hz, 8H), 0.91 (t, *J* = 7.3 Hz, 12H). ¹³C-NMR (101 MHz, DMSO-*d*₆): δ = 159.0 (q), 155.4 (q), 152.2 (q), 150.6 (q), 146.7 (q), 134.1 (q), 132.1 (+), 131.1 (+), 129.1 (+), 127.0 (+), 123.8 (+), 123.6 (+), 122.0 (+), 58.0 (-), 54.6 (-), 46.1 (+), 23.5 (-), 19.7 (-), 14.0 (+). HRMS (ESI) calcd. for (C₂₄H₂₃ClN₅O₃S⁻) [M-H]⁻: m/z = 496.1216; found 496.1220. MF: C₄₀H₅₉ClN₆O₃S. MW: 739.46 g/mol.

4.4.3 Organ-Pharmacological Testing

Preparation of the stock solutions. The stock solutions of the tested compounds and all their dilutions were prepared with DMSO.

Studies on the isolated guinea pig ileum.^[58] All organ-pharmacological experiments were carried out in accordance with national and local legislation.

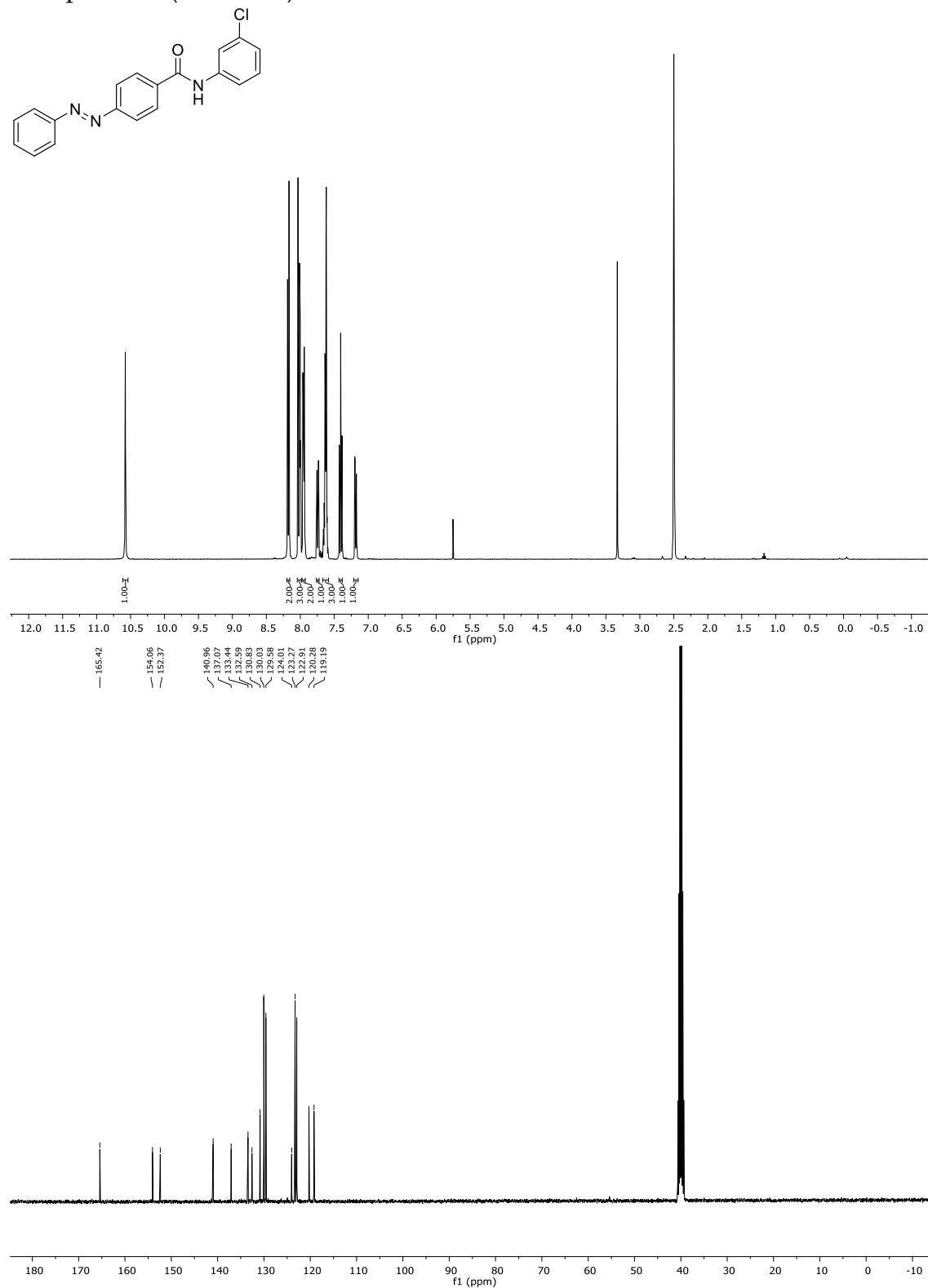
Guinea pigs of either sex (250 - 500 g) were stunned by a blow on the neck and exsanguinated. The ileum was rapidly removed, rinsed, and cut into segments of 1.5 - 2.0 cm length. The tissues were mounted isotonically (preload of 5 mN) in a jacketed 20 mL organ bath that was filled with Tyrode's solution (composition [mM]: NaCl 137, KCl 2.7, CaCl₂ 1.8, MgCl₂ 1.0, NaH₂PO₄ 0.4, NaHCO₃ 11.9, and glucose 5.0) supplemented with atropine at a concentration not affecting H₁ receptors (0.05 μ M), to block cholinergic muscarinic receptors. The bath was aerated with 95% O₂/5% CO₂ and heated at 37 °C. During an equilibration period of 80 min, the tissues were stimulated three times with histamine (2 \times 1 μ M, 1 \times 10 μ M) followed by washout. Up to four cumulative CRCs were determined on each tissue: the first by addition of histamine (0.01 - 30 μ M) and the second to fourth by addition of histamine in the presence of increasing concentrations of antagonist (pre-incubation: see below). pEC₅₀ differences were not corrected, because four successive curves for histamine were superimposable under these conditions (N > 10).

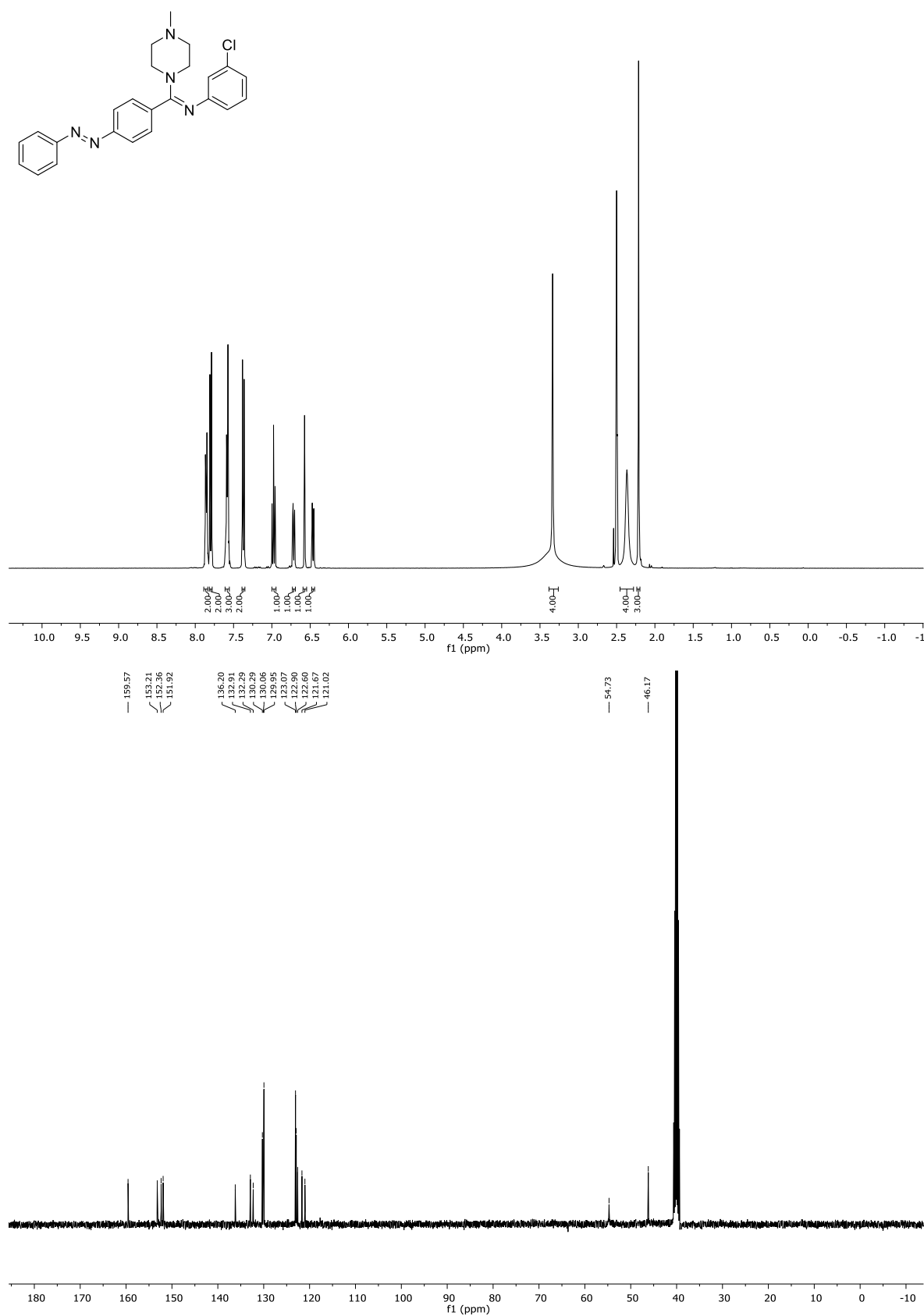
For each experiment a DMSO blank was performed simultaneously, and data were corrected. For compounds **19**, **21**, **35** and **41** pre-incubation (30 s) and the following CRC of histamine was implemented by permanent irradiation at 365 nm (**19** and **21**), 420 nm (**35**) or 400 nm (**41**). A pre-incubation and the accompanying light exposure of 15, 10, 5 and 3 min had an influence at the tissue's contractility, resulting in a depression of the CRCs of histamine. A pre-incubation of 30 s showed no difficulties, as four successive curves for histamine were superimposable under these conditions. The pA₂ values of the *trans* isomers of **19** and **21** showed no significant difference depending on the pre-incubation time (15 min *vs.* 30 s, see Table S3, Supporting Information). Therefore, incubation for **35** and **41** was set to 30 s. Data were analyzed by nonlinear regression and were best fitted to sigmoidal concentration-response curves using Prism 5.0c software (GraphPad, SanDiego, CA, USA).

4.5 Supporting Information

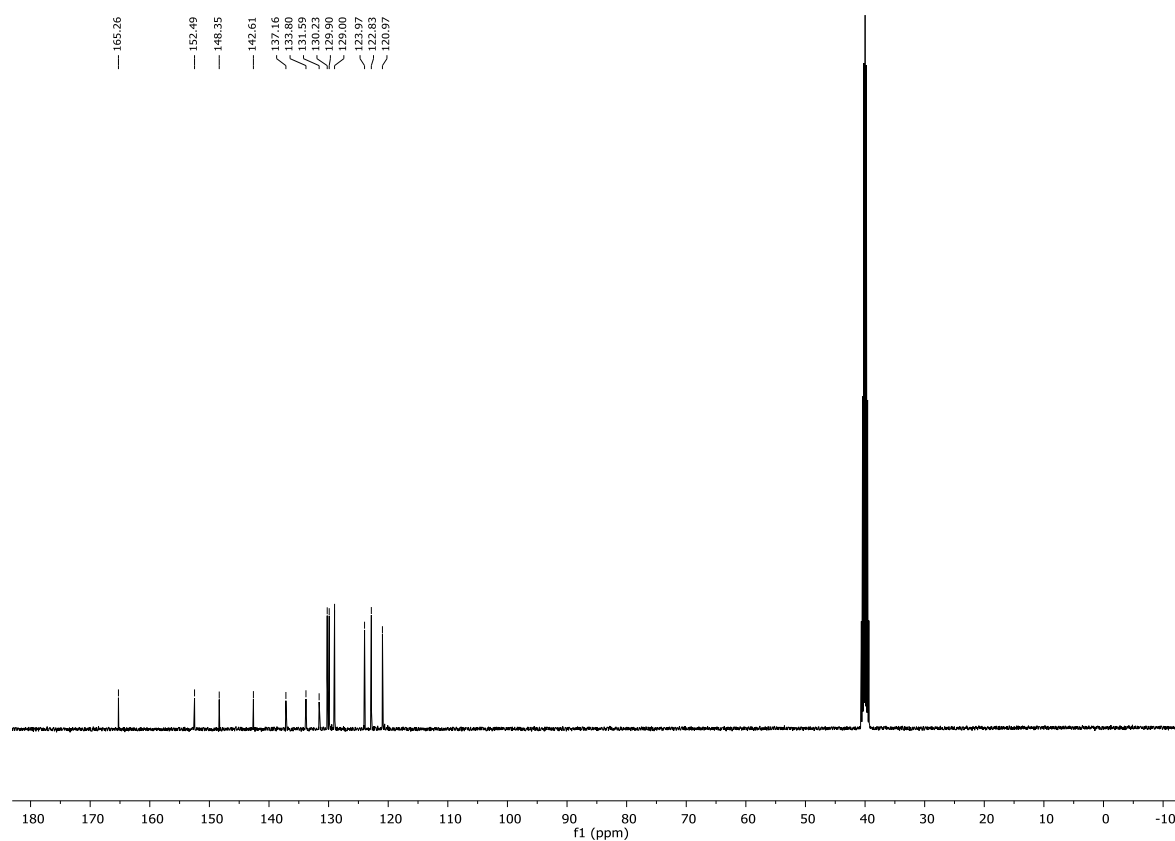
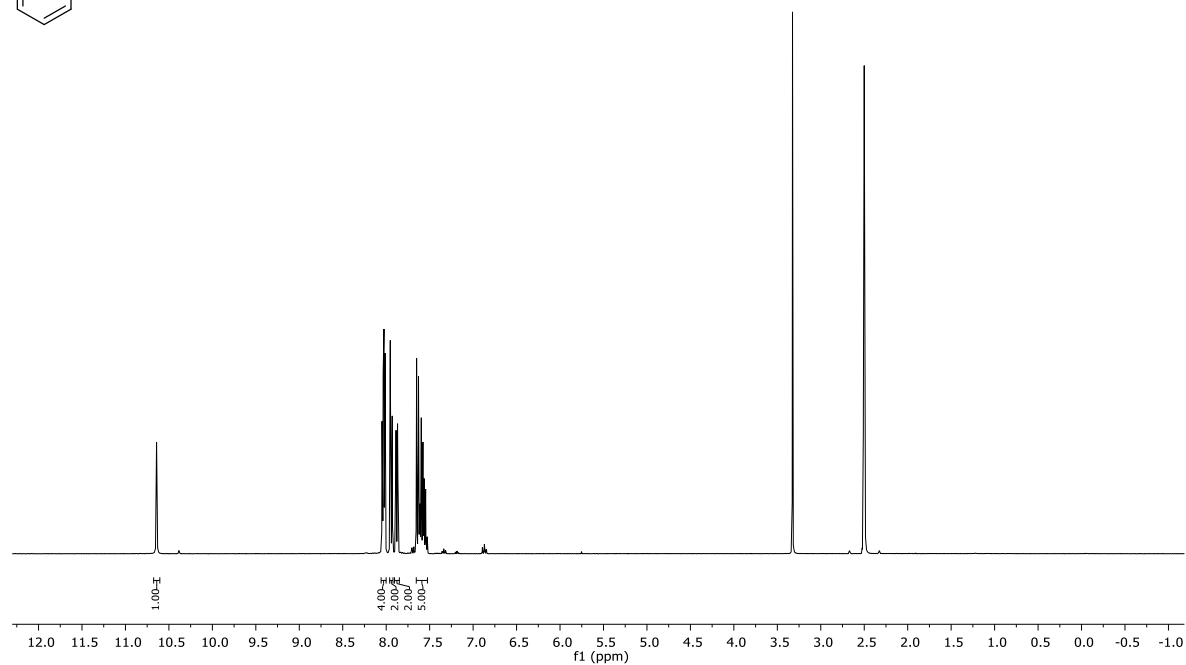
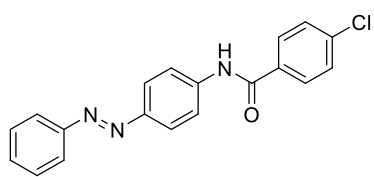
4.5.1 ¹H- and ¹³C-NMR Spectra

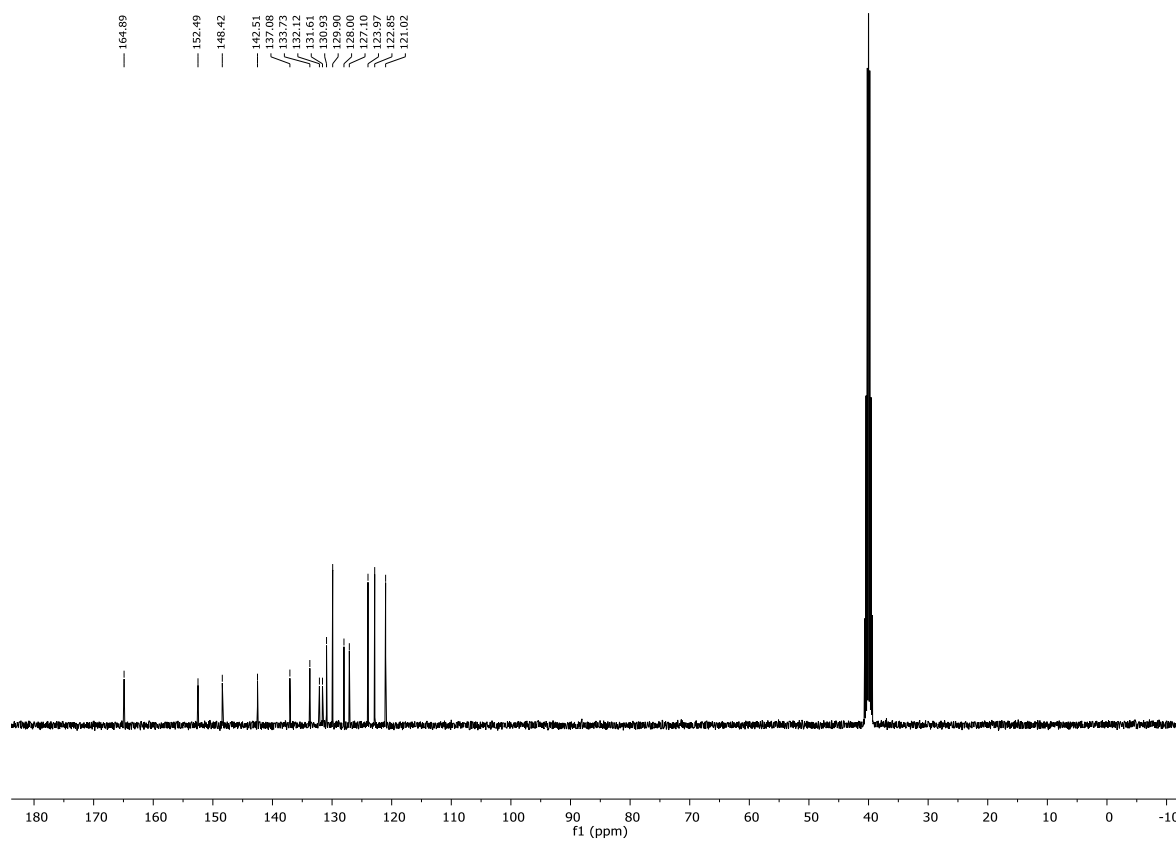
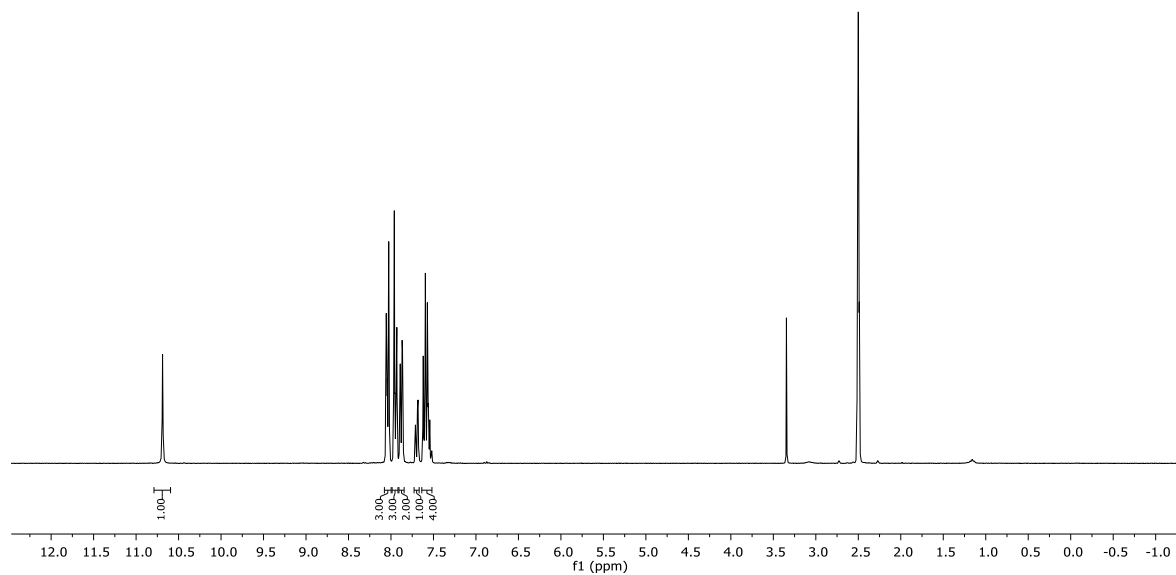
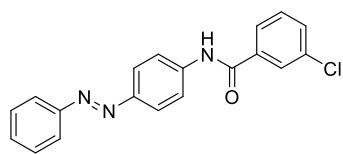
Compound 4 (DMSO-*d*₆)



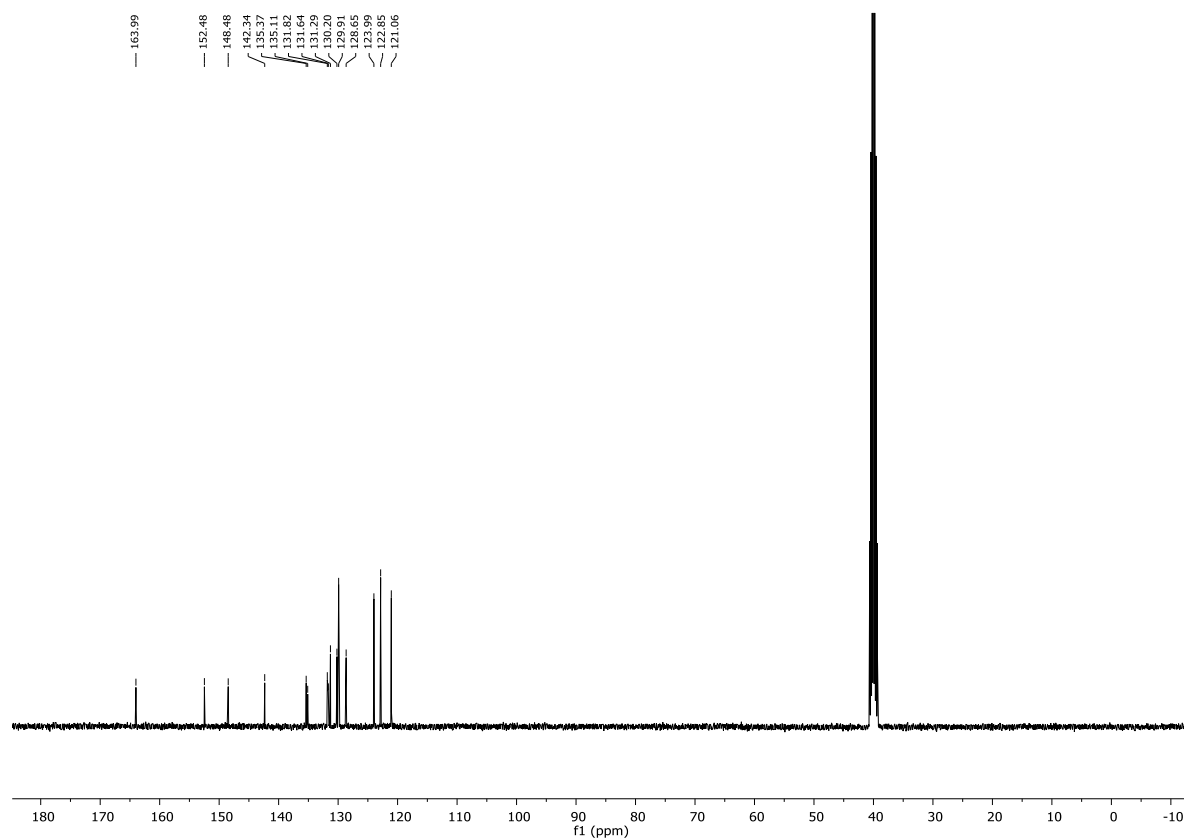
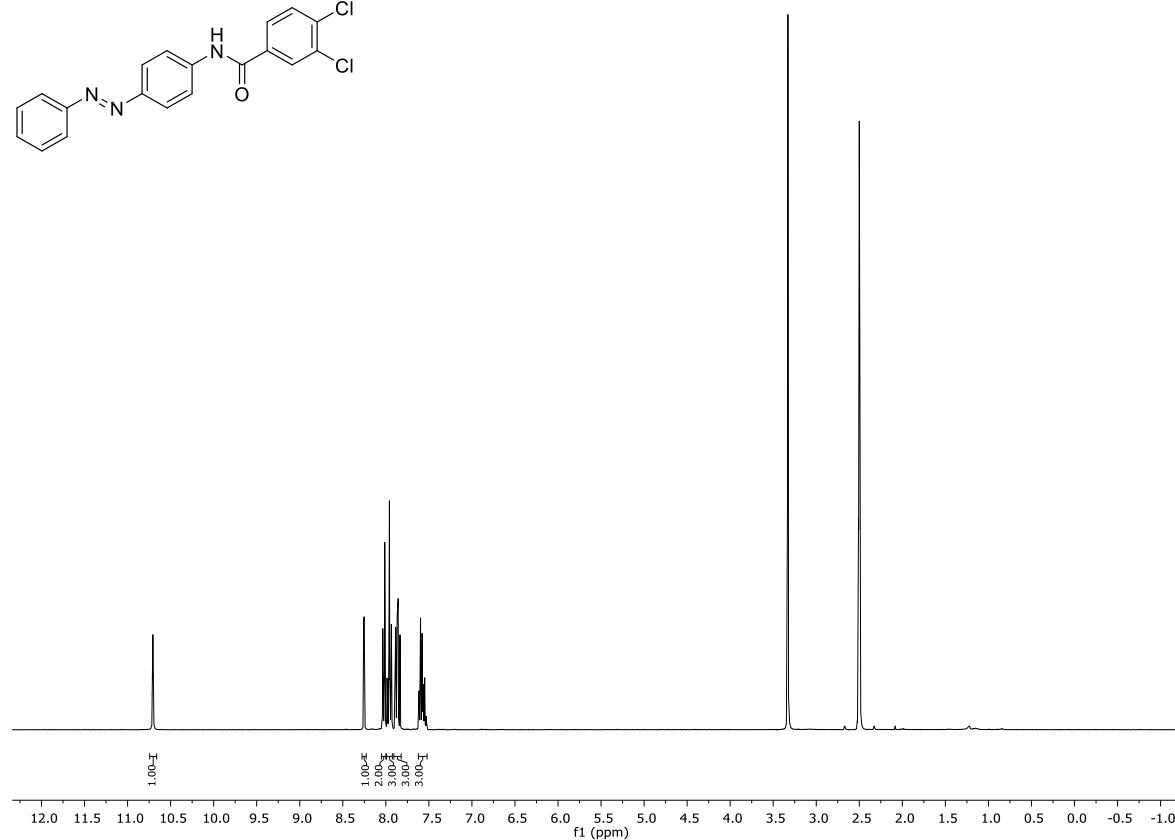
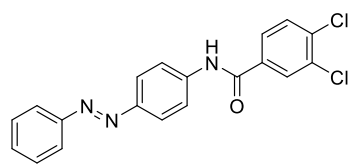
Compound 6 (DMSO-*d*₆)

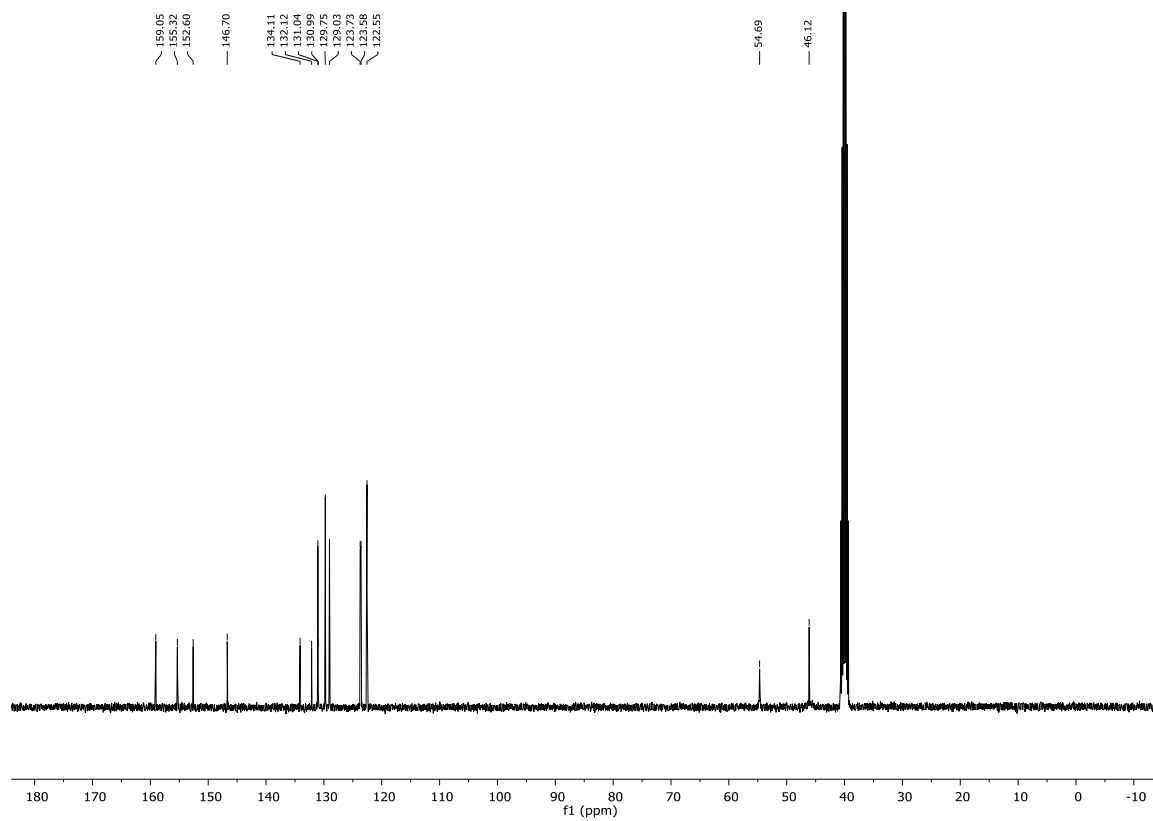
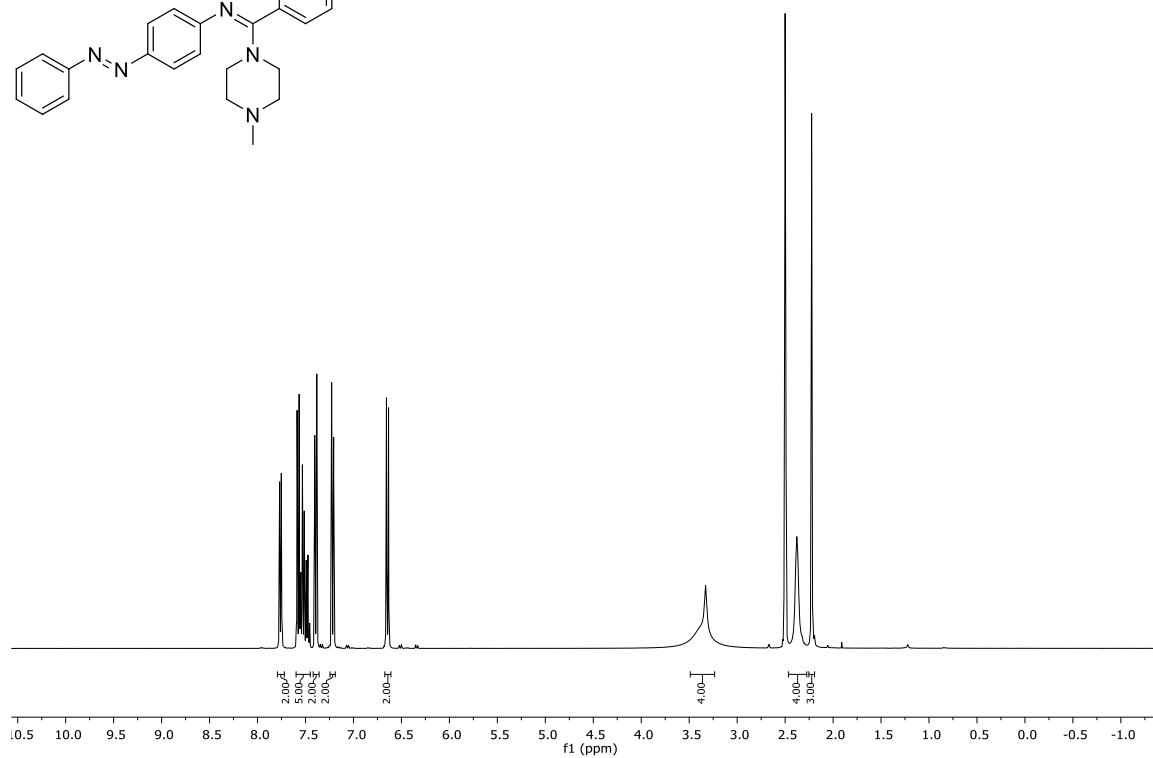
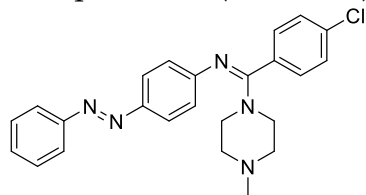
Compound **13** (DMSO-*d*₆)



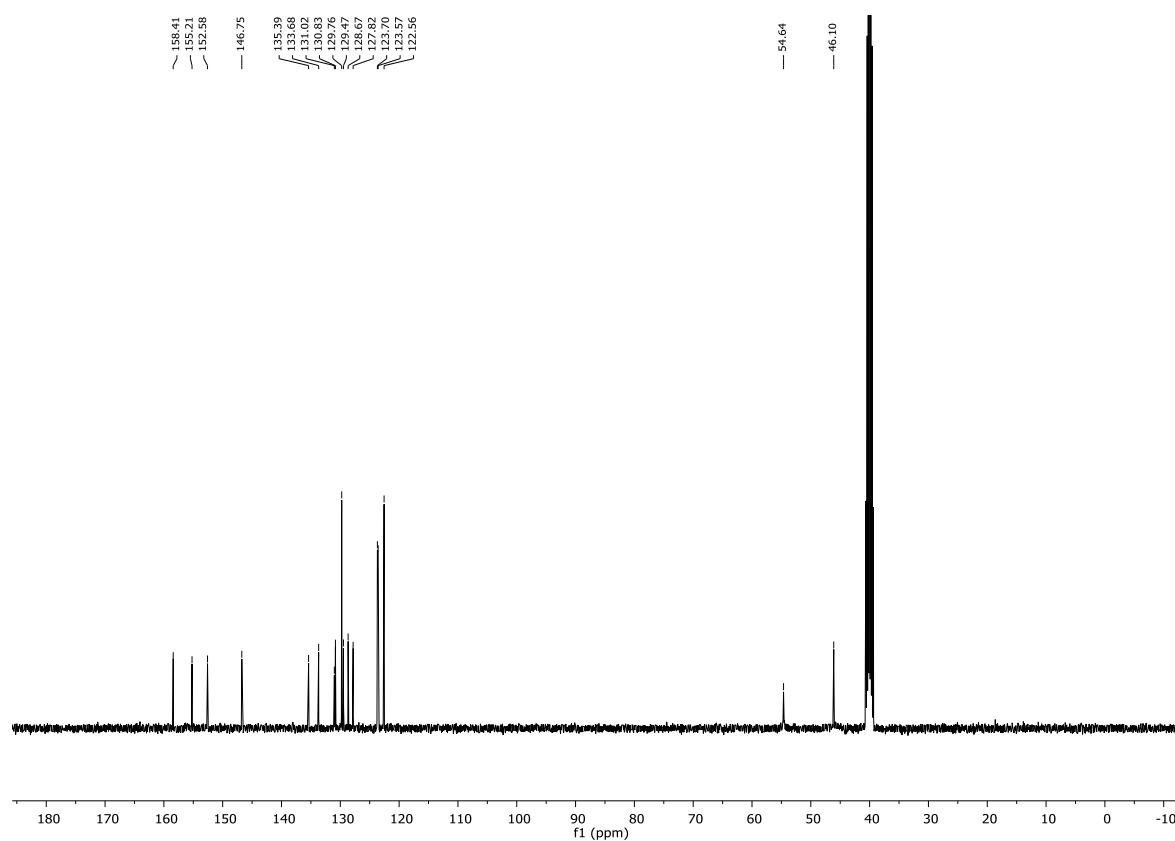
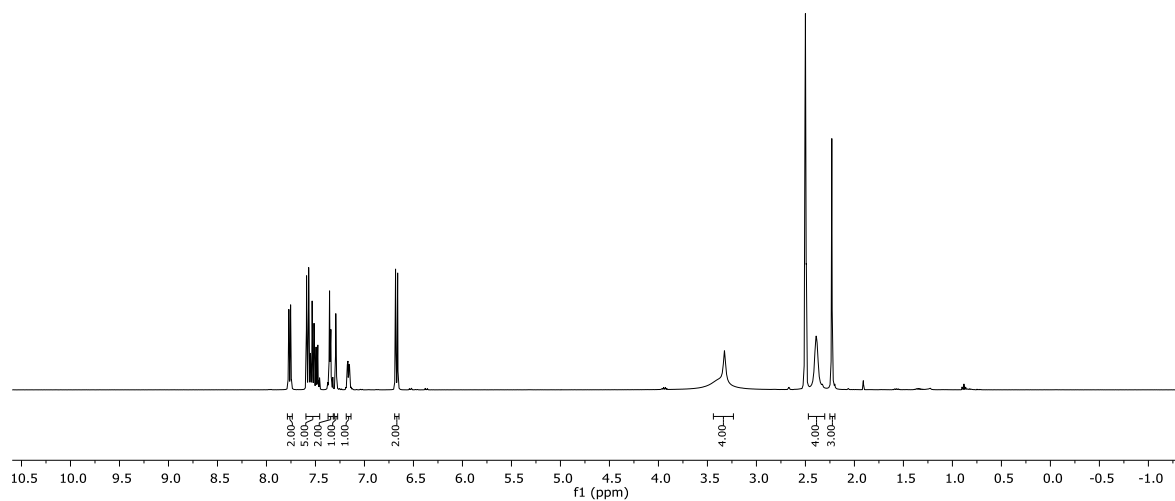
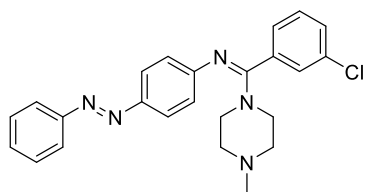
Compound **14** (DMSO-*d*₆)

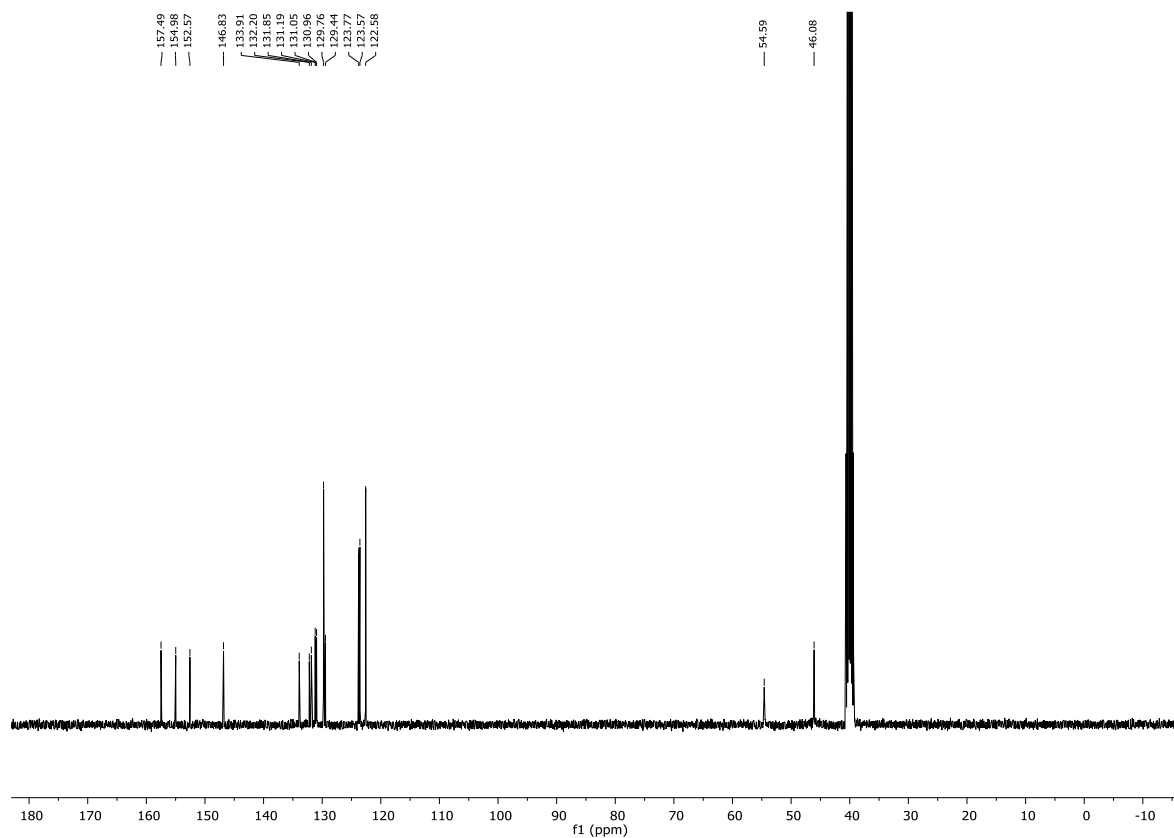
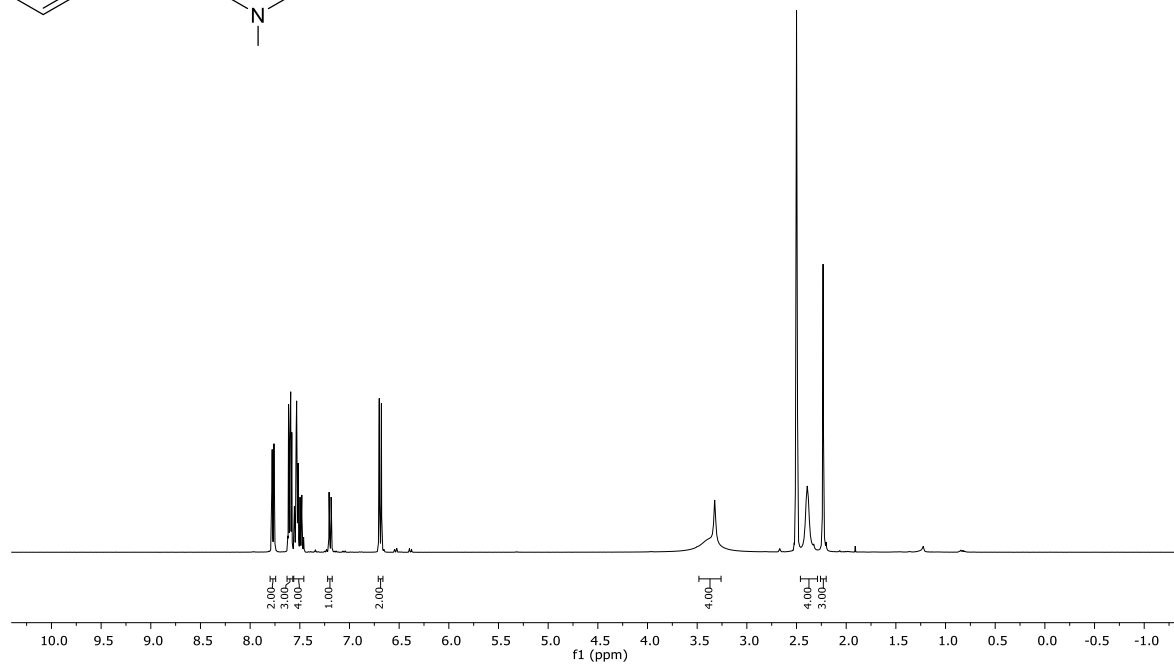
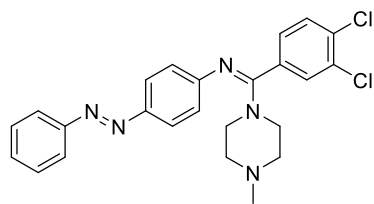
Compound 15 (DMSO-*d*₆)



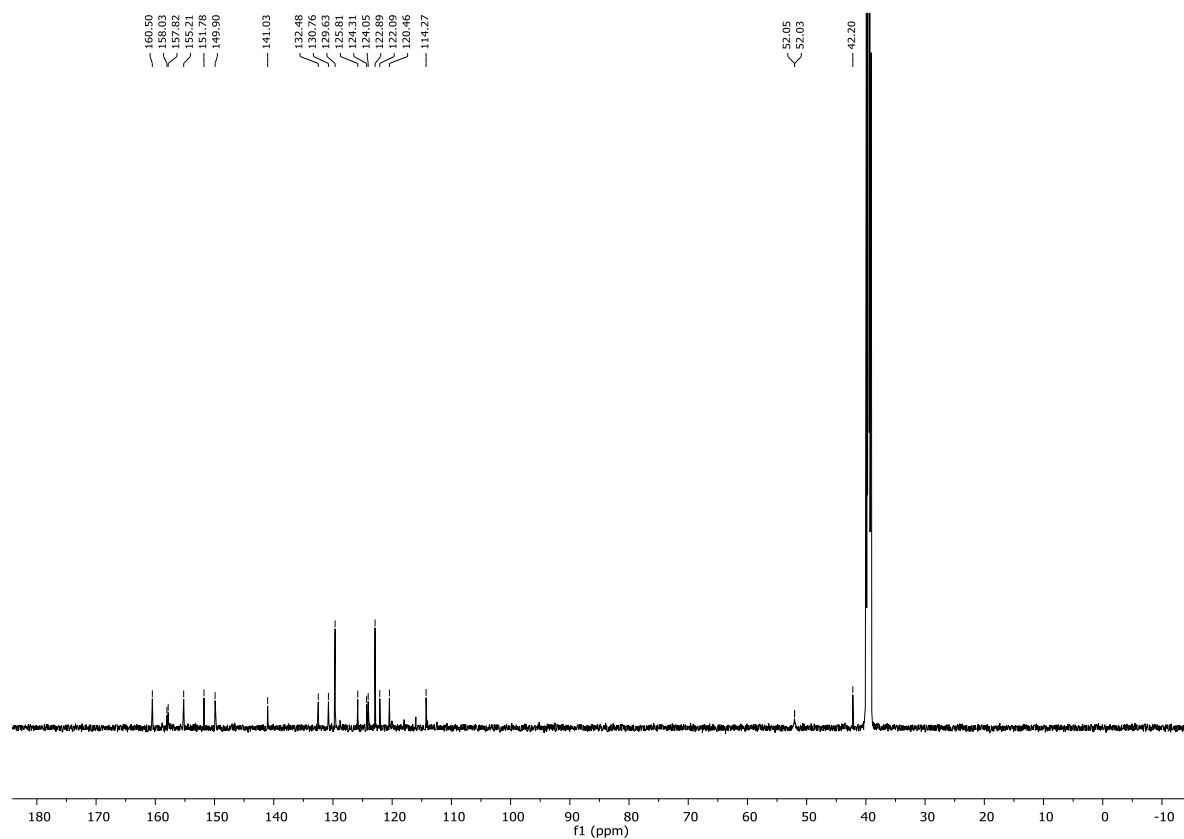
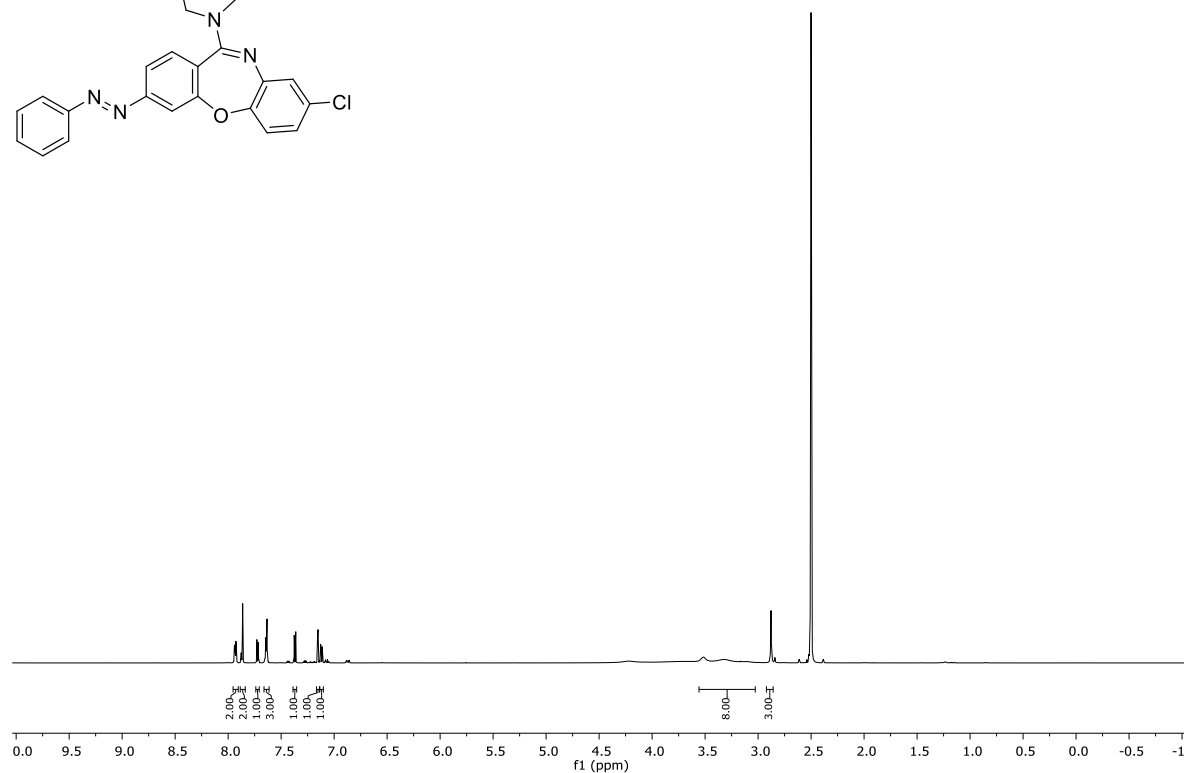
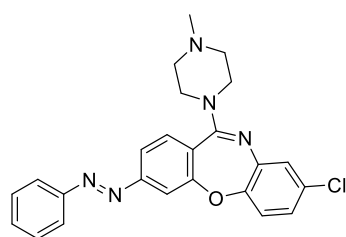
Compound **19** (DMSO-*d*₆)

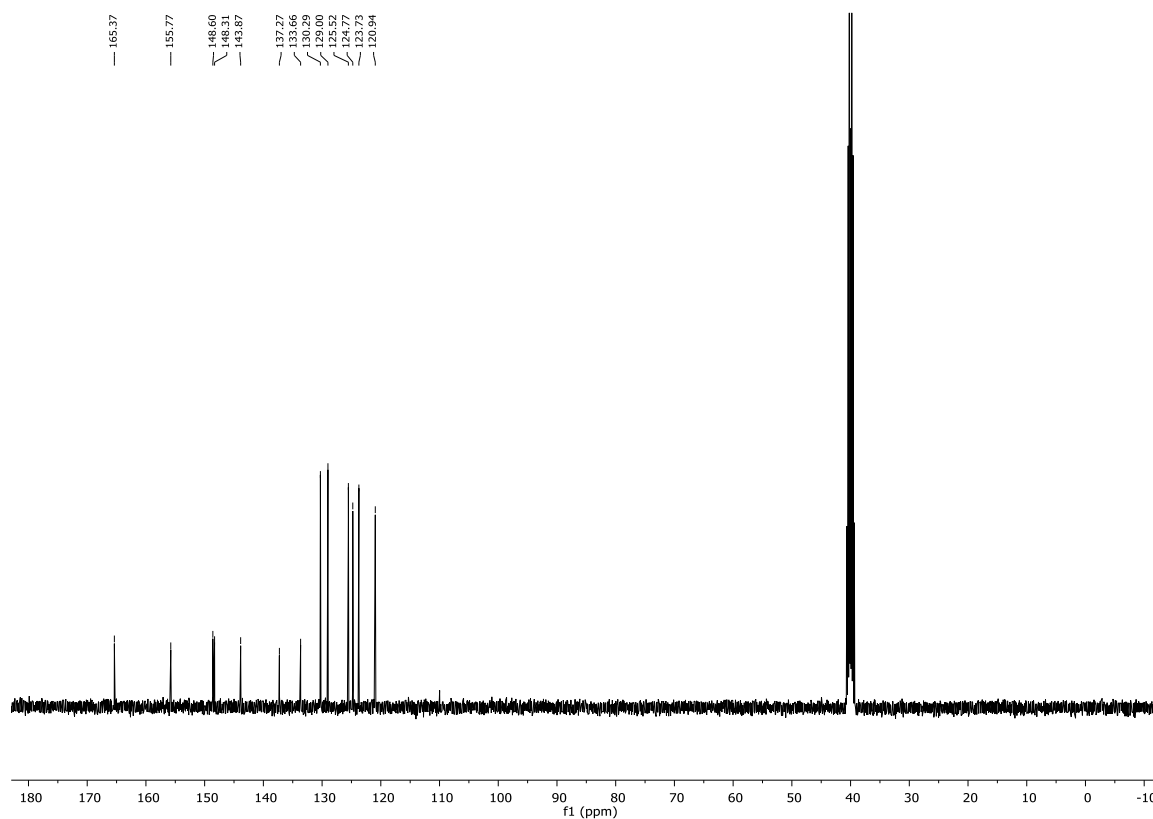
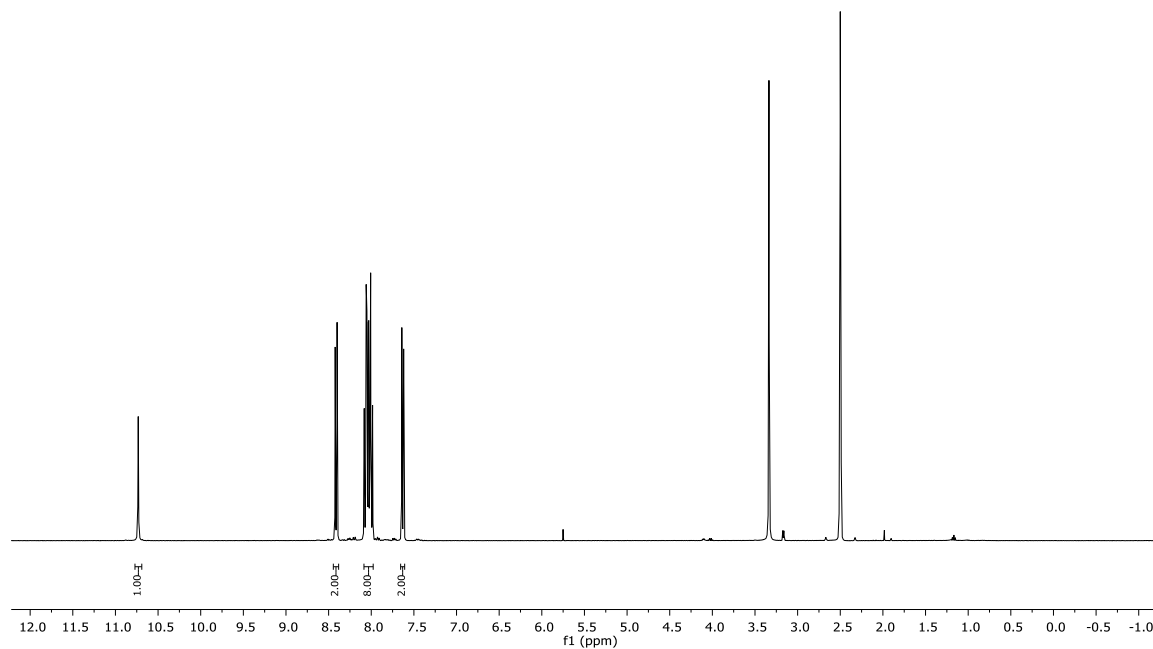
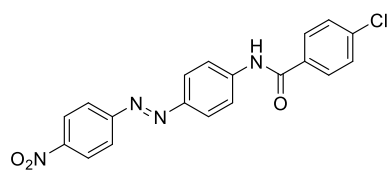
Compound **20** (DMSO-*d*₆)



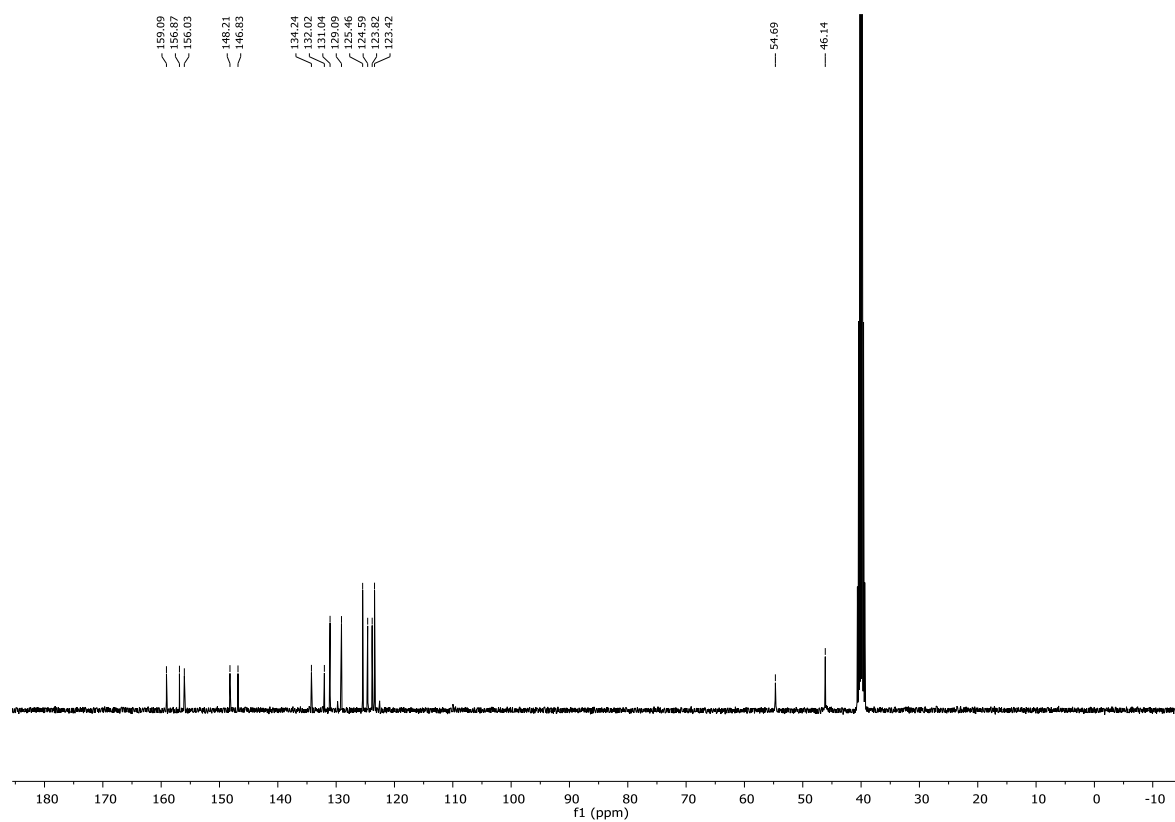
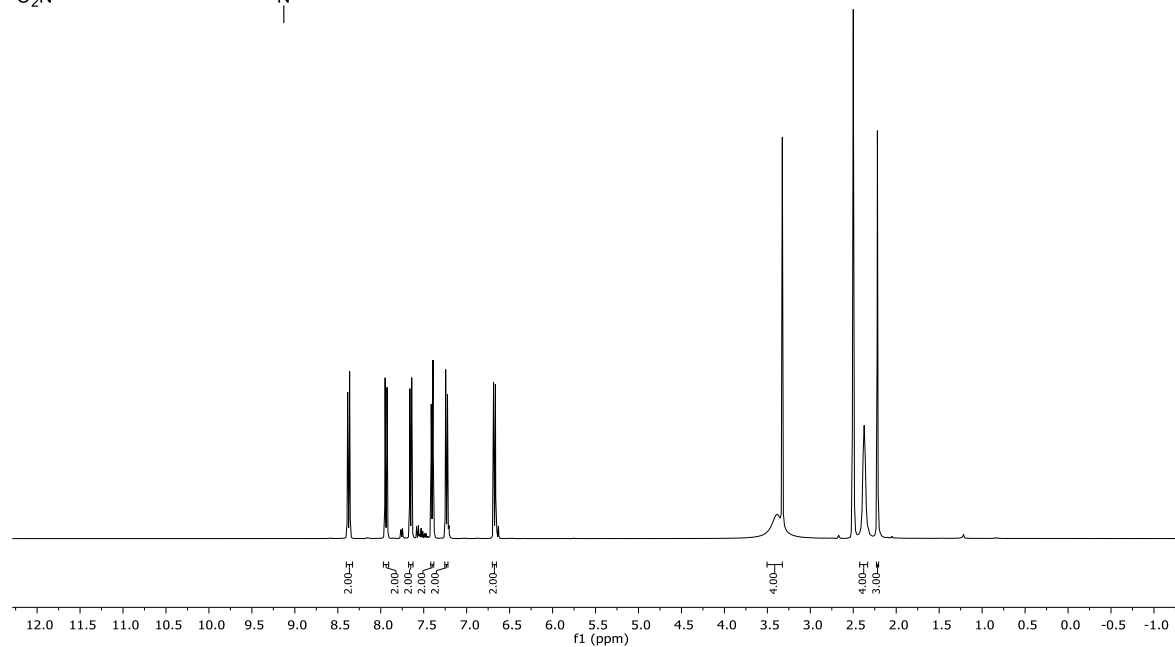
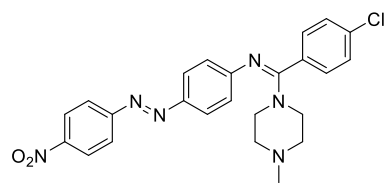
Compound **21** (DMSO-*d*₆)

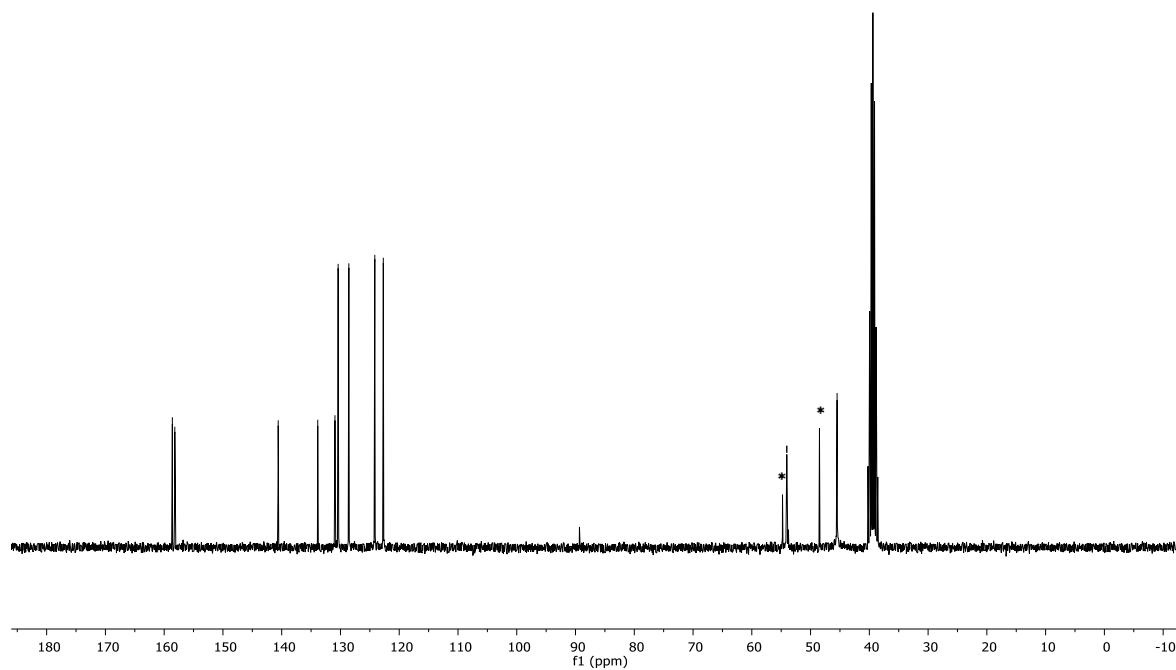
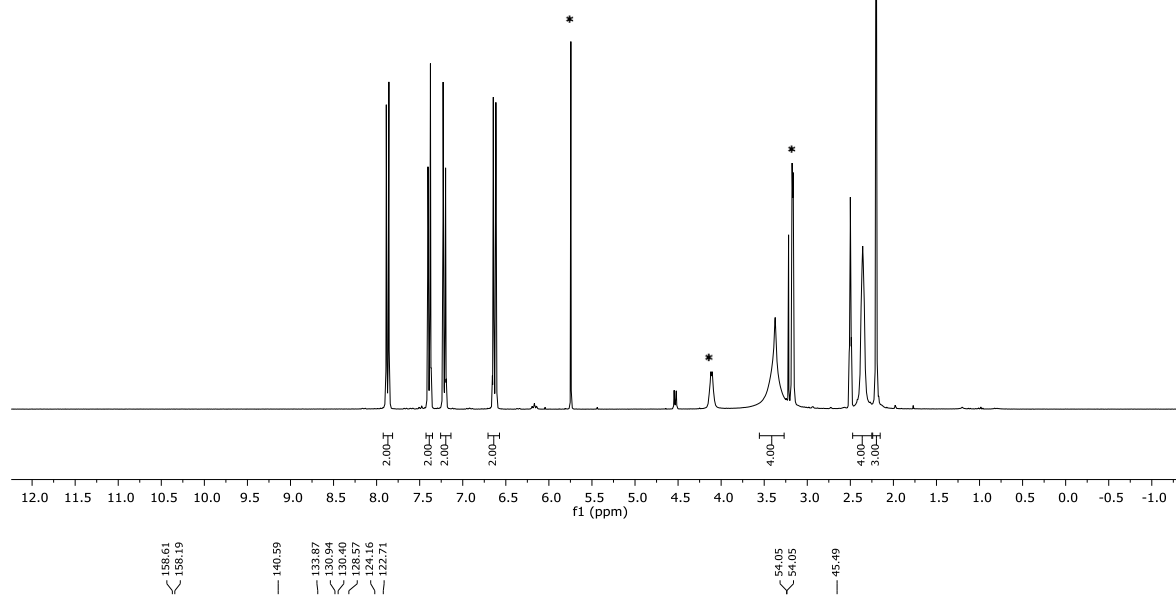
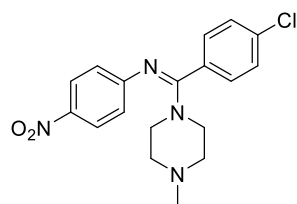
Compound **29** (DMSO-*d*₆)



Compound **32** (DMSO-*d*₆)

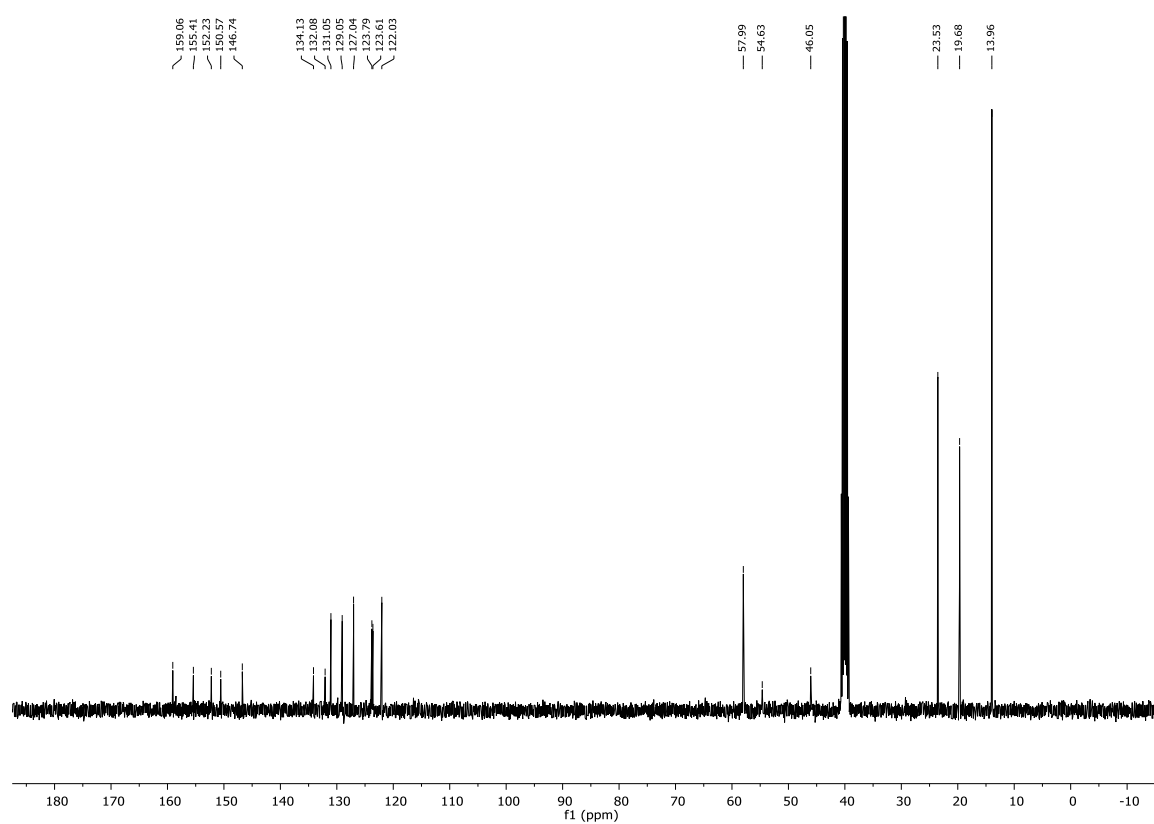
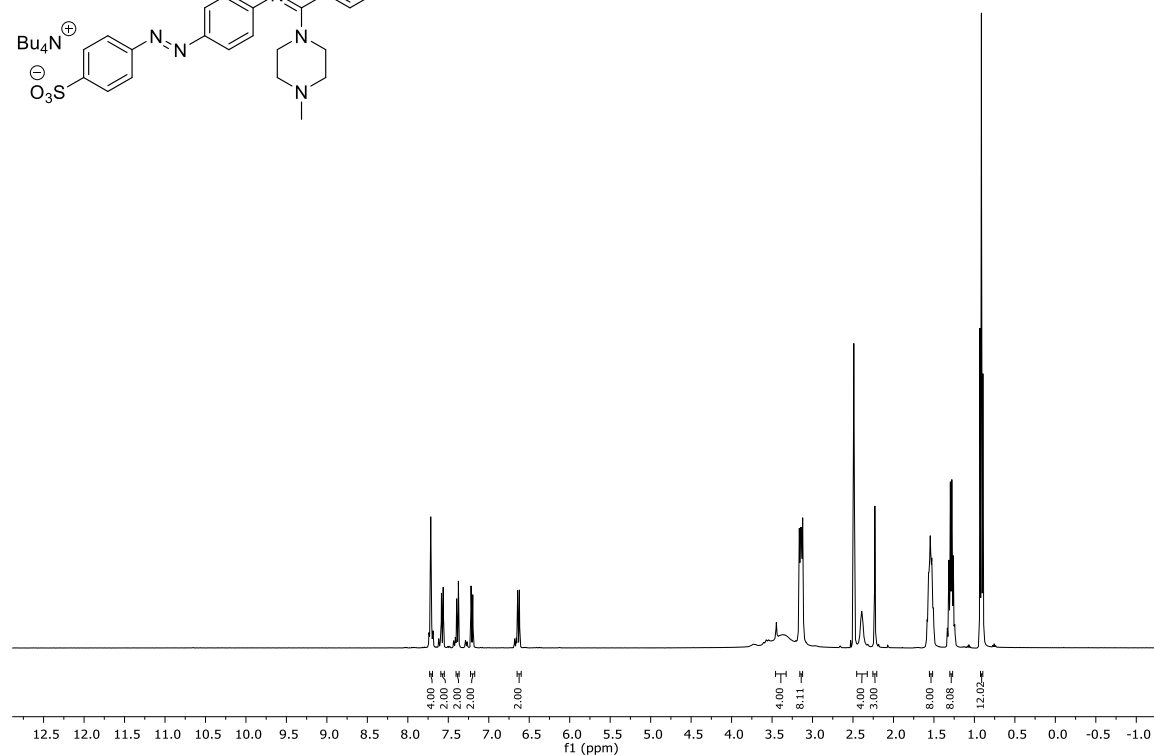
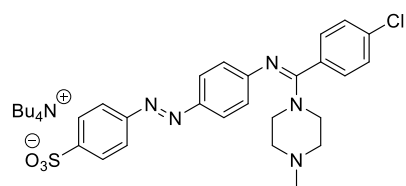
Compound **35** (DMSO-*d*₆)



Compound **38** (DMSO-*d*₆)

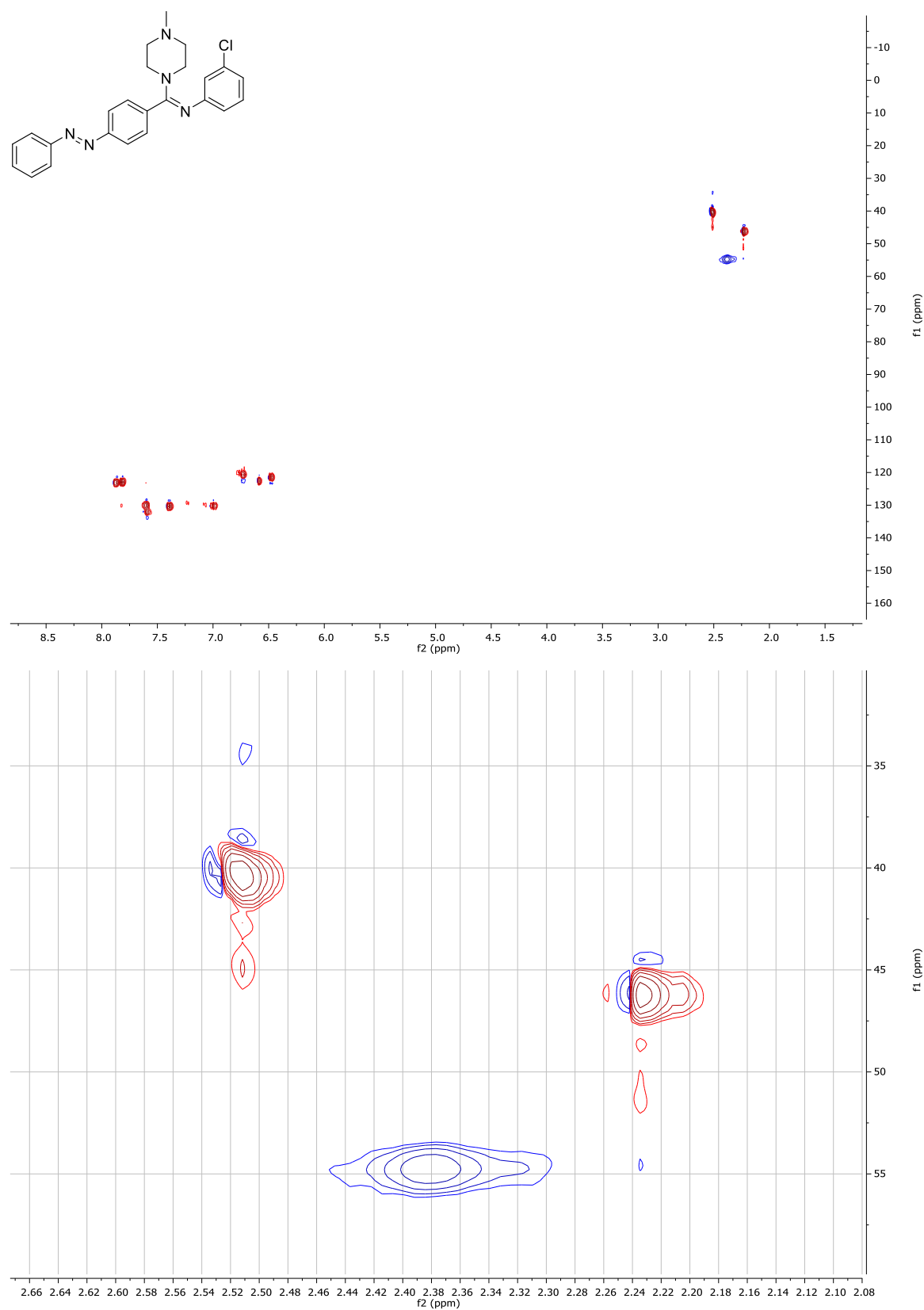
* solvent residual signals: MeOH, CH₂Cl₂

Compound **41** (DMSO-*d*₆)

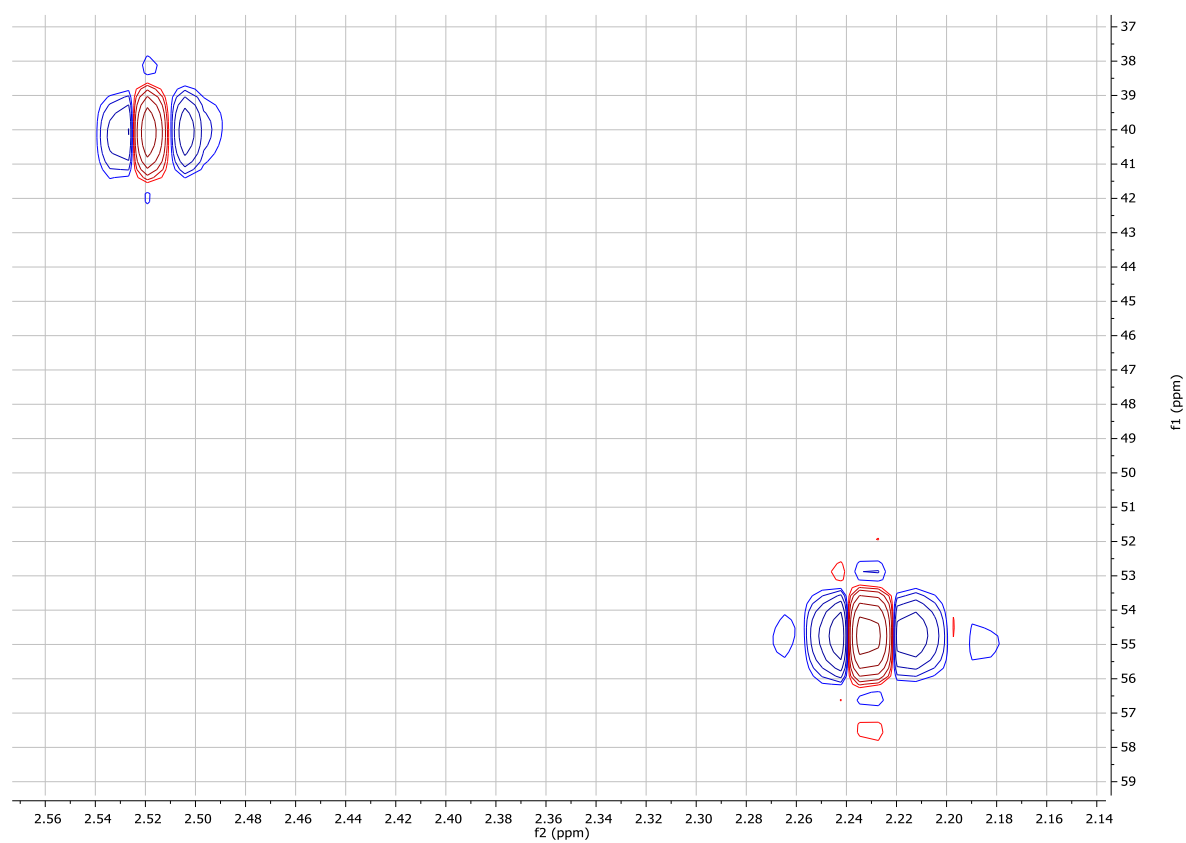
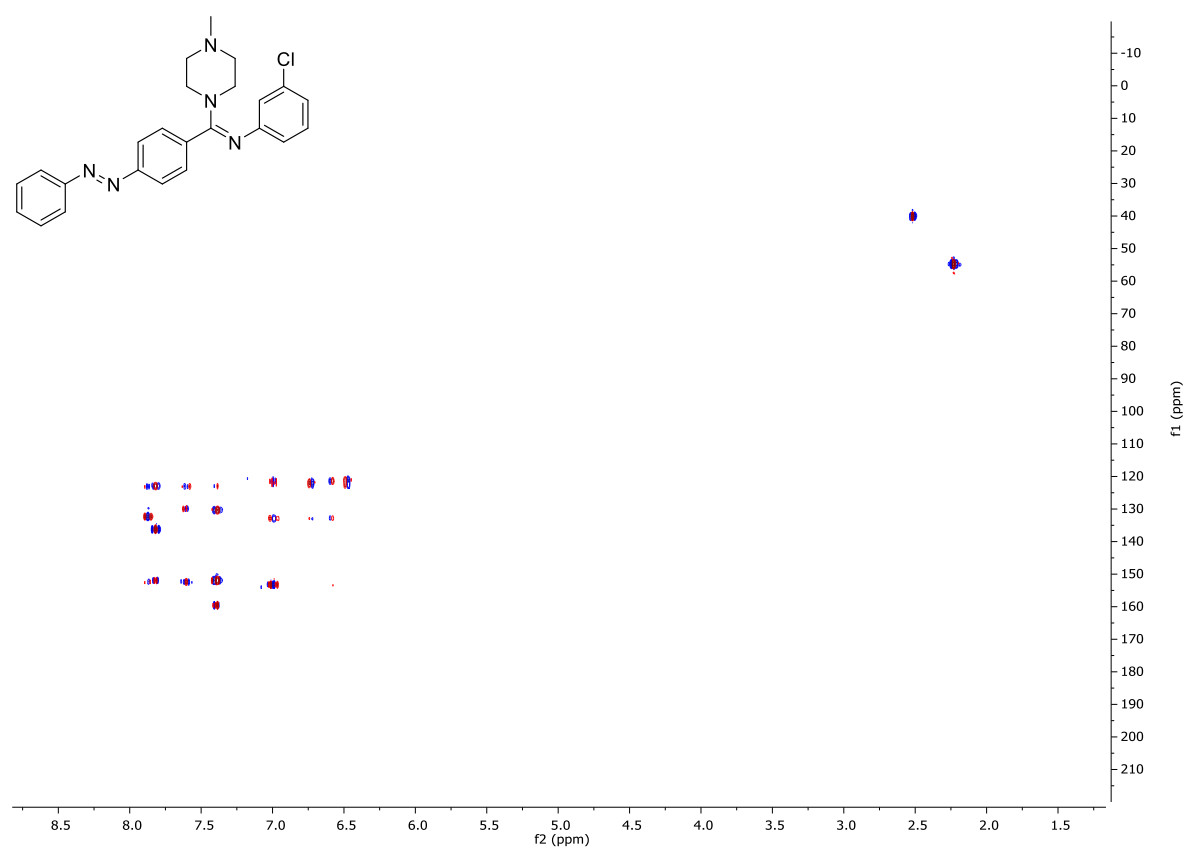


4.5.2 HSQC and HMBC spectra

HSQC spectra of compound **6** (DMSO- d_6)

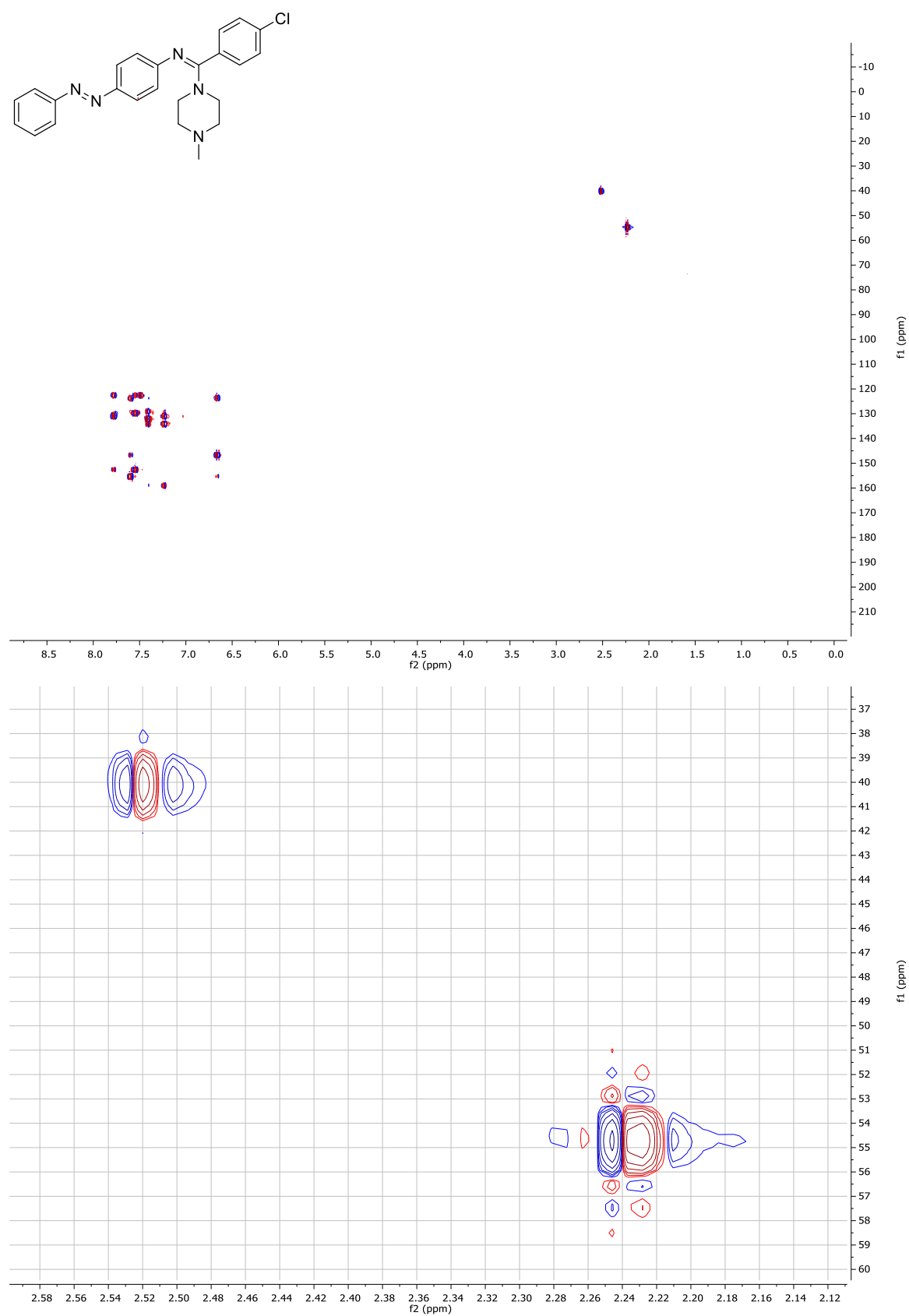


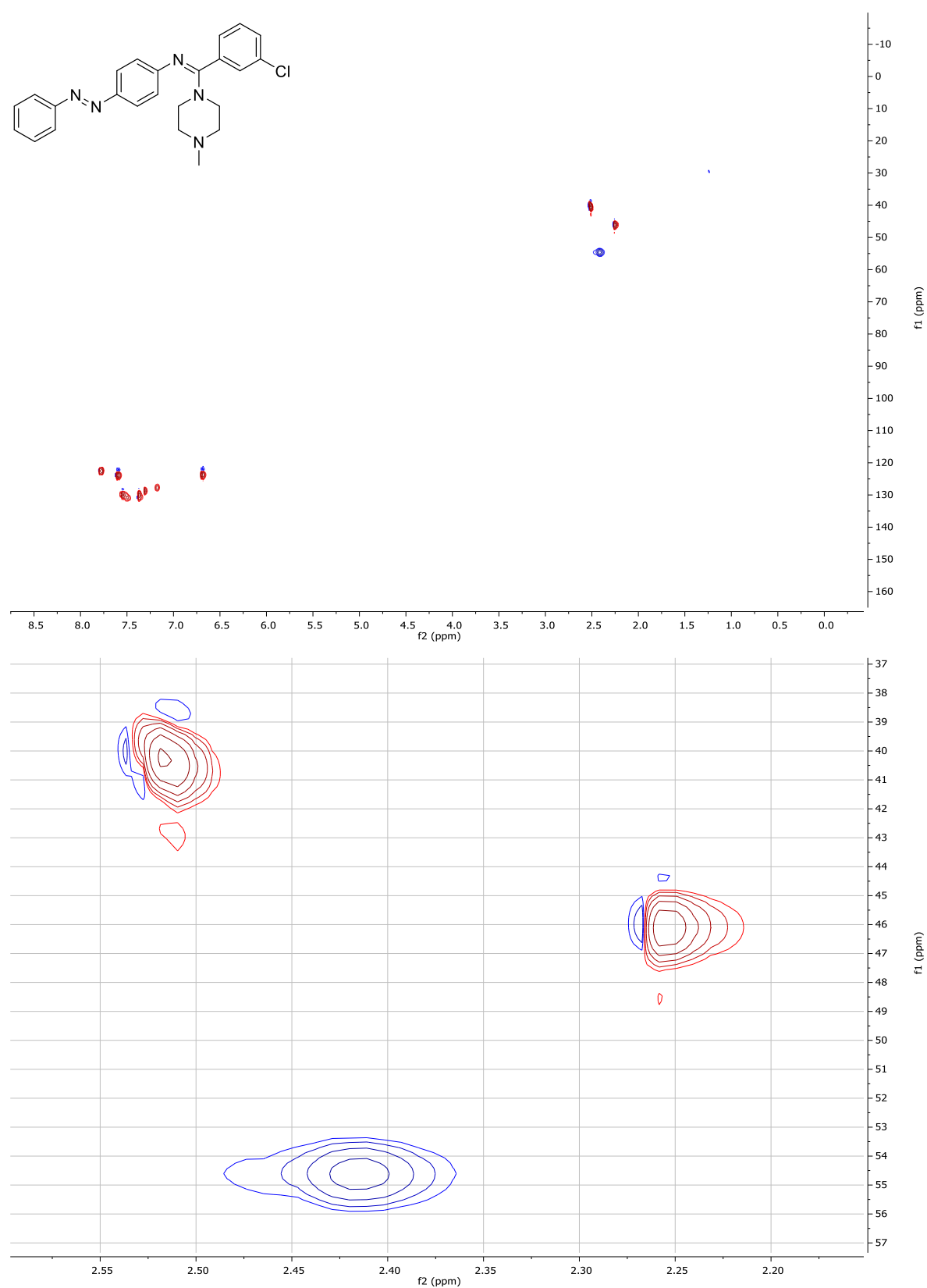
HMBC spectra of compound **6** (DMSO-*d*₆)



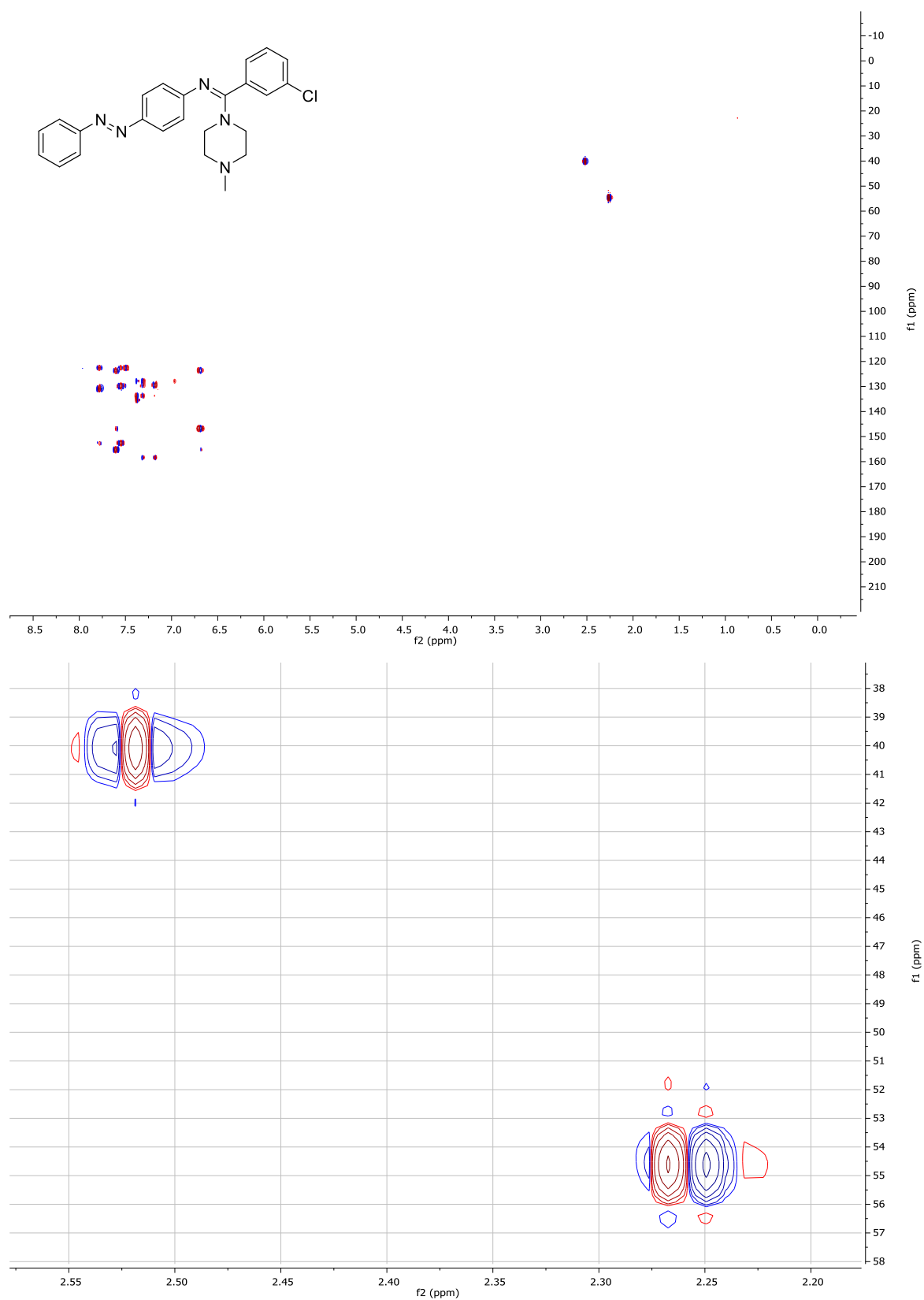
HSQC spectra of compound **19** (DMSO-*d*₆)

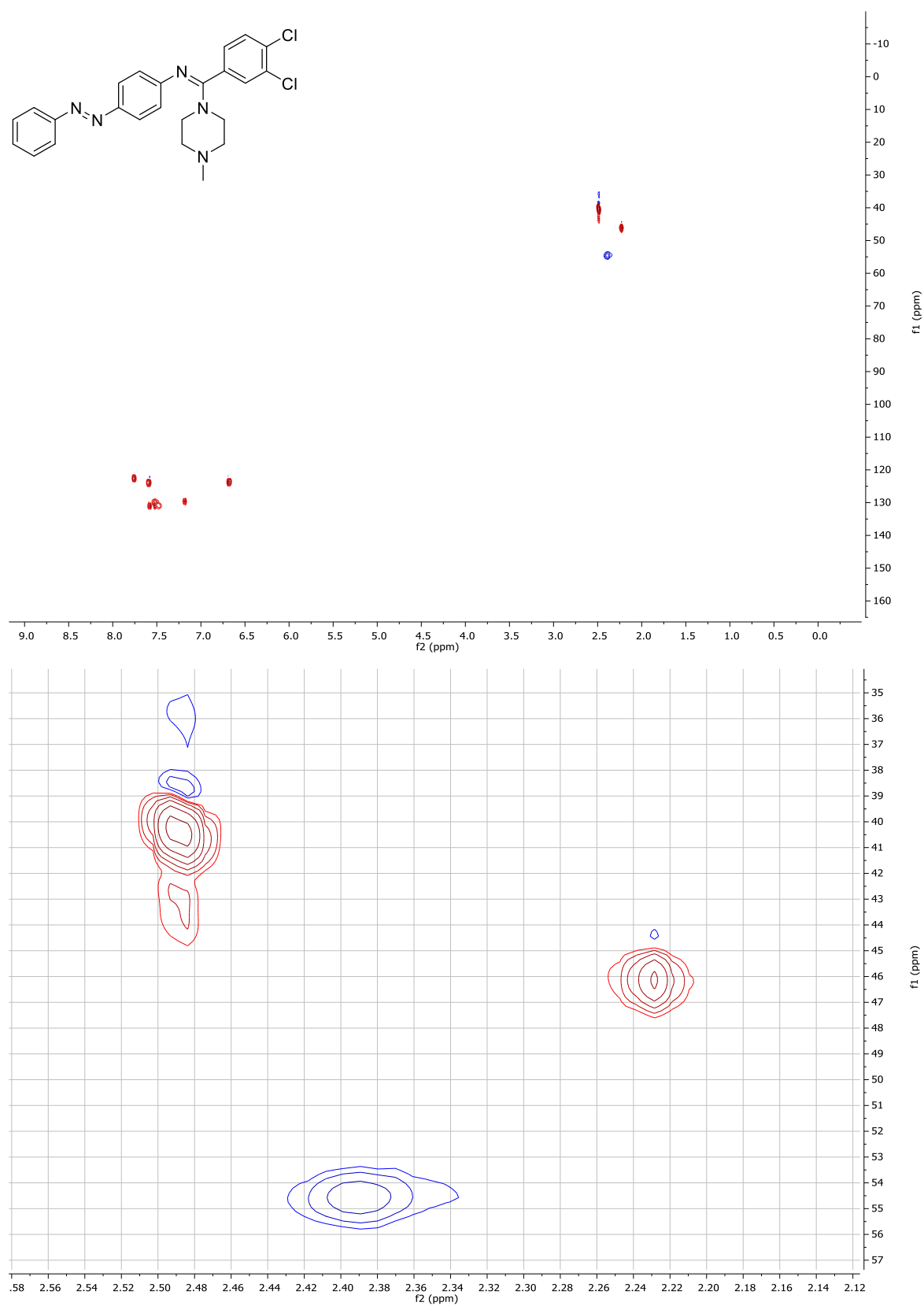
HMBC spectra of compound **19** (DMSO-*d*₆)



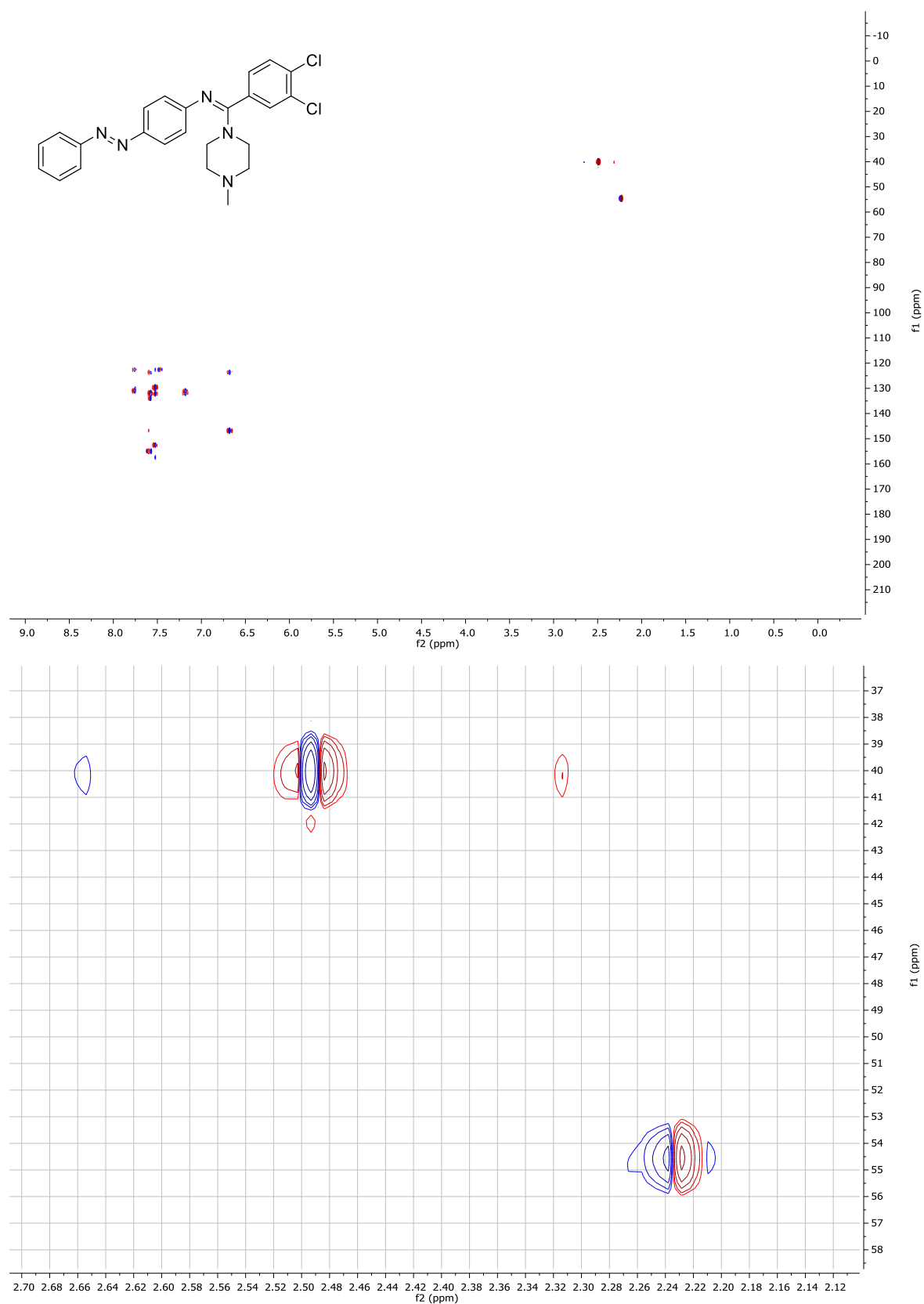
HSQC spectra of compound **20** (DMSO-*d*₆)

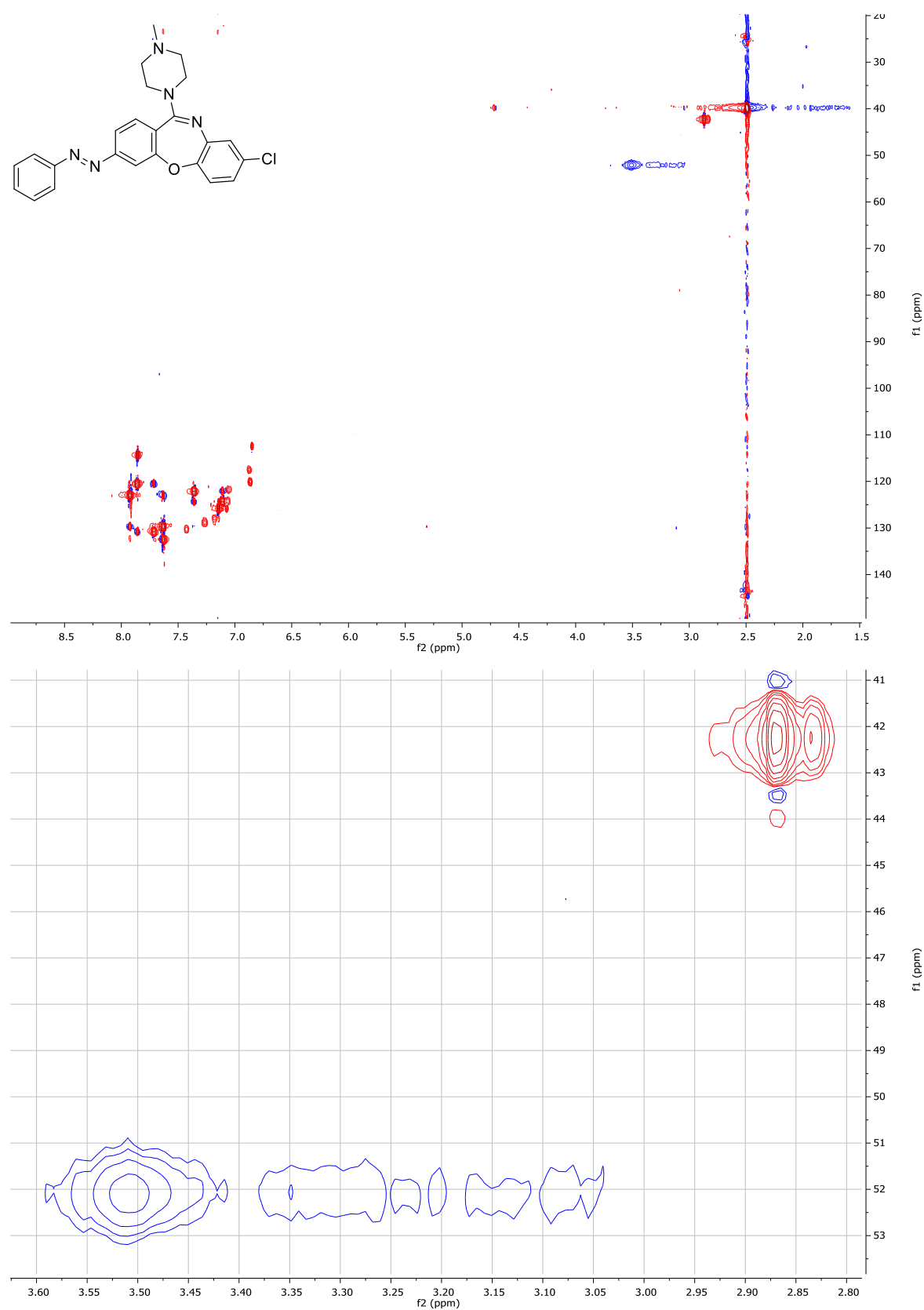
HMBC spectra of compound **20** (DMSO-*d*₆)



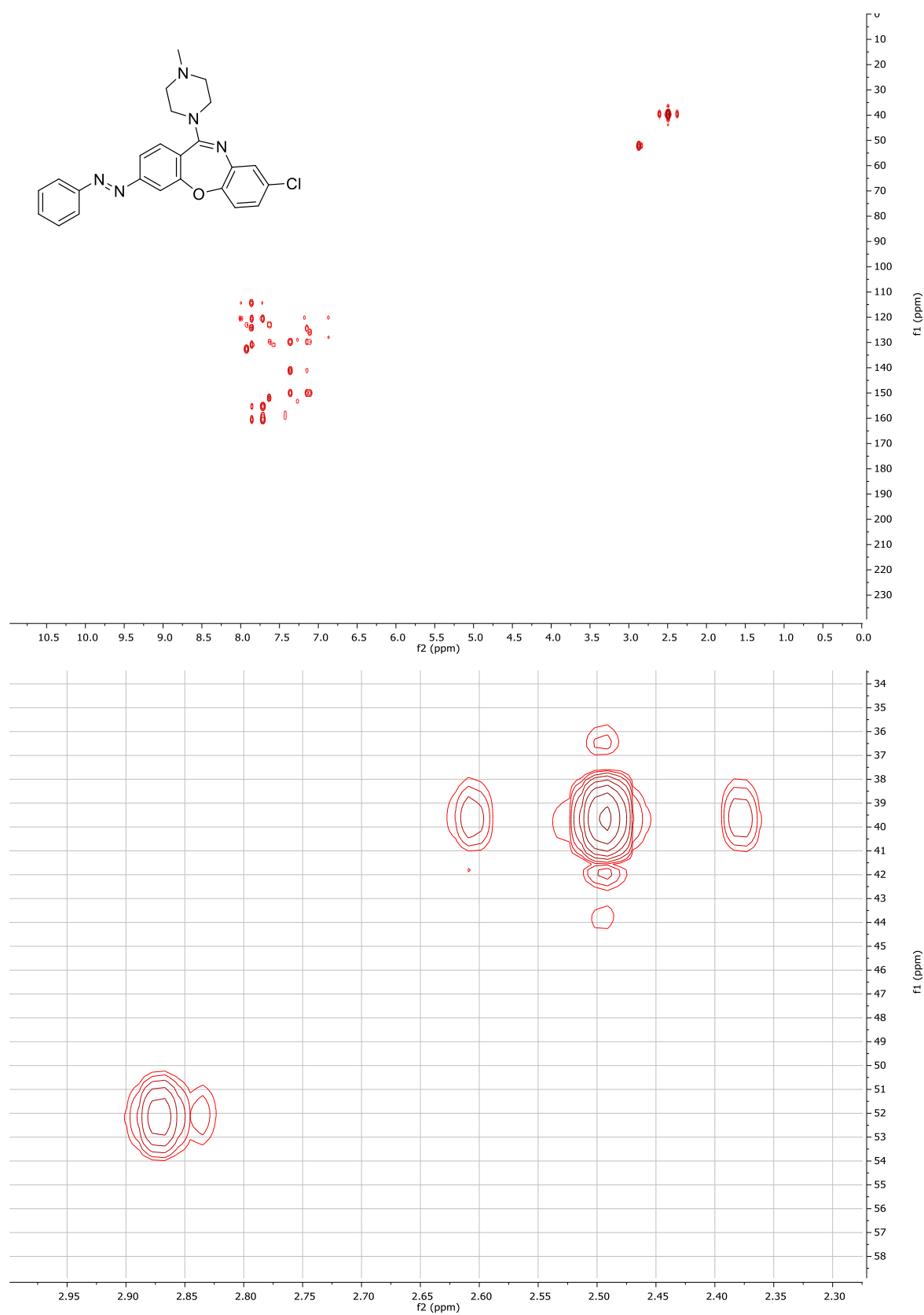
HSQC spectra of compound **21** (DMSO-*d*₆)

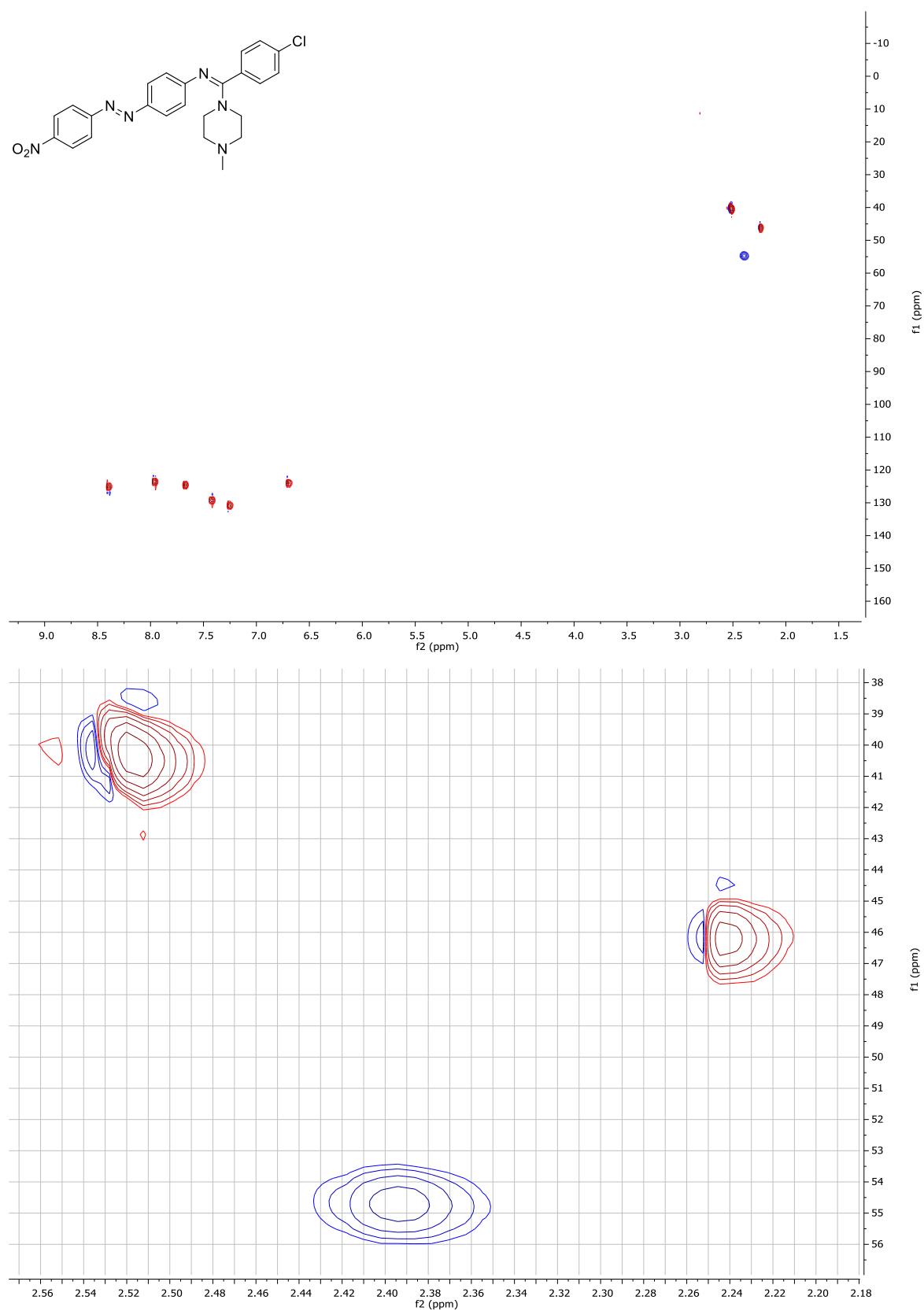
HMBC spectra of compound **21** (DMSO-*d*₆)



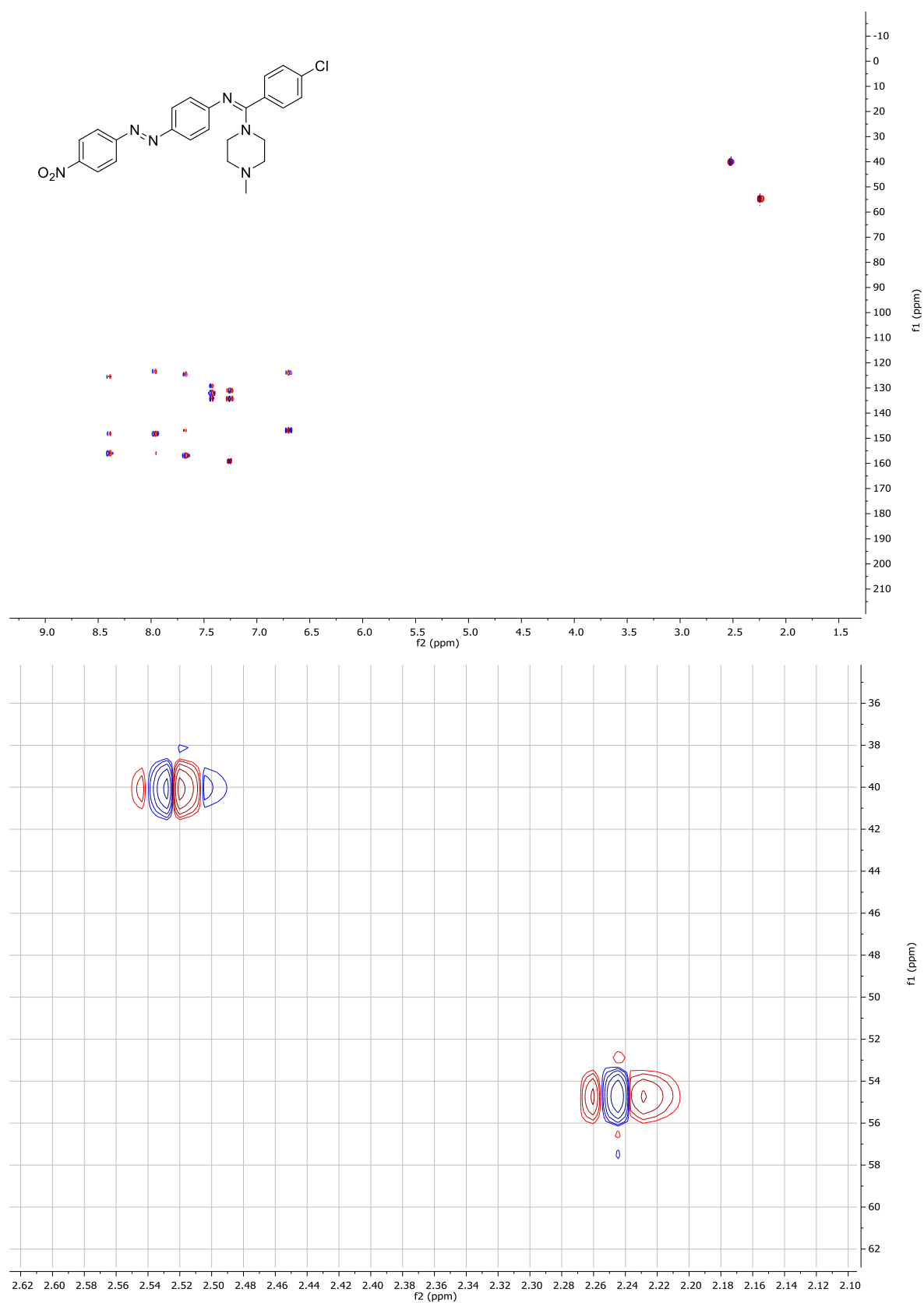
HSQC spectra of compound **29** (DMSO-*d*₆)

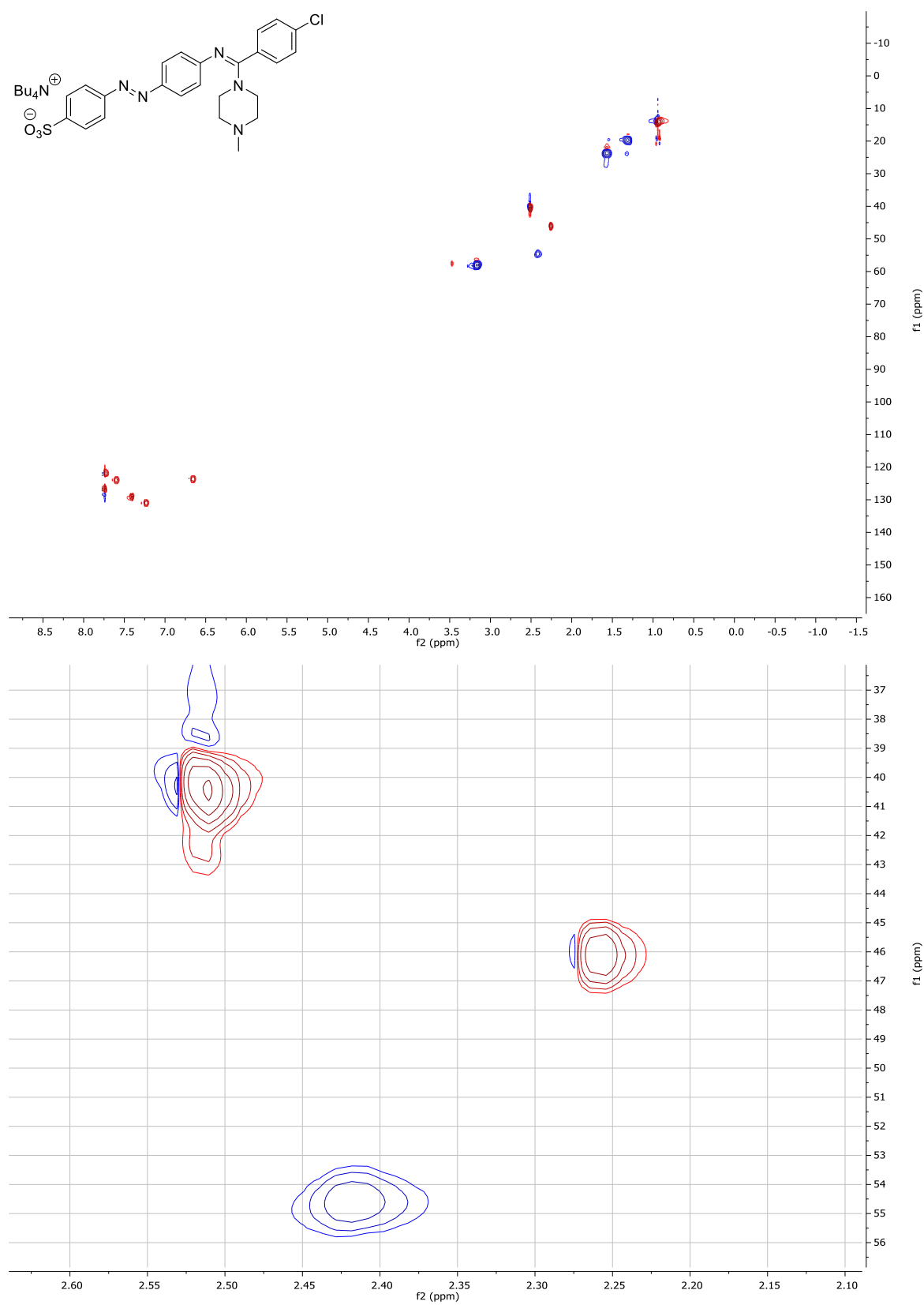
HMBC spectra of compound **29** (DMSO-*d*₆)



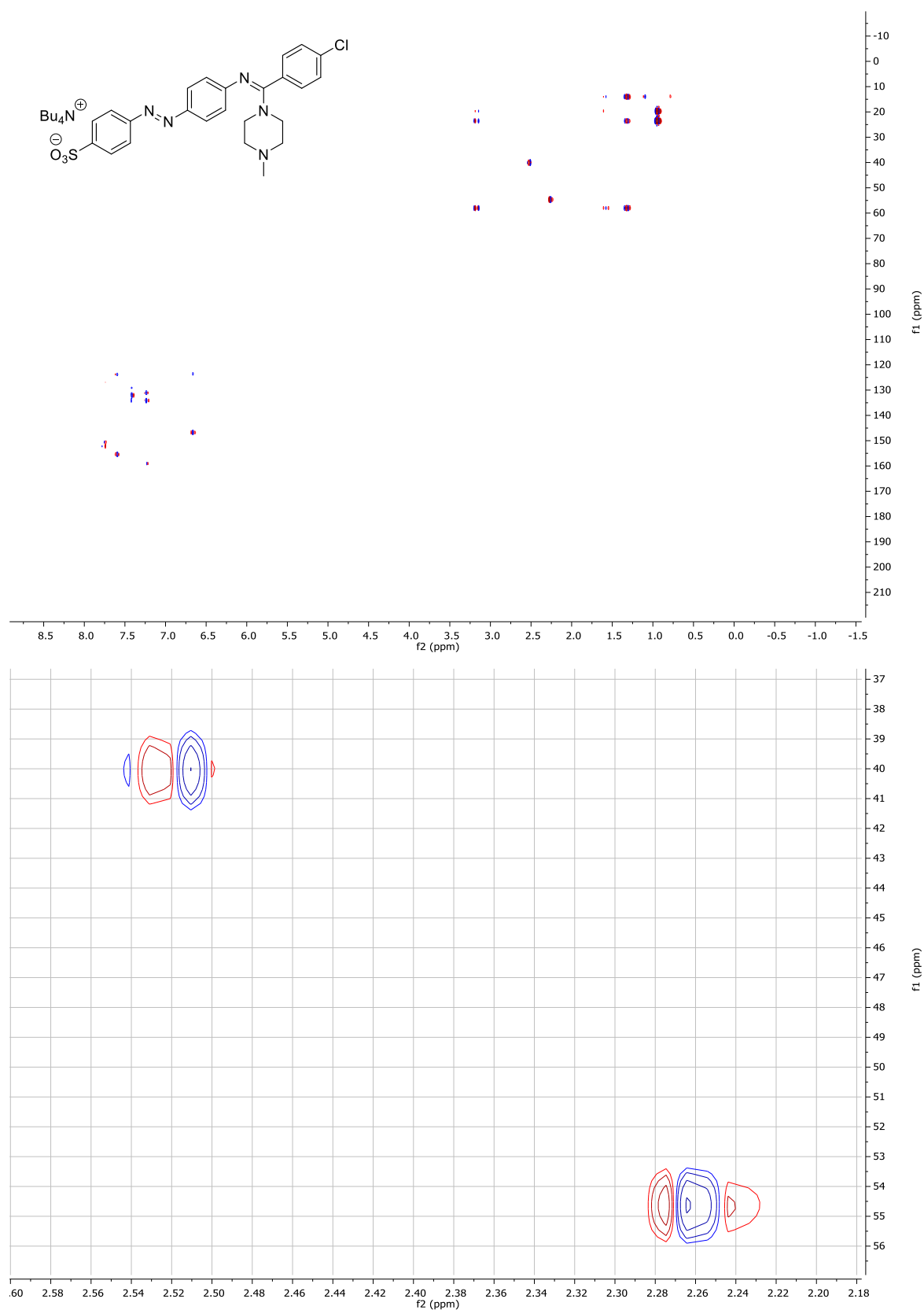
HSQC spectra of compound **35** (DMSO-*d*₆)

HMBC spectra of compound **35** (DMSO-*d*₆)



HSQC spectra of compound **41** (DMSO-*d*₆)

HMBC spectra of compound **41** (DMSO-*d*₆)



4.5.3 UV-Vis Absorption Spectra and Cycle Performances

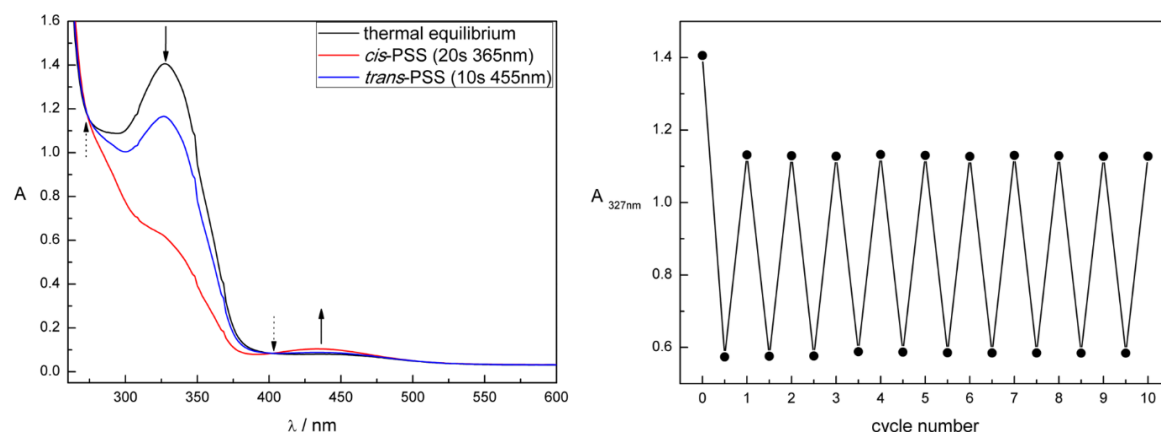


Figure S1. Compound **6** measured 50 μM in DMSO. Left: UV-Vis absorption spectra upon continuous irradiation until the PSS is reached. λ (*cis*-PSS) = 365 nm (20 s), λ (*trans*-PSS) = 455 nm (10 s). Black arrows show the changes in absorption upon *trans-cis* isomerization triggered with $\lambda = 365$ nm. Dotted black arrows indicate isosbestic points. Right: Cycle performance. Changes in absorption at 327 nm (λ_{max} of the *trans* isomer) were measured during alternate irradiation with $\lambda = 365$ nm (20 s) and $\lambda = 455$ nm (10 s) until the PSS is reached.

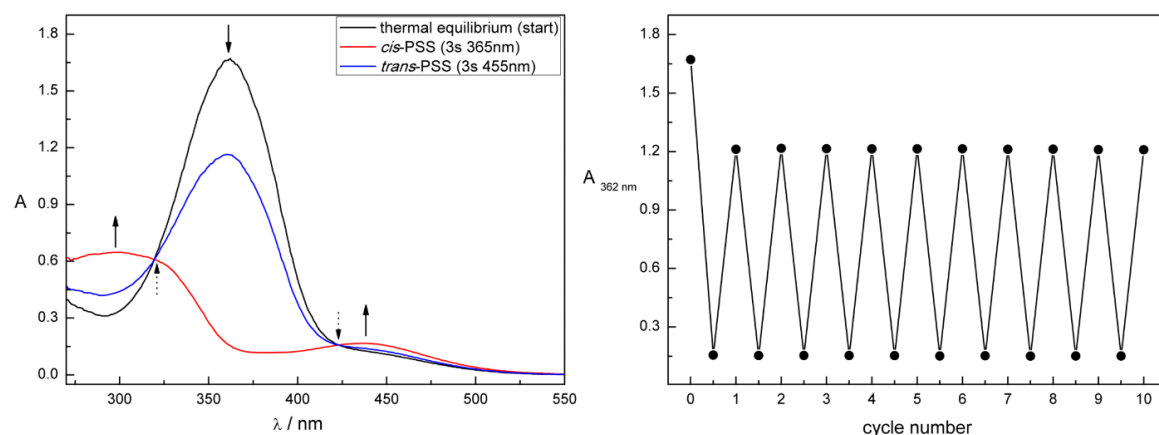


Figure S2. Compound **19** measured 50 μM in DMSO. Left: UV-Vis absorption spectra upon continuous irradiation until the PSS is reached. λ (*cis*-PSS) = 365 nm (3 s), λ (*trans*-PSS) = 455 nm (3 s). Black arrows show the changes in absorption upon *trans-cis* isomerization triggered with $\lambda = 365$ nm. Dotted black arrows indicate isosbestic points. Right: Cycle performance. Changes in absorption at 362 nm (λ_{max} of the *trans* isomer) were measured during alternate irradiation with $\lambda = 365$ nm (3 s) and $\lambda = 455$ nm (3 s) until the PSS is reached.

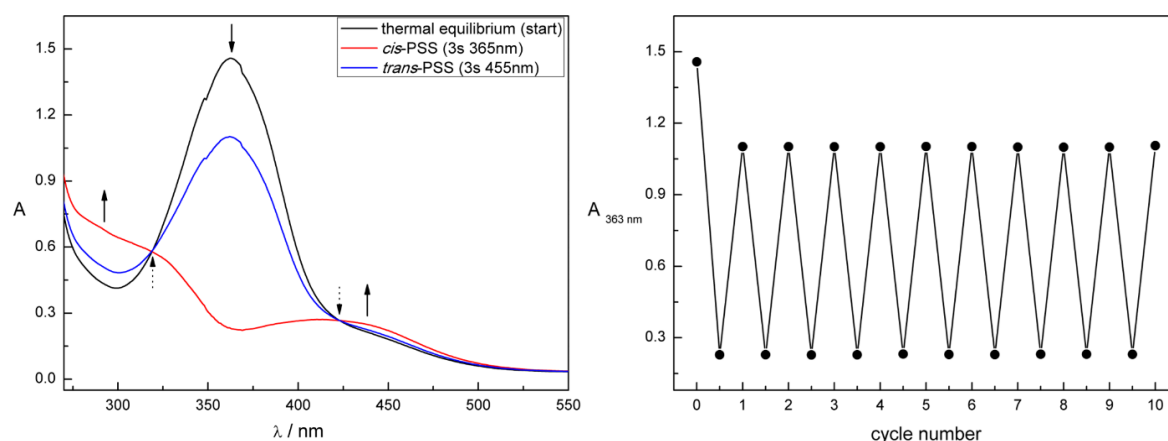


Figure S3. Compound **20** measured 50 μM in DMSO. Left: UV-Vis absorption spectra upon continuous irradiation until the PSS is reached. λ (*cis*-PSS) = 365 nm (3 s), λ (*trans*-PSS) = 455 nm (3 s). Black arrows show the changes in absorption upon *trans*-*cis* isomerization triggered with $\lambda = 365$ nm. Dotted black arrows indicate isosbestic points. Right: Cycle performance. Changes in absorption at 363 nm (λ_{max} of the *trans* isomer) were measured during alternate irradiation with $\lambda = 365$ nm (3 s) and $\lambda = 455$ nm (3 s) until the PSS is reached.

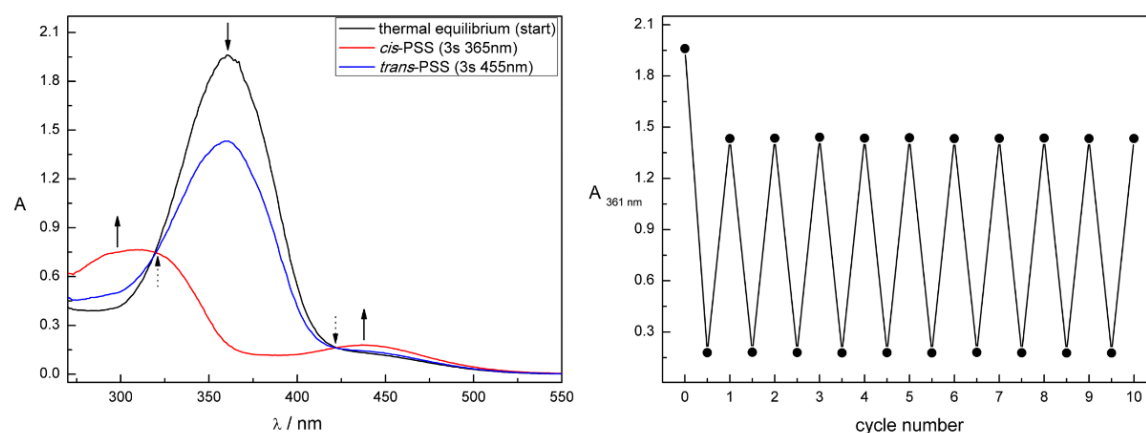


Figure S4. Compound **21** measured 50 μM in DMSO. Left: UV-Vis absorption spectra upon continuous irradiation until the PSS is reached. λ (*cis*-PSS) = 365 nm (3 s), λ (*trans*-PSS) = 455 nm (3 s). Black arrows show the changes in absorption upon *trans*-*cis* isomerization triggered with $\lambda = 365$ nm. Dotted black arrows indicate isosbestic points. Right: Cycle performance. Changes in absorption at 361 nm (λ_{max} of the *trans* isomer) were measured during alternate irradiation with $\lambda = 365$ nm (3 s) and $\lambda = 455$ nm (3 s) until the PSS is reached.

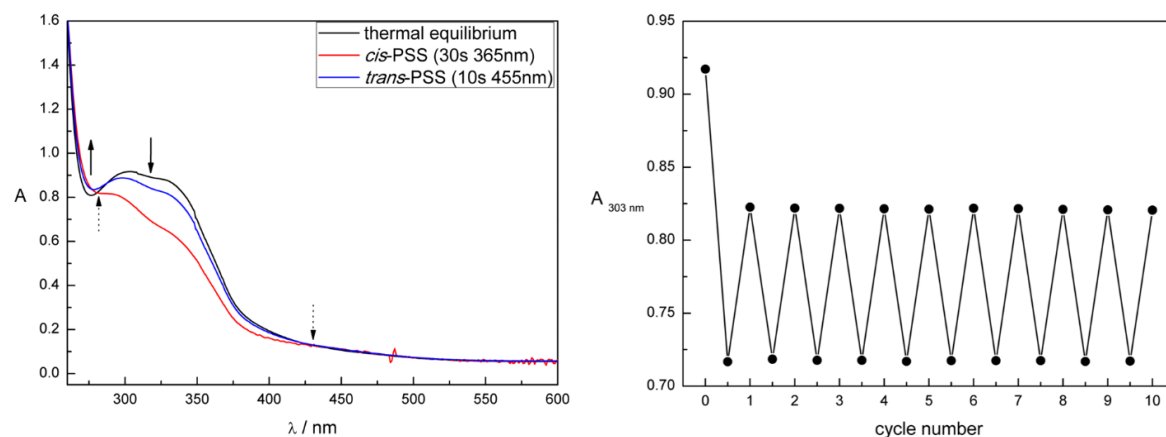


Figure S5. Compound **29** measured 50 μM in DMSO. Left: UV-Vis absorption spectra upon continuous irradiation until the PSS is reached. λ (*cis*-PSS) = 365 nm (30 s), λ (*trans*-PSS) = 455 nm (10 s). Black arrows show the changes in absorption upon *trans*-*cis* isomerization triggered with $\lambda = 365$ nm. Dotted black arrows indicate isosbestic points. Right: Cycle performance. Changes in absorption at 303 nm (λ_{max} of the *trans* isomer) were measured during alternate irradiation with $\lambda = 365$ nm (30 s) and $\lambda = 455$ nm (10 s) until the PSS is reached.

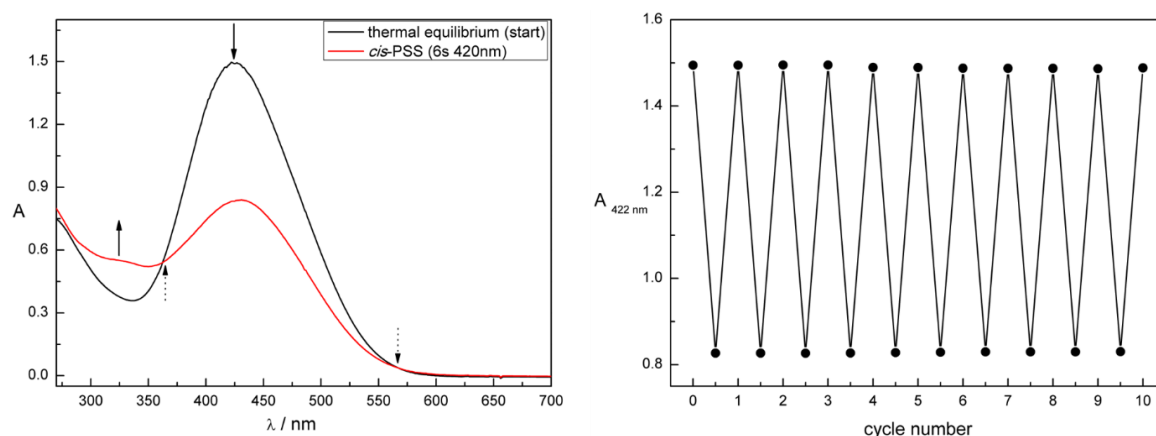


Figure S6. Compound **35** measured 50 μM in DMSO. Left: UV-Vis absorption spectra upon continuous irradiation until the PSS is reached. λ (*cis*-PSS) = 420 nm (6 s). Black arrows show the changes in absorption upon *trans*-*cis* isomerization triggered with $\lambda = 365$ nm. Dotted black arrows indicate isosbestic points. Right: Cycle performance. Changes in absorption at 422 nm (λ_{max} of the *trans* isomer) were measured during alternate irradiation with $\lambda = 420$ nm (6 s) and thermal relaxation.

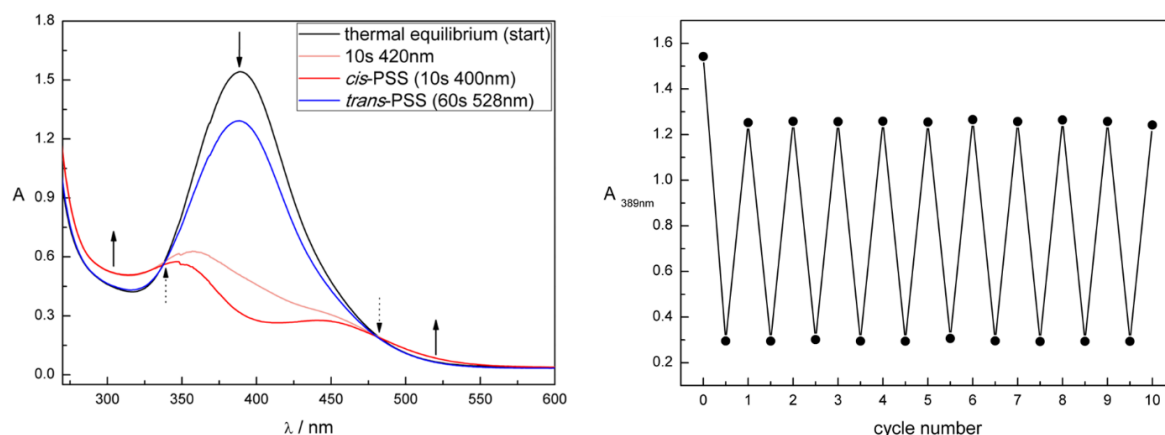


Figure S7. Compound **41** measured 50 μ M in DMSO. Left: UV-Vis absorption spectra upon continuous irradiation until the PSS is reached. λ (*cis*-PSS) = 400 nm (10 s), λ (*trans*-PSS) = 528 nm (60 s). Black arrows show the changes in absorption upon *trans-cis* isomerization triggered with λ = 400 nm. Dotted black arrows indicate isosbestic points. Right: Cycle performance. Changes in absorption at 389 nm (λ_{max} of the *trans* isomer) were measured during alternate irradiation with λ = 400 nm (10 s) and λ = 528 nm (60 s) until the PSS is reached.

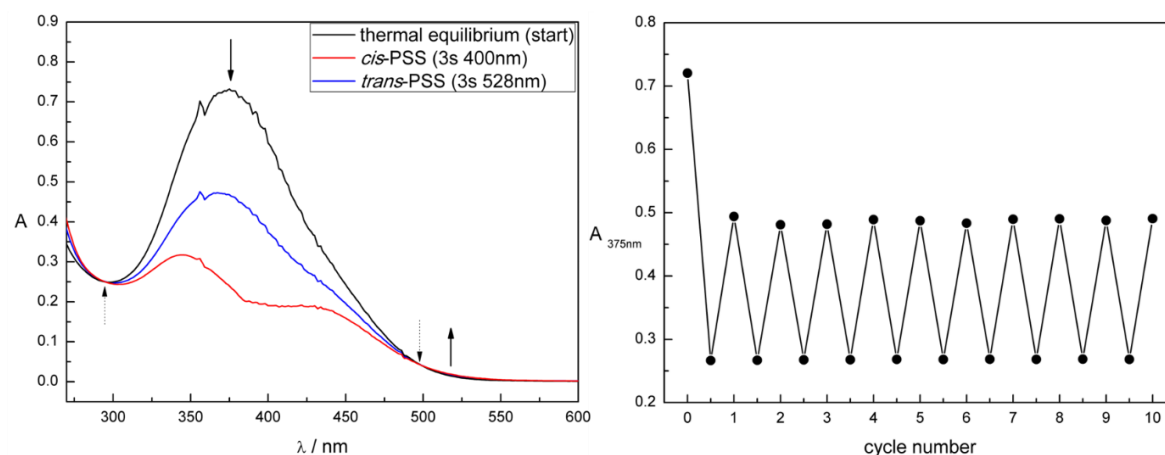


Figure S8. Compound **41** measured 50 μ M in Tyrode's solution + 0.1% DMSO. Left: UV-Vis absorption spectra upon continuous irradiation until the PSS is reached. λ (*cis*-PSS) = 400 nm (3 s), λ (*trans*-PSS) = 528 nm (3 s). Black arrows show the changes in absorption upon *trans-cis* isomerization triggered with λ = 400 nm. Dotted black arrows indicate isosbestic points. Right: Cycle performance. Changes in absorption at 375 nm (λ_{max} of the *trans* isomer) were measured during alternate irradiation with λ = 400 nm (3 s) and λ = 528 nm (3 s) until the PSS is reached.

4.5.4 Thermal Half-Lives (THL)

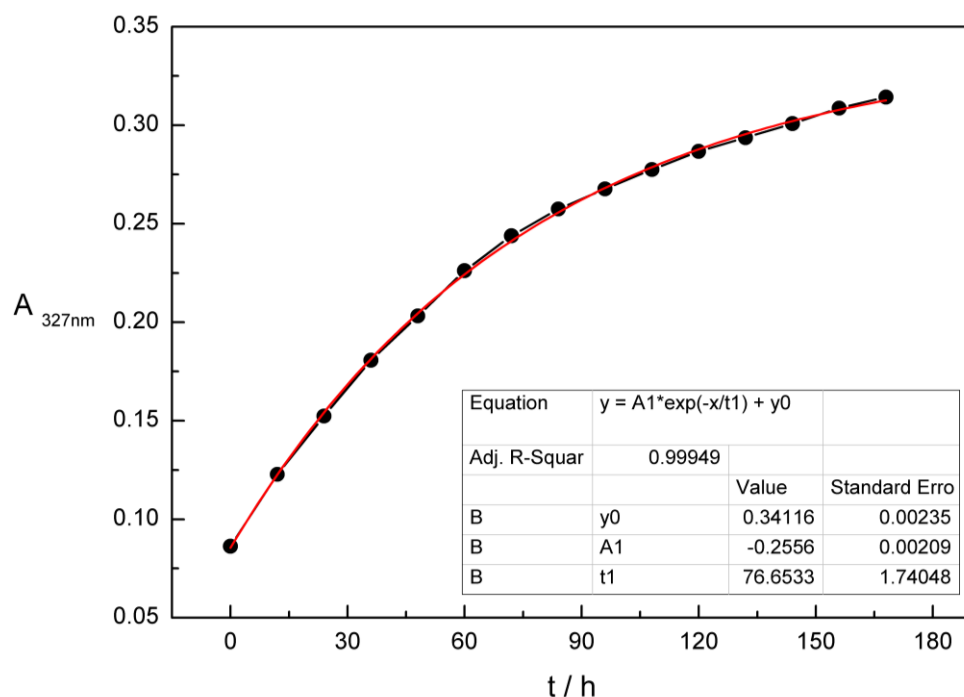


Figure S9. Thermal stability of the *cis* isomer of **6** measured 50 μM in DMSO at 25 $^{\circ}\text{C}$. Changes in the absorption at the indicated wavelength (λ_{max} of the *trans* isomer) after irradiation with $\lambda = 365$ nm and subsequent thermal relaxation are represented as black dots. The red curve represents an exponential nonlinear curve fit.

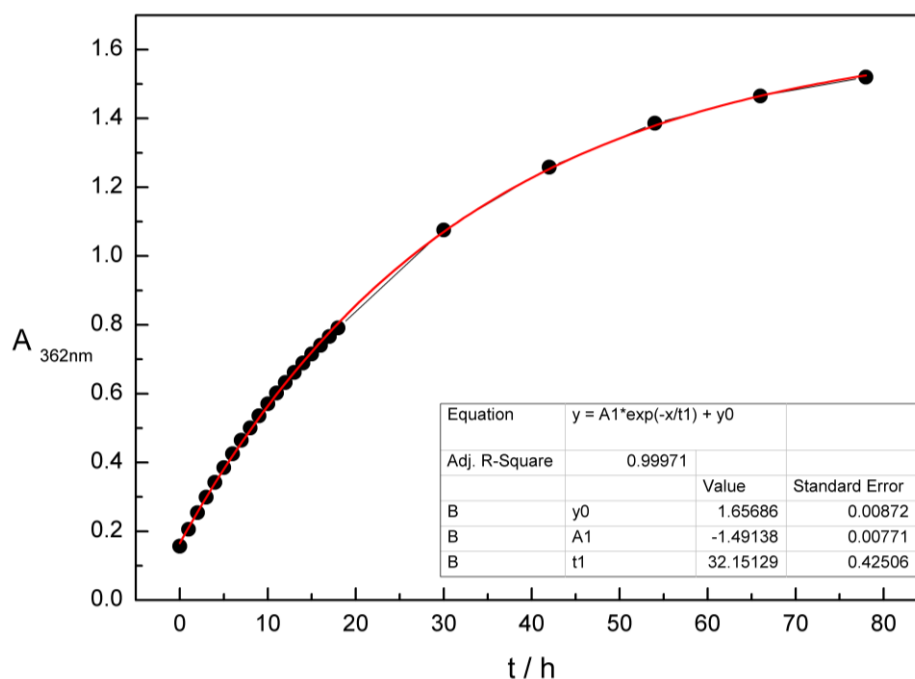


Figure S10. Thermal stability of the *cis* isomer of **19** measured 50 μM in DMSO at 25 $^{\circ}\text{C}$. Changes in the absorption at the indicated wavelength (λ_{max} of the *trans* isomer) after irradiation with $\lambda = 362$ nm and subsequent thermal relaxation are represented as black dots. The red curve represents an exponential nonlinear curve fit.

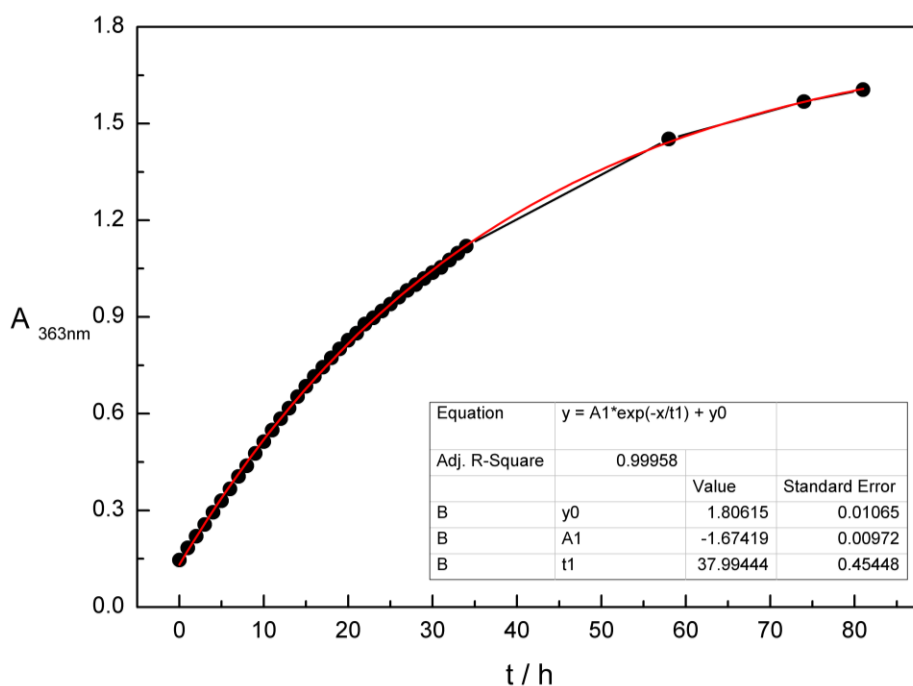


Figure S11. Thermal stability of the *cis* isomer of **20** measured 50 μ M in DMSO at 25 °C. Changes in the absorption at the indicated wavelength (λ_{max} of the *trans* isomer) after irradiation with $\lambda = 365$ nm and subsequent thermal relaxation are represented as black dots. The red curve represents an exponential nonlinear curve fit.

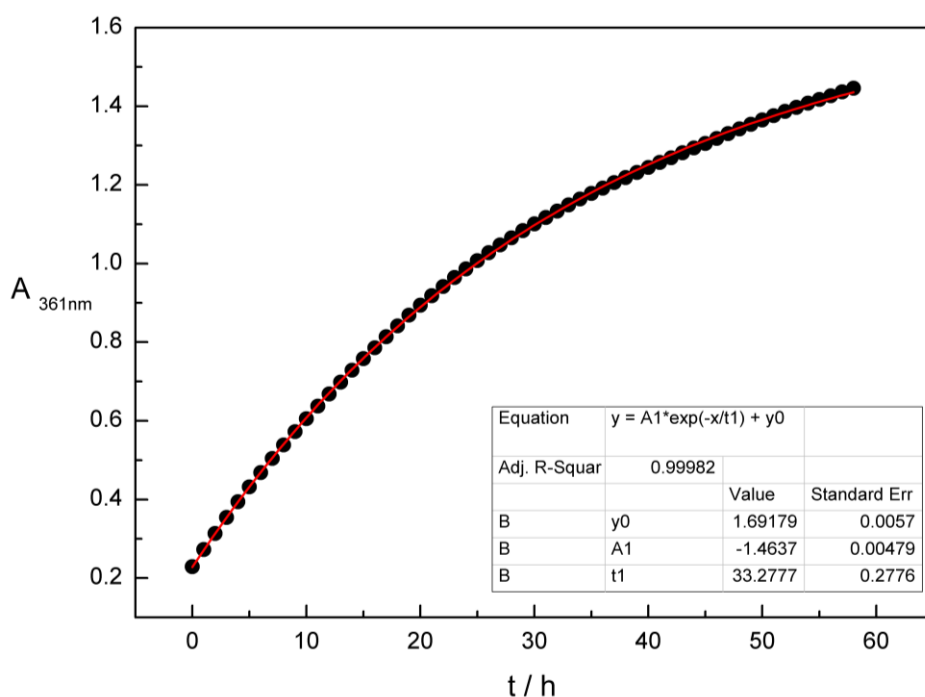


Figure S12. Thermal stability of the *cis*-isomer of **21** measured 50 μ M in DMSO at 25 °C. Changes in the absorption at the indicated wavelength (λ_{max} of the *trans* isomer) after irradiation with $\lambda = 361$ nm and subsequent thermal relaxation are represented as black dots. The red curve represents an exponential nonlinear curve fit.

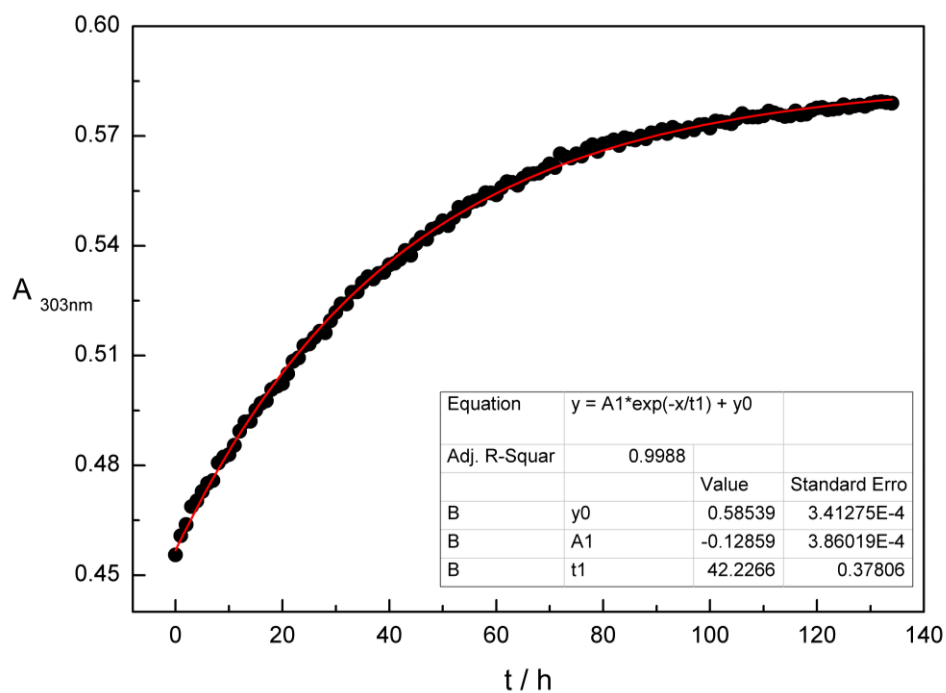


Figure S13. Thermal stability of the *cis*-isomer of **29** measured 50 μM in DMSO at 25 $^{\circ}\text{C}$. Changes in the absorption at the indicated wavelength (λ_{max} of the *trans* isomer) after irradiation with $\lambda = 365$ nm and subsequent thermal relaxation are represented as black dots. The red curve represents an exponential nonlinear curve fit.

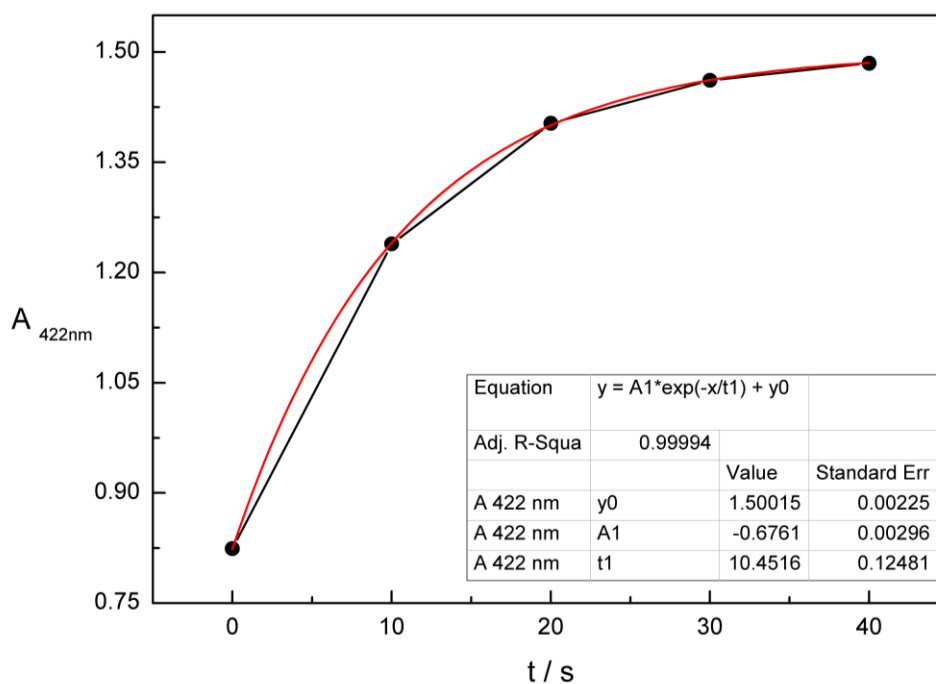


Figure S14. Thermal stability of the *cis* isomer of **35** measured 50 μM in DMSO at 25 $^{\circ}\text{C}$. Changes in the absorption at the indicated wavelength (λ_{max} of the *trans* isomer) after irradiation with $\lambda = 365$ nm and subsequent thermal relaxation are represented as black dots. The red curve represents an exponential nonlinear curve fit.

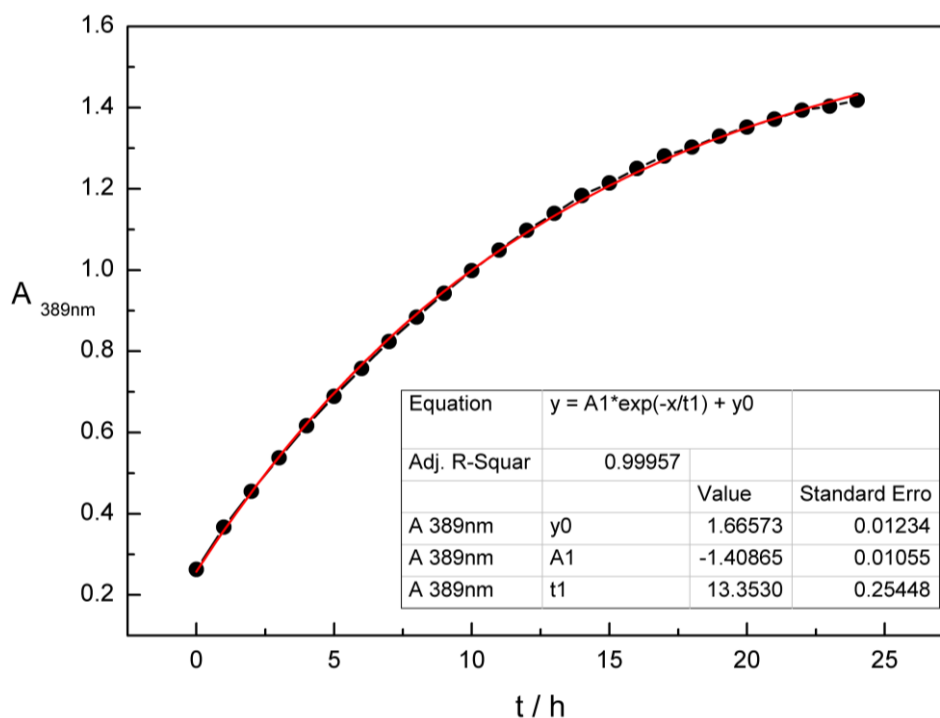


Figure S15. Thermal stability of the *cis* isomer of **41** measured 50 μ M in DMSO at 25 °C. Changes in the absorption at the indicated wavelength (λ_{\max} of the *trans* isomer) after irradiation with $\lambda = 400$ nm and subsequent thermal relaxation are represented as black dots. The red curve represents an exponential nonlinear curve fit.

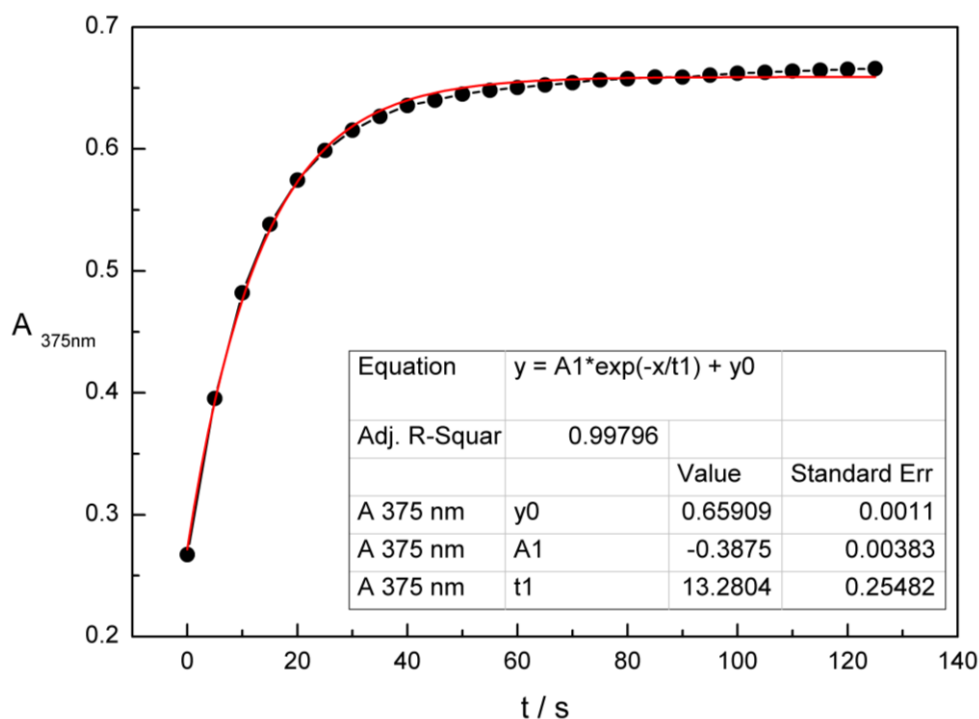


Figure S16. Thermal stability of the *cis* isomer of **41** measured 50 μ M in Tyrode's solution + 0.1% DMSO at 25 °C. Changes in the absorption at the indicated wavelength (λ_{\max} of the *trans* isomer) after irradiation with $\lambda = 400$ nm and subsequent thermal relaxation are represented as black dots. The red curve represents an exponential nonlinear curve fit.

4.5.5 Additional Photochemical Data

Table S1. Photochemical properties of photochromic histamine antagonist derivatives measured 50 μ M in DMSO at 25 °C. Cpd. = Compound.

Entry	Cpd.	λ_{max} <i>trans</i> isomer [nm]	λ_{max} <i>cis</i> isomer [nm]	Isosbestic points [nm]	λ_{irr} <i>trans</i> → <i>cis</i> [nm]	λ_{irr} <i>cis</i> → <i>trans</i> [nm]
1	6	327	435	274, 402	365	455
2	19	362	435	319, 423	365	455
3	20	363	413	319, 423	365	455
4	21	361	437	319, 422	365	455
5	29	303	-	279, 424	365	455
6	35	422	-	362, 560	420	(thermal)
7	41	389	-	337, 481	400 (420)	528

Table S2. Distribution of both isomers at their photostationary states [%]. Irradiation wavelengths indicated in brackets. Cpd. = Compound.

Entry	Cpd.	PSS distribution	THL ^(c)	Fatigue resistance
1	6	73% <i>cis</i> (365 nm), 75% <i>trans</i> (455 nm) ^(b)	53 h	excellent
2	19	84% <i>cis</i> (365 nm), 76% <i>trans</i> (455 nm) ^(a)	24 h	excellent
3	20	83% <i>cis</i> (365 nm), 75% <i>trans</i> (455 nm) ^(a)	26 h	excellent
4	21	84% <i>cis</i> (365 nm), 72% <i>trans</i> (455 nm) ^(a)	23 h	excellent
5	29	45% <i>cis</i> (365 nm), 80% <i>trans</i> (455 nm) ^(b)	29 h	excellent
6	35	n.d. <i>cis</i> (420 nm), 100% <i>trans</i> (thermal) ^(d)	7.2 s	excellent
7	41	83% <i>cis</i> (400 nm), 77% <i>trans</i> (528 nm) ^(a)	9.3 h	excellent

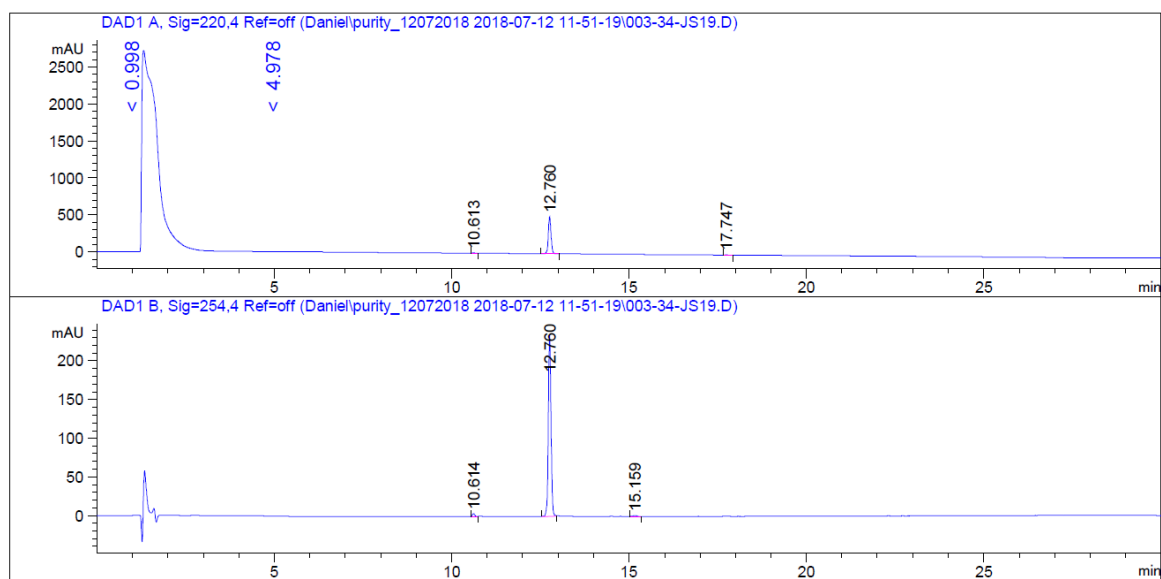
(a) Determination performed by NMR measurement of an irradiated sample. (b) Determination performed by analytical HPLC measurement of a 50 μ M solution in DMSO at the isosbestic point. (c) Thermal half-lives (THL) determined by UV-Vis absorption spectroscopy of a 50 μ M solution in DMSO at 25 °C upon irradiation with the indicated wavelength to accumulate a substantial amount of the *cis* isomer. (d) n.d.: not determined due to very fast thermal back relaxation.

Table S3. Photochemical properties of the photochromic histamine antagonist **41** measured 50 μ M in Tyrode's solution + 0.1% DMSO at 25 °C.

λ_{max} <i>trans</i> isomer [nm]	λ_{max} <i>cis</i> isomer [nm]	Isosbestic points [nm]	λ_{irr} <i>trans</i> → <i>cis</i> [nm]	λ_{irr} <i>cis</i> → <i>trans</i> [nm]	THL	Fatigue resistance
375	-	295, 498	400	528 / thermal	9.2 s	excellent

4.5.6 Analytical HPLC Traces for Purity Determination

Compound 6 (0.5 mM in DMSO, injection volume 1 µL)



t_R (*trans* isomer) = 12.8 min

Detection at 220 nm: 99%

Signal 1: DAD1 A, Sig=220,4 Ref=off

Peak #	RetTime [min]	Type	Width [min]	Area [mAU*s]	Height [mAU]	Area %
1	10.613	BB	0.0689	24.14172	5.53829	0.9237
2	12.760	VB R	0.0804	2578.88208	498.01480	98.6682
3	17.747	BB	0.0997	10.66732	1.64408	0.4081

Totals : 2613.69112 505.19717

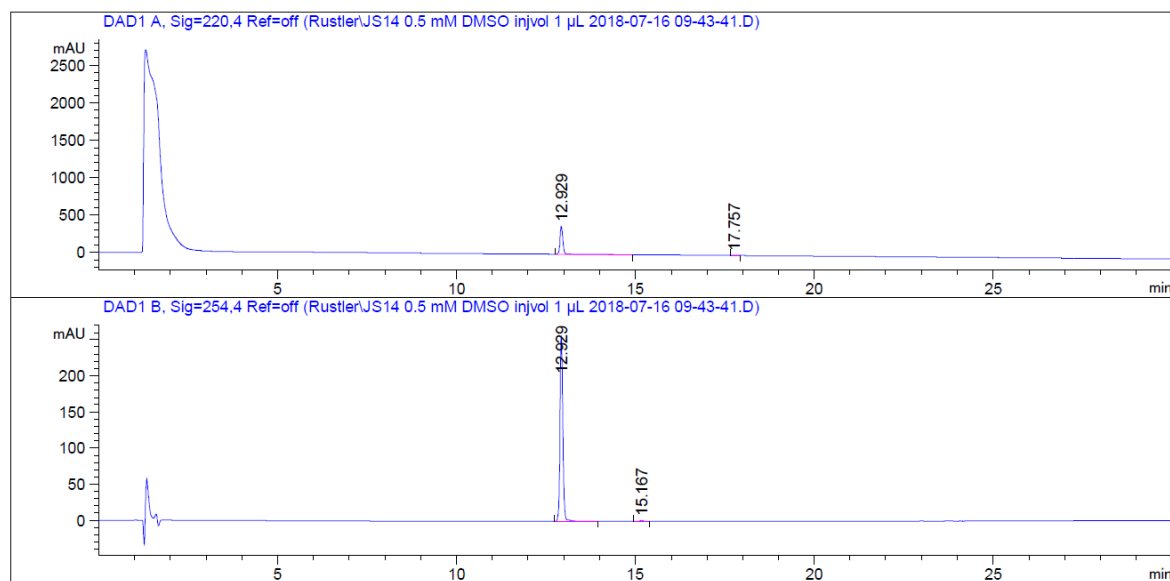
Detection at 254 nm: 98%

Signal 2: DAD1 B, Sig=254,4 Ref=off

Peak #	RetTime [min]	Type	Width [min]	Area [mAU*s]	Height [mAU]	Area %
1	10.614	BB	0.0705	17.90787	3.97915	1.4427
2	12.760	BB	0.0802	1214.00281	235.37601	97.8061
3	15.159	BB	0.1044	9.32406	1.38781	0.7512

Totals : 1241.23474 240.74297

Compound **19** (0.5 mM in DMSO, injection volume 1 μ L)



t_R (*trans* isomer) = 12.9 min

Detection at 220 nm: >99%

Signal 1: DAD1 A, Sig=220,4 Ref=off

Peak #	RetTime [min]	Type	Width [min]	Area [mAU*s]	Height [mAU]	Area %
1	12.929	BB	0.0857	2108.17432	374.33340	99.5515
2	17.757	BB	0.0958	9.49821	1.54383	0.4485

Totals : 2117.67253 375.87723

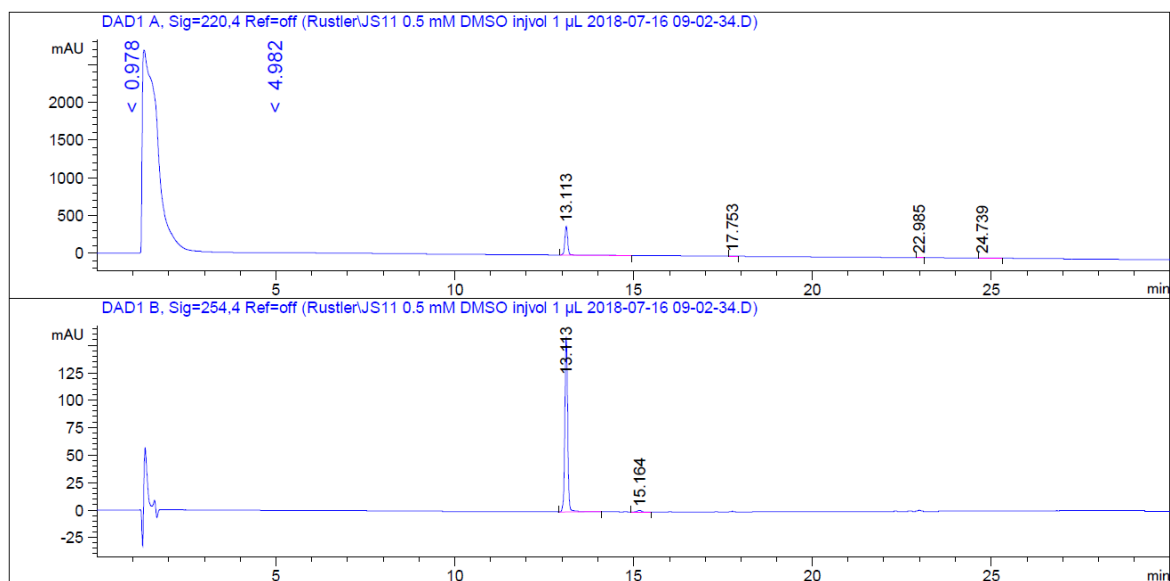
Detection at 254 nm: 99%

Signal 2: DAD1 B, Sig=254,4 Ref=off

Peak #	RetTime [min]	Type	Width [min]	Area [mAU*s]	Height [mAU]	Area %
1	12.929	BB	0.0854	1448.28516	258.41348	99.3013
2	15.167	BB	0.1071	10.19058	1.43006	0.6987

Totals : 1458.47574 259.84355

Compound **20** (0.5 mM in DMSO, injection volume 1 µL)



t_R (*trans* isomer) = 13.1 min

Detection at 220 nm: 99%

Signal 1: DAD1 A, Sig=220,4 Ref=off

Peak #	RetTime [min]	Type	Width [min]	Area [mAU*s]	Height [mAU]	Area %
1	13.113	BB	0.0868	2123.32861	382.43774	98.5309
2	17.753	BB	0.0955	9.22422	1.50546	0.4280
3	22.985	BB	0.0949	9.96733	1.64121	0.4625
4	24.739	BB	0.0983	12.46697	1.90547	0.5785

Totals : 2154.98714 387.48988

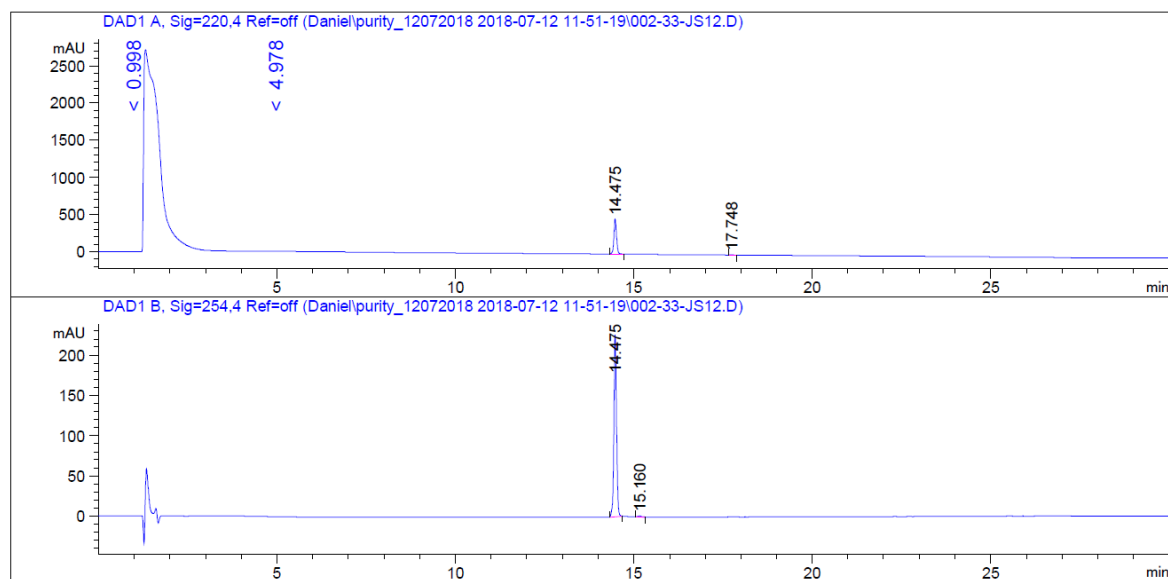
Detection at 254 nm: 99%

Signal 2: DAD1 B, Sig=254,4 Ref=off

Peak #	RetTime [min]	Type	Width [min]	Area [mAU*s]	Height [mAU]	Area %
1	13.113	BB	0.0865	882.88654	159.68443	98.8069
2	15.164	BB	0.1131	10.66132	1.42809	1.1931

Totals : 893.54785 161.11252

Compound **21** (0.5 mM in DMSO, injection volume 1 μ L)



t_R (*trans* isomer) = 14.5 min

Detection at 220 nm: >99%

Signal 1: DAD1 A, Sig=220,4 Ref=off

Peak #	RetTime [min]	Type	Width [min]	Area [mAU*s]	Height [mAU]	Area %
1	14.475	BB	0.0819	2513.17407	473.29953	99.5433
2	17.748	BB	0.1043	11.52987	1.63404	0.4567

Totals : 2524.70394 474.93357

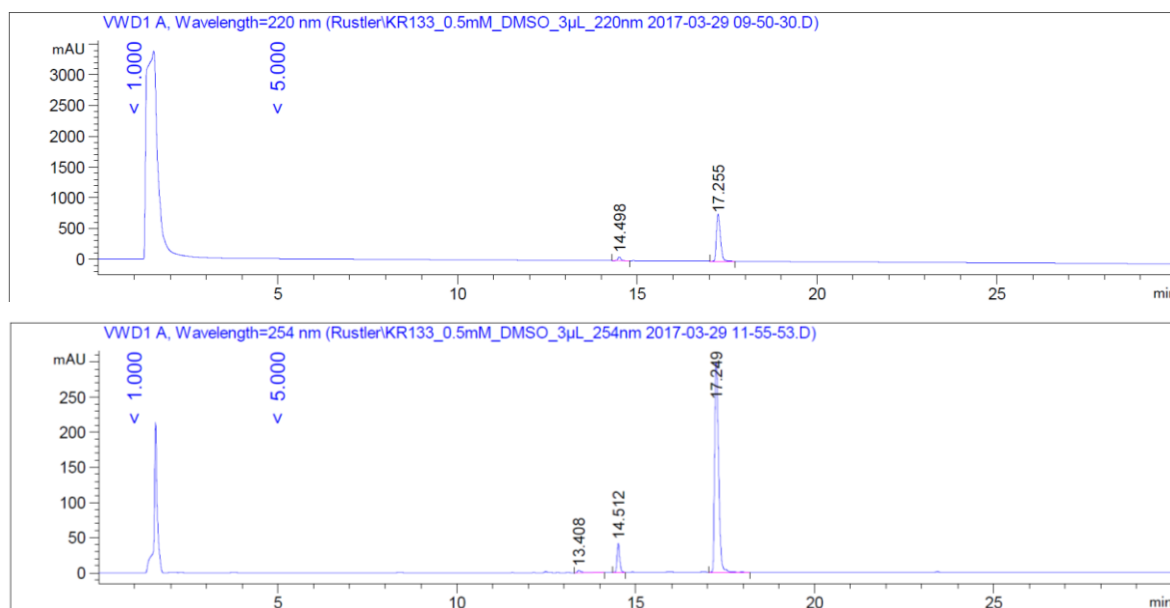
Detection at 254 nm: 99%

Signal 2: DAD1 B, Sig=254,4 Ref=off

Peak #	RetTime [min]	Type	Width [min]	Area [mAU*s]	Height [mAU]	Area %
1	14.475	BB	0.0817	1201.90039	227.16130	99.3126
2	15.160	BB	0.0973	8.31888	1.32455	0.6874

Totals : 1210.21927 228.48585

Compound **29** (0.5 mM in DMSO, injection volume 3 µL)



t_R (*trans* isomer) = 17.3 min; t_R (*cis* isomer) = 14.5 min (see HPLC PSS determination of **29** as proof for the retention time of the *cis* isomer)

Detection at 220 nm: >99% (95% *trans* isomer + 5% *cis* isomer)

Signal 1: VWD1 A, Wavelength=220 nm

Peak #	RetTime [min]	Type	Width [min]	Area [mAU*s]	Height [mAU]	Area %
1	14.498	BB	0.1026	338.33694	63.08164	5.3361
2	17.255	BB	0.1468	6002.17920	708.51471	94.6639

Totals : 6340.51614 771.59635

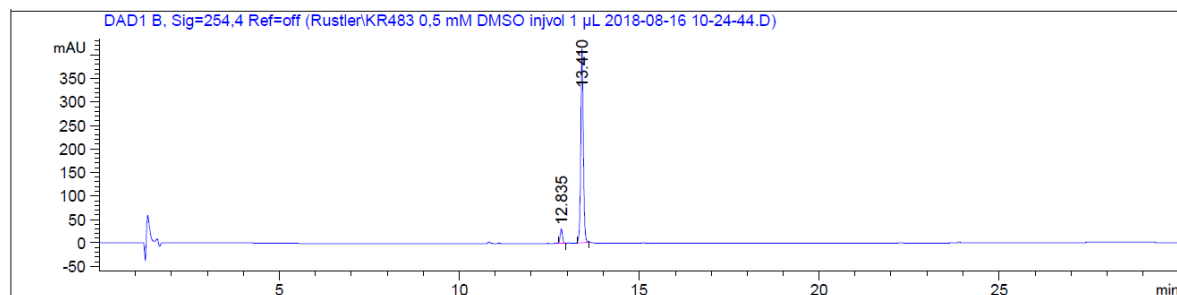
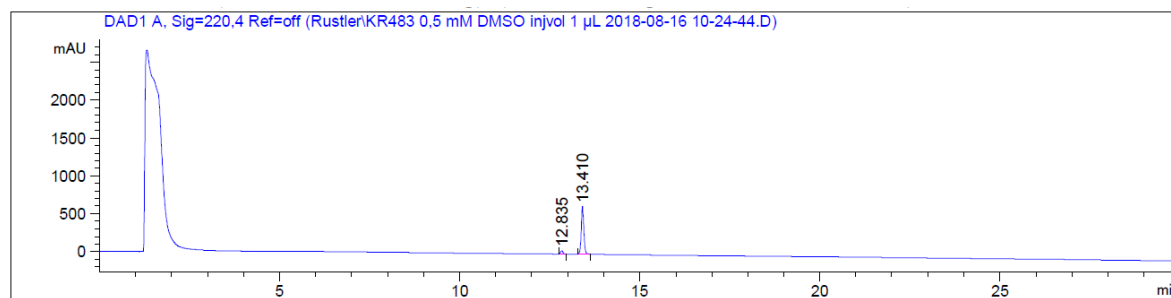
Detection at 254 nm: 99% (91% *trans* isomer + 8% *cis* isomer)

Signal 1: VWD1 A, Wavelength=254 nm

Peak #	RetTime [min]	Type	Width [min]	Area [mAU*s]	Height [mAU]	Area %
1	13.408	BV R	0.1195	27.08840	3.24091	1.0492
2	14.512	BB	0.0787	212.15456	41.42881	8.2175
3	17.249	BV R	0.1210	2342.50684	300.41037	90.7333

Totals : 2581.74979 345.08009

Compound **35** (0.5 mM in DMSO, injection volume 1 μ L)



t_R (*trans*-isomer) = 13.4 min

Detection at 220 nm: 94%

Signal 1: DAD1 A, Sig=220,4 Ref=off

Peak #	RetTime [min]	Type	Width [min]	Area [mAU*s]	Height [mAU]	Area %
1	12.835	BB	0.0710	199.54408	43.89084	5.7062
2	13.410	BB	0.0808	3297.44946	633.12482	94.2938

Totals : 3496.99355 677.01566

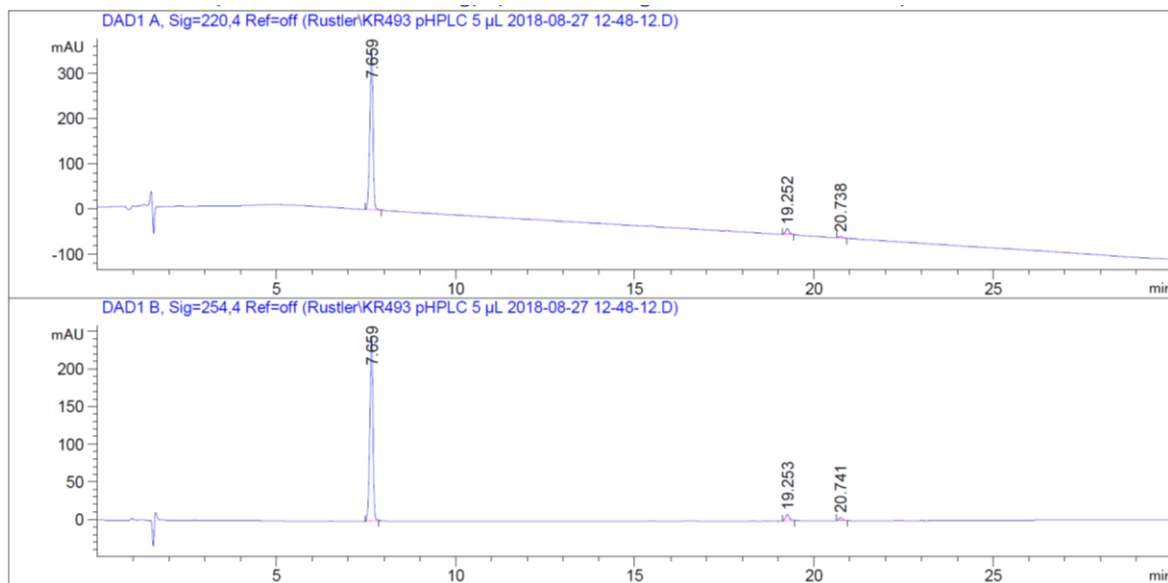
Detection at 254 nm: 94%

Signal 2: DAD1 B, Sig=254,4 Ref=off

Peak #	RetTime [min]	Type	Width [min]	Area [mAU*s]	Height [mAU]	Area %
1	12.835	BB	0.0709	137.41704	30.31804	6.0261
2	13.410	BB	0.0806	2142.93384	412.41296	93.9739

Totals : 2280.35088 442.73100

Compound **41** (50 μ M in MeCN/water, injection volume 5 μ L)



t_R (*trans* isomer) = 7.7 min.

Detection at 220 nm: 95%

Signal 1: DAD1 A, Sig=220,4 Ref=off

Peak #	RetTime [min]	Type	Width [min]	Area [mAU*s]	Height [mAU]	Area %
1	7.659	BB	0.0898	2133.59351	356.48981	95.1043
2	19.252	BB	0.1077	89.39891	12.45517	3.9849
3	20.738	BB	0.1036	20.43336	3.07134	0.9108

Totals : 2243.42578 372.01632

Detection at 254 nm: 95%

Signal 2: DAD1 B, Sig=254,4 Ref=off

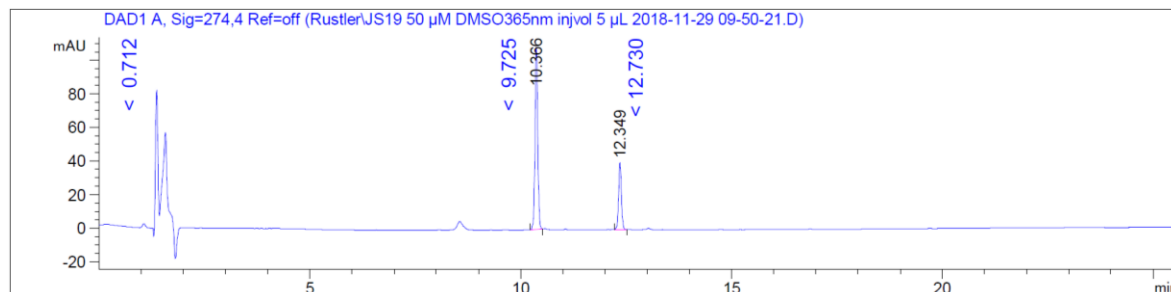
Peak #	RetTime [min]	Type	Width [min]	Area [mAU*s]	Height [mAU]	Area %
1	7.659	BB	0.0895	1469.05542	246.49878	94.5651
2	19.253	BB	0.1082	58.09341	8.05054	3.7396
3	20.741	BB	0.1058	26.33635	3.84993	1.6953

Totals : 1553.48518 258.39924

4.5.7 Analytical HPLC Traces for PSS Determination

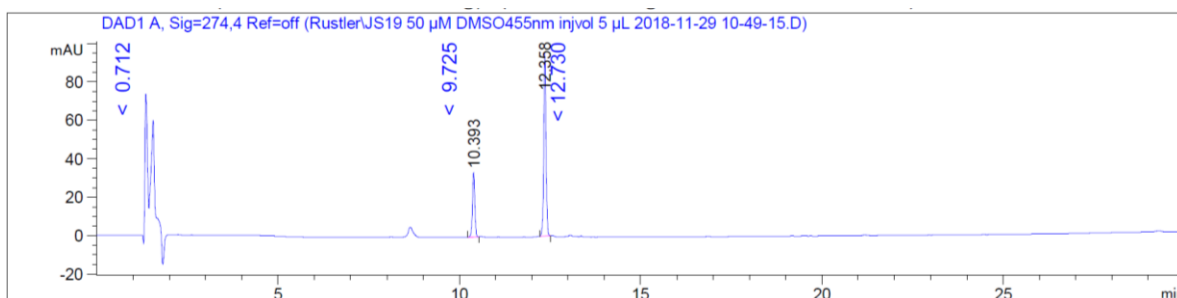
Compound **6** (50 μ M in DMSO, injection volume 5 μ L)

cis-PSS (irradiation with $\lambda = 365$ nm)



cis isomer: $t_R = 10.4$ min (73%); *trans* isomer: $t_R = 12.3$ min (27%)

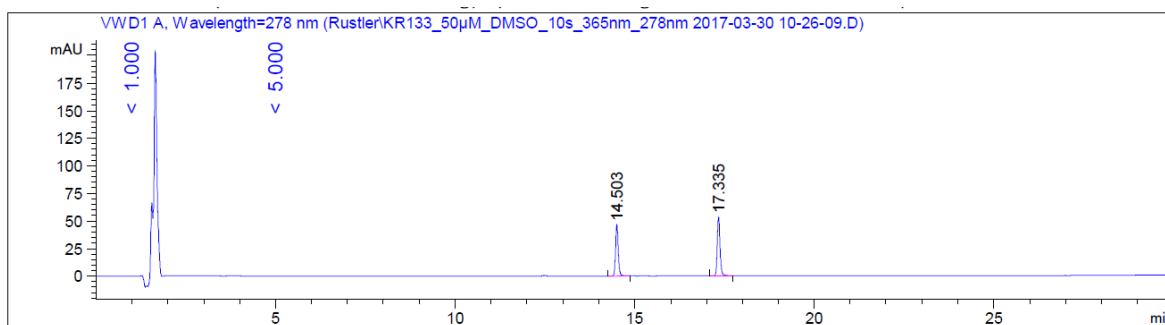
trans-PSS (irradiation with $\lambda = 455$ nm)



cis isomer: $t_R = 10.4$ min (25%); *trans* isomer: $t_R = 12.4$ min (75%)

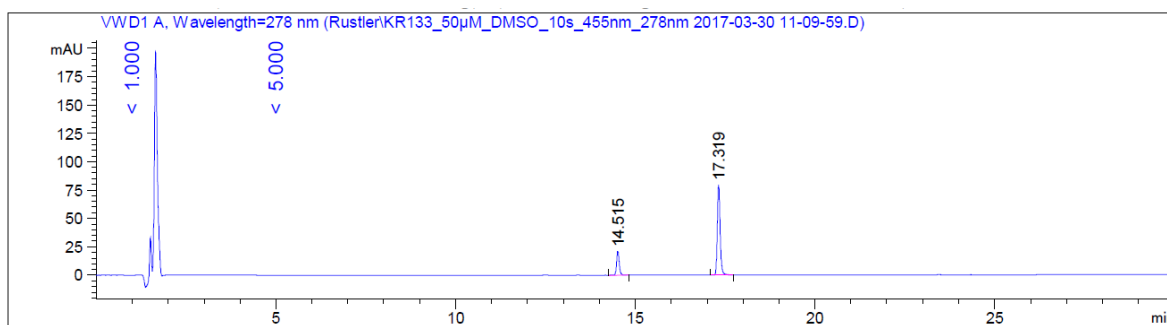
Compound **29** (50 μ M in DMSO, injection volume 5 μ L)

cis-PSS (irradiation with λ = 365 nm)



cis isomer: t_R = 14.5 min (45%); *trans* isomer: t_R = 17.3 min (55%)

trans-PSS (irradiation with λ = 455 nm)



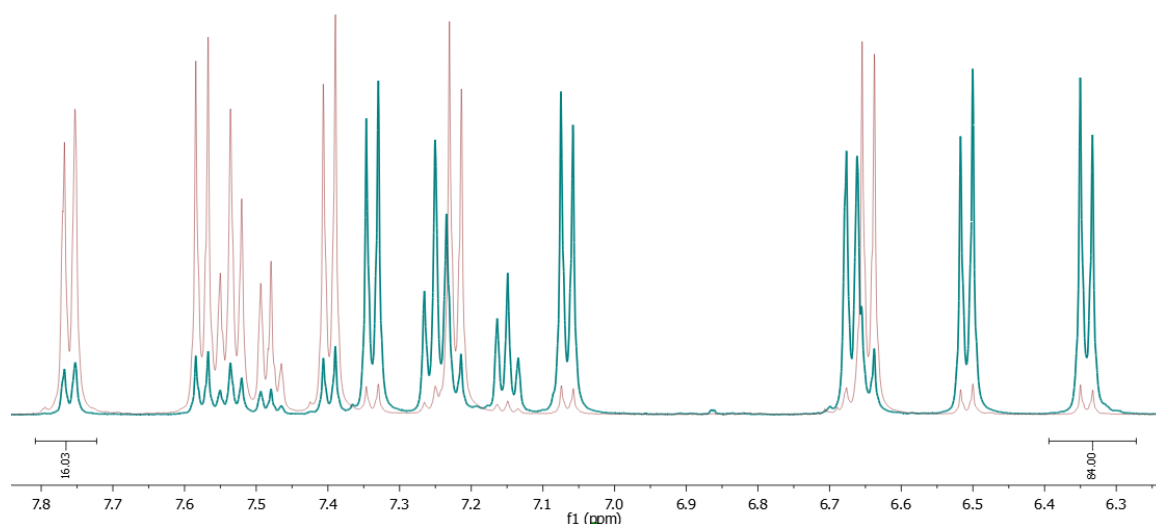
cis isomer: t_R = 14.5 min (20%); *trans* isomer: t_R = 17.3 min (80%)

4.5.8 PSS Determination *via* NMR

Compound **19** (DMSO- d_6)

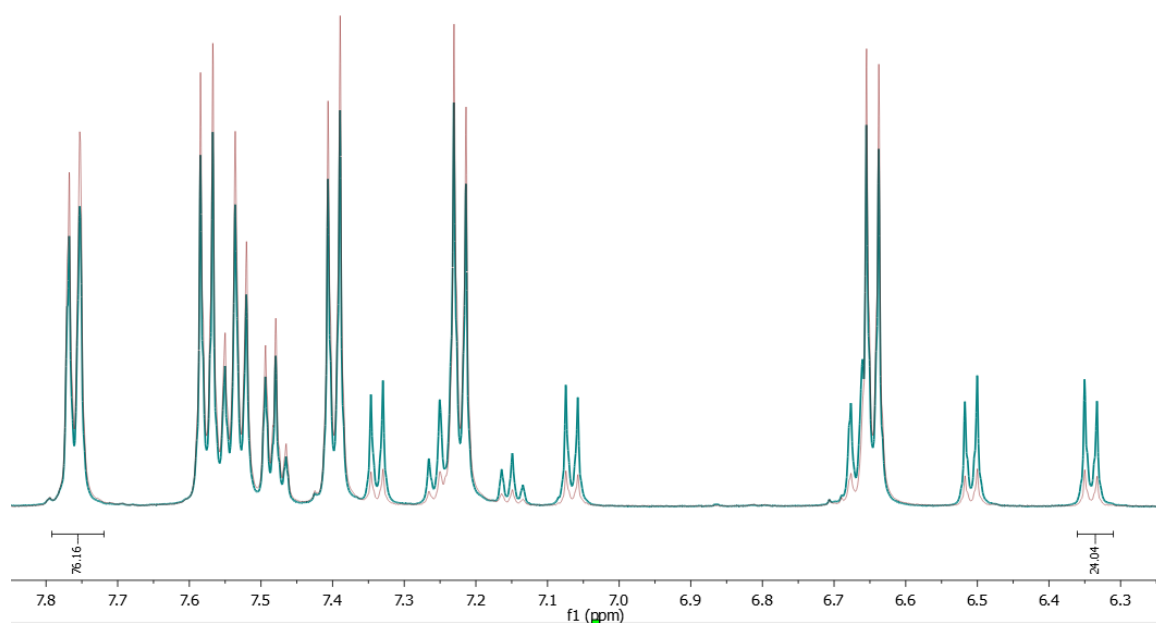
cis-PSS (irradiation with $\lambda = 365$ nm)

red spectrum = thermal equilibrium; blue spectrum = *cis*-PSS (84% *cis*)



trans-PSS (irradiation with $\lambda = 455$ nm)

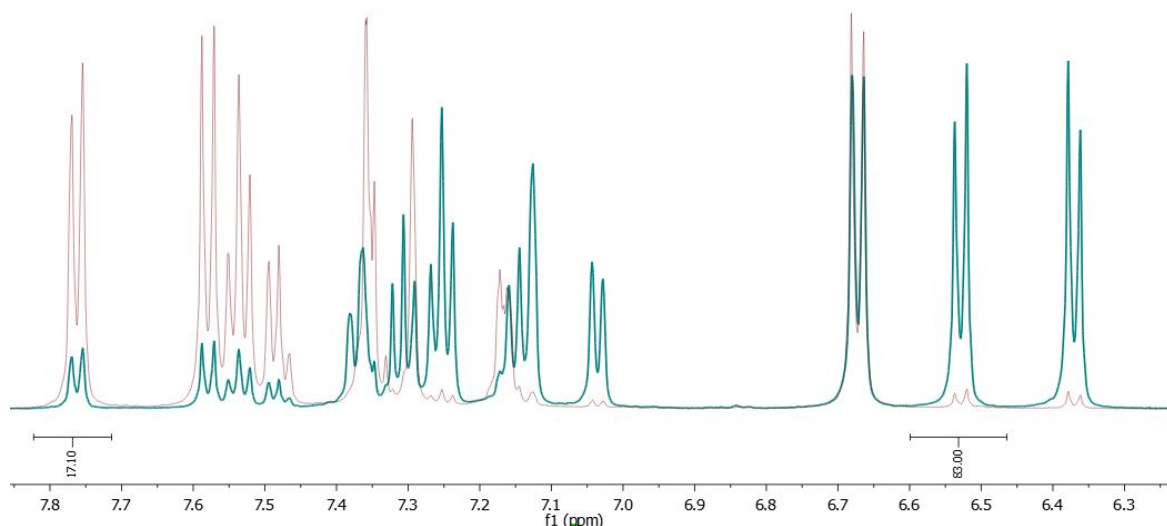
red spectrum = thermal equilibrium; blue spectrum = *trans*-PSS (76% *trans*)



Compound **20** (DMSO-*d*₆)

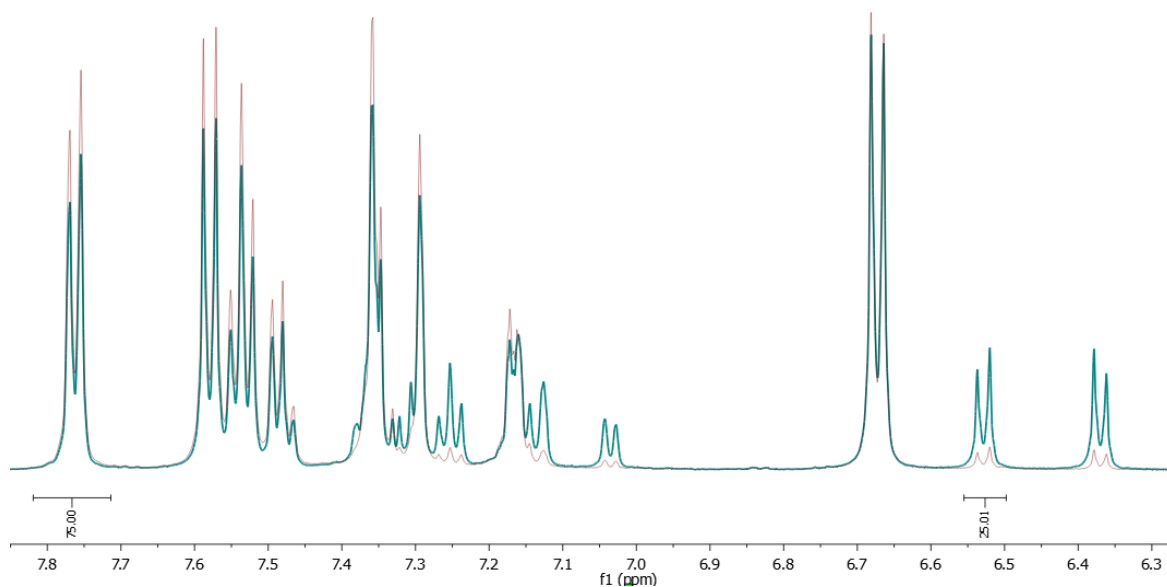
cis-PSS (irradiation with $\lambda = 365$ nm)

red spectrum = thermal equilibrium; blue spectrum = *cis*-PSS (83% *cis*)



trans-PSS (irradiation with $\lambda = 455$ nm)

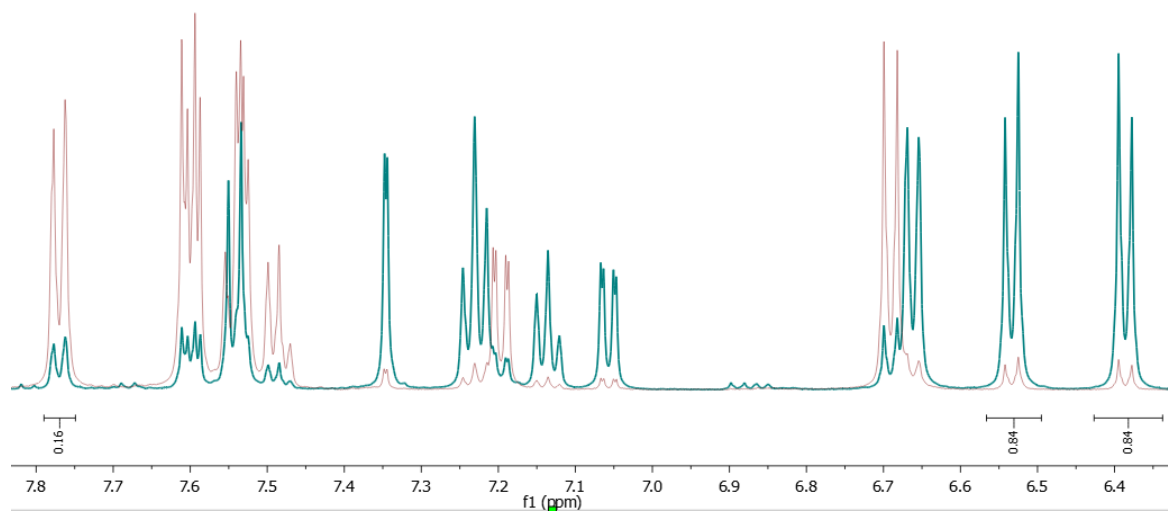
red spectrum = thermal equilibrium; blue spectrum = *trans*-PSS (75% *trans*)



Compound **21** (DMSO- d_6)

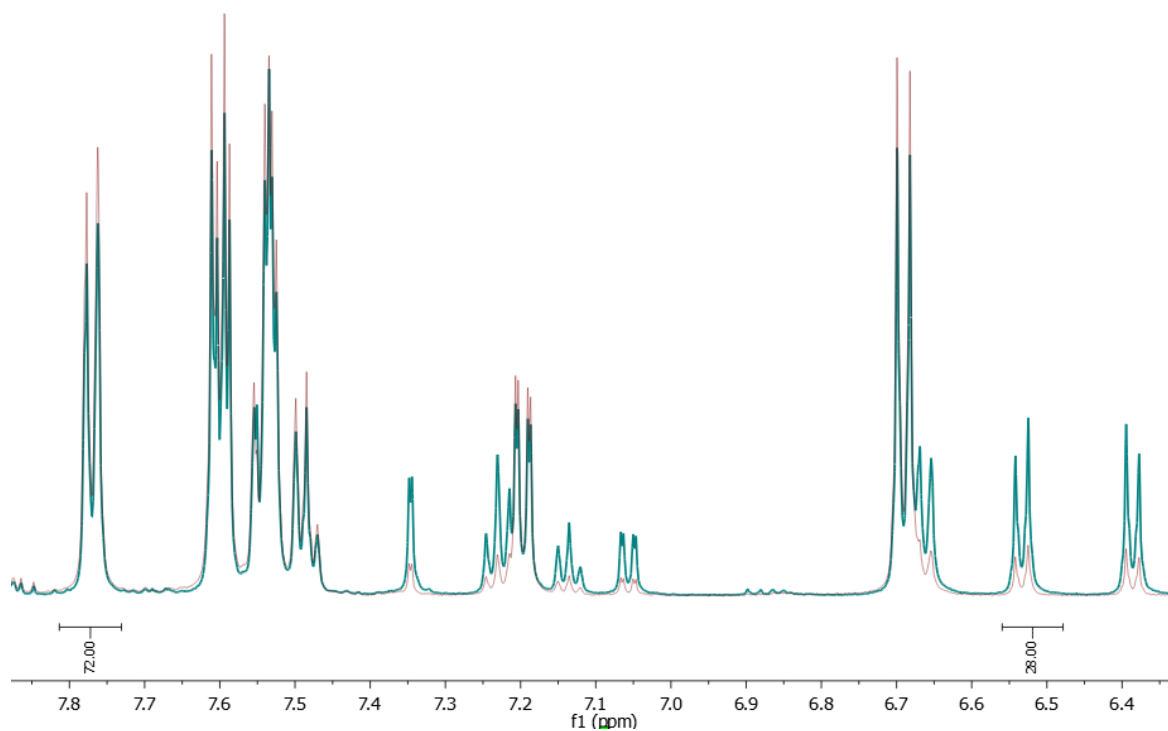
cis-PSS (irradiation with $\lambda = 365$ nm)

red spectrum = thermal equilibrium; blue spectrum = *cis*-PSS (84% *cis*)



trans-PSS (irradiation with $\lambda = 455$ nm)

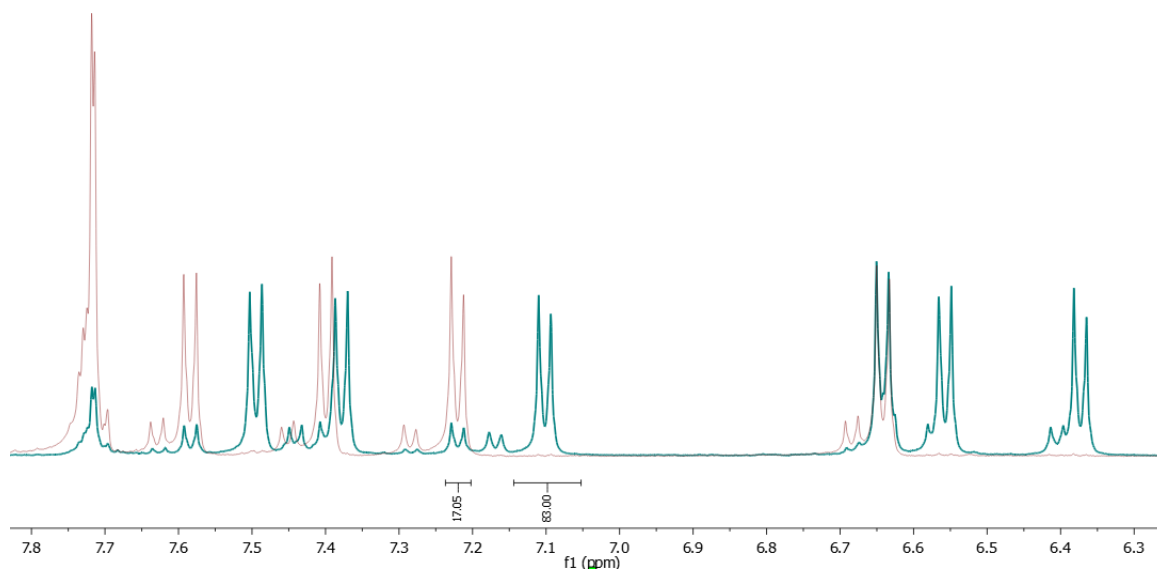
red spectrum = thermal equilibrium; blue spectrum = *trans*-PSS (72% *trans*)



Compound **41** (DMSO-*d*₆)

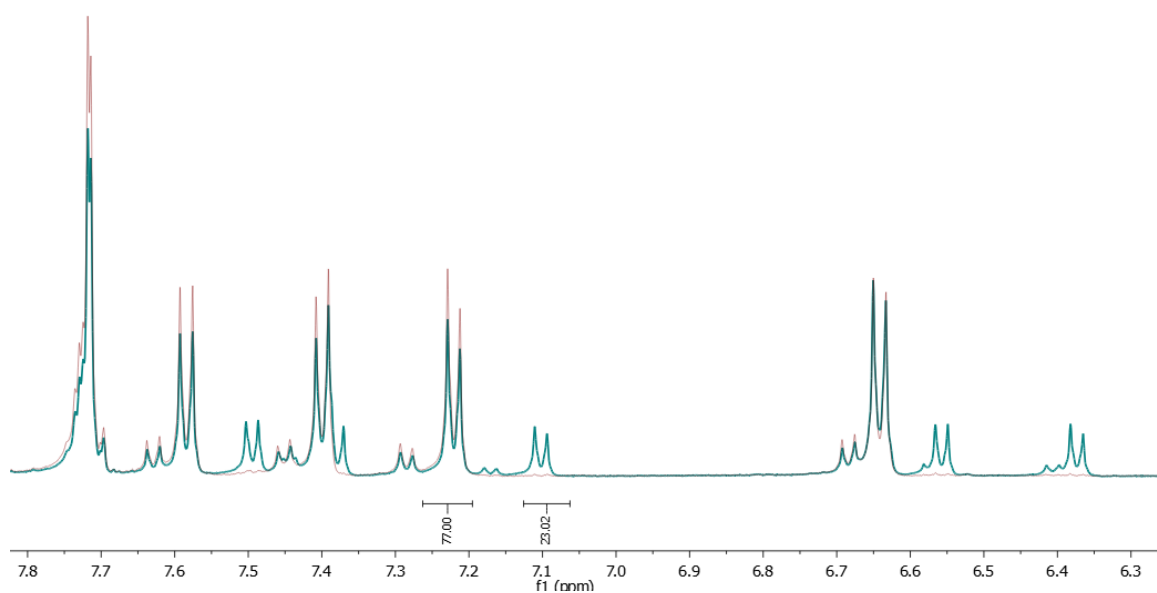
cis-PSS (irradiation with $\lambda = 410$ nm)

red spectrum = thermal equilibrium; blue spectrum = *cis*-PSS (83% *cis*)



trans-PSS (irradiation with $\lambda = 530$ nm)

red spectrum = thermal equilibrium; blue spectrum = *trans*-PSS (77% *trans*)



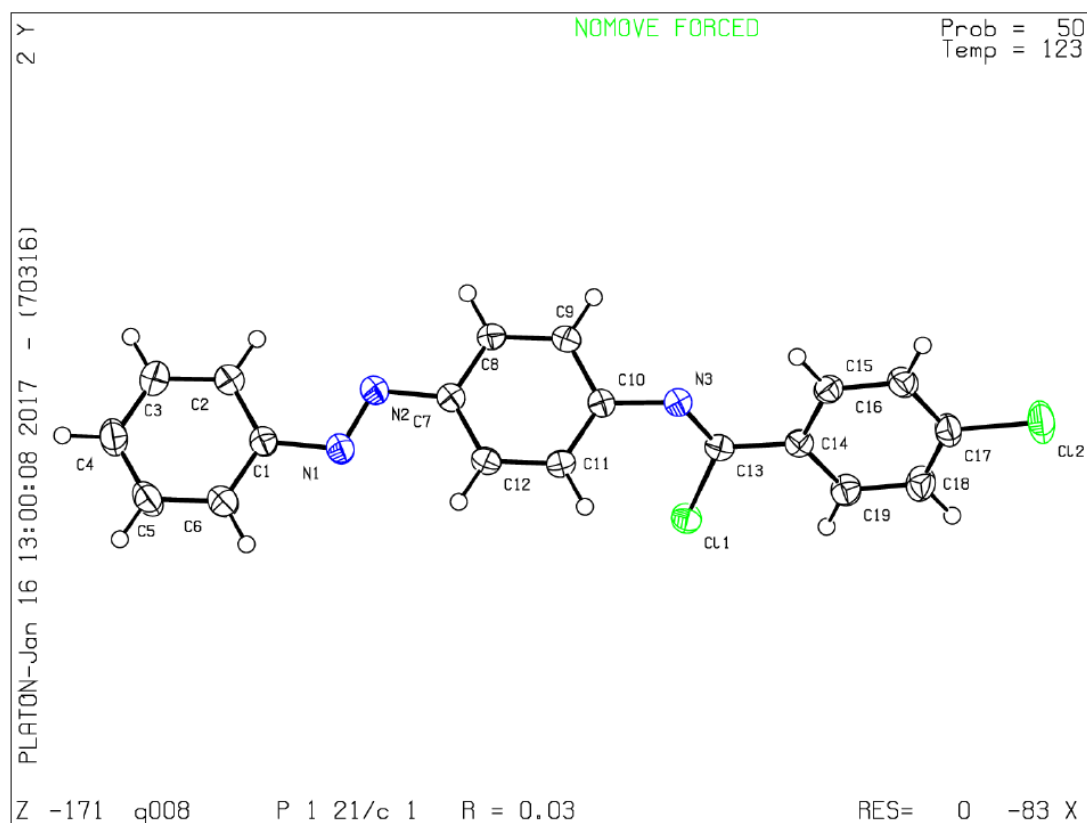
4.5.9 Single Crystal X-ray Crystallography

Compound 16

Experimental. Single clear light orange plate-shaped crystals of **16** were obtained by recrystallisation from CH_2Cl_2 . A suitable crystal ($0.22 \times 0.11 \times 0.05$) mm^3 was selected and mounted on a MITIGEN holder with inert oil on a GV 50, TitanS2 diffractometer. The crystal was kept at $T = 123$ K during data collection. Using Olex2^[59] the structure was solved with the ShelXT^[60] structure solution program, using the Intrinsic Phasing solution method. The model was refined with version 2016/6 of ShelXL^[61] using Least Squares minimization.

Crystal Data. $\text{C}_{19}\text{H}_{13}\text{Cl}_2\text{N}_3$, $M_r = 354.22$, monoclinic, $P2_1/c$ (No. 14), $a = 19.0964(7)$ Å, $b = 15.2454(4)$ Å, $c = 5.7013(2)$ Å, $\alpha = 90.0^\circ$, $\beta = 94.416(3)^\circ$, $\gamma = 90.0^\circ$, $V = 1654.91(9)$ Å³, $T = 123$ K, $Z = 4$, $Z' = 1$, $\mu(\text{CuK}\alpha) = 3.557$, 19628 reflections measured, 3290 unique ($R_{\text{int}} = 0.0605$) which were used in all calculations. The final wR_2 was 0.0859 (all data) and R_1 was 0.0328 ($I > 2(I)$).

Cambridge Structural Database CCDC. 1873233



Detailed Crystal Data.

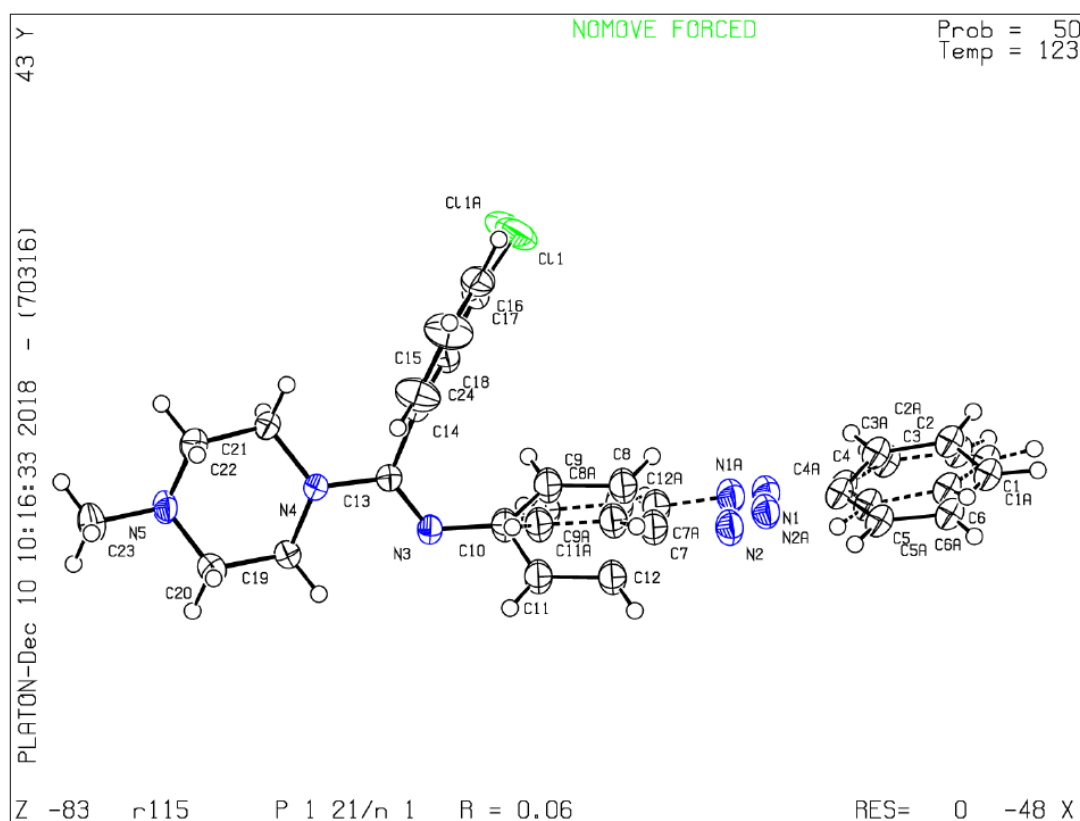
Formula	C ₁₉ H ₁₃ Cl ₂ N ₃
$D_{calc.}/\text{g cm}^{-3}$	1.422
μ/mm^{-1}	3.557
Formula Weight	354.22
Colour	clear light orange
Shape	plate
Size/ mm^3	0.22×0.11×0.05
T/K	123
Crystal System	monoclinic
Space Group	P2 ₁ /c
$a/\text{\AA}$	19.0964(7)
$b/\text{\AA}$	15.2454(4)
$c/\text{\AA}$	5.7013(2)
$\alpha/^\circ$	90.0
$\beta/^\circ$	94.416(3)
$\gamma/^\circ$	90.0
$V/\text{\AA}^3$	1654.91(9)
Z	4
Z'	1
Wavelength/ \AA	1.54184
Radiation type	CuK α
$\theta_{min}/^\circ$	3.714
$\theta_{max}/^\circ$	73.771
Measured Refl.	19628
Independent Refl.	3290
Reflections Used	2869
R_{int}	0.0605
Parameters	217
Restraints	0
Largest Peak	0.230
Deepest Hole	-0.200
GooF	1.049
wR_2 (all data)	0.0859
wR_2	0.0808
R_1 (all data)	0.0394
R_1	0.0328

Compound **19**

Experimental. Single clear orange prism-shaped crystals of **19** were obtained by recrystallisation from acetone. A suitable crystal $0.21 \times 0.14 \times 0.08 \text{ mm}^3$ was selected and mounted on a MITIGEN holder oil on a SuperNova, Single source at offset/far, Atlas diffractometer. The crystal was kept at a steady $T = 123.01(10) \text{ K}$ during data collection. The structure was solved with the ShelXT^[60] structure solution program using the Intrinsic Phasing solution method and by using Olex2^[59] as the graphical interface. The model was refined with version 2016/6 of ShelXL^[61] using Least Squares minimisation.

Crystal Data. $\text{C}_{24}\text{H}_{24}\text{ClN}_5$, $M_r = 417.93$, monoclinic, $P2_1/n$ (No. 14), $a = 12.7354(2) \text{ \AA}$, $b = 13.1621(2) \text{ \AA}$, $c = 13.0567(2) \text{ \AA}$, $\beta = 92.9670(10)^\circ$, $\alpha = \gamma = 90^\circ$, $V = 2185.69(6) \text{ \AA}^3$, $T = 123.01(10) \text{ K}$, $Z = 4$, $Z' = 1$, $\mu(\text{CuK}\alpha) = 1.698$, 24506 reflections measured, 4391 unique ($R_{\text{int}} = 0.0336$) which were used in all calculations. The final wR_2 was 0.1488 (all data) and R_1 was 0.0645 ($I > 2(I)$).

Cambridge Structural Database CCDC. 1884361



Detailed Crystal Data.

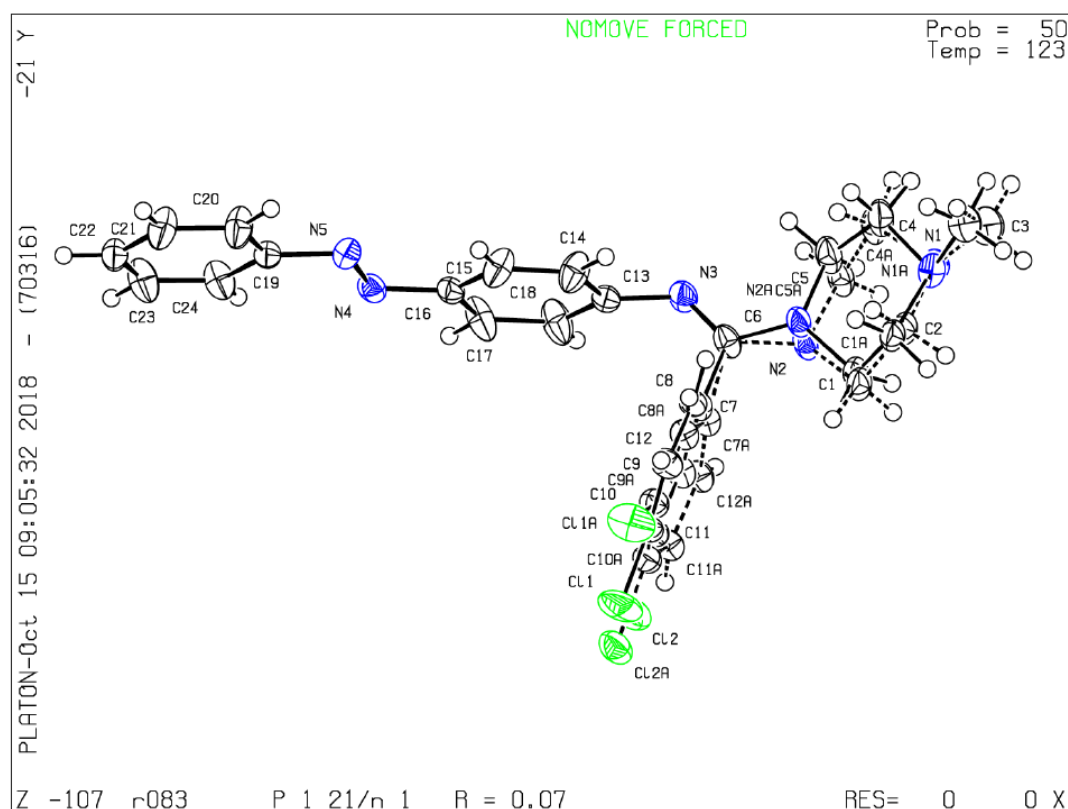
Formula	C ₂₄ H ₂₄ ClN ₅
$D_{calc.}/\text{g cm}^{-3}$	1.270
μ/mm^{-1}	1.698
Formula Weight	417.93
Colour	clear orange
Shape	prism
Size/mm ³	0.21×0.14×0.08
T/K	123.01(10)
Crystal System	monoclinic
Space Group	$P2_1/n$
$a/\text{\AA}$	12.7354(2)
$b/\text{\AA}$	13.1621(2)
$c/\text{\AA}$	13.0567(2)
$\alpha/^\circ$	90
$\beta/^\circ$	92.9670(10)
$\gamma/^\circ$	90
$V/\text{\AA}^3$	2185.69(6)
Z	4
Z'	1
Wavelength/ \AA	1.54184
Radiation type	CuK α
$\theta_{min}/^\circ$	4.730
$\theta_{max}/^\circ$	73.866
Measured Refl.	24506
Independent Refl.	4391
Reflections with $I > 2(I)$	3914
R_{int}	0.0336
Parameters	405
Restraints	384
Largest Peak	0.561
Deepest Hole	-0.355
GooF	1.027
wR_2 (all data)	0.1488
wR_2	0.1443
R_1 (all data)	0.0708
R_1	0.0645

Compound **21**

Experimental. Single clear yellow plate-shaped crystals of **21** were obtained by recrystallisation from acetone. A suitable crystal (0.44×0.23×0.07) mm³ was selected and mounted on a MITIGEN holder with inert oil on a SuperNova, Single source at offset/far, Atlas diffractometer. The crystal was kept at $T = 123$ K during data collection. Using Olex2,^[59] the structure was solved with the ShelXT^[60] structure solution program, using the Intrinsic Phasing solution method. The model was refined with version 2016/6 of ShelXL^[61] using Least Squares minimisation.

Crystal Data. C₂₄H₂₃Cl₂N₅, $M_r = 452.37$, monoclinic, P2₁/n (No. 14), $a = 9.9891(3)$ Å, $b = 20.9542(8)$ Å, $c = 10.8578(4)$ Å, $\beta = 91.030(3)^\circ$, $\alpha = \gamma = 90^\circ$, $V = 2272.32(14)$ Å³, $T = 123.00(10)$ K, $Z = 4$, $Z' = 1$, $\mu(\text{CuK}\alpha) = 2.732$, 14444 reflections measured, 4685 unique ($R_{\text{int}} = 0.0484$) which were used in all calculations. The final wR_2 was 0.1307 (all data) and R_1 was 0.0651 ($I > 2(I)$).

Cambridge Structural Database CCDC. 1873486



Detailed Crystal Data.

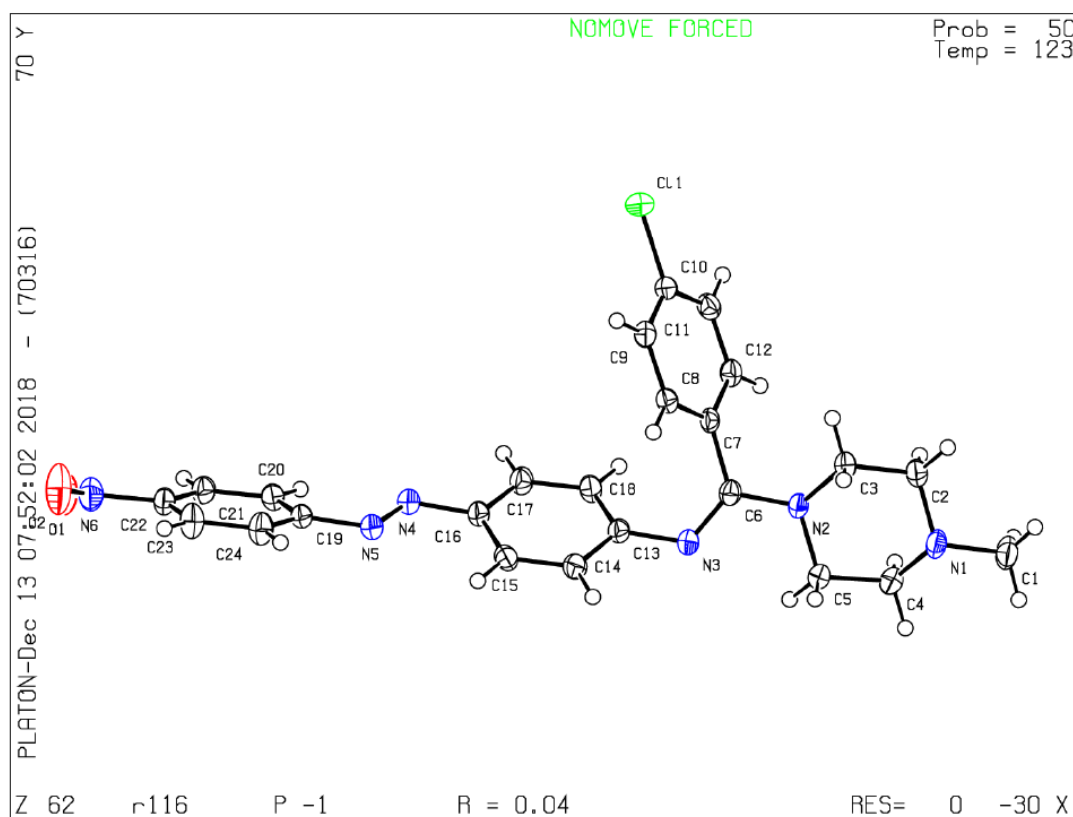
Formula	C ₂₄ H ₂₃ Cl ₂ N ₅
$D_{calc.}/\text{g cm}^{-3}$	1.322
μ/mm^{-1}	2.732
Formula Weight	452.37
Colour	clear yellow
Shape	plate
Max Size/mm	0.44
Mid Size/mm	0.23
Min Size/mm	0.07
T/K	123.00(10)
Crystal System	monoclinic
Space Group	P2 ₁ /n
$a/\text{\AA}$	9.9891(3)
$b/\text{\AA}$	20.9542(8)
$c/\text{\AA}$	10.8578(4)
$\alpha/^\circ$	90
$\beta/^\circ$	91.030(3)
$\gamma/^\circ$	90
$V/\text{\AA}^3$	2272.32(14)
Z	4
Z'	1
$\theta_{min}/^\circ$	4.220
$\theta_{max}/^\circ$	76.537
Measured Refl.	14444
Independent Refl.	4685
Reflections Used	4108
R_{int}	0.0484
Parameters	407
Restraints	240
Largest Peak	0.420
Deepest Hole	-0.513
GooF	1.172
wR_2 (all data)	0.1307
wR_2	0.1263
R_1 (all data)	0.0738
R_1	0.0651

Compound **35**

Experimental. Single clear red plate-shaped crystals of **35** were obtained by recrystallisation from acetone. A suitable crystal $0.24 \times 0.19 \times 0.08$ mm³ was selected and mounted on a MITIGEN holder oil on a SuperNova, Single source at offset/far, Atlas diffractometer. The crystal was kept at a steady $T = 123.01(10)$ K during data collection. The structure was solved with the ShelXT^[60] structure solution program using the dual solution method and by using Olex2^[59] as the graphical interface. The model was refined with version 2016/6 of ShelXL^[61] using Least Squares minimisation.

Crystal Data. C₂₄H₂₃ClN₆O₂, $M_r = 462.93$, triclinic, $P-1$ (No. 2), $a = 9.6038(3)$ Å, $b = 10.8828(3)$ Å, $c = 11.6639(3)$ Å, $\alpha = 93.930(2)^\circ$, $\beta = 105.063(3)^\circ$, $\gamma = 102.321(3)^\circ$, $V = 1140.09(6)$ Å³, $T = 123.01(10)$ K, $Z = 2$, $Z' = 1$, $\mu(\text{CuK}\alpha) = 1.765$, 24274 reflections measured, 4559 unique ($R_{\text{int}} = 0.0439$) which were used in all calculations. The final wR_2 was 0.1088 (all data) and R_1 was 0.0379 ($I > 2(I)$).

Cambridge Structural Database CCDC. 1884855



Detailed Crystal Data.

Formula	C ₂₄ H ₂₃ ClN ₆ O ₂
$D_{calc.}/\text{g cm}^{-3}$	1.349
μ/mm^{-1}	1.765
Formula Weight	462.93
Colour	clear red
Shape	plate
Size/mm ³	0.24×0.19×0.08
T/K	123.01(10)
Crystal System	triclinic
Space Group	<i>P</i> -1
$a/\text{\AA}$	9.6038(3)
$b/\text{\AA}$	10.8828(3)
$c/\text{\AA}$	11.6639(3)
$\alpha/^\circ$	93.930(2)
$\beta/^\circ$	105.063(3)
$\gamma/^\circ$	102.321(3)
$V/\text{\AA}^3$	1140.09(6)
Z	2
Z'	1
Wavelength/ \AA	1.54184
Radiation type	CuK α
$\theta_{min}/^\circ$	3.959
$\theta_{max}/^\circ$	74.052
Measured Refl.	24274
Independent Refl.	4559
Reflections with $I > 2(I)$	4064
R_{int}	0.0439
Parameters	299
Restraints	0
Largest Peak	0.256
Deepest Hole	-0.341
Goof	1.042
wR_2 (all data)	0.1088
wR_2	0.1036
R_1 (all data)	0.0431
R_1	0.0379

4.5.10 Additional Pharmacological Data

Table S3. Pharmacological data of compounds **19** and **21** at the guinea pig ileum (gpH₁R) with varying preincubation time (15 min and 30 s). Cpd. = Compound.

Cpd.	pA ₂ ± SEM ^(a) (gp-ileum) <i>trans</i> isomer ^(b) (15 min incubation)	N ^(c)	pA ₂ ± SEM ^(a) (gp-ileum) <i>trans</i> isomer ^(b) (30 min incubation)	N ^(c)
19	5.31 ± 0.10	16/(52)	5.27 ± 0.12	6/(9)
21	4.88 ± 0.04	3/(23)	4.84 ± 0.09	4/(9)

(a) Data represent mean values ± SEM (standard error of mean) from *N* experiments. Data were analysed by nonlinear regression and were best fitted to sigmoidal concentration-response curves. pA₂: $-\log c(\text{Ant}) + \log(r-1)$; where $r = 10^{\Delta \text{pEC}_{50}}$; ΔpEC_{50} was calculated from pEC₅₀ of histamine and pEC₅₀ of histamine in presence of the respective antagonist. n.a. = not active. (b) The *trans* isomer was tested in its thermal equilibrium. (c) N* represents the number of experiments in “X/(X+Y)”. Experiments were carried out in presence of the respective antagonist at a concentration range from 10^{-7.5} – 10⁻⁴. “X” represents experiments in which an effect - rightward-shift of the histamine concentration-response-curve (CRC) - could be measured. “Y” represents experiments in which no rightward-shifted histamine CRCs could be measured (especially for weak antagonists at lower concentrations).

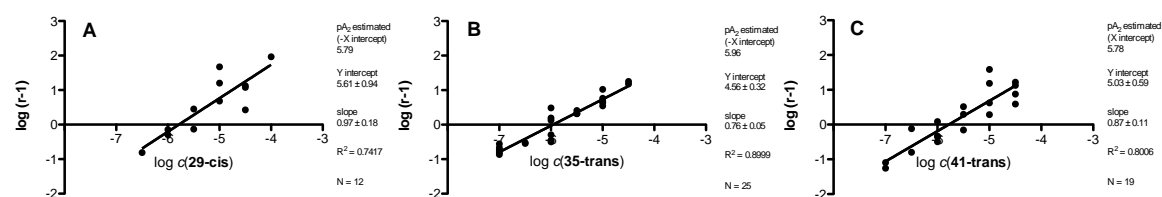
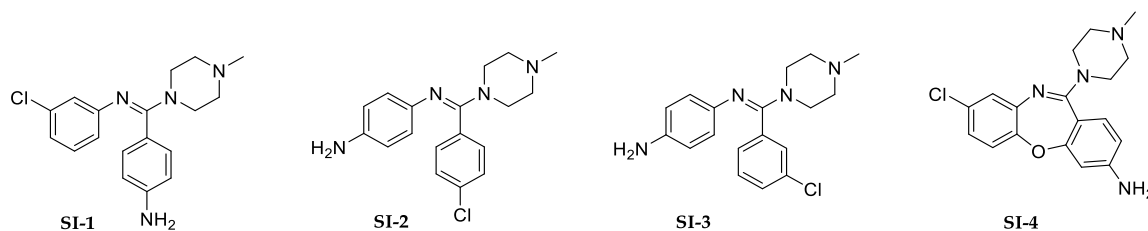


Figure S17. Schild plots for **29-cis** (A), **35-trans** (B), and **41-trans** (C) of experiments on the guinea pig ileum (gpH₁R).

4.5.11 Additional Chemical Structures



Scheme S1. Chemical structures of the reference substances.^[5,45]

4.6 References

- [1] M. Jutel, K. Blaser, C. A. Akdis, *J. Investig. Allergol. Clin. Immunol.* **2005**, 15, 1-8.
- [2] P. R. Criado, R. F. Criado, C. W. Maruta, Cd. M. Filho, *An. Bras. Dermatol.* **2010**, 85, 195-210.
- [3] L. Maint, N. Novak, *Am. J. Clin. Nutr.* **2007**, 85, 1185-1196.
- [4] R. L. Thurmond, E. W. Gelfand, P. J. Dunford, *Nat. Rev. Drug Discov.* **2008**, 7, 41-53.
- [5] F. Naporra, S. Gobleder, H.-J. Wittmann, J. Spindler, M. Bodensteiner, G. Bernhardt, H. Hübner, P. Gmeiner, S. Elz, A. Strasser, *Pharmacological Research* **2016**, 113, 610-625.
- [6] B. Jassal, S. Jupe, M. Caudy, E. Birney, L. Stein, H. Hermjakob, P. D'Eustachio, *Database (Oxford)*, **2010**, baq018.
- [7] A. S. Ash, H. O. Schild, *Br. J. Pharmacol. Chemother.* **1966**, 27, 427-439.
- [8] J. P. Overington, B. Al-Lazikani, A. L. Hopkins, *Nat. Rev. Drug Discov.* **2006**, 5, 993-996.
- [9] E. Jacoby, R. Bouhelal, M. Gerspacher, K. Seuwen, *ChemMedChem* **2006**, 1, 760-782.
- [10] A. Sharma, B. A. Hamelin, *Current Drug Metabolism* **2003**, 4, 105-129.
- [11] S. J. Hill, *Pharmacol. Rev.* **1990**, 42, 45-83.
- [12] A. del Cuvillo, J. Mullol, J. Bartra, I. Dávila, I. Jáuregui, J. Montoro, J. Sastre, A. L. Valero, *J. Investig. Allergol. Clin. Immunol.* **2006**, 16, 3-12.
- [13] S. J. Hill, C. R. Ganellin, H. Timmerman, J. C. Schwartz, N. P. Shankley, J. M. Young, W. Schunack, R. Levi, H. L. Haas, *Pharmacol. Rev.* **1997**, 49, 253-278.
- [14] J. Levitz, J. Broichhagen, P. Leippe, D. Konrad, D. Trauner, E. Y. Isacoff, *PNAS* **2017**, 114, E3546-E3554.

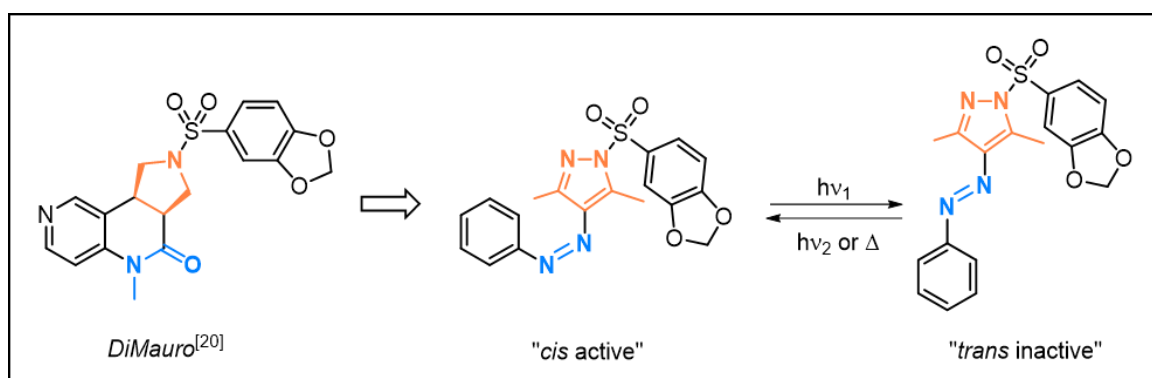
- [15] J. Broichhagen, A. Damijonaitis, J. Levitz, K. R. Sokol, P. Leippe, D. Konrad, E. Y. Isacoff, D. Trauner, *ACS Cent. Sci.* **2015**, *1*, 383-393.
- [16] N. J. Hauwert, T. A. M. Mocking, D. Da Costa Pereira, A. J. Kooistra, L. M. Wijnen, G. C. M. Vreeker, E. W. E. Verweij, A. H. De Boer, M. J. Smit, C. De Graaf, H. F. Vischer, I. J. P. de Esch, M. Wijtmans, R. Leurs, *J. Am. Chem. Soc.* **2018**, *140*, 4232-4243.
- [17] W. A. Velema, W. Szymanski, B. L. Feringa, *J. Am. Chem. Soc.* **2014**, *136*, 2178-2191.
- [18] W. Szymanski, J. M. Beierle, H. A. V. Kistemaker, W. A. Velema, B. L. Feringa, *Chem. Rev.* **2013**, *113*, 6114-6178.
- [19] M. M. Lerch, M. J. Hansen, G. M. van Dam, W. Szymanski, B. L. Feringa, *Angew. Chem. Int. Ed.* **2016**, *55*, 10978-10999.
- [20] C. Brieke, F. Rohrbach, A. Gottschalk, G. Mayer, A. Heckel, *Angew. Chem. Int. Ed. Engl.* **2012**, *51*, 8446-8476.
- [21] G. Mayer, A. Heckel, *Angew. Chem. Int. Ed.* **2006**, *45*, 4900-4921.
- [22] A. Deiters, *ChemBioChem* **2010**, *11*, 47-53.
- [23] K. Curley, D. S. Lawrence, *Pharmacol. Ther.* **1999**, *82*, 347-354.
- [24] E. A. Lemke, *ChemBioChem* **2010**, *11*, 1825-1827.
- [25] A. Reiner, E. Y. Isacoff, *Methods Mol. Biol.* **2014**, *1148*, 45-68.
- [26] P. C. Donthamsetti, N. Winter, M. Schönberger, J. Levitz, C. Stanley, J. A. Javitch, E. Y. Isacoff, D. Trauner, *J. Am. Chem. Soc.* **2017**, *139*, 18522-18535.
- [27] W.-C. Lin, M.-C. Tsai, R. Rajappa, R. H. Kramer, *J. Am. Chem. Soc.* **2018**, *140*, 7445-7448.
- [28] J. Broichhagen, J. A. Frank, D. Trauner, *Acc. Chem. Res.* **2015**, *48*, 1947-1960.
- [29] M. Irie, *Chem. Rev.* **2000**, *100*, 1685-1716.

- [30] Y. Yokoyama, *Chem. Rev.* **2000**, *100*, 1717-1740.
- [31] H. Stobbe, *Ber. Dtsch. Chem. Ges.* **1905**, *38*, 3673-3682.
- [32] H. Stobbe, *Ann. Chem.* **1911**, *380*, 1-129.
- [33] K. G. Yager, C. J. Barrett, *J. Photochem. Photobiol. A* **2006**, *182*, 250-261.
- [34] H. M. Dhammika Bandara, S. C. Burdette, *Chem. Soc. Rev.* **2012**, *41*, 1809-1825.
- [35] A. A. Beharry, G. A. Woolley, *Chem. Soc. Rev.* **2011**, *40*, 4422-4437.
- [36] E. Merino, *Chem. Soc. Rev.* **2011**, *40*, 3835-3853.
- [37] L. Laprell, I. Tochitsky, K. Kaur, M. B. Manookin, M. Stein, D. M. Barber, C. Schön, S. Michalakakis, M. Biel, R. H. Kramer, M. P. Sumser, D. Trauner, R. N. Van Gelder, *J. Clin. Invest.* **2017**, *127*, 2598-2611.
- [38] C. Pernpeintner, J. A. Frank, P. Urban, C. R. Roeske, S. D. Pritzl, D. Trauner, T. Lohmüller, *Langmuir* **2017**, *33*, 4083-4089.
- [39] M. Wegener, M. J. Hansen, A. J. M. Driessen, W. Szymanski, B. L. Feringa, *J. Am. Chem. Soc.* **2017**, *139*, 17979-17986.
- [40] B. Eisel, F. Hartrampf, T. Meier, D. Trauner, *FEBS Lett.* **2018**, *592*, 343-355.
- [41] D. Wilson, J. W. Li, N. R. Branda, *ChemMedChem* **2017**, *12*, 284-287.
- [42] R. A. Smits, H. D. Lim, B. Stegink, R. A. Bakker, I. J. P. de Esch, R. Leurs, *J. Med. Chem.* **2006**, *49*, 4512-4516.
- [43] A. Jongejan, H. D. Lim, R. A. Smits, I. J. de Esch, E. Haaksma, R. Leurs, *J. Chem. Inf. Model* **2008**, *48*, 1455-1463.
- [44] S. G. Hammer, S. Gobleder, F. Naporra, H.-J. Wittmann, S. Elz, M. R. Heinrich, A. Strasser, *Bioorg. Med. Chem. Lett.* **2016**, *26*, 292-300.
- [45] S. Gobleder, *Dissertation Universität Regensburg*, **2014**.
- [46] P. B. Marshall, *British J. Pharmacol.* **1955**, *10*, 270-278.

- [47] S. J. Hill, J. M. Young, *Mol. Pharmacol.* **1981**, 19, 379-387.
- [48] M. E. Parson, C. R. Ganellin, *British J. Pharmacol.* **2009**, 147, 127-135.
- [49] H. D. Anspon, *Org. Synth.* **1945**, 25, 86.
- [50] G. H. Coleman, G. Nichols, C. M. McCloskey, H. D. Anspon, *Org. Synth.* **1945**, 25, 87.
- [51] A. M. C. H. van den Nieuwendijk, D. Pietra, L. Heitman, A. Göblyös, A. P. IJzerman, *J. Med. Chem.* **2004**, 47, 663-672.
- [52] J. von Braun, W. Pinkernelle, *Chem. Ber.* **1934**, 67, 1218-1220.
- [53] E. Merino, M. Ribagorda, *Beilstein J. Org. Chem.* **2012**, 8, 1071-1090.
- [54] M. Schönberger, D. Trauner, *Angew. Chem. Int. Ed.* **2014**, 53, 3264-3267.
- [55] B. Priewisch, K. Rück-Braun, *J. Org. Chem.* **2005**, 70, 2350-2352.
- [56] R. Siewertsen, H. Neumann, B. Buchheim-Stehn, R. Herges, C. Näther, F. Renth, F. Temps, *J. Am. Chem. Soc.* **2009**, 131, 15594-15595.
- [57] C. E. Weston, R. D. Richardson, P. R. Haycock, A. J. P. White, M. J. Fuchter, *J. Am. Chem. Soc.* **2014**, 136, 11878-11881.
- [58] S. Pockes, D. Wifling, M. Keller, A. Buschauer, S. Elz, *ACS Omega* **2018**, 3, 2865-2882.
- [59] O. V. Dolomanov, L. J. Bourhis, R. J. Gildea, J. A. K. Howard, H. Puschmann, *J. Appl. Cryst.* **2009**, 42, 339-341.
- [60] G. M. Sheldrick, *Acta Cryst.* **2015**, C27, 3-8.
- [61] G. M. Sheldrick, *Acta Cryst.* **2015**, A71, 3-8.

CHAPTER 5

5 A Photochromic Glycine Potentiator Azolog



This chapter is a manuscript in preparation for submission.

This research is performed within the framework of the ERASynBio Modulightor project in cooperation with A. Gomila-Juaneda (Prof. P. Gorostiza, Institute for Bioengineering of Catalonia, Barcelona Institute of Science and Technology, Barcelona, Spain) and A. Nin-Hill (Prof. C. Rovira, University of Barcelona, Spain) and assistance of Dr. P. Nitschke (Prof. R. Gschwind, University of Regensburg). K. Rustler performed the synthesis and (photo-)chemical characterization of all compounds. A. Gomila-Juaneda performed *in vivo* studies. A. Nin-Hill performed docking studies. Dr. P. Nitschke measured the photostationary states *via* NMR spectroscopy under constant irradiation. Single crystal X-ray crystallography and mass spectrometry analysis were performed by the analytical department at the University of Regensburg. K. Rustler, A. Nin-Hill, and A. Gomila-Juaneda wrote the manuscript. Prof. P. Gorostiza, Prof. C. Rovira, and Prof. B. König supervised the project and will be corresponding authors.

5.1 Introduction

The field of photopharmacology emerged as a hybrid of photochemistry and pharmacology and has achieved increasing attention for the spatial and temporal regulation of biologically active targets by light.^[1,7] The use of photo-responsive molecules to trigger a certain response can be characterized by their mode of operation. In contrast to irreversible approaches (*e.g.*, caged ligands)^[8-10] or tethered ligands (*e.g.*, photoswitchable – orthogonal remotely – tethered ligands), which require genetically engineered receptors,^[11] photochromic ligands (PCLs) are freely diffusible, reversibly acting small molecules. PCLs can be isomerized between at least two different isomeric states upon irradiation with light, each characterized by certain chemical and steric properties. Besides fulgides and dithienylethenes, azobenzenes represent the most prominent PCL scaffold.^[10,12] Within the last years, especially their applications in living test systems has attracted growing attention.^[2] Their benefits include their high photostability and cycle reversibility without loss of responsiveness or degradation as well as their synthetic accessibility and tuneability concerning their photochromic properties, *e.g.*, thermal half-lives and absorption wavelengths. Upon light-induced *trans-cis* isomerization, the PCL undergoes a drastic change in sterics and electronics allowing to change the properties of the merged pharmacological ligand towards its biological target.^[10,12-15]

Although this isomerization was discovered almost 100 years ago^[16] and is henceforth experimentally and computationally deeply investigated few drawbacks remain, *e.g.*, incomplete photoswitching. Especially for biological applications, high photostationary states are desirable to unequivocally assign an effect to each of the isomers. Even though azobenzenes are successfully used in *in vitro* and *in vivo* studies, the predictability of azobenzene's photostationary states remains challenging.

A first breakthrough concerning the improvement of the photostationary states was achieved by the exchange of one of the aryl rings of conventional azobenzene

by a heterocycle. Herges reported azoindazoles with quantitative *trans* to *cis* isomerization but a *trans*-photostationary state (*trans*-PSS) of only around 50%.^[17] As further improvement, Fuchter introduced arylazo pyrazoles (AAPs) with almost quantitative switching in both directions due to a red shift of the $n\text{-}\pi^*$ absorption band of the *cis* isomer.^[18] Besides their improved photochromism, AAPs' five-membered nitrogen heterocycle provides synthetic accessibility for further functionalization and represents a significant structural component present in biological molecules and pharmaceuticals.^[19]

In particular, a highly active non-photochromic glycine potentiator has been recently reported^[20,21] that is susceptible of "azologization".^[22,23] Glycine receptors (GlyRs) are inhibitory anion selective pentameric ion channels and belong to the cysteine-loop (Cys-loop) superfamily of ligand-gated ion channels, which also include type A γ -aminobutyric acid receptors (GABA_ARs), nicotinic acetylcholine receptors (nAChRs), and serotonin type 3 receptors (5HT₃Rs). GlyRs are expressed in nerves of the spinal dorsal horn and are responsible for fast synaptic inhibitory transmission, making them potential targets for novel painkillers. Their fast kinetics are well-matched to the kinetics of synthetic photoswitches. The activation of GlyRs, in particular $\alpha 3$ GlyR, is believed to reduce the transmission of painful stimuli. Current pain treatment includes the systemic administration of agents (such as opioids) with undesirable side effects and which often lack potency.^[20,21,24-27] The identification of novel drugs devoid of these side effects or a method to localize GlyR modulation would improve medical care. Therefore, photocontrolling the activity of GlyR modulators bears great interest for neurochemistry and for medicine.^[28]

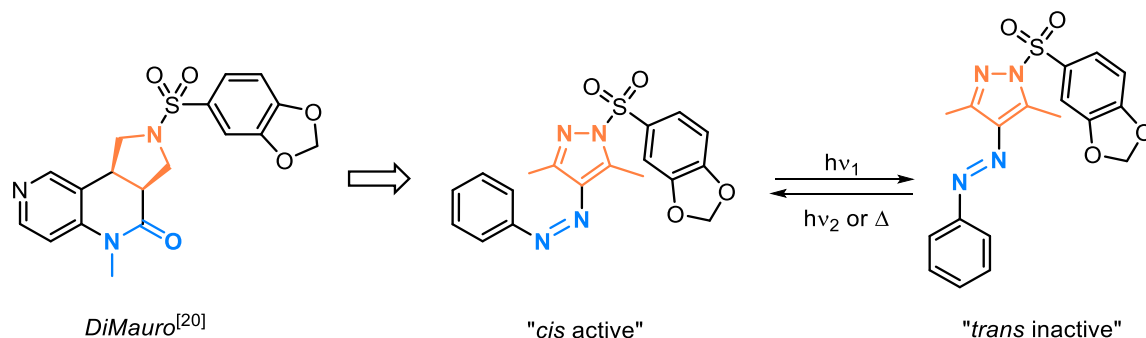
In the present work, we report the synthesis and *in vivo* evaluation of a photochromic glycine potentiator derivative based on arylazo pyrazole. The *in vivo* activity of xenopus larvae could be switched towards high excitatory states upon light-induced *trans* to *cis* isomerization and restored to vehicle activity upon re-isomerization to *trans*. Molecular modelling provides a molecular view on the binding of the photochromic ligand to its putative target receptor $\alpha 3$ GlyR and

also serves as primary screening tool to predict which of the designed molecules is more likely to exhibit a light-dependent effect.

5.2 Results and Discussion

5.2.1 Design and Syntheses

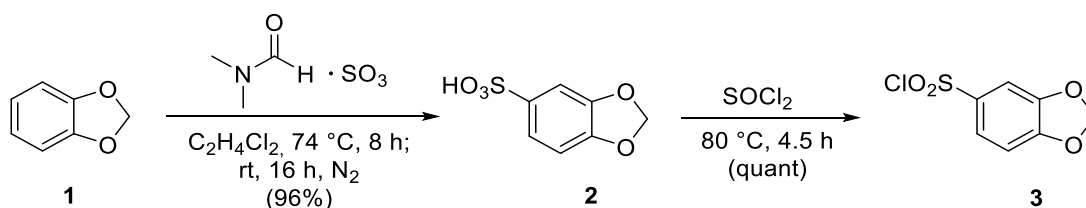
Design. Based on the chemical structure of DiMauro's^[20] optimized tricyclic sulfonamide AM3607, which functions as a high efficacy $\alpha 3$ GlyR potentiator, we designed a corresponding arylazo pyrazole derivative (Scheme 1). We envisioned that the replacement of the amide linked pyrrolidine by an aryl azo pyrazole, while maintaining the sulfonamide benzodioxole moiety would result in a highly potent arylazo pyrazole derivative. This photochromic modulator is designed to exert activity only in its *cis*-isomeric state, which resembles the "chair"-like conformation reported for the parent compound AM3607 bound to $\alpha 3$ GlyR.^[21] The steric change upon *cis* to *trans* isomerization would then result in loss of activity, which could be restored by irradiation with light. Thus, the design aimed at obtaining a *cis* active photochromic GlyR potentiator that was inert in its *trans*-isomeric state.



Scheme 1. Design of a photochromic arylazo pyrazole derivative as glycine receptor modulator based on the hit to lead optimization of DiMauro.^[20]

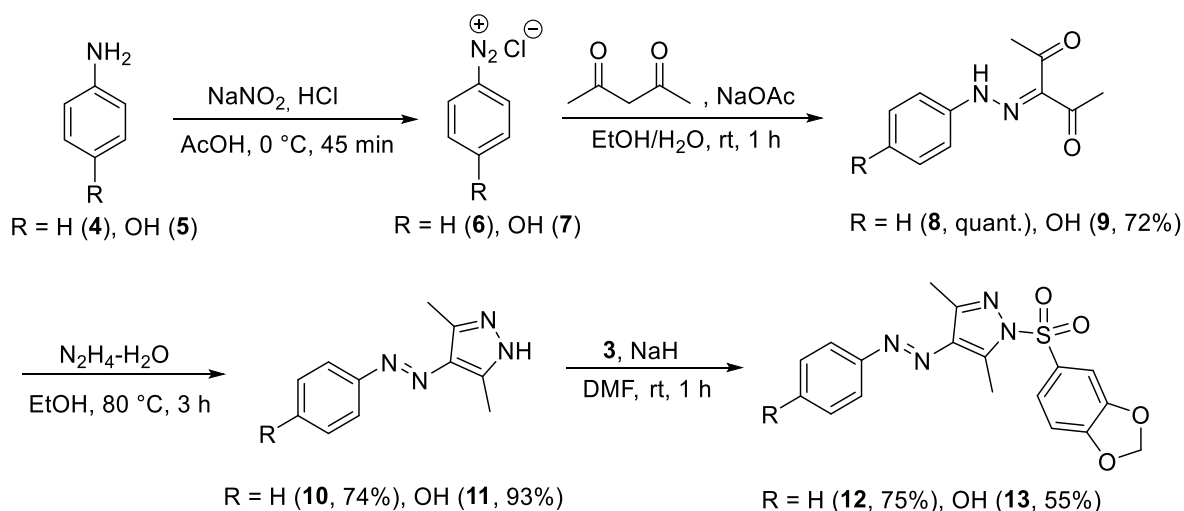
Synthesis. The synthesis of the sulfonic acid substituted benzodioxole as structural key element was performed as reported (Scheme 2).^[29] The functionalization of 1,3-benzodioxole (**1**) was performed using a sulfur trioxide-*N,N*-dimethylformamide complex. The resulting sulfonic acid **2** was converted into its corresponding

sulfonyl halide **3** upon reaction with thionyl chloride allowing the subsequent formation of an azo pyrazole sulfonamide (Scheme 3).



Scheme 2. Synthesis of the highly reactive 1,3-benzodioxole-5-sulfonyl chloride **3**.^[29]

As photochromic moiety, two different arylazo pyrazoles were synthesized as outlined in Scheme 3. Aniline (**4**) and – for improved overall solubility in aqueous media – its hydroxy derivative **5** were diazotized using sodium nitrite in the presence of hydrochloric and acetic acid and reacted with pentane-2,4-dione providing the phenylhydrazonopentane-2,4-diones **8** and **9**, respectively. The subsequent reaction with hydrazine monohydrate afforded the desired 1,3-dimethyl-arylazo pyrazoles **10** and **11**.^[30] The installation of the sulfonic acid benzodioxole **3** was achieved in the presence of sodium hydride as base affording the highly functionalized photochromic derivatives **12** and **13** in good yields.^[31]



Scheme 3. Synthesis of the pyrazole azobenzene based sulfonamides **12** and **13**.^[30,31]

5.2.2 Photochemical Characterization

The photochemical characterization of compounds **12** and **13** was performed in DMSO using UV-Vis and NMR spectroscopy as well as HPLC-assisted analysis.

Figure 1 shows exemplarily the UV-Vis absorption spectrum (left panel) and cycle performance (right panel) of the hydroxy substituted AAP sulfonamide **13**. The compounds were dissolved 50 μM in DMSO representing the *trans* isomer in its thermal equilibrium (black curve). Black arrows indicate the spectral changes upon *trans-cis* isomerization triggered by irradiation with UV light ($\lambda = 365\text{ nm}$) until the *cis*-photostationary state (*cis*-PSS; red curve) was reached. The maximum representing the *trans* isomer (black curve) decreased and a new shoulder in the visible range, characteristic for the *cis* isomer, evolved. Back isomerization to the *trans* isomer at its PSS (blue curve) is triggered by irradiation with visible light ($\lambda = 528\text{ nm}$). Dotted black arrows label the resulting isosbestic points indicating a clear two-component switching without any degradation or formation of a side product. The major photophysical properties of compounds **12** and **13** are summarized in Table 1. All compounds showed excellent photochromic properties in DMSO with high photostationary states and excellent fatigue resistance.

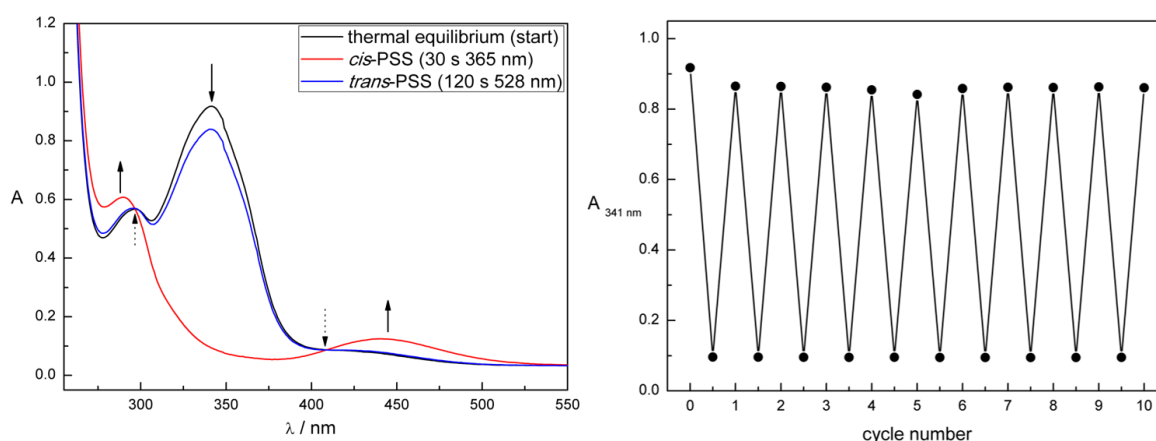


Figure 1. Photochromic properties of AAP derivative **13** (50 μM DMSO). Left panel: UV-Vis absorption spectrum upon irradiation with $\lambda = 365\text{ nm}$ until the *cis*-PSS is reached (30 s) and $\lambda = 528\text{ nm}$ until the *trans*-PSS is reached (120 s). Black arrows indicate the characteristic absorption changes upon *trans-cis* isomerization. Dotted black arrows indicate isosbestic points. Right panel: Repetitive switching cycles upon alternate irradiation with UV ($\lambda = 365\text{ nm}$) and green ($\lambda = 528\text{ nm}$) light plotted at 341 nm (λ_{max} of the *trans* isomer).

The determination of the thermal half-lives (THLs) of the *cis* isomer of compounds **12** and **13** was accomplished by monitoring the increase in absorbance at the maximum wavelength of the *trans* isomer, which corresponds to the regeneration of the *trans* isomer from a 50 μM solution of the *cis* isomer in the dark. The data

indicate moderate thermal stability of the *cis* isomers, which is beneficial because constant irradiation during the biological testing can be avoided.

Table 1. Photochemical properties of sulfonamides **12** and **13** measured 50 μ M DMSO. Cpd. = Compound.

Entry	Cpd.	λ_{max} <i>cis</i> isomer [nm]	λ_{max} <i>trans</i> isomer [nm]	Isosbestic points [nm]	THL [h]	PSS
1	12	329	439	287, 396	1.6	93% <i>cis</i> (365 nm) ^(a) 78% <i>trans</i> (455 nm) ^(a)
2	13	341	441	297, 409	2.9	86% <i>cis</i> (365 nm) ^(b) 83% <i>trans</i> (528 nm) ^(b)

(a) Determined by analytical HPLC measurement of a preirradiated 50 μ M solution at 20 °C at the isosbestic point. (b) Determined by NMR-measurement of a 50 mM solution in DMSO under constant irradiation until the PSS was reached.

5.2.3 *In Vivo* Behavioral Studies

Due to insufficient solubility of the unsubstituted AAP sulfonamide **12** only its hydroxy derivative **13** could be subjected to *in vivo* analysis in aqueous media.

Compound **13** showed a robust photoswitchable profile in animal behavioral studies. As intended by the design, the AAP sulfonamide **13** acted as a *cis*-active modulator of *xenopus* behavior (Figure 2). In its *trans*-isomeric state, compound **13** restored larvae activity to control (vehicle) activity during the relaxation period (RP) and the first visible light cycles. Upon irradiation-induced *trans* to *cis* isomerization, compound **13** induced major inactivity states to all tadpoles for the entire UV (λ = 365 nm) irradiation periods, after which the animals slowly recovered to movements corresponding to control experiments (Figure 2A). This data suggests, that the AAP sulfonamide **13** acts as a highly effective GlyR potentiator in its *cis*-isomeric state whereas its *trans*-isomeric activity resembles the control conditions (vehicle).

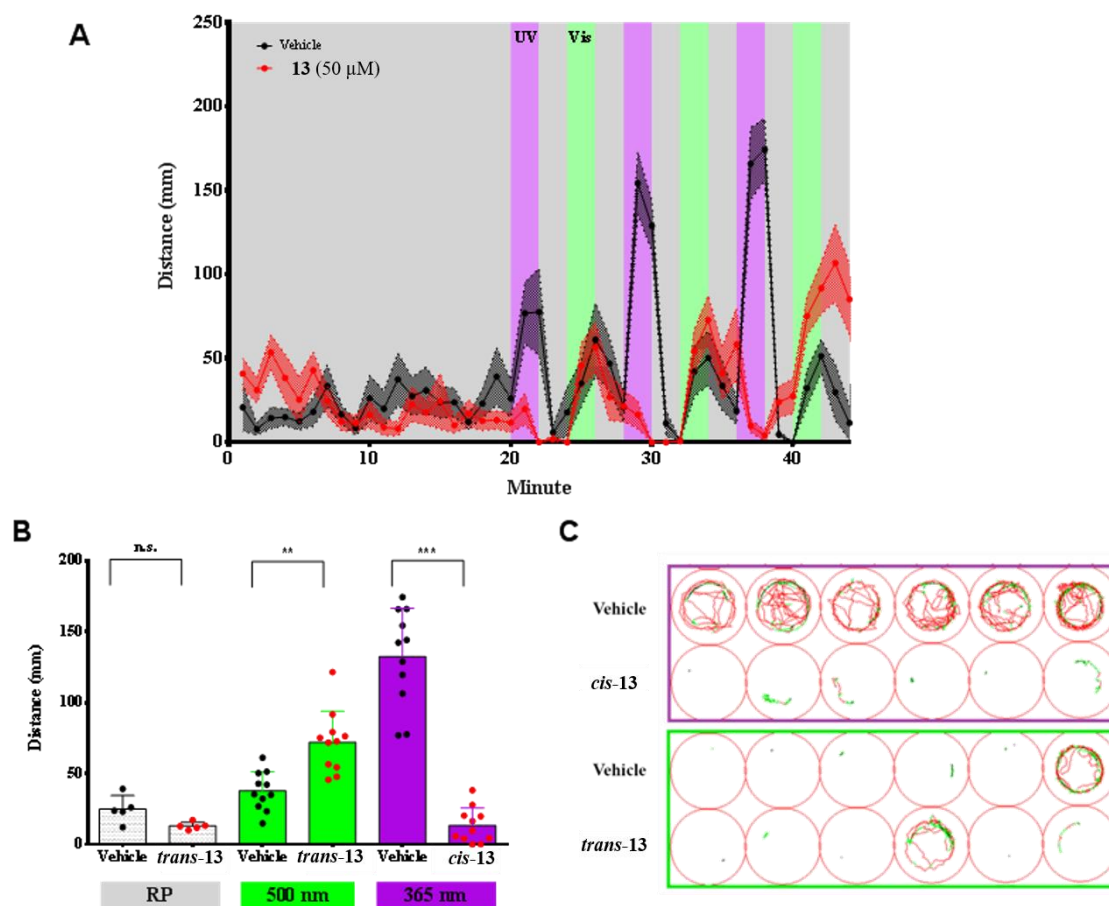


Figure 2. (A) One-minute trajectories of the average swimming distances ($n = 24$ per treatment) are shown for vehicle (0.5% DMSO) and for 50 μ M of compound **13**. For the first 20 minutes, tadpoles were undisturbed in complete darkness (relaxation period, RP). Afterwards, the larvae were irradiated with three cycles of two minutes of 365 nm and two minutes of 500 nm wavelengths, each one spared with two minutes of dark. Colored areas show the standard error of the mean (S.E.M.). (B) Light period analysis for both treated larvae. Average of the distance swam for the last five minutes of the RP and all-time irradiation periods for each wavelength (500 nm and 365 nm). Unpaired t-test was applied for each treatment and the light period was used for the statistical analysis with $p < 0.05$ for statistical significance (n.s. = not significant, ** p -value < 0.01 , *** p -value < 0.001). (C) Inset of one-minute trajectory for the same group of tadpoles and treatment corresponding to visible light (green boxed) and UV (purple boxed) irradiation period. Larvae swimming trajectories are colored traces were red traces respond to larvae movements above six mm s^{-1} and green traces for movements between two and six mm s^{-1} .

5.2.4 Molecular Docking

Compound **13** was modelled to its putative target receptor $\alpha 3$ GlyR in order to understand the molecular determinants of the different effect of the *cis* and *trans* isomers in the *in vivo* zebrafish behavioral tests. As this compound was designed based on the chemical structure of AM3607,^[20] which is an effective glycine

potentiator of $\alpha 3$ GlyR, it is expected to bind in the same allosteric pocket,^[21] located at the subunit interface in the extracellular domain.

In order to validate the applied docking protocol, AM3607^[20] was first re-docked into the crystallographically discovered allosteric pocket.^[21] The obtained docking pose accurately reproduces the X-ray binding pose of AM3607 (Figure 3). AM3607 shows two T-stacking interactions with Y78 and F32, one π - π stacking with Y161, two hydrogen bonds between the sulfonamide group and R29 and many hydrophobic contacts (Figure 4C), i.e. the obtained docking pose reproduces the main receptor-ligand interactions observed in the reported X-ray structure.^[21]

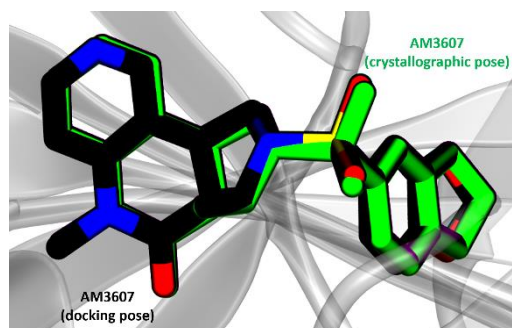


Figure 3. Binding poses of AM3607 in the crystallographic structure^[21] (green) and obtained from the docking calculation (carbon atoms in black, oxygen atoms in red and nitrogen atoms in blue) in the novel allosteric binding site.

Dockings were subsequently performed for each of the two stereoisomers of compound **13**. The *cis* isomer of compound **13** exhibits receptor-ligand interactions similar to AM3607, such as the two hydrogen bonds of the sulfonamide group with R29. Although the mentioned T-stacking interaction with F32 and some hydrophobic contacts are lost, this is easily compensated by the gain of two π - π stacking interactions with Y161 and Y78 and one hydrogen bond between K33 and the phenolic hydroxyl group of **13**.

In contrast, the *trans* isomer of compound **13** shows a binding mode, which is more different from that of AM3607. The two hydrogen bonds between R29 and the sulfonamide group (which help to secure the compound in its binding site), as well as the two π - π stacking interactions with Y78 and F32, are lost, and the hydrogen

bond with K33 is replaced by a weaker cation- π interaction. Also, fewer hydrophobic contacts are present.

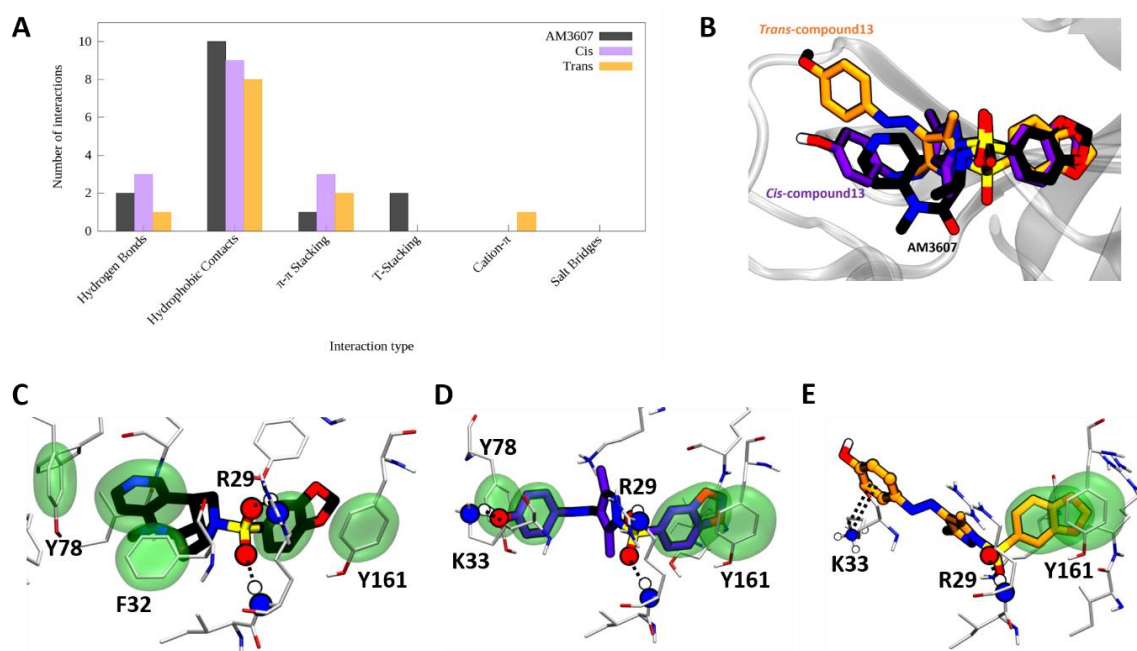


Figure 4. (A) Number of receptor-ligand interactions for AM3607 (black), *cis*-13 (pink bars) and *trans*-13 (orange) bound to α 3 GlyR. (B) Superposition of the binding modes of AM3607 (black) and of both isomers of 13 (*trans* in orange and *cis* in purple). (C) AM3607, represented with black carbon atoms and blue, yellow and red for the nitrogen, sulfur and oxygen atoms, respectively. (D) *cis*-13 bound in the novel allosteric pocket, represented with purple carbon atoms, all other atom types are colored as in (C). (E) *Trans*-13, represented with orange carbon atoms; all other atom types are colored as in (C). In panels (C-E) the residues interacting with the respective compound are shown as thin lines with carbon atoms in white. Hydrogen bonds are shown using larger spheres for the atoms involved directly in the interaction and dashed black lines connecting donor and acceptor. T- and π - π stacking interactions are displayed with green transparent surfaces around the atoms involved in the interaction, whereas cation- π interactions are represented as smaller spheres and a double dashed black line.

Altogether, the docking results indicate that the *cis* isomer of 13 binds to α 3 GlyR with a pattern of interactions more similar to AM3607 than its *trans* isomer. This is most likely due to the *cis* isomer mimicking better the “chair”- shaped conformation of AM3607^[21] than the extended *trans* isomer. Consequently, *cis*-13 is associated to the positive allosteric conformational change of GlyR α 3 proposed for AM3607. The ligand binding pocket is only 10 Å away from the glycine binding site, and hence it has been hypothesized that binding of the potentiator can stabilize the orthosteric site and increase the receptor affinity to glycine.^[21]

5.3 Conclusion

In this work, we present the design, synthesis, and (photo-)chemical characterization of an arylazo pyrazole based photochromic derivative of a reported glycine potentiator. All synthesized compounds show highly reversible photochromism with high fatigue resistance and high photostationary states. This is beneficial as an observed biological effect can clearly be assigned to one or the other isomer. *In vivo* investigations on tadpoles showed an isomer-dependent effect on their behavior. In its *cis*-isomeric state, AAP **13** induced major inactivity states, in agreement with GlyR potentiation. Reisomerization to *trans* AAP **13** provoked the restoration of the larvae activity to vehicle activity. Molecular docking analysis provide a rational guidance to design and understand the observed isomer-dependent *in vivo* activities in comparison to the reported^[20,21] results.

5.4 Experimental Part

5.4.1 General Procedures and Materials

Commercial reagents and starting materials were purchased from the commercial suppliers abcr, Acros Organics, Alfa-Aesar, Fisher Scientific, Merck, Sigma Aldrich, TCI, or VWR and used without any further purification. Solvents were used in p.a. quality and dried according to common procedures, if necessary. Dry nitrogen was used as an inert gas atmosphere. Flash column chromatography was performed using Sigma Aldrich MN silica gel 60 M (40-63 μm , 230-400 mesh) for normal phase chromatography. Reaction monitoring *via* thin layer chromatography was performed on alumina plates coated with silica gel (Merck silica gel 60 F₂₅₄, layer thickness 0.2 mm). Melting points were determined using a Stanford Research System OptiMelt MPA 100 and are uncorrected. NMR spectra were measured on a Bruker Avance 300 (¹H 300.13 MHz, ¹³C 75.48 MHz), Bruker Avance III HD 400 (¹H 400.13 MHz, ¹³C 100.61 MHz), Bruker Avance III HD 600 (¹H 600.25 MHz, ¹³C 150.95 MHz) and Bruker Avance III 600 (¹H 600.25 MHz, ¹³C

150.95 MHz). The spectra are referenced against the NMR-solvent (DMSO- d_6 : δ_H = 2.50 ppm, δ_C = 39.52 ppm) and chemical shifts δ are reported in ppm. Resonance multiplicity is abbreviated as: s (singlet), d (doublet), t (triplet) and m (multiplet). Carbon NMR signals are assigned using DEPT 135 and 1H - ^{13}C HSQC spectra with (+) for primary/tertiary, (-) for secondary, and (q) for quaternary carbons. Mass spectra were recorded on a Finnigan MAT-SSQ 710 A, ThermoQuest Finnigan TSQ 7000, Agilent Q-TOF 6540 UHD, or a Jeol AccuTOF GCX instrument. UV-Vis absorption spectroscopy was performed in 10 mm quartz cuvettes using an Agilent 8543, Agilent Cary 100, or Agilent Varian Cary 50 spectrometer. Analytical HPLC measurements were performed using an Agilent 1220 Infinity LC (column: Phenomenex Luna 3 μm C₁₈(2) 100 Å, 150 x 2.00 mm; flow 0.3 mL min⁻¹ at 20 °C or 30 °C; solvent A: MilliQ water with 0.05 wt% TFA; solvent B: MeCN). The ratios at the PSSs were determined *via* analytical HPLC at 20 °C at the isosbestic points or *via* NMR spectroscopy under constant irradiation. An Agilent 1260 system (column: Phenomenex Luna 10 μm C₁₈(2) 100 Å, 250 x 21.2 mm; flow: 22 mL min⁻¹; solvent A: MilliQ water; solvent B: MeCN) was used for preparative HPLC purification. Light sources for irradiation: λ = 365 nm (Seoul Viosys CUN6GB1A, 1000 mA, 1.4 W), λ = 455 nm (Osram OSOLON SSL 80 LD-CQ7P-1U3U, 1000 mA, 0.45 W), and λ = 528 nm (Osram LTCP7P-KXKZ, 350 mA, 71 lm). The power of the light source is given based on the specifications supplied by the company when the LEDs were purchased. All tested final compounds possess a purity $\geq 94\%$ determined by HPLC measurements at 30 °C with detection at 220 nm or 254 nm, respectively.

Compounds **2**,^[29] **3**,^[29] **8**,^[30] **9**,^[30] **10**,^[30] and **11**^[30] were prepared according to reported procedures.

5.4.2 Synthetic Procedures and Characterization

General procedure for the synthesis of 12 and 13. Compounds **12** and **13** were prepared *via* an adapted literature procedure.^[31] A solution of the respective azo pyrazole (1.0 eq) in DMF (10 mL pro mmol) was cooled to 0 °C under a nitrogen

atmosphere. Sodium hydride (60% suspension in paraffin oil, 1.1 eq) was added and the mixture stirred for 15 minutes at 0 °C and 15 minutes at room temperature. The substituted sulfonyl chloride (1.3 eq) was added and the reaction stirred at room temperature for one hour. The mixture was poured on ice and the solid collected by filtration. Purification by column chromatography using CH₂Cl₂ + 5% MeOH as eluent and subsequent preparative HPLC afforded the desired product.

(E)-1-(benzo[d][1,3]dioxol-5-ylsulfonyl)-3,5-dimethyl-4-(phenyldiazenyl)-1H-pyrazole (12). Orange solid (0.36 g, 0.93 mmol, 75%). Gradient 0-10 min 50%-98% MeCN, t_R = 11.1 min. M.p.: 158 °C. ¹H-NMR (400 MHz, DMSO-*d*₆): δ = 7.82 – 7.76 (m, 2H), 7.65 (dd, J = 8.3, 2.0 Hz, 1H), 7.59 – 7.49 (m, 4H), 7.17 (d, J = 8.4 Hz, 1H), 6.21 (s, 2H), 2.88 (s, 3H), 2.38 (s, 3H). ¹³C-NMR (101 MHz, DMSO-*d*₆): δ = 153.3 (q), 152.5 (q), 148.5 (q), 145.5 (q), 144.8 (q), 135.9 (q), 131.0 (+), 129.4 (+), 129.2 (q), 124.7 (+), 122.0 (+), 108.9 (+), 107.1 (+), 103.3 (-), 14.7 (+), 10.9 (+). HRMS (ESI) calcd. for (C₁₈H₁₇N₄O₄S⁺) [M+H]⁺: m/z = 385.0965; found 385.0970. MF: C₁₈H₁₆N₄O₄S. MW: 384.41 g/mol.

(E)-4-((1-(benzo[d][1,3]dioxol-5-ylsulfonyl)-3,5-dimethyl-1H-pyrazol-4-yl)diaz-enyl)phenol (13). Orange solid (264 mg, 0.66 mmol, 55%). Gradient 0-20 min 10%-98% MeCN, t_R = 16.2 min. M.p.: 156 °C. ¹H-NMR (400 MHz, DMSO-*d*₆): δ = 12.88 (s, 1H), 7.72 – 7.68 (m, 2H), 7.41 (d, J = 1.9 Hz, 1H), 7.35 (dd, J = 8.2, 2.0 Hz, 1H), 7.19 – 7.15 (m, 2H), 7.11 (d, J = 8.3 Hz, 1H), 6.22 (s, 2H), 3.31 (s, 6H). ¹³C-NMR (101 MHz, DMSO-*d*₆): δ = 153.4 (q), 152.0 (q), 149.7 (q), 148.9 (q), 141.3 (q), 141.3 (q), 134.7 (q), 127.1 (q), 125.5 (+), 123.4 (+), 123.2 (+), 109.1 (+), 108.1 (+), 103.6 (-), 12.3 (+), 12.3 (+). HRMS (ESI) calcd. for (C₁₈H₁₇N₄O₅S⁺) [M+H]⁺: m/z = 401.0914; found 401.0910. MF: C₁₈H₁₆N₄O₅S. MW: 400.41 g/mol.

5.4.3 *In Vivo* Behavioral Studies

Animal housing and photoswitchable behavioral assays. *Xenopus tropicalis* embryos (Nasco) were obtained by natural mating and maintained till 3-4 dpf in 0.1 × Marc's modified Ringer's (MMR) solution in agarose coated petri dishes (10-15 cm diameter) in a dark incubator (24°C). Animals were transferred to tanks

containing *Xenopus* water, which was prepared by adding eight grams of instant ocean salt (Instant Ocean) to 20 L of distilled water. Conductivity and pH were 800 μS and 7.0-7.5, respectively. Tadpoles were kept at a density of 30-50 animals L^{-1} , at 25°C and fed daily with spirulina. Tadpoles were recorded and video analyzed using the Zebrabox and Zebralab software (ViewPoint Life Sciences). For all experiments, tadpoles of stage 43 to 47^[32] were left undisturbed for 40 minutes in 200 μL fresh UV filtered water and in darkness. Continuously, 100 μL were removed and replaced with a double concentrated treatment solution and data and video recording begun. For the first 20 minutes, tadpoles were kept in darkness measuring basal activity, named as the relaxation period (RP). After the RP, three double light irradiation cycles were applied; two minutes of 365 nm (UV light) and two minutes of darkness followed by two minutes 500 nm (visible light) and two minutes of darkness.

Data analysis and statistics. *X. tropicalis* tracking was performed in real time and data acquisition integrated one-minute intervals using the Zebralab software (ViewPoint Life Science). Data statistical analysis was performed using GraphPad Prism 6 software. Selective irradiation was performed with two ordered based (evenly distributed) arrays of twelve light emitting diodes (LEDs) for each wavelength placed twelve cm afar of the multiwell plate. The light intensities, measured with an optical power meter (model Newport 1916-C), were 5.92 W m^{-2} for 365 nm (UV) and 2.2 W m^{-2} for 500 nm (Visible-Blue). Distance activity was measured as the sum of swimming distances (in millimeters) during burst activities (larvae swimming velocities higher than 6 mm s^{-1}) over one-minute integration. Data was analyzed following unpaired t-test with Welch's correction (p-value 0.05) and are presented as mean \pm standard error of the mean (s.e.m.) with the number of larvae (*n*) indicated in each case.

5.4.4 Molecular Docking

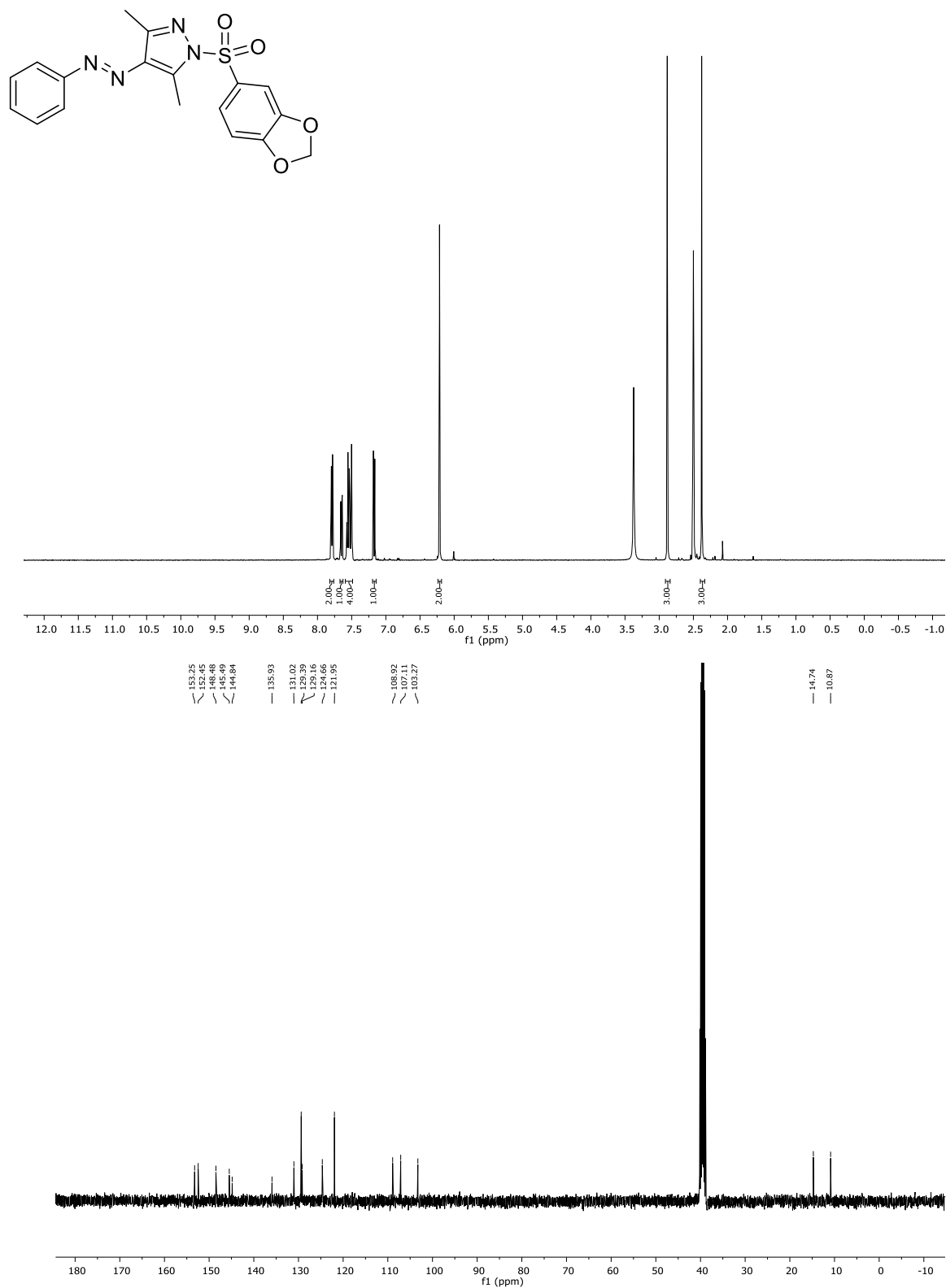
The initial structures of compound **13** (*cis* and *trans*) were created employing Avogadro (version 1.1.1).^[33] The structure of the $\alpha 3$ GlyR was taken from the

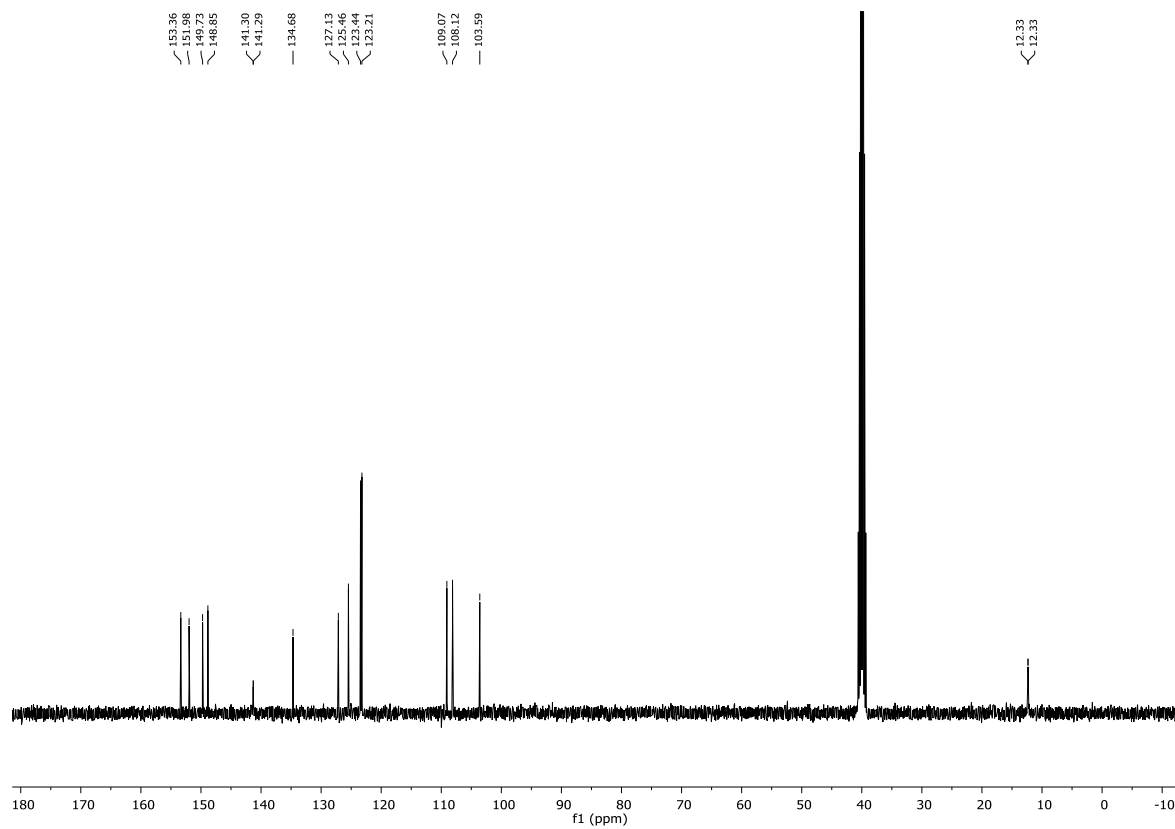
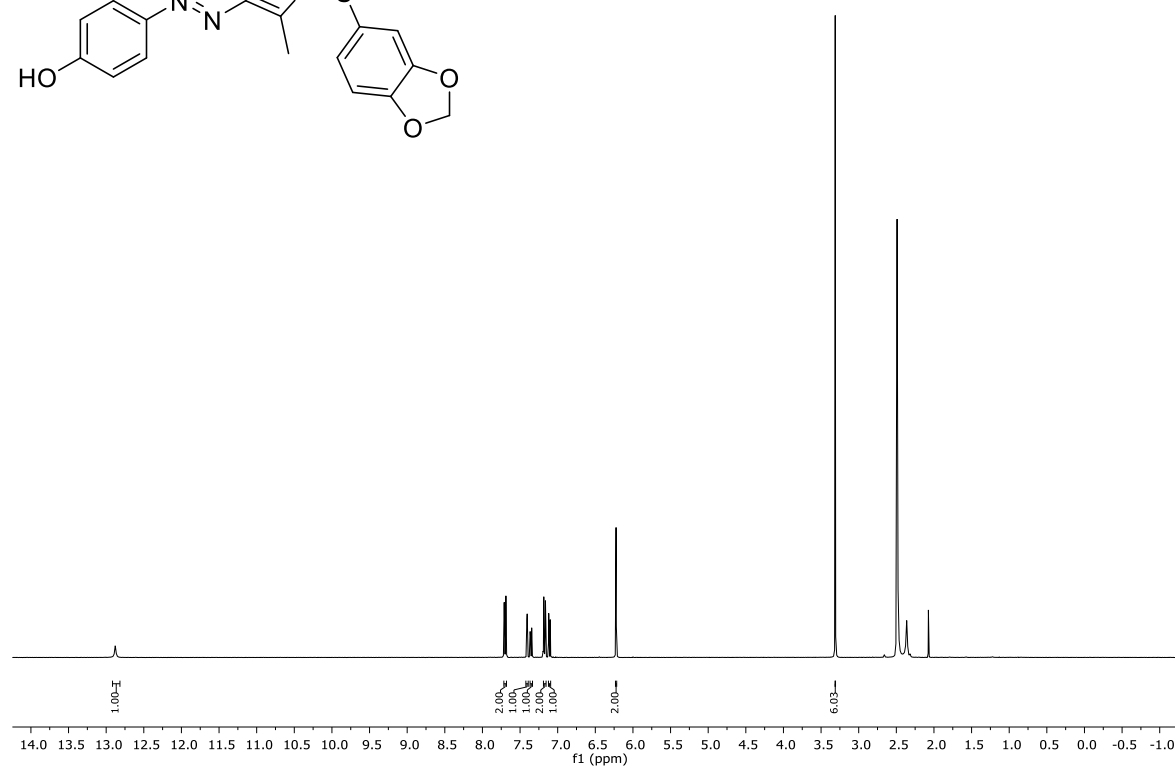
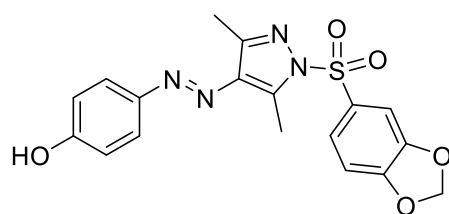
recently published crystal structure (PDB code 5TIO).^[21] Docking was performed into the novel allosteric pocket found for AM3607, located at the subunit interface in the extracellular domain. Given the pentameric symmetry of GlyR, only one site was considered. The program Autodock Vina^[34] was used for the docking calculations, using default values. This docking protocol was repeated ten times, starting with different random seeds, so that a total number of 90 binding modes was obtained for each of the two possible isomers of compound **13**. Both compound **13** and some receptor residues were treated as flexible. In particular, the protein residues chosen as flexible are the ones surrounding the photochromic moiety attached to the pharmacologically active sulfonamide benzodioxole (see Scheme 1), in order to allow the protein to adjust to the ligand modifications. A similar docking protocol was used for the re-docking experiment of AM3607. The criteria to select the best docking pose are: (i) the sulfonamide benzodioxole moiety is placed as the AM3607 potentiator,^[21] in order to maximize the interactions with the allosteric binding pocket residues, and (ii) the pose has the highest binding energy, according to the AutoDock Vina scoring function.^[34] Protein-ligand interactions (such as hydrogen bonds, π - π stacking, and hydrophobic interactions) were analyzed using the Binana algorithm.^[35] All images were generated using the VMD program.^[36]

5.5 Supporting Information

5.5.1 ^1H - and ^{13}C -NMR Spectra

Compound **12** ($\text{DMSO}-d_6$)



Compound **13** (DMSO-*d*₆)

5.5.2 UV-Vis Absorption Spectra and Cycle Performances

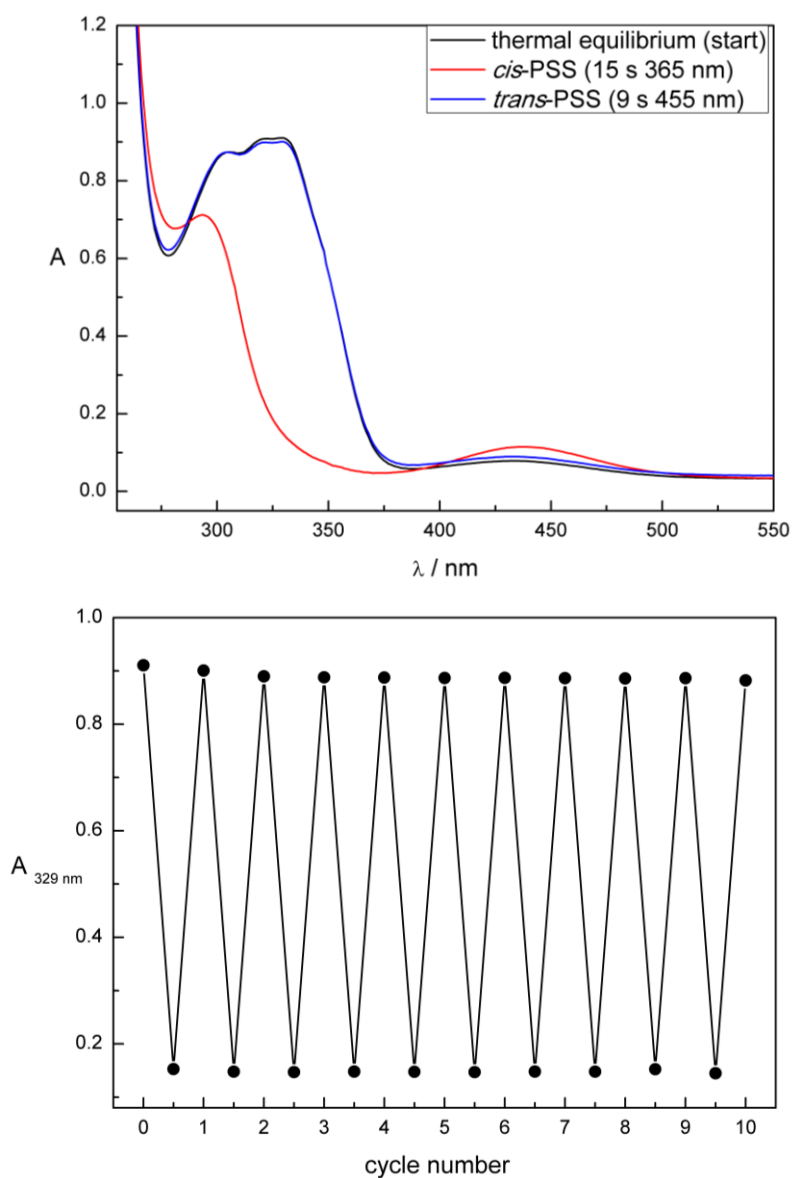


Figure S1. Compound **12** measured 50 μM in DMSO. Upper panel: UV-Vis absorption spectra upon continuous irradiation until the PSS is reached. λ (*cis*-PSS) = 365 nm (15 s), λ (*trans*-PSS) = 455 nm (9 s). Lower panel: Cycle performance. Changes in absorption at 348 nm (λ_{max} of the *trans* isomer) were measured during alternate irradiation with λ = 365 nm (10 s) and λ = 455 nm (10 s) until the PSS is reached.

5.5.3 Thermal Half-Lives

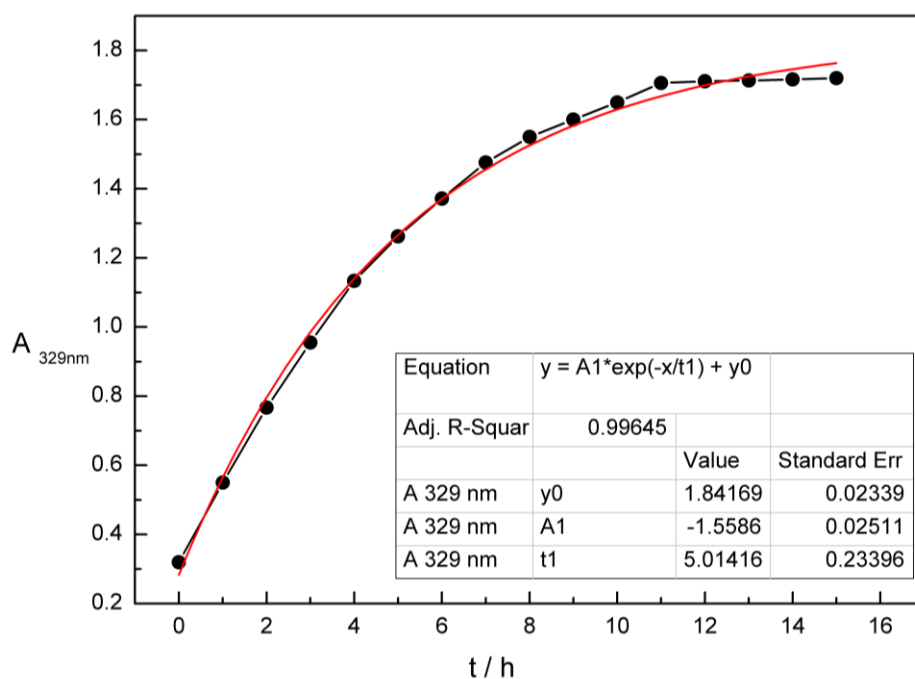


Figure S2. Thermal stability of the *cis* isomer of **12** measured 50 μ M in DMSO at 25 $^{\circ}$ C. Changes in the absorption at the indicated wavelength (λ_{max} of the *trans* isomer) after irradiation with $\lambda = 365$ nm and subsequent thermal relaxation are represented as black dots. The red curve represents an exponential nonlinear curve fit.

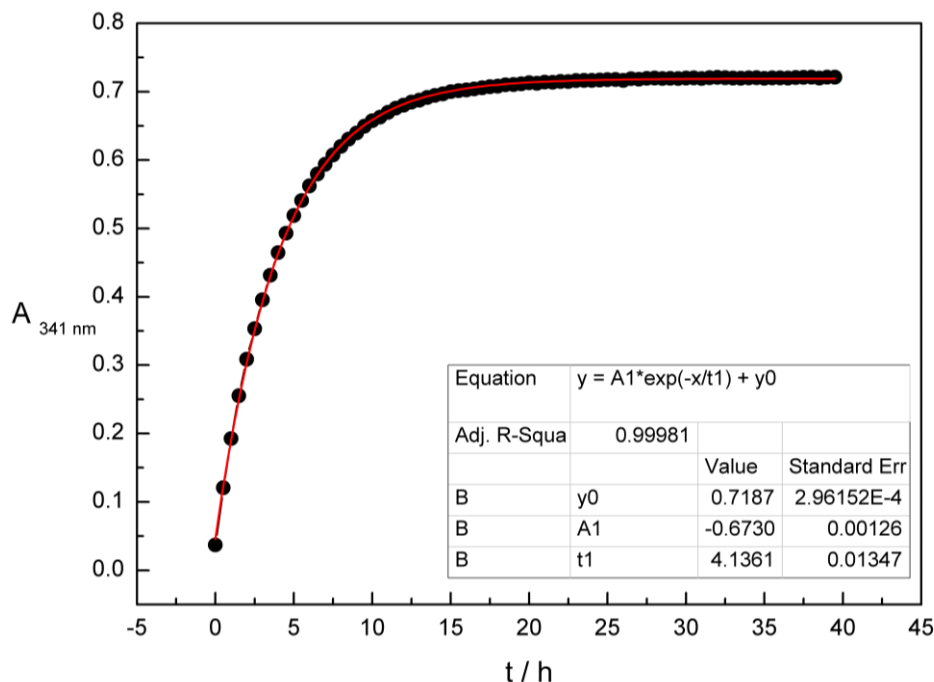
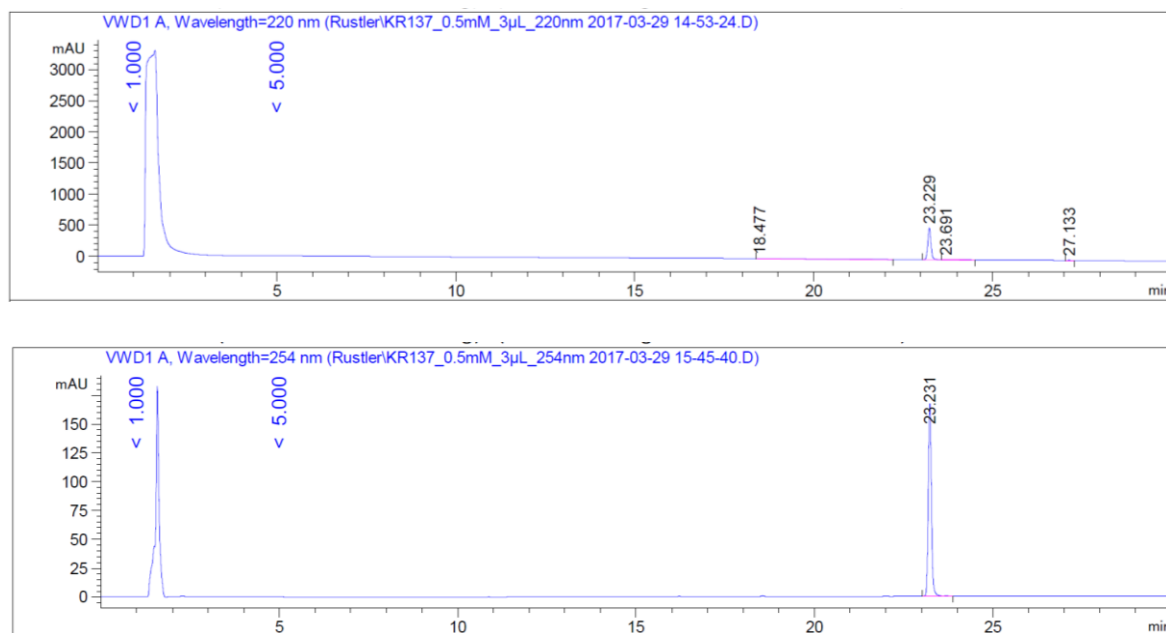


Figure S3. Thermal stability of the *cis* isomer of **13** measured 50 μ M in DMSO at 25 $^{\circ}$ C. Changes in the absorption at the indicated wavelength (λ_{max} of the *trans* isomer) after irradiation with $\lambda = 365$ nm and subsequent thermal relaxation are represented as black dots. The red curve represents an exponential nonlinear curve fit.

5.5.4 Analytical HPLC Traces for Purity Determination

Compound **12** (0.5 mM in DMSO, injection volume 3 μ L)



t_R (*trans* isomer) = 23.2 min

Detection at 220 nm: 97%

Signal 1: VWD1 A, Wavelength=220 nm

Peak #	RetTime [min]	Type	Width [min]	Area [mAU*s]	Height [mAU]	Area %
1	18.477	VB	0.4324	61.07616	1.71549	1.8747
2	23.229	BV R	0.0949	3168.53076	514.48987	97.2560
3	23.691	VB E	0.1215	16.45184	1.91022	0.5050
4	27.133	BBA	0.0930	11.86827	1.97762	0.3643

Totals : 3257.92703 520.09319

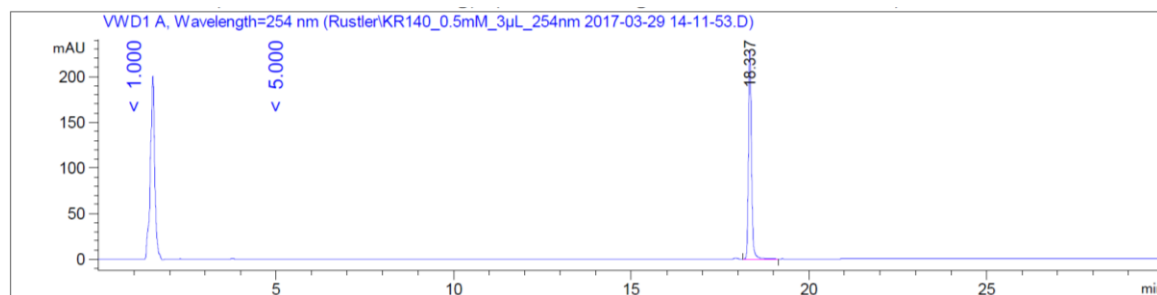
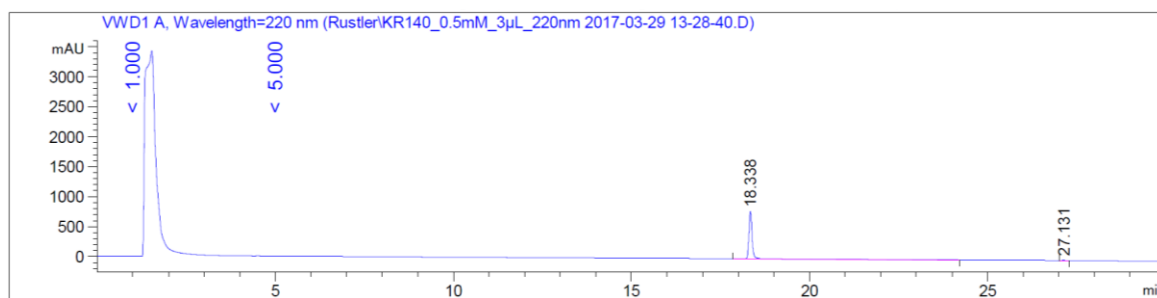
Detection at 254 nm: >99%

Signal 1: VWD1 A, Wavelength=254 nm

Peak #	RetTime [min]	Type	Width [min]	Area [mAU*s]	Height [mAU]	Area %
1	23.231	BV R	0.0935	1026.43823	167.40030	100.0000

Totals : 1026.43823 167.40030

Compound **13** (0.5 mM in DMSO, injection volume 3 μ L)



t_R (*trans* isomer) = 18.3 min

Detection at 220 nm: >99%

Signal 1: VWD1 A, Wavelength=220 nm

Peak #	RetTime [min]	Type	Width [min]	Area [mAU*s]	Height [mAU]	Area %
1	18.338	VV R	0.0933	4853.29102	793.66156	99.6672
2	27.131	BBA	0.0931	16.20477	2.69875	0.3328

Totals : 4869.49579 796.36031

Detection at 254 nm: >99%

Signal 1: VWD1 A, Wavelength=254 nm

Peak #	RetTime [min]	Type	Width [min]	Area [mAU*s]	Height [mAU]	Area %
1	18.337	BB	0.0912	1360.14001	229.15797	100.0000

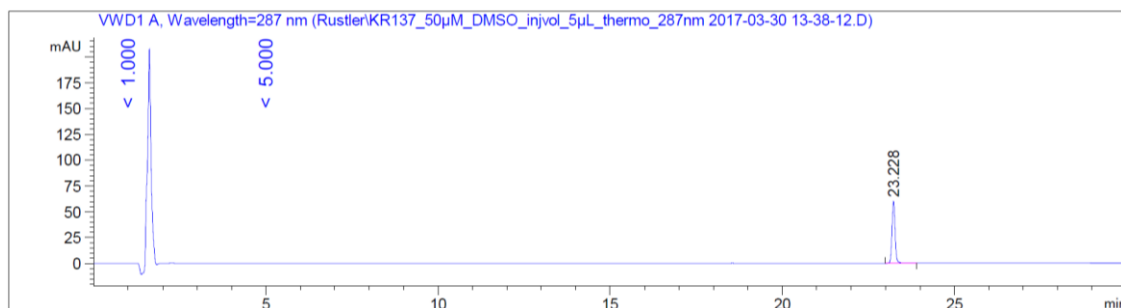
Totals : 1360.14001 229.15797

5.5.5 Analytical HPLC Traces for PSS Determination

Compound 12

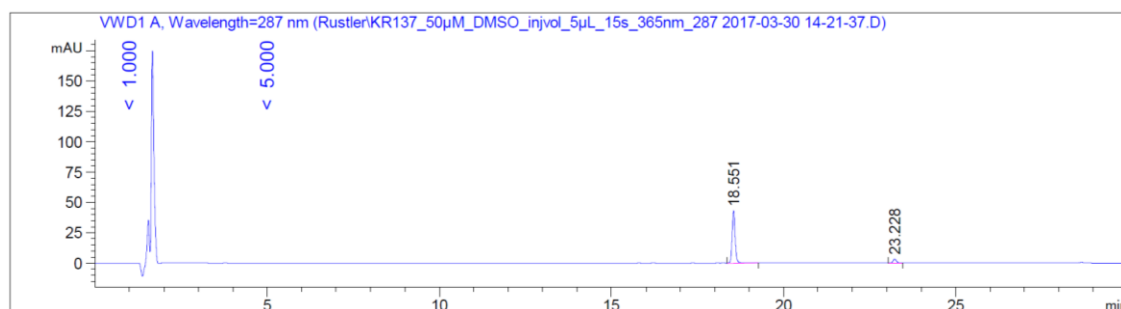
Thermal equilibrium (50 μ M solution in DMSO, injection volume 5 μ L):

100% *trans* isomer



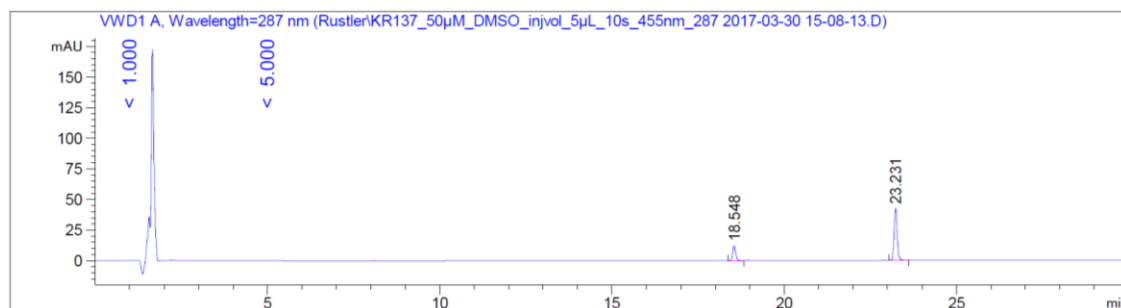
cis-PSS (50 μ M solution in DMSO, injection volume 5 μ L; 365 nm):

93% *cis* isomer; 7% *trans* isomer



trans-PSS (50 μ M solution in DMSO, injection volume 5 μ L; 455 nm):

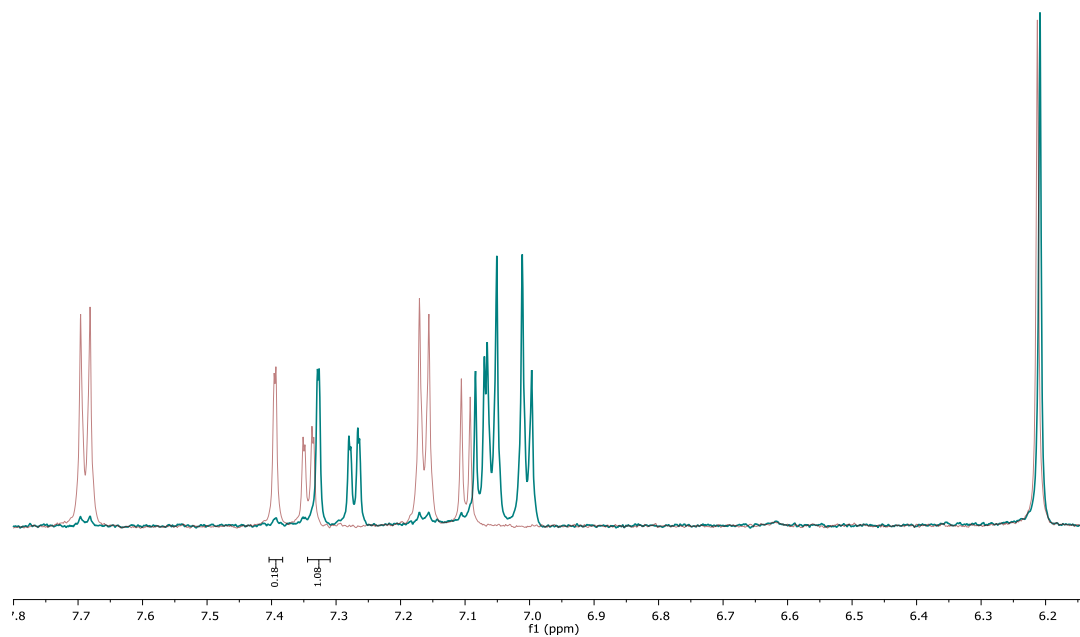
22% *cis* isomer; 78% *trans* isomer



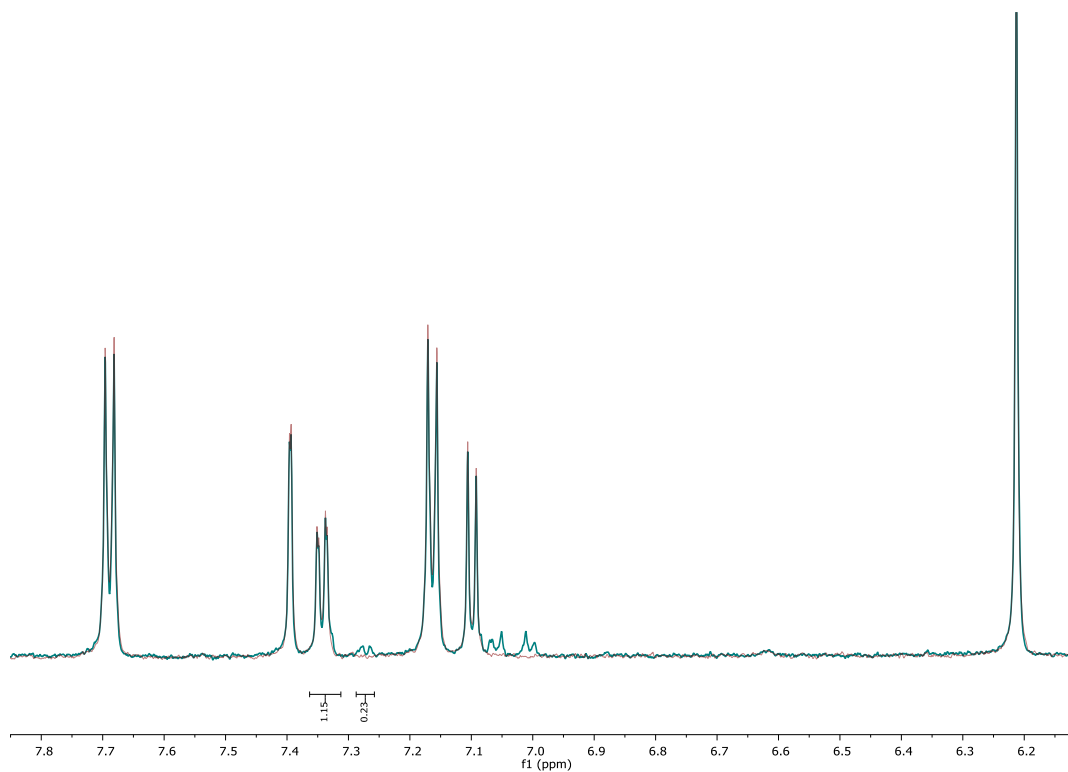
5.5.6 PSS Determination *via* NMR

Compound 13

cis-PSS (86%; blue spectrum) compared to thermal equilibrium (red spectrum)



trans-PSS (83%; blue spectrum) compared to thermal equilibrium (red spectrum)



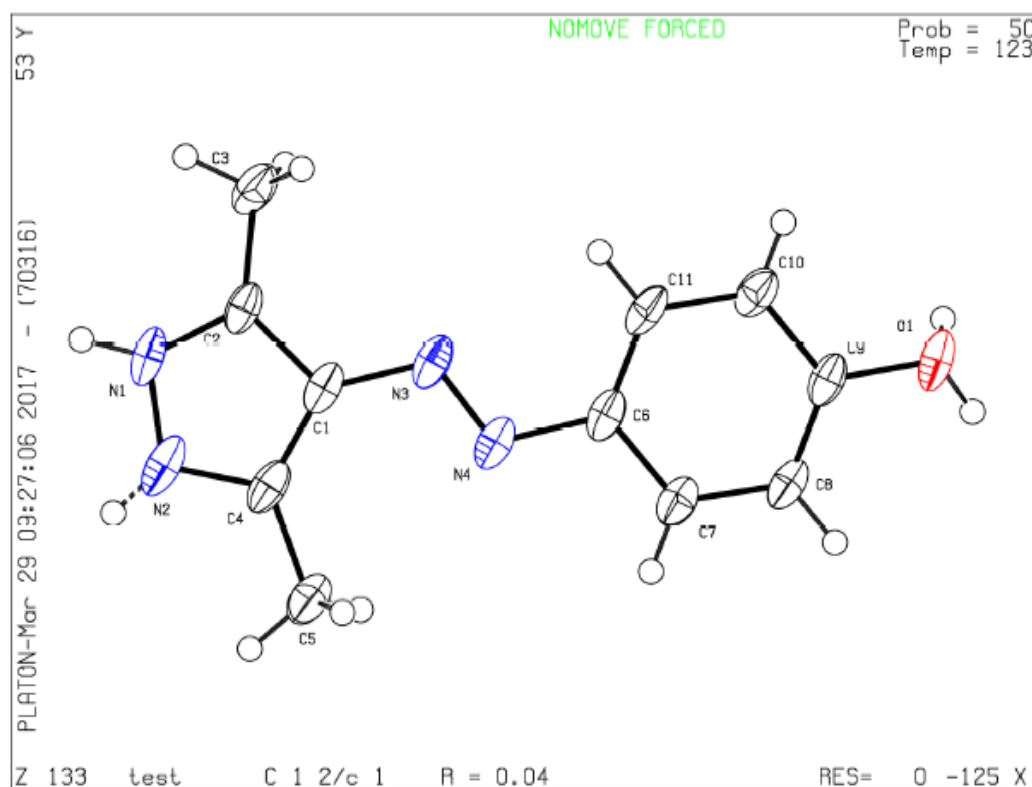
5.5.7 Single Crystal X-ray Crystallography

Compound 11

Experimental. Single clear light-yellow prism-shaped crystals of **11** were obtained by recrystallisation from ethanol. A suitable crystal (0.25×0.08×0.06) mm³ was selected and mounted on a MITIGEN holder oil on a SuperNova, Single source at offset, Atlas diffractometer. The crystal was kept at T = 122.99(10) K during data collection. Using Olex2,^[37] the structure was solved with the ShelXT^[38] structure solution program, using the Intrinsic Phasing solution method. The model was refined with version 2016/6 of ShelXL^[39] using Least Squares minimization.

Crystal Data. C₁₁H₁₂N₄O, *M_r* = 216.25, monoclinic, C2/c (No. 15), *a* = 11.1476(2) Å, *b* = 9.5888(2) Å, *c* = 20.3006(4) Å, β = 92.376(2)°, α = γ = 90°, *V* = 2168.11(7) Å³, *T* = 122.99(10) K, *Z* = 8, *Z'* = 1, μ(CuKα) = 0.735, 23381 reflections measured, 2182 unique (*R_{int}* = 0.0488) which were used in all calculations. The final *wR*₂ was 0.0985 (all data) and *R*₁ was 0.0357 (*I* > 2(*I*)).

Cambridge Structural Database CCDC. 1942445



Detailed Crystal Data.

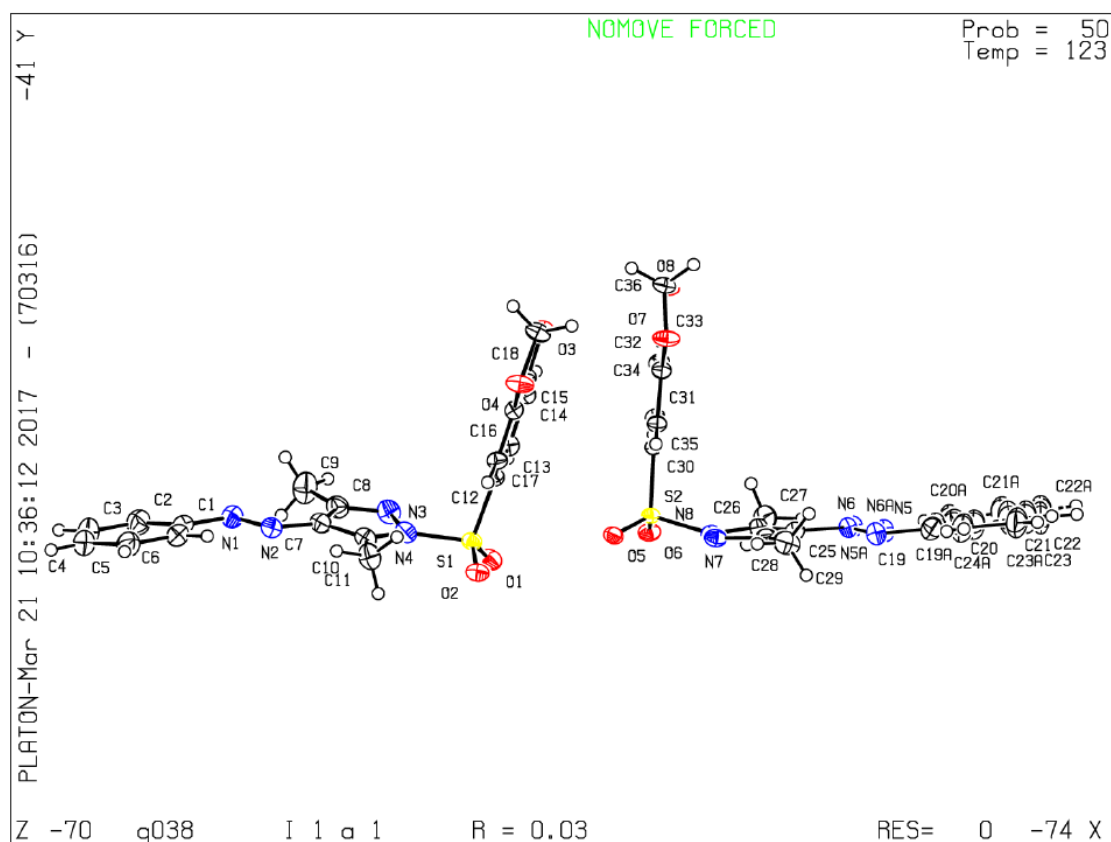
Formula	C ₁₁ H ₁₂ N ₄ O
$D_{\text{calc.}}/\text{g cm}^{-3}$	1.325
μ/mm^{-1}	0.735
Formula Weight	216.25
Colour	clear light yellow
Shape	prism
Size/mm ³	0.25×0.08×0.06
T/K	122.99(10)
Crystal System	monoclinic
Space Group	C2/c
$a/\text{\AA}$	11.1476(2)
$b/\text{\AA}$	9.5888(2)
$c/\text{\AA}$	20.3006(4)
$\alpha/^\circ$	90
$\beta/^\circ$	92.376(2)
$\gamma/^\circ$	90
$V/\text{\AA}^3$	2168.11(7)
Z	8
Z'	1
Wavelength/ \AA	1.54184
Radiation type	CuK α
$\theta_{\text{min}}/^\circ$	4.360
$\theta_{\text{max}}/^\circ$	73.758
Measured Refl.	23381
Independent Refl.	2182
Reflections Used	1890
R_{int}	0.0488
Parameters	157
Restraints	0
Largest Peak	0.223
Deepest Hole	-0.249
GooF	1.035
wR_2 (all data)	0.0985
wR_2	0.0941
R_1 (all data)	0.0414
R_1	0.0357

Compound **12**

Experimental. Single clear yellow prism-shaped crystals of **12** were obtained by recrystallisation from CH_2Cl_2 . A suitable crystal ($0.23 \times 0.12 \times 0.11$) mm^3 was selected and mounted on a MITIGEN holder oil on a SuperNova, Single source at offset, Atlas diffractometer. The crystal was kept at $T = 122.99(12)$ K during data collection. Using Olex2,^[37] the structure was solved with the ShelXT^[38] structure solution program, using the Intrinsic Phasing solution method. The model was refined with ShelXL^[39] using Least Squares minimization.

Crystal Data. $\text{C}_{18}\text{H}_{16}\text{N}_4\text{O}_4\text{S}$, $M_r = 384.41$, monoclinic, Ia (No. 9), $a = 12.34620(10)$ Å, $b = 8.95780(10)$ Å, $c = 32.9428(4)$ Å, $\beta = 98.9220(10)^\circ$, $a = \gamma = 90^\circ$, $V = 3599.22(7)$ Å³, $T = 122.99(12)$ K, $Z = 8$, $Z' = 2$, $\mu(\text{CuK}\alpha) = 1.891$, 39474 reflections measured, 7168 unique ($R_{\text{int}} = 0.0328$) which were used in all calculations. The final wR_2 was 0.0707 (all data) and R_1 was 0.0262 ($I > 2(I)$).

Cambridge Structural Database CCDC. 1942441



Detailed Crystal Data.

Formula	C ₁₈ H ₁₆ N ₄ O ₄ S
$D_{calc.}/\text{g cm}^{-3}$	1.419
μ/mm^{-1}	1.891
Formula Weight	384.41
Colour	clear yellow
Shape	prism
Max Size/mm	0.23
Mid Size/mm	0.12
Min Size/mm	0.11
T/K	122.99(12)
Crystal System	monoclinic
Flack Parameter	0.012(8)
Hooft Parameter	0.000(3)
Space Group	Ia
$a/\text{\AA}$	12.34620(10)
$b/\text{\AA}$	8.95780(10)
$c/\text{\AA}$	32.9428(4)
$\alpha/^\circ$	90
$\beta/^\circ$	98.9220(10)
$\gamma/^\circ$	90
$V/\text{\AA}^3$	3599.22(7)
Z	8
Z'	2
$\Theta_{min}/^\circ$	5.121
$\Theta_{max}/^\circ$	73.726
Measured Refl.	39474
Independent Refl.	7168
Reflections Used	7014
R_{int}	0.0328
Parameters	540
Restraints	194
Largest Peak	0.263
Deepest Hole	-0.182
GooF	1.016
wR_2 (all data)	0.0707
wR_2	0.0700
R_1 (all data)	0.0270
R_1	0.0262

5.6 References

- [1] W. A. Velema, W. Szymanski, B. L. Feringa, *J. Am. Chem. Soc.* **2014**, *136*, 2178-2191.
- [2] K. Hüll, J. Morstein, D. Trauner, *Chem. Rev.* **2018**, *118*, 10710-10747.
- [3] J. Morstein, D. Trauner, *Curr. Opin. Chem. Biol.* **2019**, *50*, 145-151.
- [4] M. M. Lerch, M. J. Hansen, G. M. van Dam, W. Szymanski, B. L. Feringa, *Angew. Chem. Int. Ed.* **2016**, *55*, 10978-10999.
- [5] H. Cheng, J. Yoon, H. Tian, *Coord. Chem. Rev.* **2018**, *372*, 66-84.
- [6] J. Broichhagen, J. A. Frank, D. Trauner, *Acc. Chem. Res.* **2015**, *48*, 1947-1960.
- [7] D. Fornasari, *Pain Ther.* **2017**, *6*, 25-33.
- [8] P. Klán, T. Šolomek, C. G. Bochet, A. Blanc, R. Givens, M. Rubina, V. Popik, A. Kostikov, J. Wirz, *Chem. Rev.* **2013**, *113*, 119-191.
- [9] M. J. Hansen, W. A. Velema, M. M. Lerch, W. Szymanski, B. L. Feringa, *Chem. Soc. Rev.* **2015**, *44*, 3358-3377.
- [10] C. Brieke, F. Rohrbach, A. Gottschalk, G. Mayer, A. Heckel, *Angew. Chem. Int. Ed.* **2012**, *51*, 8446-8476.
- [11] J. Broichhagen, A. Damijonaitis, J. Levitz, K. R. Sokol, P. Leippe, D. Kontrad, E. Y. Isacoff, D. Trauner, *ACS Cent Sci.* **2015**, *1*, 383-393.
- [12] W. Szymanski, J. M. Beierle, H. A. V. Kistemaker, W. A. Velema, B. L. Feringa, *Chem. Rev.* **2013**, *113*, 6114-6178.
- [13] O. Sadovski, A. A. Beharry, F. Zhang, G. A. Woolley, *Angew. Chem. Int. Ed. Engl.* **2009**, *48*, 1484-1486.
- [14] A. A. Beharry, G. A. Woolley, *Chem. Soc. Rev.* **2011**, *40*, 4422-4437.
- [15] D. Bléger, S. Hecht, *Angew. Chem. Int. Ed.* **2015**, *54*, 11338-11349.
- [16] G. S. Hartley, *Nature* **1937**, *140*, 281.

- [17] C. Schütt, G. Heitmann, T. Wendler, B. Krahwinkel, R. Herges, *J. Org. Chem.* **2016**, *81*, 1206-1215.
- [18] C. E. Weston, R. D. Richardson, P. R. Haycock, A. J. P. White, M. J. Fuchter, *J. Am. Chem. Soc.* **2014**, *136*, 11878-11881.
- [19] R. D. Taylor, M. MacCoss, A. D. G. Lawson, *J. Med. Chem.* **2014**, *57*, 5845-5859.
- [20] H. Bregman, J. R. Simard, K. L. Andrews, S. Ayube, H. Chen, H. Gunaydin, A. Guzman-Perez, J. Hu, L. Huang, X. Huang, P. H. Krolikowski, S. G. Lehto, R. T. Lewis, K. Michelsen, P. Pegman, M. H. Plant, P. L. Shaffer, Y. Teffera, S. Yi, M. Zhang, J. Gingras, E. F. DiMauro, *J. Med. Chem.* **2017**, *60*, 1105-1125.
- [21] X. Huang, P. L. Shaffer, S. Ayube, H. Bregman, H. Chen, S. G. Lehto, J. A. Luther, D. J. Matson, S. I. McDonough, K. Michelsen, M. H. Plant, S. Schneider, J. R. Simard, Y. Teffera, S. Yi, M. Zhang, E. F. DiMauro, J. Gingras, *Nat. Struct. Mol. Biol.* **2017**, *24*, 108-113.
- [22] M. Schönberger, A. Damijonaitis, Z. Zhang, D. Nagel, D. Trauner, *ACS Chem. Neurosci.* **2014**, *5*, 514-518.
- [23] S. Pittolo, X. Gómez-Santacana, K. Eckelt, X. Rovira, J. Dalton, C. Goudet, J. P. Pin, A. Llobet, J. Giraldo, A. Llebaria, P. Gorostiza, *Nat. Chem. Biol.* **2014**, *10*, 813-815.
- [24] C. F. Burgos, G. E. Yévenes, L. G. Aguayo, *Mol. Pharmacol.* **2016**, *90*, 318-325.
- [25] C.-M. Becker, *The Neuroscientist* **1995**, *1*, 130-141.
- [26] J. W. Lynch, *Physiol. Rev.* **2004**, *84*, 1051-1095.
- [27] J. W. Lynch, Y. Zhang, S. Talwar, A. Estrada-Mondragon, *Adv. Pharmacol.* **2017**, *79*, 225-253.
- [28] A. M. J. Gomila, K. Rustler, G. Maleeva, A. Nin-Hill, D. Wutz, A. Bautista-Barrufet, X. Rovira, M. Bosch, E. Mukhametova, M. Mukhamedyarov, F. Peiretti,

M. Alfonso-Prieto, C. Rovira, B. König, P. Bregestovski, P. Gorositz, *bioRxiv* **2019**, <http://dx.doi.org/10.1101/744391>.

[29] W. D. Miller, E. V. P. Tao, Patent **1995**, Synthesis of bicyclic aromatic sulfonic acids sulfonyl chlorides and sulfonamides, *US5387681A*.

[30] L. Stricker, E. C. Fritz, M. Peterlechner, N. L. Doltsinis, B. J. Ravoo, *J. Am. Chem. Soc.* **2016**, *138*, 4547-4554.

[31] P. J. Conn, C. W. Lindsley, C. R. Hopkins, C. M. Nilswender, R. D. Gogliotti, Patent **2011**, MGLUR4 Allosteric Potentiators, Compositions, and Methods of Treating Neurological Dysfunction, *WO/2011/050305*.

[32] P. D. Nieuwkoop, J. Faber, *Normal table of Xenopus laevis (Daudin): A Systematical and Chronological Survey of the Development from the Fertilized Egg till the end of Metamorphosis*. **1994**.

[33] M. D. Hanwell, D. E. Curtis, D. C. Lonie, T. Vandermeersch, E. Zurek, G. R. Hutchison, *J. cheminformatics* **2012**, *4*(1), 17.

[34] O. Trott, A. J. Olson, *J. Comp. Chem.* **2010**, *31*(2), 455-461.

[35] J. D. Durrant, J. A. McCammon, *J. Mol. Graph. Model.* **2011**, *29*(6), 888-893.

[36] W. Humphrey, A. Dalke, K. Schulten, *J. Mol. Graph. Model.* **1996**, *14*(1), 33-38.

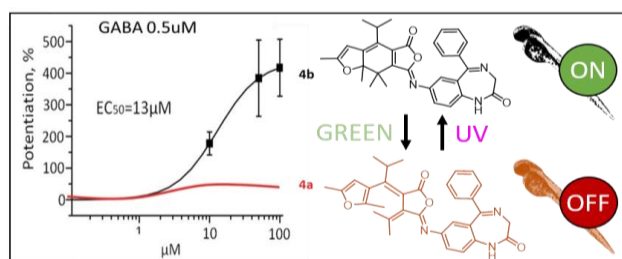
[37] O.V. Dolomanov, L.J. Bourhis, R.J. Gildea, J.A.K. Howard, H. Puschmann, *J. Appl. Cryst.* **2009**, *42*, 339-341.

[38] G. M. Sheldrick, *Acta Cryst.* **2015**, *A71*, 3-8.

[39] G. M. Sheldrick, *Acta Cryst.* **2015**, *C27*, 3-8.

CHAPTER 6

6 Fulgazepam: A Fulgimide-Based Potentiator of GABA_A Receptors



This chapter has been published as:

K. Rustler, G. Maleeva, A. Gomila-Juaneda, P. Gorostiza, P. Bregestovski, B. König, *ChemRxiv* **2019**, DOI: 10.26434/chemrxiv.9906194.v1.

This research was performed within the framework of the ERASynBio Modulightor project in cooperation with Dr. G. Maleeva (Prof. P. Bregestovski, Aix-Marseille University, France) and A. Gomila-Juaneda (Prof. P. Gorostiza, Institute for Bioengineering of Catalonia, Barcelona Institute of Science and Technology, Barcelona, Spain). K. Rustler performed the synthesis and (photo-)chemical investigation of all compounds. A. Gomila-Juaneda performed *in vivo* studies. Dr. G. Maleeva performed *in vitro* studies. Single crystal X-ray crystallography and mass spectrometry analysis were performed by the analytical department at the University of Regensburg. K. Rustler, A. Gomila-Juaneda, and Dr. G. Maleeva wrote the manuscript and contributed equally to the work. Prof. P. Bregestovski, Prof. P. Gorostiza, and Prof. B. König supervised the project. Prof. P. Bregestovski, Prof. P. Gorostiza, and Prof. B. König are corresponding authors.

6.1 Introduction

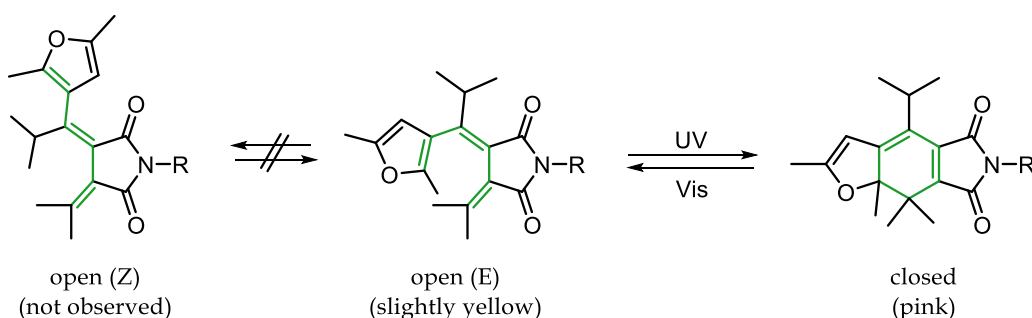
In nature, various receptors and biochemical processes evolved provoked by light.^[1,2] Photons as non-invasive, abundant input signal may trigger a system's response with high spatial and temporal resolution.^[3,4] Their use as a control element for biological systems is highly suitable as light matches perfectly with fast signal transduction, especially of ion channels.^[3-6] One profoundly investigated example is represented by γ -aminobutyric acid (GABA) gated chloride channels, the major mediators of inhibitory neurotransmission in the mammalian central nervous system. Besides GABA_A receptors (GABA_ARs) the Cys-loop family of pentameric ligand-gated ion channels also includes glycine, serotonin and nicotinic acetylcholine receptors.^[7] GABA_ARs display a broad variety regarding their subunit composition and connected physiological functions as cognition, learning, and memory.^[8,9] Owing to their complexity, misfunction of these receptors leads to epilepsy, anxiety, depression and sleep disorders.^[9] Ligand-gated chloride channels, such as GABA type A receptors (GABA_ARs), mediate fast inhibition of neural activity and determine the bulk of synaptic transmission controlling all behavioral relevant circuitry.^[10] Thus, GABA_ARs represent an important drug target and object of current research aiming for suitable therapeutics for improved medical care. For instance, benzodiazepine-based pharmaceuticals act *via* allosteric modulation potentiating GABA_ARs function. Despite successful clinical administration, improved drugs with reduced side effects or tools allowing further receptor investigation and mechanistic studies are desirable.^[11-13]

Light allows superior spatiotemporal resolution and enables delimited manipulation onto protein targets. Several optogenetic strategies have been addressed to control inhibitory (GABA-releasing) neurons, giving much insight on brain-wide inhibitory circuits using photoswitchable tethered ligands (PTLs) – usually needing a genetically engineered cysteine near the GABA-binding site.^[14,15] Another optogenetic approach for inhibitory circuit studies would be to

use light-gated chloride anion channels,^[16,17] although improvement in cell level expression and channel conductance^[18] must be addressed for map circuitry and *in vivo* purposes. Light-caged GABA compounds have shown a remarkable action onto neuronal spines and seizure control. Unfortunately, toxicity levels on neuronal culture must be corrected prior to *in vivo* applications.^[19]

To overcome genetic manipulation, the use of exogenous proteins and non-toxic by-products, we focused on the advantages of photopharmacology to synthesize a photoswitchable modulator for endogenous neurotransmission, inactive prior to irradiation and fully reversible with light. Photopharmacology allows orthogonal control to most cellular processes.^[3-6] Triggered by irradiation with light, a photochromic ligand may reversibly be interconverted between at least two isomeric states with different absorption spectra. Depending on the targeted field of application, various photochromic scaffolds emerged, amongst which azobenzenes, dithienylethenes, and fulgimides are the most prominent examples.^[3-6,20] Our quest for photochromic derivatives of benzodiazepines has led to the serendipitous identification of a pore blocker of GABA_A receptors (Azo-NZ1)^[21], and a selective inhibitor of the structurally related glycine receptors (Glyght).^[22] However, it has failed to preserve the allosteric potentiator profile of GABA_ARs that is characteristic of benzodiazepines. Azobenzenes have been successfully used as photochromic scaffolds for biological applications^[21-28] due to their synthetic accessibility and their large change in geometry and dipole moment upon switching.^[3-6,20,29] However, several drawbacks limit their range of application. Their photoinduced *cis* isomer is thermally bistable and its half-life strongly solvent- and substitution-dependent.^[30,31] Determined by the exact photochromic scaffold, incomplete photoconversion due to a substantial overlap of the absorption maxima of both isomers may be considered, but structural optimization (*e.g.*, arylazo pyrazoles) for a better $n-\pi^*$ and $\pi-\pi^*$ band separation is possible.^[32] Furthermore, the stability of azobenzenes towards glutathione reductase in biological systems is controversial.^[33-35]

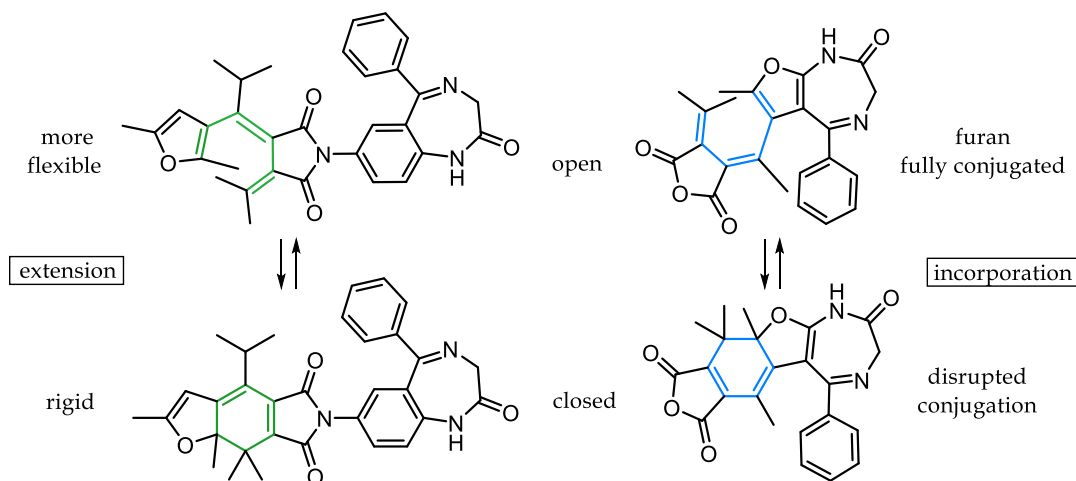
In contrast, dithienylethenes, fulgides and their fulgimide-named amide derivatives generally feature high photostationary states (PSS) with both photoisomers being thermally stable.^[3,20] As dithienylethenes often lack of switching efficiency and stability in polar solvents due to a twisted intramolecular electron charge transfer,^[36-38] fulgi(mi)des were chosen as photochromic scaffold in this study. Both subtypes can be interconverted between their flexible, less-coloured ring-open and their rigid, more coloured ring-closed isomer upon light-induced conrotatory 6π -electrocyclic rearrangement (Scheme 1).^[20,39] Although switching from the open to the closed form is usually triggered using UV light, this might be avoided by the isolation and separate application of both isomers. In addition, this ensures the application of quantitative amounts of either the open or the closed form. Thereby, a biological effect can clearly be assigned to one or the other conformation and enabling a photopharmacological profile corresponding to a pure modulator, without agonist or antagonist^[40,41] or antagonist activities^[42] which could interfere with endogenous neurotransmission. Synthetic investigations revealed the beneficial effects of an isopropyl group in the alpha bridge position of the fulgide, as the *E-Z* isomerization of the open isomer is suppressed due to steric hindrance and consequently only two distinct isomers are observed (Scheme 1).^[43]



Scheme 1. Furan-fulgimide in its open and closed isomeric state interconvertible by irradiation with UV- and visible light.^[20,39]

One advantage of fulgimides over fulgides is their improved switching in aqueous solutions and high stability. Furthermore, the two-step transformation of fulgides towards fulgimides *via* nucleophilic ring-opening of the anhydride by a primary amine and subsequent recyclization allows the smooth introduction of amino-

functionalized biomolecules.^[20,43] Recently, few examples using fulgi(mi)des in a biological context are reported.^[44-46] The transformation of a known ligand into a photoresponsive molecule is typically achieved by either extending the pharmacophore with a photoswitch or *via* incorporation of the photochromic scaffold as part of the drug's chemical structure. Once introduced, ideally one isomeric state is biologically active whereas the other loses its required interactions. In the presented work, both approaches were pursued. On the one hand, a furan-fulgide photochromic scaffold is merged with an amino-benzodiazepine under fulgimide formation (Scheme 2, left panel). A difference in activity arises from the different flexibility of both isomeric states. On the other hand, a functionalized diazepine was synthesized aiming for a photochromic benzodiazepine core (Scheme 2, right panel). The difference in activity was expected to be given by the different conjugation of the pharmacophore's aromatic system upon switching. Unfortunately, the latter modified pharmacophore (compound **9**, Scheme 4) was inactive in patch-clamp studies (data not shown) and the synthesis towards the photoswitch was not further pursued.

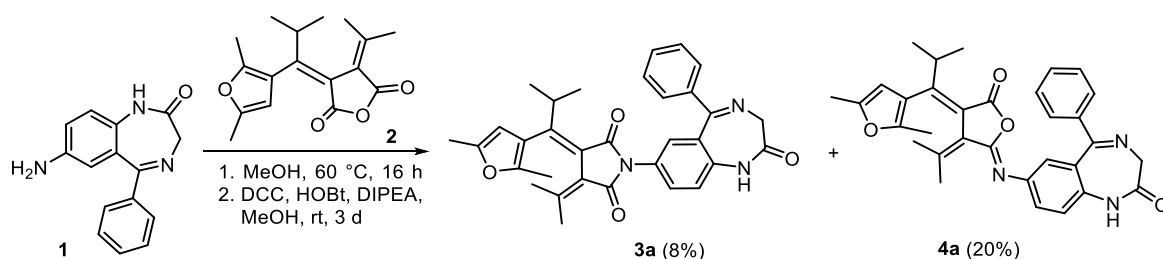


Scheme 2. Left: Pharmacophore nitrazepam and its extension towards a photochromic fulgimide. Right: Derivatization towards a photochromic diazepine fulgide hybrid.

6.2 Results and Discussion

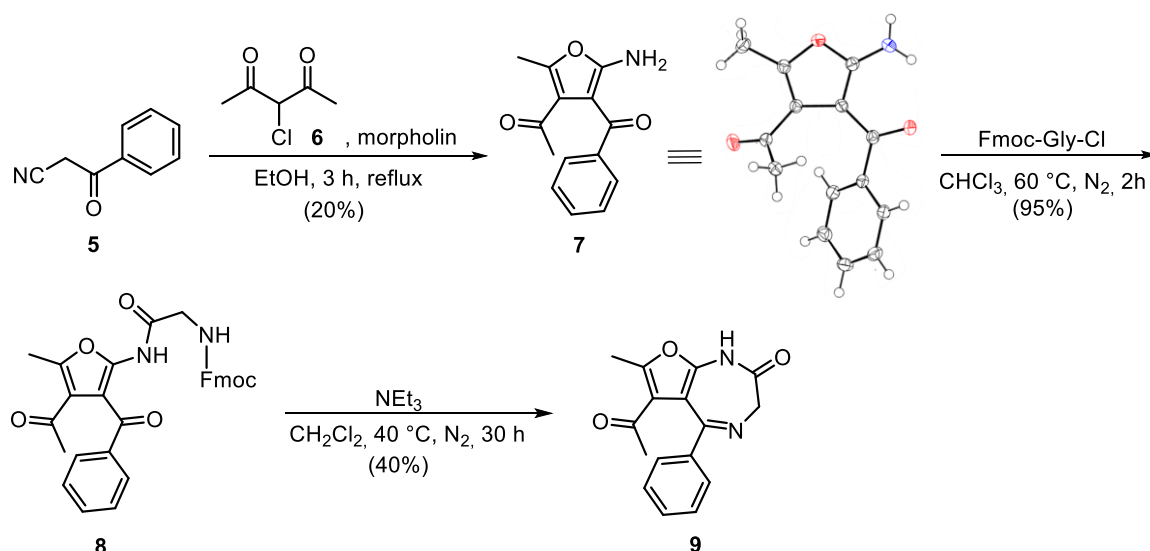
6.2.1 Syntheses

The reaction of furano-fulgide **2**^[45] with amino-nitrazepam **1**^[47] upon addition of dicyclohexylcarbodiimide (DCC), diisopropylethylamine (DIPEA), and 1-hydroxybenzotriazole (HOBt) in methanol afforded the desired benzodiazepine-furano-fulgimide **3a** and its iso-fulgimide derivative **4a**.



Scheme 3. Synthesis of fulgimide-nitrazepam **3a** and its iso-fulgimide derivative **4a**.

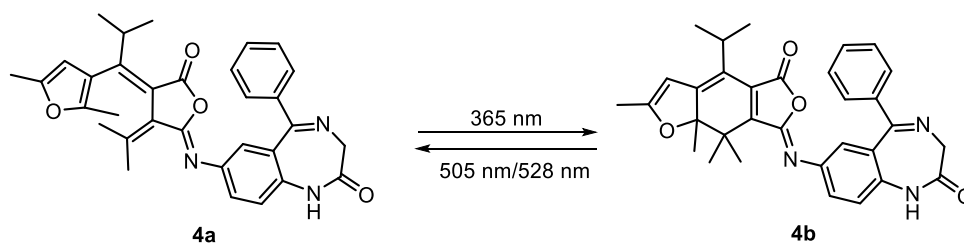
To obtain a photochromic pharmacophore core, we envisioned a functionalized diazepine derivative (**7**) providing an acetyl group in position 3 required for Stobbe^[48-50] condensation towards fulgide formation and a methyl-group in position 2 beneficial for the fulgide's switching performance.^[45] For diazepine formation, the highly functionalized precursor **7** requires in addition a primary amine in position 5 and a phenone substitution in position 4.^[47] Based on the literature known Gewald-reaction^[51] and screening of solvents and bases the desired functionalized furan **7** was obtained in good yield in a one-step synthesis starting from commercially available benzoylacetonitrile **5** and 3-chloroacetylaceton **6** (Scheme 4).^[52,53] The following ring closure required for diazepine formation of **9** was performed in analogy to literature reports.^[47]



Scheme 4. Synthesis of the highly functionalized furan **7** and its diazepine formation towards compound **9**.^[37,44-46]

6.2.2 Photochemical Characterization

The introduction of the bulky isopropyl group on the 1,3,5-hexatriene system of the fulgide avoided the undesired UV light induced *E-Z* isomerization of the open *E*-fulgimide isomer (Scheme 1). Only the *E*-isomer undergoes a photocyclization reaction to the thermally stable closed isomer (Scheme 5). The colorless open isomers **3a** and **4a** were converted to their strongly colored ring closed isomers **3b** and **4b** upon irradiation with UV light of $\lambda = 365$ nm. The absorption maximum of the open isomer around 340 nm decreased and a new maximum around 520 nm representing the closed isomer formed (Figure 1). Both compounds show almost quantitative ring-closing (93% for **3b** and 95% for **4b**, measured 50 μ M in DMSO) and quantitative ring-reopening using green light ($\lambda = 505$ nm or 528 nm).



Scheme 5. Irradiation induced ring-closing (**4b**) and ring-opening (**4a**) of iso-fulgimide **4**.

Figure 1 shows exemplarily the UV-Vis absorption spectrum and cycle performance of iso-fulgimide **4** upon irradiation with 365 nm and 505 nm. Black

arrows indicate the spectral evolution upon irradiation. Dotted black arrows label isosbestic points indicating a clear two component switching. After 10 s irradiation at $\lambda = 365$ nm the closed-PSS was reached and 93% of the closed-isomer are accumulated. Quantitative reopening was achieved within 120 s irradiation at $\lambda = 505$ nm or 528 nm, respectively. Both compounds show a high fatigue resistance over ten measured cycles upon alternate irradiation with 365 nm for closing and 528 nm for opening.

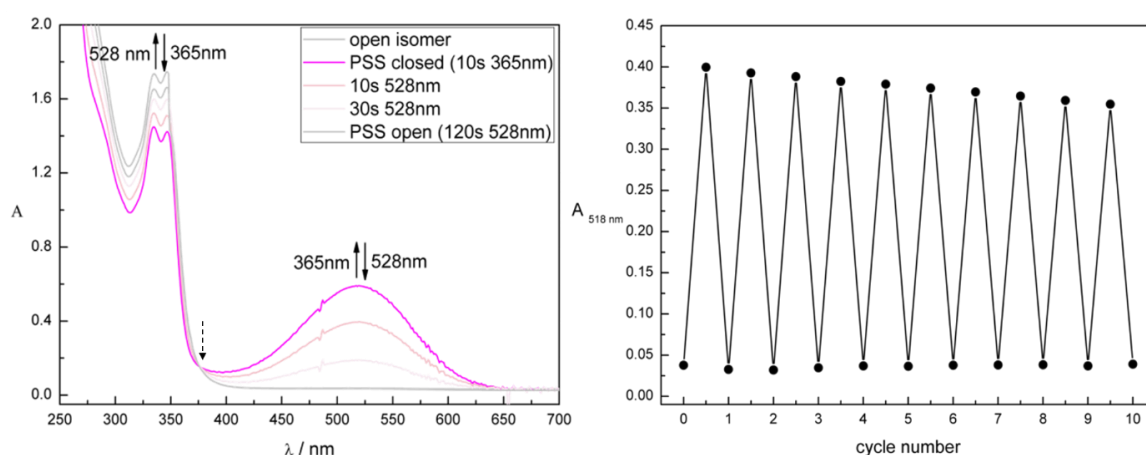


Figure 1. Photochromic properties of iso-fulgimide **4** measured 50 μ M in DMSO. Left: Spectral evolution of **4a** (open isomer; grey spectrum) upon irradiation with 365 nm and re-opening of **4b** (closed isomer; purple spectrum) upon irradiation with 528 nm. Right: Cycle performance of **4** upon alternate irradiation with 365 nm (ring closing) and 528 nm (ring opening) detected at 518 nm (λ_{max} closed isomer).

The photochromic properties of compounds **3** and **4** measured 50 μ M in DMSO are summarized in Table 1. The photostationary states were determined *via* analytical HPLC measurement of an irradiated sample and detected at the wavelength of the isosbestic point.

Table 1. Photochemical properties of fulgimide-based benzodiazepine derivatives **3** and **4** measured 50 μ M in DMSO at 25 °C. Cpd. = Compound. PSS = Photostationary state.

Entry	Cpd.	λ_{max} open [nm]	λ_{max} closed [nm]	Isosbestic point [nm]	PSS
1	3	-	521	375	95% closed (UV); 99% open (green)
2	4	335, 347	518	377	93% closed (UV); 99% open (green)

6.2.3 *In Vitro* Patch-Clamp Testing

All experiments were performed on cells transiently expressing alpha1/beta2/gamma2 subunits of the GABA_A receptor. This receptor possesses the canonical benzodiazepine allosteric site and its EC₅₀ for GABA is about 8 μM.^[21] The effects of the fulgimide-based benzodiazepine derivatives **3** and **4** on the receptor's function were studied upon co-application of 0.5 μM GABA, *i.e.* the concentration, which is below the EC₅₀ (close to EC₃) and allows to observe allosteric potentiation of GABA_AR-mediated currents.^[54]

Application of compound **4a** (open isomer) (10 μM) caused no significant effect on GABA_A-mediated currents, while application of **4b** (closed isomer), generated by pre-irradiation with UV light (365 nm), induced an increase of GABA_A-mediated current amplitudes (Figure 2A). Thus, two different isomers of compound **4** differently interact with GABA_A receptors: being inactive in its open form and potentiatory in its closed form. Analysis of a series of dose-response curves established that the EC₅₀ for **4b** was 13 μM ($n = 6$; Figure 2B).

Figure 2C demonstrates that UV irradiation can induce a live-time switching of compound's **4** conformation and a prominent increase of the amplitude of GABA-induced currents. In average during isomerization of 10 μM of **4a** into **4b** under UV irradiation the currents amplitude increased on 228±41% (Figure 2D; $n = 11$).

Compound **3a** in its open state co-applied with GABA (0.5 μM) induced a powerful potentiation of GABA_AR-mediated currents (Figure S3A). This potentiation was not sensitive to irradiation by UV light and subsequent isomerization to the closed isomer **3b** (Figure S3B) and the kinetics of compound **3b**'s development (slow wash-in and slow wash-out) was similar to the one of **4b**. Application of 10 μM of **3a** increased the current amplitude on 292±65%, while 50 μM of **3a** increased the current amplitude on 544±107% ($n = 11$). The EC₅₀ for **3a** was as well similar to the one of compound **4b** – it comprised 12 μM (Figure S3C, $n = 11$). The degree of the potentiation by **3a** markedly varied for different cells (*cf.* A and B in Figure S3). The similar feature was also characteristic for the action of **4b** on GABA_ARs. We

suggest that this effect reflects the variability in the EC_{50} for GABA on different cells, as it has been shown that allosteric potentiation decreases with an elevation of the effective GABA concentration.^[55]

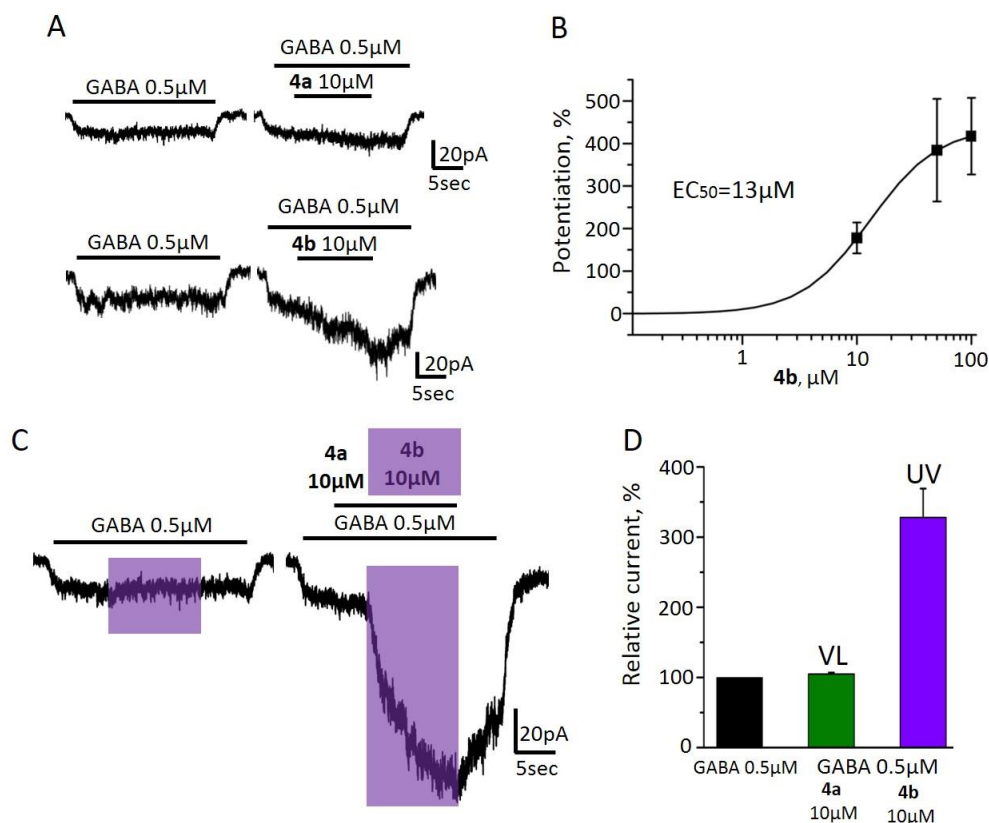


Figure 2. The effect of compounds **4a** and **4b** on GABA_A-mediated currents. (A) Upper panel: representative traces of currents induced by application of GABA 0.5 μM and by mixture of GABA 0.5 μM with **4a** 10 μM; lower panel: representative traces of currents induced by application of GABA 0.5 μM and by mixture of GABA 0.5 μM with **4b** 10 μM. Durations of applications of GABA and compound **4** are indicated by black bars above the traces. (B) Cumulative dose-response curve for the compound **4b** ($n = 6$). (C) Representative traces demonstrating the effect of **4a** upon photoswitching on the amplitude of GABA-induced currents. On the left: current was induced by application of GABA 0.5 μM; on the right: at the same trace current was induced subsequently by GABA 0.5 μM, by a mixture of GABA with **4a** 10 μM at visible light and upon irradiation with UV light (isomerization to **4b**). Duration of UV irradiation is indicated by violet rectangle. Note the prominent increase of the GABA-induced current in the presence of **4** during irradiation with UV light, which triggered ring-closing (**4b**). (D) Cumulative graph representing mean relative amplitude of currents induced by application of GABA 0.5 μM (black column), GABA 0.5 μM + **4a** 10 μM (green column) and GABA 0.5 μM + **4b** 10 μM (violet column) upon irradiation with UV light ($n = 11$).

6.2.4 *In Vivo* Behavioral Studies

Behavioral analysis on zebrafish larvae show that fulgazepam **4** influences their behavior, which is most likely driven by isomerization and can be maintained for

dark periods over time. As both compound states are stable in the dark, larvae behaviors could be studied using pre-irradiated compounds in dark and under direct irradiation using 365 and 500 nm wavelengths. Pre-irradiated solutions showed a dose dependent difference on undisturbed larvae during the resting period, where **4b** at 100 μ M concentration evoked an increase in swimming distance (Figure 3B, top). For all three concentrations of **4a**, UV irradiation (isomerization to **4b**) showed a significant increase in motility, highly potentiated on their following dark periods and reduced to vehicle levels once they were irradiated with visible light (Figure 3A). This photoswitching behavior was also observed for all **4b** concentrations upon irradiation, showing even higher swimming distances over larvae incubated with **4a** (Figure 3B, bottom) and were controlled with visible light. Therefore, these changes in larvae motility are triggered by conformational changes of compound **4** rather than by natural photoresponsive behaviors. An increase in larvae activity over vehicle levels is enhanced when **4b** increases and lowered to natural activities when **4a** is recovered.

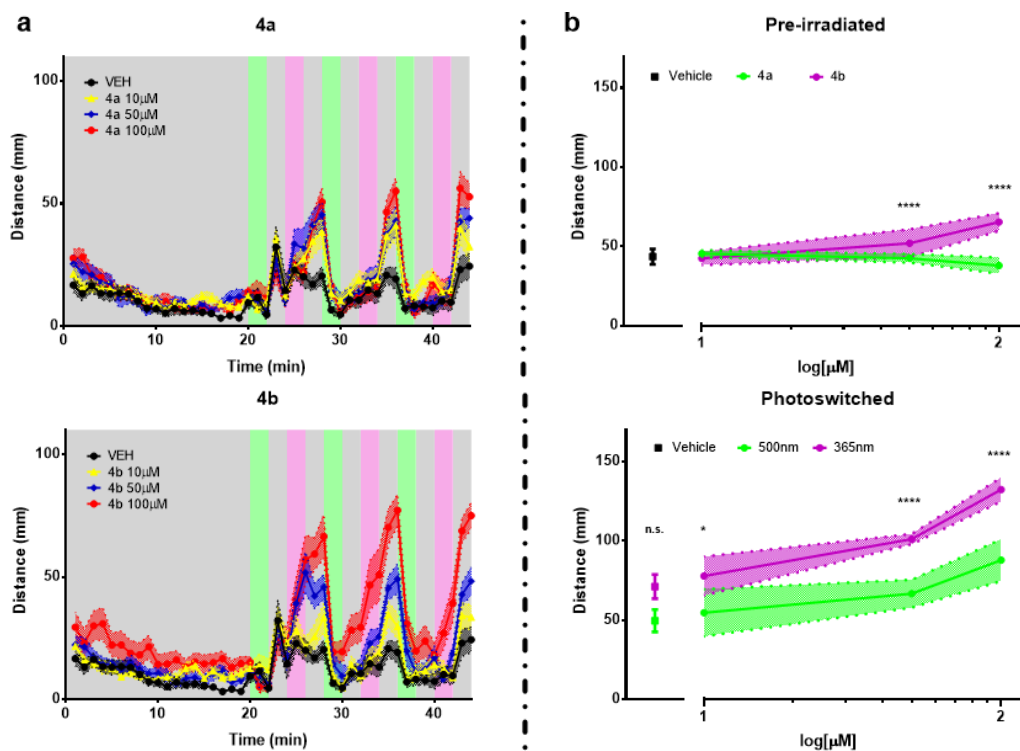


Figure 3. (a) One-minute trajectories of average swimming distances ($n = 12$ per treatment) are shown for vehicle (1% DMSO) and three different concentrations of compound **4** (**4a** (Top) and **4b** (Bottom)). For the first 20 minutes, larvae were undisturbed in complete darkness (Relaxation

period, RP), therefore maintaining stable states. Following RP larvae were irradiated with three consecutive cycles of visible light (500 nm) and UV (365 nm) with discrete dark between each wavelength and compound transit between both conformations. Colored areas show standard error of the mean (S.E.M.). (b) Top: Quantification of swimming distances over the last 5 minutes of the RP (darkness) from two independent experiments ($n = 24$ per treatment) for both pre-irradiated compounds **4a** (green trace) and **4b** (violet trace) and vehicle (1% DMSO). Bottom: Quantification of swimming distances over the light periods after UV irradiation (violet traces) and visible light irradiation (green trace) ($n = 12$ per treatment) for compound **4** and vehicle (1% DMSO). n.s. no significance, * p -value <0.05 , **** p -value <0.0001 . Colored areas show standard deviation (S.D.).

6.3 Conclusion

In summary, we successfully functionalized the benzodiazepine nitrazepam into a light-controllable molecule *via* extension by a photochromic fulgimide and report the first photochromic switch-on potentiator of GABA_A receptors based on a fulgimide scaffold. The synthesized fulgimides **3** and **4** (Fulgazepam) displayed good photochromic properties and high photostationary states. Both fulgimides preserve the GABA_A potentiator behavior that is characteristic of benzodiazepines, indicating that it is a pharmacologically tolerable substitution, in contrast to azobenzenes at the same position. Remarkably, both fulgimides are photochromic but only Fulgazepam **4** enables controlling the pharmacological activity with light. The open conformation of Fulgazepam (**4a**) did not influence the amplitude of GABA-induced currents, while being switched to its closed form **4b** by UV irradiation resulted in a prominent potentiating effect. The open (**4a**) and closed (**4b**) conformation of iso-fulgimide **4** produced different behavioral outcomes on *Danio rerio* larvae. The ring-open isomer **4a** did not alter larvae swimming activities, neither with undisturbed long-term larvae nor upon irradiation cycles. *Vice versa*, the closed conformation **4b** produced an increase in larvae motility in a dose dependent manner during prolonged dark periods and under UV irradiation. Hence, the photoswitching between both conformations of Fulgazepam **4** controls the behavior of larvae, producing high activity swimming upon UV irradiation, which persists for continuous dark periods, and lowering it to control levels upon ring-opening *via* visible light irradiation.

Here we have developed a novel compound to study and control GABA_AR activity. Fulgazepam **4** possesses some unique characteristics as a direct result of its photochromic (fulgimide) and pharmacological (diazepam) moieties: (i) the fulgimide scaffold imparts complete reversible switching of the Fulgazepam conformation; (ii) both Fulgazepam states are stable and can be easily obtained by irradiation with light of the appropriate wavelengths; (iii) Fulgazepam is a soluble photochromic compound successfully used to photocontrol of endogenous GABA_ARs *in vitro* – in its closed form it is a pure potentiator of GABA_ARs without agonist or antagonist activity; (iv) Fulgazepam allows to photocontrol the zebrafish behavior *in vivo*.

6.4 Experimental Part

6.4.1 General Procedures and Materials

Commercial reagents and starting materials were purchased from the commercial suppliers abcr, Acros Organics, Alfa-Aesar, Fisher Scientific, Merck, Sigma Aldrich, TCI, or VWR and used without any further purification. Solvents were used in p.a. quality and dried according to common procedures, if necessary. Dry nitrogen was used as an inert gas atmosphere. Flash column chromatography was performed using Sigma Aldrich MN silica gel 60 M (40-63 μ m, 230-400 mesh) for normal phase chromatography. Reaction monitoring *via* thin layer chromatography was performed on alumina plates coated with silica gel (Merck silica gel 60 F₂₅₄, layer thickness 0.2 mm). Melting points were determined using a Stanford Research System OptiMelt MPA 100 and are uncorrected. NMR spectra were measured on a Bruker Avance 300 (¹H 300.13 MHz, ¹³C 75.48 MHz), Bruker Avance III HD 400 (¹H 400.13 MHz, ¹³C 100.61 MHz), Bruker Avance III HD 600 (¹H 600.25 MHz, ¹³C 150.95 MHz) and Bruker Avance III 600 (¹H 600.25 MHz, ¹³C 150.95 MHz). The spectra are referenced against the NMR-solvent (DMSO-*d*₆: δ_{H} = 2.50 ppm, δ_{C} = 39.52 ppm; CDCl₃-*d*: δ_{H} = 7.26 ppm, δ_{C} = 77.16 ppm) and chemical shifts δ are reported in ppm. Resonance multiplicity is abbreviated as: s (singlet), d (doublet), t (triplet) and m (multiplet). Carbon NMR signals are assigned using

DEPT 135 and ^1H - ^{13}C HSQC spectra with (+) for primary/tertiary, (-) for secondary, and (q) for quaternary carbons. Mass spectra were recorded on a Finnigan MAT-SSQ 710 A, ThermoQuest Finnigan TSQ 7000, Agilent Q-TOF 6540 UHD, or a Jeol AccuTOF GCX instrument. UV-Vis absorption spectroscopy was performed in 10 mm quartz cuvettes using an Agilent Cary 100 or Agilent Varian Cary 50 spectrometer. Analytical HPLC measurements were performed using an Agilent 1220 Infinity LC (column: Phenomenex Luna 3 μm C₁₈(2) 100 Å, 150 x 2.00 mm; flow 0.3 mL min⁻¹ at 30 °C; solvent A: MilliQ water with 0.05 wt% TFA; solvent B: MeCN). The ratios at the PSSs were determined *via* analytical HPLC at 20 °C at the isosbestic points. An Agilent 1260 system (column: Phenomenex Luna 10 μm C₁₈(2) 100 Å, 250 x 21.2 mm; flow: 22 mL min⁻¹; solvent A: MilliQ water with 0.05 wt% TFA; solvent B: MeCN) was used for preparative HPLC purification. Light sources for irradiation: λ = 365 nm (Herolab hand-held lamp UV-6 L, 6W; Seoul Viosys CUN6GB1A, 1000 mA, 1.4 W), λ = 505 nm (Osram LVCK7P-JYKZ, 350 mA, 112 lm), λ = 528 nm (Osram LTCP7P-KXKZ, 350 mA, 71 lm). The power of the light source is given based on the specifications supplied by the company when the LEDs were purchased. All tested final compounds possess a purity $\geq 95\%$ determined by analytical HPLC measurements with detection at 220 nm and 254 nm, respectively. Compounds **1**^[47] and **2**^[45] were synthesized following literature reported procedures.

6.4.2 Synthetic Procedures and Characterization

(Iso-)fulgimide synthesis. A solution of fulgide **2**^[45] (0.25 g, 0.87 mmol, 1.0 eq) and amino-nitrazepam **1**^[47] (0.24 g, 0.96 mmol, 1.1 eq) in methanol (10 mL) was heated to 60 °C and stirred for 16 h. The mixture was cooled to room temperature. Then, DCC (0.23 g, 1.1 mmol, 1.3 eq), HOBT (0.15 g, 1.1 mmol, 1.3 eq) and DIPEA (0.20 mL, 0.15 g, 1.1 mmol, 1.3 eq) were added and the mixture stirred at room temperature for three days. The reaction mixture was filtered and concentrated *in vacuo*. Purification by column chromatography (petroleum ether/ethyl acetate 1/1) and

subsequent preparative HPLC (55% - 98% MeCN in 12 min) yielded fulgimide **3a** (t_R = 7.2 min, 8%) and iso-fulgimide **4a** (t_R = 11.2 min, 20%) as slightly yellow solids.

(E)-3-(1-(2,5-dimethylfuran-3-yl)-2-methylpropylidene)-1-(2-oxo-5-phenyl-2,3-dihydro-1H-benzo[e][1,4]diazepin-7-yl)-4-(propan-2-ylidene)pyrrolidine-2,5-dione (3a). M.p.: 115 °C. $^1\text{H-NMR}$ (600 MHz, $\text{DMSO-}d_6$): δ = 10.79 (s, 1H), 7.64 (dd, J = 8.7, 2.3 Hz, 1H), 7.60 – 7.56 (m, 2H), 7.56 – 7.53 (m, 1H), 7.48 (m, 2H), 7.37 (d, J = 8.7 Hz, 1H), 7.33 (d, J = 2.3 Hz, 1H), 6.14 (s, 1H), 4.39 – 4.36 (m, 1H), 4.18 (s, 2H), 2.23 (s, 3H), 2.18 (s, 3H), 1.86 (s, 3H), 1.30 (s, 3H), 1.25 (d, J = 7.1 Hz, 3H), 0.78 (d, J = 6.8 Hz, 3H). $^{13}\text{C-NMR}$ (151 MHz, $\text{DMSO-}d_6$): δ = 169.9 (q), 166.3 (q), 158.3 (q), 158.0 (q), 152.0 (q), 149.7 (q), 148.0 (q), 146.5 (q), 139.3 (q), 131.3 (+), 131.0 (+), 129.7 (+), 129.7 (+), 128.4 (+), 126.5 (q), 125.3 (q), 125.3 (q), 122.8 (q), 122.7 (q), 121.5 (+), 119.2 (q), 106.3 (+), 56.3 (-), 29.1 (+), 26.7 (+), 22.8 (+), 21.5 (+), 20.4 (+), 13.0 (+), 12.5 (+). HRMS (ESI) calcd. for $\text{C}_{32}\text{H}_{31}\text{N}_3\text{O}_4\text{Na}$ $[\text{M}+\text{Na}]^+$: m/z = 544.2207, found 544.2206. MF: $\text{C}_{32}\text{H}_{31}\text{N}_3\text{O}_4$. MW: 521.62 g/mol.

7-(((2Z,4E)-4-(1-(2,5-dimethylfuran-3-yl)-2-methylpropylidene)-5-oxo-3-(propan-2-ylidene)dihydrofuran-2(3H)-ylidene)amino)-5-phenyl-1,3-dihydro-2H-benzo[e][1,4]diazepin-2-one (4a). M.p.: 146 °C. $^1\text{H-NMR}$ (600 MHz, $\text{DMSO-}d_6$): δ = 12.16 (s, 1H), 7.59 – 7.52 (m, 2H), 7.45 (tt, J = 7.5, 1.3 Hz, 1H), 7.36 (d, J = 8.6 Hz, 1H), 7.32 (d, J = 7.5 Hz, 2H), 7.15 (dd, J = 8.5, 2.2 Hz, 1H), 6.76 (d, J = 2.1 Hz, 1H), 6.11 (s, 1H), 4.35 – 4.31 (m, 1H), 4.02 (s, 2H), 2.21 (s, 3H), 2.13 (s, 3H), 1.84 (s, 3H), 1.28 (s, 3H), 1.22 (d, J = 7.1 Hz, 3H), 0.75 (d, J = 6.8 Hz, 3H). $^{13}\text{C-NMR}$ (101 MHz, $\text{DMSO-}d_6$): δ = 167.2 (q), 158.1 (q), 152.1 (q), 150.2 (q), 148.2 (q), 146.8 (q), 135.0 (q), 135.0 (q), 131.9 (q), 130.2 (+), 123.0 (+), 128.5 (+), 126.6 (q), 124.5 (+), 123.4 (q), 123.3 (q), 122.2 (q), 122.0 (+), 119.7 (q), 118.3 (q), 115.7 (+), 110.0 (-), 106.8 (+), 29.5 (+), 27.1 (+), 23.3 (+), 21.9 (+), 20.9 (+), 13.5 (+), 13.0 (+). HRMS (ESI) calcd. for $\text{C}_{32}\text{H}_{31}\text{N}_3\text{O}_4\text{Na}$ $[\text{M}+\text{Na}]^+$: m/z = 544.2207, found 544.2210. MF: $\text{C}_{32}\text{H}_{31}\text{N}_3\text{O}_4$. MW: 521.62 g/mol.

1-(5-amino-4-benzoyl-2-methylfuran-3-yl)ethan-1-one (7). Morpholine (2.9 g, 33 mmol, 1.1 eq) was added to a suspension of benzoylacetonitrile (4.4 g, 30 mmol, 1.0 eq) in EtOH (30 mL). 3-Chloro-2,4-diketo-pentan (4.0 g, 30 mmol, 1.0 eq) was

added dropwise. The solution was heated to reflux for three hours.^[51-53] Evaporation of the solvent and purification by column chromatography (petroleum ether/ethyl acetate 1/1) afforded the desired product as yellow solid (1.5 g, 6.0 mmol, 20%). M.p.: 86 °C. ¹H-NMR (400 MHz, CDCl₃-*d*): δ = 7.65 – 7.58 (m, 2H), 7.52 – 7.45 (m, 1H), 7.42 – 7.35 (m, 2H), 6.29 (s, 2H), 2.30 (s, 3H), 1.58 (s, 3H). ¹³C-NMR (101 MHz, CDCl₃-*d*): δ = 196.9 (q), 189.5 (q), 162.6 (q), 146.3 (q), 140.6 (q), 131.8 (+), 128.7 (+), 127.9 (+), 122.8 (q), 97.4 (q), 30.3 (+), 12.4 (+). HRMS (ESI) calcd. for C₁₄H₁₄NO₃ [M+H]⁺: m/z = 244.0968, found 244.0967. MF: C₁₄H₁₃NO₃. MW: 243.26 g/mol.

6-Acetyl-7-methyl-5-phenyl-1,3-dihydro-2H-furo[2,3-*e*][1,4]diazepin-2-one (9).

Compound **9** was synthesized *via* an adapted literature procedure^[47] starting from tetrasubstituted furan **7** (0.50 g, 2.1 mmol, 1.0 eq) and Fmoc-Glycine (0.61 g, 2.1 mmol, 1.0 eq). Purification by column chromatography (CH₂Cl₂ + 10% MeOH) and subsequent preparative HPLC (10% - 98% MeCN in 25 min, t_R = 10.1 min) afforded the desired product as slightly yellow solid (0.23 g, 0.80 mmol, 38% over two steps). M.p.: decomposition over 300 °C. ¹H-NMR (400 MHz, DMSO-*d*₆): δ = 11.32 (s, 1H), 7.72 – 7.67 (m, 2H), 7.60 – 7.54 (m, 1H), 7.50 – 7.45 (m, 2H), 4.57 (s, 2H), 2.30 (s, 3H), 1.93 (s, 3H). ¹³C-NMR (101 MHz, DMSO-*d*₆): δ = 194.4 (q), 188.5 (q), 173.3 (q), 140.1 (q), 139.5 (q), 132.2 (+), 129.2 (q), 128.6 (+), 128.5 (+), 122.1 (q), 100.9 (q), 47.5 (-), 30.3 (+), 11.5 (+). HRMS (ESI) calcd. for C₁₆H₁₅N₂O₃ [M+H]⁺: m/z = 283.1077, found 283.1076. MF: C₁₆H₁₄N₂O₃. MW: 282.30 g/mol.

6.4.3 In Vitro Studies

Cell culture and transfection. GABA_A receptors were heterologously expressed in cultured Chinese hamster ovary (CHO) cells obtained from the American Type Tissue Culture Collection (ATCC, Molsheim, France) that were maintained in culture conditions as previously described.^[56] Cells were simultaneously transfected with cDNAs of alpha1, beta2 and gamma2 subunits (concentrations 0.9-1.2 µg/µl). One day before transfection, cells were plated on the cover slips (12 mm in diameter) and placed inside 35 mm cell culture dishes with 2 ml of

medium. Transfection was performed using the Lipofectamine 3000 protocol (Life Technology, USA). To facilitate identification of transfected cells a green fluorescent protein (GFP, 0.5 µg/µl) was added to the transfection mixture. Electrophysiological recordings were performed in the fluorescent cells 24-72 hours after transfection.

Electrophysiological recordings on CHO cells. Whole-cell recordings were performed at room temperature (20-25 °C) using an EPC-9 amplifier (HEKA Elektronik, Germany). Cells were continuously superfused with external solution containing (mM): NaCl 140, CaCl₂ 2, KCl 2.8, MgCl₂ 4, HEPES 20, glucose 10; pH 7.4; 320-330 mOsm. Intracellular solution used for filling recording pipettes contained (mM): KCl 140, MgCl₂ 2, MgATP 2, HEPES 10, BAPTA (tetrapotassium salt) 2; pH 7.3; 290 mOsm. Recording pipettes were pulled from borosilicate glass capillaries (Harvard Apparatus Ltd, USA) and had resistances of 5-10 MOhms. For the rapid replacement of the solutions, the fast application system was used. Three parallel rectangular tubes (100x100 µm) were positioned 40-50 µm above the recorded cell. The movement of the tubes was controlled by a computer-driven fast exchange system (SF 77A Perfusion Fast-Step, Warner, USA) allowing a 10–90% solution exchange in 3–5 ms, as measured by open electrode controls (1/10 external solution/water). Cells with low input resistance (<150 MOhms) and a rapid run-down (>30% with repetitive application) were excluded from analysis. Recordings were performed at holding potential (V_{hold}) of -30 mV. Pure agonist was applied during five seconds at the beginning and at the end of the trace; the mixture of the agonist with studied compounds was applied during 15 seconds in the middle of the trace. UV light (365 nm) was applied during five seconds in the middle of the trace. UV light emitting diode (Thorlabs) was placed at the distance of 4-5 cm from the recorded cell. The power of UV light was reaching 0.6 mW/mm², which was determined using an optical power meter (Thorlabs).

6.4.4 Behavioral Studies

Animal housing and photoswitchable behavioral assays. Tupfel-Lon *Danio rerio* embryos were raised in darkness for 6 days post fertilization (dpf) in UV filtered tap water in petri dishes (daily cleaned and refilled) at 28.5 °C. Larvae were recorded and video analyzed using the Zebrabox and Zebralab software (ViewPoint Life Sciences). For all experiments, 7 dpf larvae were left undisturbed for 40 minutes in 200 μ L fresh UV filtered water and in darkness. Continuously, 100 μ L were removed and replaced with a double concentrated treatment solution and data and video recording begun. For the first 20 minutes, larvae were kept in darkness measuring basal activity, named as the relaxation period (RP). After the RP, three double light irradiation cycles were applied; 2 minutes 500 nm (visible light) and 2 minutes of darkness followed by 2 minutes of 365 nm (UV light) and 2 minutes of darkness. Hence, it was assured that solutions for compound **4** transit between their respective open (**4a**) and closed states (**4b**). As both opened and closed photostationary states are stable in dark, larvae were applied each solution independently. Original compound solution was received as a full opened state solution and was kept in dark before the addition to larvae wells. Closed state was achieved by irradiating with 365 nm lamp original solution for 5 minutes before the addition as double concentrated solution to larvae. Data and video recording lasted for 48 minutes in order to acquire a RP and light transition measurements.

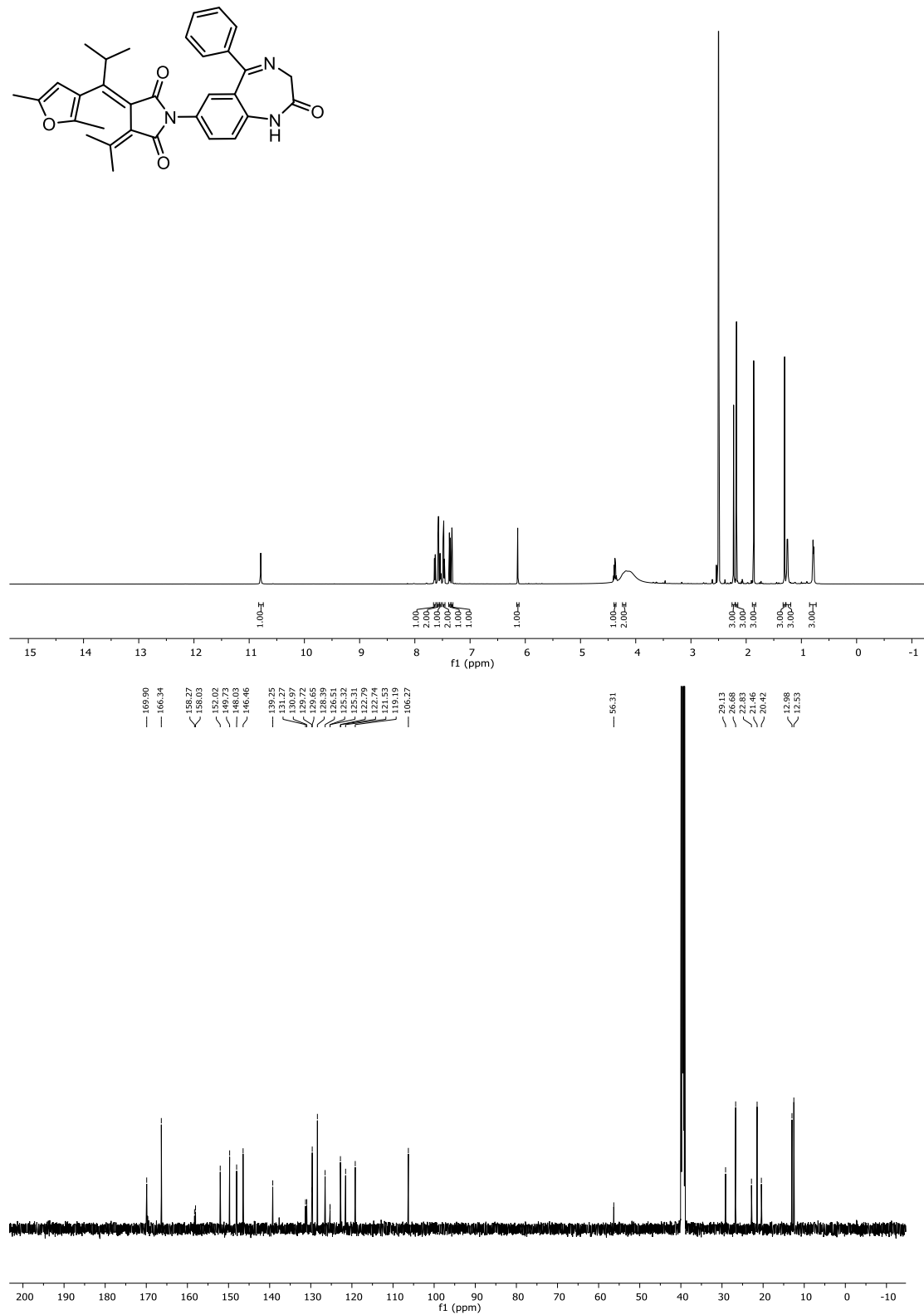
Data analysis and statistics. Zebrafish tracking was performed in real time and data acquisition integrated one-minute intervals using the Zebralab software (ViewPoint Life Science). Data statistical analysis were performed using GraphPad Prism 6 software. Selective irradiation was performed with two ordered based [evenly distributed] arrays of 12 light emitting diodes (LEDs) for each wavelength placed 12 cm afar of the multiwell plate. The light intensities, measured with an optical power meter (model Newport 1916-C), were 5.92 Wm^{-2} for 365 nm (UV) and 2.2 Wm^{-2} for 500 nm (Visible-Blue). Distance activity was measured as the sum of swimming distances (in millimeters) during burst activities (larvae swimming velocities higher than 6 mms^{-1}) over one-minute integration. Data was analyzed

following two-way ANOVA (p-value 0.05) and are presented as mean \pm standard error of the mean (s.e.m.) or standard deviation (s.d.) with the number of larvae (*n*) indicated in each case.

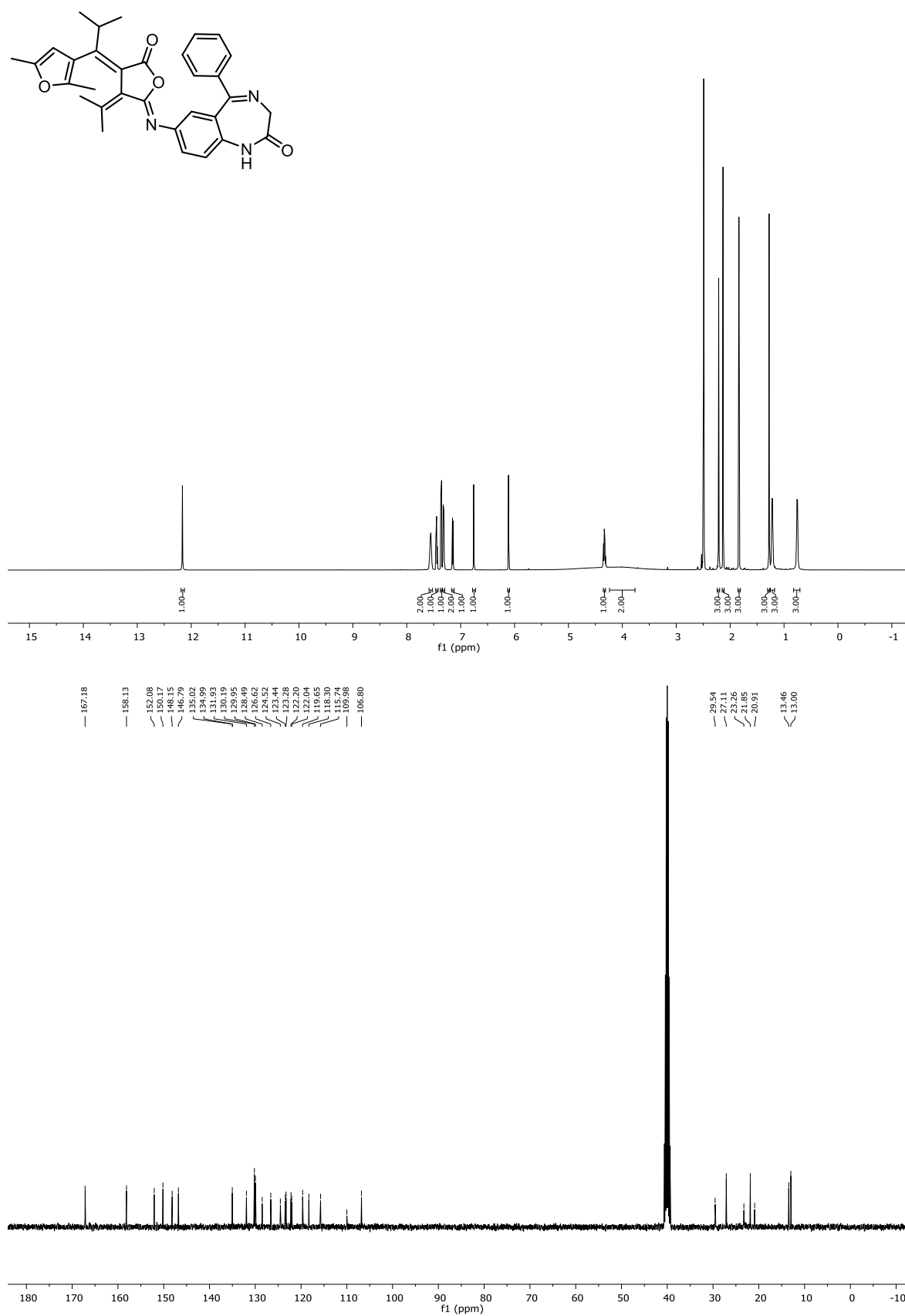
6.5 Supporting Information

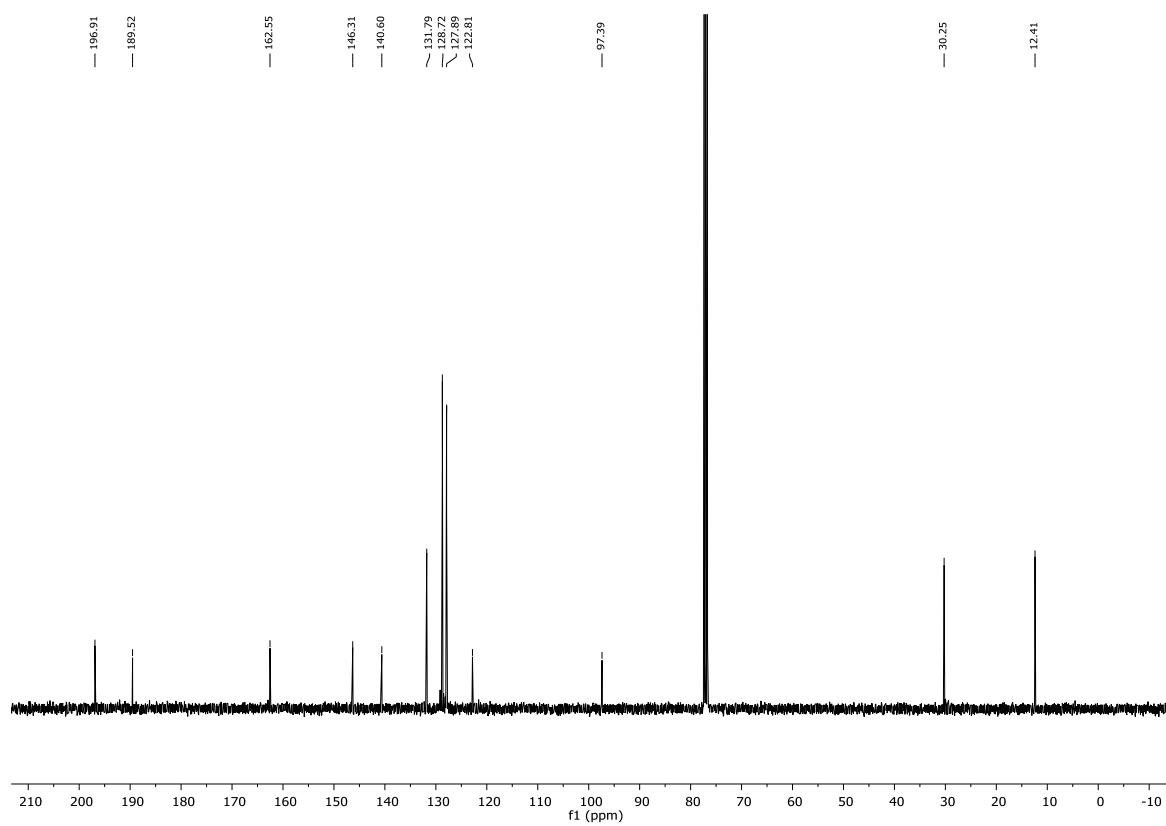
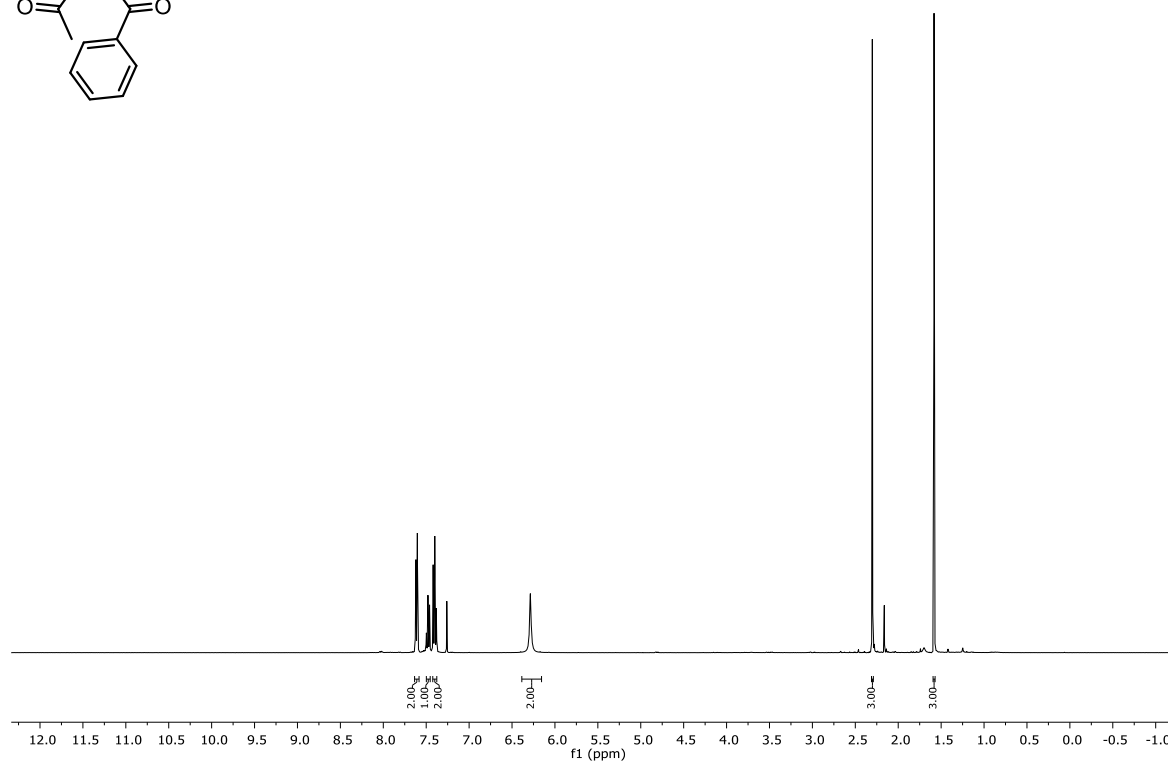
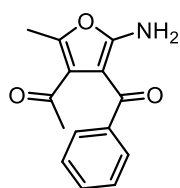
6.5.1 ^1H - and ^{13}C -NMR Spectra

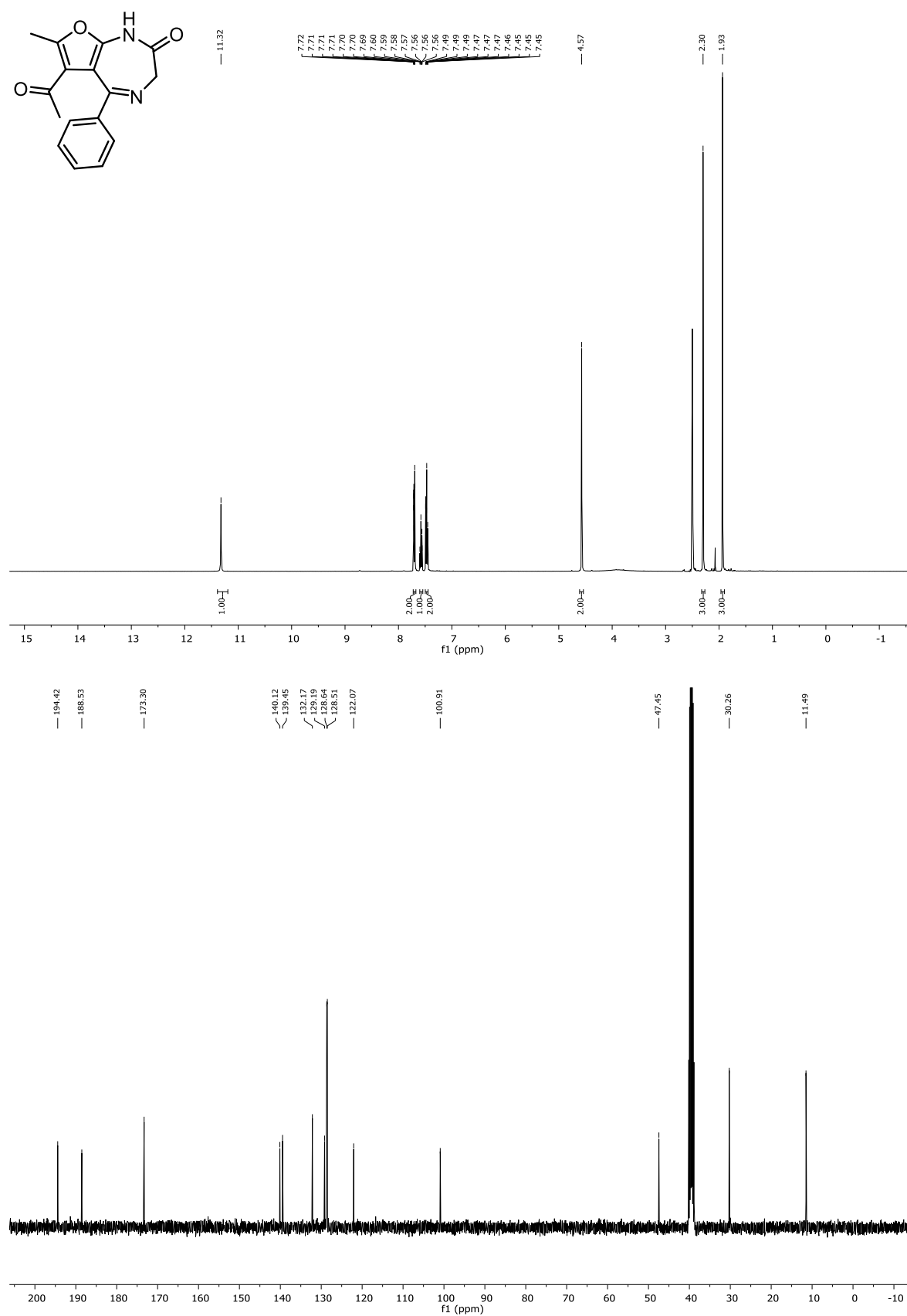
Compound **3a** ($\text{DMSO}-d_6$)



Compound **4a** (DMSO-*d*₆)



Compound 7 (CDCl₃-d)

Compound **9** (DMSO-*d*₆)


6.5.2 UV-Vis Absorption Spectra and Cycle Performances

Compound 3

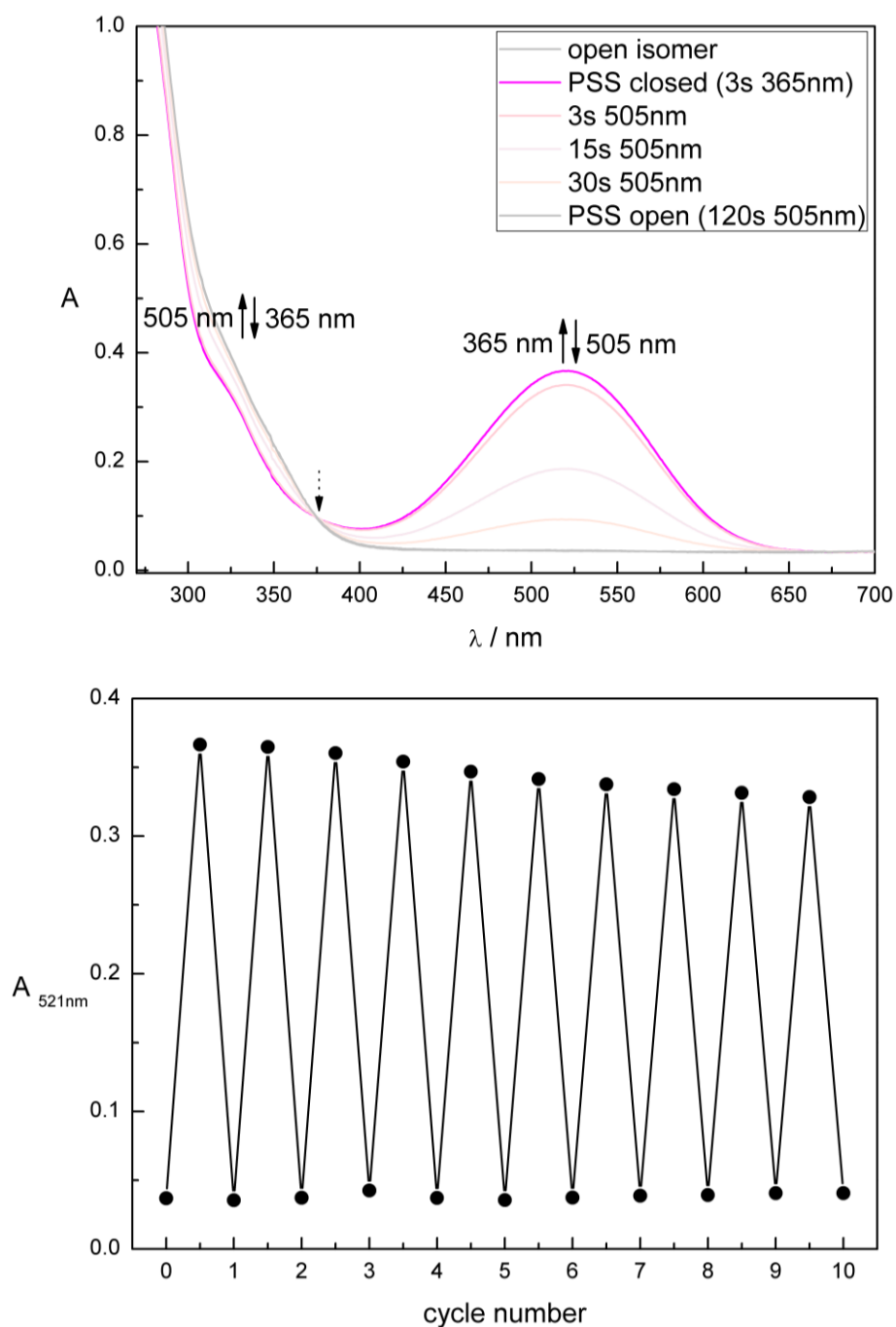


Figure S1. Upper panel: UV-Vis absorption spectrum of fulgimide **3**. Transformation of the colorless ring-open isomer (**3a**) to its purple ring-closed isomer (**3b**) upon irradiation with 365 nm. Reopening upon irradiation with 505 nm. Lower panel: Repetitive cycle performance of **3** upon alternate irradiation with 365 nm and 505 nm.

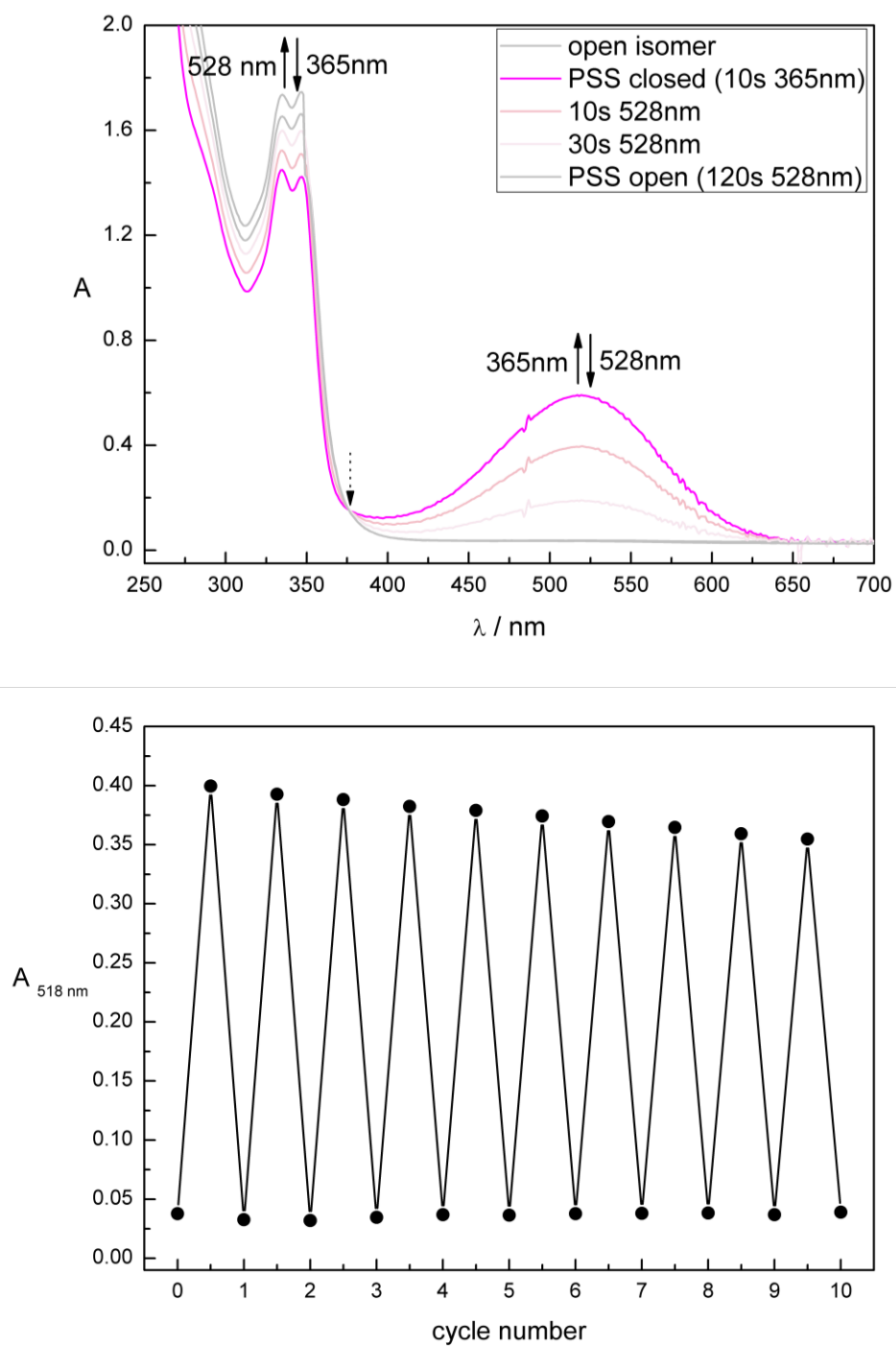
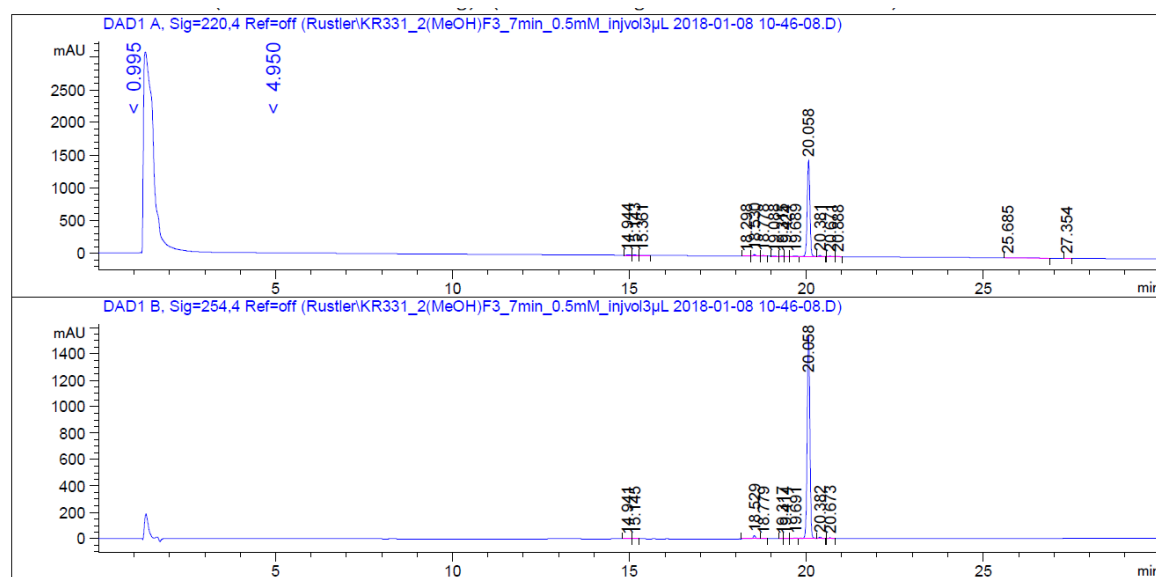
Compound **4**

Figure S2. Upper panel: UV-Vis absorption spectrum of iso-fulgimide **4**. Transformation of the colorless ring-open isomer (**4a**) to its purple ring-closed isomer (**4b**) upon irradiation with 365 nm. Reopening upon irradiation with 528 nm. Lower panel: Repetitive cycle performance of **4** upon alternate irradiation with 365 nm and 528 nm.

6.5.3 Analytical HPLC Traces for Purity Determination

Compound **3a** (0.5 mM in DMSO, injection volume 3 μ L)



Detection at 220 nm: 95% purity

Detection at 254 nm: 97% purity

Signal 1: DAD1 A, Sig=220,4 Ref=off

Peak #	RetTime [min]	Type	Width [min]	Area [mAU*s]	Height [mAU]	Area %
1	14.944	BV	0.1043	20.30099	2.74506	0.2528
2	15.143	VV	0.0929	24.00655	3.95144	0.2989
3	15.361	VB	0.0877	10.76981	1.85496	0.1341
4	18.298	BV	0.0894	16.78782	2.90794	0.2091
5	18.530	VV	0.0819	114.85024	21.65755	1.4302
6	18.778	VB	0.0815	40.79560	7.73744	0.5080
7	19.088	BB	0.1041	9.67722	1.52325	0.1205
8	19.315	BV	0.0854	11.43824	2.03939	0.1424
9	19.424	VB	0.0793	7.09037	1.39420	0.0883
10	19.689	BV T	0.1034	24.48545	3.59901	0.3049
11	20.058	VV R	0.0810	7623.84668	1457.50513	94.9382
12	20.381	VB T	0.0765	59.39925	12.26160	0.7397
13	20.671	BB	0.0790	38.39948	7.58809	0.4782
14	20.888	BB	0.0795	6.37989	1.25011	0.0794
15	25.685	BB	0.1774	16.28838	1.20757	0.2028
16	27.354	BBA	0.0852	5.81392	1.07282	0.0724

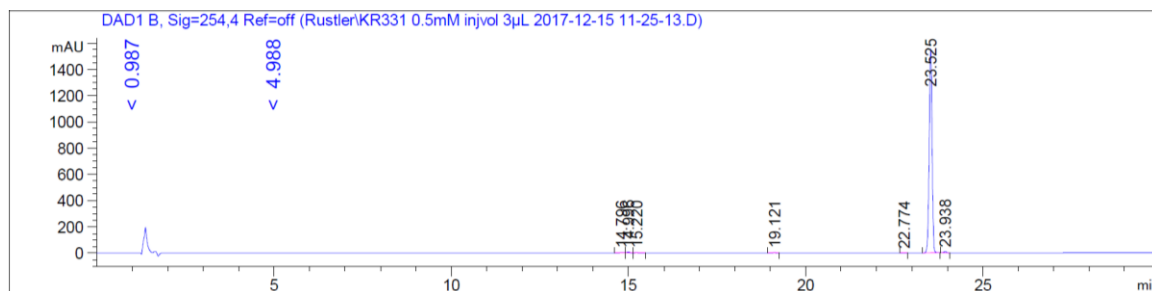
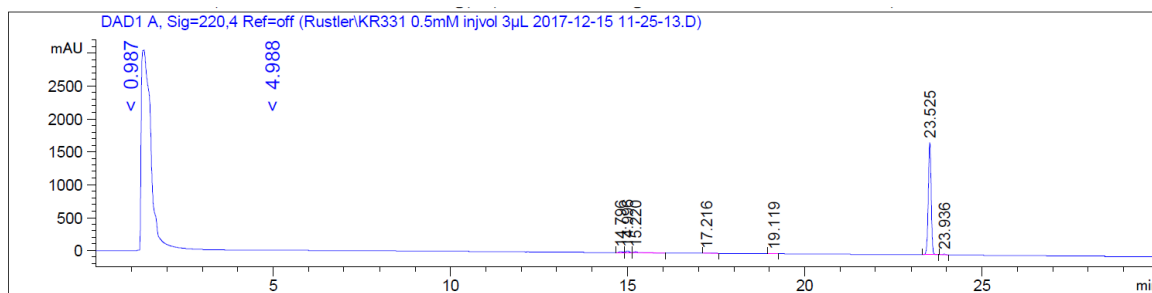
Totals : 8030.32991 1530.29553

Signal 2: DAD1 B, Sig=254,4 Ref=off

Peak #	RetTime [min]	Type	Width [min]	Area [mAU*s]	Height [mAU]	Area %
1	14.941	BV	0.0950	7.74013	1.17203	0.0926
2	15.145	VB	0.0855	6.42651	1.18136	0.0769
3	18.529	VV R	0.0774	127.75799	25.09272	1.5282
4	18.779	VB T	0.0794	10.23114	2.07885	0.1224
5	19.317	BV	0.0767	5.97865	1.18849	0.0715
6	19.414	VB	0.0866	7.49186	1.31197	0.0896
7	19.691	BV T	0.0981	22.28177	3.41614	0.2665
8	20.058	VV R	0.0811	8087.13916	1545.29724	96.7343
9	20.382	VB T	0.0760	51.49631	10.73422	0.6160
10	20.673	BB	0.0771	33.61602	6.63975	0.4021

Totals : 8360.15953 1598.11276

Compound **4a** (0.5 mM in DMSO, injection volume 3 μ L)



Detection at 220 nm: 95% purity

Detection at 254 nm: 98% purity

Signal 1: DAD1 A, Sig=220,4 Ref=off

Peak #	RetTime [min]	Type	Width [min]	Area [mAU*s]	Height [mAU]	Area %
1	14.796	BV	0.1162	118.11269	14.32794	1.1939
2	14.996	VV	0.0994	173.31990	26.13495	1.7519
3	15.220	VB	0.1076	95.90490	13.07767	0.9694
4	17.216	BB	0.1015	11.20386	1.60394	0.1132
5	19.119	BB	0.0875	21.09451	3.64496	0.2132
6	23.525	BB	0.0864	9418.38379	1704.98877	95.1999
7	23.936	BB	0.0900	55.24893	9.48264	0.5584

Totals : 9893.26858 1773.26088

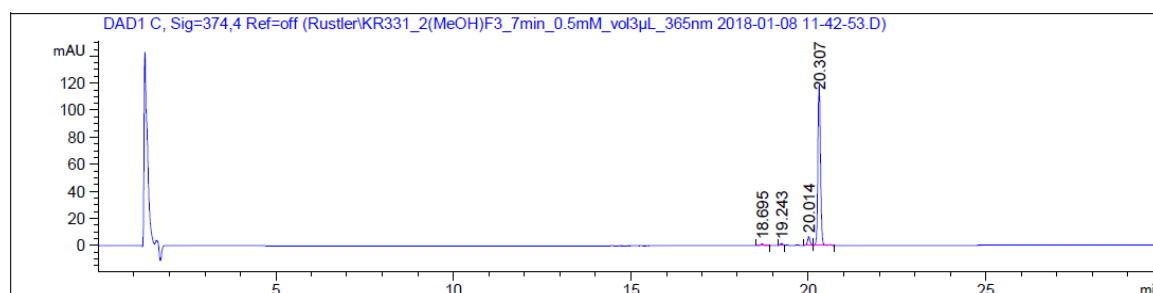
Signal 2: DAD1 B, Sig=254,4 Ref=off

Peak #	RetTime [min]	Type	Width [min]	Area [mAU*s]	Height [mAU]	Area %
1	14.796	BV	0.1202	44.76250	5.21297	0.5071
2	14.996	VV	0.0990	55.74607	8.44625	0.6315
3	15.220	VB	0.0949	26.13252	4.18356	0.2960
4	19.121	BB	0.0875	23.32179	4.03348	0.2642
5	22.774	BB	0.0851	8.56763	1.58528	0.0971
6	23.525	BB	0.0865	8611.23633	1557.81189	97.5530
7	23.938	BB	0.0879	57.47643	10.17249	0.6511

Totals : 8827.24325 1591.44591

6.5.4 Analytical HPLC Traces for PSS Determination

Compound **3** (0.5 mM solution in DMSO, injection volume 3 μ L)



Irradiation with $\lambda = 365$ nm for open \rightarrow closed isomerization.

Detection at 374 nm: t_R open = 20.0 min (5%), t_R closed = 20.3 min (93%)

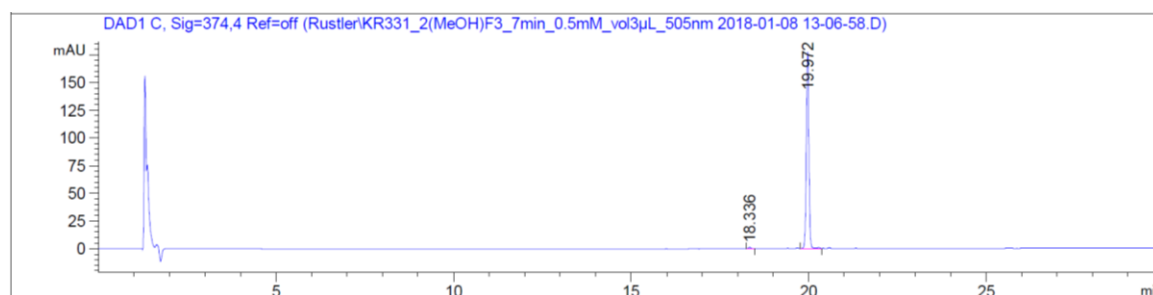
Signal 3: DAD1 C, Sig=374,4 Ref=off

Peak #	RetTime [min]	Type	Width [min]	Area [mAU*s]	Height [mAU]	Area %
1	18.695	BB	0.0741	5.67112	1.17847	0.8531
2	19.243	BB	0.0725	6.11693	1.30850	0.9202
3	20.014	BV	0.0802	33.22660	6.44082	4.9983
4	20.307	VV R	0.0811	619.74103	118.31590	93.2284

Totals : 664.75568 127.24368

Irradiation with $\lambda = 505$ nm for closed \rightarrow open isomerization.

Detection at 374 nm: t_R open = 20.0 min (99%)

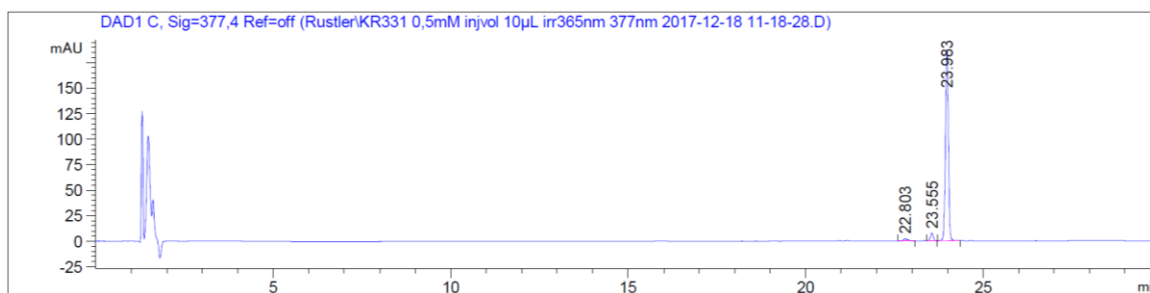


Signal 3: DAD1 C, Sig=374,4 Ref=off

Peak #	RetTime [min]	Type	Width [min]	Area [mAU*s]	Height [mAU]	Area %
1	18.336	BB	0.0684	5.76978	1.28472	0.6268
2	19.972	BV R	0.0782	914.68585	177.40359	99.3732

Totals : 920.45563 178.68832

Compound **4** (0.5 mM solution in DMSO, injection volume 10 μ L)



Irradiation with $\lambda = 365$ nm for open \rightarrow closed isomerization.

Detection at 377 nm: t_R open = 23.6 min (4%), t_R closed = 24.0 min (95%)

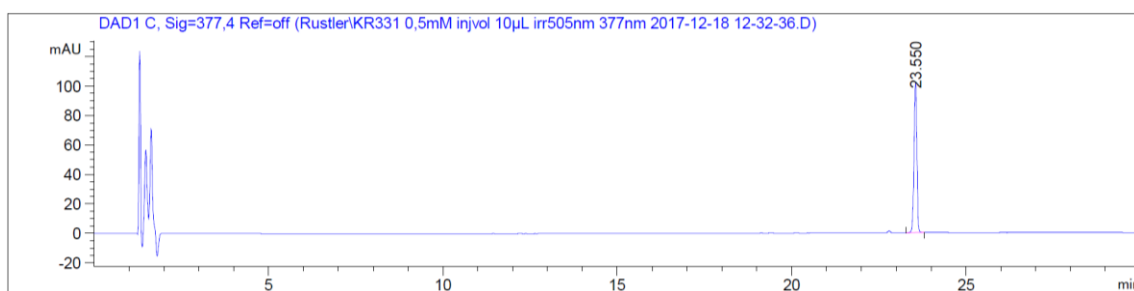
Signal 1: DAD1 C, Sig=377,4 Ref=off

Peak #	RetTime [min]	Type	Width [min]	Area [mAU*s]	Height [mAU]	Area %
1	22.803	BB	0.1073	16.79935	2.24548	1.5172
2	23.555	BB	0.0860	40.16666	7.32464	3.6276
3	23.983	BB	0.0874	1050.27759	187.22672	94.8552

Totals : 1107.24361 196.79684

Irradiation with $\lambda = 505$ nm for closed \rightarrow open isomerization.

Detection at 374 nm: t_R open = 23.6 min (100%)



Signal 1: DAD1 C, Sig=377,4 Ref=off

Peak #	RetTime [min]	Type	Width [min]	Area [mAU*s]	Height [mAU]	Area %
1	23.550	BB	0.0853	571.35895	102.11843	100.0000

Totals : 571.35895 102.11843

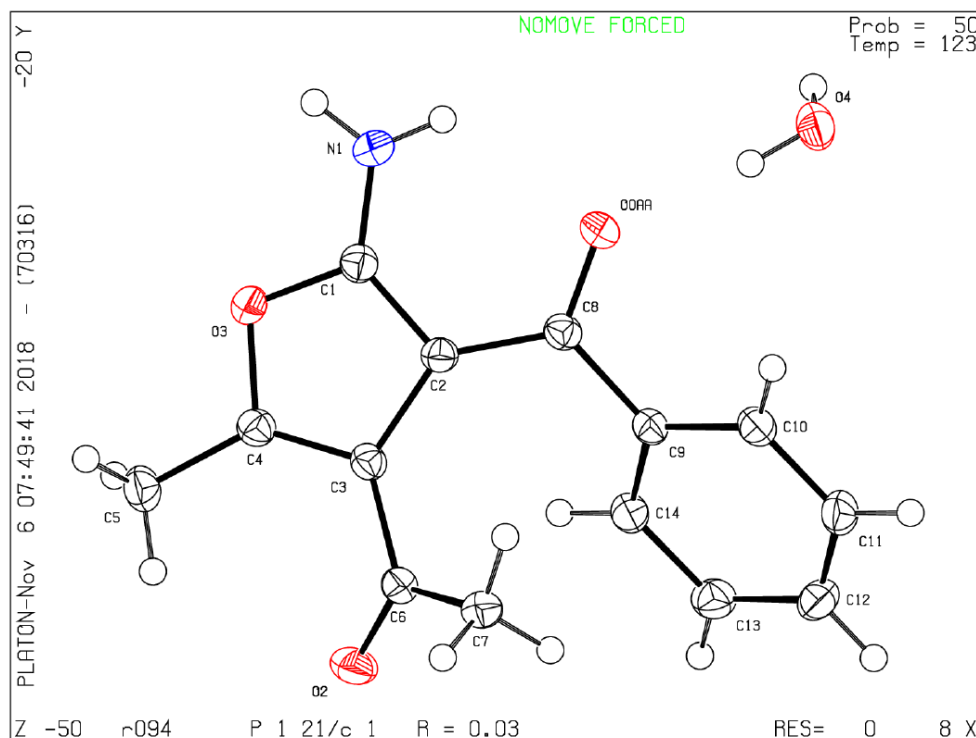
6.5.5 Single Crystal X-ray Crystallography

Compound 7

Experimental. Single metallic yellow prism-shaped crystals of **7** were obtained by recrystallisation from acetone. A suitable crystal $0.23 \times 0.18 \times 0.14 \text{ mm}^3$ was selected and mounted on a MITIGEN holder oil on an GV1000, TitanS2 diffractometer. The crystal was kept at a steady $T = 123.0(3) \text{ K}$ during data collection. The structure was solved with the ShelXT^[57] structure solution program using the Intrinsic Phasing solution method and by using Olex2^[58] as the graphical interface. The model was refined with version 2016/6 of ShelXL^[59] using Least Squares minimisation.

Crystal Data. $\text{C}_{14}\text{H}_{15}\text{NO}_4$, $M_r = 261.27$, monoclinic, $P2_1/c$ (No. 14), $a = 16.7096(5) \text{ \AA}$, $b = 13.2785(2) \text{ \AA}$, $c = 7.0935(2) \text{ \AA}$, $\beta = 126.945(4)^\circ$, $\alpha = \gamma = 90^\circ$, $V = 1257.88(8) \text{ \AA}^3$, $T = 123.0(3) \text{ K}$, $Z = 4$, $Z' = 1$, $\mu(\text{CuK}) = 0.613$, 14196 reflections measured, 2534 unique ($R_{\text{int}} = 0.0216$) which were used in all calculations. The final $wR2$ was 0.0879 (all data) and $R1$ was 0.0333 ($I > 2(I)$).

Cambridge Structural Database CCDC. 1942472



Detailed Crystal Data.

Formula	C ₁₄ H ₁₅ NO ₄
$D_{calc.}/\text{g cm}^{-3}$	1.380
μ/mm^{-1}	0.613
Formula Weight	261.27
Colour	metallic yellow
Shape	prism
Size/mm ³	0.23×0.18×0.14
T/K	123.0(3)
Crystal System	monoclinic
Space Group	$P2_1/c$
$a/\text{\AA}$	16.7096(5)
$b/\text{\AA}$	13.2785(2)
$c/\text{\AA}$	7.0935(2)
$\alpha/^\circ$	90
$\beta/^\circ$	126.945(4)
$\gamma/^\circ$	90
$V/\text{\AA}^3$	1257.88(8)
Z	4
Z'	1
Wavelength/ \AA	1.39222
Radiation type	Cu K
$\theta_{min}/^\circ$	4.240
$\theta_{max}/^\circ$	60.099
Measured Refl.	14196
Independent Refl.	2534
Reflections with $I > 2(I)$	2348
R_{int}	0.0216
Parameters	178
Restraints	0
Largest Peak	0.305
Deepest Hole	-0.217
GooF	1.037
wR_2 (all data)	0.0879
wR_2	0.0862
R_1 (all data)	0.0354
R_1	0.0333

6.5.6 Additional *in Vitro* Patch-Clamp Data of Compound 3

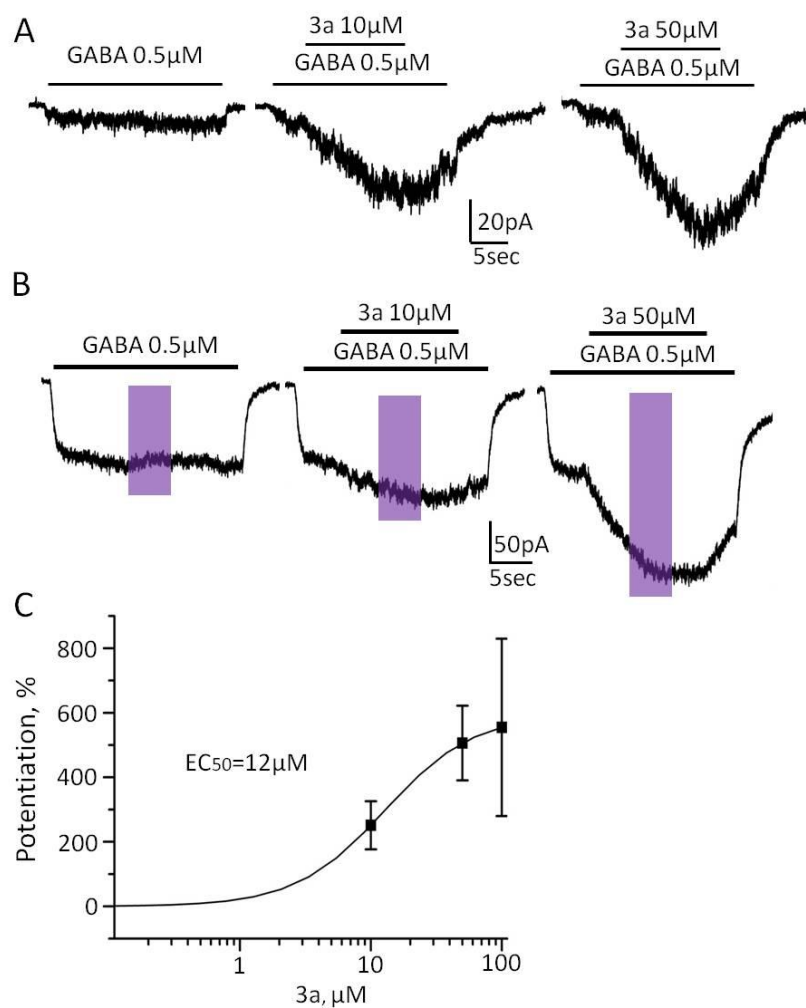


Figure S3. The effect of **3** on GABA_A-mediated currents upon application in its open state (**3a**) and irradiation with UV light for light-triggered ring-closing (highlighted in purple) (**3b**). (A) Representative traces of currents induced by application of GABA 0.5 μ M (left), by mixture of GABA with **3a** 10 μ M (center) and by mixture of GABA with **3a** 50 μ M (right) (B) Representative traces demonstrating the absence of the effect of UV light irradiation (triggering ring closing) on the amplitude of currents induced by application of GABA 0.5 μ M (left), by mixture of GABA with **3a** 10 μ M (center) and by mixture of GABA with **3a** 50 μ M (right). (C) Cumulative dose-response curve for the compound **3a** ($n = 4-11$).

6.6 References

- [1] J. McClendon, *Earth Sci. Rev.* **1999**, 47, 71-93.
- [2] D. W. Deamer, *Mirobiol. Mol. Biol. Rev.* **1997**, 61, 239-261.
- [3] W. Szymanski, J. M. Beierle, H. A. V. Kistemaker, W. A. Velema, B. L. Feringa, *Chem. Rev.* **2013**, 113, 6114-6178.
- [4] W. A. Velema, W. Szymanski, B. L. Feringa, *J. Am. Chem. Soc.* **2014**, 136, 2178-2191.
- [5] K. Hüll, J. Morstein, D. Trauner, *Chem. Rev.* **2018**, 118, 10710-10747.
- [6] J. Broichhagen, J. A. Frank, D. Trauner, *Acc. Chem. Res.* **2015**, 48, 1947-1960.
- [7] T. Lynagh, S. A. Pless, *Front. Physiol.* **2014**, 5 (160), 1-12.
- [8] S. P. H. Alexander, J. A. Peters, E. Kelly, N. Marrion, H. E. Benson, E. Faccenda, A. J. Pawson, J. L. Sharman, C. Southan, J. A. Davies, *Br. J. Pharmacol.* **2015**, 172, 5870-5903.
- [9] G. A. Johnston, M. Chebib, J. R. Hanrahan, K. N. Mewett, *Curr. Drug. Targets CNS Neurol. Disord.* **2003**, 2, 260-268.
- [10] E. Engin, R. S. Benham, U. Rudolph, *Trends Pharmacol. Sci.* **2018**, 39, 710-732.
- [11] W. Sieghart, *Adv. Pharmacol.* **1994**, 98, 11623-11627.
- [12] K. R. Tan, U. Rudolph, C. Lüscher, *Trends neurosci.* **2011**, 34, 188-197.
- [13] W. Sieghart, *Adv. Pharmacol.* **2015**, 72, 53-96.
- [14] W. C. Lin, M. C. Tsai, C. M. Davenport, C. M. Smith, J. Veit, N. M. Wilson, H. Adesnik, R. H. Kramer, *Neuron* **2015**, 88, 879-891.
- [15] W. C. Lin, C. M. Davenport, A. Mourot, D. Vytla, C. M. Smith, K. A. Medeiros, J. J. Chambers, R. H. Kramer, *ACS Chem. Biol.* **2014**, 9, 1414-1419.
- [16] E. G. Govorunova, O. A. Sineshchekov, R. Janz, X. Liu, J. L. Spudich, *Science* **2015**, 349, 647-650.

- [17] J. Wietek, J. S. Wiegert, N. Adeishvili, F. Schneider, H. Watanabe, S. P. Tsunoda, A. Vogt, M. Elstner, T. G. Oertner, P. Hegemann, *Science* **2014**, *344*, 409-412.
- [18] M. Mahn, L. Gibor, P. Patil, K. C.-K. Malina, S. Oring, Y. Printz, R. Levy, I. Lampl, O. Yizhar, *Nat. Commun.* **2018**, *9*, 4125.
- [19] X. Yang, D. L. Rode, D. S. Peterka, R. Yuste, S. M. Rothman, *Ann. Neurol.* **2012**, *71*, 68-75.
- [20] C. Brieke, F. Rohrbach, A. Gottschalk, G. Mayer, A. Heckel, *Angew. Chem. Int. Ed. Engl.* **2012**, *51*, 8446-8476.
- [21] G. Maleeva, D. Wutz, K. Rustler, A. Nin-Hill, C. Rovira, E. Petukhova, A. Bautista-Barrufet, A. Gomila-Juaneda, P. Scholze, F. Peiretti, M. Alfonso-Prieto, B. König, P. Gorostiza, P. Bregestovski, *Brit. J. Pharmacol.* **2019**, *176*, 2661-2677.
- [22] A. M. J. Gomila, K. Rustler, G. Maleeva, A. Nin-Hill, D. Wutz, A. Bautista-Barrufet, X. Rovira, M. Bosch, E. Mukhametova, M. Mukhamedyarov, F. Peiretti, M. Alfonso-Prieto, C. Rovira, B. König, P. Bregestovski, P. Gorositza, *bioRxiv* **2019**, <http://dx.doi.org/10.1101/744391>.
- [23] X. Gómez-Santacana, S. M. de Munnik, P. Vijayachandran, D. Da Costa Pereira, J. P. M. Bebelman, I. J. P. de Esch, H. F. Fischer, M. Wijtmans, R. Leurs, *Angew. Chem. Int. Ed.* **2018**, *57*, 11608-11612.
- [24] N. J. Hauwert, T. A. M. Mocking, D. Da Costa Pereira, A. J. Kooistra, L. M. Wijnen, G. C. M. Vreeker, E. W. E. Verweij, A. H. De Boer, M. J. Smit, C. De Graff, H. F. Vischer, I. J. P. de Esch, M. Wijtmans, R. Leurs, *J. Am. Chem. Soc.* **2018**, *140*, 4232-4243.
- [25] K. Rustler, M. J. Mickert, J. Nazet, R. Merkl, H. H. Gorris, B. König, *Org. Biomol. Chem.* **2018**, *16*, 7430-7437.

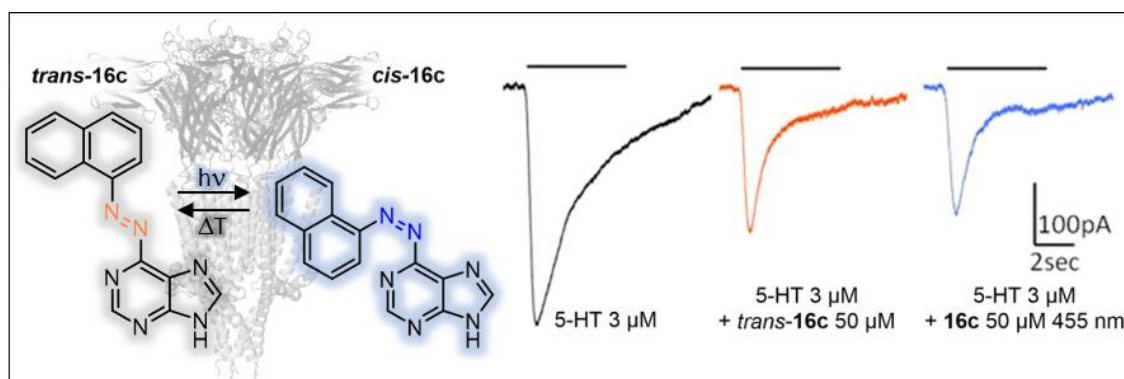
- [26] M. H. Berry, A. Holt, J. Levitz, J. Broichhagen, B. M. Gaub, M. Visel, C. Stanley, K. Aghi, Y. J. Kim, K. Cao, R. H. Kramer, D. Trauner, J. Flannery, E. Y. Isacoff, *Nat. Commun.* **2017**, *8*, 1862-1873.
- [27] B. Eisel, F. W. W. Hartrampf, T. Meier, D. Trauner, *FEBS Letters* **2018**, *592*, 343-355.
- [28] C. Pernpeintner, J. A. Frank, P. Urban, C. R. Roeske, S. D. Pritzl, D. Trauner, T. Lohmüller, *Langmuir* **2017**, *33*, 4083-4089.
- [29] E. Merino, *Chem. Soc. Rev.* **2011**, *40*, 3835-3853.
- [30] P. Bortolus, S. Monti, *J. Phys. Chem.* **1979**, *83*, 648-652.
- [31] T. Halicioglu, O. Sinanoglu, *Ann. N. Y. Acad. Sci.* **1969**, *158*, 308-317.
- [32] C. E. Weston, R. D. Richardson, P. R. Haycock, A. J. P. White, M. J. Fuchter, *J. Am. Chem. Soc.* **2014**, *136*, 11878-11881.
- [33] S. Samanta, A. A. Beharry, O. Sadovski, T. M. McCormick, A. Babalhavaeji, V. Tropepe, G. A. Wooley, *J. Am. Chem. Soc.* **2013**, *135*, 9777-9784.
- [34] S. Samanta, T. M. McCormick, S. K. Schmidt, D. S. Seferos, G. A. Woolley, *Chem. Commun.* **2013**, *49*, 10314-10316.
- [35] A. Heckel, G. Mayer, *The chemical biology of nucleic acids* **2010**, 279-306.
- [36] T. Yamaguchi, K. Uchida, M. Irie, *J. Am. Chem. Soc.* **1997**, *119*, 6066-6071.
- [37] M. Irie, K. Sayo, *J. Phys. Chem.* **1992**, *96*, 7671-7674.
- [38] C. Fleming, P. Remón, S. Li, N. A. Simeth, B. König, M. Grøtli, J. Andréasson, *Dyes Pigm.* **2017**, *137*, 410-420.
- [39] A. Santiago, R. S. Becker, *J. Am. Chem. Soc.* **1968**, *90*, 3654-3658.
- [40] M. Stein, S. J. Middendorp, V. Carta, E. Pejo, D. E. Raines, S. A. Forman, E. Sigel, D. Trauner, *Angew. Chem. Int. Ed.* **2012**, *51*, 10500-10504.

- [41] L. Yue, M. Pawlowski, S. S. Dellal, A. Xie, F. Feng, T. S. Otis, K. S. Bruzik, H. Qian, D. R. Pepperberg, *Nat. Comm.* **2012**, DOI: 10.1038/ncomms2094.
- [42] M. T. Richers, J. M. Amatrudo, J. P. Olson, G. C. Ellis-Davies, *Angew. Chem. Int. Ed. Engl.* **2017**, 56, 193-197.
- [43] F. Strübe, *Dissertation Universität Bielefeld* **2011**.
- [44] N. A. Simeth, L.-M. Altmann, N. Wössner, E. Bauer, M. Jung, B. König, *J. Org. Chem.* **2018**, 83, 7919-7927.
- [45] D. Wutz, D. Gluhacevic, A. Chakrabarti, K. Schmidtkunz, D. Robaa, E. Erdmann, C. Romier, W. Sippl, M. Jung, B. König, *Org. Biomol. Chem.* **2017**, 15, 4882-4896.
- [46] D. Lachmann, C. Studte, B. Männel, H. Hübner, P. Gmeiner, B. König, *Chem. Eur. J.* **2017**, 23, 13423-13434.
- [47] L. Guandalini, C. Cellai, A. Laurenzana, S. Scapecchi, F. Paoletti, M. N. Romanelli, *Bioorg. Med. Chem. Lett.* **2008**, 18, 5071-5074.
- [48] H. Stobbe, *Chem. Ber.* **1905**, 38, 3673-3682.
- [49] H. Stobbe, *Chem. Ber.* **1907**, 40, 3372-3382.
- [50] H. Stobbe, *Liebigs Ann. Chem.* **1911**, 380, 1-2.
- [51] K. Gewald, E. Schinke, H. Böttcher, *Chem. Ber.* **1966**, 99, 94-100.
- [52] J. Backes, E. Brunner, W. Eberbach, A. Gossauer, C. Jutz, *Houben Weyl Methods of Organic Chemistry* **2014**, E6a, 227.
- [53] C. Valant, L. Aurelio, S. M. Devine, T. D. Ashton, J. M. White, P. M. Sexton, A. Christopououlos, P. J. Scammells, *J. Med. Chem.* **2012**, 55, 2367-2375.
- [54] A. C. May, W. Fleischer, O. Kletke, H. L. Haas, O. A. Sergeeva, *Brit. J. Pharmacol.* **2013**, 170, 222-232.
- [55] R. J. Walters, S. H. Hadley, K. D. Morris, J. Amin, *Nat. Neurosci.* **2000**, 3, 1274.

- [56] G. Maleeva, S. Buldakova, P. Bregestovski, *Front. Mol. Neurosci.* **2015**, 8, 64.
- [57] G. M. Sheldrick, *Acta Cryst.* **2015**, C27, 3-8.
- [58] O.V. Dolomanov, L.J. Bourhis, R.J. Gildea, J.A.K. Howard, H. Puschmann, *J. Appl. Cryst.* **2009**, 42, 339-341.
- [59] G. M. Sheldrick, *Acta Cryst.* **2015**, A71, 3-8.

CHAPTER 7

7 Azologization of Serotonin 5-HT₃ Receptor Antagonists



This chapter has been published as:

K. Rustler, G. Maleeva, P. Bregestovski, B. König, *Beilstein J. Org. Chem.* **2019**, 15, 780-788.

This research is performed within the framework of the ERASynBio Modulightor project in cooperation with Dr. G. Maleeva (Prof. P. Bregestovski, Aix-Marseille University, France). K. Rustler performed the synthesis and (photo-)chemical investigation of all compounds. Dr. G. Maleeva performed *in vitro* analysis. Single crystal X-ray crystallography and mass spectrometry analysis were performed by the analytical department at the University of Regensburg. K. Rustler and Dr. G. Maleeva wrote the manuscript. Prof. P. Bregestovski and Prof. B. König supervised the project. Prof. B. König is corresponding author.

7.1 Introduction

5-Hydroxytryptamine (5-HT), commonly known as serotonin^[1,2] or enteramine,^[3,4] is a monoamine neurotransmitter and hormone which is produced in the brain and in intestines and regulates a large variety of physiological functions in the mammalian central and peripheral nervous system.^[1,5] In the central nervous system (CNS), it modulates sleep–wake cycles, emesis, appetite, mood, memory, breathing, cognition and numerous other functions.^[6–9] In the gastrointestinal (GI) tract, it causes peristalsis *via* either smooth muscle contraction or enteric nerve depolarization.^[10] It is also found in the platelets, where it is presumably involved in blood coagulation and vasoconstriction. Furthermore, serotonin is one of the first neurotransmitters to appear during development^[11] and may have an organizing function in the development of the mammalian CNS being involved in cell division, differentiation, survival, neuronal migration^[12,13] and synaptogenesis.^[14] Dysfunction of the 5-HT receptor (5-HTR) signalling during early developmental stages may lead to altered cognitive ability, neurodevelopmental disorders, and increased incidence of psychopathologies such as autism and schizophrenia.^[15,16]

Serotonin operates *via* seven classes of 5-HT receptors of which six are G protein-coupled receptors (GPCRs) and only one, the 5-HT₃R, is a ligand-gated cation channel.^[5,6,17] When this receptor was identified and cloned,^[18–20] it became clear that 5-HT₃ takes a unique position as pentameric ligand-gated cation-selective ion channel belonging to the Cys-loop receptor subfamily. In vertebrates, this family also includes nicotinic acetylcholine receptors (nAChRs), γ -aminobutyric acid type A receptors (GABA_ARs), and glycine receptors (GlyRs). To date, five subunits of the 5-HT₃ receptor are identified (5-HT₃A–5-HT₃E).^[21] Functional receptors are either constructed as 5-HT₃A homopentamers or as heteropentamers containing 5-HT₃A and 5-HT₃B receptor subunits.^[22–24] 5-HT₃ receptors are highly expressed in the brainstem, especially in areas involved in the vomiting reflex and in the dorsal horn of the spinal cord.^[25] These receptors are also expressed

presynaptically providing regulation of the neurotransmitters release.^[21,22] Besides targeting of 5-HT₃Rs for the treatment of psychiatric disorders, they are object to counteract postoperative nausea and chemo-/radiotherapy provoked emesis.^[26-29] In the early 1990s, the first potent and selective 5-HT₃ receptor antagonist ondansetron was initially developed.^[26] Since then the development of 5-HT₃R antagonists progressed. The first-generation antagonists are structurally categorized in three major classes: (I) carbazole derivatives (*e.g.*, ondansetron), (II) indazoles (*e.g.*, granisetron), and (III) indoles (*e.g.*, dolasetron).^[26,30] Generally, 5-HT₃R antagonists share a basic amine, a rigid (hetero-)aromatic system and a carbonyl group or isosteric equivalent which is coplanar to the aromatic system. Although the antagonists show a general structural motive, they differ in their binding affinities, dose responses, and side effects.^[22]

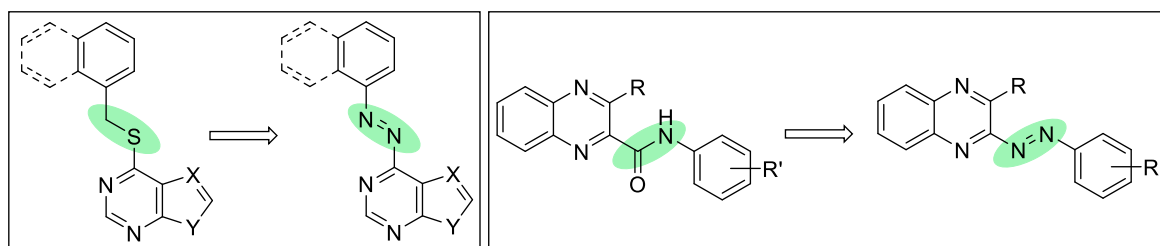
To improve prospective antagonists and obtain a systematic tool for receptor investigation, spatial and temporal restriction of ligand binding and concomitant activity regulation is desirable. Fuelled by light, the growing field of photopharmacology provides a noninvasive method to trigger a drug's pharmacological response on demand.^[31-33] To introduce photoresponsiveness into a biological system, different approaches are feasible, *e.g.*, the use of caged ligands (CL),^[34-37] photoswitchable tethered ligands (PTLs),^[38-40] photoswitchable orthogonal remotely tethered ligands (PORTLs)^[41] or photochromic ligands (PCLs).^[31,42] The latter ones represent small molecules, which can either be engineered *via* extension of the chemical structure of a known pharmacophore towards a photochromic moiety or *via* replacement of certain parts of the biomolecule to generate a photochromic hybrid biomolecule. In this context, various photochromic scaffolds including diethienylethenes, fulgi(mi)des, and azobenzenes are investigated.^[31,42] The latter ones were already discovered in 1834 by E. Mitscherlich^[43] but it took around another 100 years till G. S. Hartley^[44] revealed their photo-induced *trans*-*cis* isomerization representing the time of birth of the azobenzene photoswitch. Benefiting of their accessible synthesis, large change in polarity and geometry upon switching, excellent photochromic

properties and tuneability, azobenzenes are amongst the most widely used photochromic scaffolds.^[31,42,45-47] Since their first use in a biological environment in the late 1960s for the photoregulation of the enzymatic activity of chymotrypsin,^[48] their applications in biology widely expanded towards receptor control^[49-52] and fields as bacterial growth,^[53] vision restoration,^[53-55] the respiratory chain^[56] and lipids.^[57-58] Owing to the reported serotonin antagonists' chemical structures, the use of azobenzene as photochromic scaffold in the presented work seemed axiomatic. Therefore, the primary design of our photochromic derivatives is based on the direct "azologization"^[59] of reported non-photochromic antagonists^[60,61] *via* replacement of the benzene-ring connecting amide bond and thioether, respectively, by an azo bridge.

7.2 Results and Discussion

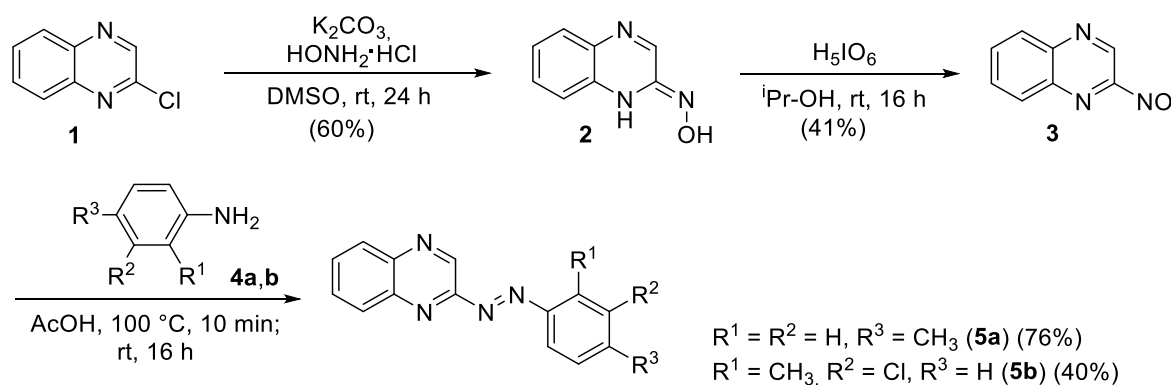
7.2.1 Design and Syntheses

Design. The reported^[60,61] scaffolds of 5-HT₃R antagonists are based on an aromatic system either connected to a purine/pyrimidine moiety *via* a thioether bridge or a quinoxaline moiety *via* an amide bond. Referring to this work performed by the groups of DiMauro^[60] and Jensen,^[61] we envisioned that the replacement of the thioether or amide bond (Scheme 1) by an azo bridge would result in highly active photochromic serotonin 5-HT₃R antagonists controllable by irradiation with light. Based on the suggested receptor binding mode reported for one potent non-photochromic antagonist (lead structure of **16c**)^[61] we expected the extended *trans* isomer as biologically active configuration whereas its bent *cis* isomer should be inactive.



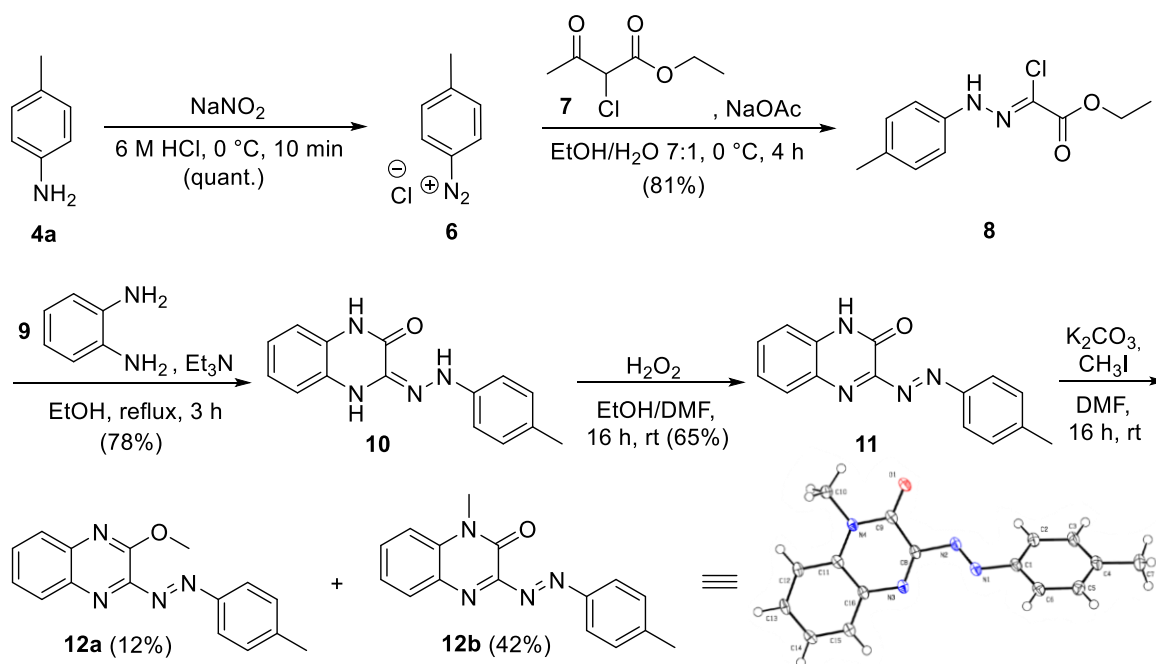
Scheme 1. Approach of the direct azologization of reported^[60,61] serotonin 5-HT₃R antagonists *via* replacement of a thioether or amide bond by an azo bridge.

Synthesis of the quinoxaline-based azobenzenes. The synthesis of the unsubstituted quinoxaline-based azobenzene derivatives **5a** and **5b** is based on a Baeyer^[62]–Mills^[63] reaction (Scheme 2). Therefore, nitrosoquinoxaline **3** was synthesized in a two-step procedure starting from 2-chloroquinoxaline (**1**), which was transformed into its oxime **2** using hydroxylammonium chloride.^[64] The subsequent oxidation was performed using periodic acid as oxidant.^[65] The subsequent reaction with differently substituted anilines in acetic acid^[65] provided both quinoxaline azobenzene derivatives in good yields.



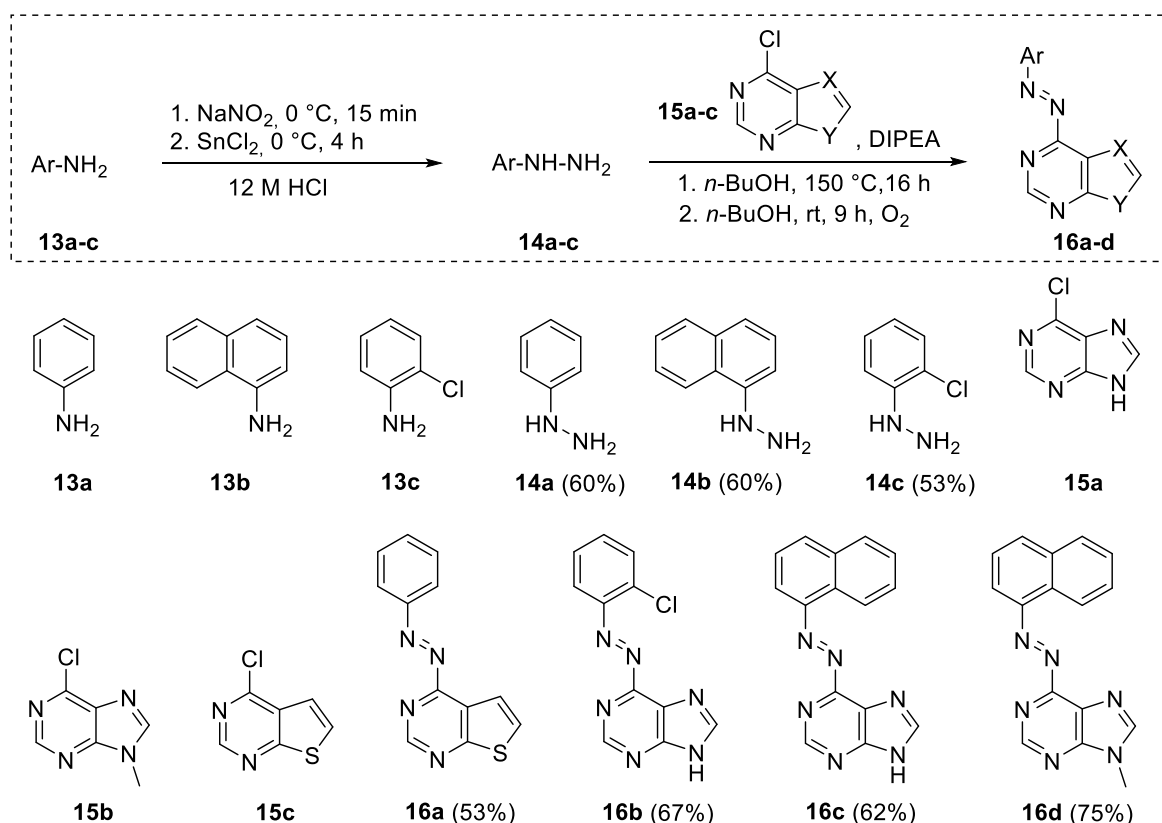
Scheme 2. Synthesis of the differently substituted quinoxaline azobenzene derivatives **5a** and **5b** via Baeyer^[62]–Mills^[63] reaction.^[64,65]

The methoxy-substituted quinoxaline azobenzene derivative **12a** was synthesized via a different synthetic route depicted in Scheme 3. In a first step, *p*-toluidine (**4a**) was diazotized using sodium nitrite and subsequently reacted with the 2-chloroacetylacetone ester derivative **7** providing hydrazine **8**.^[66] Upon reaction of the chloro-ester **8** with phenylenediamine (**9**) in the presence of triethylamine the quinoxaline moiety was formed.^[67] Oxidation of the hydrazine derivative **10** using hydrogen peroxide under an oxygen atmosphere afforded the quinoxaline azobenzene derivative **11**.^[68] Subsequent methylation using methyl iodide^[69] mainly resulted in the formation of the *N*-methylated non-photochromic product **12b** but in low yields also the desired photochromic methoxy-substituted quinoxaline azobenzene derivative **12a**.



Scheme 3. Synthesis of the methoxy substituted quinoxaline derivative **12a** *via* diazotization.^[66-69]

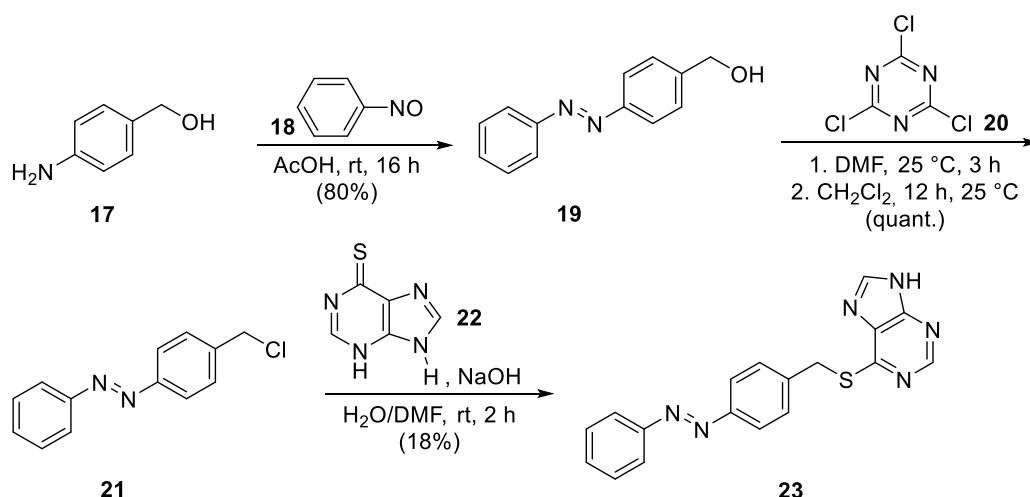
Synthesis of the purine and thienopyrimidine-based derivatives. Scheme 4 depicts the general procedure applied for the synthesis of differently substituted purine and thienopyrimidine azobenzene derivatives. Differently substituted non-photochromic antagonists were chosen as lead structures delivering photochromic derivatives with varying electronic and thus photochromic properties. The respective arylamines **13a-c** were converted into their corresponding hydrazines **14a-c** *via* diazonium-salt formation using sodium nitrite and subsequent reduction using tin(II)chloride.^[70] The following nucleophilic substitution at a chloro-substituted purine (**15a,b**) or thienopyrimidine (**15c**), respectively, and subsequent oxidation of the hydrazine moiety afforded the corresponding azobenzene derivatives **16a-d**.^[71]



Scheme 4. General procedure for the synthesis of purine- and thienopyrimidine-substituted arylazobenzenes and depiction of the corresponding structures.^[70,71]

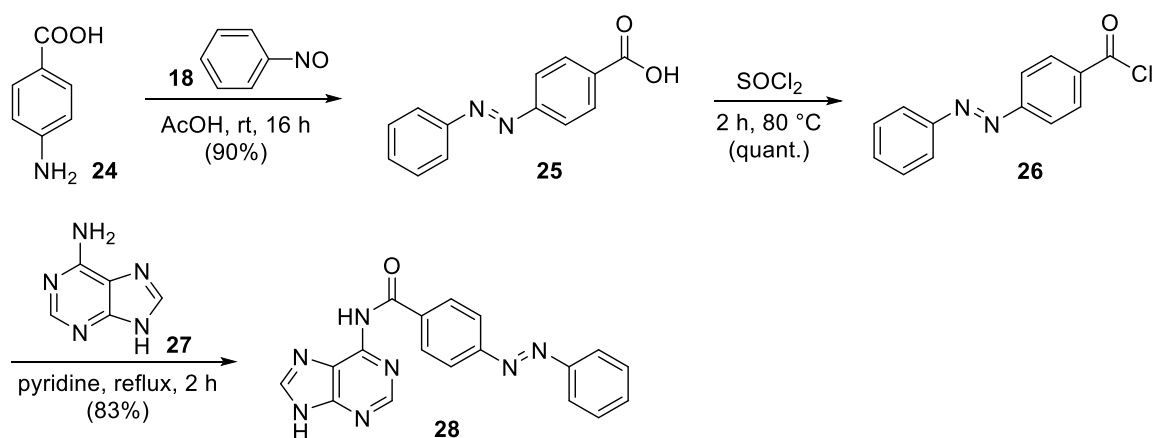
Synthesis of azobenzene-extended thiopurine derivatives. To further tune the photochromism and compare the properties of direct azologization to azo-extension, two additional derivatives of the *in vitro* most promising naphthalene azopurine **16c** were synthesized either by keeping the original thioether (Scheme 5) or replacing it by an amide bond (Scheme 6) known as common structural feature of 5-HT₃R antagonists.

Scheme 5 reflects the synthesis of the azo-extended thiomethylpurine **23** starting with the synthesis of hydroxymethylazobenzene **19**^[72] in a Baeyer^[62]–Mills^[63] reaction and subsequent nucleophilic substitution using cyanuric chloride (**20**)^[73] providing chloromethyl azobenzene **21**. The introduction of the thiopurine moiety in **23** was accomplished upon reaction of **21** with dihydropurinethione **22**.^[74]



Scheme 5. Synthesis of the thiomethyl-linked purine azobenzene **23**.^[62,63,72-74]

The amide-linked derivative of thiomethylpurine azobenzene **23** was synthesized *via* Baeyer^[62]–Mills^[63] formation of the carboxylated azobenzene **25** starting from aminobenzoic acid **24** and nitrosobenzene (**18**).^[75] Activation using thionyl chloride^[76] afforded the acid chloride **26** and allowed amide-bond formation^[77] for the generation of **28** (Scheme 6).



Scheme 6. Synthesis of the amide-linked azobenzene purine **28**.^[62,63,75-77]

7.2.2 Photochemical Characterization

The investigation of the photochromic properties of the potential 5-HT₃R antagonists **5a**, **5b**, **12a**, **16a–d**, **23**, and **28** was performed in DMSO and depending on their solubility in phosphate buffer + 0.1% DMSO (**16a–d**) by UV-Vis absorption spectroscopy. The compounds were dissolved at 50 μ M in the respective solvent and irradiated with the indicated wavelengths to generate a substantial amount of

their *cis* isomer. This process can be followed by a decrease of the *trans* absorption maximum at around 350–400 nm and an increase in absorption at around 450–500 nm in the UV-Vis spectrum representing the *cis*-isomer (Figure 1, black arrows). The absorption bands of the *trans* and *cis* isomers of compounds **12a**, **16c**, and **16d** overlap to such an extent, that no new maximum representing the *cis* isomer was observed and thus *cis*–*trans* isomerization only occurs thermally and is not triggerable by irradiation with visible light. Back-isomerization was triggered by irradiation with visible light (**5a**, **5b**, **16a**, **16b**, **23**, and **28**) of the indicated wavelength or by thermal relaxation (**5a**, **5b**, **12a**, **16a–d**, **23**, and **28**). Irradiation times were determined by following the UV-Vis spectrum upon isomerization until no more changes in absorption were observed and the photostationary state (PSS) was reached. The points of intersection in the absorption spectrum upon switching (= isosbestic points) indicate a clear two-component switching between *trans* and *cis* species without any degradation or formation of a side-product (Figure 1, dotted black arrows). The UV-Vis absorption spectra of all compounds are depicted in Supporting Information, Figures S1–S10 and the data are summarized in Table S1 and Table S2. A comparison of the differently substituted purine azobenzene derivatives revealed the beneficial effect of an *o*-chloro substitution on the photochromic properties of **16b** compared to **16c** as the electron density at the nitrogen-rich purine core is reduced. Further reduction of the electron density was achieved by using a thienopyrimidine (**16a**) instead of a purine core (**16b–d**). Nevertheless, the photochromic properties of those heterocyclic, especially purine-based azobenzenes, are rather poor. In addition to direct azologization, two azo-extended purine derivatives **23** and **28** were synthesized resulting in excellent photochromic properties. Figure 1 compares exemplarily the UV-Vis absorption spectra of the naphthalene-azo-purine **16c** (left) and its azo-extended azobenzene thioether purine **23** (right). The determination of the thermal half-lives (THL) of the *cis* isomers of compounds **5a**, **5b**, **12a**, **16a–d**, **23**, and **28** was accomplished by monitoring the increase in absorbance which corresponds to the evolution of the *trans* isomer after irradiation

and exposure to dark. In contrast to the heterocyclic compounds **5a**, **5b**, **12a**, and **16a–d** with a thermal half-life in the seconds to minutes range, the azo-extended compounds **23** and **28** showed only slow thermal back-isomerization (day range) at room temperature. Depending on the desired application, both properties may be of benefit. For thermally unstable compounds, only one wavelength for switching is required. In case of thermally stable *cis* isomers constant irradiation to maintain a substantial amount of the *cis* isomer can be avoided.

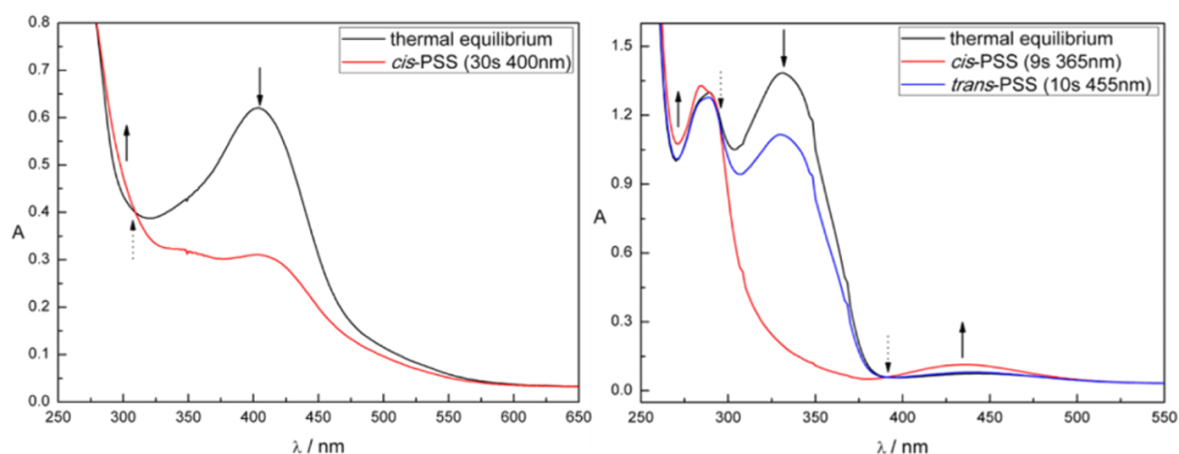


Figure 1. UV-Vis absorption spectra measured at 50 μM in DMSO. Left: Purine derivative **16c**; Right: azo-extended derivative **23**.

7.2.3 In Vitro Patch-Clamp Studies

The synthesized azo antagonist derivatives **5a**, **5b**, **12a**, **16a–d**, **23**, and **28** were tested for their inhibitory activity using patch-clamp technique on heterologously expressed ionotropic homopentameric 5-HT_{3A} receptors. Only upon addition of **16c** the amplitude of the 5-HT_{3A} mediated currents was decreased (Figure 2, left). Application of a 50 μM solution of *trans*-**16c** in its thermal equilibrium decreased the amplitude of 5-HT induced currents on $54 \pm 3\%$ ($n = 4$). However, irradiation-induced *trans*–*cis* isomerization with light of $\lambda = 530$ nm and 455 nm, respectively, had no significant effect on the amplitude of 5-HT_{3A}-mediated currents (Figure 2, right).



Figure 2. On the left panel representative traces of currents induced by the application of 3 μM 5-HT (black trace), by 3 μM 5-HT and 50 μM *trans*-16c (red trace), by 5-HT and 16c under constant irradiation (455 nm, blue trace), and again by pure 5-HT – wash-out of the studied compound (black trace) are shown. On the right panel, a graph representing the relative amplitudes of currents in control (black column), at application of *trans*-16c (red column), at application of 16c irradiated with blue light (blue column) and at wash-out (gray column) are shown. $P > 0.05$, paired t-test.

7.3 Conclusion

In the presented work, we address the design, synthesis, photochromic characterization and *in vitro* investigation of in total nine azobenzene-based derivatives of reported 5-HT₃R antagonists. Initially, seven photoligands (**5a**, **5b**, **12a**, and **16a–d**) either based on quinoxaline (**5a**, **5b**, and **12a**) or purine derivatives (**16a–d**) with varying electronic and thus photochromic properties were synthesized by direct azologization of the respective leads. Especially the purine-based azobenzenes displayed high solubility in aqueous media. The beneficial effect of substituents reducing the overall electron density of the purine moiety (**16a**, **16b**) resulted in higher photostationary states and better band separation compared to **16c** and **16d**. Still, only one compound (**16c**) showed antagonistic activity in patch-clamp studies. This might be explained by the fact that its corresponding non-photochromic lead is the inhibitory most active reported^[61] antagonist among the investigated ones. The partial rigidization of the thioether *via* incorporation of an azo bridge might result in a vast loss of activity. Thereby, azologization of the less potent leads resulted in complete loss of inhibitory activity (**5a**, **5b**, **12a**, **16a**, **16b**, **16d**) and only the originally most potent derivative **16c** kept recordable antagonistic activity. The missing significant difference in activity upon irradiation-induced *trans–cis* isomerization of **16c** is probably due to its moderate

photochromic properties and slow *trans*–*cis* isomerization (Figure 1, left). During the patch-clamp analysis, the cells are continuously superfused with external solution resulting in a fast exchange of the surrounding media and co-applied tested compounds. Thus, the *cis*-PSS of **16c** might not be reached by irradiation within the short time of compound application despite continuous irradiation. Therefore, two azobenzene-extended derivatives (**23** and **28**) with improved photochromic properties were synthesized but lost antagonistic activity probably due to their increased steric demand.

In ongoing studies, detailed molecular modelling is used to design potential photochromic antagonists fitting the requirements of the receptor's binding pocket. Regarding the analysis method, compounds will be optimized towards either thermally stable *cis*-isomers to be tested separately upon prior irradiation or faster switching compounds.

7.4 Experimental Part

7.4.1 General Procedures and Materials

Commercially reagents and starting materials were purchased from the commercial suppliers abcr, Acros Organics, Alfa-Aesar, Fisher Scientific, Merck, Sigma Aldrich, TCI, or VWR and used without any further purification. Solvents were used in p.a. quality and dried according to standard procedures, if necessary. Dry nitrogen was used as an inert gas atmosphere. Flash column chromatography was performed using Sigma Aldrich MN silica gel 60 M (40–63 μm , 230–400 mesh) for normal phase chromatography. Reaction monitoring *via* thin layer chromatography was performed on alumina plates coated with silica gel (Merck silica gel 60 F₂₅₄, layer thickness 0.2 mm). Melting points were determined using a Stanford Research System OptiMelt MPA 100 and are uncorrected. NMR spectra were measured on a Bruker Avance 300 (¹H 300.13 MHz, ¹³C 75.48 MHz), Bruker Avance III HD 400 (¹H 400.13 MHz, ¹³C 100.61 MHz), Bruker Avance III HD 600 (¹H 600.25 MHz, ¹³C 150.95 MHz) and Bruker Avance III 600 (¹H 600.25 MHz, ¹³C 150.95 MHz). The spectra are referenced against the NMR solvent (DMSO-*d*₆: δ_{H} =

2.50 ppm, $\delta_{\text{C}} = 39.52$ ppm; CDCl_3 -*d*: $\delta_{\text{H}} = 7.26$ ppm, $\delta_{\text{C}} = 77.16$ ppm) and chemical shifts δ are reported in ppm. Resonance multiplicity is abbreviated as: s (singlet), d (doublet), t (triplet) and m (multiplet). Carbon NMR signals are assigned using DEPT 135 and ^1H - ^{13}C HSQC spectra with (+) for primary/tertiary, (-) for secondary, and (q) for quaternary carbons. Mass spectra were recorded on a Finnigan MAT-SSQ 710 A, ThermoQuest Finnigan TSQ 7000, Agilent Q-TOF 6540 UHD, or a Jeol AccuTOF GCX instrument. UV-vis absorption spectroscopy was performed in 10 mm quartz cuvettes using an Agilent 8543, Agilent Cary 100, or Agilent Varian Cary 50 spectrometer. Analytical HPLC measurements were performed using an Agilent 1220 Infinity LC (column: Phenomenex Luna 3 μm C₁₈(2) 100 Å, 150 \times 2.00 mm; flow 0.3 mL min⁻¹ at 20 °C or 30 °C; solvent A: MilliQ water with 0.05 wt% TFA; solvent B: MeCN). The ratios at the PSSs were determined *via* analytical HPLC at 20 °C at the isosbestic points or *via* NMR spectroscopy. An Agilent 1260 system (column: Phenomenex Luna 10 μm C₁₈(2) 100 Å, 250 \times 21.2 mm; flow: 22 mL min⁻¹; solvent A: MilliQ water; solvent B: MeCN) was used for preparative HPLC purification. Light sources for irradiation: $\lambda = 365$ nm (Seoul Viosys CUN6GB1A, 1000 mA, 1.4 W), $\lambda = 385$ nm (Seoul Viosys CUN8GF1A, 1000 mA, 1.6 W), $\lambda = 400$ nm (Luxeon 400 nm SZ-01-S2, 500 mA, 0.48 W), $\lambda = 455$ nm (Osram OSOLON SSL 80 LD-CQ7P-1U3U, 1000 mA, 0.45 W). The power of the light is given based on the specifications supplied by the company when the LEDs were purchased.

Compounds **2**,^[64] **3**,^[65] **6**,^[66] **8**,^[66] **10**,^[67] **11**,^[68] **14a-c**,^[70] **19**,^[72] **21**,^[73] **25**,^[75] and **26**^[76] were synthesized following adapted reported procedures.

7.4.2 Synthetic Procedures and Characterization

(E)-2-(*p*-tolylidiazanyl)quinoxaline (5a). This compound was synthesized *via* an adapted literature reported procedure.^[65] Nitrosoquinoxaline **3** (0.48 g, 3.0 mmol, 1.0 eq) and *p*-toluidine (**4a**, 0.36 g, 3.4 mmol, 1.1 equiv) were suspended in acetic acid (10 mL), refluxed for 10 min and stirred at room temperature for additional 16 hours. Purification by flash column chromatography using CH_2Cl_2 as the eluent

afforded the desired product as red solid (0.57 g, 2.3 mmol, 76%). M.p.: 135 °C. $^1\text{H-NMR}$ (300 MHz, $\text{DMSO-}d_6$): δ = 9.32 (s, 1H), 8.26 – 8.19 (m, 2H), 8.01 – 7.96 (m, 4H), 7.50 (d, J = 8.6 Hz, 1H), 2.45 (s, 3H). $^{13}\text{C-NMR}$ (75 MHz, $\text{DMSO-}d_6$): δ = 155.6 (q), 150.7 (q), 144.8 (q), 142.9 (q), 141.0 (q), 138.5 (+), 131.9 (+), 131.8 (+), 130.8 (+), 130.3 (+), 129.4 (+), 123.9 (+), 21.7 (+). HRMS (ESI) calcd. for $(\text{C}_{15}\text{H}_{13}\text{N}_4)^+$ $[\text{M}+\text{H}]^+$: m/z = 249.1135; found 249.1138. MF: $\text{C}_{15}\text{H}_{12}\text{N}_4$. MW: 248.29 g/mol.

(E)-2-((3-chloro-2-methylphenyl)diazenyl)quinoxaline (5b). This compound was synthesized *via* an adapted literature reported procedure.^[65] Nitrosoquinoxaline **3** (0.48 g, 3.0 mmol, 1.0 eq) and aniline (**4b**, 0.48 g, 3.4 mmol, 1.1 eq) were mixed in acetic acid (10 mL) and heated to reflux for 10 min. The mixture was then heated at 50 °C for additional 16 hours. Purification by flash column chromatography using CH_2Cl_2 as the eluent afforded the target compound as red solid (40%). M.p.: 140 °C. $^1\text{H-NMR}$ (300 MHz, $\text{DMSO-}d_6$): δ = 9.35 (s, 1H), 8.32 – 8.18 (m, 2H), 8.06 – 7.94 (m, 2H), 7.74 (dd, J = 23.8, 8.1 Hz, 2H), 7.46 (t, J = 7.9 Hz, 1H), 2.81 (s, 3H). $^{13}\text{C-NMR}$ (101 MHz, $\text{DMSO-}d_6$): δ = 155.6 (q), 151.7 (q), 143.1 (q), 141.0 (q), 138.4 (+), 137.9 (q), 135.7 (q), 133.9 (+), 132.2 (+), 131.9 (+), 130.3 (+), 129.5 (+), 128.3 (+), 114.5 (+), 14.7 (+). HRMS (ESI) calcd. for $(\text{C}_{15}\text{H}_{12}\text{ClN}_4)^+$ $[\text{M}+\text{H}]^+$: m/z = 283.0745; found 283.0745. MF: $\text{C}_{15}\text{H}_{11}\text{ClN}_4$. MW: 282.73 g/mol.

(E)-2-methoxy-3-(*p*-tolyl diazenyl)quinoxaline (12a) and (E)-1-methyl-3-(*p*-tolyl diazenyl)quinoxalin-2(1H)-one (12b). These compounds were synthesized *via* an adapted literature reported procedure.^[69] Compound **11** (0.36 g, 1.4 mmol, 1.0 eq) and potassium carbonate (0.19 g, 1.4 mmol, 1.0 eq) were suspended in DMF (6.0 mL). Then methyl iodide (0.19 g, 1.4 mmol, 1.0 eq) was added and the mixture stirred at room temperature for 16 hours. Water (2.0 mL/mmol) was added to the mixture and the aqueous layer extracted with ethyl acetate for three times. The combined organic layers were washed with brine, dried over magnesium sulfate, filtered and the solvent evaporated. Purification by flash column chromatography using petroleum ether/ethyl acetate 1:1 as eluent afforded the products **12a** and **12b**. Characterization of **12a**. Red solid (45 mg, 0.16 mmol, 12%). Gradient 0-13 min: MeCN/ H_2O 45:55 – 98:2, t_R = 12.2 min. M.p.: 137 °C. $^1\text{H-NMR}$ (600 MHz,

DMSO-*d*₆): δ = 8.07 (dd, J = 8.2, 1.4 Hz, 1H), 7.97 – 7.88 (m, 3H), 7.82 (ddd, J = 8.4, 6.9, 1.5 Hz, 1H), 7.70 (ddd, J = 8.4, 7.0, 1.4 Hz, 1H), 7.48 (d, J = 8.1 Hz, 2H), 4.15 (s, 3H), 2.46 (s, 3H). ¹³C-NMR (75 MHz, CDCl₃): δ = 154.2 (q), 151.6 (q), 149.4 (q), 144.0 (q), 141.5 (q), 137.8 (q), 130.5 (+), 130.2 (+), 129.9 (+), 127.4 (+), 126.8 (+), 124.1 (+), 54.4 (+), 21.8 (+). HRMS (ESI) calcd. for (C₁₆H₁₅N₄O⁺) [M+H]⁺: m/z = 279.1240; found 279.1243. MF: C₁₆H₁₄N₄O. MW: 278.32 g/mol. Characterization of **12b**. Orange solid (0.16 g, 0.57 mmol, 42%). Gradient 0-10 min 45:55-90:10, t_R = 7.5 min. M.p.: 132 °C. ¹H-NMR (400 MHz, DMSO-*d*₆): δ = 7.87 (d, J = 8.4 Hz, 3H), 7.73 – 7.64 (m, 2H), 7.49 – 7.40 (m, 3H), 3.72 (s, 3H), 2.45 (s, 3H). ¹³C-NMR (101 MHz, DMSO-*d*₆): δ = 157.4 (q), 152.2 (q), 150.8 (q), 144.5 (q), 134.6 (q), 131.6 (+), 131.3 (q), 130.7 (+), 130.7 (+), 124.6 (+), 123.8 (+), 115.6 (+), 29.7 (+), 21.7 (+). HRMS (ESI) calcd. for (C₁₆H₁₅N₄O⁺) [M+H]⁺: m/z = 279.1240; found 279.1243. MF: C₁₆H₁₄N₄O. MW: 278.32 g/mol.

(E)-4-(phenyldiazenyl)thieno[2,3-*d*]pyrimidine (16a). This compound was synthesized *via* an adapted literature reported procedure.^[71] 4-chlorothieno[2,3-*d*]pyrimidine (**15c**, 0.20 g, 1.2 mmol, 1.0 eq), phenylhydrazine (**13b**, 0.15 g, 1.4 mmol, 1.2 eq), DIPEA (0.76 g, 5.9 mmol, 5.0 equiv) and *n*-BuOH (5.0 mL) were mixed and stirred at 150 °C for 16 hours. The reaction mixture was cooled to room temperature and exposed to pure oxygen (balloon) for 24 hours. Purification by flash column chromatography using CH₂Cl₂ as the eluent afforded the desired product as red solid (0.15 g, 0.60 mmol, 53%). M.p.: 106 °C. ¹H-NMR (400 MHz, DMSO-*d*₆): δ = 9.25 (s, 1H), 8.18 (d, J = 6.0 Hz, 1H), 8.13 – 8.10 (m, 2H), 7.89 (d, J = 6.0 Hz, 1H), 7.74 – 7.69 (m, 3H). ¹³C-NMR (101 MHz, DMSO-*d*₆): δ = 172.1 (q), 161.4 (q), 153.7 (+), 152.7 (q), 134.4 (+), 131.9 (+), 130.3 (+), 124.0 (+), 121.7 (q), 120.6 (+). HRMS (ESI) calcd. for (C₁₂H₉N₄S⁺) [M+H]⁺: m/z = 241.0542; found 241.0540. MF: C₁₂H₈N₄S. MW: 240.28 g/mol.

(E)-6-((2-chlorophenyl)diazenyl)-9H-purine (16b). This compound was synthesized *via* an adapted literature reported procedure.^[71] 6-Chloro-9-isopropyl-9H-purine (0.37 g, 2.4 mmol, 1.0 eq), *o*-chlorophenylhydrazine (0.41 g, 2.9 mmol, 1.2 eq), DIPEA (1.6 g, 12 mmol, 5.0 eq) and *n*-BuOH (16 mL) were mixed and stirred

in a sealed glass vial at 150 °C for 16 hours. The reaction mixture was cooled to room temperature and exposed to pure oxygen (balloon) for 24 hours. The solvent was removed and the product purified by flash column chromatography using CH₂Cl₂ + 5% MeOH to afford **16b** as red solid (0.42 g, 1.6 mmol, 67%). M.p.: 179 °C. ¹H-NMR (400 MHz, DMSO-*d*₆): δ = 13.26 (s, 1H), 9.10 (s, 1H), 8.83 (s, 1H), 7.82 – 7.78 (m, 2H), 7.73 – 7.69 (m, 1H), 7.60 – 7.55 (m, 1H). ¹³C-NMR (101 MHz, DMSO-*d*₆): δ = 152.3 (+), 149.0 (q), 135.8 (q), 135.2 (+), 131.5 (+), 128.7 (+), 118.2 (+). HRMS (ESI) calcd. for (C₁₁H₈ClN₆)⁺ [M+H]⁺: m/z = 259.0493; found 259.0493. MF: C₁₁H₇ClN₆. MW: 258.67 g/mol.

(E)-6-(naphthalen-1-yl diazenyl)-9H-purine (16c). This compound was synthesized *via* an adapted literature reported procedure.^[71] A mixture of chloroadenine **15a** (93 mg, 0.60 mmol, 1.0 eq), hydrazine **14b** (0.11 g, 0.72 mmol, 1.2 eq) and DIPEA (0.39 g, 0.52 mL, 3.0 mmol, 5.0 eq) in *n*-BuOH (4.0 mL) was stirred at 150 °C for 16 hours. After cooling to room temperature, the solution was exposed to an oxygen atmosphere (balloon) for 24 hours. The product was purified by column chromatography using CH₂Cl₂ + 5% MeOH as the eluent and subsequent preparative HPLC (gradient 0 20 min: MeCN/H₂O 10:90 – 98:2) and afforded adenine-azo **16c** as red solid (*t_R* = 11.47 min, 92.0 mg, 0.37 mmol, 62%). M.p.: 110 °C. ¹H-NMR (400 MHz, DMSO-*d*₆): δ = 13.53 (s, 1H), 9.14 (s, 1H), 8.91 (d, *J* = 8.4 Hz, 1H), 8.85 (s, 1H), 8.31 (d, *J* = 8.0 Hz, 1H), 8.13 (d, *J* = 8.0 Hz, 1H), 7.99 (d, *J* = 7.5 Hz, 1H), 7.80 – 7.70 (m, 3H). ¹³C-NMR (151 MHz, DMSO-*d*₆): δ = 155.0 (q), 151.8 (+), 149.3 (q), 147.7 (+), 134.0 (+), 133.9 (q), 130.2 (q), 128.2 (+), 128.0 (+), 127.0 (+), 125.8 (+), 123.3 (+), 113.6 (q). HRMS (ESI) calcd. for (C₁₅H₁₁N₆)⁺ [M+H]⁺: m/z = 275.1040; found 275.1044. MF: C₁₅H₁₀N₆. MW: 274.29 g/mol.

(E)-9-methyl-6-(naphthalen-1-yl diazenyl)-9H-purine (16d). This compound was synthesized *via* an adapted literature reported procedure.^[71] A mixture of methylated chloro-adenin **15b** (0.10 g, 0.60 mmol, 1.0 eq), hydrazine **14b** (0.11 g, 0.72 mmol, 1.2 equiv) and DIPEA (0.39 g, 0.52 mL, 3.0 mmol, 5.0 equiv) in *n*-butanol (4.0 mL) was stirred at 150 °C for 16 hours. After cooling to room temperature, the solution was exposed to an oxygen atmosphere (balloon) for 24 hours. The product

was purified by column chromatography using CH₂Cl₂ + 5% MeOH as eluent and subsequent preparative HPLC (gradient 0 20 min: MeCN/H₂O 10:90 – 98:2) and afforded the methylated azoadenine **16d** as red solid (*t_R* = 12.91 min, 0.13 g, 0.45 mmol, 75%). M.p.: 186 °C. ¹H-NMR (400 MHz, CDCl₃-*d*): δ = 9.13 (s, 1H), 9.08 (d, *J* = 7.3 Hz, 1H), 8.27 (s, 1H), 8.09 (d, *J* = 7.8 Hz, 2H), 7.94 (d, *J* = 7.8 Hz, 1H), 7.71 – 7.66 (m, 1H), 7.62 – 7.58 (m, 2H), 4.00 (s, 3H). ¹³C-NMR (101 MHz, CDCl₃-*d*): δ = 158.0 (q), 155.6 (q), 152.7 (+), 148.6 (q), 147.5 (+), 134.3 (q), 134.1 (+), 132.0 (q), 127.9 (+), 127.9 (+), 126.8 (+), 126.0 (q), 125.4 (+), 123.9 (+), 113.0 (+), 30.2 (+). HRMS (ESI) calcd. for (C₁₆H₁₃N₆⁺) [M+H]⁺: *m/z* = 289.1196; found 289.1198. MF: C₁₆H₁₂N₆. MW: 288.31 g/mol.

(E)-6-((4-(phenyldiazenyl)benzyl)thio)-7H-purine (23). This compound was synthesized *via* an adapted literature reported procedure.^[74] A solution of chloromethylated azobenzene **21** (0.80 g, 3.5 mmol, 1.1 eq) in DMF (10 mL) was added to a solution of 6-mercaptopurine **22** (0.15 g, 3.2 mmol, 1.0 eq) in 2 M NaOH (10 mL) and the mixture stirred at room temperature for 3 hours. The solvent was evaporated, and the product purified by flash column chromatography using CH₂Cl₂ + 5% MeOH as the eluent. Evaporation of the solvent afforded the desired product as orange solid (215 mg, 0.62 mmol, 18%). M.p.: 212 °C. ¹H-NMR (400 MHz, DMSO-*d*₆): δ = 13.55 (s, 1H), 8.76 (s, 1H), 8.46 (s, 1H), 7.89 – 7.83 (m, 4H), 7.68 (d, *J* = 8.4 Hz, 2H), 7.59 – 7.55 (m, 3H), 4.76 (s, 2H). ¹³C-NMR (101 MHz, DMSO-*d*₆): δ = 158.3 (q), 152.4(q), 151.9 (+), 151.4 (q), 149.9 (q), 143.6 (q), 142.4 (q), 132.0 (+), 130.5 (+), 129.9 (+), 123.2 (+), 123.0 (+), 31.7 (-). HRMS (ESI) calcd. for (C₁₈H₁₅N₆S⁺) [M+H]⁺: *m/z* = 347.1073; found 347.1077. MF: C₁₈H₁₄N₆S. MW: 346.41 g/mol.

(E)-4-(phenyldiazenyl)-N-(9H-purin-6-yl)benzamide (28). This compound was synthesized *via* an adapted literature reported procedure.^[77] Chlorocarbonylazobenzene **26** (0.64 g, 2.6 mmol, 1.1 eq) was added dropwise over 30 minutes to a stirred suspension of adenine **27** (0.32 g, 2.4 mmol, 1.0 eq) in dry pyridine and stirring was continued for two hours at 100 °C. The mixture was cooled to room temperature and stirred for additional 16 hours. The reaction was

quenched with methanol and the solvents were removed under reduced pressure. Purification by column chromatography using CH_2Cl_2 as eluent afforded the desired product as orange solid (0.68 g, 2.0 mmol, 83%). M.p.: 271 °C. ^1H -NMR (400 MHz, $\text{DMSO}-d_6$): δ = 11.69 (s, 1H), 8.76 (s, 1H), 8.54 (s, 1H), 8.32 (d, J = 8.3 Hz, 2H), 8.03 (d, J = 8.3 Hz, 2H), 7.97 – 7.94 (m, 2H), 7.67 – 7.62 (m, 3H). ^{13}C -NMR (101 MHz, $\text{DMSO}-d_6$): δ = 166.2 (q), 154.5 (q), 152.4 (q), 151.6 (+), 146.3 (+), 135.5 (q), 132.7 (+), 130.5 (+), 130.1 (+), 123.3 (+), 122.9 (+). HRMS (ESI) calcd. for $(\text{C}_{18}\text{H}_{14}\text{N}_7\text{O}^+)$ $[\text{M}+\text{H}]^+$: m/z = 344.1254; found 344.1257. MF: $\text{C}_{18}\text{H}_{13}\text{N}_7\text{O}$. MW: 343.35 g/mol.

7.4.3 *In Vitro* Studies

Cell culture and transfection. The subtype A of 5-HT₃ receptors was heterologously expressed in cultured chinese hamster ovary (CHO) cells obtained from the American Type Tissue Culture Collection (ATCC, Molsheim, France). Transfection with cDNA of 5-HT_{3A} receptors was performed using the Lipofectamine 3000 protocol (Life Technology, USA). For identification of transfected cells a cDNA of green fluorescent protein (GFP) was co-transfected with cDNA of 5-HT₃ARs. Three hours after the initial exposure of cells to the cDNAs the culture medium was replaced with fresh medium. Electrophysiological recordings were carried out on fluorescent cells 24-72 hours after transfection.

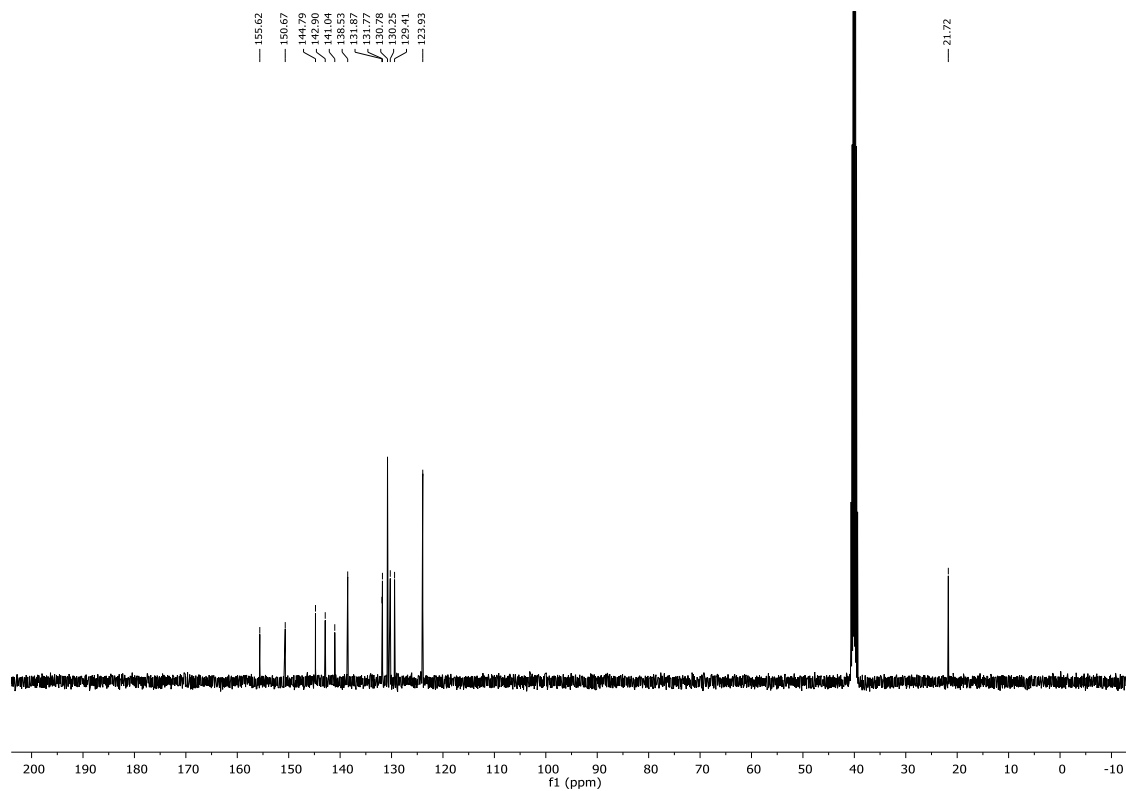
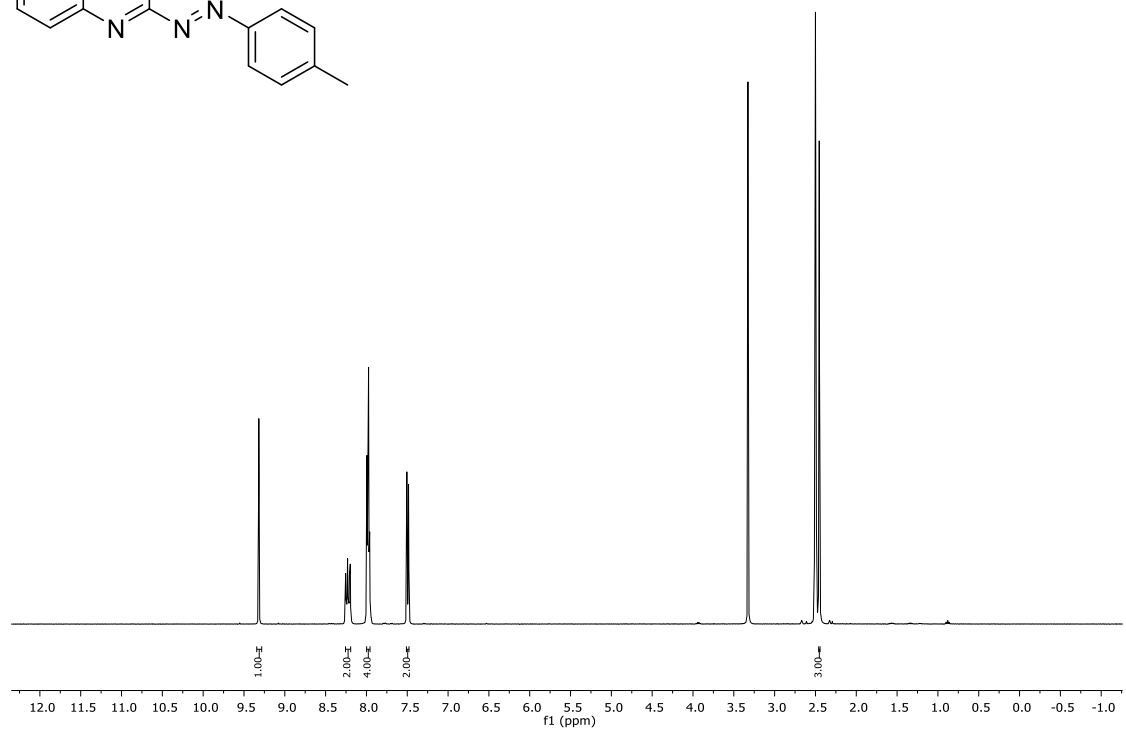
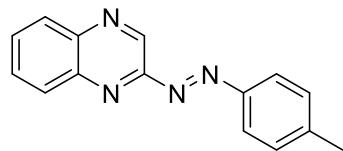
Electrophysiological recordings. Whole-cell patch-clamp recordings were held at room temperature (20-25 °C) using an EPC-9 amplifier (HEKA Elektronik, Germany). Cells were continuously superfused with external solution containing (mM): NaCl 140, CaCl_2 2, KCl 2.8, MgCl_2 4, HEPES 20, glucose 10; pH 7.4; 320-330 mOsm. Intracellular solution used for filling recording patch pipettes contained (mM): KCl 140, MgCl_2 2, MgATP 2, BAPTA (tetrapotassium salt) 2; pH 7.3; 290 mOsm. Recording pipettes were pulled from borosilicate glass capillaries (Harvard Apparatus Ltd, USA) and had resistances of 5-10 MOhm. Rapid replacement of solutions was provided by fast application system (SF 77A Perfusion Fast-Step, Warner, USA), placed 40-50 μm above the recorded cell. Cells

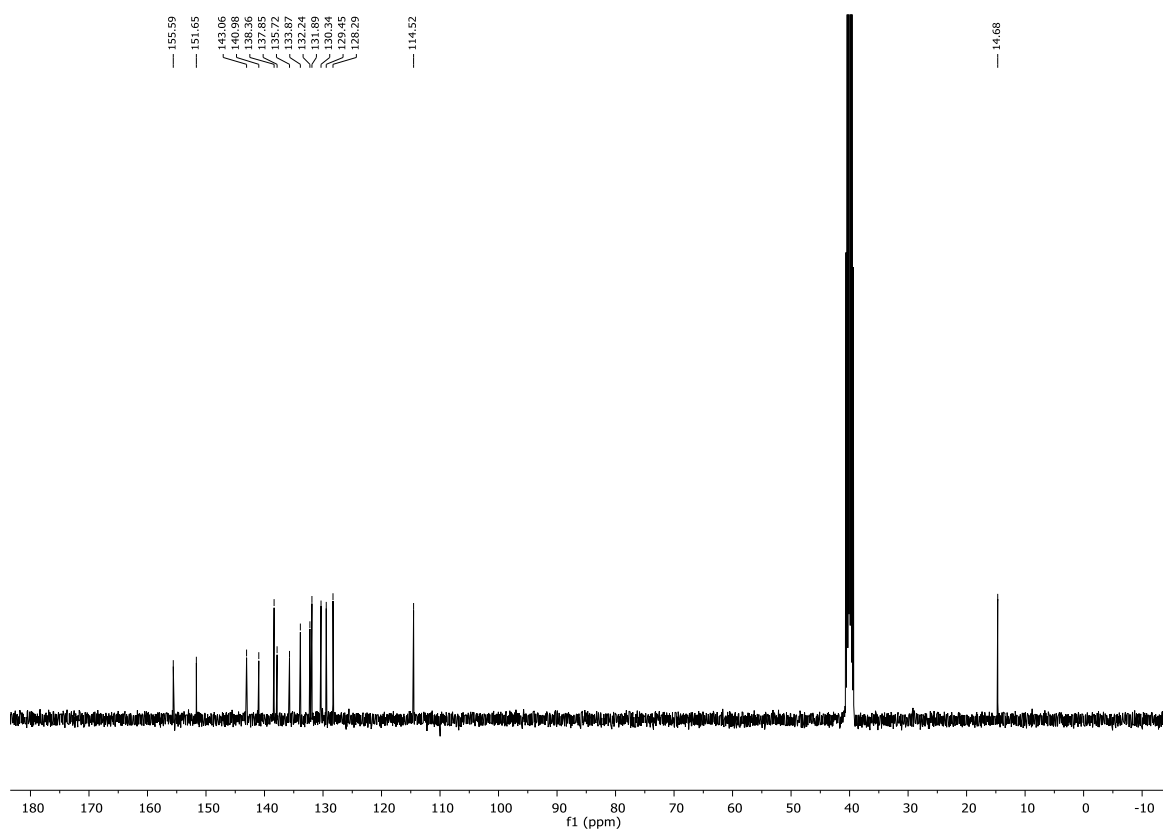
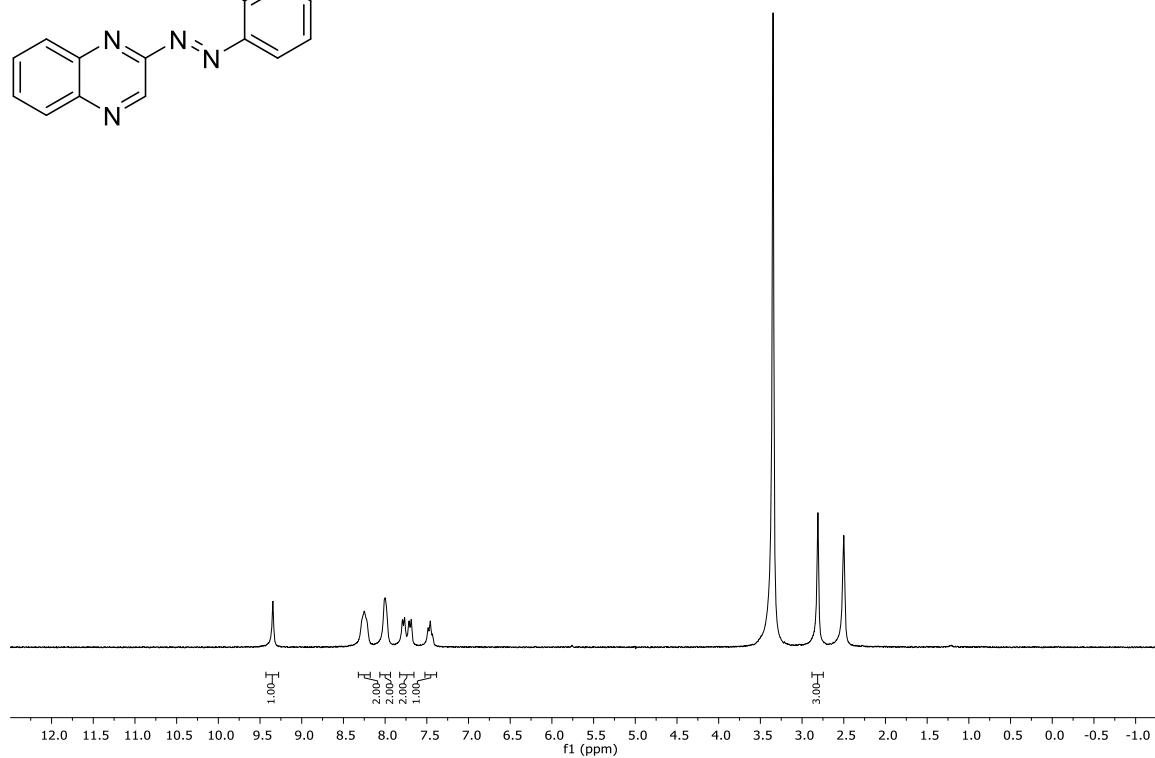
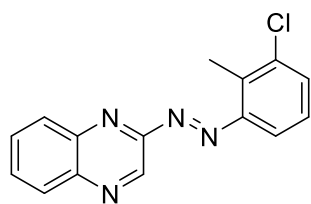
with low input resistance (<150 MOhm) and a rapid run-down (>30% with repetitive application) were excluded from analysis. The agonist 5-HT for the activation was applied alone or mixed with studied compounds during 5 s. Irradiation with the light of 455 nm or 530 nm was provided by LEDs (Thorlabs) placed at the distance of 4-5 cm from the studied cell.

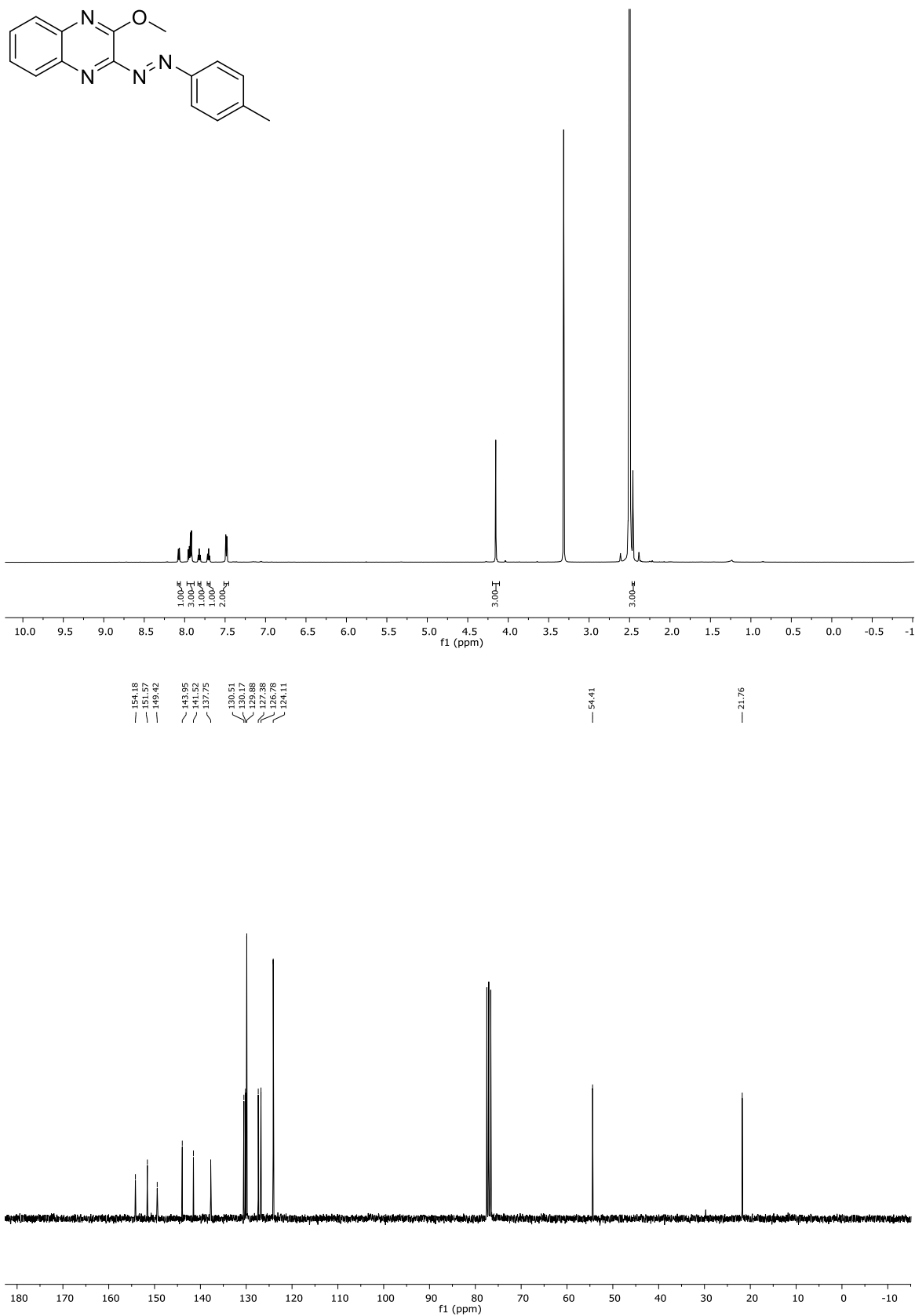
7.5 Supporting Information

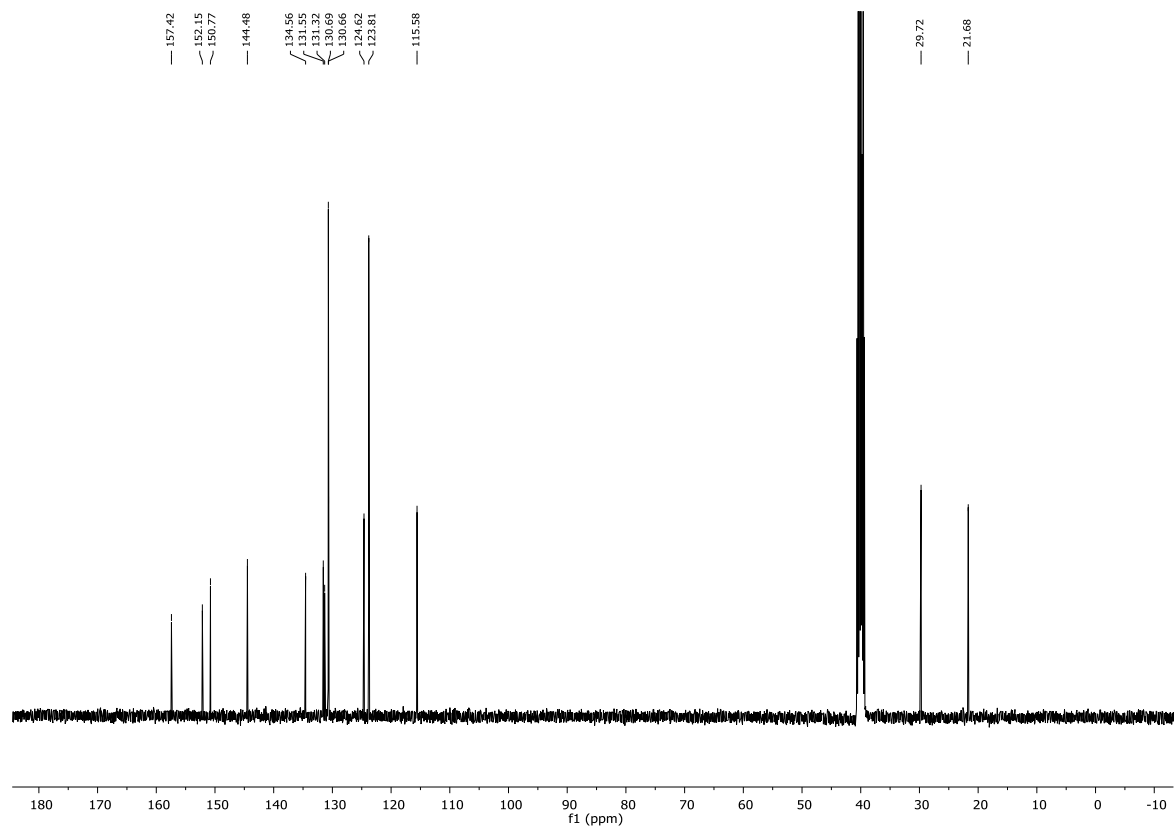
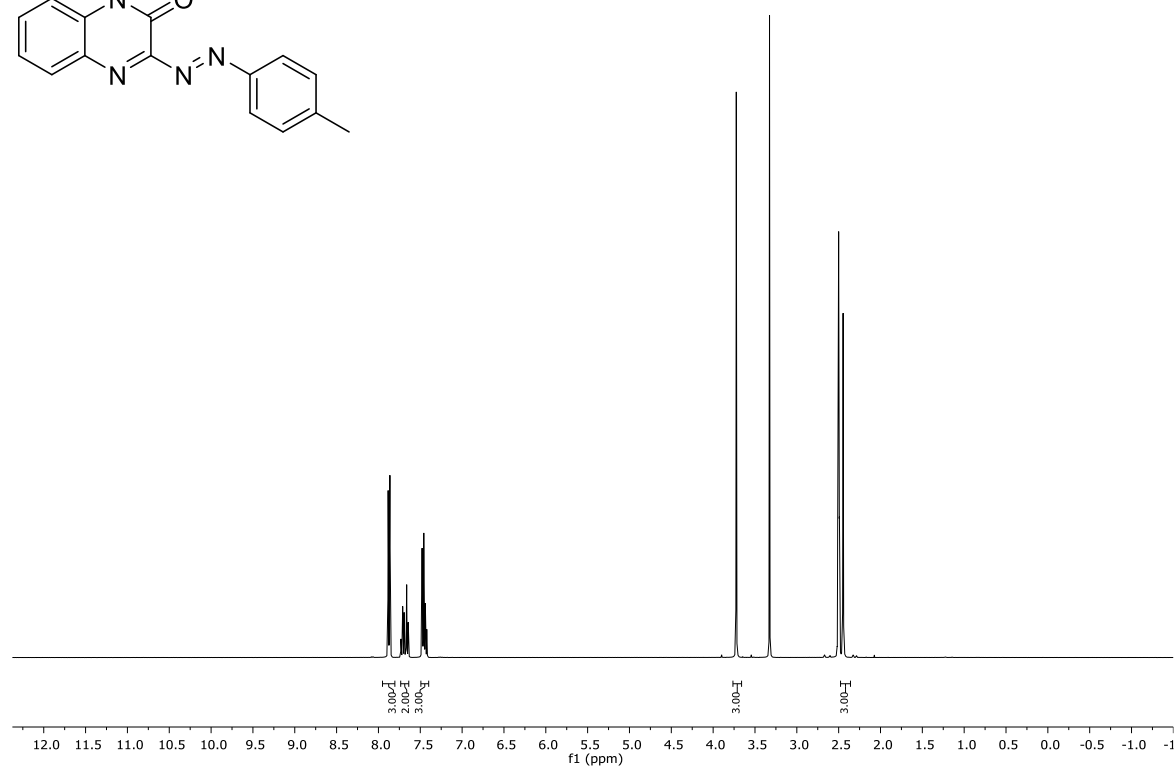
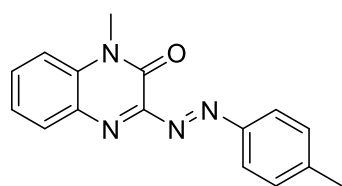
7.5.1 ^1H - and ^{13}C -NMR Spectra

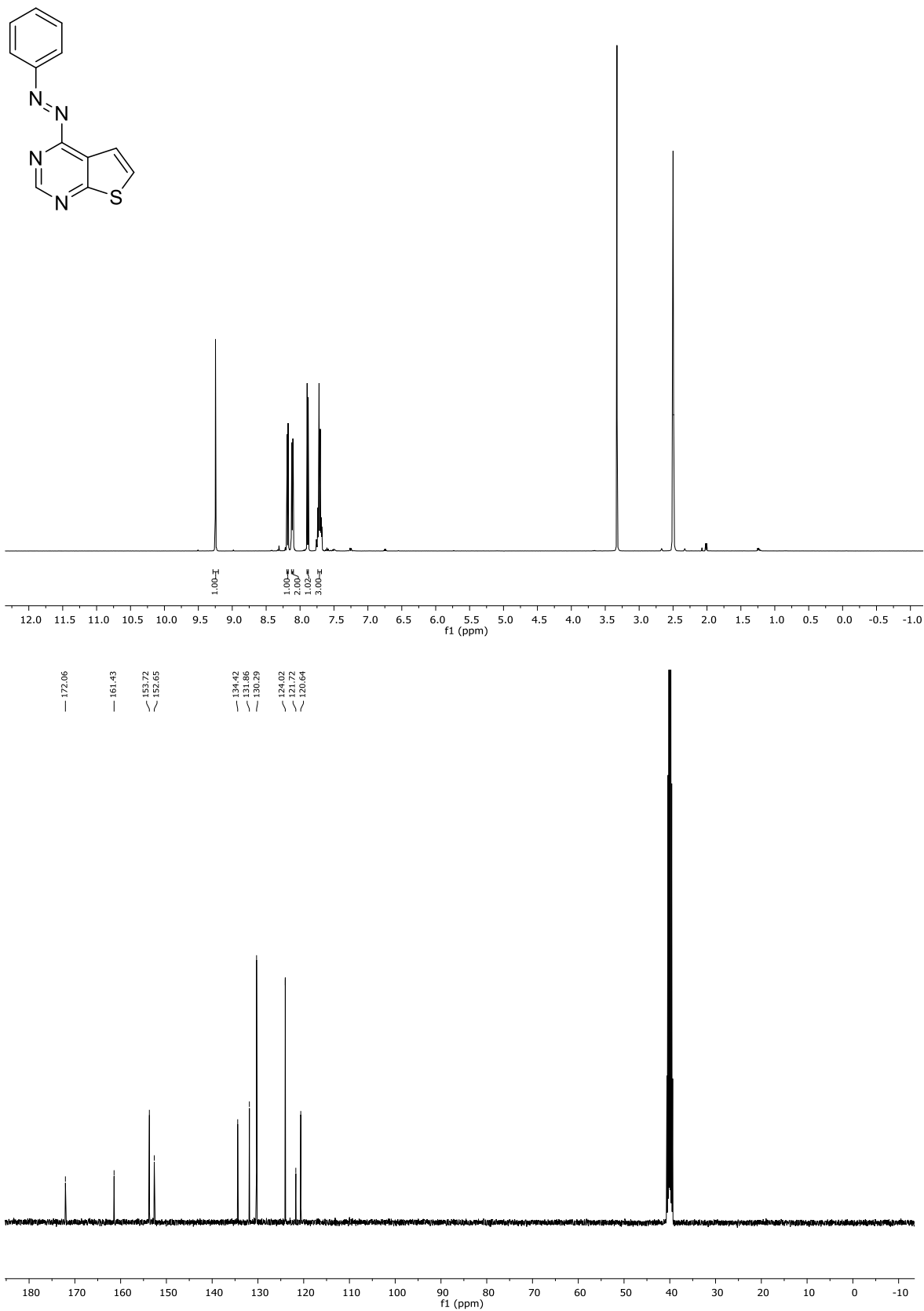
Compound 5a (DMSO- d_6)

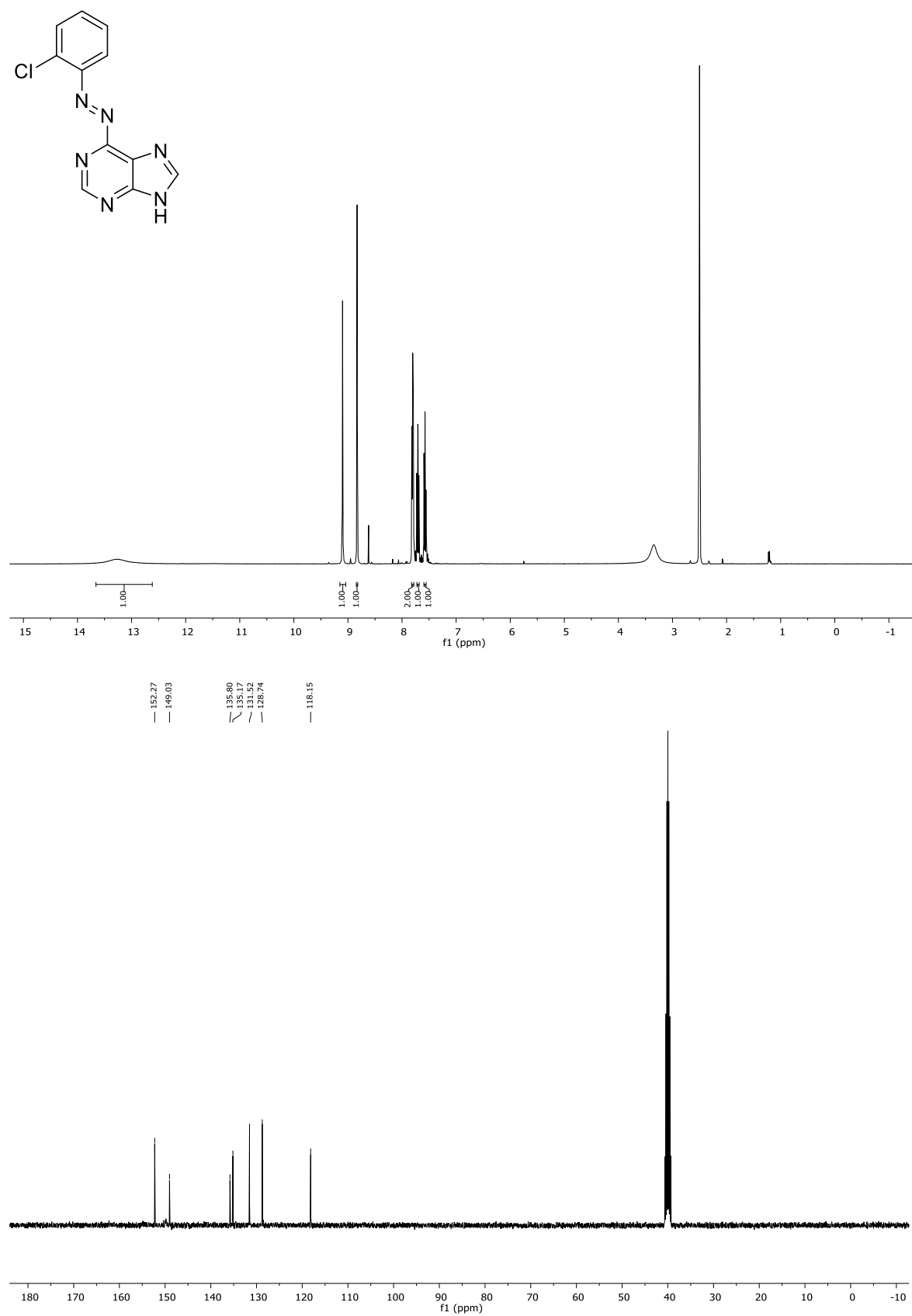


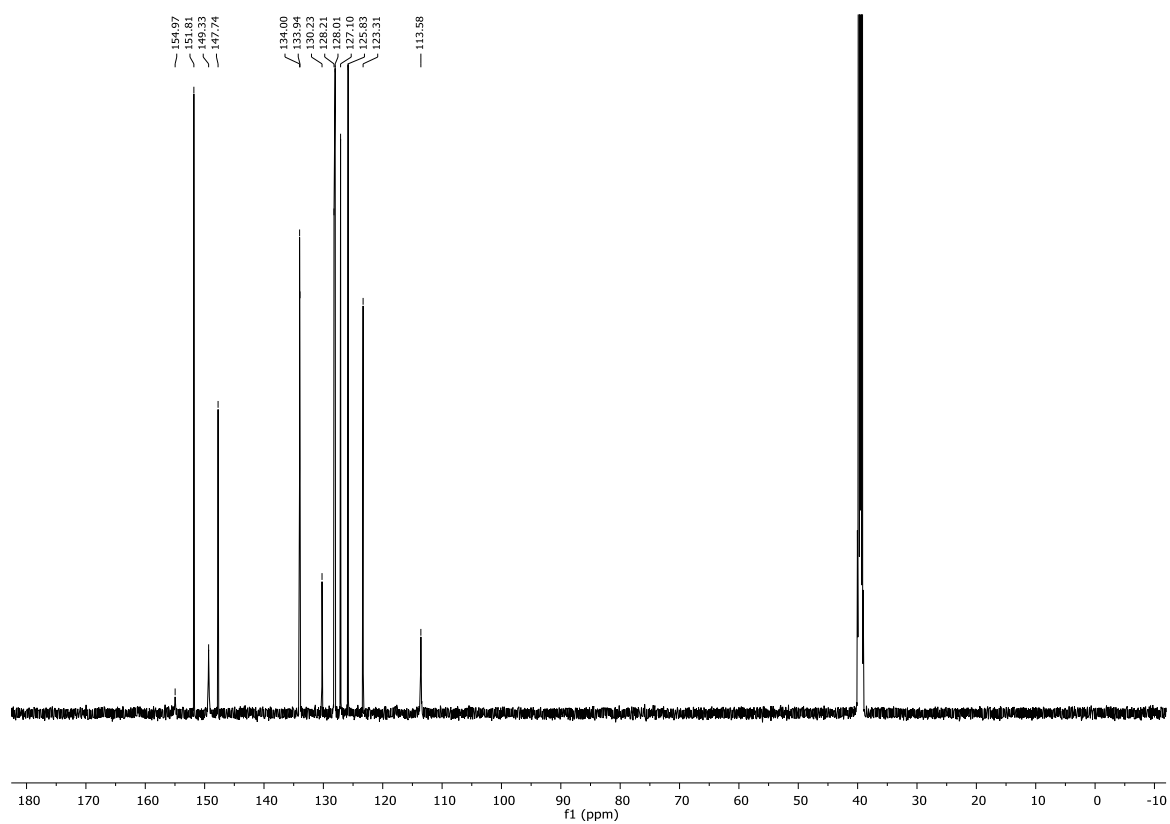
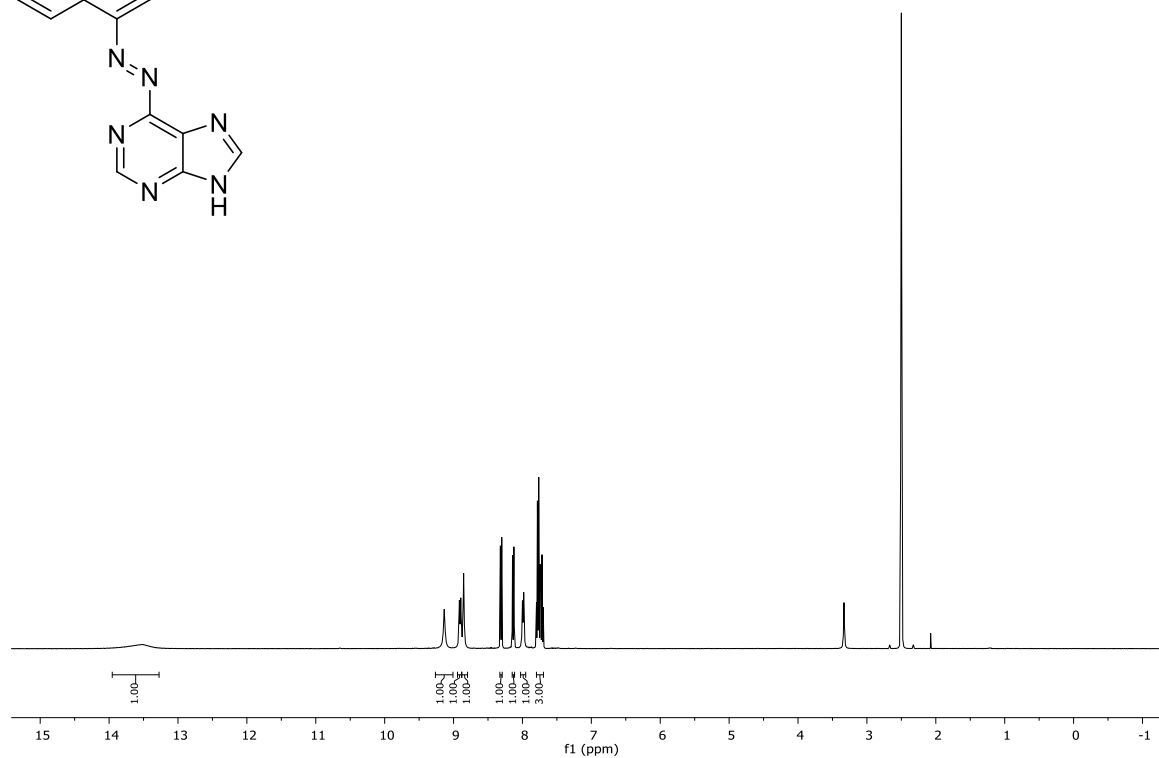
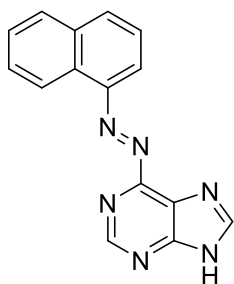
Compound **5b** (DMSO-*d*₆)


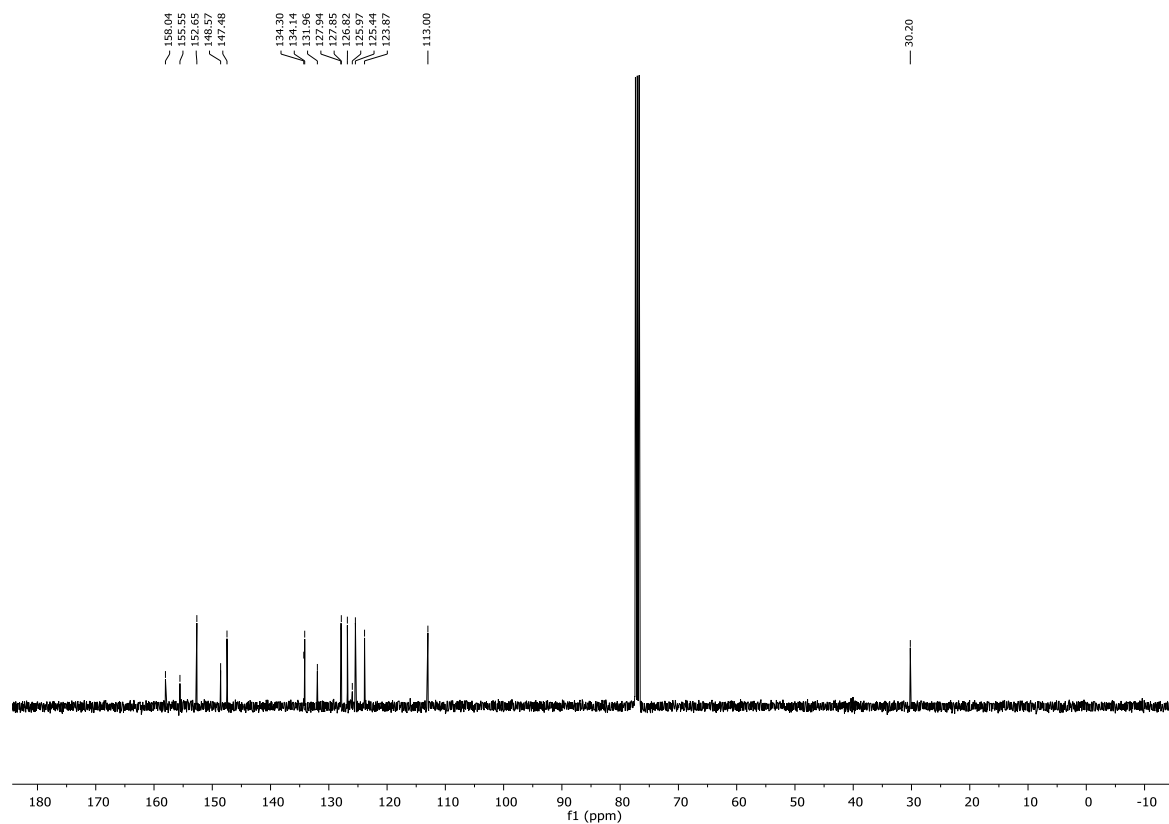
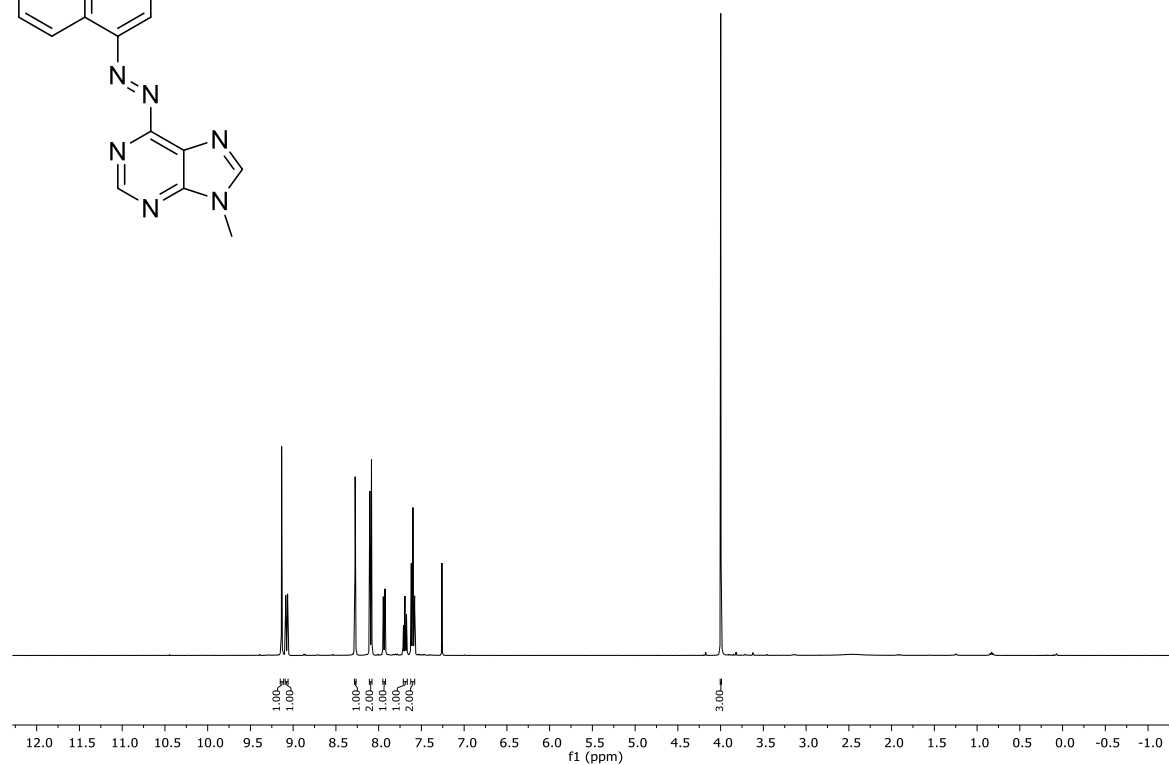
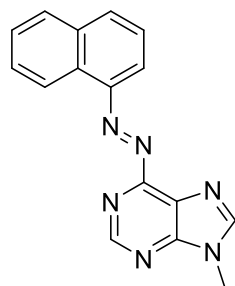
Compound **12a** (^1H DMSO- d_6 , ^{13}C CDCl_3 - d)

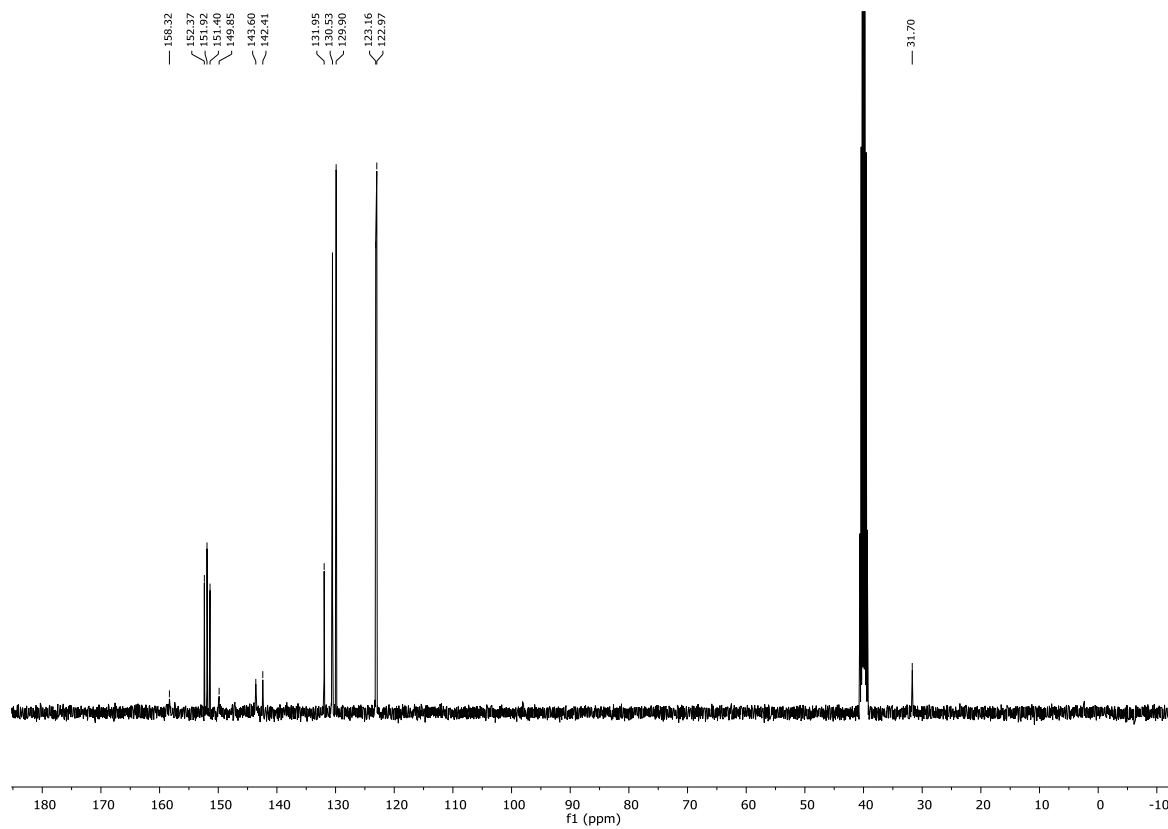
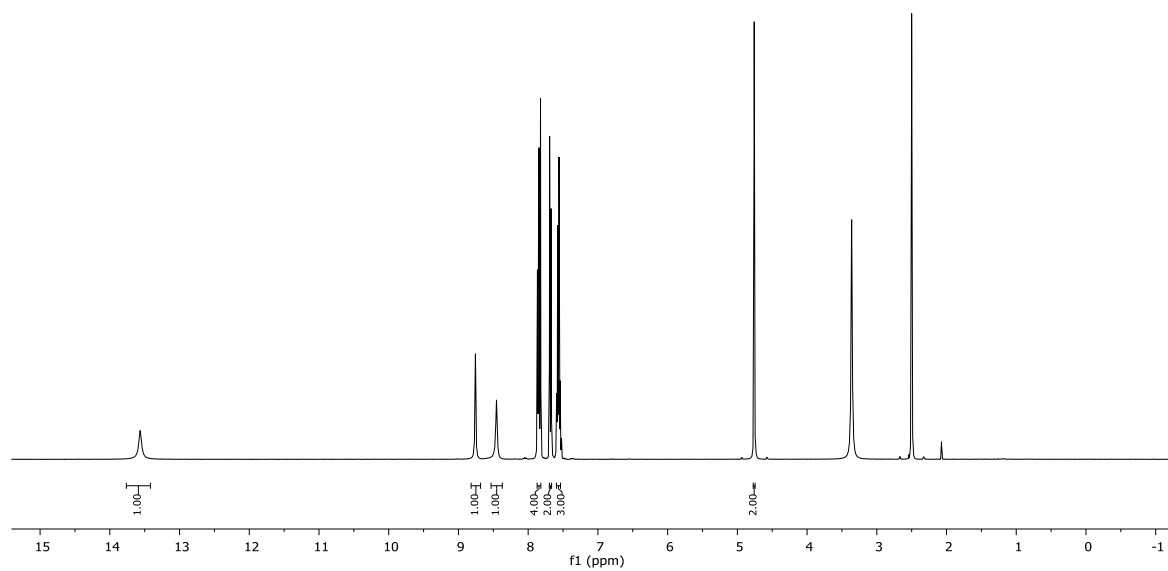
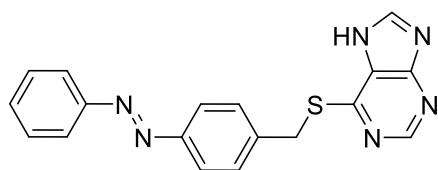
Compound **12b** (DMSO-*d*₆)

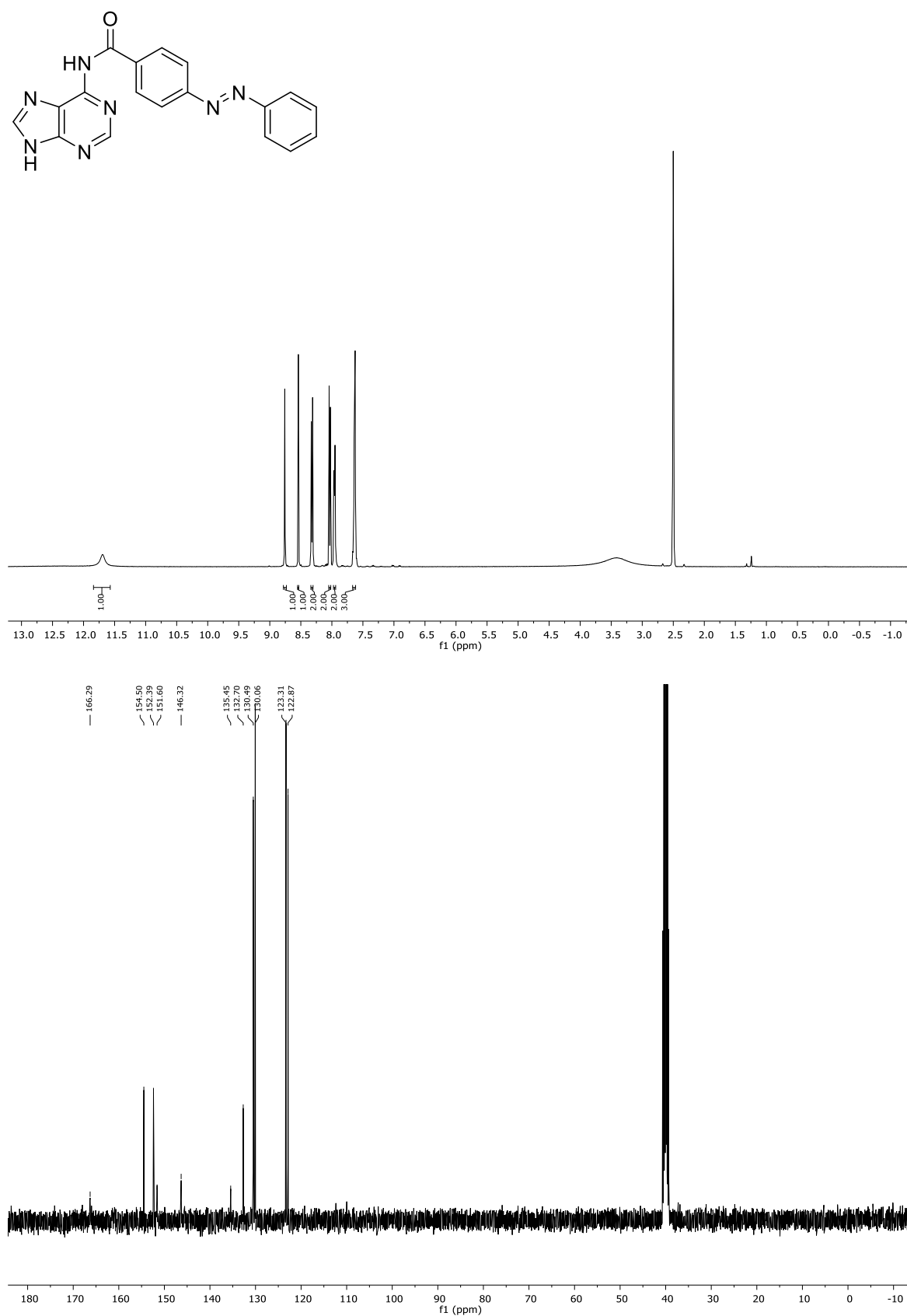
Compound **16a** (DMSO-*d*₆)

Compound **16b** (DMSO-*d*₆)




Compound **16d** (CDCl₃-*d*)


Compound **23** (DMSO-*d*₆)

Compound **28** (DMSO-*d*₆)

7.5.2 UV-Vis Absorption Spectra, Cycle Performances, and Thermal Half-Lives

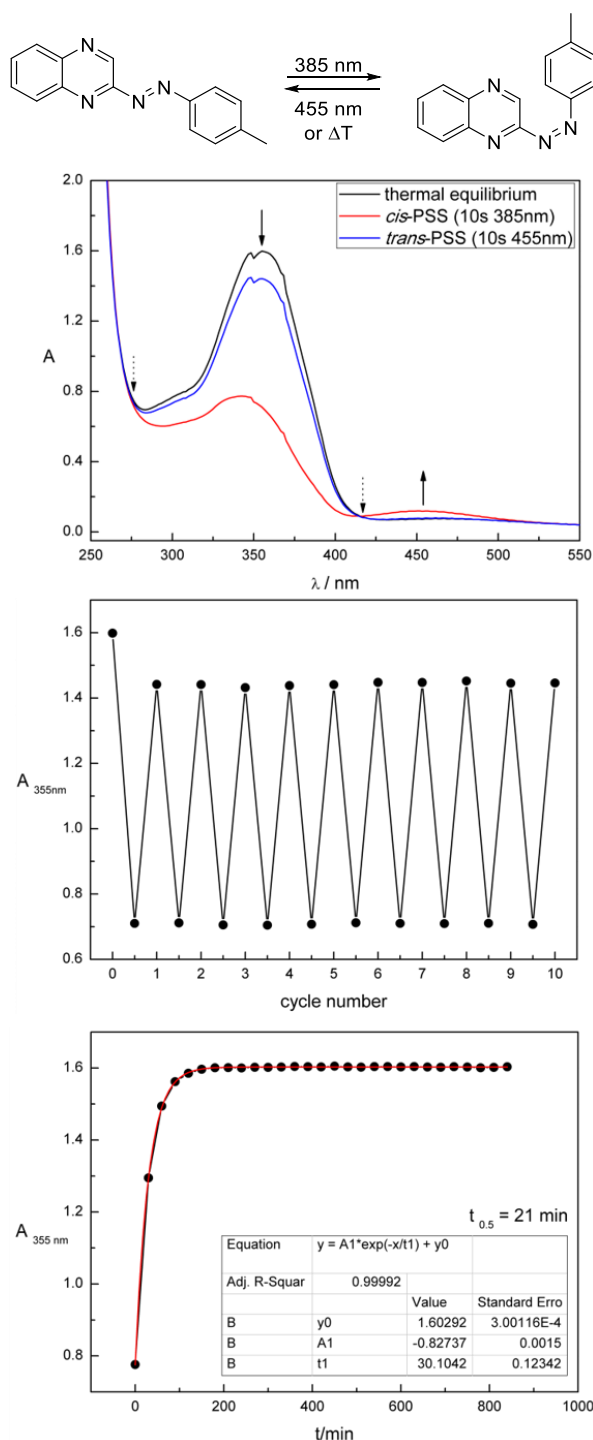


Figure S1. UV-Vis absorption spectroscopic characterization of compound **5a** measured at 50 μM in DMSO. Upper panel: UV-Vis absorption spectrum upon continuous irradiation with the indicated wavelengths until the PSS is reached. Black arrows indicate the changes in the absorption upon *trans*-*cis* isomerization. Dotted black arrows indicate isosbestic points. Middle panel: Cycle performance. Changes in absorption at λ_{max} of the *trans* isomer were measured during alternate irradiation with the indicated wavelengths. Lower panel: Thermal half-life determined at λ_{max} of the *trans* isomer.

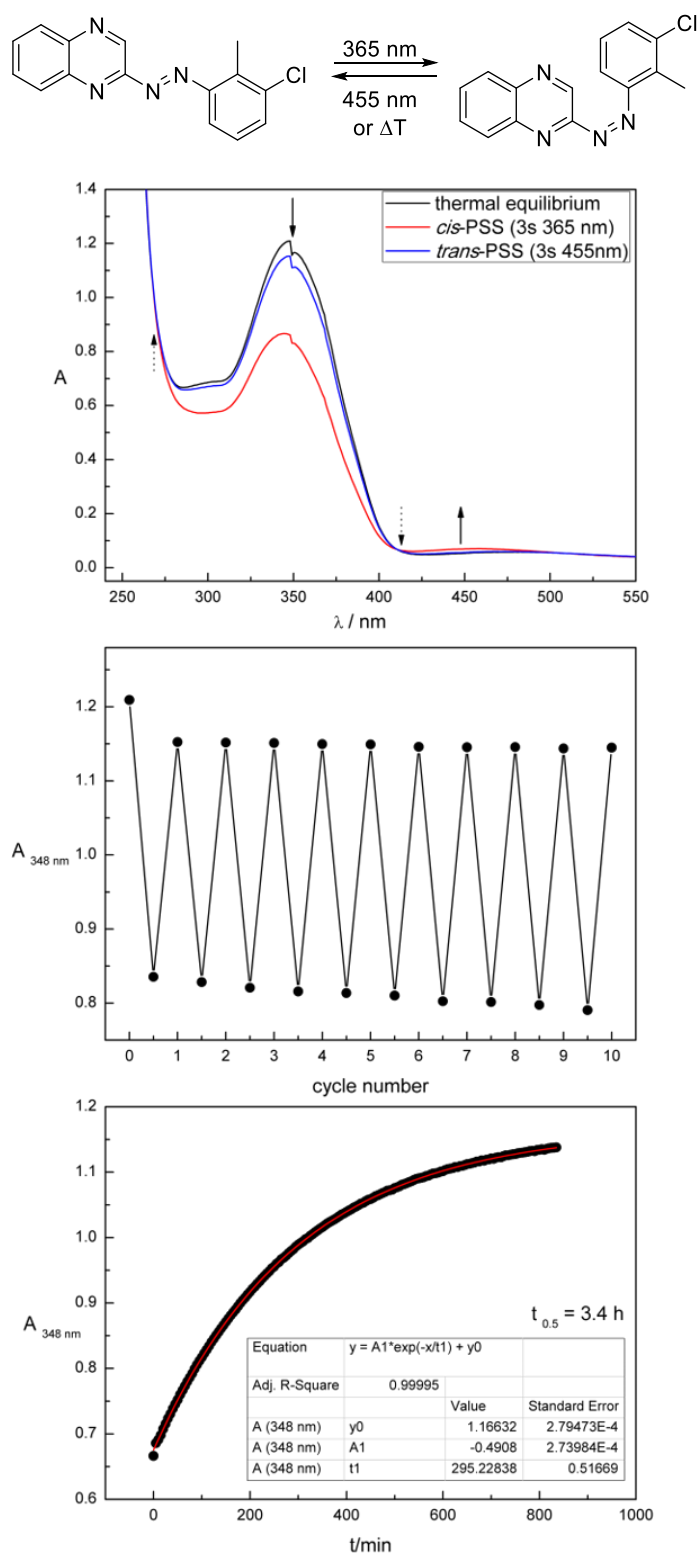


Figure S2. UV-Vis absorption spectroscopic characterization of compound **5b** measured at 50 μM in DMSO. Upper panel: UV-Vis absorption spectrum upon continuous irradiation with the indicated wavelengths until the PSS is reached. Black arrows indicate the changes in the absorption upon *trans*-*cis* isomerization. Dotted black arrows indicate isosbestic points. Middle panel: Cycle performance. Changes in absorption at λ_{max} of the *trans* isomer were measured during alternate irradiation with the indicated wavelengths. Lower panel: Thermal half-life determined at λ_{max} of the *trans* isomer.

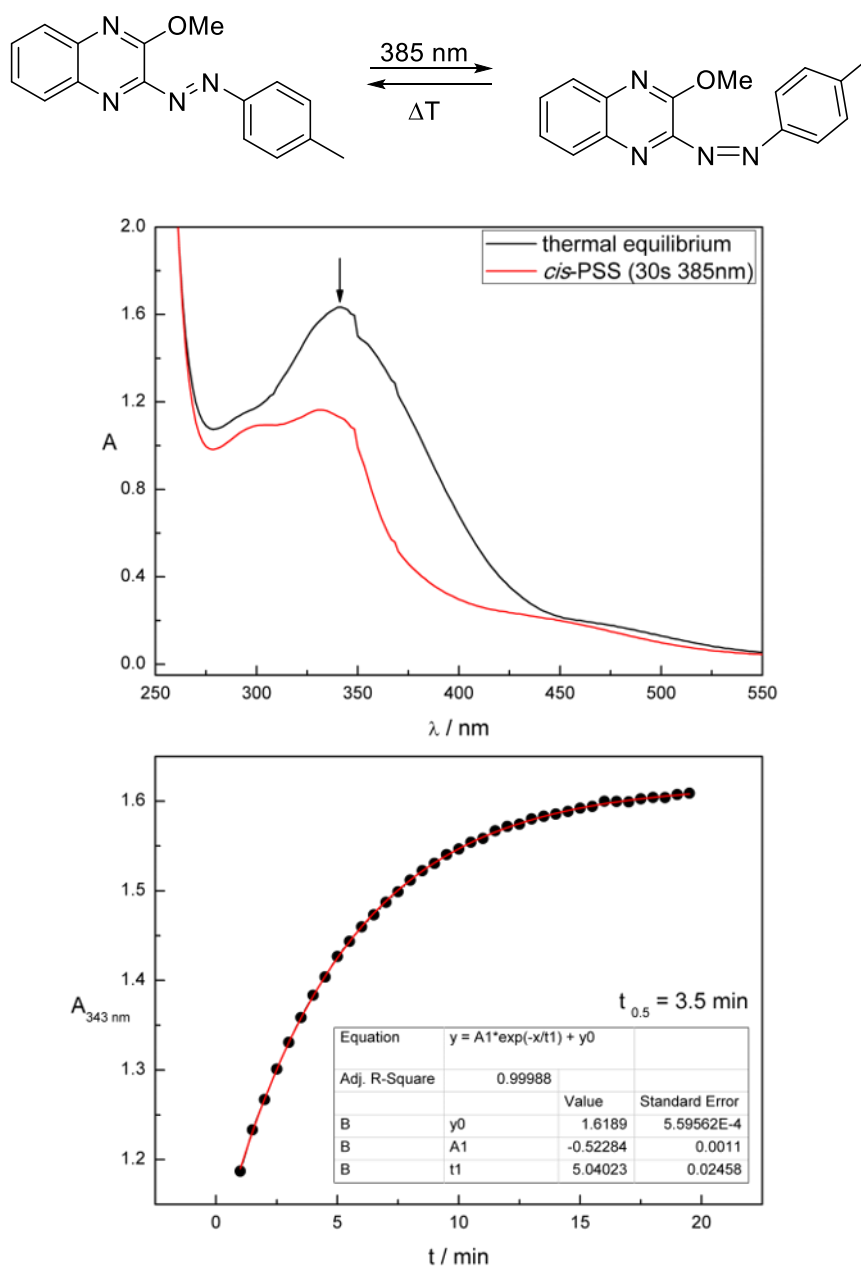


Figure S3. UV-Vis absorption spectroscopic characterization of compound **12a** measured at 50 μM in DMSO. As the *cis-trans* back isomerization is not triggerable by irradiation with light no cycle performance was recorded. Upper panel: UV-Vis absorption spectrum upon continuous irradiation with the indicated wavelength until the PSS is reached. Black arrow indicates the change in the absorption upon *trans-cis* isomerization. Lower panel: Thermal half-life determined at λ_{max} of the *trans* isomer.

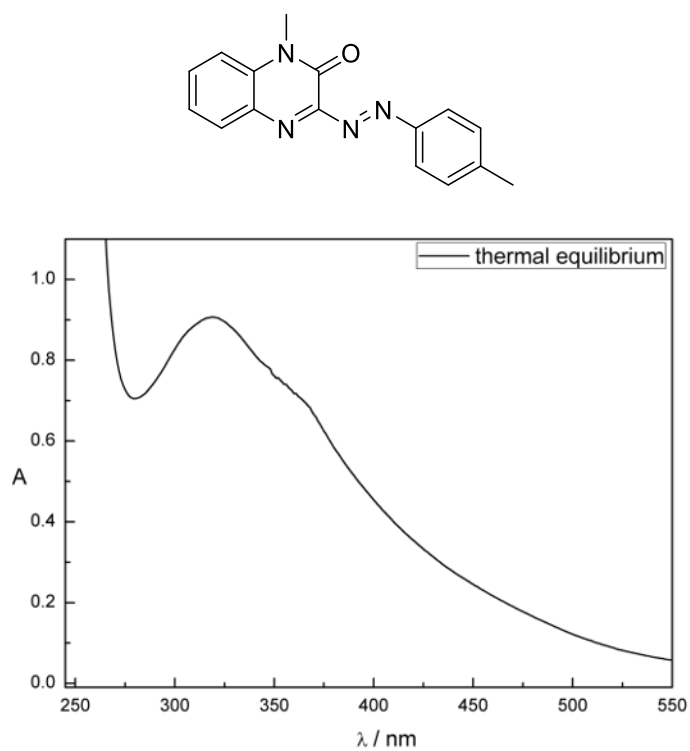


Figure S4. UV-Vis absorption spectrum of non-photochromic compound **12b** measured at 50 μ M in DMSO.

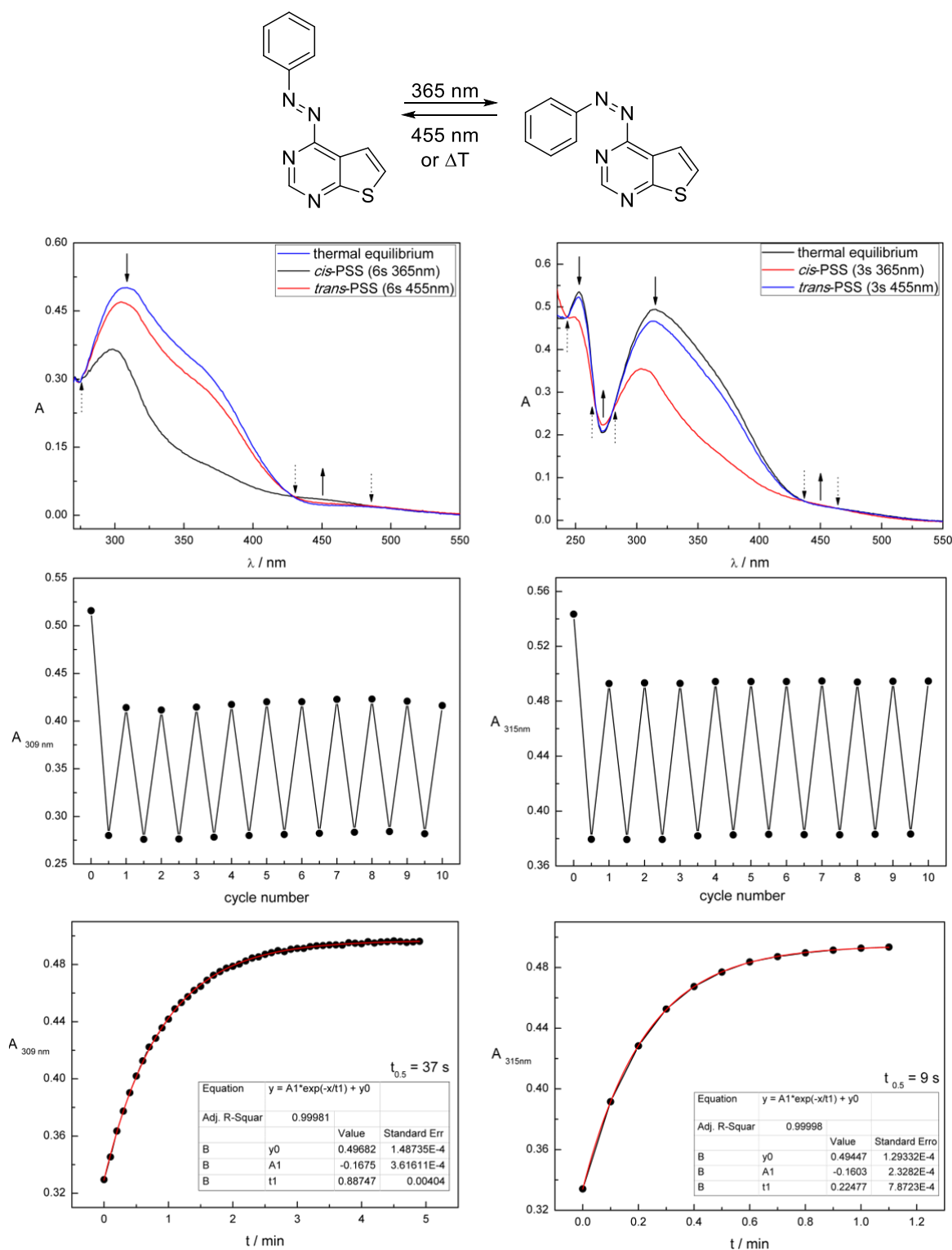


Figure S5. UV-Vis absorption spectroscopic characterization of compound **16a** measured at 50 μ M in DMSO (left) and phosphate buffer + 0.1% DMSO (right), respectively. Upper panel: UV-Vis absorption spectra upon continuous irradiation with the indicated wavelengths until the PSS is reached. Black arrows indicate the changes in the absorption upon *trans*-*cis* isomerization. Dotted black arrows indicate isosbestic points. Middle panel: Cycle performances. Changes in absorption at λ_{\max} of the *trans* isomer were measured during alternate irradiation with the indicated wavelengths. Lower panel: Thermal half-lives determined at λ_{\max} of the *trans* isomer.

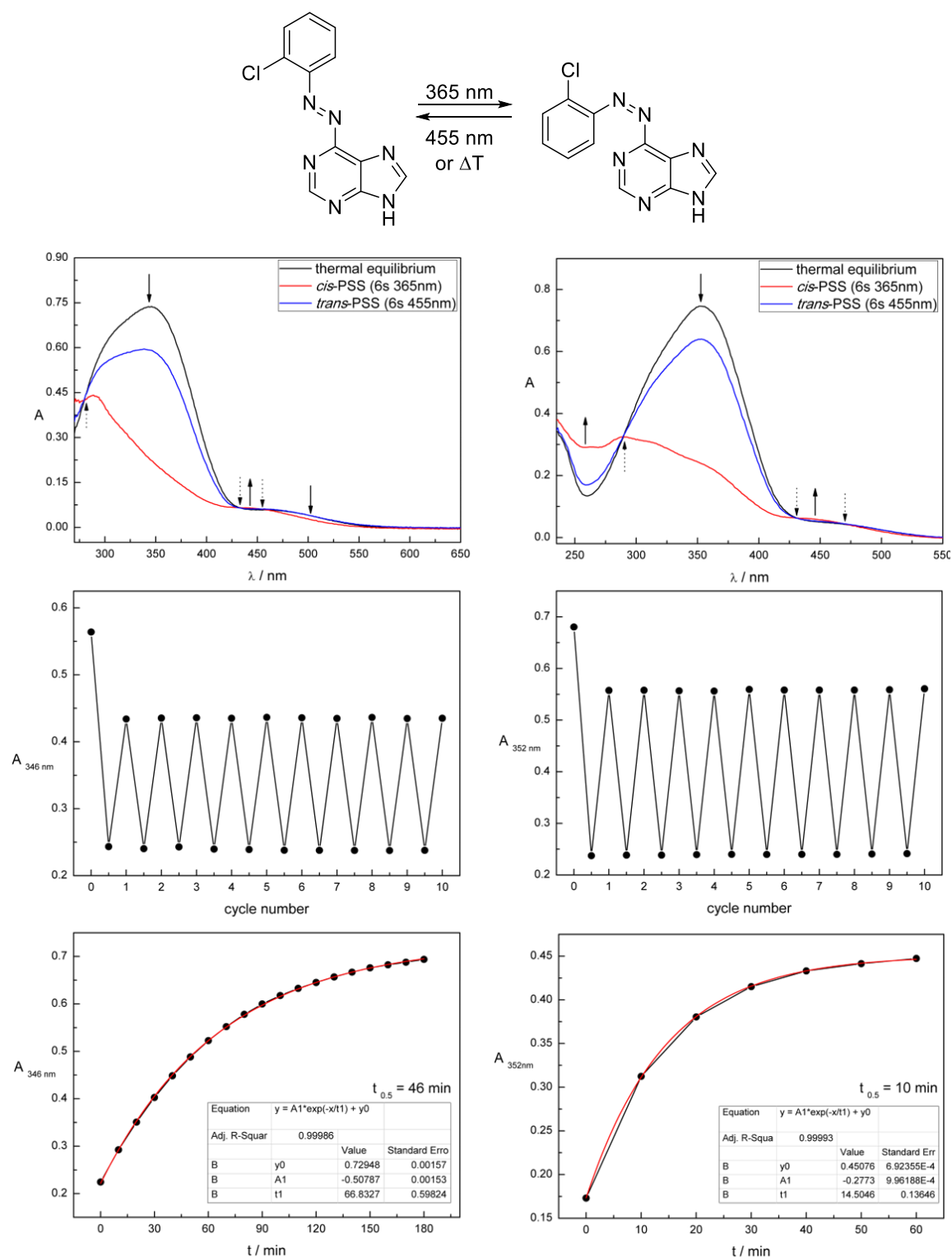


Figure S6. UV-Vis absorption spectroscopic characterization of compound **16b** measured at 50 μM in DMSO (left) and phosphate buffer + 0.1% DMSO (right), respectively. Upper panel: UV-Vis absorption spectra upon continuous irradiation with the indicated wavelengths until the PSS is reached. Black arrows indicate the changes in the absorption upon *trans-cis* isomerization. Dotted black arrows indicate isosbestic points. Middle panel: Cycle performances. Changes in absorption at λ_{max} of the *trans* isomer were measured during alternate irradiation with the indicated wavelengths. Lower panel: Thermal half-lives determined at λ_{max} of the *trans* isomer.

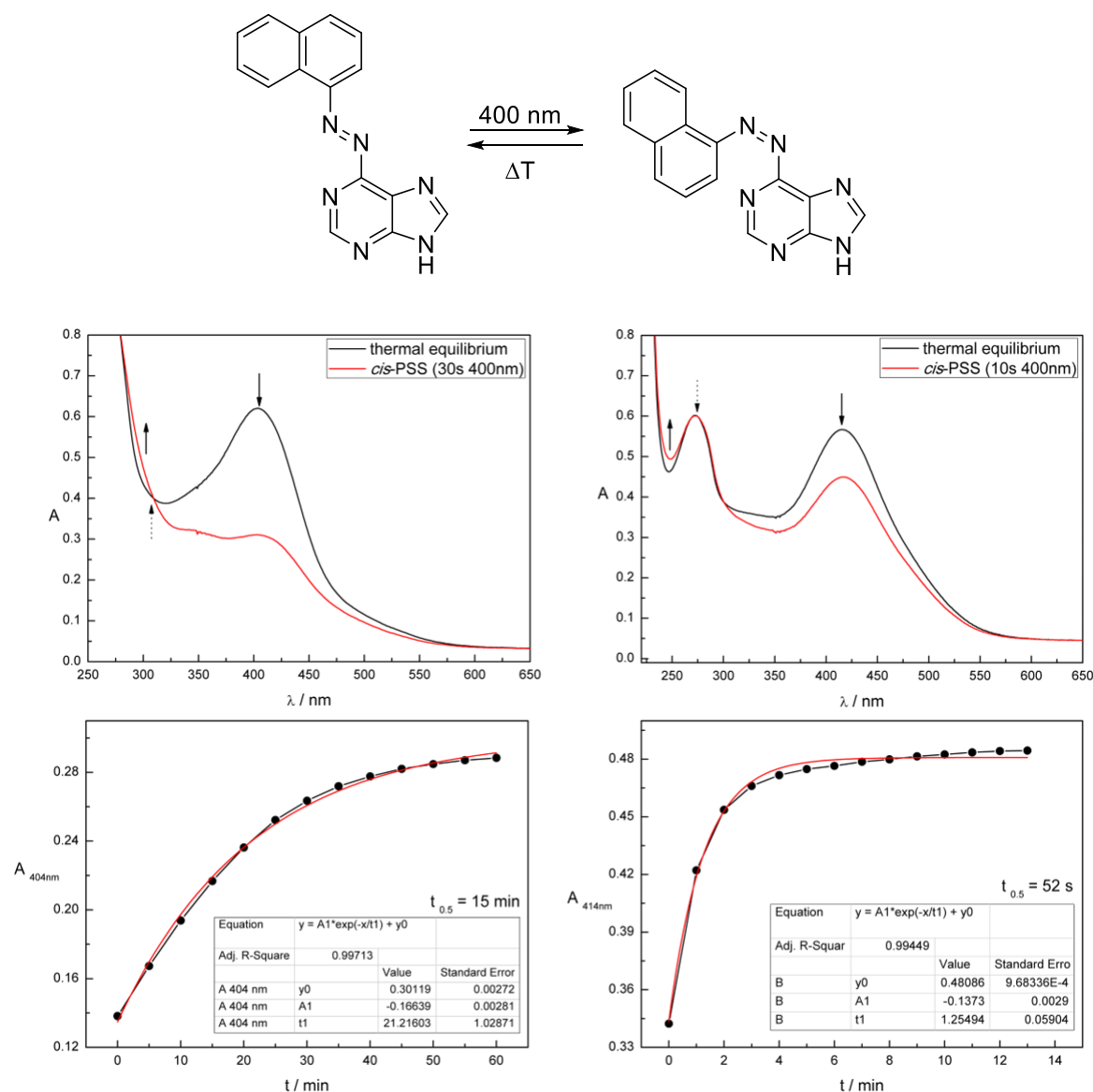


Figure S7. UV-Vis absorption spectroscopic characterization of compound **16c** measured at 50 μM in DMSO (left) and phosphate buffer + 0.1% DMSO (right), respectively. As the *cis-trans* back isomerization is not triggerable by irradiation with light no cycle performances were recorded. Upper panel: UV-Vis absorption spectra upon continuous irradiation with the indicated wavelength until the PSS is reached. Black arrows indicate the change in the absorption upon *trans-cis* isomerization. Lower panel: Thermal half-lives determined at λ_{\max} of the *trans* isomer.

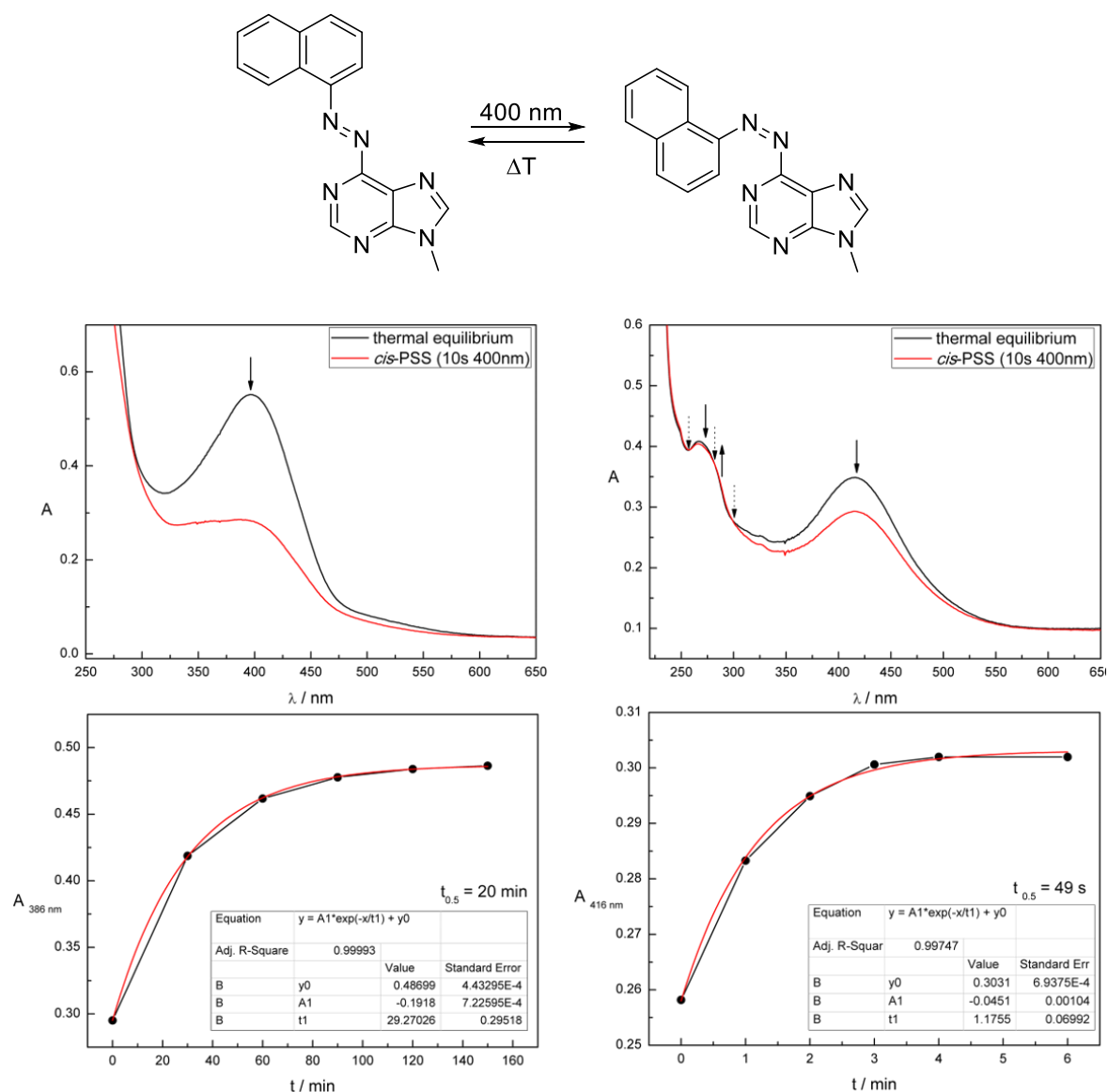


Figure S8. UV-Vis absorption spectroscopic characterization of compound **16d** measured at 50 μM in DMSO (left) and phosphate buffer + 0.1% DMSO (right), respectively. As the *cis-trans* back isomerization is not triggerable by irradiation with light no cycle performances were recorded. Upper panel: UV-Vis absorption spectra upon continuous irradiation with the indicated wavelength until the PSS is reached. Black arrows indicate the change in the absorption upon *trans-cis* isomerization. Dotted black arrows indicate isosbestic points. Lower panel: Thermal half-lives determined at λ_{max} of the *trans*-isomer.

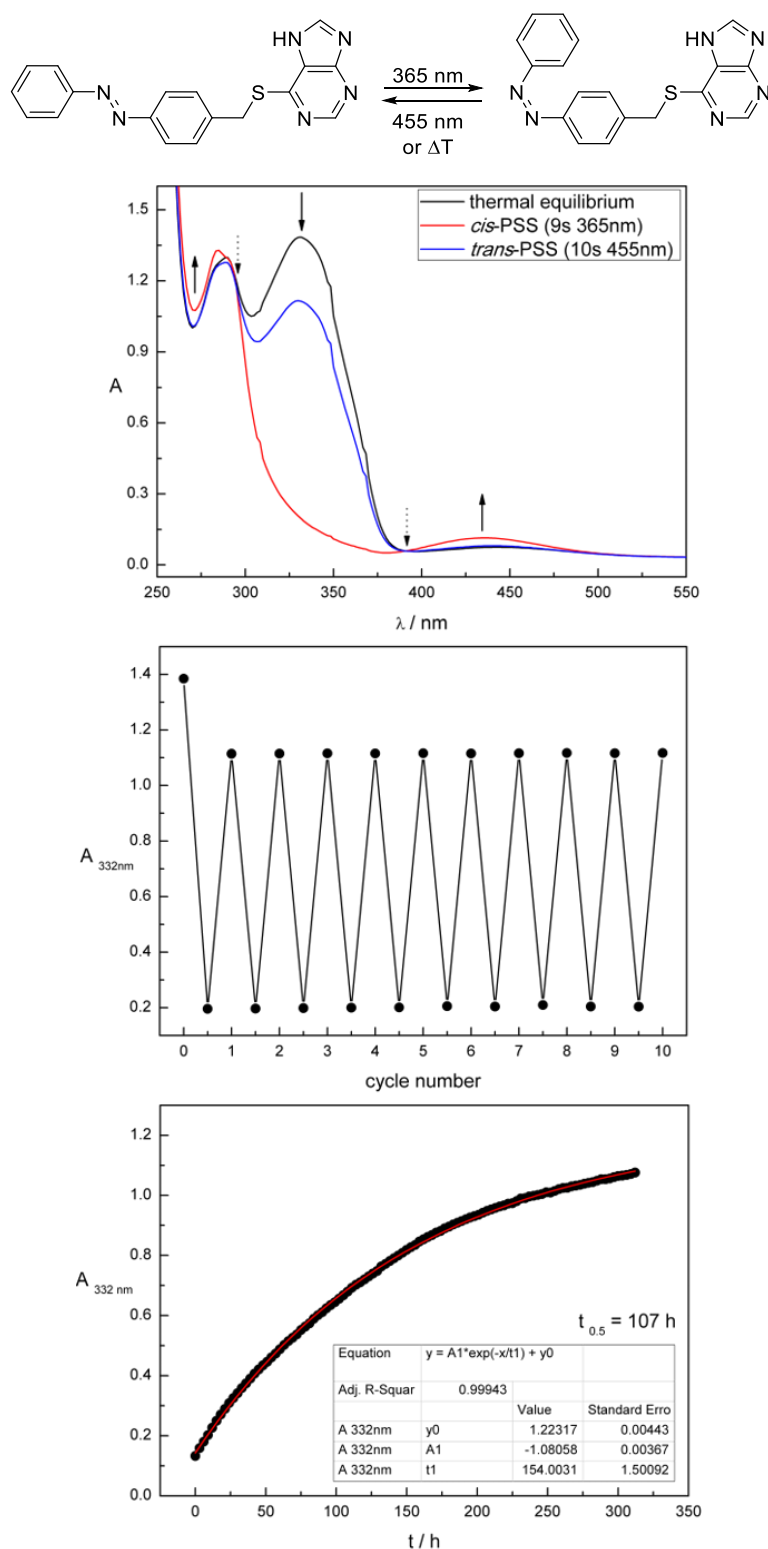


Figure S9. UV-Vis absorption spectroscopic characterization of compound **23** measured at 50 μM in DMSO. Upper panel: UV-Vis absorption spectrum upon continuous irradiation with the indicated wavelengths until the PSS is reached. Black arrows indicate the changes in the absorption upon *trans*-*cis* isomerization. Dotted black arrows indicate isosbestic points. Middle panel: Cycle performance. Changes in absorption at λ_{max} of the *trans* isomer were measured during alternate irradiation with the indicated wavelengths. Lower panel: Thermal half-life determined at λ_{max} of the *trans* isomer.

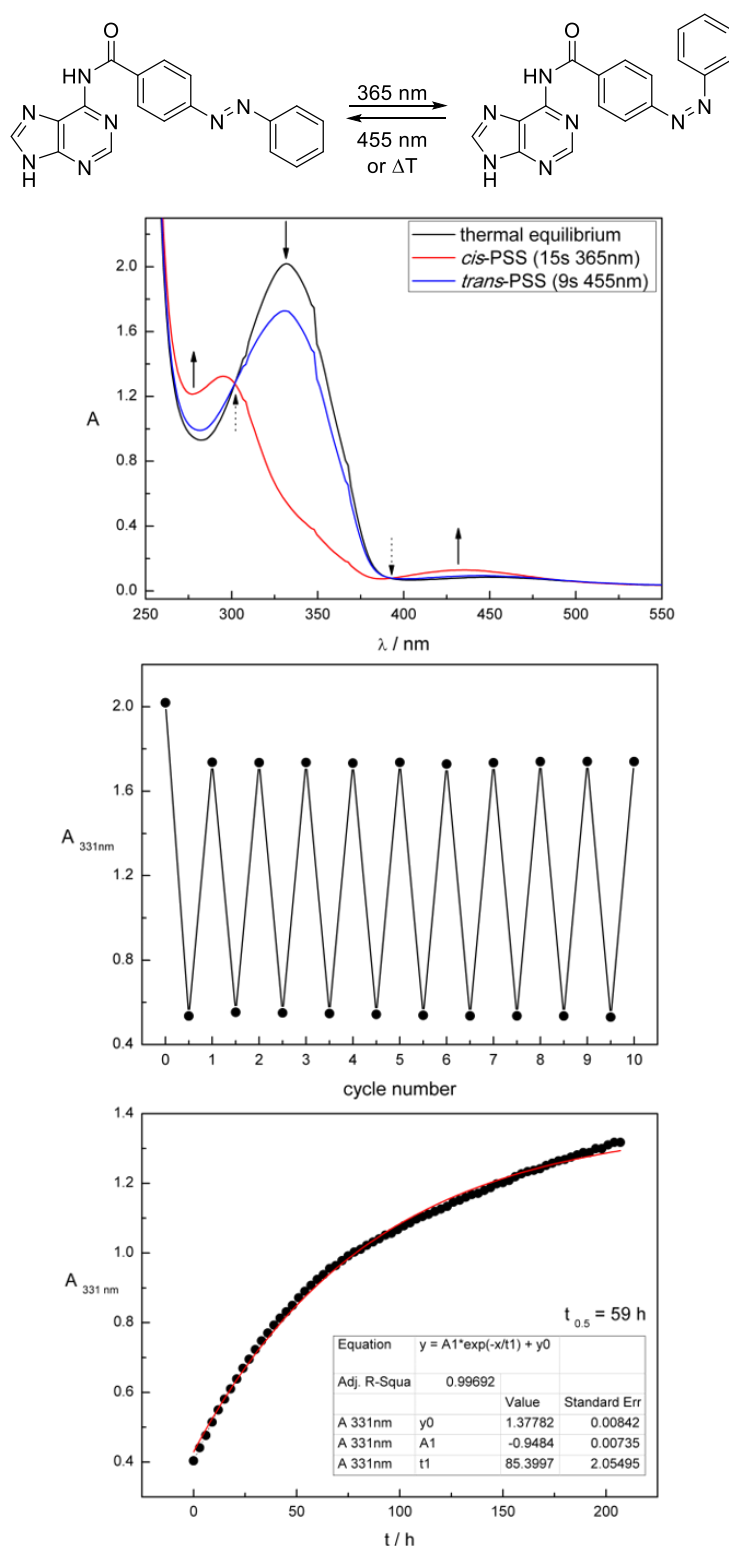


Figure S10. UV-Vis absorption spectroscopic characterization of compound **28** measured at 50 μM in DMSO. Upper panel: UV-Vis absorption spectrum upon continuous irradiation with the indicated wavelengths until the PSS is reached. Black arrows indicate the changes in the absorption upon *trans*-*cis* isomerization. Dotted black arrows indicate isosbestic points. Middle panel: Cycle performance. Changes in absorbance at λ_{max} of the *trans* isomer were measured during alternate irradiation with the indicated wavelengths. Lower panel: Thermal half-life determined at λ_{max} of the *trans* isomer.

7.5.3 Tabular Summarized Photochemical Data

Table S1. Photochemical properties of azobenzene-based serotonin 5-HT₃R antagonists determined at 50 μ M in DMSO. Cpd. = Compound.

Entry	Cpd.	λ_{\max} <i>trans</i> isomer [nm]	λ_{\max} <i>cis</i> isomer [nm]	Isosbestic points [nm]	THL
1	5a	355	452	268, 415	21 min
2	5b	348	455	266, 411	3.4 h
3	12a	343	-	-	3.5 min
4	12b	319	-	-	-
5	16a	309	-	275, 430, 489	37 s
6	16b	346	-	279, 432, 459	46 min
7	16c	404	-	309	15 min
8	16d	386	-	309	20 min
9	23	332	437	289, 391	107 h
10	28	331	434	302, 392	59 h

Table S2. Photochemical properties of azobenzene-based serotonin 5-HT₃R antagonists determined at 50 μ M in phosphate buffer + 0.1% DMSO. Cpd. = Compound.

Entry	Cpd.	λ_{\max} <i>trans</i> isomer [nm]	λ_{\max} <i>cis</i> isomer [nm]	Isosbestic points [nm]	THL
1	16a	315	-	243, 267, 280, 438, 466	9 s
2	16b	352	-	289, 431, 470	10 min
3	16c	414	-	306	52 s
4	16d	416	-	314	49 s

Table S3. Determination of the photostationary states for the thermally more stable compounds **23** and **28** (at 50 μ M DMSO) using analytical HPLC at the isosbestic point at 20 °C.

Entry	Compound	PSS-distribution
1	23	91% <i>cis</i> (365 nm); 81% <i>trans</i> (455 nm)
2	28	69% <i>cis</i> (365 nm); 84% <i>trans</i> (455 nm)

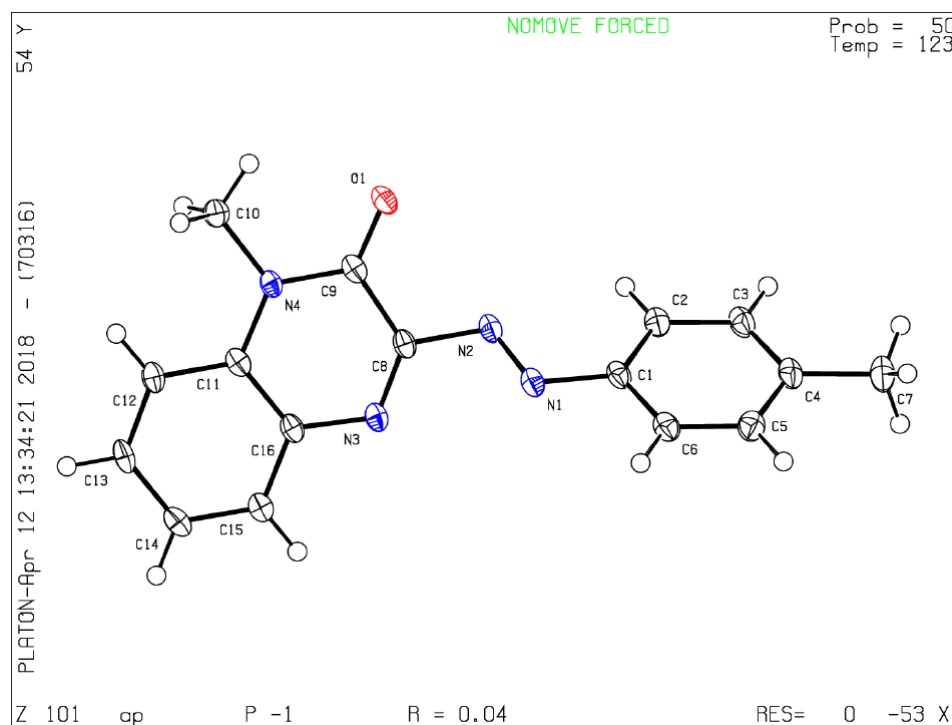
7.5.4 Single Crystal X-ray Crystallography

Compound **12b**

Experimental. Single clear red plate-shaped crystals of **12b** were obtained by recrystallisation from acetone. A suitable crystal (0.088×0.195×0.309) mm³ was selected and mounted on a MITIGEN holder with inert oil on a SuperNova, Single source at offset/far, Atlas diffractometer. The crystal was kept at T = 123 K during data collection. Using Olex2,^[78] the structure was solved with the ShelXT^[79] structure solution program, using the Intrinsic Phasing solution method. The model was refined with version 2016/6 of ShelXL^[80] using Least Squares minimization.

Crystal Data. C₁₆H₁₄N₄O, *M_r* = 279.31, triclinic P-1 (No. 2), *a* = 7.3051(5) Å, *b* = 9.2030(6) Å, *c* = 11.3965(8) Å, α = 100.804(5)°, β = 97.060(5)°, γ = 113.159(6)°, *V* = 675.35(9) Å³, *T* = 123(1) K, *Z* = 1 λ=(CuKα) = 2.732, 395 reflections measured, 2567 unique (*R*_{int} = 0.0305) which were used in all calculations. The final *wR*₂ was 0.1266 (all data) and *R*₁ was 0.0522 (*I* > 2(*I*)).

Cambridge Structural Database CCDC. 1890055



Detailed Crystal Data.

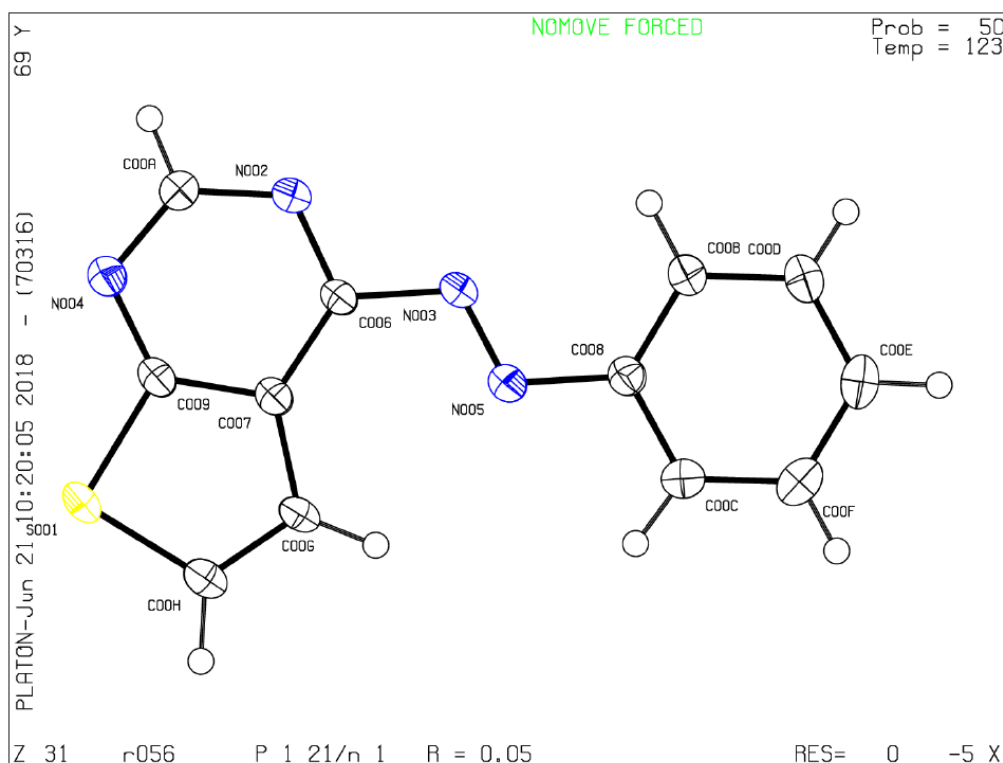
Empirical formula	C ₁₆ H ₁₄ N ₄ O
Formula weight	278.31
Temperature/K	123(1)
Crystal system	triclinic
Space group	P-1
a/Å	7.3051(5)
b/Å	9.2030(6)
c/Å	11.3965(8)
α/°	100.804(5)
β/°	97.060(5)
γ/°	113.159(6)
Volume/Å ³	675.35(9)
Z	1
ρ _{calc} /g/cm ³	0.684
μ/mm ⁻¹	0.362
F(000)	146.0
Crystal size/mm ³	0.309 × 0.195 × 0.088
Radiation	CuKα (λ = 1.54184)
2Θ range for data collection/°	8.092 to 146.842
Index ranges	-8 ≤ h ≤ 8, -7 ≤ k ≤ 11, -14 ≤ l ≤ 11
Reflections collected	3951
Independent reflections	2567 [R _{int} = 0.0305, R _{sigma} = 0.0405]
Data/restraints/parameters	2567/0/192
Goodness-of-fit on F ²	1.036
Final R indexes [I ≥ 2σ (I)]	R ₁ = 0.0443, wR ₂ = 0.1179
Final R indexes [all data]	R ₁ = 0.0522, wR ₂ = 0.1266
Largest diff. peak/hole / e Å ⁻³	0.24/-0.29

Compound **16a**

Experimental. Single clear orange plate-shaped crystals of **16a** were obtained by recrystallisation from CH₂Cl₂. A suitable crystal 0.29×0.24×0.04 mm³ was selected and mounted on a suitable support on an GV1000, TitanS2 diffractometer. The crystal was kept at a steady $T = 123.01(13)$ K during data collection. The structure was solved with the ShelXT^[79] structure solution program using the Intrinsic Phasing solution method and by using Olex2^[78] as the graphical interface. The model was refined with version 2016/6 of ShelXL^[80] using Least Squares minimization.

Crystal Data. C₁₂H₈N₄S, $M_r = 240.28$, monoclinic, $P2_1/n$ (No. 14), $a = 7.0586(3)$ Å, $b = 7.5744(2)$ Å, $c = 20.8479(9)$ Å, $\beta = 98.124(3)^\circ$, $\alpha = \gamma = 90^\circ$, $V = 1103.44(7)$ Å³, $T = 123.01(13)$ K, $Z = 4$, $Z' = 1$, $\mu(\text{CuK}\alpha) = 2.445$, 7909 reflections measured, 2196 unique ($R_{\text{int}} = 0.0606$) which were used in all calculations. The final wR_2 was 0.1380 (all data) and R_1 was 0.0465 ($I > 2(I)$).

Cambridge Structural Database CCDC. 1889897



Detailed crystal data.

Formula	C ₁₂ H ₈ N ₄ S
$D_{\text{calc.}}/\text{g cm}^{-3}$	1.446
μ/mm^{-1}	2.445
Formula Weight	240.28
Colour	clear orange
Shape	plate
Size/mm ³	0.29×0.24×0.04
T/K	123.01(13)
Crystal System	monoclinic
Space Group	$P2_1/n$
$a/\text{\AA}$	7.0586(3)
$b/\text{\AA}$	7.5744(2)
$c/\text{\AA}$	20.8479(9)
$\alpha/^\circ$	90
$\beta/^\circ$	98.124(3)
$\gamma/^\circ$	90
$V/\text{\AA}^3$	1103.44(7)
Z	4
Z'	1
Wavelength/ \AA	1.54184
Radiation type	CuK α
$\theta_{\text{min}}/^\circ$	4.284
$\theta_{\text{max}}/^\circ$	74.411
Measured Refl.	7909
Independent Refl.	2196
Reflections with $I > 2(I)$	1981
R_{int}	0.0606
Parameters	186
Restraints	0
Largest Peak	0.344
Deepest Hole	-0.369
GooF	1.099
wR_2 (all data)	0.1380
wR_2	0.1321
R_1 (all data)	0.0516
R_1	0.0465

7.6 References

- [1] N. M. Barnes, J. F. Neumaier, *Tocris Bioscience Scientific Review Series* **2015**, 34, 1-16.
- [2] M. M. Rapport, *J. Biol. Chem.* **1949**, 180, 961-969.
- [3] V. Erspamer, B. Asero, *Nature* **1952**, 169, 800-801.
- [4] V. Erspamer, *Archiv f. experiment. Path. u. Pharmacol.* **1940**, 196, 343-365.
- [5] N. M. Barnes, T. Sharp, *Neuropharmacology* **1999**, 38, 1083-1152.
- [6] M. Berger, J. A. Gray, B. L. Roth, *Annu. Rev. Med.* **2009**, 60, 355-366.
- [7] J. M. Davis, N. L. Alderson, R. S. Welsh, *Am. J. Clin. Nutr.* **2000**, 72, 573S-8S.
- [8] R. S. Ray, A. E. Corcoran, R. D. Brust, J. C. Kim, G. B. Richerson, E. Nattie, S. M. Dymecki, *Science* **2011**, 333, 637-642.
- [9] J. D. McCorvy, B. L. Roth, *Pharm. Ther.* **2015**, 150, 129-142.
- [10] M. D. Gershon, P. R. Wade, A. L. Kirchgessner, H. Tamir, *Neuropharmacology* **1990**, 3, 385-395.
- [11] J. M. Lauder, *Annals of the New York Academy of Science* **1990**, 600, 297-313.
- [12] E. C. Azmitia, *Brain Res. Bull.* **2001**, 56, 413-424.
- [13] T. Vitalis, O. Cases, S. Passemard, J. Callebert, J. G. Parnavelas, *Eur. J. Neurosci.* **2007**, 26, 331-334.
- [14] M. Matsukawa, K. Nakadate, I. Ishihara, N. Okada, *Neuroscience* **2003**, 122, 627-635.
- [15] M. Engel, M. P. Schmidt, J. A. van Hooft, *Front. Cell. Neurosci.* **2013**, 7, 1-8.
- [16] P. M. Whitaker-Azmitia, *Brain Res. Bull.* **2001**, 56, 479-485.
- [17] D. Hoyer, D. E. Clarke, J. R. Fozard, P. R. Hartig, G. R. Martin, E. J. Mylecharane, P. R. Saxena, P. P. A. Humphrey, *Pharmacol. Rev.* **1994**, 46, 157-203.

- [18] V. Derkach, A. Surprenant, R. A. North, *Nature* **1989**, 339, 706-709.
- [19] A. V. Maricq, A. S. Peterson, A. J. Brake, R. M. Myers, D. Julius, *Science* **1991**, 254, 432-437.
- [20] G. J. Kilpatrick, B. J. Jones, M. B. Tyers, *Nature* **1987**, 330, 746-748.
- [21] S. C. R. Lummis, *J. Biol. Chem.* **2012**, 23, 40239-40245.
- [22] A. J. Thompson, S. C. R. Lummis, *Curr. Pharm. Des.* **2006**, 12, 3615-3630.
- [23] P. A. Davies, M. Pistis, M. C. Hanna, J. A. Peters, J. J. Lambert, T. G. Hales, E. F. Kirkness, *Nature* **1999**, 397, 359-363.
- [24] A. E. Dubin, R. D. Huvar, M. R. Andrea, J. Pyati, J. Y. Zhu, K. C. Joy, S. J. Wilson, J. E. Galindo, C. A. Glass, L. Luo, M. R. Jackson, T. W. Lovenberg, M. G. Erlander, *J. Biol. Chem.* **1999**, 274, 30799-30810.
- [25] M. C. Miquel, M. B. Emerit, A. Noejean, A. Simon, P. Rumajogee, M. J. Brisorgueil, E. Doucet, M. Hamon, D. Vergé, *Eur. J. Neurosci.* **2002**, 15, 449-457.
- [26] H. S. Smith, L. R. Cox, E. J. Smith, *Ann. Palliat. Med.* **2012**, 1, 115-120.
- [27] P. S. Miller, T. G. Smart, *Trends Pharmacol. Sci.* **2010**, 31, 161-174.
- [28] N. M. Barnes, T. G. Hales, S. C. Lummis, J. A. Peters, *Neuropharmacology* **2009**, 56, 273-284.
- [29] J. Walstab, G. Rappold, B. Niesler, *Pharmacol. Ther.* **2010**, 128, 146-169.
- [30] K. Y. Ho, T. J. Gan, *Curr. Opin. Anaesthesiol.* **2006**, 19, 606-611.
- [31] W. Szymanski, J. M. Beierle, H. A. V. Kistemaker, W. A. Velema, B. L. Feringa, *Chem. Rev.* **2013**, 113, 6114-6178.
- [32] M. M. Lerch, M. J. Hansen, G. M. van Dam, W. Szymanski, B. L. Feringa, *Angew. Chem. Int. Ed.* **2016**, 55, 10978-10999.
- [33] J. Broichhagen, J. A. Frank, D. Trauner, *Acc. Chem. Res.* **2015**, 48, 1947-1960.
- [34] G. Mayer, A. Heckel, *Angew. Chem. Int. Ed.* **2006**, 45, 4900-4921.

- [35] A. Deiters, *ChemBioChem* **2010**, *11*, 47-53.
- [36] K. Curley, D. S. Lawrence, *Pharmacol. Ther.* **1999**, *82*, 347-354.
- [37] E. A. Lemke, *ChemBioChem* **2010**, *11*, 1825-1827.
- [38] A. Reiner, E. Y. Isacoff, *Methods Mol. Biol.* **2014**, *1148*, 45-68.
- [39] P. C. Donthamsetti, N. Winter, M. Schönberger, J. Levitz, C. Stanley, J. A. Javitch, E. Y. Isacoff, D. Trauner, *J. Am. Chem. Soc.* **2017**, *139*, 18522-18535.
- [40] W.-C. Lin, M.-C. Tsai, R. Rajappa, R. H. Kramer, *J. Am. Chem. Soc.* **2018**, *140*, 7445-7448.
- [41] J. Broichhagen, A. Damijonaitis, J. Levitz, K. R. Sokol, P. Leippe, D. Konrad, E. Y. Isacoff, D. Trauner, *ACS Cent. Sci.* **2015**, *1*, 383-393.
- [42] C. Brieke, F. Rohrbach, A. Gottschalk, G. Mayer, A. Heckel, *Angew. Chem. Int. Ed.* **2012**, *51*, 8446-8476.
- [43] E. Mitscherlich, *Ann. Pharm.* **1834**, *12*, 311-314.
- [44] G. S. Hartley, *Nature* **1937**, *140*, 281-282.
- [45] M. Dong, A. Babalhavaeji, S. Samanta, A. A. Beharry, G. A. Woolley, *Acc. Chem. Res.* **2015**, *48*, 2662-2670.
- [46] A. A. Beharry, O. Sadoski, G. A. Woolley, *J. Am. Chem. Soc.* **2011**, *133*, 19684-19687.
- [47] C. E. Weston, R. D. Richardson, P. R. Haycock, A. J. P. White, M. J. Fuchter, *J. Am. Chem. Soc.* **2014**, *136*, 11878-11881.
- [48] H. Kaufman, S. M. Vratsanos, B. F. Erlanger, *Science* **1968**, *162*, 1487-1489.
- [49] W. J. Deal, B. F. Erlanger, D. Nachmansohn, *Proc. Natl. Acad. Sci. U. S. A.* **1969**, *64*, 1230-1234.
- [50] M. Volgraf, P. Gorostiza, R. Numano, R. H. Kramer, E. Y. Isacoff, D. Trauner, *Nat. Chem. Biol.* **2006**, *2*, 47-62.

- [51] M. Volgraf, P. Gorostiza, S. Szobota, M. R. Helix, E. Y. Isacoff, D. J. Trauner, *J. Am. Chem. Soc.* **2007**, 129, 260-261.
- [52] N. J. Hauwert, T. A. M. Mocking, D. da Costa Pereira, A. J. Kooistra, L. M. Wijnen, G. C. M. Vreeker, E. W. E. Verweij, A. H. de Boer, M. J. Smit, C. de Graaf, H. F. Vischer, I. J. P. de Esch, M. Wijtmans, R. Leurs, *J. Am. Chem. Soc.* **2018**, 140, 4232-4243.
- [53] M. Wegener, M. J. Hansen, A. J. M. Driessen, W. Szymanski, B. L. Feringa, *J. Am. Chem. Soc.* **2017**, 139, 17979-17986.
- [54] A. Polosukhina, J. Litt. I. Tochitsky, J. Nemargut, Y. Sychev, I. de Kochkovski, T. Huang, K. Borges, D. Trauner, R. N. van Gelder, R. H. Kramer, *Neuron* **2012**, 75, 271-282.
- [55] I. Tochitsky, A. Polosukhina, V. E. Degtyar, N. Gallerani, C. M. Smith, A. Friedman, R. N. van Gelder, D. Trauner, D. Kaufer, R. H. Kramer, *Neuron* **2014**, 81, 800-813.
- [56] N. A. Simeth, A. C. Kneuttinger, R. Sterner, B. König, *Chem. Sci.* **2017**, 8, 6474-6483.
- [57] J. A. Frank, H. G. Franquelim, P. Schwille, D. Trauner, *J. Am. Chem. Soc.* **2016**, 138, 12981-12986.
- [58] C. Pernpeintner, J. A. Frank, P. Urban, C. R. Roeske, S. D. Pitzl, D. Trauner, T. Lohmüller, *Langmuir* **2017**, 33, 4083-4089.
- [59] M. Schönberger, A. Damijonaitis, Z. Zhang, D. Nagel, D. Trauner, *ACS Chem. Neurosci.* **2014**, 5, 514-518.
- [60] B. A. Sparling, E. F. DiMauro, *Bioorg. Med. Chem. Lett.* **2017**, 27, 3207-3218.
- [61] S. M. Trattnig, K. Harpsøe, S. B. Thygesen, L. M. Rahr, P. K. Ahring, T. Balle, A. A. Jensen, *J. Biol. Chem.* **2012**, 287, 25241-25254.
- [62] A. Baeyer, *Chem. Ber.* **1874**, 7, 1638-16463]0.

- [63] C. J. Mills, *J. Chem. Soc.* **1895**, 67, 925-933.
- [64] M. v. Wantoch Rekowski, A. Pyriochou, N. Papapetropoulos, A. Stössel, A. Papapetropoulos, A. Giannis, *Bioorg. Med. Chem.* **2010**, 18, 1288-1296.
- [65] K. Harsányi, C. Gönczi, D. Korbonits, *Liebigs Ann. Chem.* **1973**, 2, 190-194.
- [66] S. Murarka, P. Martín-Gago, C. Schultz-Fademrecht, A. Al Saabi, M. Baumann, E. K. Fansa, S. Ismail, P. Nussbaumer, A. Wittinghofer, H. Waldmann, *Chem. Eur. J.* **2017**, 23, 6083-6093.
- [67] V. Colotta, D. Catarzi, F. Varano, L. Cecchi, G. Filachhioni, A. Galli, C. Costagli, *Arch. Pharm. Pharm. Med. Chem.* **1997**, 330, 387-391.
- [68] C. Párkányi, A. O. Abdelhamid, *J. Heterocyclic Chem.* **1984**, 21, 521-524.
- [69] S. Pierau, G. Dale, *Assignee Morphochem Aktiengesellschaft fuer Kombinatorische Chemie Germany*, International Publication Date 2 March **2006**, WO2006021448 A1, Title: Novel Compounds having an anti-bacterial Activity.
- [70] X. Wang, Y.-F. Chen, W. Yan, L.-L. Cao, Y.-H. Ye, *Molecules* **2016**, 21, 1574-1588.
- [71] D. Kolarski, W. Szymanski, B. L. Feringa, *Org. Lett.* **2017**, 19, 5090-5093.
- [72] P. Stawski, M. Sumser, D. Trauner, *Angew. Chem. Int. Ed.* **2012**, 51, 5748-5751.
- [73] J. Del Barrio, P. N. Horton, D. Lairez, G. O. Lloyd, C. Toprakcioglu, O. A. Sherman, *J. Am. Chem. Soc.* **2013**, 135, 11760-11763.
- [74] S. A. Laufer, D. M. Domeyer, T. R. F. Scior, W. Albrecht, D. R. J. Hauser, *J. Med. Chem.* **2005**, 48, 710-722.
- [75] F.-N. Meng, Z.-Y. Li, Y.-L. Ying, S.-C. Liu, J. Zhang, Y.-T. Long, *Chem. Com.* **2017**, 53, 9462-9465.
- [76] G. H. Coleman, G. Nichols, C. M. McCloskey, H. D. Anson, *Org. Synth.* **1945**, 25, 87-89.

[77] C. F. Liu, Y. Zeng, X. W. Lu, *Assignee Nanyang Technological University*, International Publication Date 11 March **2010**, WO2010027326 A1, Title: Peptide Nucleic Acid Monomers and Oligomers.

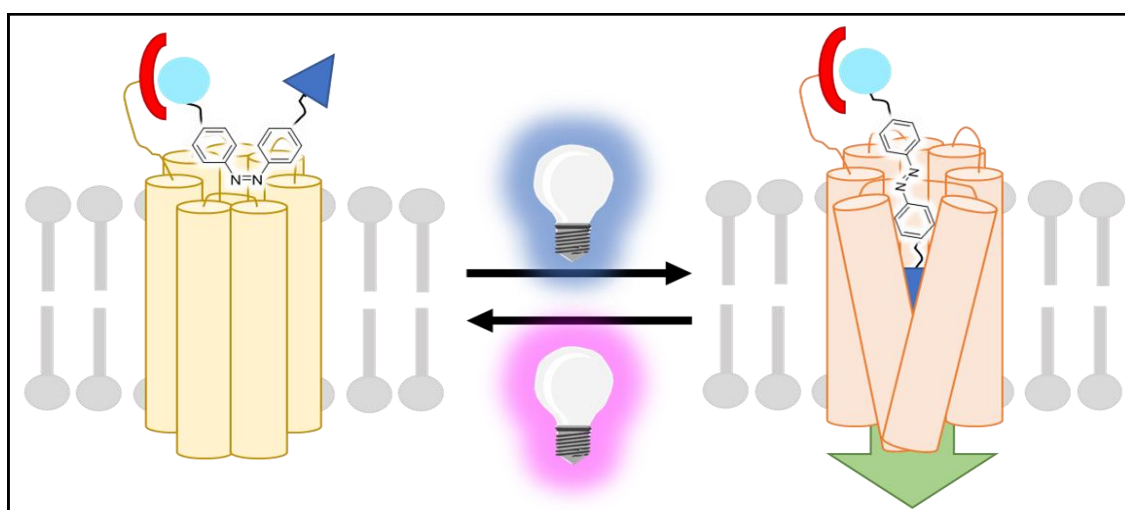
[78] O.V. Dolomanov, L.J. Bourhis, R.J. Gildea, J.A.K. Howard, H. Puschmann, *J. Appl. Cryst.* **2009**, 42, 339-341.

[79] G. M. Sheldrick, *Acta Cryst.* **2015**, A71, 3-8.

[80] G. M. Sheldrick, *Acta Cryst.* **2015**, C27, 3-8.

CHAPTER 8

8 Photochromic Metal Complex-Agonist Conjugates



This chapter has not been published.

This research was performed in collaboration with Prof. R. Kubota (Prof. I. Hamachi, University of Kyoto, Japan) within the framework of the JSPS summer program. K. Rustler performed the synthesis, (photo-)chemical characterization, and *in vitro* calcium measurements under assistance of Prof. R. Kubota. Mass spectrometry analysis were partially performed by the analytical department at the University of Regensburg and partially at the University of Kyoto. Metal chelator **22** and ligand **24** were provided by the Hamachi laboratory. Prof. I. Hamachi and Prof. B. König supervised the project.

8.1 Introduction

The human genome is expressing genes for over 800 different G protein-coupled receptors, which are the largest superfamily of membrane receptors.^[1-4] A conserved feature of all known GPCRs is their heptahelical transmembrane domain, which undergoes conformational changes upon ligand binding allowing for interaction with intracellular proteins and initiation of downstream signalling cascades.^[5] Their embedding in diverse cellular processes explains their importance as drug target. Around 34% of the medications approved by the US Food and Drug Administration (FDA) trigger around 100 different GPCRs.^[6] Amongst them are mainly family A GPCRs which are representing 85% of the GPCR superfamily.^[7] So called orphan GPCRs are of unknown function and their endogenous ligands remain unknown. Furthermore, their identification is made more difficult, as GPCRs are woven into the cell membrane and are difficult to purify. This emphasizes the importance of GPCRs, especially of class A, as a research target as it is likely that various untreated diseases are provoked by their dysfunction.^[8]

One approach for GPCR investigation is represented by designer receptors exclusively activated by designer drugs (DREADDs) or receptors activated solely by a synthetic ligand (RASSLs). As their name implies, these systems use engineered GPCRs, which are exclusively sensitive to synthetic ligands and no longer to their natural ones. This method allows receptor selectivity and cell type specificity but as it is based on mutated receptors, it is unreliable how far new findings can be applied for their natural counterparts.^[9-11] The desire to unravel deeper understanding on native receptors led to the development of new tools, *e.g.*, in the field of photopharmacology, using light as non-invasive abundant trigger orthogonal to cellular processes to control a drug's activity.^[12] Photocaged and photoswitchable ligands are soluble molecules of which the biological activity can be regulated in high spatiotemporal resolution by irradiation induced cleavage of a protecting group or isomerization.^[13] Unfavourable, their kinetics are diffusion

limited, which often limits their specificity and activity. To overcome those drawbacks, the ligands are covalently tethered to a bioconjugation motif at the targeted protein placing the ligand in proximity to its binding pocket. Usually, an engineered cysteine is selectively expressed in the cells of interest and reacts to a maleimide motive of the photochromic ligand. Those photochromic tethered ligands (PTLs) allow to control the ligand's position towards or away from the binding pocket. Nevertheless, the given cell and subtype specificity is restricted by conjugation to free thiols (*e.g.*, glutathione, native cysteines) in intracellular environments and the instability of maleimides towards hydrolyzation under physiological conditions. Improvement is provided *via* tethering of a photochromic ligand to a benzylguanine able to react with a SNAP-tag encoded at an arranged site providing a photoswitchable orthogonal remotely tethered ligand (PORTL). Beneficial is the high stability of the tethering group and high selectivity and orthogonality to native reactions.^[14] Another suitable approach useful for class A GPCRs but lacking photo responsiveness is reported by chemogenetic coordination tethering. Typically, the native agonist is linked to a metal chelator *via* a polyethyleneglycol moiety providing flexibility and solubility in aqueous media. This metal complex-agonist conjugate (MAC) binds with high affinity to an engineered His₄ tag providing 10-100-fold lower EC₅₀ values for ligand-binding at the designed receptors compared to the wildtype as the ligand is selectively placed close to its binding site. The length of the linker is crucial for the accessibility of the agonist towards its binding pocket. If the linker is too short, the site is not reached. If the linker is too long, the efficacy of the binding is reduced. Release of the ligand is driven by diffusion or complete wash-out of the MAC as it is not covalently bound.^[15] More insight into the dynamics of the addressed class A GPCRs would be provided if binding and unbinding of the ligand could be further regulated *via* incorporation of a photochromic moiety.

We envisioned, that the incorporation of an azobenzene as part of the MAC leads to an irradiation inducible change of the linker length upon *trans-cis* isomerization and thus to an adjustable high affinity ligand binding and unbinding (Figure 1). In

this case, the change in biological activity of the photochromic metal complex-agonist conjugate (PMAC) does not result from a change in the efficacy of the ligand itself as it does for PCLs or caged compounds, but from a change in the accessibility of the ligand to its binding site.

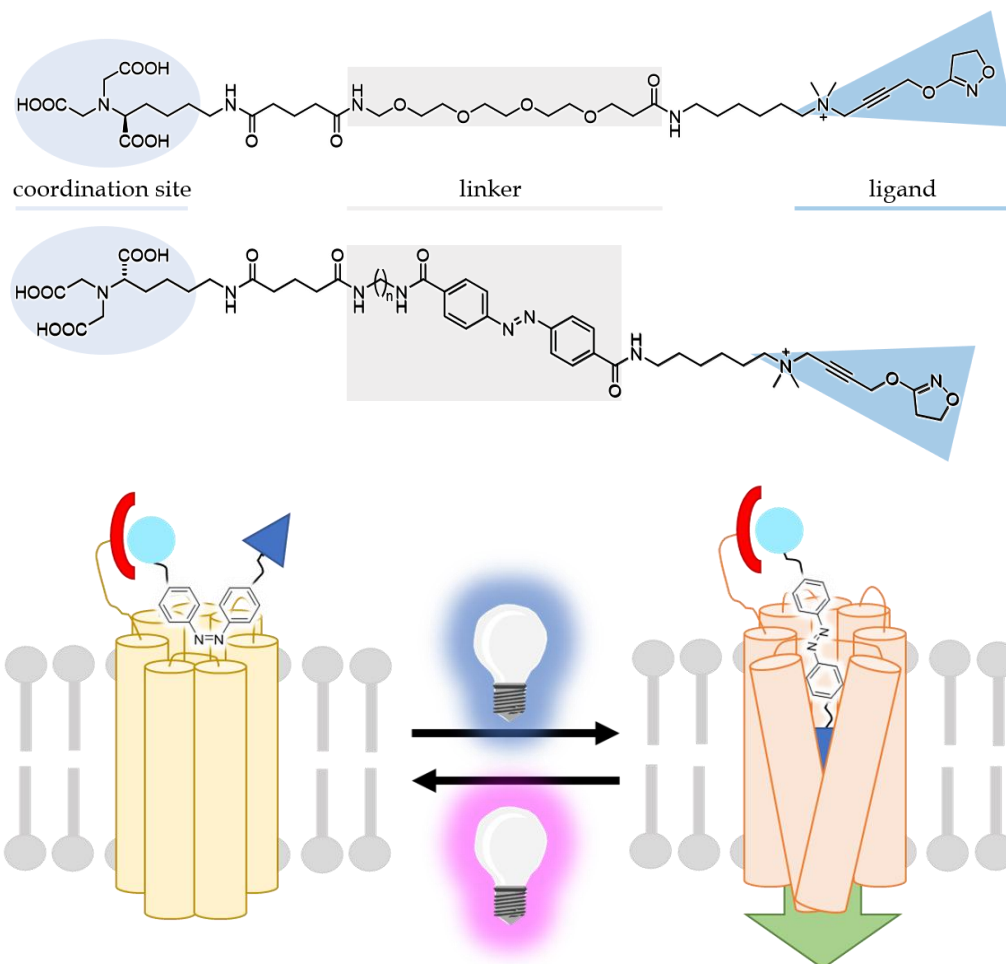


Figure 1. Upper panel: MAC designed by the Hamachi group and PMAC design attempted in this work. Lower panel: Schematic drawing of a PMAC acting on an engineered His₄-tagged class A GPCR.

8.2 Results and Discussion

8.2.1 Design and Syntheses

Design. The choice of the photochromic scaffold is essential for the photochromic properties of the final metal complex-agonist conjugate. As it is reported^[15] by the Hamachi group that the linker length is crucial for the biological activity of the MAC, azobenzene was chosen as photochromic scaffold as its light-induced *trans*-

cis isomerization leads to a change in end-to-end distance, which might influence ligand binding.^[13,16,17] The photophysical properties of azobenzene, *e.g.*, the wavelengths required for isomerization and the thermal stability of the *cis* isomer can be classified based on its substitution pattern. Unsubstituted azobenzenes undergo *trans* to *cis* isomerization upon irradiation with UV light and show long thermal half-lives of their *cis* isomers. The addition of an electron donating group (EDG) in *para* position or even an additional electron withdrawing group (EWG) in *para'* position leads to a bathochromic shift of the absorption spectrum and reduced thermal stability of the *cis* isomers.^[18] To avoid continuous irradiation during the *in vitro* assay an azobenzene scaffold is required, of which the *cis* isomer is thermally stable enough to be tested upon prior irradiation. In analogy to the design of a MAC reported^[15] by the Hamachi group, the azobenzene is linked to the coordination site and the ligand *via* amide bonds. Using a *para para'* dicarboxy azobenzene allows the required functionalization for PMAC formation and provides the desired photochromic properties.

To keep the length of the azobenzene linker in accordance to the reported tetraethyleneglycol linker, Chem3D was used to calculate the end-to-end distances of different azobenzene linkers. This led to the design of a dicarboxy azobenzene moiety with an amide linked butylamine (Figure 2).

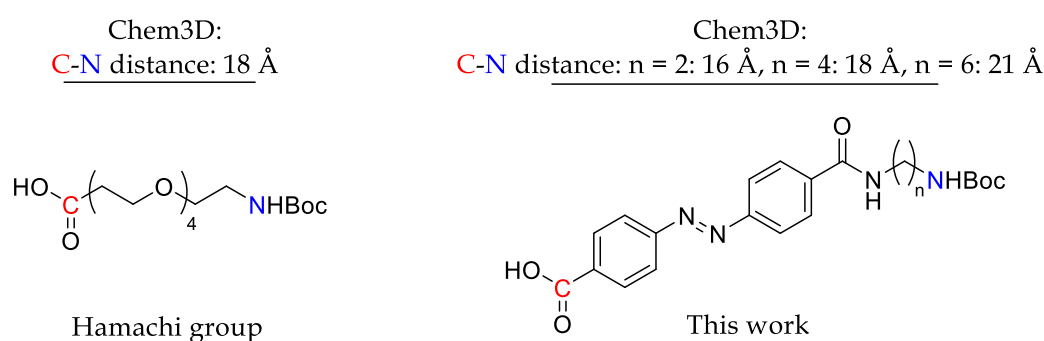
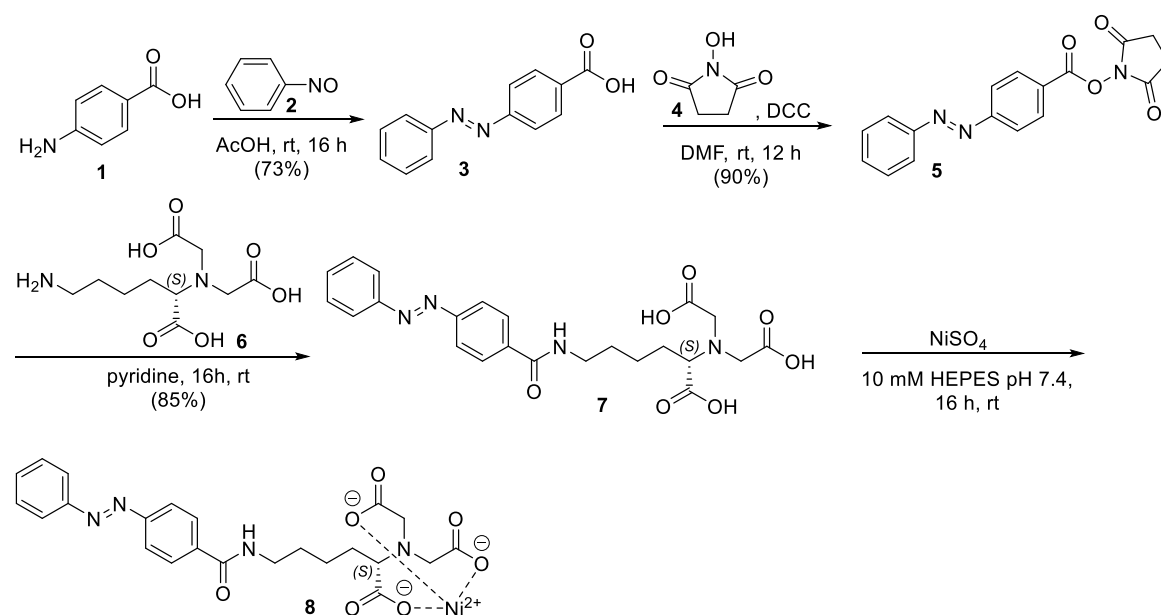


Figure 2. Rough estimation of the linker length using Chem3D.

Synthesis of the control compound. To assure that the photoisomerization of the latter photochromic metal complex-agonist conjugate is not altered upon coordination of nickel, the simplified photochromic metal chelator **5** based on

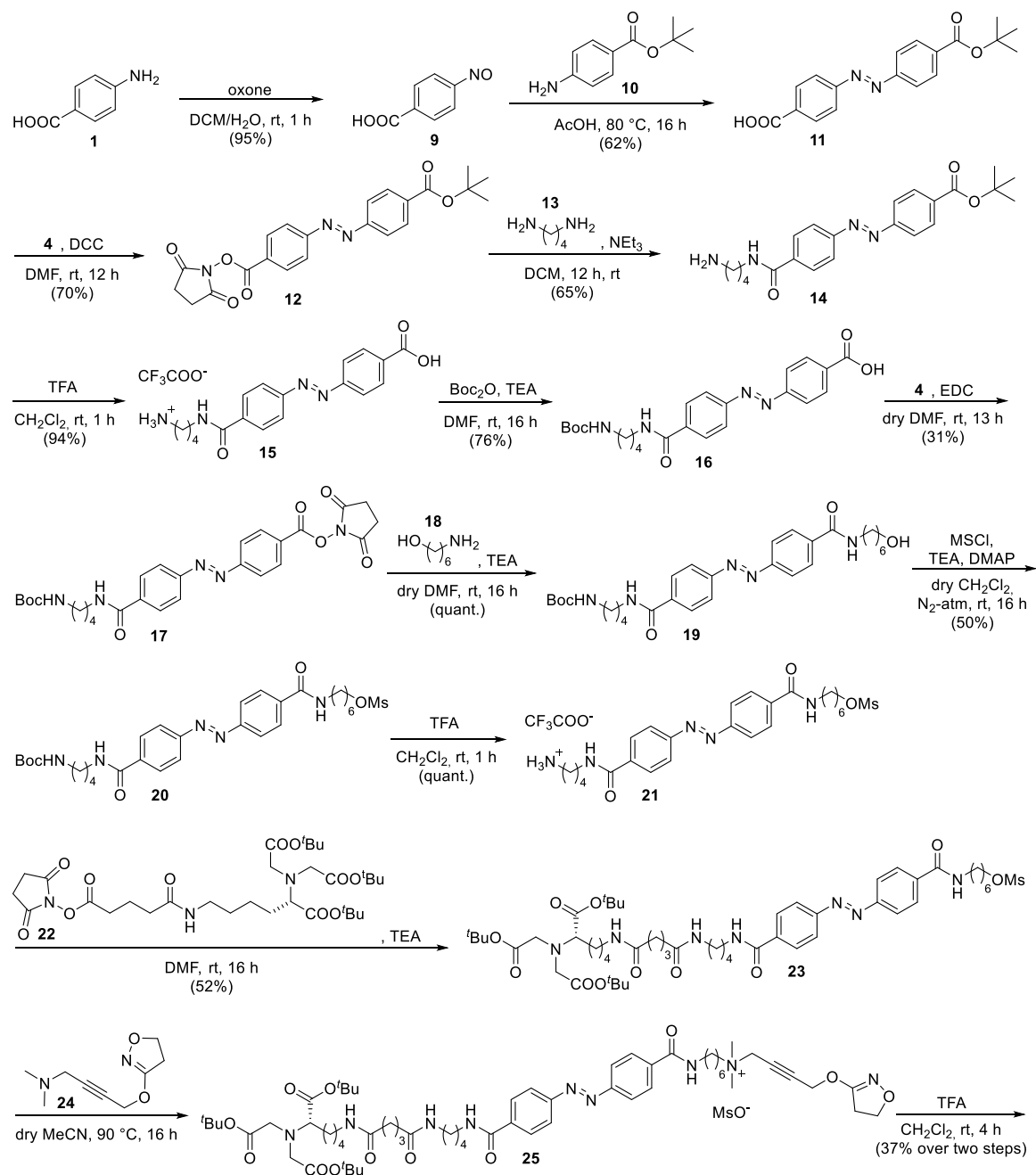
carboxy azobenzene was synthesized (Scheme 1). In a first synthetic step, the carboxylic acid azobenzene **3** was synthesized using a Mills reaction starting from amino benzoic acid **1** and nitrosobenzene **2**.^[19] Conversion to its highly reactive NHS-ester **5** allowed its subsequent reaction with the alkyl amine linked triacid **6** providing the photochromic metal chelator **7**.^[20] Nickel coordination was achieved by addition of an equimolar amount of nickel(II)sulfate in Hepes buffered saline (HBS) at pH 7.4, which represents the solvent required during *in vitro* testing.^[15]

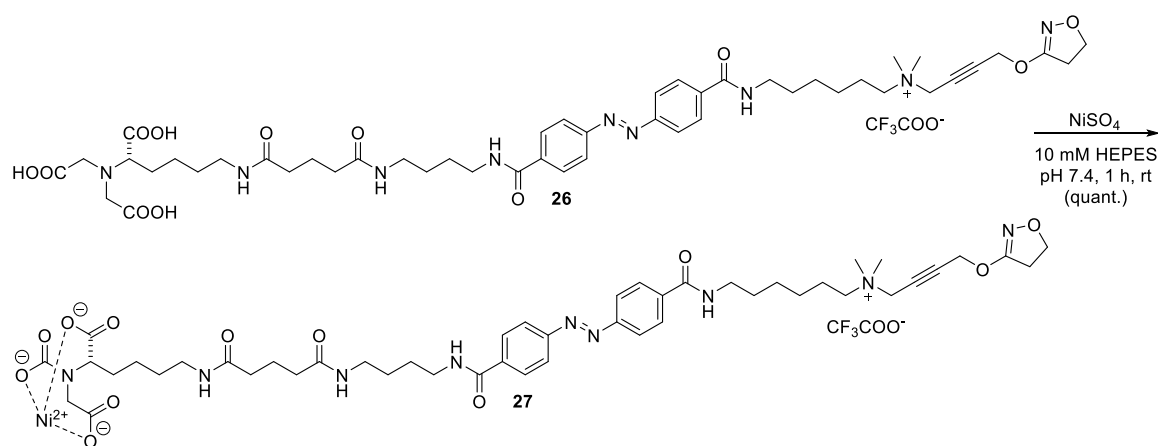


Scheme 1. Synthesis of the azobenzene metal conjugate **8** and its non-coordinated precursor **7**.^[15,19,20]

Synthesis of the photochromic metal complex-agonist conjugate (PMAC). The overall synthesis (Scheme 2) of the photochromic metal complex-agonist was designed in analogy to the reported MAC synthesis. Therefore, *para* carboxy *para'* *tert* butyl ester azobenzene **11** was synthesized *via* Mills reaction. Amino benzoic acid **1** was oxidized to its nitroso derivative **9** using oxone in a biphasic solvent mixture preventing overoxidation.^[21] Subsequent addition of the *tert* butyl ester substituted aniline **10** in acetic acid allowed the formation of azobenzene **11**. Transformation of the *para* carboxylic acid **11** to its NHS-ester **12** allowed its reaction with butyldiamine **13** providing the *para* amino butylamide azobenzene **14**.^[20] Upon cleavage of the *para'* *tert* butyl ester of **14** using trifluoro acetic acid the free amino group of **15** was Boc protected. The carboxylic acid of **16** was selectively

NHS-activated (**17**) and subsequently reacted with the amino substituted hexanol **18** providing its linked derivative **19** required for the latter addition of the agonist moiety. The hydroxy group of **19** is activated using methansulfonylchloride and deprotection of its Boc amine allowed the introduction of the NHS-activated metal chelator precursor **22** providing **23**. In the next step, the iperoxo ligand **24** was introduced and the carboxylic acid groups of **25** deprotected providing the PMAC **26** with its free carboxylic acid groups required for nickel-coordination.^[15]





Scheme 2. Synthesis of the photochromic metal complex-agonist conjugate **27**.^[15,20,21]

8.2.2 Photochemical Characterization

Control experiments. Initially, the photochromic properties of control compound **7** were investigated by absorption spectroscopy in HEPES buffer before (**7**) and upon nickel coordination (**8**). The black curve in Figure 3, left panel, shows the spectrum of compound **7** at its thermal equilibrium. Upon irradiation with UV light ($\lambda = 365$ nm) a substantial amount of the *cis* isomer was accumulated, until no more changes in the spectrum despite ongoing irradiation could be observed (= *cis*-photostationary state; Figure 3, red curve). Thereby, the maximum around 330 nm representing the *trans* isomer decreased and a new maximum in the visible range representing the *cis* isomer is formed. Regeneration of the *trans* isomer is achieved by irradiation with blue light ($\lambda = 455$ nm) until the *trans*-photostationary state (blue curve) is reached. To this solution, an equimolar amount of nickel(II)sulfate was added and the mixture incubated at room temperature for 12 h. The solution containing nickel-coordinated compound **8** could be isomerized by irradiation with UV and visible light of the same wavelengths as required for the non-coordinated compound **7** and the *cis*- and *trans*-photostationary states of **7** could nearly be regenerated showing that the nickel coordination has no effect on the switching performance. To proof the thermal stability of the basic photochromic MAC scaffold represented by the prefunctionalized azobenzene **14**, the thermal recovery of its *cis* isomer was determined proving high thermal stability in the day range (Figure 3, right panel).

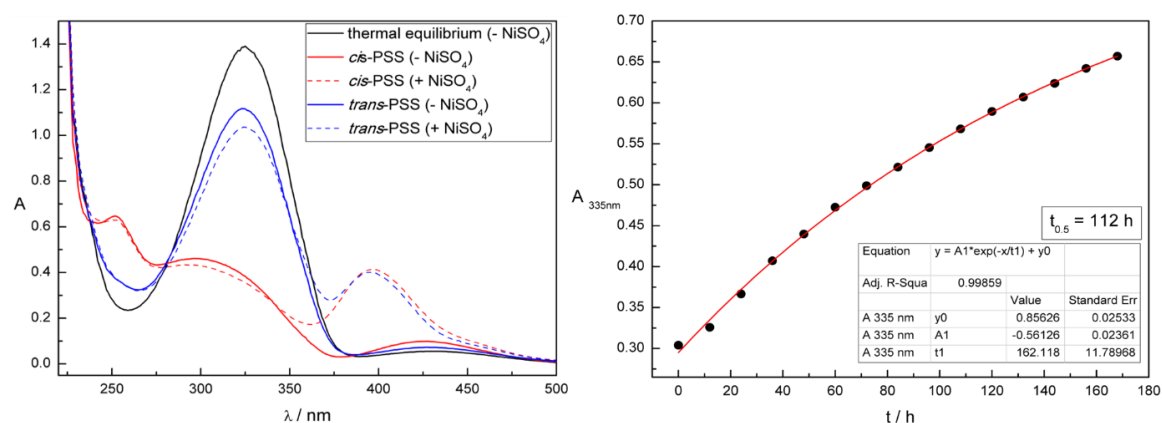


Figure 3. Left panel: Switching performance of triacid **7** (-NiSO₄) and upon nickel coordination (compound **8**, +NiSO₄) measured in 10 mM HBS pH 7.4. Right panel: Thermal half-life of the functionalized azobenzene linker **14** measured 50 μM in DMSO.

Photochromic metal complex-agonist conjugate. The investigation of the photochromic properties of PMAC **26** was performed by absorption spectroscopy in DMSO (Figure S2, Supporting Information) and in HBS (Figure 4) prior to (**26**) and upon (**27**) nickel coordination (1.0 eq; 1 h incubation at rt). The results underline that the nickel coordination has neither an effect on the switching efficiency nor on the absorption bands of the spectrum. Furthermore, the absorption spectrum shows the same characteristic maxima as control compound **7** and the prefucionalized derivate **14** highlighting that the photochromic properties of azobenzenes are mainly determined by the substituents directly attached to the phenyl rings. Black arrows in Figure 4 indicate the characteristic changes in the absorption spectrum upon isomerization. Upon irradiation with UV light, the maximum of the *trans* isomer in its thermal equilibrium (black curve) is decreasing and a new maximum in the visible range representing the *cis*-photostationary state (PSS) is formed (red curve). Reisomerization to the *trans*-PSS (blue curve) is triggered using blue light ($\lambda = 455$ nm). Due to a substantial overlap of the absorption bands of both isomeric states, a quantitative generation of one or the other species by irradiation is not feasible. The points of intersection (= isosbestic points) in the absorption spectra of non-coordinated compound **26** and coordinated compound **27** upon isomerization indicate a clear two component switching between *trans* and *cis* isomer without any degradation

or formation of a side-product (Figure 4, dotted black arrows). The repetitive cycle performance of compound **26** shows high fatigue resistance (Figure 4, right panel).

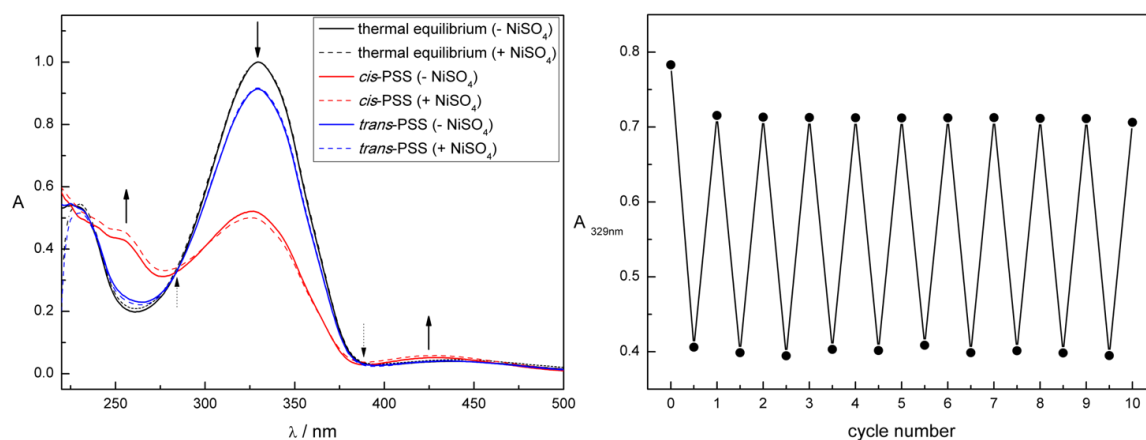


Figure 4. Left panel: Switching performance of iperoxo azobenzene triacid prior to (- NiSO₄, **26**) and upon nickel coordination (+NiSO₄, 1 h incubation, **27**) measured in HBS. Right panel: Cycle performance of compound **26** (-NiSO₄) measured in HBS.

Table 1 summarizes the characteristic photochromic data (absorption maxima, isosbestic points) for azobenzenes **7**, **8**, **14**, **26**, and **27**.

Table 1. Summary of the characteristic photochemical properties of azobenzenes **7**, **8**, **14**, **26**, and **27**. Cpd. = Compound.

Entry	Cpd.	λ_{\max} <i>trans</i> isomer [nm]	λ_{\max} <i>cis</i> isomer [nm]	Isosbestic points [nm]	solvent	NiSO ₄
1	7	325	426	281, 383	1xHBS	-
2	8	324	397	281, 387	1xHBS	+ (1.0 eq) ^(a)
3	14	335	433	287, 391	DMSO	-
4	26	337	434	287, 392	DMSO	-
5	26	329	428	284, 391	1xHBS	-
6	27	329	428	285, 387	1xHBS	+ (1.0 eq) ^(b)

Incubation with an equimolar amount of NiSO₄ at room temperature for (a) 12 hours, (b) 1 hour.

8.2.3 In Vitro Fluorescence Ca²⁺ Imaging

To validate the biological activity of the synthesized photochromic metal complex-agonist conjugate, both isomeric states were examined on the native and the His-tagged muscarinic acetylcholine receptor (mAChR) M1R as representative of a class A GPCR in the presence and absence of nickel. The activities of the wildtype M1R and His-tagged M1R transiently expressed in CHO cells were evaluated

using fluorescence Ca^{2+} imaging.^[15] The obtained preliminary results will be discussed in the following.

The positive controls (Figure S4, Supporting Information) proved the activity of Fluo4 and Fura2 as calcium sensing fluorescence reporters as well as the possibility of ligand (Iperoxo) wash-out and subsequent reactivation of the investigated cells.

The *trans* isomer was tested in its thermal equilibrium. The concentration dependence for activating the His-tagged receptor showed an increased efficiency by a factor of 100 in the presence of nickel (Figure S6, Supporting Information) compared to the His-tagged receptor activation under absence of nickel (Figure S5, Supporting Information). The evoked response on the His-tagged cells without addition of nickel corresponded to the activation response on wildtype cells upon addition of nickel (Figure S8, Supporting Information). In absence of nickel, the response of the wildtype receptor (Figure S7, Supporting Information) was even further reduced by a factor of 10. These preliminary data confirm the beneficial effect of high-affinity nickel complex formation of compound **27** towards the His-tagged receptor. This implies that the incorporation of *trans* azobenzene as part of the MAC kept the linker length within an acceptable range for ligand induced receptor activation upon coordination to the His-tag.

As the *cis* isomer was tested at its photostationary state background activity of the remaining *trans* isomer needs to be kept in mind. Furthermore, back-isomerization of the *cis* PMAC upon adhesion to the cell and the receptor, respectively, cannot be ruled out. Due to aging of the cells no reliable results could be achieved for the testing of the *cis* isomer and the measurements need to be repeated with younger cells in ongoing tests.

The Ca^{2+} responses evoked by different concentrations of the photochromic metal complex-agonist conjugate in the absence (compound **26**) and presence (compound **27**) of nickel for the *trans* isomer are summarized in Table 2.

Table 2. Summarized Ca^{2+} response evoked by different concentrations of the photochromic metal-complex agonist conjugate in the absence (compound **26**) and presence (compound **27**) of NiSO_4 for the *trans* isomer in its thermal equilibrium. n.a.: not active. *n* = number of individual measurements. Cpd. = Compound.

Entry	Cpd.	1.0 nM	10 nM	0.10 μM	1.0 μM	Ni ^(a)	Type ^(b)	<i>n</i>
1	26 <i>trans</i>	n.a.	n.a.	active	active	-	His	2
2	27 <i>trans</i>	active	active	active	active	+	His	3 (<i>n</i> =2; 1.0 nM, 1.0 μM)
3	26 <i>trans</i>	n.a.	n.a.	n.a.	active	-	WT	3
4	27 <i>trans</i>	n.a.	-(c)	active	active	+	WT	1

(a) A 10 mM solution of the compound and NiSO_4 was incubated for 60 min at rt prior to testing and dilution; in cases of “+” an equimolar amount of NiSO_4 was added. (b) Wildtype receptor: M1R; His-tagged receptor: M1R(1.18H4). (c) No clear effect can be assigned.

8.3 Conclusion

In the presented work, we address the design, synthesis and (photo-)chemical characterization of a photochromic metal-complex agonist conjugate (PMAC) derivative of a reported non-photochromic metal-complex agonist conjugate investigated by the Hamachi group. Due to their large change in geometry and end-to-end distance upon light-induced *trans-cis* isomerization azobenzenes were chosen as photochromic scaffold to be incorporated as part of the linker between the agonist and the metal chelator. The synthesized derivative displayed high fatigue in aqueous media regardless the presence or absence of nickel(II)sulfate. Its high thermal stability is beneficial as constant irradiation during the *in vitro* cell testing is not required, which might harm the cells. Furthermore, the synthesized PMAC was subjected to *in vitro* calcium measurements upon and prior to addition of NiSO_4 and coordination to its engineered receptor site. The efficiency of the binding is increased by a factor of 100 upon coordination and proofed the general principle of coordination tethering. Furthermore, this verifies the calculation of the linker length. If the azobenzene incorporated linker is too short, the tethered ligand would not be able to bind to its receptor site. If it's too long, the efficiency wouldn't be increased upon nickel coordination as the binding would rather be diffusion driven. The investigation of the agonist binding upon *trans* to *cis* isomerization performed by the Hamachi group is ongoing. Due to a change in linker length and

geometry the binding efficiency of the tethered ligand might be reduced compared to its *trans*-isomeric state. This would lead to a light controlled high-efficiency activation of class A GPCRs represented by the muscarinic acetylcholine receptor (mAChR) M1R.

8.4 Experimental Part

8.4.1 General Procedures and Materials

Commercial reagents and starting materials were purchased from the commercial suppliers abcr, Acros Organics, Alfa-Aesar, Fisher Scientific, Fluorochem, Merck, Sigma Aldrich, TCI, or VWR and used without any further purification. Solvents were used in p.a. quality and dried according to common procedures, if necessary. Flash column chromatography was performed using Sigma Aldrich MN silica gel 60 M (40-63 μm , 230-400 mesh) or Kanto Chemical silica gel 60N (40-50 μm) for normal phase chromatography. Reaction monitoring *via* thin layer chromatography was performed on alumina plates coated with silica gel (Merck silica gel 60 F₂₅₄, layer thickness 0.2 mm). NMR spectra were measured on a Bruker Avance 300 and a Varian Mercury 400. The spectra are referenced against the NMR-solvent (DMSO-*d*₆: δ_{H} = 2.50 ppm, δ_{C} = 39.52 ppm; CDCl₃-*d*: δ_{H} = 7.26 ppm, δ_{C} = 77.16 ppm) or tetramethyl silane as internal reference and chemical shifts δ are reported in ppm. Resonance multiplicity is abbreviated as: b (broad), s (singlet), d (doublet), t (triplet), and m (multiplet). Carbon NMR signals are assigned using DEPT 135 and ¹H-¹³C HSQC spectra with (+) for primary/tertiary, (-) for secondary, and (q) for quaternary carbons. Mass spectra were recorded on a Finnigan MAT-SSQ 710 A, ThermoQuest Finnigan TSQ 7000, Agilent Q-TOF 6540 UHD, a Jeol AccuTOF GCX instrument, or a Thermo Scientific Exactive. UV-Vis absorption spectroscopy was performed in 10 mm quartz cuvettes using an Agilent 8543, Agilent Cary 100, Agilent Varian Cary 50 or a Shimadzu UV-2600 spectrometer. Light sources for irradiation: λ = 365 nm (Seoul Viosys CUN6GB1A, 1000 mA, 1.4 W), and λ = 455 nm (Osram OSOLON SSL 80 LD-CQ7P-1U3U, 1000 mA, 0.45 W). The power of the light is given based on the specifications

supplied by the company when the LEDs were purchased. Reversed phase HPLC was carried out on an Agilent 1260 system (column: Phenomenex Luna 10 μm C₁₈(2) 100 Å, 250 x 21.2 mm; flow: 22 mL min⁻¹; solvents: MilliQ water with 0.05% aqueous TFA; MeCN) or on a Hitachi Chromaster system equipped with a diode array (column: YMC-Pack Triart C18 or ODS-A; solvents: 0.1% aqueous TFA; MeCN containing 0.1% TFA). The control expression vector pCI-neo, wildtype mAChR expressing vector HA-M1R-pCI neo (WT), and His tag-fused mAChR expression vector HA-M1R(1.18H₄)-pCI neo were provided by the Hamachi Laboratory.

8.4.2 Synthetic Procedures and Characterization

(E)-4-(phenyldiazenyl)benzoic acid (3). This compound was synthesized following a literature reported procedure.^[19] 4-amino benzoic acid (**1**, 0.55 g, 4.0 mmol, 1.2 eq) was dissolved in acetic acid (5.0 mL). A solution of nitrosobenzene (**2**, 0.50 g, 3.3 mmol, 1.0 eq) dissolved in acetic acid (10 mL) was added dropwise. The reaction mixture was stirred for 24 h at room temperature. The solvent was evaporated, and the product recrystallized from ethyl acetate. Drying *in vacuo* afforded the product **3** as gold solid (0.54 g, 2.4 mmol, 73%). The analytical data are in agreement with the reported ones. ¹H-NMR (300 MHz, DMSO-*d*₆): δ = 13.25 (s, 1H), 8.19 – 8.09 (m, 2H), 8.00 – 7.88 (m, 4H), 7.62 (dd, *J* = 5.1, 1.9 Hz, 3H). ¹³C-NMR (75 MHz, DMSO-*d*₆): δ = 166.6 (q), 154.1 (q), 151.8 (q), 132.7 (q), 132.1 (q), 130.5 (+), 129.5 (+), 122.7 (+), 122.4 (+). MF: C₁₃H₁₀N₂O₂. MW: 226.24 g/mol.

2,5-dioxopyrrolidin-1-yl(E)-4-(phenyldiazenyl)benzoate (5). The compound was synthesized following a literature reported procedure.^[20] Carboxy azobenzene **3** (1.0 g, 4.4 mmol, 1.0 eq), *N*-hydroxy succinimide (0.51 g, 4.4 mmol, 1.0 eq), and dicyclohexylcarbodiimid (0.91 g, 4.4 mmol, 1.0 eq) were stirred in DMF (20 mL) at room temperature for 12 hours. The reaction mixture was filtered, and the solvent evaporated. The crude was recrystallized from CH₂Cl₂ to afford the product as orange solid (1.3 g, 4.0 mmol, 90%). The analytical data are in agreement with the

reported ones. $^1\text{H-NMR}$ (300 MHz, $\text{DMSO-}d_6$): δ = 8.37 – 8.24 (m, 2H), 8.15 – 8.04 (m, 2H), 8.02 – 7.94 (m, 2H), 7.70 – 7.56 (m, 3H), 2.92 (s, 4H). $^{13}\text{C-NMR}$ (75 MHz, $\text{DMSO-}d_6$): δ = 170.7 (q), 161.7 (q), 156.0 (q), 152.3 (q), 133.2 (+), 132.1 (+), 130.1 (+), 126.6 (q), 123.7 (+), 123.5 (+), 26.0 (-). MF: $\text{C}_{17}\text{H}_{13}\text{N}_3\text{O}_4$. MW: 323.31 g/mol.

(*S,E*) - 2,2' - ((1-carboxy-5-(4-(phenyldiazenyl)benzamido)pentyl)azanediyl)diacetic acid (7). This compound was synthesized *via* an adapted literature reported procedure. NHS azobenzene **5** (0.20 g, 0.62 mmol, 1.0 eq), triacid **6** (0.32 g, 1.2 mmol, 2.0 eq), and triethylamine (63 mg, 0.62 mmol, 1.0 eq) were mixed in CH_2Cl_2 (10 mL) and stirred at room temperature for 12 hours.^[20] The solvent was evaporated, and the product purified by preparative HPLC to afford the desired product as orange solid in 85% yield. $^1\text{H-NMR}$ (300 MHz, $\text{DMSO-}d_6$): δ = 12.41 (s, 3H), 8.63 (t, J = 5.6 Hz, 1H), 8.11 – 8.00 (m, 2H), 7.98 – 7.84 (m, 4H), 7.62 (dd, J = 5.1, 2.2 Hz, 3H), 3.54 – 3.22 (m, 8H), 1.69 – 1.38 (m, 5H). $^{13}\text{C-NMR}$ (75 MHz, $\text{DMSO-}d_6$): δ = 174.4 (q), 173.6 (q), 165.8 (q), 153.6 (q), 152.4 (q), 137.4 (q), 132.4 (+), 130.0 (+), 128.9 (+), 123.2 (+), 122.8 (+), 64.7 (+), 53.7 (-), 39.7 (-), 29.8 (-), 29.2 (-), 23.7 (-). MF: $\text{C}_{23}\text{H}_{26}\text{N}_4\text{O}_7$. MW: 470.48 g/mol.

(*E*)-4-((4-(*tert*-butoxycarbonyl)phenyl)diazenyl)benzoic acid (11). Under a nitrogen atmosphere, amino benzoic acid **1** (3.0 g, 22 mmol, 1.0 eq) was dissolved in CH_2Cl_2 (100 mL). A solution of oxone (13 g, 22 mmol, 1.0 eq) in water (0.10 L) was added and the biphasic reaction mixture stirred at room temperature for one hour. The precipitate was collected by filtration and dried under vacuum.^[21] The crude nitroso benzoic acid **9** was dissolved in acetic acid (0.15 L) and *tert*-butyl aniline **10** (4.2 g, 22 mmol, 1.0 eq) was added. The reaction mixture was stirred at room temperature for 16 hours. The precipitate was collected and dried *in vacuo* (4.4 g, 14 mmol, 62%). $^1\text{H-NMR}$ (300 MHz, $\text{DMSO-}d_6$): δ = 8.17 – 8.09 (m, 4H), 8.02 – 7.97 (m, 4H), 1.57 (s, 9H). $^{13}\text{C-NMR}$ (75 MHz, $\text{DMSO-}d_6$): δ = 167.1 (q), 164.6 (q), 154.6 (q), 154.5 (q), 134.2 (q), 133.8 (q), 131.1 (+), 130.8 (+), 123.3 (+), 123.3 (+), 81.8 (q), 28.2 (+). HRMS (ESI) calcd. for $(\text{C}_{18}\text{H}_{19}\text{N}_2\text{O}_4)^+$ $[\text{M}+\text{H}]^+$: m/z = 327.1339; found 327.1343. MF: $\text{C}_{18}\text{H}_{18}\text{N}_2\text{O}_4$. MW: 326.35 g/mol.

***Tert*-butyl(*E*)-4-((4-(((2,5-dioxopyrrolidin-1-yl)oxy)carbonyl)phenyl)diazenyl)benzoate (12).** The substituted carboxy azobenzene **11** (4.4 g, 13 mmol, 1.0 eq), *N*-hydroxy succinimide **4** (1.6 g, 13 mmol, 1.0 eq) and dicyclohexylcarbodiimid (2.8 g, 13 mmol, 1.0 eq) were stirred in DMF (0.10 L) at room temperature for 12 hours.^[20] The reaction mixture was filtered, and the solvent evaporated. The crude product was purified by column chromatography using CH₂Cl₂ as eluent providing the product as orange solid (4.0 g, 9.5 mmol, 70%). ¹H-NMR (300 MHz, DMSO-*d*₆): δ = 8.39 – 8.28 (m, 2H), 8.18 – 8.09 (m, 4H), 8.07 – 8.01 (m, 2H), 2.93 (s, 4H), 1.58 (s, 9H). ¹³C-NMR (75 MHz, DMSO-*d*₆): δ = 170.7 (q), 164.6 (q), 162.7 (q), 161.7 (q), 155.8 (q), 154.5 (q), 134.6 (q), 132.1 (+), 130.9 (+), 124.0 (+), 123.5 (+), 81.9 (q), 28.2 (+), 26.0 (-). HRMS (ESI) calcd. for (C₂₂H₂₂N₃O₆⁺) [M+H]⁺: *m/z* = 424.1503; found 424.1507. MF: C₂₂H₂₁N₃O₆. MW: 423.43 g/mol.

***Tert*-butyl (*E*)-4-((4-((4aminobutyl)carbamoyl)phenyl)diazenyl)benzoate (14).** NHS azobenzene **12** (1.1 g, 2.6 mmol, 1.0 eq) and triethylamine (0.27 g, 2.6 mmol, 1.0 eq) were dissolved in CH₂Cl₂ (50 mL). A solution of butyldiamine **13** (0.69 g, 7.8 mmol, 2.5 eq) in CH₂Cl₂ (10 mL) was added dropwise.^[20] The reaction mixture was stirred at room temperature for 12 hours and the product was purified by column chromatography using CH₂Cl₂ + 5% MeOH as eluent (0.67 g, 1.7 mmol, 65%). ¹H-NMR (300 MHz, DMSO-*d*₆): δ = 8.78 (t, *J* = 5.7 Hz, 1H), 8.14 – 8.05 (m, 4H), 8.02 – 7.96 (m, 4H), 7.86 (s, 2H), 3.46 (s, 2H), 3.38 – 3.27 (m, 2H), 2.89 – 2.79 (m, 2H), 1.64 – 1.60 (m, 2H), 1.57 (s, 9H). ¹³C-NMR (75 MHz, DMSO-*d*₆): δ = 165.8 (q), 164.7 (q), 154.6 (q), 153.6 (q), 137.7 (q), 134.1 (q), 130.8 (+), 129.0 (+), 123.2 (+), 123.1 (+), 81.8 (q), 39.1 (-), 39.1 (-), 28.2 (+), 26.5 (-), 25.1 (-). HRMS (ESI) calcd. for (C₂₂H₂₉N₄O₃⁺) [M+H]⁺: *m/z* = 397.2234; found 397.2239. MF: C₂₂H₂₈N₄O₃. MW: 396.49 g/mol.

(*E*)-4-(4-((4-carboxyphenyl)diazenyl)benzamido)butan-1-aminiumtrifluoroacetate (15). Alkylamine azobenzene **14** (0.50 g, 1.3 mmol, 1.0 eq) was dissolved in CHCl₃ (8.0 mL) and trifluoro acetic acid (TFA, 2.5 mL) was added dropwise. The reaction mixture was stirred at room temperature for 1 hour.^[15] The solvent was evaporated and residual trifluoro acetic acid co-evaporated from toluene for three

times affording the product as its TFA salt (1.2 g, 2.7 mmol, 94%). ¹H-NMR (400 MHz, DMSO-*d*₆): δ = 8.74 (t, *J* = 5.7, 1H), 8.18 – 8.15 (m, 2H), 8.09 – 8.05 (m, 2H), 8.04 – 7.98 (m, 4H), 7.70 (s, 2H), 3.35 – 3.29 (m, 2H), 2.88 – 2.78 (m, 2H), 1.64 – 1.55 (m, 4H). MF: C₂₀H₂₁F₃N₄O₅. MW: 454.41 g/mol.

(E)-4-((4-((4-((*tert*-butoxycarbonyl)amino)butyl)carbamoyl)phenyl)diazenyl)benzoic acid (16). Trifluoro acetate amino azobenzene **15** (1.2 g, 2.7 mmol, 1.0 eq) was dissolved in a mixture of DMF (10 mL) and water (0.10 L). Boc anhydride (0.60 g, 2.7 mmol, 1.0 eq) and triethylamine (1.1 mL, 8.2 mmol, 3.0 eq) were added. The reaction mixture was stirred at room temperature for 16 hours.^[15] A solution of 5% citric acid (0.10 L) and CH₂Cl₂ (0.15 L) was added. The product was extracted for ten times. The combined organic phases were dried over Na₂SO₄, filtered, and the solvent evaporated yielding the product as orange solid (0.92 g, 2.1 mmol, 76%). ¹H-NMR (400 MHz, DMSO-*d*₆): δ = 8.65-8.70 (b, 1H), 7.95-8.25 (m, 8H), 6.75-6.85 (b, 1H), 2.80-3.20 (m, 4H), 1.41-1.55 (m, 2H), 1.30-1.40 (s, 9 H), 1.15-1.30 (m, 2H). MF: C₂₀H₂₁F₃N₄O₅. MF: C₂₃H₂₈N₄O₅. MW: 440.50 g/mol.

2,5-dioxopyrrolidin-1-yl(E)-4-((4-((4-((*tert*-butoxycarbonyl)amino)butyl)carbamoyl)phenyl)diazenyl)benzoate (17). Carboxylic acid azobenzene **16** (0.92 g, 2.1 mmol, 1.0 eq), *N*-hydroxy succinimide (0.37 g, 3.2 mmol, 1.5 eq), and WSC·HCl (0.61 g, 3.2 mmol, 1.5 eq) were dissolved in DMF (50 mL) and stirred at room temperature for 13 hours.^[15] The solvent was evaporated, and the product purified by column chromatography using CH₂Cl₂ + 0-20% MeOH as eluent. Evaporation of the solvent afforded the product as orange solid (0.34 g, 0.64 mmol, 31%). ¹H-NMR (400 MHz, CDCl₃-*d*): δ = 8.41 – 8.20 (m, 2H), 8.10 – 7.94 (m, 8H), 4.82 – 4.57 (m, 1H), 3.80 – 3.62 (m, 1H), 3.62 – 3.46 (m, 2H), 3.30 – 3.03 (m, 4H), 1.76 – 1.62 (m, 4H), 1.54 – 1.40 (m, 9H). MF: C₂₇H₃₁N₅O₇. MW: 537.57 g/mol.

***Tert*-butyl(E)-4-(4-((4-((6-hydroxyhexyl)carbamoyl)phenyl)diazenyl)benzamido)butyl)carbamate (19).** NHS azobenzene **17** (0.34 g, 0.64 mmol, 1.0 eq) was dissolved in DMF (5.0 mL). Triethylamine (0.19 g, 1.9 mmol, 3.0 eq) and 6-amino-1-hexanol (**18**, 0.23 g, 2.0 mmol, 3.0 eq) were added and the mixture stirred at room

temperature for 16 hours.^[15] The solvent was evaporated, and the residue dissolved in CH₂Cl₂. The organic phase was washed with a 1:1 mixture of brine and 5% citric acid (3x). The combined organic phases were dried over Na₂SO₄, filtered, and the solvent evaporated to yield the product in quantitative yield (0.35 g, 0.64 mmol). ¹H-NMR (400 MHz, DMSO-*d*₆): δ = 8.73 – 8.65 (m, 2H), 8.10 – 8.04 (m, 4H), 8.00 – 7.96 (m, 4H), 6.81 (t, 1H), 4.44 – 4.30 (m, 1H), 3.41 – 3.38 (m, 2H), 3.30 – 3.26 (m, 4H), 2.97 – 2.90 (m, 2H), 1.56 – 1.40 (m, 8H), 1.37 (s, 9H), 1.33 – 1.28 (m, 4H). MF: C₂₉H₄₁N₅O₅. MW: 539.68 g/mol.

(E)-6-(4-((4-((4-((*tert*-butoxycarbonyl)amino)butyl)carbamoyl)phenyl)diazenyl)benzamido)hexylmethanesulfonate (20). Hydroxyalkane azobenzene **19** (0.35 g, 0.64 mmol, 1.0 eq) was dissolved in DMF (6.0 mL) under a nitrogen atmosphere and cooled to 0 °C. Dimethyl aminopyridine (24 mg, 0.20 mmol, 0.3 eq), Triethylamine (0.19 g, 1.9 mmol, 3.0 eq), and MSCL (0.22 g, 1.9 mmol, 3.0 eq) were added and the reaction mixture allowed to warm to room temperature. The reaction mixture was stirred for 16 hours.^[15] The solvent was evaporated and the crude mixture purified by column chromatography using CH₂Cl₂ + 5% MeOH as eluent. Evaporation of the solvent afforded the desired product as orange solid (0.20 g, 0.32 mmol, 50%). ¹H-NMR (400 MHz, DMSO-*d*₆): δ = 8.65 (t, *J* = 5.7 Hz, 2H), 8.06 (d, *J* = 8.5 Hz, 4H), 7.98 (d, *J* = 8.5 Hz, 4H), 6.81 (t, *J* = 5.6 Hz, 1H), 4.20 (t, *J* = 6.5 Hz, 2H), 3.31 – 3.25 (m, 4H), 3.16 (s, 3H), 3.00 – 2.91 (m, 2H), 2.57 – 2.52 (m, 2H), 1.73 – 1.65 (m, 2H), 1.59 – 1.51 (m, 4H), 1.46 – 1.40 (m, 4H), 1.37 (s, 9H). HRMS (ESI) calcd. for (C₃₀H₄₃N₅O₇SN⁺) [M+Na]⁺: *m/z* = 640.2775; found 640.2774. MF: C₃₀H₄₃N₅O₇S. MW: 617.76 g/mol.

(E)-4-(4-((4-((6-((methylsulfonyl)oxy)hexyl)carbamoyl)phenyl)diazenyl)benzamidobutan-1-aminiumtrifluoroacetate (21). Methane sulfonate alkane azobenzene **20** (80 mg, 0.13 mmol, 1.0 eq) was dissolved in CH₂Cl₂ (1.0 mL). Trifluoroacetic acid (1.0 mL) was added as deprotecting agent. The mixture was stirred at room temperature for one hour.^[15] The solvent was evaporated and residual trifluoro acetic acid removed by threefold co-evaporation from CH₂Cl₂. The crude product was obtained in quantitative yield (82 mg, 0.13 mmol). ¹H-NMR

(400 MHz, DMSO-*d*₆): δ = 8.82 – 8.57 (m, 2H), 8.08 – 8.04 (m, 4H), 8.01 – 7.96 (m, 4H), 7.66 (s, 2H), 4.20 (t, 2H), 3.35 – 3.27 (m, 4H), 3.16 (s, 3H), 2.88 – 2.79 (m, 2H), 1.75 – 1.65 (m, 2H), 1.61 – 1.57 (m, 4H), 1.57 – 1.51 (m, 2H), 1.41 – 1.33 (m, 4H). MF: C₂₇H₃₆F₃N₅O₇S. MW: 613.67 g/mol.

***Tert*-butyl (*S,E*)-19-(2-(*tert*-butoxy)-2-oxoethyl)-18-(*tert*-butoxycarbonyl)-1-(4-((4-((6-((methylsulfonyl)oxy)hexyl)carbamoyl)phenyl)diazenyl)phenyl)-1,8,12-trioxo-2,7,13,19-tetraaza-henicosan-21-oate (23).** Methane sulfonate azobenzene **21** (40 mg, 0.063 mmol, 1.0 eq) was dissolved in DMF (1.0 mL). The protected triacid NHS ester **22** (53 mg, 0.082 mmol, 1.3 eq) and triethylamine (19 mg, 0.19 mmol, 3.0 eq) were added and the mixture stirred at room temperature for 16 hours.^[15] The solvent was removed under reduced pressure, the residue dissolved in CHCl₃ and washed with 5% citric acid, saturated aq. NaHCO₃, and brine. The organic phase was dried over Na₂SO₄, filtered, and the solvent removed *in vacuo*. The crude reaction mixture was purified by column chromatography using CH₂Cl₂ + 5% MeOH as eluent. Evaporation of the solvent afforded the desired product **21** in 52% yield (0.033 mmol, 35 mg). ¹H-NMR (400 MHz, CDCl₃-*d*): δ = 8.02 – 8.01 (m, 1H), 8.00 – 7.95 (m, 8H), 7.94 – 7.92 (m, 2H), 7.92 – 7.89 (m, 1H), 4.25 (t, *J* = 6.4 Hz, 2H), 3.53 – 3.48 (m, 5H), 3.43 – 3.42 (m, 2H), 3.41 – 3.40 (m, 2H), 3.33 – 3.29 (m, 4H), 3.01 (s, 3H), 2.30 – 2.26 (m, 4H), 2.00 – 1.95 (m, 2H), 1.81 – 1.77 (m, 2H), 1.67 – 1.64 (m, 13H), 1.43 (s, 27H). MF: C₅₂H₈₁N₇O₁₃S. MW: 1044.32 g/mol.

(*S,E*)-6-(4-((4-((6-(2-(*tert*-butoxy)-2-oxoethyl)-7-(*tert*-butoxycarbonyl)-2,2-dimethyl-4,13,17-trioxo-3-oxa-6,12,18-triazadocosan-22-yl)carbamoyl)phenyl)diazenyl)benzamido)-*N*-(4-((4,5-dihydroisoxazol-3-yl)oxy)but-2-yn-1-yl)-*N,N*-dimethylhexan-1-aminium methanesulfonate (25). Azobenzene **23** (40 mg, 0.038 mmol, 1.0 eq) and the Iperoxo ligand **24** (7.7 mg, 0.042 mmol, 1.1 eq) were suspended in dry acetonitrile (0.50 mL) and refluxed for 23 hours.^[15] Thin layer chromatography indicated incomplete reaction. Even under addition of up to 3.0 eq of Iperoxo ligand no further conversion of the starting material was achieved. The solvent was evaporated and the crude product used in the next

reaction step without further purification. $^1\text{H-NMR}$ (400 MHz, $\text{MeOD-}d_4$): δ = 8.02 (s, 8H), 4.80 (t, J = 1.9 Hz, 4H), 4.38 – 4.36 (m, 2H), 3.48 – 3.41 (m, 8H), 3.39 – 3.36 (m, 4H), 3.28 – 3.21 (m, 3H), 3.17 (s, 6H), 3.06 – 2.96 (m, 5H), 2.72 – 2.65 (m, 2H), 2.21 (t, J = 7.4 Hz, 4H), 1.91 – 1.85 (m, 2H), 1.84 – 1.77 (m, 2H), 1.71 – 1.58 (m, 10H), 1.54 – 1.51 (m, 4H), 1.46 – 1.44 (m, 27H). MF: $\text{C}_{61}\text{H}_{95}\text{N}_9\text{O}_{15}\text{S}$. MW: 1226.54 g/mol.

(*S,E*)-6-(4-((4-((4-(5-((5-(bis(carboxymethyl)amino)-5-carboxypentyl)amino)-5-oxopentanamido)butyl)carbamoyl)phenyl)diazenyl)benzamido)-*N*-(4-((4,5-dihydroisoxazol-3-yl)oxy)but-2-yn-1-yl)-*N,N*-dimethylhexan-1-aminium (26).

Crude tri *tert*-butyl ester **25** (53 mg) was suspended in CH_2Cl_2 (2.0 mL) and trifluoro acetic acid (1.0 mL) was added. The solution was stirred at room temperature for four hours.^[15] The solvent was evaporated and residual TFA removed by co-evaporation from CH_2Cl_2 for three times. Purification by preparative RP-HPLC (gradient: 100% 0.05% aq. TFA 0-10 min; 0-100% MeCN + 0.05% TFA 10-60 min; t_R = 36 min) afforded the desired product as orange solid (22 mg, 0.021 mmol, 37% over two steps). $^1\text{H-NMR}$ (400 MHz, $\text{MeOD-}d_4$): δ = 8.15 – 7.96 (m, 8H), 5.00 – 4.92 (m, 8H), 4.50 – 4.30 (m, 4H), 3.80 – 3.62 (m, 4H), 3.56 – 3.34 (m, 8H), 3.26 – 3.22 (m, 2H), 3.17 (s, 6H), 3.02 (t, J = 9.6 Hz, 1H), 2.31 – 2.16 (m, 4H), 1.94 – 1.85 (m, 2H), 1.84 – 1.77 (m, 2H), 1.74 – 1.65 (m, 4H), 1.64 – 1.58 (m, 2H), 1.57 – 1.45 (m, 6H). HRMS (ESI) calcd. for $(\text{C}_{48}\text{H}_{68}\text{N}_9\text{O}_{12})^+ [\text{M}]^+$: m/z = 962.4982; found 962.4964. MF: $\text{C}_{50}\text{H}_{68}\text{F}_3\text{N}_9\text{O}_{14}$. MW: 1076.14 g/mol.

8.4.3 *In Vitro* Studies

Culture and transfection of CHO cells. CHO cells were maintained in Dulbecco's modified Eagle's medium (DMEM-F12, Sigma-Aldrich) with 10% fetal bovine serum (FBS) (Gibco), 100 unit/mL penicillin, 100 $\mu\text{g/mL}$ penicillin, 100 $\mu\text{g/mL}$ streptomycin, and 0.25 $\mu\text{g/mL}$ amphotericin B (Gibco) at 37 °C in a humidified atmosphere of 95% air and 5% CO_2 . For M1R, CHO cells were transiently transfected with plasmids (WT M1R, the M1R mutants, or the control vector) using Lipofectamine2000 transfection reagent in DMEM-F12, supplemented with 10% FBS according to the manufacturer's instruction. The cells were co-transfected with

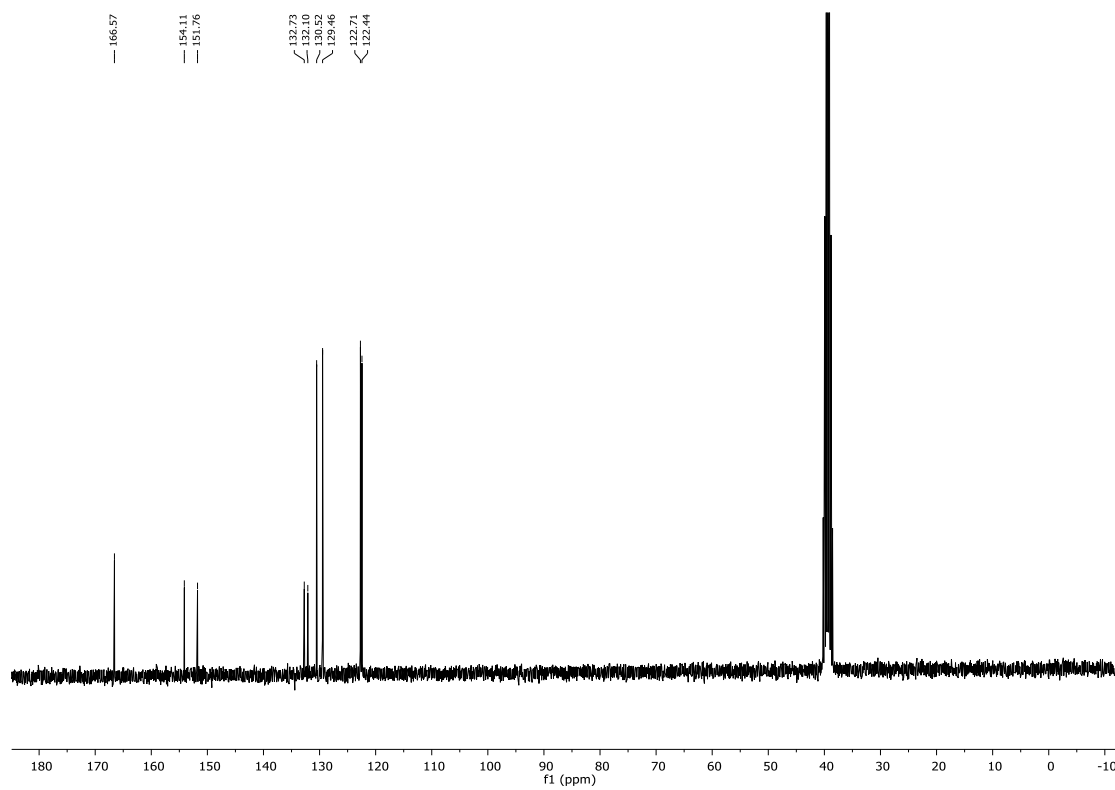
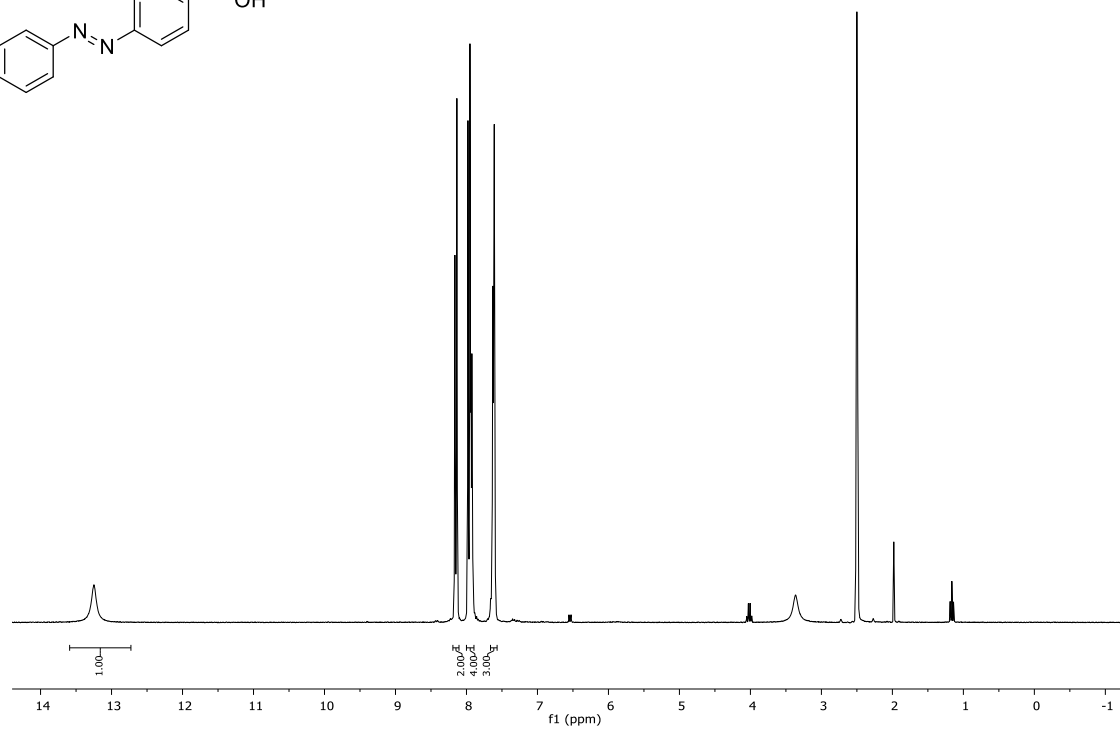
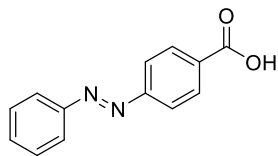
pEGFP-F (Clontech) or pmCherry-F as a transfection marker. For Ca^{2+} imaging, the cells were grown for 24-36 h, seeded on glass coverslips (Matsunami) coated with poly-L-lysine solution (Sigma-Aldrich), and subjected to Ca^{2+} imaging 4-12 h after seeding.

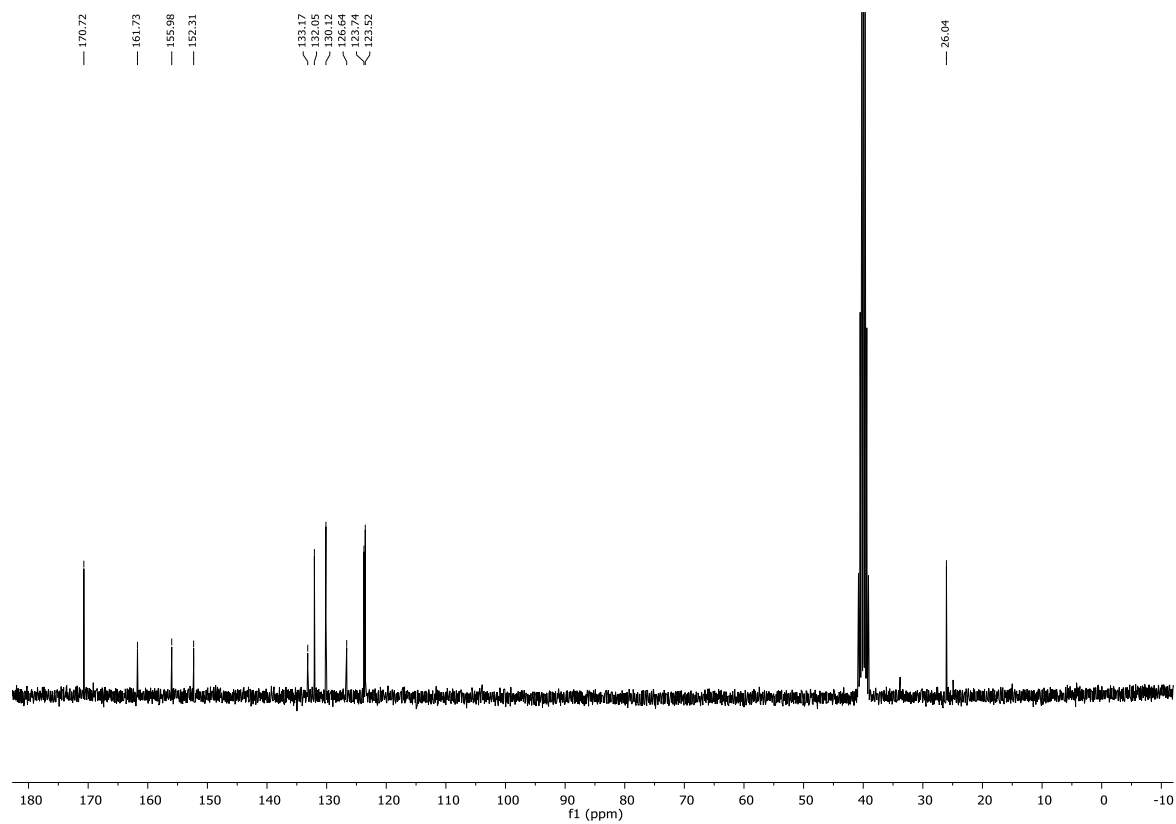
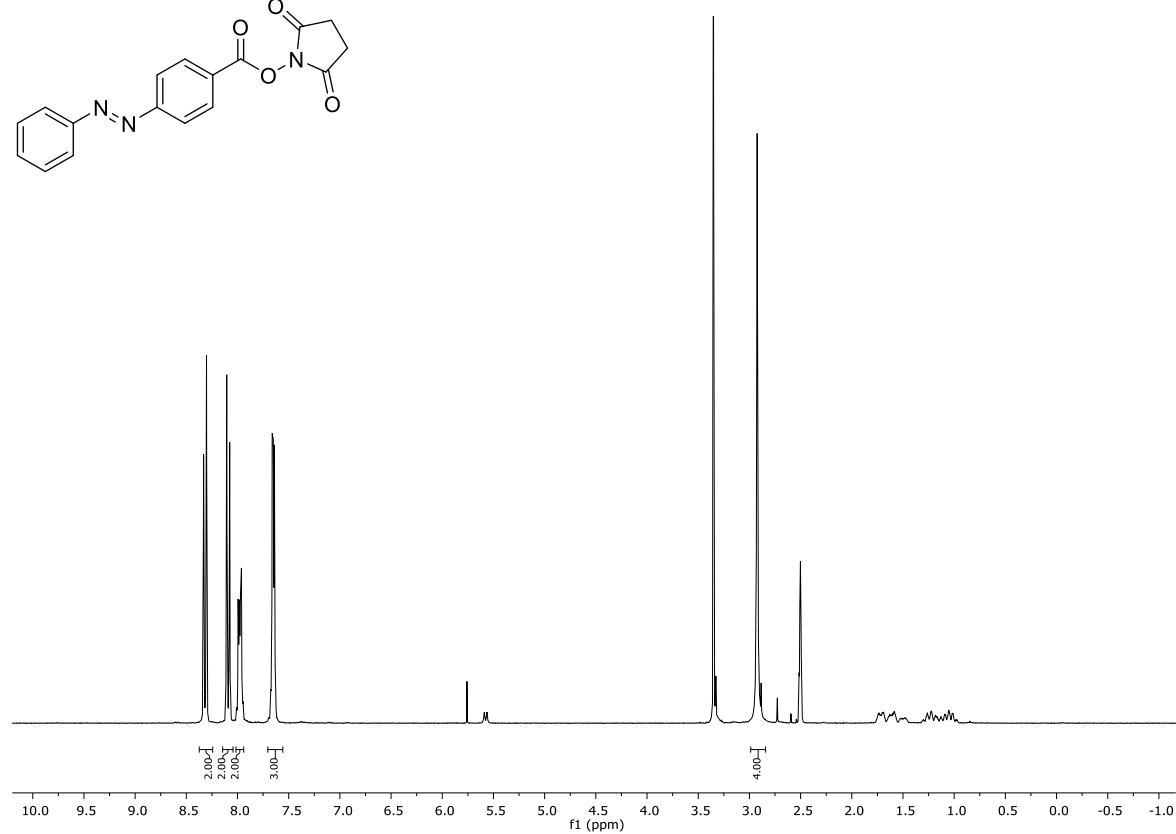
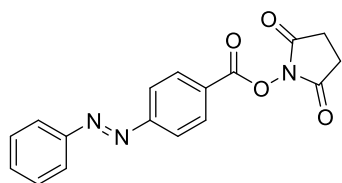
Fluorescence Ca^{2+} imaging. CHO cells were loaded with 5 μM Fura-2 AM (absorption maximum Ca^{2+} -bound 340 nm; Ca^{2+} -free 380 nm; emission maximum 510 nm) or 5 μM Fluo-4 AM (absorption maximum Ca^{2+} -bound 480 nm excitation; emission maximum 516 nm), respectively, for 20-30 min in growth medium. The fluorescence was measured in HBS (107 mM NaCl, 6 mM KCl, 1.2 mM MgSO_4 , 11.5 mM glucose, 0.2 mM CaCl_2 , and 20 mM HEPES at pH 7.4), respectively. The photochromic metal chelator agonist **26** stock solution was prepared 10 mM in millipore water. Dilutions were prepared in HBS. For nickel positive experiments, compound **26** and 1.0 eq of NiSO_4 (both 10 mM) were mixed 60 min before fluorescence Ca^{2+} imaging providing complex **27**. Iperoxo was dissolved in HBS from 1000x H_2O stocks. Fluorescence images were obtained using a fluorescence microscope (IX71, Olympus) equipped with a CMOS camera (ORCA-flash 4.0, Hamamatsu Photonics) under xenon lamp irradiation, and analyzed with a video imaging system (CellSens Dimension, Olympus) according to the manufacturer's protocol.

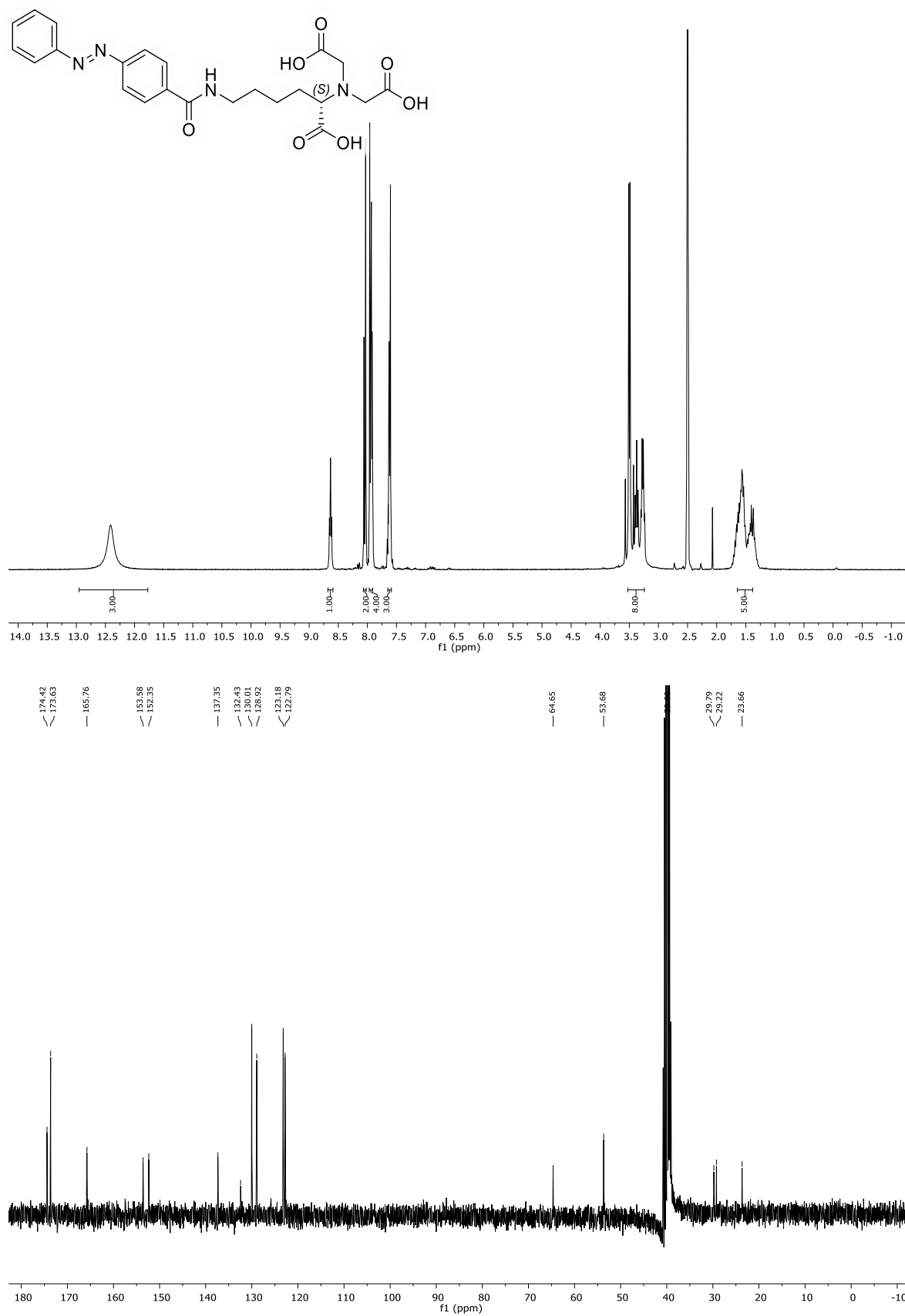
8.5 Supporting Information

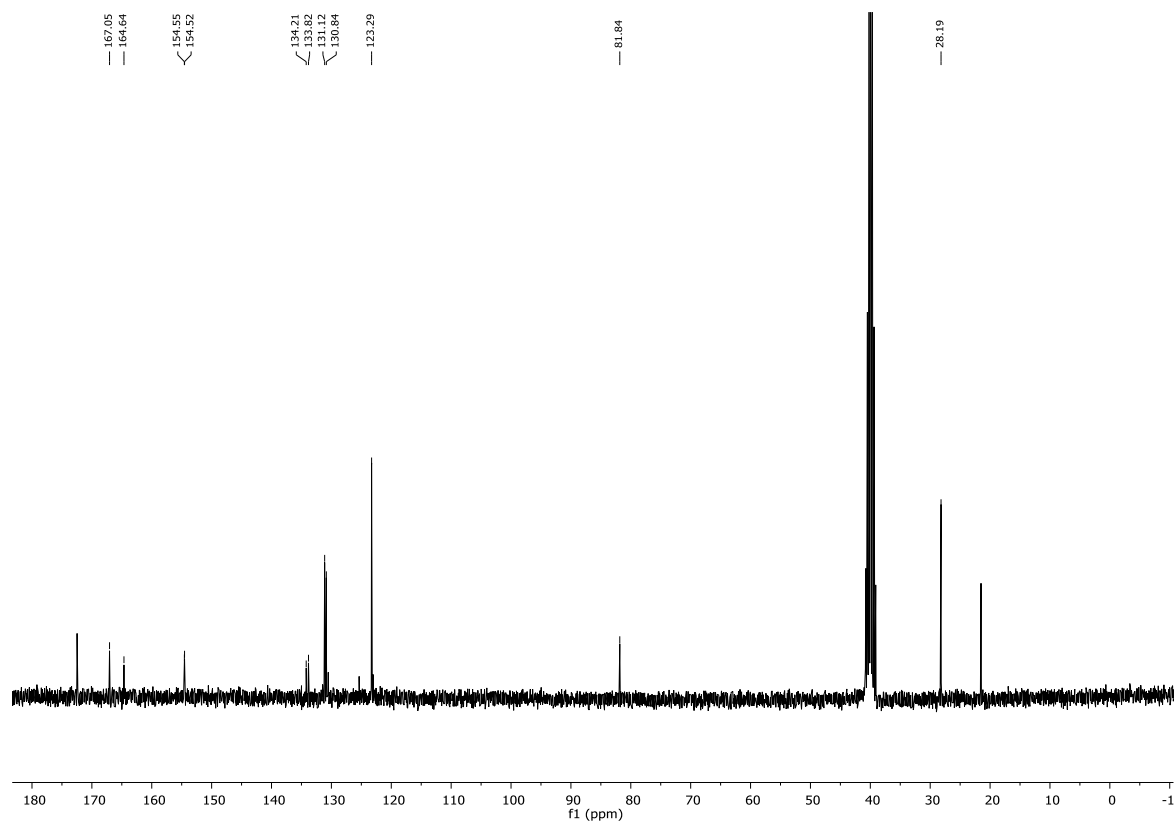
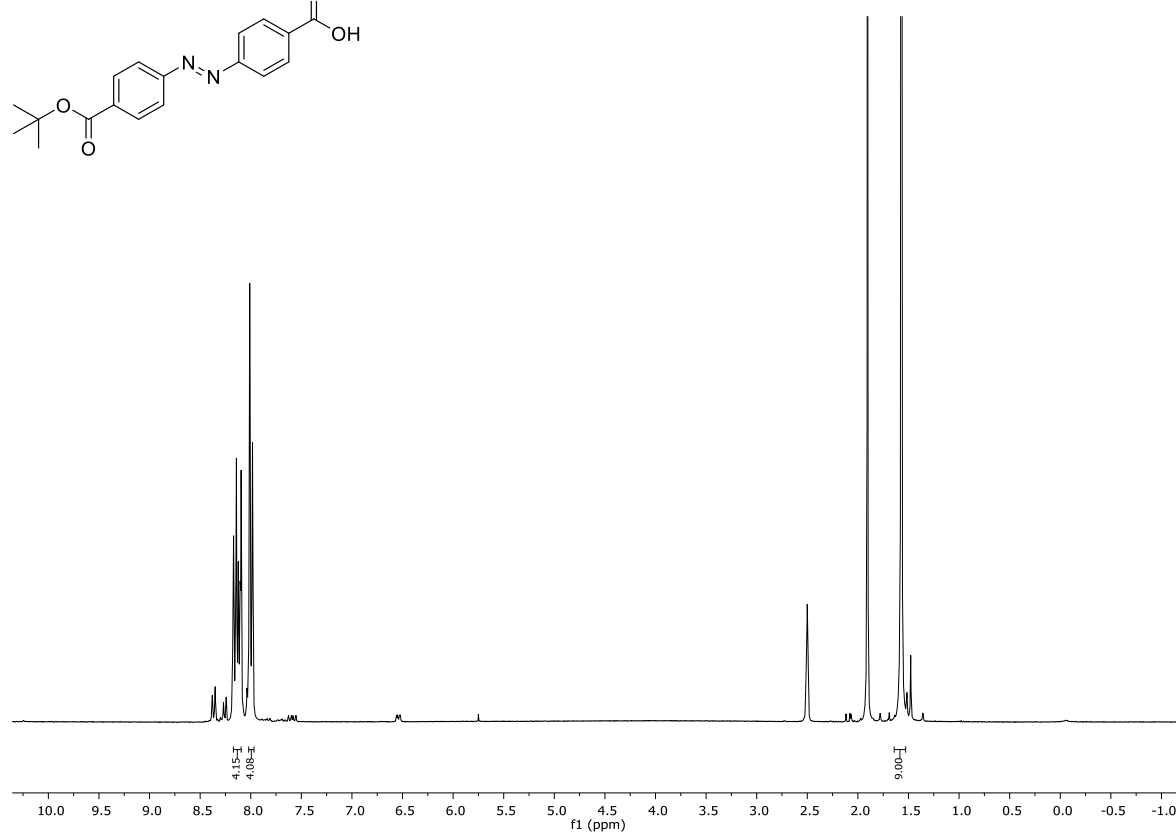
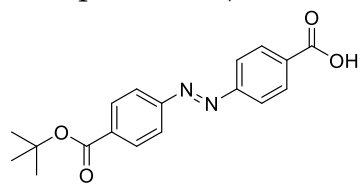
8.5.1 ^1H - and ^{13}C -NMR Spectra

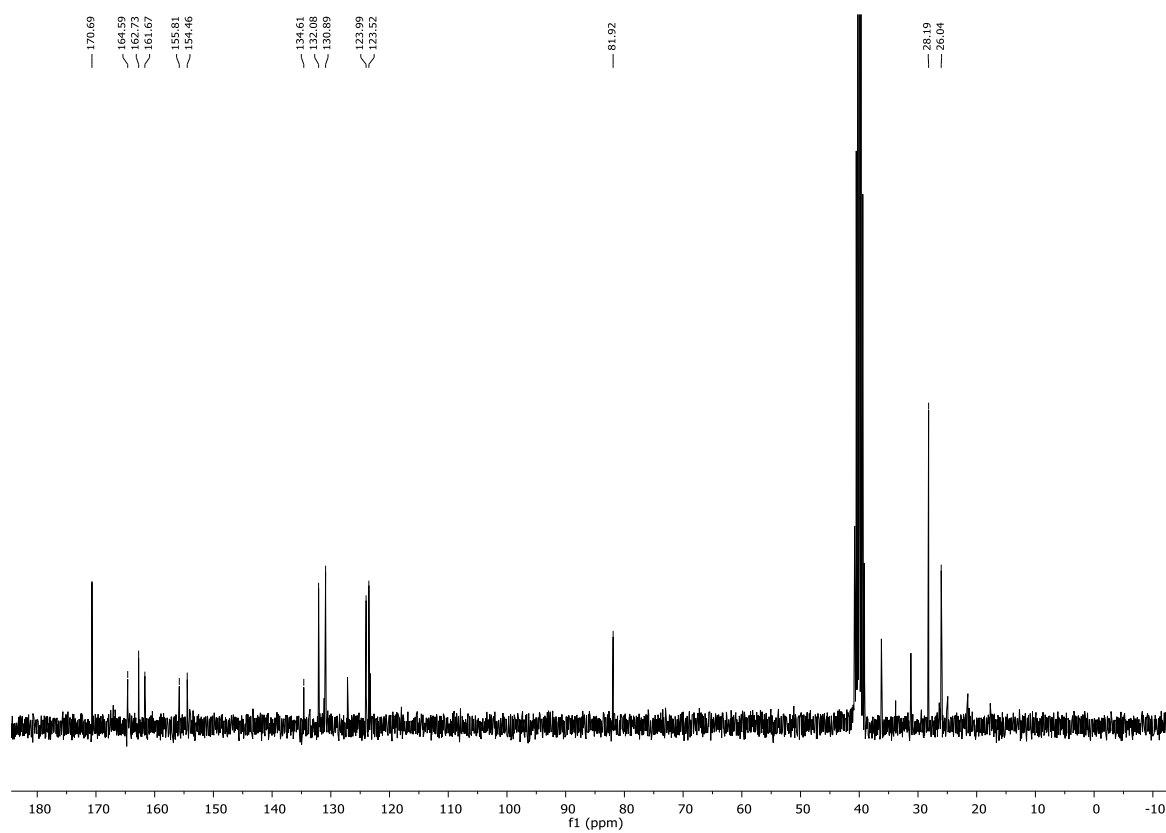
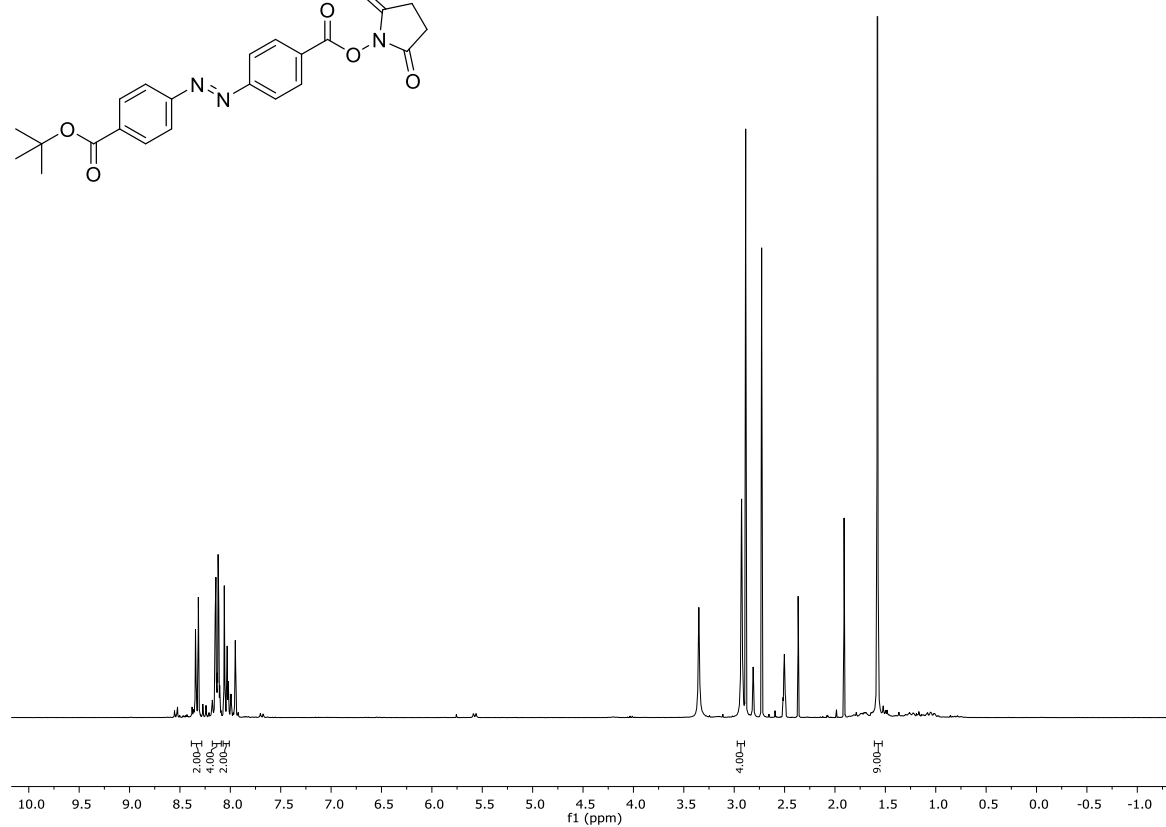
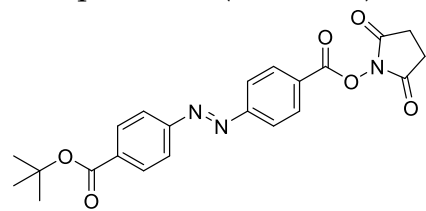
Compound 3 (DMSO- d_6)

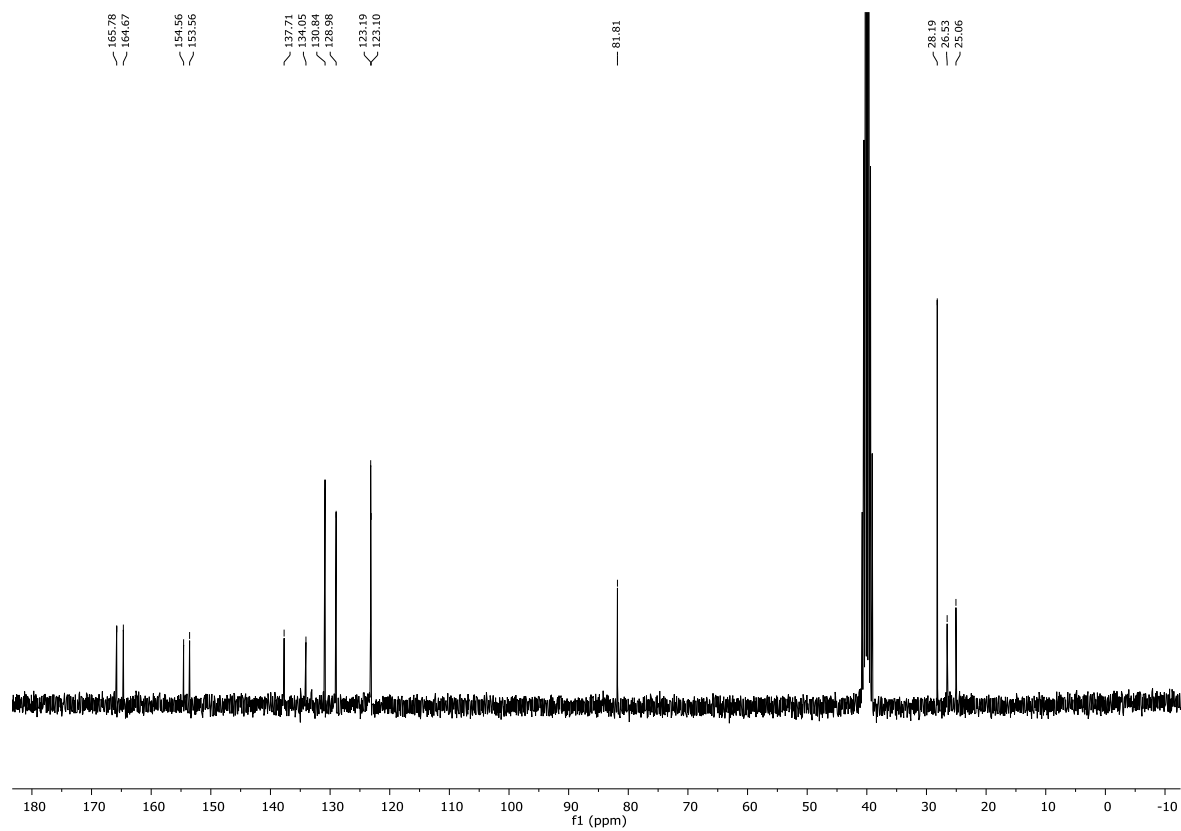
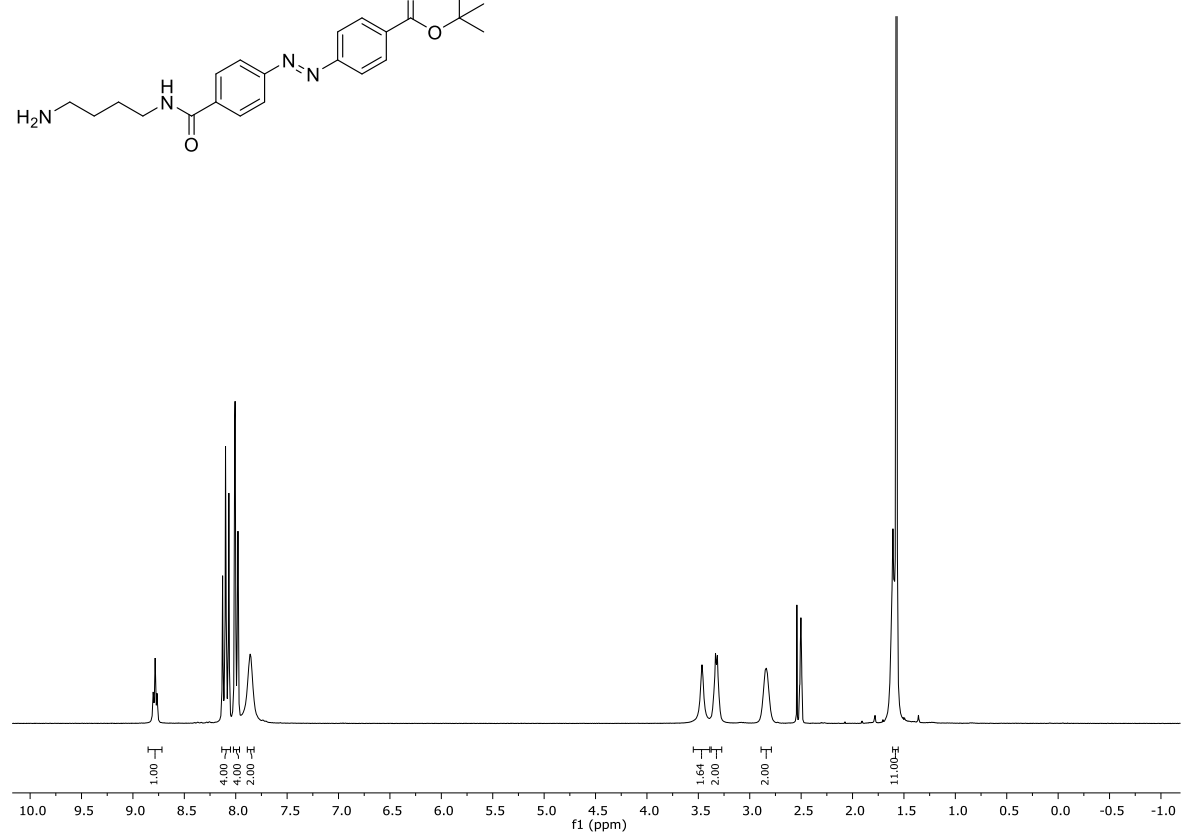
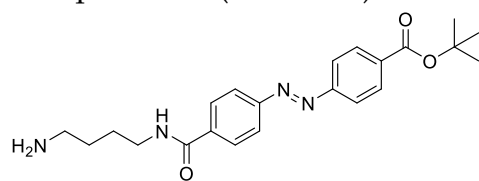


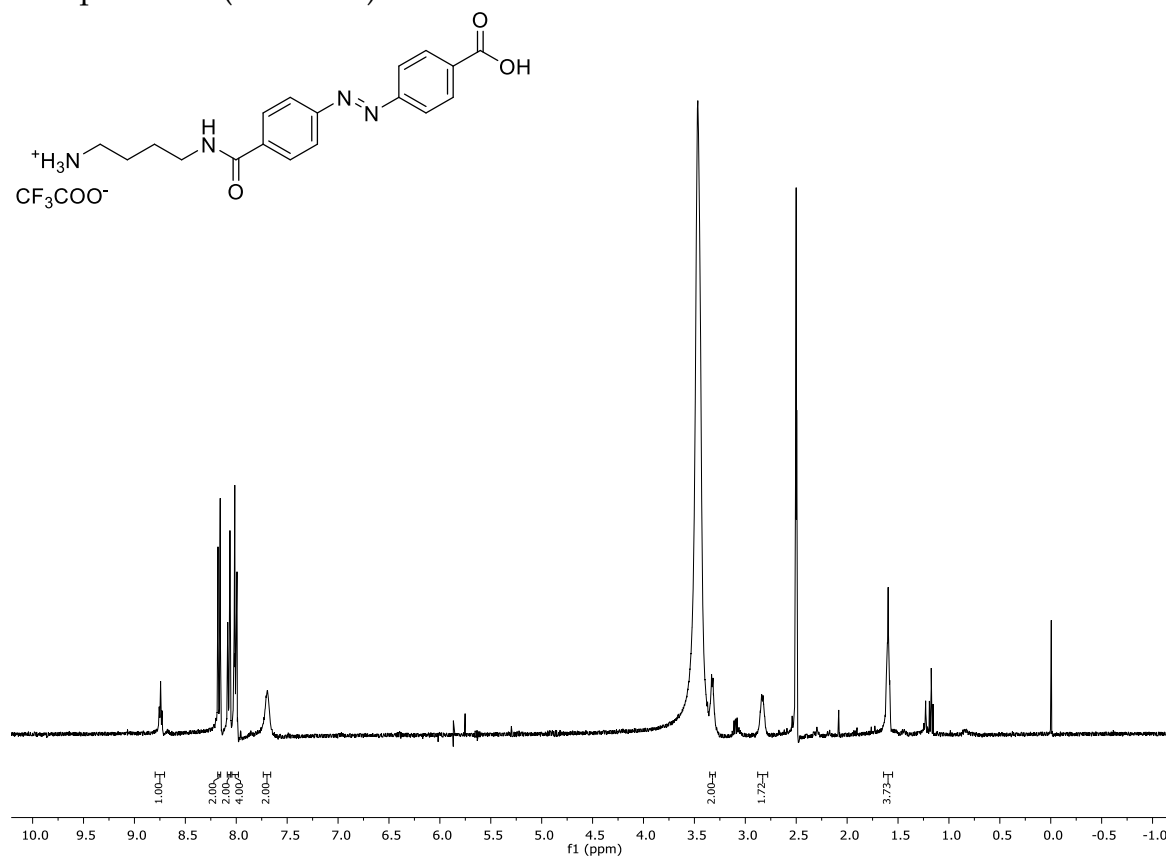
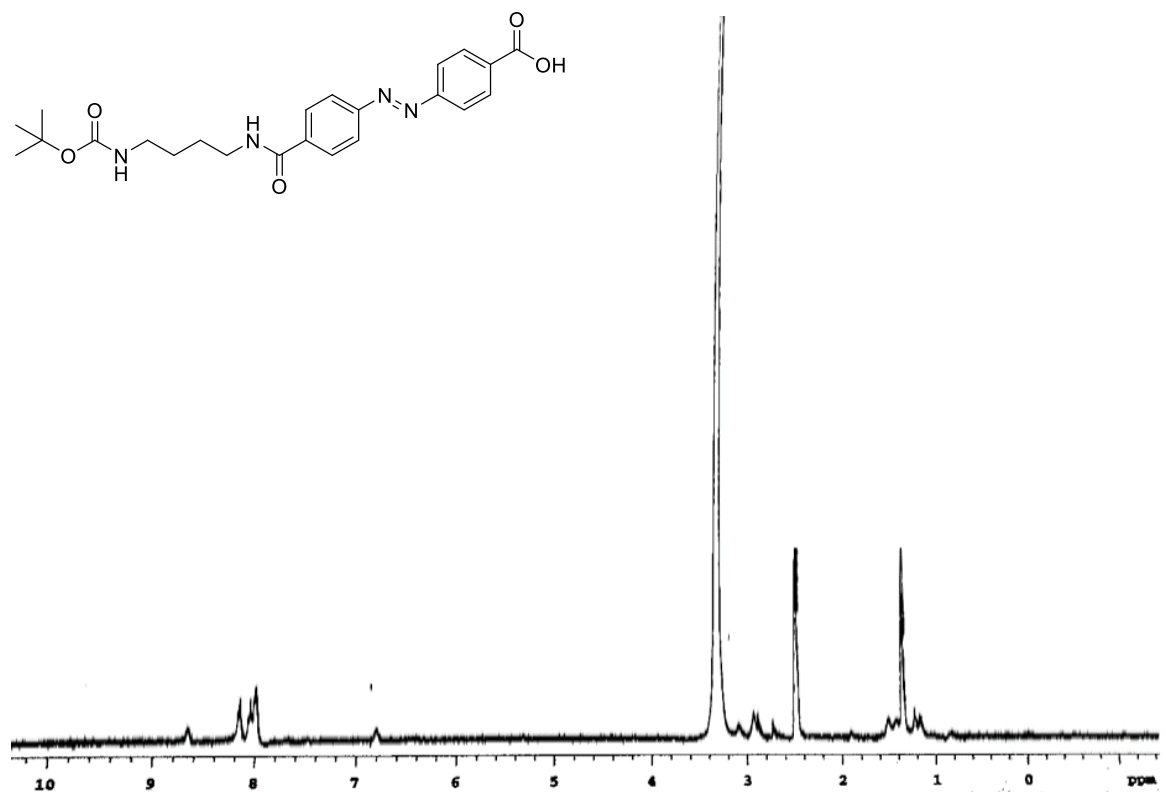
Compound 5 (DMSO-*d*₆)


Compound 7 (DMSO-*d*₆)

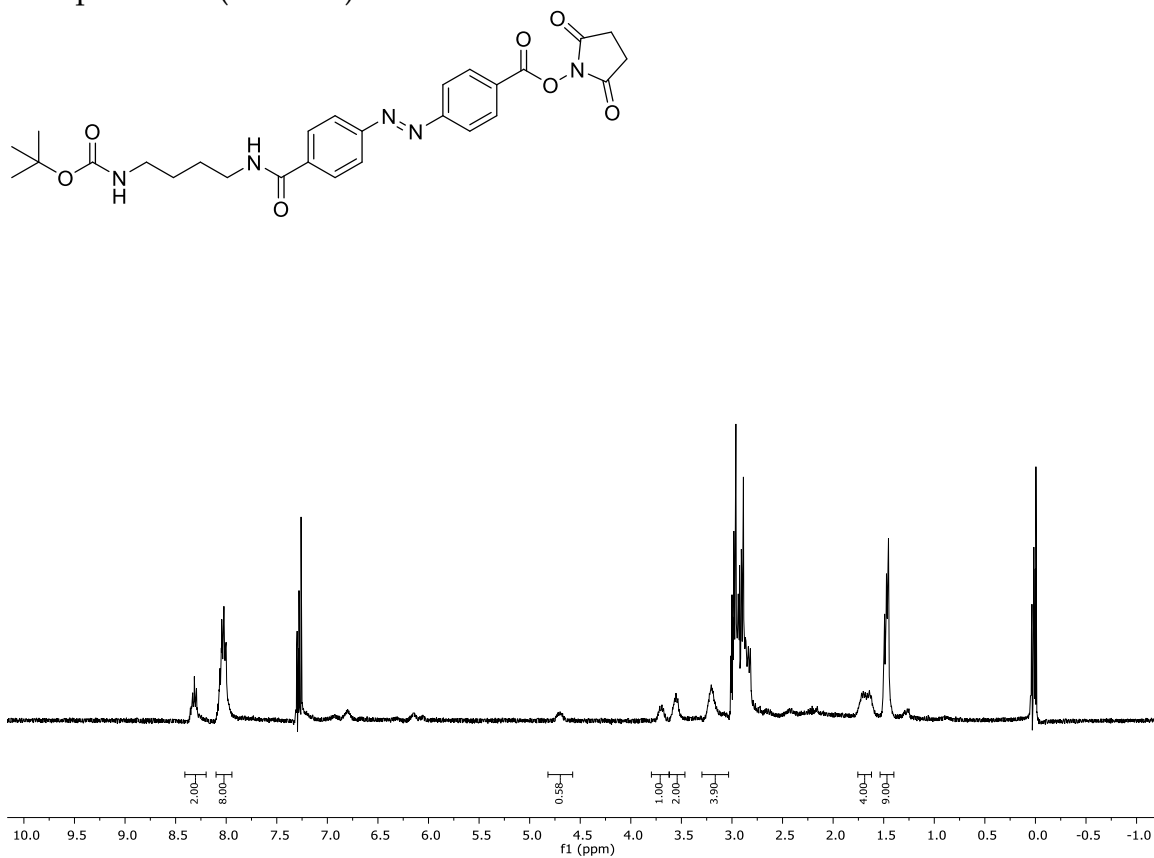
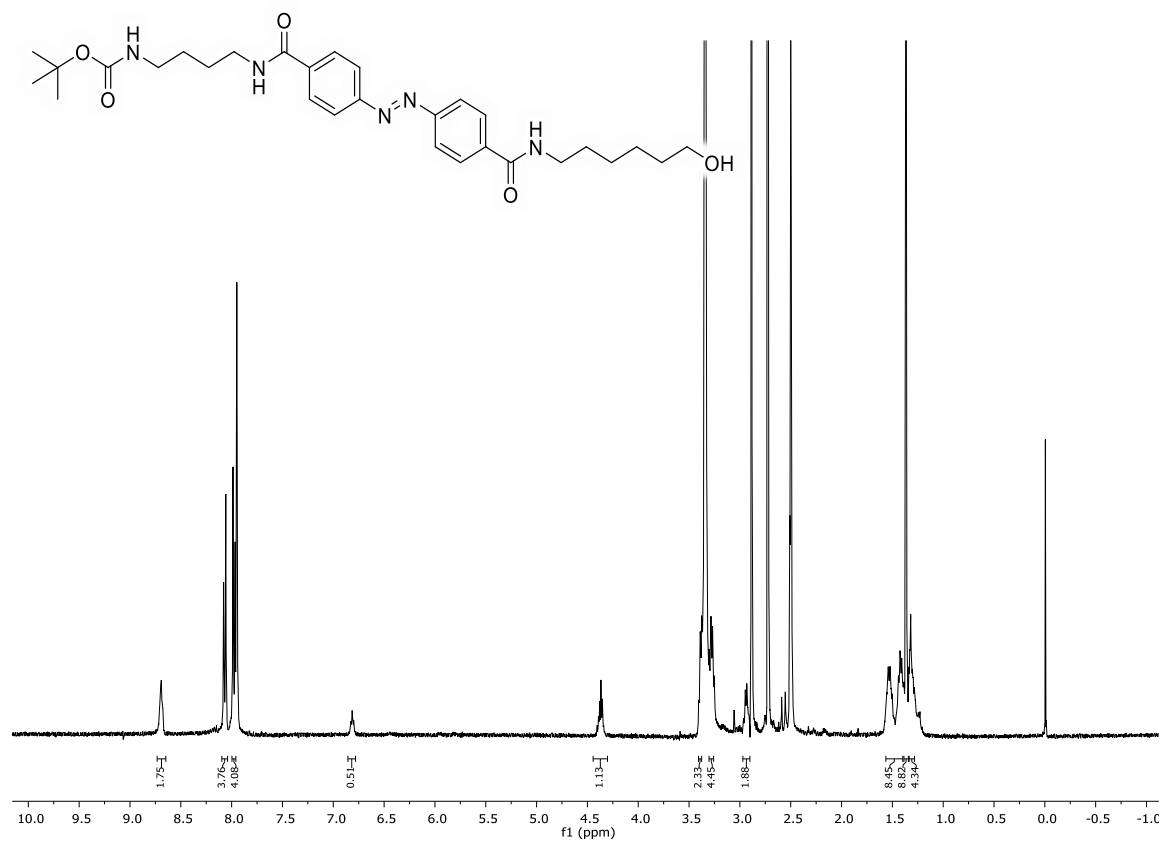
Compound **11** (DMSO-*d*₆)


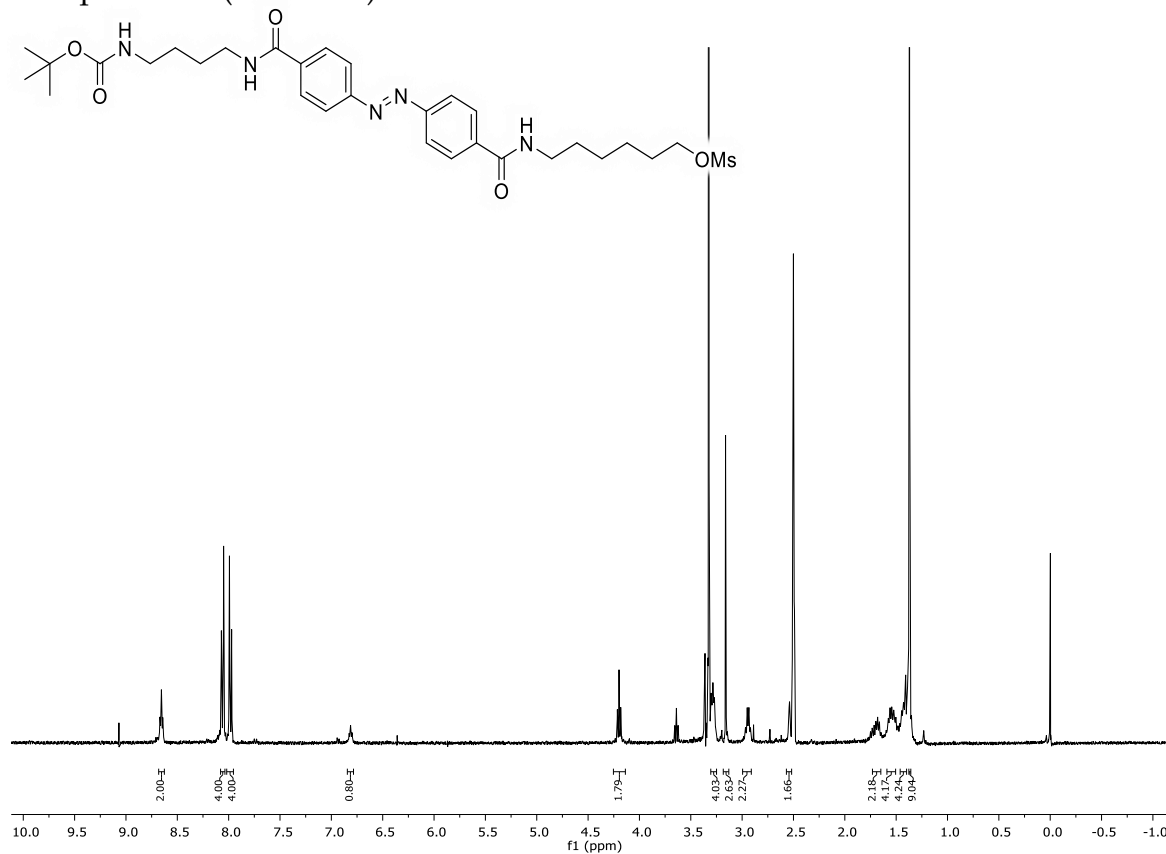
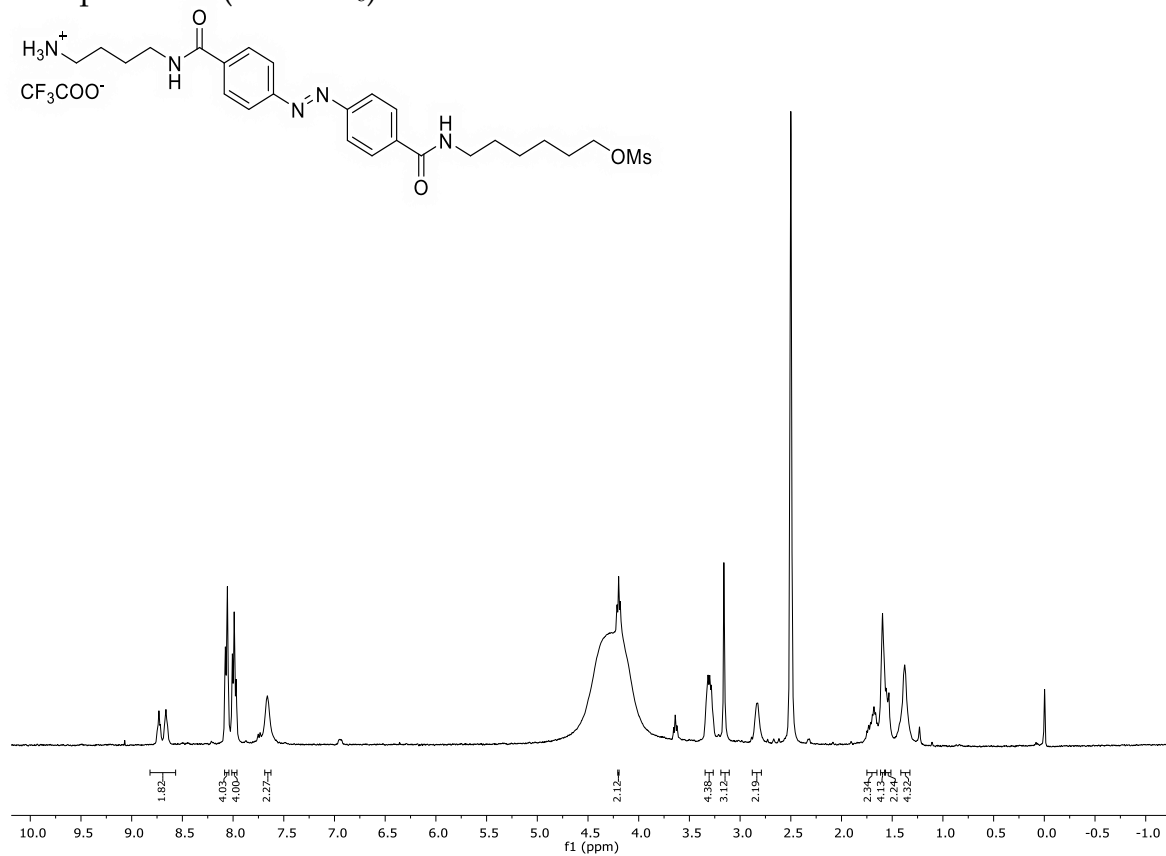
Compound **12** (DMSO-*d*₆)

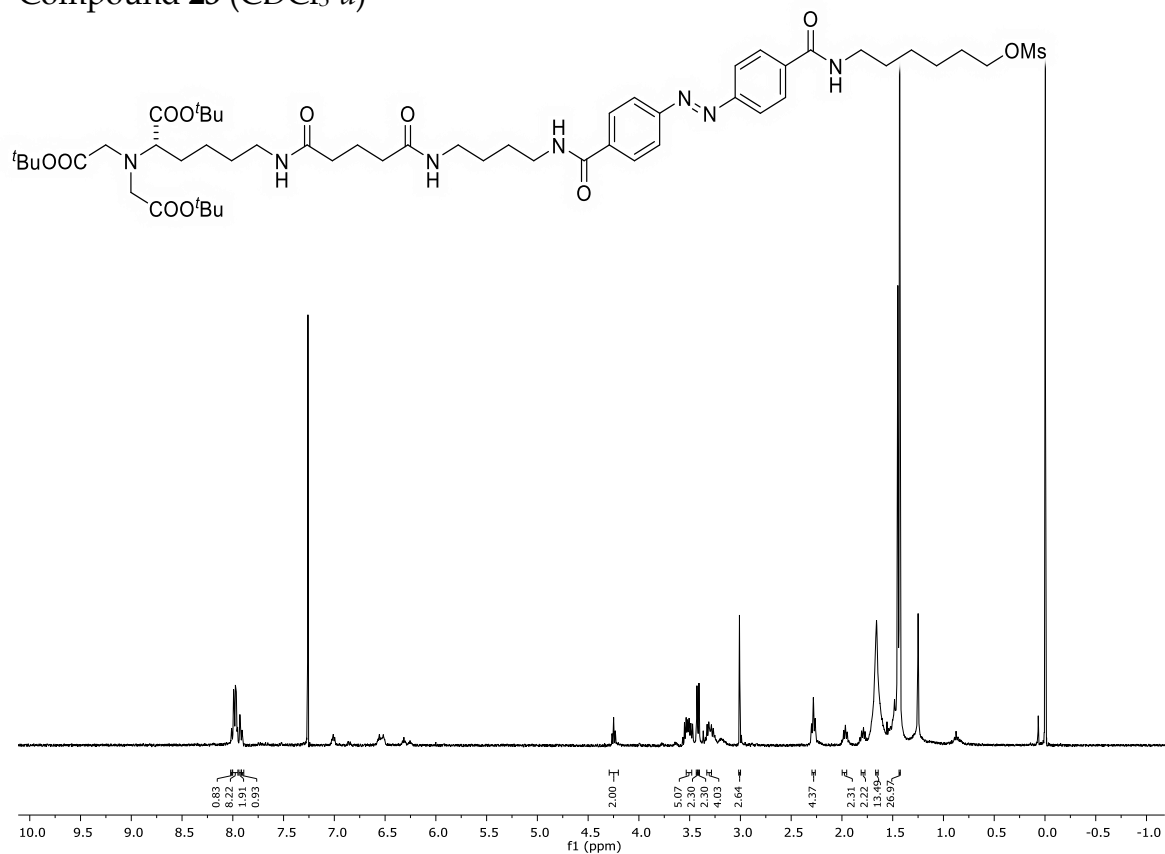
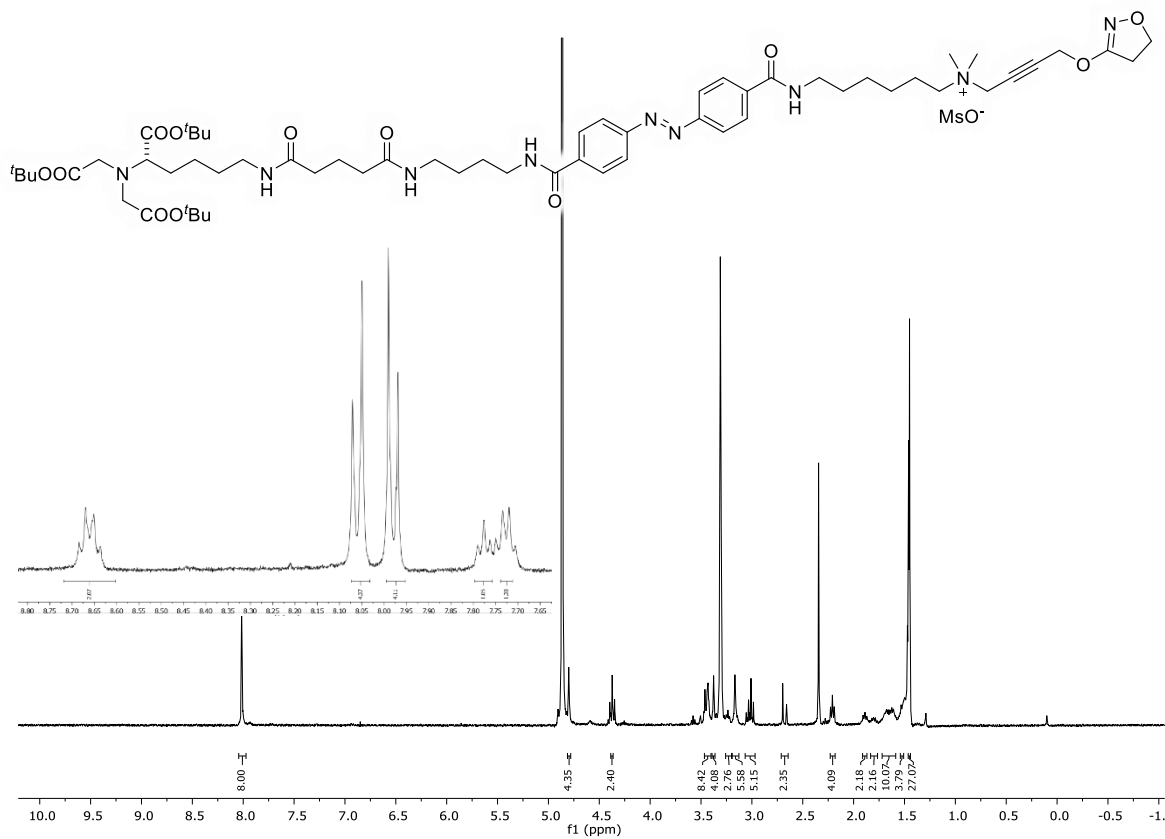
Compound **14** (DMSO-*d*₆)


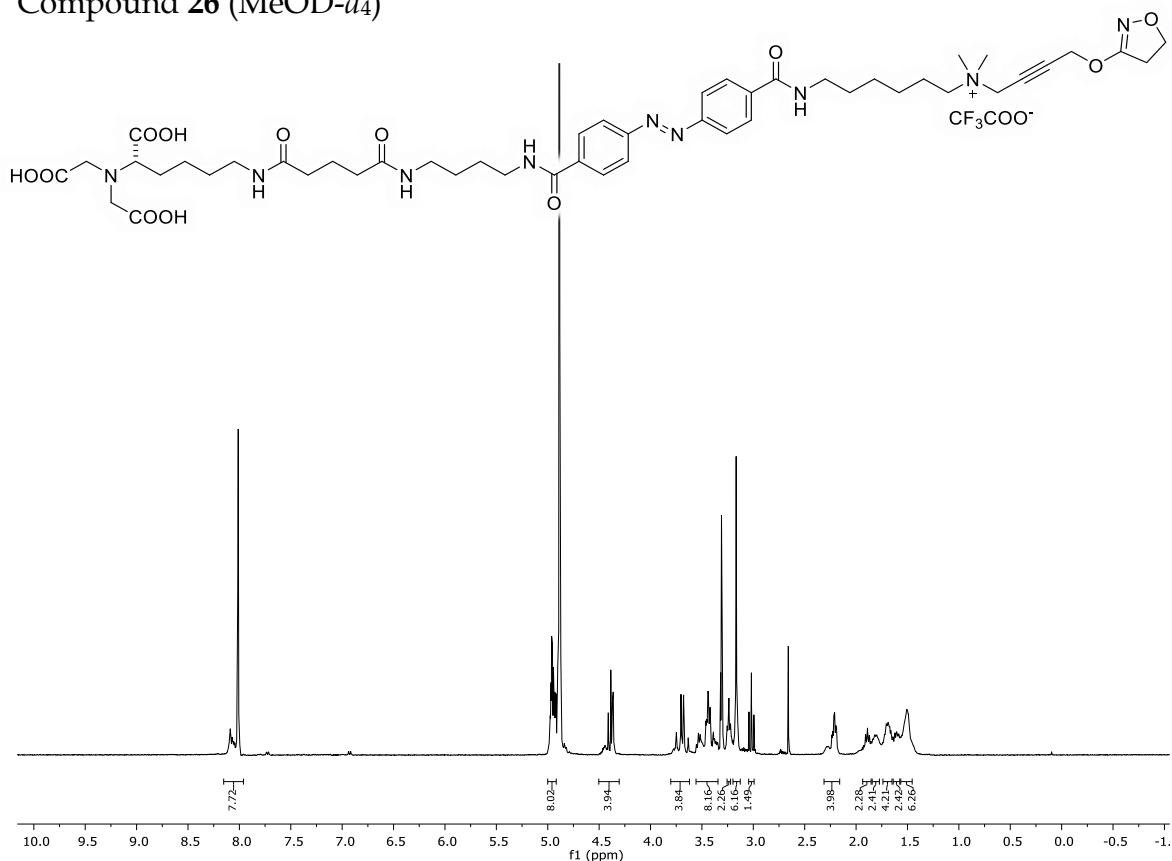
Compound **15** (DMSO-*d*₆)Compound **16** (DMSO-*d*₆)*

*copied print-out

Compound 17 (CDCl₃-d)

 Compound 19 (DMSO-d₆)


Compound **20** (DMSO-*d*₆)Compound **21** (DMSO-*d*₆)

Compound **23** (CDCl₃-d)

 Compound **25** (MeOD-d₄) (Zoom for visualization of amide groups in DMSO-d₆)


Compound **26** (MeOD-*d*₄)

8.5.2 UV-Vis Absorption Spectra, Cycle Performances, and Thermal Half-Lives

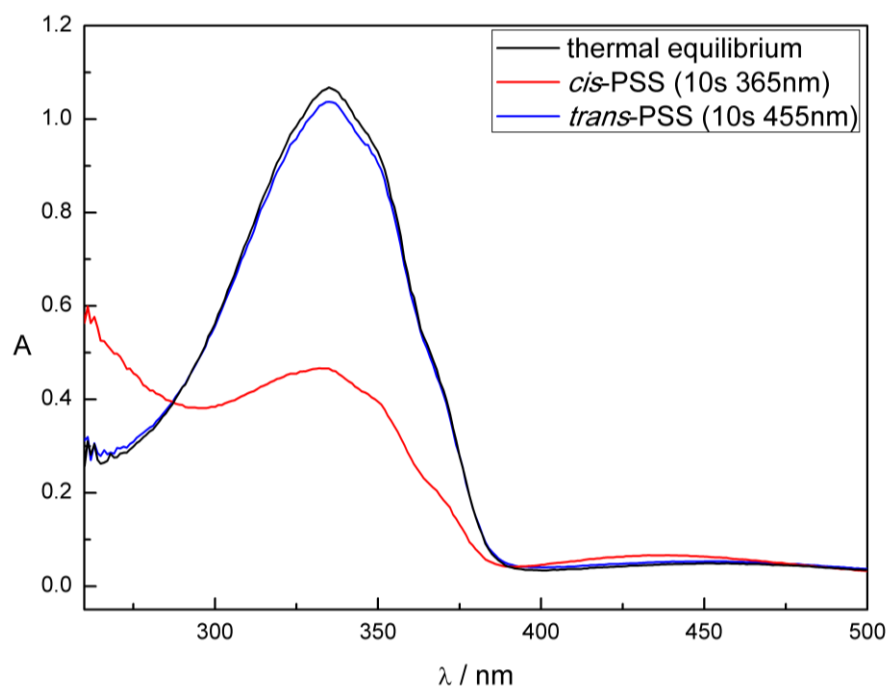


Figure S1. UV-Vis absorption spectrum of compound **14** measured in DMSO. Thermal equilibrium (black curve). *Cis*-PSS (red curve). *Trans*-PSS (blue curve).

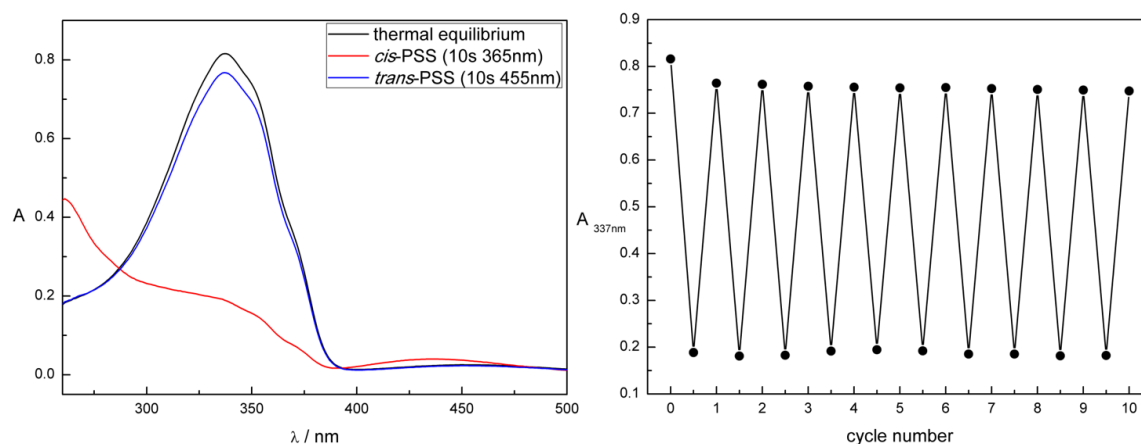


Figure S2. Left panel: UV-Vis absorption spectrum of compound **27** measured in DMSO. Thermal equilibrium (black curve). *Cis*-PSS (red curve). *Trans*-PSS (blue curve). Right panel: Repetitive cycle performance measured at λ_{\max} of the *trans* isomer.

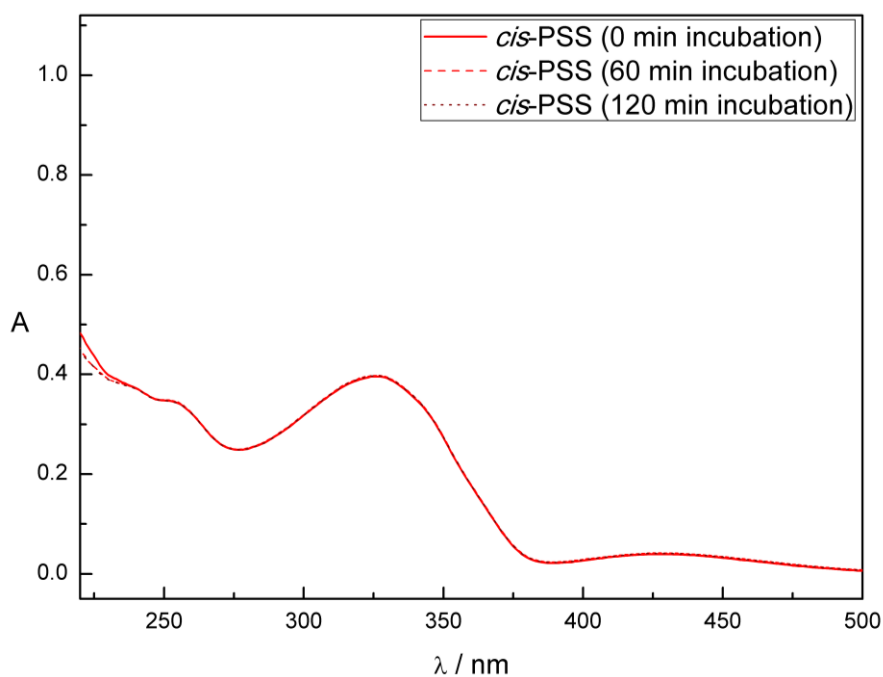


Figure S3. Thermal recovery of compound **18** measured in HBS in the dark. No changes in the absorption spectrum detected over 2 hours of measurement at 24 °C.

8.5.3 *In Vitro* Fluorescence Ca^{2+} Imaging

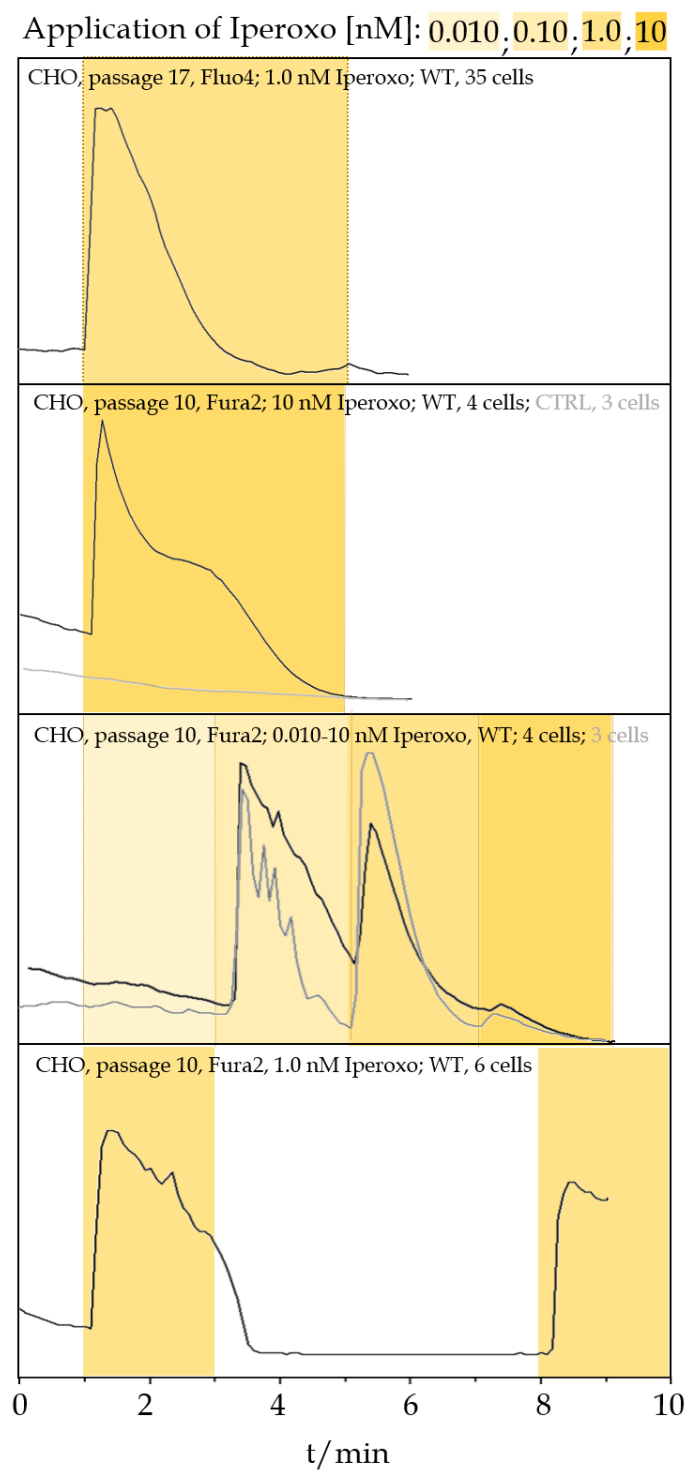


Figure S4. Evoked responses at wildtype CHO-cells upon addition of different concentrations of the iperoxo ligand in the presence of Fura2 and Fluo4, respectively, as fluorescence reporter for GPCR activation. Plots represent average activity of all analyzed cells.

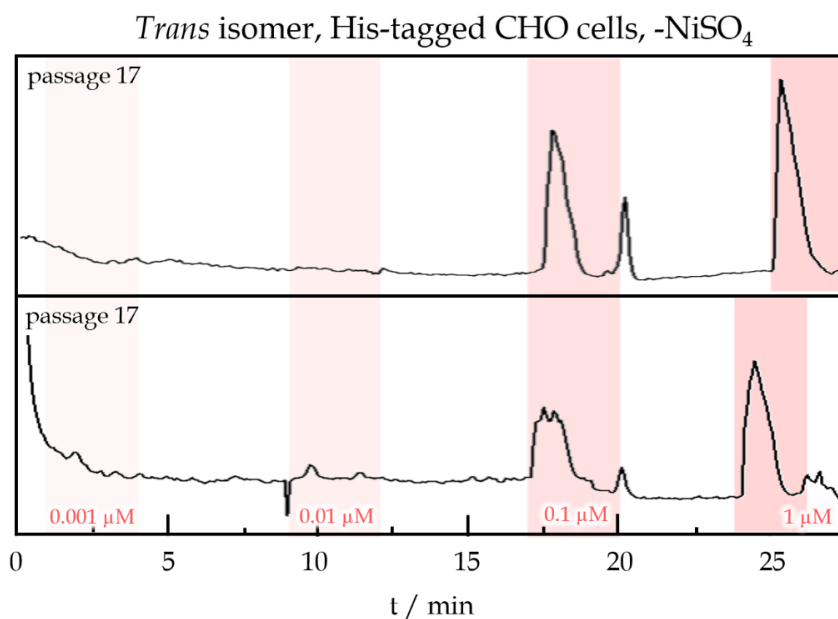


Figure S5. Evoked responses at His-tagged CHO-cells in the absence of nickel upon addition of different concentrations of *trans* **26**. Plots represent average activity of all analyzed cells.

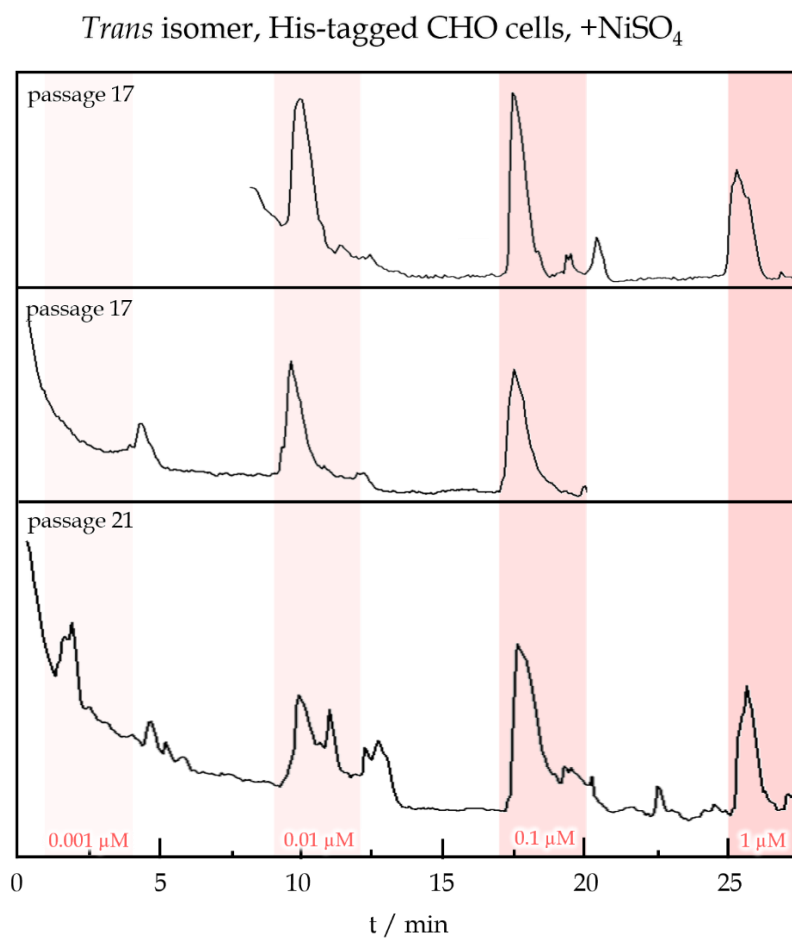


Figure S6. Evoked responses at His-tagged CHO-cells in the presence of nickel upon addition of different concentrations of *trans* **27**. Plots represent average activity of all analyzed cells.

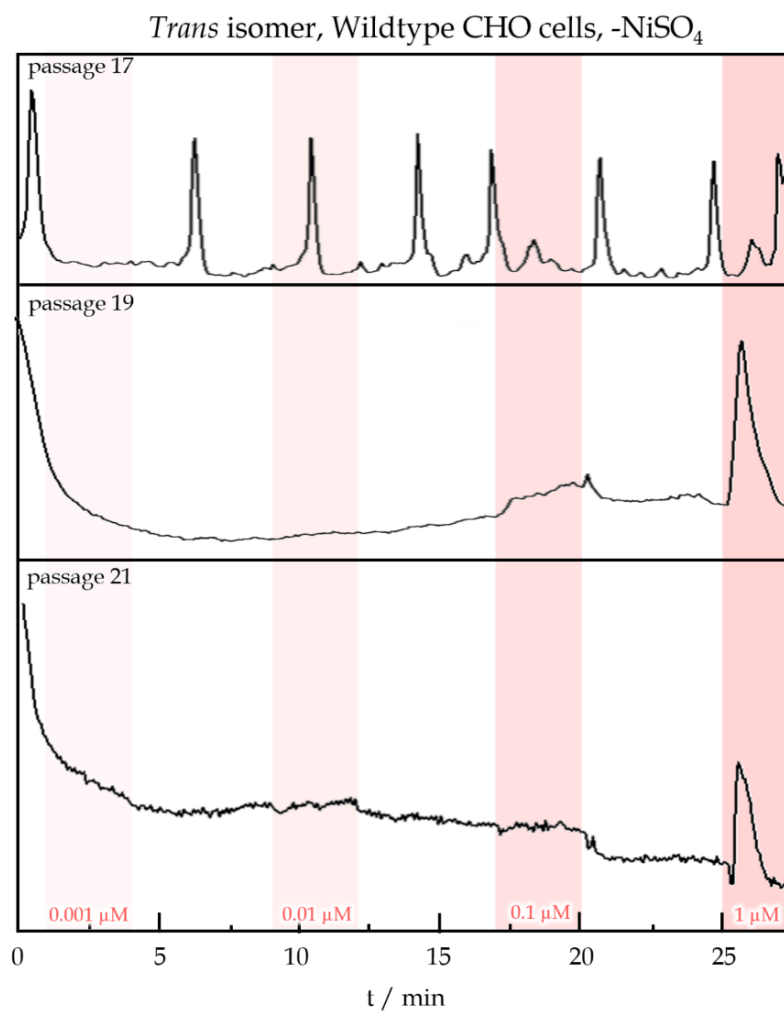


Figure S7. Evoked responses at wildtype CHO-cells in the absence of nickel upon addition of different concentrations of *trans* 26. Plots represent average activity of all analyzed cells.

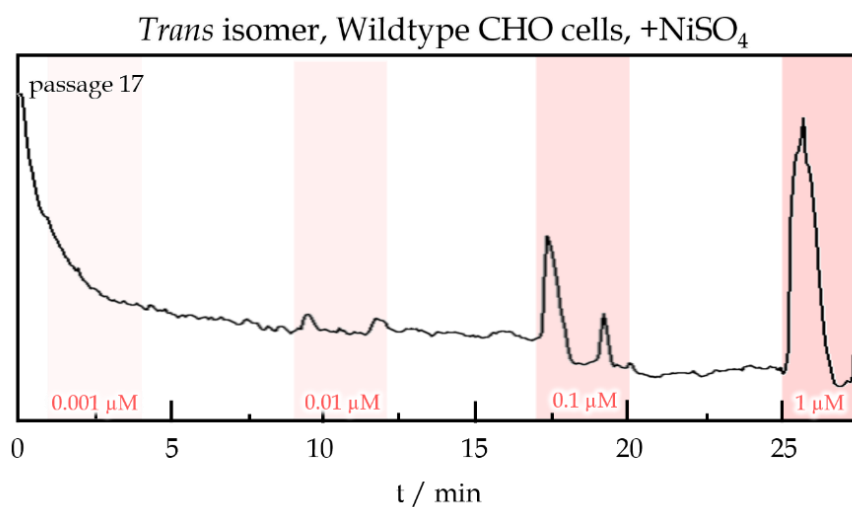


Figure S8. Evoked responses at wildtype CHO-cells in the presence of nickel upon addition of different concentrations of *trans* 27. Plots represent average activity of all analyzed cells.

8.6 References

- [1] S. B. Gacasan, D. L. Baker, A. L. Parrill, *AIMS Biophys.* **2017**, 4, 491-527.
- [2] J. C. Venter, M. D. Adams, E. W. Myers, *et al.*, *Science* **2001**, 291, 1304-1351.
- [3] E. S. Lander, L. M. Linton, B. Birren, *et al.*, *Nature*, **2001**, 409, 860-921.
- [4] R. Fredriksson, M. C. Lagerström, L. G. Lundin, H. B. Schiöth, *Mol. Pharmacol.* **2003**, 63, 1256-1272.
- [5] K. L. Pierce, R. T. Premont, R. J. Lefkowitz, *Nat. Rev. Mol. Cell Biol.* **2002**, 3, 639-650.
- [6] A. S. Hauser, M. M. Attwood, M. Rask-Andersen, H. B. Schiöth, D. E. Gloriam, *Nature Reviews Drug Discovery* **2017**, 16, 829-842.
- [7] M. C. Lagerstrom, H. B. Schioth, *Nat. Rev. Drug Discovery* **2008**, 7, 339.
- [8] X. Tang, Y. Wang, D. Li, J. Luo, M. Liu, *Acta Pharmacologica Sinica* **2012**, 33, 363-371.
- [9] D. J. Urban, B. L. Roth, *Annu. Rev. Pharmacol. Toxicol.* **2015**, 55, 399-417.
- [10] B. L. Roth, *Neuron* **2016**, 89, 683-694.
- [11] B. R. Conklin, E. C. Hsiao, S. Claeysen, A. Dumuis, S. Srinivasan, J. R. Forsayeth, J. M. Guettier, W. C. Chang, Y. Pei, K. D. Mc. Carthy, R. A. Nissenson, J. Wess, J. Bockaert, B. L. Roth, *Nature Methods* **2008**, 5, 673-678.
- [12] W. A. Velema, W. Szymanski, B. L. Feringa, *J. Am. Chem. Soc.* **2014**, 136, 2178-2191.
- [13] C. Brieke, F. Rohrbach, A. Gottschalk, G. Mayer, A. Heckel, *Angew. Chem. Int. Ed.* **2012**, 51, 2-33.
- [14] J. Broichhagen, A. Damijonaitis, J. Levitz, K. R. Sokol, P. Leippe, D. Konrad, E. Y. Isacoff, D. Trauner, *ACS Cent. Sci.* **2015**, 1, 383-393.

- [15] R. Kubota, W. Nomura, T. Iwasaka, K. Ojima, S. Kiyonaka, I. Hamachi, *ACS Cent. Sci.* **2018**, *4*, 1211-1221.
- [16] H. M. Dhammika Bandara, S. C. Burdette, *Chem. Soc. Rev.* **2012**, *41*, 1809-1825.
- [17] W. Szymanski, J. M. Beierle, H. A. V. Kistemaker, W. A. Velema, B. L. Feringa, *Chem. Rev.* **2013**, *113*, 6114-6178.
- [18] A. Goulet-Hanssens, C. J. Barrett, *Wiley Periodicals, Inc. J. Polym. Sci., Part A: Polym. Chem.* **2013**, *51*, 3058-3070.
- [19] P. Fatás, E. Longo, F. Rastrelli, M. Crisma, C. Toniolo, A. I. Jiménez, C. Cativiela, A. Moretto, *Chem. Eur. J.* **2011**, *17*, 12606-12611.
- [20] M. Zhou, S. Haldar, J. Franses, J.-M. Kim, D. H. Thompson, *Supramolecular Chemistry* **2005**, *17*, 101-111.
- [21] G. Ieronimo, G. Palmisano, A. Maspero, A. Marzorati, L. Scapinello, N. Masciocchi, G. Cravotto, A. Barge, M. Simonetti, K. L. Ameta, K. M. Nicholas, A. Penoni, *Org. Biomol. Chem.* **2018**, *16*, 6853-6859.

SUMMARY

9 Summary

This thesis presents the synthesis and (photo-)chemical characterization of (functionalized) photochromic scaffolds and their application for the deeper understanding of (bio-)chemical problems.

Chapter I deals with the synthesis of azobenzene surfactants bearing a polar head group and a hydrophobic tail. Variation of the substitution pattern led to the development of tool compounds with different photochromic, electronic, and steric properties. The group of Prof. Motschmann performed the photophysical analysis of the derivatives using the drop shape analysis. The influence of the light-induced *trans-cis* isomerization of a monolayer of the photochromic surfactant on the surface tension of a hanging drop resulted only in minor changes, which disqualified the compounds for further investigations.

A novel class of photochromic scaffolds based on arylazo NH-pyrazoles is presented in **Chapter II**. As so far mainly their methylated derivatives are reported, we performed UV-Vis studies to investigate this unexplored photochromic scaffold. Advantages of this compound class are overall good photostationary states, fast photoswitching with high fatigue and thermal stability of the corresponding *cis* isomers. Furthermore, the free NH allows for post functionalization and coordination. In addition, pyrazoles represent an important building block of many drugs and natural products.

In **Chapter III**, photoswitchable inhibitors for the tetrameric enzyme β -galactosidase are designed and analyzed for their inhibitory activity in cooperation with the group of PD. Dr. Gorris. This enzyme plays an important role in biochemistry and single molecule studies. Despite the recent advances in photopharmacology and the wide-spread use of azobenzenes, there are no photochromic inhibitors reported. Based on the molecular structures of 2-phenylethyl- β -D-thiogalactoside (PETG) and β -D-galactosylamine we designed light-responsive derivatives showing excellent photochromic properties in polar solvents. One optimized compound worked as strong competitive inhibitor with a

change in its inhibitory constant between 60 nM (*trans*) and 290 nM (*cis*) upon isomerization.

Chapter IV deals with light-switchable antagonists for the histamine H₁ receptor at the isolated guinea pig ileum. Variation in the position of the azobenzene moiety and of the chloro substitution pattern allowed the investigation of sterically and photochemically different derivatives of a reported histamine antagonist. In cooperation with Dr. Pockes an irradiation setup for tissue testing at the isolated guinea pig ileum was developed. One compound maintained the pharmacological activity compared to its non-photochromic reference and served as lead for further optimization. The two most promising derivatives showed increased antagonistic activity of their *trans* isomers compared to their non-photochromic reference. Upon irradiation-induced *trans-cis* isomerization the antagonistic activity of one compound dropped remarkably by a factor of even 46.

The azologization of a reported highly active glycine receptor potentiator and its use for light-triggered *in vivo* studies is discussed in **Chapter V**. Arylazo pyrazoles are used as photochromic scaffold as their photochromism benefits of almost quantitative switching in both directions, which is especially beneficial for biological applications, as an effect can clearly be assigned to one or the other isomer. One derivative showed sufficient solubility in aqueous media and was subjected to *in vivo* behavioral analysis performed in the group of Prof. Gorostiza. The tested compound acted as *cis* activator of tadpole excitatory activity and displaying inertness in its thermally stable *trans*-isomeric state. Molecular docking gave a rational for the observed differences between the two isomers in comparison to the reported reference.

In **Chapter VI**, fulgides are used as photochromic scaffold and merged with the molecular structure of amino-nitrazepam. As both isomeric states of fulgides are thermally stable, they can be isolated and tested separately. The synthetic conditions provided a fulgide-nitrazepam and its iso-fulgimide isomer. *In vitro* patch-clamp measurements were performed in the group of Prof. Bregestovski.

The iso-fulgimide showed a potentiating effect on GABA induced currents at the GABA_A receptor in its closed state, whereas the open conformation did not influence the amplitude of GABA-induced currents. *In vivo* analysis performed in the group of Prof. Gorostiza showed that both isomeric states produce different behavioral outcomes on *Danio rerio* larvae fitting both the results of the *in vitro* patch-clamp analysis and the expected effect of the benzodiazepine nitrazepam.

Chapter VII addresses the design, synthesis, photochromic characterization and *in vitro* investigation of azobenzene-based derivatives of reported antagonists of the serotonin receptor 5-HT₃. The photoligands either based on a quinoxaline or purine scaffold vary in their electronic and photochromic properties. Especially the purine-based azobenzenes displayed high solubility in aqueous media. Despite structural optimization for improved photochromism, only one derivative retained its antagonistic activity in patch-clamp studies performed in the group of Prof. Bregestovski. The effect was not controllable by irradiation induced isomerization, which might be explained by the low photostationary state of this compound and its slow switching.

The synthesis of a photochromic metal complex-agonist conjugate is content of **Chapter VIII**. This work is performed in cooperation with Prof. Hamachi reporting about coordination tethering of ligands to engineered receptors. A metal complex-agonist conjugate (MAC) bearing a highly active GPCR agonist is linked to a metal chelator *via* a flexible tether. This locates the ligand in proximity to its binding pocket. We envisioned that the introduction of an azobenzene as part of the linker results in binding and unbinding of the ligand due a change in end-to-end distance upon isomerization. In this case, the change in biological response of the photochromic MAC does not result from a change in the activity of the ligand itself but from a change in the accessibility of the ligand to its binding site. *In vitro* investigations for the *trans*-isomeric state are performed. The investigations on the *cis* isomers of the compound are ongoing.

ZUSAMMENFASSUNG

10 Zusammenfassung

Das Ziel dieser Doktorarbeit umfasst die Synthese und (photo-)chemische Charakterisierung (funktionalisierter) photochromer Grundgerüste sowie deren Anwendung zur Aufklärung (bio-)chemischer Fragestellungen.

Kapitel I behandelt die Synthese von Azobenzolen, die durch eine polare Kopfgruppe und einen hydrophoben Rest als einfache Tenside fungieren. Durch Änderungen im Substitutionsmuster konnten Verbindungen unterschiedlicher photochromer, elektronischer und sterischer Eigenschaften gewonnen werden. Die photophysikalische Testung der Substanzen mittels Tropfenstrukturanalyse wurde in der Gruppe von Prof. Motschmann durchgeführt. Die lichtinduzierte *trans-cis* Isomerisierung einer Monoschicht der photochromen Tenside rief nur eine geringe Änderung der Oberflächenspannung eines hängenden Tropfens hervor, weshalb keine weiteren Experimente durchgeführt wurden.

Eine neue Klasse photochromer Arylazo *NH*-Pyrazole ist in **Kapitel II** dargestellt. Da sich bisherige Studien vor allem mit ihren methylierten Derivaten befassen, wurden UV-Vis Experimente durchgeführt, um neues Wissen über dieses verborgene Schaltergerüst zu generieren. Vorteile dieser Klasse sind allgemein gute photostationäre Zustände, eine schnelle wiederholbare Photoisomerisierung sowie moderate thermische Halbwertszeiten ihrer *cis* Isomere. Desweiteren ermöglicht die freie *NH*-Gruppe Postfunktionalisierung und Koordination. Zudem sind Pyrazole ein wichtiger Strukturbaustein vieler Medikamente und Naturstoffe.

Kapitel III behandelt die Entwicklung photochromer Inhibitoren des tetrameren Enzyms β -Galactosidase sowie deren Testung in Zusammenarbeit mit der Arbeitsgruppe von PD Dr. Gorris. Das Enzym spielt eine Schlüsselrolle in der Biochemie und für Einzelmolekülstudien. Trotz der Fortschritte im Feld der Photopharmakologie und der weitreichenden Verwendung von Azobenzolen gibt es bisher keinen photochromen Inhibitor dieses Enzyms. Basierend auf den

molekularen Strukturen von 2-Phenylethyl- β -D-thiogalactosid (PETG) und β -D-Galactosylamin haben wir licht-regulierbare Derivate mit hervorragenden photochromen Eigenschaften in polaren Lösemitteln entwickelt. Eine optimierte Verbindung fungierte als effektiver kompetitiver Inhibitor und zeigte eine isomer-abhängige Änderung der Inhibitorkonstante zwischen 60 nM (*trans*) und 290 nM (*cis*).

Kapitel IV behandelt schaltbare Antagonisten des Histamin H₁ Rezeptors getestet am isolierten Meerschweinchendarm. Die Änderung der Position der Azobenzol Einheit und des Chlor Substitutionsmusters ermöglicht die Untersuchung sterisch und photochemisch unterschiedlicher Derivate eines publizierten Histamin Antagonisten. In Zusammenarbeit mit Dr. Pockes wurde ein Belichtungsapparat für Gewebetestungen am isolierten Meerschweinchendarm entwickelt. Für eine der analysierten Verbindungen konnte die inhibitorische Aktivität gegenüber ihrer nicht-photochromen Referenzsubstanz aufrechterhalten werden. Diese diente als Leitmotiv für weitere Strukturoptimierungen. Die beiden vielversprechendsten Derivate zeigten eine verstärkte antagonistische Aktivität ihrer *trans* Isomere im Vergleich zur nicht-photochromen Referenz. Durch die *trans-cis* Photoisomerisierung sank die antagonistische Aktivität einer Verbindung sogar um den Faktor 46.

Die Azologisierung eines literaturbekannten hochaktiven Verstärkers des Glycin Rezeptors und dessen Anwendung für licht-regulierte *in vivo* Studien ist in **Kapitel V** diskutiert. Arylazopyrazole als photochrome Grundgerüste zeichnen sich durch ihre nahezu quantitative Photoisomerisierung aus. Diese ist besonders für biologische Anwendungen von Vorteil, da ein Effekt eindeutig dem ein oder anderen Isomer zugeordnet werden kann. Ein Derivat war ausreichend wasserlöslich und wurde in der Gruppe von Prof. Gorostiza mittels *in vivo* Verhaltensstudien getestet. Die untersuchte Verbindung agierte als *cis* aktiver Verstärker der Kaulquappenaktivität, welche in ihrem thermisch stabilen *trans* Zustand inaktiv ist. Computerbasierte Strukturanalysen erklärten die

beobachteten Aktivitätsunterschiede beider Isomere im Vergleich zur Referenzsubstanz.

In **Kapitel VI** dienen Fulgide als Grundgerüst zur Synthese eines photochromen Aminonitrazepam Derivates. Da beide Fulgidisomere thermisch stabil sind, können diese isoliert und separat getestet werden. Die Synthesebedingungen führten zur Bildung eines Fulgimidnitrazepams und dessen iso-Fulgimidisomers. *In vitro* Patch-Clamp Analysen beider Substanzen wurden in der Gruppe von Prof. Bregestovski durchgeführt. Das geschlossene iso-Fulgimidisomer wirkte als Verstärker von GABA induzierten Ionenströmen am GABA_A Rezeptor, wohingegen das ringoffene Isomer keinen Einfluss nimmt. In der Gruppe von Prof. Gorostiza durchgeführte *in vivo* Analysen zeigten, dass beide Isomere des Isofulgimids unterschiedliche Verhaltensantworten bei *Danio rerio* Larven hervorrufen. Diese stimmen mit den Ergebnissen der *in vitro* Testung und der erwarteten Wirkung des Benzodiazepins Aminonitrazepam überein.

Kapitel VII behandelt das Design, die Synthese, die photochrome Charakterisierung und *in vivo* Untersuchung von azobenzolbasierten Antagonisten des Serotonin 5-HT₃ Rezeptors. Die Photoliganden basieren auf einem Quinoxalin oder Purin Gerüst und unterscheiden sich in ihren elektronischen und photochromen Eigenschaften. Besonders die purinbasierten Azobenzole sind in wässrigem Medium gut löslich. Trotz struktureller Optimierungen zur Verbesserung der Photochemie zeigte nur ein Derivat antagonistische Aktivität in Patch-Clamp Studien, welche in der Gruppe von Prof. Bregestovski durchgeführt wurden. Der Effekt war nicht photoregulierbar, was durch einen niedrigen photostationären Zustand und langsames Schalten begründet werden kann.

Die Synthese eines photochromen Metallkomplex-Agonist Konjugats wird in **Kapitel VIII** behandelt. Diese Arbeit wurde in Kooperation mit Prof. Hamachi durchgeführt, der über Koordinationsbindung von Liganden an modifizierte Rezeptoren berichtete. Ein Metall Komplex-Agonist Derivat trägt einen hoch

aktiven GPCR Agonisten, welcher über einen flexiblen Linker an einen Metallchelator gebunden ist. Dadurch ist der Ligand in räumlicher Nähe zu seiner Bindestelle am Rezeptor lokalisiert. Azobenzol als Teil des Linkers sollte es ermöglichen, die Bindung des Liganden durch isomer abhängige Zugänglichkeit zu regulieren. Dabei resultiert die Änderung des biologischen Effekts nicht von einer Änderung der Aktivität des Liganden, sondern dessen Zugänglichkeit. *In vitro* Studien des *trans* Isomers wurden durchgeführt. Die Analyse des *cis* Isomers ist ausstehend.

APPENDIX

11 Appendix

11.1 Abbreviations

°C	degrees Celsius
Å	Ångström (10^{-10} m)
3D	three-dimensional
5-HT	5-hydroxytryptamine
A	absorbance
AAP	arylazo pyrazole
aq.	aqueous
c	concentration
calcd.	calculated
cDNA	complementary deoxyribonucleic acid
<i>cf</i>	compare with/see also (<i>lat.</i> confer)
CHO	chinese hamster ovary
CL	caged ligand
cm	centimeter
cmc	critical micelle concentration
CNS	central nervous system
Cpd.	compound
CRC	concentration response curve
Cys	cysteine
δ	chemical shift
DCC	dicyclohexylcarbodiimide
DIPEA	diisopropylethylamin
DMF	dimethylformamide
DMSO	dimethylsulfoxide
dpf	days post fertilization
DSA	drop shape analysis
DTE	dithienylethene

ε	molar extinction coefficient
EA	ethyl acetate
<i>E. coli</i>	<i>Escherichia coli</i>
EC ₅₀	half-maximal effective concentration
EDG	electron donating group
<i>e.g.</i>	for example (<i>lat. exempli gratia</i>)
eq	equivalent
ESI	electrospray ionization
<i>et al.</i>	and others (<i>lat. et alii</i>)
EWG	electron withdrawing group
F	phenylalanine
FBS	fetal bovine serum
g	gram
γ	surface tension
GABA	gamma aminobutyric acid
GABA _A R	gamma aminobutyric acid receptor subtype A
GFP	green fluorescent protein
GI	gastrointestinal
GlyR	glycine receptor
gp	guinea pig
GPCR	G protein-coupled receptor
h	hour
HEPES	2-(4-(2-hydroxyethyl-1-piperazinyl)-ethansulfonsäure
His	histidine
HMBC	heteronuclear multiple bond correlation
<i>hν</i>	incident photon energy
HOBt	1-hydroxybenzotriazol
HPLC	high pressure liquid chromatography
HR	high resolution
HSQC	heteronuclear single quantum coherence spectroscopy

ID	identification number
J	coupling constant
K_i	inhibitory constant
K_M	Michaelis constant
L	liter
LED	light-emitting diode
λ_{Em}	emission wavelength
λ_{Ex}	excitation wavelength
λ_{irr}	irradiation wavelength
lm	lumen
log	logarithm
M	molar (mol/L)
m	meter
mA	milli ampere
mAChR	muscarinic acetylcholine receptor
MeCN	acetonitrile
MeOH	methanol
MF	molecular formula
mg	milligram
min	minute
mL	milliliter
mM	millimolar (mmol/L)
mm	millimeter
μ M	micromolar
mmol	millimole
MMR	Marc's modified ringer
mN	milli Newton
mOsm	milliosmole
M.p.	melting point
MS	mass spectrometry

mV	milli volt
mW	milli watt
MW	molecular weight
<i>n</i>	number
n.a.	not active
n.d.	not detected
NACHR	nicotinic acetylcholine receptor
NHS	<i>N</i> -hydroxy succinimid
nm	nanometer
NMR	nuclear magnetic resonance
ns	nanosecond
oxone	potassium peroxy sulfate
p.a.	pro analysi
PBS	phosphate-buffered saline
PCL	photochromic ligand
PDB	protein data bank
PE	petroleum ether
PETG	polyethylene terephthalate glycol
PMAC	photochromic metal complex-agonist conjugate
PORTL	photoswitchable orthogonal remotely tethered ligand
ppm	parts per million
PSS	photostationary state
PTL	photochromic tethered ligand
R	arginine
ppm	parts per million
R	arginine
RP	relaxation period
rt	room temperature
s	second
s.d.	standard deviation

SEM	standard error of the mean
T	temperature
t	time
t _{0.5}	half-life
TFA	trifluoroacetic acid
THL	thermal half-life
TLC	thin layer chromatography
t _R	retention time
UV	ultra violet
Vis	visible
WT	wildtype
wt%	weight percent
<i>X. tropicalis</i>	<i>Xenopus tropicalis</i>
Y	tyrosine

11.2 Curriculum Vitae

PERSONAL DATA

Name: Karin Rustler
Date of birth: 04.08.1992
Place of birth: Regensburg
Nationality: German

EDUCATION

11/2016 – 11/2019 **Ph. D. thesis** at the Institute of Organic Chemistry, University of Regensburg (Supervisor: Prof. Dr. B. König)
“Functionalized Photochromic Scaffolds”
10/2014 – 09/2019 **Master of Science** in Biochemistry, University of Regensburg
Master thesis: “Azobenzene Modified Muscimol Derivatives as Photochromic Modulators for GABA Ion Channels” (Supervisor: Prof. Dr. B. König)
10/2011 – 09/2014 **Bachelor of Science** in Biochemistry, University of Regensburg
Bachelor thesis: “Influence of the LMX1B target genes *Abra* and *Arl4c* on the RhoA signaling cascade” (Supervisor: Prof. Dr. R. Witzgall)
09/2002 – 05/2011 **Allgemeine Hochschulreife** (general university entrance qualification) at the Johann-Michael-Fischer Gymnasium Burglengenfeld

INTERNSHIPS

06/2019 – 08/2019 Department of Synthetic Chemistry and Biological Chemistry, **Kyoto University**, Japan (Supervisor: Prof. Dr. I. Hamachi)
“Photochromic Metal Complex-Agonist Conjugates”
06/2016 **Institute for Bioengineering of Catalonia (IBEC)**, Barcelona, Spain (Supervisor: Prof. Dr. P. Gorostiza)
“*In vivo* characterization of photochromic ligands for GABA_AR and GlyR in freely behaving tadpoles and zebrafish larvae”
09/2015 – 11/2015 **Helmholtz Zentrum München** (German Research Center for Environmental Health), Germany (Supervisor: Dr. A. Wolf)
“Homo-Oligomerization and Substrate-Binding of Ribosomale Oxygenases”

CONFERENCES

11/2018 **14th International Kyoto Conference on New Aspects of Organic Chemistry**, Kyoto, Japan (poster presentation)

11/2018	2nd International Symposium on Photopharmacology , Vic, Spain (poster presentation)
09/2018	9th Summerschool "Medicinal Chemistry" , Regensburg, Germany (poster presentation)
09/2018	26th Lecture Conference on Photochemistry , Munich, Germany (poster presentation)
04/2018	3rd Modulightor Meeting , Regensburg, Germany (oral presentation)
07/2017	2nd Modulightor Meeting , Marseille, France (oral presentation)
06/2017	ACS National Organic Chemistry Symposium , Davis, California, America (poster presentation)
02/2017	International Symposium on Photopharmacology , Groningen, Netherlands (poster presentation)
11/2016	PSL*Chemical Biology Symposium , Paris, France (poster presentation)
09/2016	8th Summerschool "Medicinal Chemistry" , Regensburg, Germany (poster presentation)
06/2016	1st Modulightor Meeting , Barcelona, Spain (oral presentation)

PUBLICATIONS

K. Rustler, G. Maleeva, A. Gomila-Juaneda, P. Gorostiza, P. Bregestovski, B. König, „Fulgazepam: A Fulgimide-Based Potentiator of GABA_A Receptors.“ *ChemRxiv* **2019**, DOI: 10.26434/chemrxiv.9906194.v1.

A. Gomila-Juaneda, K. Rustler, G. Maleeva, A. Nin-Hill, D. Wutz, A. Bautista-Barrufet, X. Rovira, M. Bosch, E. Mukhametova, M. Mukhamedyarov, F. Peiretti, M. Alfonso-Prieto, C. Rovira, B. König, P. Bregestovski, P. Gorostiza, „Photocontrol of endogenous glycine receptors in vivo.“ *BioRxiv* **2019**, DOI: 10.1101/744391.

G. Maleeva, D. Wutz, K. Rustler, A. Nin-Hill, M. Alfonso-Prieto, E. Petukhova, A. Bautista-Barrufet, A. Gomila-Juaneda, P. Scholze, F. Peiretti, C. Rovira, B. König, P. Gorostiza, P. Bregestovski, „A photoswitchable GABA receptor channel blocker.“ *Brit. J. Pharmacol.* **2019**, 176, 2661-2677.

K. Rustler, G. Maleeva, P. Bregestovski, B. König, „Azologization of serotonin 5-HT₃ receptor antagonists.“ *Beilstein J. Org. Chem.* **2019**, 15, 780-788.

K. Rustler, S. Pockes, B. König, „Light-switchable antagonists for the histamine H₁ receptor at the isolated guinea pig ileum.“ *ChemMedChem* **2019**, 14, 636-644.

K. Rustler, M. J. Mickert, J. Nazet, R. Merkl, H. H. Gorris, B. König, „Development of photoswitchable inhibitors for β -galactosidase.“ *Org. Biomol. Chem.* **2018**, 16, 7430-7437.

DANKSAGUNG

12 Danksagung

Allen voran gilt ein besonderer Dank meinem Doktorvater Prof. Dr. Burkhard König für die Betreuung meiner Dissertation und die Möglichkeit, diese Arbeit im Feld der Photochemie an der Schnittstelle zur Biochemie im Rahmen zahlreicher Kooperationen durchzuführen. Ich bedanke mich herzlichst für seine Unterstützung, seine positive und motivierende Art und die mir gewährten Freiheiten. Danke für die Hilfe zur Organisation meines Auslandsaufenthaltes an der Universität in Kyoto. Großer Dank gilt hierbei Prof. Dr. Itaru Hamachi und Prof. Dr. Ryou Kubota für die exzellente Betreuung vor Ort. *Domo arigatou gozaimashita.*

Für die Übernahme des Zweitgutachtens danke ich PD Dr. Hans-Heiner Gorris. Vielen Dank an Prof. Dr. Frank-Michael Matysik und Prof. Dr. Julia Rehbein, dass sie sich die Zeit genommen haben in meinem Prüfungsausschuss mitzuwirken.

Ich danke dem Bundesministerium für Bildung und Forschung für die Teilfinanzierung meiner Promotion im Rahmen des „MODULIGHTOR“ Projektverbundes sowie der Japan Society for the Promotion of Science für die Finanzierung meines Japan Auslandsaufenthaltes.

Besonderer Dank gilt meinen Kooperationspartnern Prof. Dr. Pau Gorostiza, Prof. Dr. Carme Rovira, Prof. Dr. Piotr Bregestovski, Prof. Dr. Hubert Motschmann, PD Dr. Hans-Heiner Gorris, Dr. Steffen Pockes, Dr. Stefano Crespi, Dr. Philipp Nitschke, Dr. Galina Maleeva, Dr. Mercedes Alfonso-Prieto, Alexandre Gomila-Juaneda, Alba Nin-Hill, Alexander-Anton Dietz, Julian Nazet und Matthias Mickert für die vielen fachlichen Diskussionen und ohne deren Mitwirken diese Arbeit nicht zustande gekommen wäre.

Den Mitarbeitern der Zentralen Analytik der Universität Regensburg danke ich für die stets zuverlässige und gewissenhafte Messung meiner Aufträge, insbesondere Josef Kiermaier und Wolfgang Söllner für die zahlreichen MS

Messungen sowie der Röntgenstrukturanalyse für die unermüdlichen Versuche messbare Kristalle in meinen Proben zu finden.

Vielen Dank an alle Festangestellten des AK Königs für jegliche Hilfe und Unterstützung bei technischen, organisatorischen und bürokratischen Angelegenheiten sowie den gelegentlichen Small-Talk.

Meinen Praktikanten, Bachelor- und Masteranden Sebastian Graf, Ran An, Wolfgang Haumer, Jessica Stahl, Oaikhena-Zekeri Esezobor, Ann-Kathrin Baier, und besonders Ulrike Wirth danke ich für die Mitarbeit an meinen Forschungsprojekten.

Ganz besonderer Dank gilt den ehemaligen und derzeitigen Mitgliedern des Arbeitskreises, vor allem meinen – nicht nur – Laborkollegen Karsten Donabauer und Anna Berger für das angenehme Arbeitsklima und alle Aktivitäten drum herum, für Ihre Hilfsbereitschaft, gemeinsame Pausen, erholsame Abende, schöne Urlaube und auch die ein oder andere fachliche Diskussion. Danke an Manuel Bause und Simone Stark, die mich für die Synthesechemie begeistert haben sowie an Daniel Wutz, Daniel Lachmann und Nadja Simeth für Ihre Unterstützung.

Von ganzem Herzen danke ich meinen Eltern und meinen Brüdern für Ihren Rückhalt. Besonderer Dank geht an Thomas und an meine langjährigen Freundinnen Felicitas und Carolin – Danke, dass wir uns nie aus den Augen verloren haben und ihr mich auf meinem Weg begleitet und immer für mich da seid.

„Leider lässt sich eine wahrhafte Dankbarkeit mit Worten nicht ausdrücken.“

- Johann Wolfgang von Goethe

Danke